Department of Imaging and Applied Physics

Geological Histories from 4372 Ma to 26 Ma Recorded in Siliciclastic Metasedimentary Rocks from the Central Yilgarn Craton

Eric Royal Thern

This thesis is presented for the Degree of
Doctor of Philosophy
of
Curtin University

October 2012

0.1 Declaration

To the best of my knowledge and belief this thesis contains no material previously published by any other person except where due acknowledgement has been made.

This thesis contains no material which has been accepted for the award of any other degree or diploma in any university.

Signature: 

Date: June 24, 2013

0.2 Abstract

This study presents an investigation of detrital, metamorphic, and hydrothermal minerals from siliciclastic metasedimentary rocks of the Illaara and Maynard Hills greenstone belts, central Yilgarn Craton. This research assesses how 4.3 to 3.0 Ga detrital zircon populations came to be found in dispersed metasedimentary rocks, how these rock occurrences relate to each other and what this may reveal about early Earth and the formation of the Yilgarn Craton.

Hadean zircons from the greenstone belts show complex age structures that have been investigated via Sensitive High Resolution Ion Microprobe (SHRIMP) spot analysis, traverses and depth profiling, Electron Probe Microanalysis (EPMA), Quantitative Evaluation of Minerals by Scanning electron microscopy (QEMSCAN), and cathodoluminescence (CL) imaging techniques. SHRIMP analyses on >4300 Ma detrital zircon cores show concordant $^{207}Pb/^{206}Pb$ dates which span >50 M.y., a significantly larger range than expected from analytical uncertainty. Later (<3800 Ma) metamorphic events have modified the $^{207}Pb/^{206}Pb$ dates obtained on many detrital grains. Evidence is presented that late-stage overprinting of thermal events has left distinct signatures in the Hadean grains and that only the most pristine 'cores' of the zircons can be used when interpreting age results. The observed range of $^{207}Pb/^{206}Pb$ dates on pristine Hadean zircon cores suggests early heterogeneous (>3900 Ma) Pb-redistribution between annealed and radiation-damaged zones or channels during periodic post-crystallization thermal events.

In order to assess the provenance of the Hadean zircons, a multivariate approach using a similarity matrix derived from >5500 UPb zircon analyses was used to investigate the complex and overlapping detrital zircon age structure within ca. 3 Ga metasedimentary rocks from the Yilgarn Craton, Western Australia. Detrital zircon analyses were grouped by their $^{207}Pb/^{206}Pb$ dates using a robust Chi-square grouping method which produced 74 Yilgarn-wide age groups from a pool of >3500 analyses and that were correlated between different metasedimentary rocks. Principal component analysis (PCA) was then used on a calculated similarity matrix of >65 samples which contained these age groups. PCA indicates that the main age populations of the detrital zircons in the ca. 3 Ga metasedimentary rocks were derived in varying portions from the Narryer and Yarlarweelor Gneiss Complexes. Differences between the age structure of >3.9 Ga zircon populations within the Mt. Alfred metasedimentary rocks with those from Mt. Narryer, Jack Hills and Maynard Hills localities is best explained by their derivation from two distinct Hadean terranes which were joined by ca. 3.7 Ga.

The presence of detrital Hadean zircons in ca. 3.0 Ga metasedimentary rocks of the Illaara and Maynard Hills greenstone belts implies a genetic link to the ca. 3.0 Ga metasedimentary rocks of the Narryer Terrane, which also contain abundant Hadean zircons. As granites and gneisses older than the youngest detrital zircons within these metasedimentary rocks have not been identified within the Southern Cross Terrane, the metasedimentary rocks of the Maynard Hills, Illaara and Gum Creek greenstone belts may be the oldest rocks yet identified within this terrane. Well preserved sedimentary structures are rare, as upper-greenschist to middle-amphibolite facies metamorphism and shearing has obscured primary relationships between the greenstone-hosted metasedimentary rock occurrences. More than 1000 detrital zircons from twelve samples within

these belts were analyzed to determine the age and composition of their provenance sources and to better constrain their stratigraphic relationships.

Depositional ages are currently constrained by the youngest zircons from Mt. Alfred's eastern (3318±6 Ma) and western (3264±7 Ma) horizons, and Maynard Hills ca. 3060 to 2960 Ma analyses. A minimum depositional age of ca. 2939 Ma has been calculated by the use of $^{40}Ar/^{39}Ar$ plateau ages using tourmalines from stratiform quartz-tourmaline veins within the outcrops. Increasing age complexity and maximum depositional age 'younging' is common across the Mt. Alfred locality from East (almost exclusively 3700-3780 Ma) to West (3300-3700 Ma and >3800 Ma). The western-most horizon at Mt. Alfred contains abundant >3800 Ma zircons, but lacks the prominent 3500 to 3300 Ma ages common to Jack Hills Hadean-zircon bearing metasedimentary rocks. This Hadean-zircon bearing horizon at Mt. Alfred is most similar in detrital zircon age characteristics to the metasedimentary rocks at Mt. Narryer but without the younger zircon ages (of Eurada and Dugel gneiss affinity; 3480-3300 Ma) found in abundance at Mt. Narryer. This makes Mt. Alfred a unique source for detrital Hadean zircons.

The detrital zircon age similarities within greenstone-hosted metasedimentary rocks throughout the Yilgarn Craton, including the Illaara, Maynard Hills and Gum Creek Greenstone Belts of the Southern Cross Terrane, the Jack Hills and Mt. Narryer of the Narryer Terrane, and the Toodyay Lake Grace Domain within the South West Terrane, strongly suggest a shared provenance of these ca. >2940 Ma metasedimentary rocks. It is likely they were deposited contemporaneously between ca. 3300 and 2940 Ma, later separated by multiple younger ca. 2950 to 2630 Ma granite-greenstone formations during rifting and collision episodes, and occur today as 'rafts' within younger ca. 2730-2640 Ma granite-greenstones.

A minimum depositional age, that also constrains the end-stages of deposition of the early Archean metasedimentary rocks, has been determined at ca. 2939±15 Ma (95% confidence) via multiple robust $^{40}Ar/^{39}Ar$ plateau ages on tourmalines within post-depositional stratiform layers. An initial indication of Ar closure temperature in tourmaline was experimentally calculated to be >600 °C by a single step-heating experiment. The association of barite and rhythmites in parallel metasedimentary units, indications of relatively enriched $\delta^{11}B$ within tourmaline, and their 2939±15 Ma $^{40}Ar/^{39}Ar$ dates suggest the host sediments were deposited prior to 2939±15 Ma within a marine-intertidal-evaporitic environment. Younger stratiform tourmaline, crystallized on the margins of late-stage quartz veins, give an age of 2622±20 Ma, defining the timing of the quartz veining, and a second stage of tourmaline growth from B-rich fluids.

The post-depositional thermal history of ca. 3.0 Ga Illaara and Maynard Hills greenstone belt siliciclastic metasedimentary rocks are characterized by a combination of SHRIMP U-Pb rutile, $^{40}Ar/^{39}Ar$ and (U-Th)/He geochronology. SHRIMP U-Pb rutile analyses from 8 siliciclastic metasedimentary rock samples reveal a complex history of events between deposition of their host sandstones (ca. 3.0 Ga) and the subsequent intrusions of mafic-ultramafics at ca. 2.8 Ga, folding, thrusting and granitic intrusions (ca. 2730 to 2630 Ma, regional D1 to D3 events). Some individual rutile grains yield multiple U-Pb dates which span from before the maximum depositional age of the metasedimentary rocks at ca. 3060 Ma to the last major metamorphic and granitic event at ca. 2630 Ma. These rutiles exhibit weakly defined core-rim younging profiles which have been interpreted to represent multiple stages of metamorphic growth and crystallization and

a possible Pb-loss overprinting. The results suggest that under protracted upper greenschist to pulses of mid-amphibolite metamorphic conditions, rutile can retain signatures of multiple thermal events and even retain some of their original detrital ages and characteristics. $^{40}Ar/^{39}Ar$ plateau ages on muscovites from both greenstone belts show that late to post-deformation, planar-foliation recrystalization at 2610±15 Ma (possibly coeval with the end of D3) marks the end of high-grade stabilizing tectono-thermal events and temperatures above 350−400°C. Zircon (U−Th)/He dates of 230±13 Ma define the age of exhumation, with temperatures <180°C for the siliciclastic metasedimentary rocks, similar to fission track results from the northern Yilgarn. Goethite (U−Th)/He dates of 25±2 Ma are probably coeval with Fe-rich meteoric fluid influx and associated zero-age Pb-loss and Fe enrichment in metamict zones of both rutile and zircon.

0.3 Acknowledgements

I gratefully acknowledge the assistance of the following:

David R. Nelson, who supervised this thesis and guided many aspects of the research direction. I especially thank his resolve when his guiding influence was ignored, and his input when tangential research yielded results. It's impossible to summarize in a few sentences the level of support provided; but from help with the scholarship application process all the way through critical editing of this manuscript, he was always available and for that I am greatly appreciative.

Other supervisory support from Neal McNaughton, Bob Loss and Robert Pidgeon has helped with smoothing the path towards completion, and honing in on specific aspects of this research.

Special thanks to Fred Jourdan of the West Australian Argon Isotope Facility (WAAIF) for the $^{39}Ar/^{40}Ar$ lab time and discussions on not just all things Argon, but also relating to the overall thesis during my candidature. Without this support, the post-depositional component of this thesis would have assuredly been meagre.

Invaluable discussions and support from within the Curtin University Geology department, especially Birger Rasmussen, Simon Wilde, Ian Fletcher, Alexander Nemchin and others have helped many aspects of this research.

This research has benefited from invaluable scientific (and perhaps some random) discussions with, to name a few (and in no particular order), Wulf Mueller†, James K.W. Lee, Greg Hitchen, Chi V. Ly, Jeff Chiarenzelli, Dustin Trail, Nick Tailby, Bruce Watson, Andreas Möller, Thorsten Geisler, Martina Menneken, and Falko Langenhorst.

Discussions with numerous people at the Goldschmidt Geochemistry Conference (Prague, 2011) has helped this research, especially the rutile and post-depositional components. Thanks goes to Thomas Zack, Delia Rösel, Matthijs Smit, Ellen Kooijman, and Tanya Ewing.

Noreen Evans, Brad McDonald and Martin Danišík are thanked for the (U−Th)/He analyses and discussions about these results.

I would like to acknowledge the support from within the John de Laeter SHRIMP lab, especially that of Hao Gao, Adin Sehic, Richard Taylor and Allen Kennedy. Further, I acknowledge help from Neal McNaughton, Richard Taylor and Allen Kennedy for the Windmill Hill rutile standards used in Chapter 6.

Many thanks to Adam Frew, Adam Freeman, Stefan Klaric, Anna van der Helder and Renee Bingham for providing excellent support on multiple sampling trips to the Maynard Hills and Illaara Greenstone Belts. Honorable mention goes to the Klaric family and Rudi Klaric†, for the loan of a binocular mineral-picking microscope, which was used in the preparation of nearly all samples throughout this study.

Special acknowledgement is due for the contributions of Adam Frew for help during fieldwork, his insistence on collecting the quartz-tourmaline sample MA08, and help within the WAAIF $^{40}Ar/^{39}Ar$ lab including valuable discussions on sample preparation and instrumental analysis.

The St. Lawrence University Geology Department is thanked for access to laboratory and XRD equipment, with support from the James Street Fund of St. Lawrence University. Jill Pflugheber of the St. Lawrence University Microscopy Laboratory provided invaluable assistance and support with the SEM imaging and EDS analytical techniques.

All SHRIMP analyses were carried out on the SHRIMP II at the John de Laeter Centre for Isotope Research at Curtin University of Technology, operated by a consortium consisting of Curtin University of Technology, the Geological Survey of Western Australia and the University of Western Australia.

All electron microprobe (EPMA) analyses were carried out by Greg Hitchen at CSIRO.

Financial support was provided by a Curtin University Postgraduate Scholarship (CUPS), for which I thank Curtin University and the Australian taxpayer.

I would like to thank my family for their understanding and support while I've been on the other side of the planet. Mom, Dad, Rachel and Sarah - glad you've listened to me and provided feedback even when you didn't necessarily want to listen any longer.

Finally, extra special thanks to Renee, who has been there for me through thick and thin, and will be thankful when this can become a doorstop.

TABLE OF CONTENTS

LIST OF FIGURES

LIST OF TABLES

CHAPTER 1
INTRODUCTION

The oldest materials that survive on Earth, >4000 Ma zircons, are found within ca. 3 Ga metasedimentary rocks throughout the Yilgarn Craton. These zircons, with ages up to ca. 4400 Ma, have been found within the metasedimentary rocks of Mt. Narryer (Froude et al., 1983; Kinny et al., 1990; Crowley et al., 2005; Pidgeon and Nemchin, 2006), Jack Hills (Compston et al., 1985; Wilde et al., 2001; Peck et al., 2001; Cavosie et al., 2004; Crowley et al., 2005; Cavosie et al., 2006), Maynard Hills (Nelson, 2002a; Wyche et al., 2004) and the Mt. Alfred locality of the Illaara Greenstone Belt (Nelson, 2005; Wyche, 2007); this study; see Figure 1.1. The metasedimentary rocks at Jack Hills are among the most-studied on Earth with sample site W74 having well over 100,000 zircons analyzed thus far (Holden et al., 2009). More recently, zircons with ages older than 4000 Ma have been found within ca. 3.0 Ga Southern Cross Terrane metasedimentary rocks within the Illaara (Nelson, 2005; Wyche, 2007) and Maynard Hills (Nelson, 2002b; Wyche et al., 2004) greenstone belts. These ancient zircons are of unknown provenance, and their distribution throughout multiple disparate metasedimentary rocks >400 km apart within granite greenstone terranes and high grade gneiss complexes makes their relation to one another at time of deposition difficult to assess.

1.1 Overview and Thesis Structure

This thesis presents an investigation of detrital, metamorphic, and hydrothermal minerals from siliciclastic metasedimentary rocks of the Illaara and Maynard Hills greenstone belts, central Yilgarn Craton. This research assesses how 4.3 to 3.0 Ga detrital zircon populations came to be found in dispersed metasedimentary rocks, how these rock occurrences relate to each other and what this may reveal about the early Earth and the formation of the Yilgarn Craton.

Each chapter of this thesis consists of a self-contained investigation, in publication or manuscript form, into an aspect of this problem, with a summary of events in the conclusions chapter 7. The final chapter, chapter 8, is a series of in-press supplemental studies which have helped in the interpretation of data throughout this thesis.

This section presents an overview of each chapter, highlighting the aims and direction of each study in reference to the overall thesis structure.

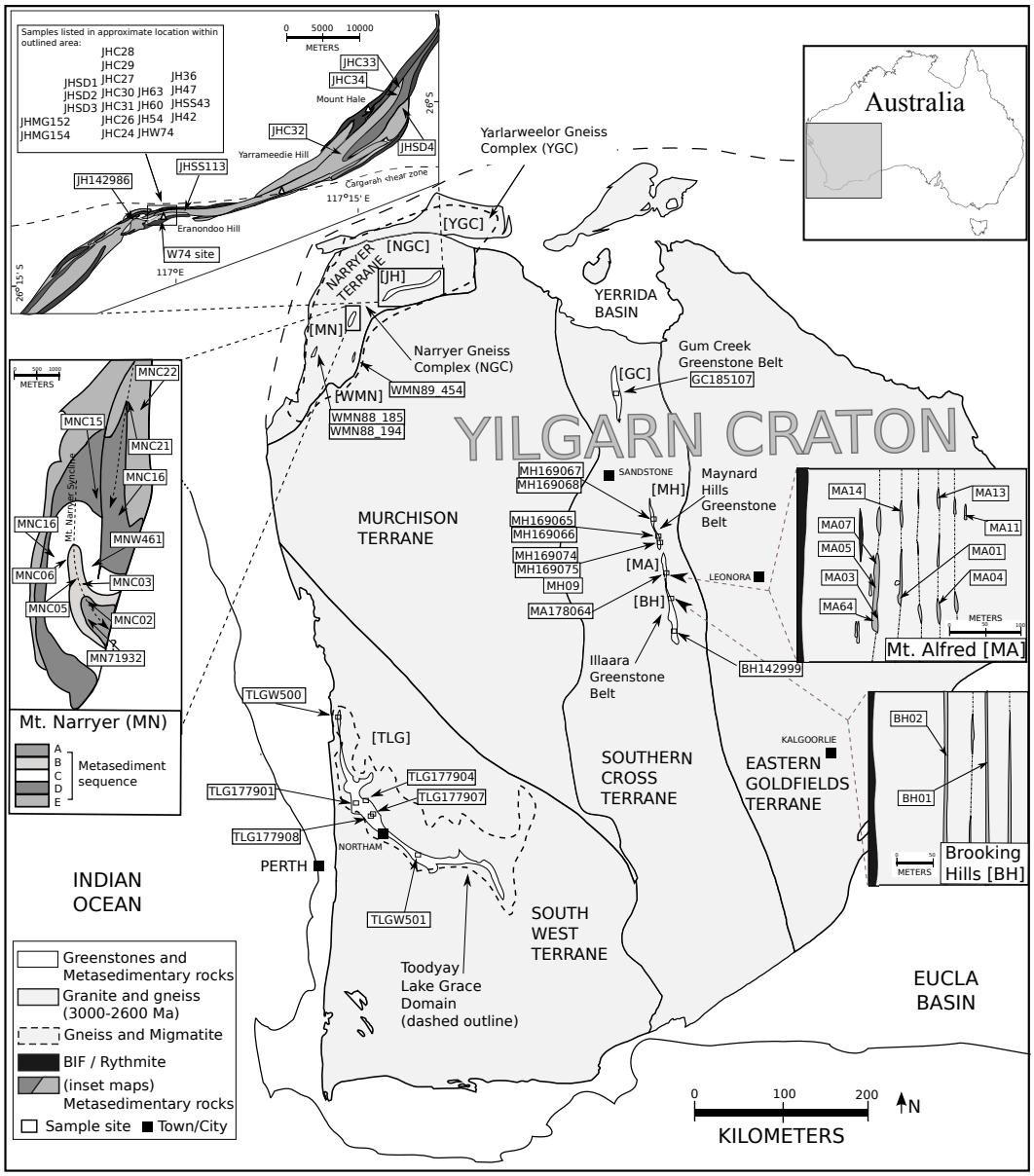

Figure 1.1: Map of the Yilgarn Craton, Western Australia, showing locations of ca. 3.0 Ga metasedimentary rocks (Toodyay Lake Grace Domain, Jack Hills, Mt. Narryer, Gum Creek, Maynard Hills, Illaara), greenstone belts, granites and gneisses. Samples used in this study have been prefixed with locality information: [JH] Jack Hills, [MN] Mt. Narryer, [WMN] West of Mt. Narryer, [TLG] Toodyay Lake Grace, [BH] Brooking Hills, [MA] Mt. Alfred, [MH] Maynard Hills and [GC] Gum Creek. Locations where >4300 Ma zircons have been found are at Mt. Narryer, Jack Hills, Mt. Alfred and Maynard Hills.

1.1.1 Chapter Two: Hadean Zircons

The antiquity of the Hadean zircons found within the Yilgarn metasedimentary rocks make them interesting targets for early Earth research. It has been noted (e.g. Nelson, 2000c; Wilde et al., 2001; Nemchin et al., 2006) that many of these Hadean detrital zircons exhibit complex $^{207}Pb/^{206}Pb$ age variations within their cores. Interpretation of these complex zircon ages can be assessed by studying their microstructure and isotopic compositions. As of yet, no study has established a model for the $^{207}Pb/^{206}Pb$ variation observed within these ancient zircons.

In chapter two of this thesis, a number of >4300 Ma zircons from the Illaara and Maynard Hills greenstone belts have been studied in detail. Their apparent range of $^{207}Pb/^{206}Pb$ dates are assessed to help determine the extent of their age variation and to help formulate a model to explain this variation. Further, the extent of younger, post-Hadean age, thermal event overprinting is assessed when using $^{207}Pb/^{206}Pb$ dates obtained on these Hadean grains to decipher conditions of the early Earth. Sensitive High Resolution Ion Microprobe (SHRIMP) spot analysis, traverses and depth profiling, Electron Probe Microanalysis (EPMA), Quantitative Evaluation of Minerals by SCANning electron microscopy (QEMSCAN), and cathodoluminescence (CL) imaging techniques are used to investigate complex age structures within these Hadean detrital zircons.

1.1.2 Chapter Three: 3.0 Ga Yilgarn Metasedimentary Rocks

Early Archean siliciclastic metasedimentary rocks are found throughout the Narryer Terrane, Southern Cross Terrane, and Toodyay Lake Grace Domain. The abundance of current data has been concentrated on one particular site at Jack Hills, with over 100,000 zircons analyzed from sample site W74 (Holden et al., 2009). Recent studies (e.g. Crowley et al., 2005; Pidgeon et al., 2010) into the Mt. Narryer, Jack Hills and other localities of the Yilgarn Craton, such as the Toodyay Lake Grace Domain, have revealed interesting structures within the zircon age populations of the metasedimentary rocks, suggesting possible links to deposition from a Narryer-like, or extant Narryer Terrane. The detrital zircon populations found within the Southern Cross metasedimentary rocks have some commonalities with the Narryer Terrane, including similar age groups to Mt. Narryer and Jack Hills metasedimentary rocks (Nelson, 2004c; Wyche et al., 2004; Wyche, 2007). The overall similarities observed within detrital age populations of these metasedimentary rocks are difficult to assess, as the depositional ages, source environments and correlateable age groups across geologically dispersed samples are not well constrained.

This chapter works to resolve some of these complexities by comparing all zircon age data from ca. 3.0 Ga metasedimentary rocks throughout the Yilgarn Craton. This study uses statistical analysis to decipher the potential makeup of the provenance of these zircons from the Illaara and Maynard Hills greenstone belts using data collected during this thesis research, as well as assessing the overall age structures found within these samples when compared to other ca. 3.0 Ga metasedimentary rocks throughout the Yilgarn Craton. Hadean age gaps in the data when comparing Mt. Alfred data to Jack Hills and Mt. Narryer, leads to a discussion on pre-3800 Ma land masses, and evidence that the source of these ancient zircons was a composite Hadean terrane.

1.1.3 Chapter Four: Detrital Zircon Provenance

Throughout the Southern Cross, Murchison, and South West Terranes, ca. 3.0 Ga metasedimentary rocks occur within ca. 2730 to 2600 Ma granites and gneisses, and greenstones of >2900 Ma, ca. 2800 Ma and ca. 2730 Ma ages. Similar metasedimentary rocks within the Narryer Terrane at Mt. Narryer and Jack Hills occur within >3.0 Ga granites and gneisses as well as >2900 Ma greenstones, granites and gneisses, respectively. These greenstones are distributed along N−S trending elongate belts throughout the Yilgarn Craton. These >3.0 Ga metasedimentary rocks commonly contain abundant zircons with ages older than 3250 Ma, older than any known rocks within the Yilgarn Craton outside of the Narryer Gneiss Complex within the Narryer Terrane. With the exception of those at Mt. Narryer, the metasedimentary rocks are located on the margins or within greenstone 'rafts' throughout the Yilgarn and their relationship to one another and to the Narryer Gneiss Complex has remained problematic.

The presence of Hadean zircons within the siliciclastic metasedimentary rocks of the Illaara and Maynard Hills greenstone belts is unique to these central Yilgarn rocks. The source of these early Archean zircons are unknown, as is their relation to the early Archean to Hadean detrital zircons found within Jack Hills and at Mt. Narryer of the Narryer Terrane in Western Australia. Searching for more Hadean zircons from this new area, including in-depth sampling and geochronology has led to new insight about the complexity of these early Archean metamorphosed sandstones. This chapter discusses >1000 analyses on detrital zircons obtained from samples throughout the Illaara and Maynard Hills greenstone belts. The new data reveal insights into the provenance of these early Archean and Hadean detrital zircons, as well as the geographical distribution of these metasedimentary rock occurrences, and provides constraints on the depositional ages of the host metasedimentary rocks. A model is proposed, based on these detrital zircon ages, for the formation of the Yilgarn Craton.

1.1.4 Chapter Five: Depositional Age and Environment

Stratiform tourmalines found at the Mt. Alfred and Brooking Hills localities of the Illaara greenstone belt provide an interesting target for study, as their field relations suggest they were formed post depositionally, but that they pre-date nearly all of the tectonic folding and metamorphic activity within the area. Stratiform tourmalines in metasedimentary rocks are often formed from post-depositional hydrothermal or metamorphic fluid flow (Marschall and Jiang, 2011). They can record information about depositional environment in their B isotopic signatures, with high δ^{11}B values interpreted as being derived from evaporitic or meta-evaporitic environments (Cook and Ashley, 1992; Harraz and El-Sharkawy, 2001). Evidence for evaporitic environmental depositional settings can also be constrained by the presence of barite (Cook and Ashley, 1992; Sugitani et al., 2003; Hesse and Schacht, 2011). Studies utilizing the ^{40}Ar/^{39}Ar dating technique on tourmaline are rare (Marschall and Jiang, 2011), with only one recent study within the past decade on ca. 300 Ma tourmalines (Martínez-Martínez et al., 2010). The Ar closure temperature is not well constrained, with initial estimates of closure temperatures of ca. 600 °C.

Chapter five presents tourmaline ^{40}Ar/^{39}Ar plateau ages and boron isotopic data to elucidate geological events from within the Mt. Alfred and Brooking Hills localities of the Illaara Greenstone Belt. These tourmalines occur as post-depositional stratiform layers within the metasedimentary rocks, and may have grown during a period of diagenesis, or enhanced heating and hydrothermal fluid flow. The stratiform nature of the tourmalines, along with the association of barite in parallel metasedimentary units and their elevated δ^{11}B isotopic ratios places constraints on a possible depositional environment of these metasedimentary rocks. This study also discusses the issue of Ar closure temperature in tourmaline. The tourmaline ^{40}Ar/^{39}Ar dates obtained can be used for assigning minimum depositional ages to these sedimentary units, constraining the timing of deposition.

1.1.5 Chapter Six: Post-depositional Thermal History

Other post depositional events can be assessed through geochronology applied to rutile, muscovite-fuchsites and (U−Th)/He dating of zircons and goethite. Rutile is a common accessory mineral in detrital sediments (Force, 1991; Meinhold, 2010) and is found in abundance in the Archean metasedimentary rocks of the Illaara and Mayanard Hills greenstone belts. Rutile from other ca. 3.0 Ga metasedimentary rocks at the Jack Hills revealed SHRIMP ages of ca. 2500 Ma which correspond to a regional metamorphic event, and older 'detrital' ages were not present (Harrison et al., 2007). This suggests rutile was either reset, or grew during this event, and that ages obtained on rutiles from ca. 3.0 Ga metasedimentary rocks throughout the Yilgarn may be difficult to assess due

to their protracted histories. Metamorphic rutile growth in metasedimentary rocks can occur through the breakdown of ilmenite during greenschist facies or higher (Luvizotto and Zack, 2009; Meinhold, 2010). Higher grade events, amphibolite or granulite facies, can also cause considerable amounts of Pb diffusion within rutiles, causing measurable core-rim younging and impacting on the overall U-Pb and Pb-Pb ages determined on smaller grains (Mezger et al., 1989; Kooijman et al., 2010).

Chapter six discusses geochronological results on rutiles, muscovites, zircons and goethites, and reveals a broad and varied post-depositional history of the Illaara and Maynard Hills Greenstone Belt metasedimentary rocks. Rutile SHRIMP Pb-Pb age data constrains rutile growth episodes after deposition of the host sediments. Imaging and microstructural studies show metamorphic and detrital features in these rutiles, and what this reveals about the metamorphic history of these greenstone belts is discussed. The timing of late-stage tectonic shearing is revealed by muscovite-fuchsite $^{40}Ar/^{39}Ar$ geochronology, and younger events are determined through $(U-Th)/He$ analyses on zircon and goethite. An overview of post-depositional events defines not only the thermal history of the metasedimentary rocks in these two greenstone belts, but advances the model of Yilgarn Craton formation as presented in Chapter Four.

1.1.6 Chapter Seven: Conclusions

A brief timeline of events in the conclusions chapter summarizes the findings of this thesis, and offers a number of future directions for further research. This final synthesis briefly elucidates the nature of these early Hadean zircons, their provenance sources, and the Yilgarn and proto-Yilgarn Craton formation by summarizing the timing of events from 4,372 to 26 million years ago.

1.1.7 Chapter Eight: Supporting and Collaborative Publications

A collection of in-press publications is presented in this chapter which collates work undertaken during candidature. These published papers present geochronological studies, many of which involve zircons, and include discussion and interpretation on zircon isotopic response to contrasting thermal-hydrothermal and metamorphic conditions.

1.2 Justification of Paper Authorship

In chapters 2 through 4, this thesis is composed of three manuscripts (to be submitted), one submitted paper (under review), and one published paper, respectively. Chapters 5 and 6 are composed of self-contained studies in the same manuscript-style

format as the other chapters. Chapter 8, in contrast, is composed of five in-press studies which were undertaken during candidature.

The first manuscript, comprising chapter 2, has been authored by the candidate (Eric R. Thern) and co-authored by David R. Nelson, Greg Hitchen and Chi V. Ly. The candidate collected, processed, and analyzed the samples. Greg Hitchen collected the EPMA analyses, and Chi V. Ly collected the QEMSCAN images. With editorial support from David R. Nelson, the manuscripts and figures were entirely produced by the candidate, with scientific discussions and advice in relation to the interpretation of the data therein undertaken with the support of the co-authors.

Eric R. Thern, David R. Nelson, Greg Hitchen and Chi V. Ly; Age structure within >4300 Ma zircons and implications for conditions on the Hadean Earth.

The first and second papers, comprising chapters 3 and 4, have been authored by the candidate (Eric R. Thern) and co-authored by David R. Nelson. The candidate collected, processed, and analyzed the samples, and wrote any software associated with the first paper (chapter 3). With editorial support from David R. Nelson, the manuscripts and figures were entirely produced by the candidate, with scientific discussions and advice in relation to the interpretation of the data therein undertaken with the support of the co-author.

Thern, E. R., Nelson, D. R., (2012). Detrital zircon age structure within ca. 3 Ga metasedimentary rocks, Yilgarn Craton: elucidation of Hadean source terranes by principal component analysis. Precambrian Research; v.214215; p. 2843

Thern, E. R., Nelson, D. R., Provenance of ca. 4372−3000 Ma detrital zircons within Early Archean siliciclastic metasedimentary rocks from the Illaara and Maynard Hills Greenstone Belts, Western Australia, submitted to Precambrian Research

The second and third manuscripts, in chapter format, comprise chapters 5 and 6.

The third paper (chapter 8) is first authored by J. Chiarenzelli and co-authored by M. Lupulescu, B. Cousens, E. Thern, L. Coffin and S. Regan. J. Chiarenzelli is the primary author. M. Lupulescu undertook the geochemistry analyses. B. Cousens analyzed the samples and obtained Nd results. The candidate collected U-Pb zircon SHRIMP data, processed, and interpreted these results. L. Coffin provided petrography for samples. S. Regan provided field assistance. All authors provided editorial support during the submission of the manuscript.

Chiarenzelli, J., Lupulescu, M., Cousens, B., Thern, E., Coffin, L., Regan, S. (2010) Enriched Grenvillian Lithospheric Mantle as a Consequence of Long-Lived Subduction Beneath Laurentia. Geology, February 2010; v.38; no. 2; p.

151-154.

The fourth paper is first authored by J. Chiarenzelli and co-authored by D. Valentino, M. Lupulescu, E. Thern and S. Johnston. D. Valentino introduced the problem and collected the original samples. The first author processed separates for analysis, and conducted the analyses. The candidate analyzed the zircons using the SEM (Cathodoluminescence imaging) as well as SHRIMP Pb-Pb and U-Pb dating, and processed and interpreted the results within their geological context. D. Valentino and M. Lupulescu provided scientific advice throughout the manuscript process. LA-MC-ICPMS data was processed by S. Johnston, who also provided logistical support during the analyses. All authors provided editorial support during the submission of the manuscript.

J. Chiarenzelli, D. Valentino, M. Lupulescu, E. Thern, and S. Johnston (2011) Differentiating Shawinigan and Ottawan orogenesis in the Central Adirondacks. Geosphere, Feb 2011; 7: 222.

The fifth paper (chapter 8) is first authored by Jeff Chiarenzelli and co-authored by Marian Lupulescu, Eric Thern and Brian Cousens. The first author collected the samples, processed separates for analysis, and conducted analyses using LA-MC-ICPMS. The candidate analyzed the zircons using the SEM (Cathodoluminescence imaging) as well as SHRIMP Pb-Pb and U-Pb dating, and processed and interpreted the results within their geological context. M. Lupulescu provided scientific advice throughout the manuscript process. Nd data was processed by Brian Cousens, who also provided logistical support during the analyses. All authors provided editorial support during the submission of the manuscript.

J. Chiarenzelli, M. Lupulescu, E. Thern, and B. Cousens (2011) Tectonic implications of the discovery of a Shawinigan ophiolite (Pyrites Complex) in the Adirondack Lowlands. Geosphere, April 1, 2011; 7(2): 333 356

The sixth paper (chapter 8) is first authored by W. Siebel and co-authored by C. K. Shang, E. Thern, M. Danišík and J. Rohrmuller. The first author collected the samples, and processed separates for analysis, and conducted U-Pb ID-TIMS analyses and obtained all SEM images on the zircons. The candidate analyzed the zircons, obtaining SHRIMP U-Pb and Pb-Pb ages, processed the data and helped with their geological interpretations. C. K. Shang, M. Danišík and J. Rohrmuller provided scientific advice and editorial support throughout the manuscript process.

W. Siebel, C. K. Shang, E. Thern, M. Danišík and J. Rohrmuller (2012) Zircon response to high-grade metamorphism as revealed by U−Pb and cathodoluminescence studies. Int J Earth Sci (Geol Rundsch), 22 April 2012; DOI 10.1007/s00531-012-0772-5

The seventh paper (chapter 8) is first authored by Noreen J. Evans and co-authored

by Brent I. A. McInnes, Brad McDonald, Martin Danišík, Fred Jourdan, Celia Mayers, Eric Thern and Dudley Corbett. Evans conducted the ICPMS analyses, and interpreted processed data from (U−Th)/He and SHRIMP analyses, along with B. McInnes. Samples were collected by Brent I. A. McInnes, Dudley Corbett and Brad McDonald. Brad McDonald conducted the (U−Th)/He analyses and provided technical support. Martin Danišík developed and performed the zircon etching protocols. Fred Jourdan analyzed the phlogopite and processed the data relating to the $^{40}Ar/^{39}Ar$ method. Celia Mayers performed all the microscopy and helped with the presentation of the (U−Th)/He results within the manuscript. The candidate provided support during the acquisition of zircon data on the SHRIMP, processed the data, produced plots and data tables, and helped with interpretations. All authors provided editorial support during the submission of the manuscript.

Noreen J. Evans, Brent I. A. McInnes, Brad McDonald, Martin Danišík, Fred Jourdan, Celia Mayers, Eric Thern, Dudley Corbett. (2012) Emplacement age and thermal footprint of the diamondiferous Ellendale E9 lamproite pipe, Western Australia. Miner Deposita, 14 July 2012; DOI 10.1007/s00126-012-0430-7

1.3 Conventions and Nomenclature

1.3.1 Constants and Abbreviations Used

Table 1.1: Constants used

$\lambda_{U238} = 1.55125 \text{ x } 10^{-10}\text{y}^{-1}$
$\lambda_{U235} = 9.8485 \text{ x } 10^{-10}\text{y}^{-1}$
$\lambda_{Th232} = 4.9475 \text{ x } 10^{-11}\text{y}^{-1}$
Broken Hill common-Pb $^{204}Pb/^{206}Pb = 0.0625$
Broken Hill common-Pb $^{207}Pb/^{206}Pb = 0.9618$
Broken Hill common-Pb $^{208}Pb/^{206}Pb = 2.2285$
CZ3 zircon standard $^{207}Pb/^{206}Pb = 0.05892$
CZ3 zircon standard $Pb*/U = 0.0914$
CZ3 zircon standard U concentration = 551 ppm
CZ3 zircon standard Th concentration = 31 ppm

Table 1.2: Abbreviations used

% concordance =	100 x (^{206}Pb/^{238}U date)/(^{207}Pb/^{206}Pb date)
SHRIMP	Sensitive High Resolution Ion MicroProbe
EPMA	Electron Probe Microanalysis
WDS	Wavelength Dispersive Spectrometer
QEMSCAN	Quantitative Evaluation of Minerals by SCANning electron microscopy
PCA	Principal Component Analysis

1.3.2 Terminology

A number of terms are used when referring to the location of particular analyses by either SHRIMP or EPMA techniques. A SHRIMP `analysis site` refers to the ablation pit the $^{16}O_2^-$ primary beam creates, typically forming a 20μm Kohler spot which equates to the amount of sample analyzed. An EPMA `analysis site` is used to refer to the location of X-ray generation on a sample that is bombarded by an electron beam. When a linear series of analysis sites are obtained across a single grain or sample, the result is referred to as an EPMA or SHRIMP `traverse`.

The results throughout this thesis refer to Pb-Pb, U-Pb and Th-Pb *dates* as opposed to *ages*. A 'date' is a term applied to an initial analysis of a sample from the lab (in this case from the SHRIMP or EPMA via CHIME). An 'age' is a term that can only be used when the 'date' holds geological significance. Concordant data may increase the confidence of a particular *date* obtained, thus proving its geological significance to most. It is the author's view that the complex early histories of these >4300 Ma zircon grains are not constrained well enough to refer to any *date* obtained on these zircons as an *age*, even when there are numerous dates or the obtained dates are concordant.

Samples are discussed as 'metasedimentary rocks', but nearly all original sedimentary features have been lost due to shearing and late stage metamorphic recrystallization, and is compounded by growth of metamorphic minerals such as muscovite and fuchsite. The term 'siliciclastic metasedimentary rock' is used for what could be described as quartz arenites, or quartzites, however the abundance of muscovite-fuchsite and occurrence of andalusite within some of these quartz arenites requires a more generalized term which encompasses a broad range of possible original sedimentological characteristics.

The term "Terrane" is used descriptively and is not intended to imply that the geological unit may not share parts of its geological history with that of adjacent terranes.

CHAPTER 2
HADEAN ZIRCONS

This chapter presents a draft manuscript that was a collaboration with Dr. David Nelson, Greg Hitchen and Chi Ly and uses geochronology and microstructural analysis on Hadean zircons to further our understanding of their isotopic systematics. Geochronological data from a number of ca. 4300 Ma zircons are assessed, with an emphasis on interpreting their apparent range of $^{207}Pb/^{206}Pb$ dates.

2.1 Manuscript 1: Age structure within >4300 Ma zircons and implications for conditions on the Hadean Earth

Eric R. Thern, David R. Nelson, Greg Hitchen and Chi V. Ly; Age structure within >4300 Ma zircons and implications for conditions on the Hadean Earth.

E.R. Thern[a*], D.R. Nelson[b], G. Hitchen[c], Chi V. Ly[d]

[a] Department of Imaging and Applied Physics, Curtin University of Technology, GPO Box U1987, Perth, WA 6001, Australia (*eric@thern.org)

[b] School of Natural Sciences, University of Western Sydney, Locked Bag 1797, Penrith, NSW 2751, Australia

[c] CSIRO Exploration and Mining, Australian resources Research Centre, Box 1130, Bentley WA 6102, Australia

[d] CSIRO Minerals Waterford, PO Box 90, Bentley, WA 6982, Australia

2.2 Abstract

New Ion-Microprobe U-Pb age data and characterization of >4300 Ma detrital zircons from siliciclastic metasedimentary rocks of the Maynard Hills and Illaara Greenstone Belt, Yilgarn Craton, are presented. Sensitive High Resolution Ion Microprobe (SHRIMP) analyses on >4300 Ma detrital zircon cores show concordant $^{207}Pb/^{206}Pb$ dates which span >50 M.y. The range of dates do not correspond with obvious structural features within the grain and lie on what should be isochemical cathodoluminescence zones. This age range is significantly larger than can be attributable to analytical uncertainty alone.

The extent of younger, post-Hadean age, thermal overprinting is assessed. The application of numerous analytical methods, including SHRIMP spot analysis, traverses and depth profiling, EPMA, QEMSCAN, and cathodoluminescence imaging are used to assess these ancient zircons and their complex age structures.

Later (<3800 Ma) metamorphic, tectonic and hydrothermal events have modified the $^{207}Pb/^{206}Pb$ dates obtained on many detrital grains, including many Hadean grains. Further research into these later events is ongoing in an effort to decouple earlier thermal histories during Hadean times with Archean and younger thermal events. Evidence is mounting that late-stage overprinting of thermal events has left distinct signatures in these Hadean grains and that only the most pristine 'cores' of these zircons can be used when interpreting age results.

However, the existence of a range of $^{207}Pb/^{206}Pb$ dates within a well preserved >4300 Ma igneous zircon core is difficult to assess, as it is not consistent with the operation of simple chemical redistribution mechanisms such as volume diffusion alone. It is also not related to simple modification processes such as recrystallization, as these zircons retain their original igneous CL and BSE zoning. Surface mapping of a Hadean zircon using QEMSCAN did not reveal any micro-inclusions, indicating that the range cannot be attributed to inclusions from phosphates or other Pb-bearing minerals. The observed range of $^{207}Pb/^{206}Pb$ dates suggests an early heterogeneous (>3900 Ma) Pb-redistribution between annealed and radiation-damaged zones or channels within these Hadean zircon cores during periodic post-crystallization thermal events.

2.3 Introduction

Little is directly known about the first 500 million years of Earth's history. There are models of planet formation between 4571-4500 Ma (Chambers and Wetherill, 1998;

Wetherill, 1996; Canup, 2004) and of an impact with a Mars-sized object between 4550 to 4500 Ma (Halliday, 2000; Lee et al., 2002; Nelson, 2004b) which led to the formation of the moon. A global magma ocean could have existed for hundreds of millions of years after Earth formation (Yutaka Abe et al., 2000; Debaille et al., 2007) with peak temperatures ≥10000 K (Melosh, 1989). There are also models of substantial meteorite bombardment of Earth between 4500 to 4200 Ma (Wetherill, 1975; Hartmann et al., 2000). With such a violent early history, there should be no surprise that little is left of the Hadean rock record to study.

The oldest remnants of the terrestrial rock record found are >4300 Ma detrital zircons from Western Australia (locations shown on map in Figure 2.1). These Hadean zircons are the only known surviving terrestrial material from early Earth's history (from 4404 Ma to 4030 Ma) and are uniquely pertinent to ancient Earth studies. These zircons older than >4000 Ma have been found within the ca. 3 Ga metasedimentary rocks dispersed throughout the Yilgarn Craton at Mt. Narryer (Froude et al., 1983; Kinny et al., 1990; Crowley et al., 2005; Pidgeon and Nemchin, 2006), Jack Hills (Compston et al., 1985; Wilde et al., 2001; Peck et al., 2001; Cavosie et al., 2004; Crowley et al., 2005; Cavosie et al., 2006), Maynard Hills (Nelson, 2002a; Wyche et al., 2004) and the Mt. Alfred locality of the Illaara Greenstone Belt (Nelson, 2005; Wyche, 2007). Of these localities, only three locations so far have identified zircons older than 4300 Ma; the Jack Hills (Narryer Terrane) (Wilde et al., 2001; Peck et al., 2001; Cavosie et al., 2004) the Maynard Hills (Nelson, 2002b; Wyche et al., 2004) and the Mt. Alfred locality of the Illaara Greenstone Belt. These ancient zircons are of unknown provenance, and their distribution throughout multiple disparate metasedimentary rocks >400 km apart within granite greenstone terranes and high grade gneiss complexes makes their relation to one another at time of deposition difficult to assess.

Initial investigations of these >4300 Ma grains imply an igneous origin based on their oscillatory zoning, Th/U ratios and REE abundances (Wilde et al., 2001; Peck et al., 2001; Nelson, 2002b; Cavosie et al., 2004; Cavosie et al., 2006). Evidence of elevated $\delta^{18}O$ in a ca. 4364 Ma (with a single 4404 Ma analysis) zircon from the Jack Hills (Wilde et al., 2001; Peck et al., 2001) was interpreted to indicate that the igneous source was derived from crustal material that had interacted with the hydrosphere, implying the existence of ancient oceans (Valley et al., 2002). Water-saturated crustal material has also been suggested as the dominant source for Hadean zircons, based on Ti-in-zircon thermometry which yields zircon crystallization temperatures of 680-720°C, consistent with near water-saturated minimum melts under prograde conditions (Watson and Harrison, 2005; Harrison and Schmitt, 2007). Harrison (2005) discussed the possibility that deviations in the $^{176}Hf/^{177}Hf$ ratios from the bulk Earth within these >4000 Ma zircons provides evidence for continental crust and recycling of this crust into the mantle. Hadean era subduction processes with a thick continental lithosphere

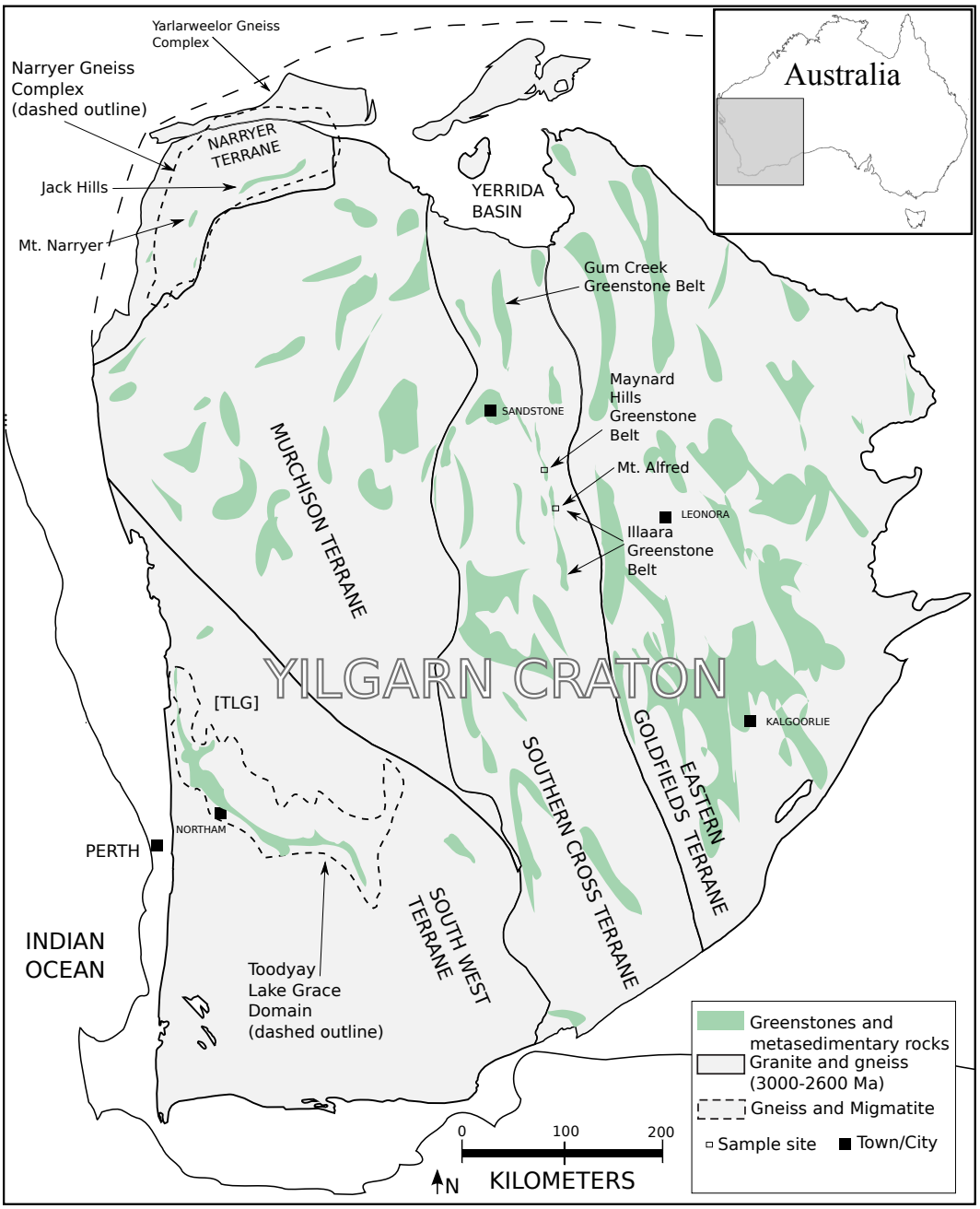

Figure 2.1: Map of the Yilgarn Craton, Western Australia, showing locations of ca. 3 Ga metasedimentary rocks and of gneisses examined in this study. Inset maps are of Mt. Narryer (after Crowley, 2005), Jack Hills (after Spaggiari, 2007), Mt. Alfred and Brooking Hills. Samples used in this study have been prefixed with locality information: [JH] Jack Hills, [MN] Mt. Narryer, [WMN] West of Mt. Narryer, [TLG] Toodyay Lake Grace, [BH] Brooking Hills, [MA] Mt. Alfred, [MH] Maynard Hills and [GC] Gum Creek. Locations where >4300 Ma zircons have been found are at Mt. Narryer, Jack Hills, Mt. Alfred and Maynard Hills.

have also been interpreted from the identification of diamond inclusions within ca. 4250 Ma zircons; it was argued that these diamonds resemble those formed under ultrahigh-pressure metamorphic conditions (Menneken et al., 2007).

Whereas many conclusions have been drawn from these Hadean zircons, there are also questions as to the relevance of the dates obtained from them. Ion microprobe data on individual zircons show that many of these Hadean detrital zircons exhibit complex $^{207}Pb/^{206}Pb$ age variations within their cores (e.g. Nelson, 2000c; Wilde et al., 2001; Nemchin et al., 2006) . This range of $^{207}Pb/^{206}Pb$ dates has previously been interpreted to be due to either growth of new rim zircon, late radiogenic Pb-loss (Wilde et al., 2001; Peck et al., 2001), interaction with low-temperature fluids (Hoskin, 2005; Nemchin et al., 2006) or diffusive Pb-loss during episodic metamorphic events in the Hadean (Nemchin et al., 2006). As of yet, no study has established a conclusive model for the $^{207}Pb/^{206}Pb$ variation observed within these ancient zircons. A better understanding of the observed age complexity on Hadean zircons is important when using their obtained ages to interpret geological events.

In order to best understand the apparent $^{207}Pb/^{206}Pb$ date variation within these ancient zircons, the aims of this study are to: (1) Investigate alternative possibilities that might explain detectable SHRIMP $^{207}Pb/^{206}Pb$ date variation within individual zircon crystals; (2) Nominate a preferred model for the $^{207}Pb/^{206}Pb$ variation observed in these ancient zircons; and (3) Discuss the implications this may have for conditions on the early Earth.

2.4 Sample Selection

Three detrital zircon grains with radiogenic $^{207}Pb/^{206}Pb$ core ages older than 4300 Ma were selected from siliciclastic metasedimentary rocks of the Illaara and Maynard Hills greenstone belts. Sample localities and brief descriptions of host rocks are outlined in Table 2.1. Zircon MH09-10, (which is the same grain as 169075-10), is a ca. >4300 Ma zircon from the Maynard Hills metasedimentary rocks. Zircon MA64-41, (which is the same grain as 178064-41), and zircon MA03-72 are both ca. >4300 Ma zircons from the Mt. Alfred locality within the Illaara Greenstone Belt. Zircon MA64-48, (which is the same grain as 178064-48), is a ca. 3770 Ma grain, used for comparison purposes to the Hadean zircons, and is also from the Mt. Alfred locality within the Illaara Greenstone Belt.

Table 2.1: List of sample localities and brief descriptions

Sample	South	East	Lithology and Description
Mt. Alfred [MA] – Southern area of the Northern Illaara Granite Greenstone Belt			
MA03	S 28° 50.694'	E 119° 59.977'	metasandstone; a pale greenish-white, medium- to coarse-grained, quartzite from the western margin of a 20 m-thick, bedded quartzite unit; 2 m-east of GSWA sample 178064.
MA64	S 28° 50.694'	E 119° 59.971'	coarse sandstone; a pale pinkish-white, medium- to coarse- and even-grained, well-sorted quartz sandstone from a 20 m-thick, bedded quartzite unit; GSWA sample 178064 (Nelson, 2005).
Maynard Hills [MH] – Southern section of the Maynard Hills Granite Greenstone Belt			
MH09	S 28° 29.316'	E 119° 49.050'	quartzite; a pale pinkish-grey, coarse grained massively recrystallized quartzite with thin (<1 mm thick) reddish-yellow clay-rich layers; GSWA sample 169075 (Nelson, 2002b).

2.5 Analytical Procedures

2.5.1 SHRIMP U-Th-Pb

SHRIMP operating conditions were similar to those described in (Nelson, 2001, 2004c). A standard SHRIMP session included 7 scans of the following mass peaks and integration times: $^{196}Zr_2O^+$ (2 s), $^{204}Pb^+$ (10 s), $^{204.045}$Background (10 s), $^{206}Pb^+$ (10 s), $^{207}Pb^+$ (20 s), $^{208}Pb^+$ (10 s), $^{238}U^+$ (5 s), $^{232}Th^{16}O^+$ (2 s), $^{238}U^{16}O^+$ (2 s) and $^{238}U^{16}O_2{}^+$ (2 s). All SHRIMP U-Th-Pb analyses have been reduced using CONCH software (Nelson, 2006).

2.5.2 SHRIMP REE

Rare earth elements were measured on the SHRIMP using 3 scans of the following runtable: ^{96}Zr (2 s) [ref peak], $^{104}Ca_2$ (2 s), $^{96}Zr^{16}O$ (2 s) [ref peak], ^{138}Ba (2 s), ^{139}La (30 s), ^{140}Ce (10 s),^{141}Pr (10 s), ^{143}CaP (10 s), ^{143}Nd (15 s), ^{146}Nd (15 s), ^{147}Sm (10 s), ^{149}Sm (10 s), ^{151}Eu (10 s), ^{153}Eu (10 s), ^{155}Gd (10 s), ^{157}Gd (10 s), ^{159}Tb (10 s), ^{161}Dy (10 s), ^{163}Dy (10 s), ^{165}Ho (10 s) [ref peak], ^{166}Er (10 s), ^{167}Er (10 s), ^{169}Tm (8 s) [ref peak], ^{171}Yb (8 s), ^{172}Yb (10 s), ^{175}Lu (10 s), ^{178}Hf (4 s) and ^{180}Hf (4 s). ^{96}Zr was used as the reference peak and $^{96}Zr^{16}O$ was used to monitor the $^{96}Zr/^{96}Zr^{16}O$ ratio. During the analytical session the REE standard zircon (P.D. Kinny, personal communication; values shown in Table 2.5) and the CZ3 standard zircon was analyzed. SHRIMP REE data was reduced by relating the raw counts on the unknowns to the raw counts on a REE zircon standard and to CZ3.

2.5.3 SHRIMP and EPMA Mapping, Traverses and QEM-SCAN imaging

The SHRIMP mapping functionality provides qualitative sub-ppb level isotopic concentration maps and traverses of the surface of a sample. SHRIMP maps can create a grid or line of analysis points which measure a single isotope at a time in 3.3μm stage increments with reproducibility of $\pm$3μm. The limitations of such a technique are the SHRIMP's large spot size (about 20-30μm), stage position reproducibility, lack of secondary beam monitoring and surface topology impacting secondary extraction yield.

Zircon grain MH09-10 within the SHRIMP mount was cleaned, gold coated, and analyzed with a linear SHRIMP traverse for REE and U-Th-Pb, respectively. Typical running conditions on the SHRIMP included a primary beam (O_2^-) of 3nA and sensitivity of >12 cps/ppm/nA of ^{206}Pb in zircon. A pre-analysis raster on the Zr peak

Table 2.2: Trace element EPMA peak summary

Crystal:	PET	PET	LIF
Pressure	1atm	1atm	3atm
Group 1:	U (Mα)	Y (Lα)	Sm (Lα)
Group 2:	Th (Mα)	Pb (Mβ)	Yb (Lα)
Group 3:	Pb (Mα)	U (Mβ)	Dy (Lα)
Beam:	35kV, 200nA, Spot: 1μm		

(consisting of single or multiple runs) was used in order to stabilize count rates while burning through the conductive gold coat.

Linear traverses of analysis points across zircon grains were obtained using a Cameca SX-50 electron microprobe (EPMA) located at CSIRO (Bentley, WA) with CSIRO-Trace software (Robinson and Graham, 1992). The EPMA technique yielded a spot size of 1-5μm and a stage stepping size of about 1μm with reproducibility of $\pm$1μm. Each linear traverse was comprised of single spot analyses consisting of ten 100 second cycles, which resulted in each elemental peak on each spot being counted for 1000 seconds. The peaks used are summarized in Table 2.2. Traverse locations were selected based on (1) previous SHRIMP spots (2) grain surface topology, and (3) CL response. Samples that were prepared and dated by SHRIMP were cleaned and carbon coated prior to electron microprobe analysis.

The QEMSCAN scanning electron microprobe has been proven to detect and map inclusions of phosphates, apatite and other minerals on a sub-micron scale. The QEMSCAN was used to produce an elemental map at a 0.5 μm resolution of the surface of grain MH09-10. Operating conditions used were a 25kV beam acceleration voltage, 5nA specimen current and 1.7nA probe current. The QEMSCAN operates by scanning a selected area on the sample (in this case, the entire grain of MH09-10) by deflecting the beam across the area. The spatial resolution is much better than that of a SHRIMP or EPMA, but the QEMSCAN has lower detection limits. This approach resulted in detailed maps of the major and some minor elemental concentrations on the surface of the grain, but did not allow for trace element concentration maps along CL zones, which would require sub-ppm level detection limits.

2.5.4 Detection of diffusion events

The EPMA traverses were set up to span across, along and slightly oblique to CL zones within the >4300 Ma zircon grain in order to explore for chemical gradients that might be attributable to diffusion processes. The overall goal of this approach is to detect slope variances within these zones that differ for a set of rare earth elements that have different diffusion coefficients. The elements chosen were (from lowest diffusion coefficient to highest) Sm, Y, U, Yb, Pb, Dy, U and Th.

2.5.5 SHRIMP U-Th-Pb Depth Profiling

Zircon MH09-10 was selected for depth profiling following methods similar to those in Trail et al. (2007). A set of standards was also used to assess the $^{206}Pb/^{238}U$ calibration, $^{207}Pb/^{206}Pb$ dates and U concentration (standard zircons BR266, 91500, and $^{207}Pb/^{206}Pb$ standard zircon OGC-1).

The mount was prepared by having a small section of double-thick double sided tape in the central region of the mount area where grains were added in order to provide extra relief for grains surrounding the unknowns during polishing. This setup allowed for the inner zircons to remain unpolished while the standards around the edge were polished. Selected grains were analyzed using a standard U-Th-Pb runtable on the SHRIMP for three cycles each; masses and (count integration times): $^{196}Zr_2O^+$ (2 s), $^{204}Pb^+$ (10 s), $^{204.045}$Background (10 s), $^{206}Pb^+$ (10 s), $^{207}Pb^+$ (20 s), $^{208}Pb^+$ (10 s), $^{238}U^+$ (5 s), $^{232}Th^{16}O^+$ (2 s), $^{238}U^{16}O^+$ (2 s) and $^{238}U^{16}O_2{}^+$ (2 s).

2.5.6 Grouping of $^{207}Pb/^{206}Pb$ dates

All dates obtained have been grouped by CONCH using the Chi-Square (χ^2) reduction method. χ^2 tests whether the observed frequencies differ significantly from the expected frequencies (Moroney, 1984). A low near unity χ^2 value indicates that there are no additional sources of uncertainty and the data are consistent within counting statistics, whereas a χ^2 value >1 indicates that there are additional (geological) sources of uncertainty. A χ^2 value significantly less than one indicates that analytical uncertainties have been over-estimated compared with those based on counting statistics. The data presented in this study has been parsed using CONCH, which uses a default χ^2 grouping limit value of 1.75. This will only identify the minimum number of clearly resolvable dates based on the uncertainty limits assigned to each individual analysis. The grouping method for CONCH is explained in detail in Nelson (2006).

2.6 Results

2.6.1 SHRIMP U-Pb and Pb-Pb Data

Isotopic and chemical data from zircons MH09-10, MA64-41, MA64-48 and MA03-72 are presented in Table 2.3. An overview of analysis site numbers, split by SHRIMP analytical session are presented in Figure 2.2. Wetherill diagrams, and an overview Gaussian summation probability plot are shown in Figure 2.3.

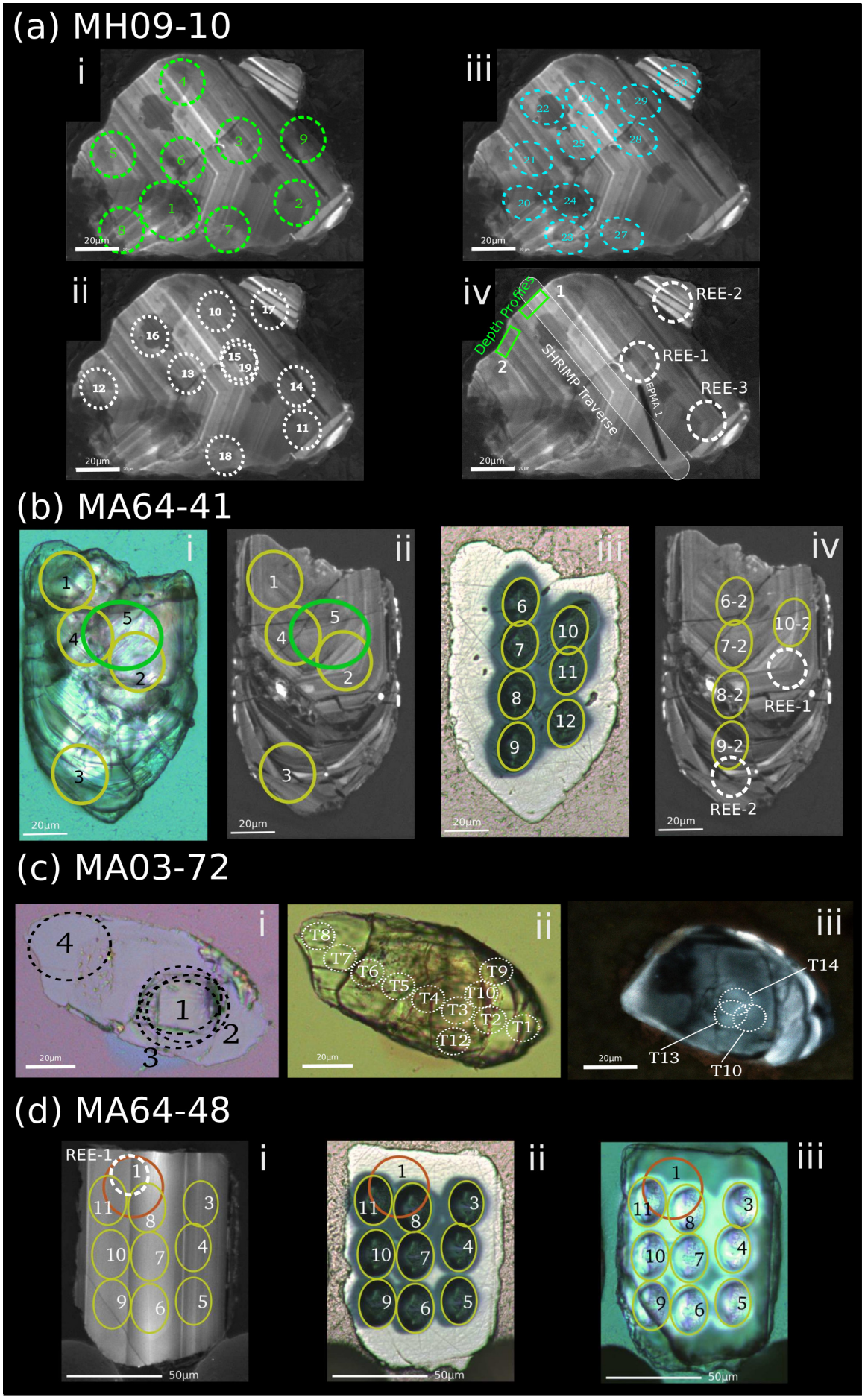

Figure 2.2: see next page for full description

Figure 2.2: SHRIMP analyses and sessions for (a) zircon MH09-10 (i) session 1, (ii) session 2, (iii) session 3, (iv) REE analysis sites, SHRIMP traverse, EPMA traverse locations, and two SHRIMP depth profile sites; (b) zircon MA64-41 (i) session 1, (ii) session 2, (iii) session 3, including REE sites (dashed circles); (c) zircon MA03-72 (i) session 1 reflected light, (ii) session 2 transmitted light; (iii) session 2 CL (d) zircon MA64-48 (i) session 1 CL, including REE site (dashed circle), (ii) session 1 transmitted, (iii) session 1 reflected.

Table 2.3: SHRIMP analytical results for Hadean zircons

						Ratios									Dates (Ma)					
						^{207}Pb		^{208}Pb		^{206}Pb		^{207}Pb			^{206}Pb		^{207}Pb		^{207}Pb	
Grain .spot	U ppm	Th ppm	Th/U	Pb ppm	$f206\%$	^{206}Pb 204corr	$\pm1\sigma$ (%)	^{206}Pb 204corr	$\pm1\sigma$ (%)	^{238}U 204corr	$\pm1\sigma$ (%)	^{235}U 204corr	$\pm1\sigma$ (%)	%c	^{238}U date	$\pm1\sigma$ (Ma)	^{235}U date	$\pm1\sigma$ (Ma)	^{206}Pb date	$\pm1\sigma$ (Ma)
Sample MH09 zircon grain 10 (104 analyses)																				
MH09-10.30	424	169	0.40	177	0.067	0.4496	0.37	0.0590	1.54	0.320	4.01	19.834	4.07	44	1790	63	3083	39	4084	6
MH09-10.9*	892	663	0.74	293	0.764	0.4557	0.23	0.1297	0.99	0.236	1.01	14.816	1.06	33	1365	12	2804	10	4104	3
MH09-10.17	534	235	0.44	205	0.541	0.4711	0.35	0.0775	2.09	0.284	1.02	18.426	1.12	39	1610	15	3012	11	4153	5
MH09-10.14	656	484	0.74	305	0.388	0.4972	0.29	0.1533	0.90	0.324	1.02	22.217	1.10	43	1810	16	3193	11	4233	4
MH09-10.12	340	148	0.44	173	0.779	0.5045	0.39	0.1709	1.41	0.343	1.04	23.892	1.16	45	1903	17	3264	11	4254	6
MH09-10.11	299	194	0.65	337	0.058	0.5136	0.24	0.1661	0.54	0.779	1.06	55.139	1.11	87	3712	30	4090	11	4281	4
MH09-10.18	234	149	0.64	278	0.107	0.5139	0.31	0.1599	0.79	0.820	1.09	58.097	1.17	90	3860	32	4142	12	4281	4
MH09-P-2.34	148	952	6.44	210	0.217	0.5143	0.99	0.1248	3.42	1.003	4.72	71.124	4.94	105	4478	152	4344	50	4283	15
MH09-10.28	192	104	0.54	205	0.085	0.5226	0.52	0.1347	1.28	0.745	4.03	53.687	4.13	83	3589	111	4063	41	4306	8
MH09-P-2.31	156	980	6.30	256	0.224	0.5239	0.88	0.1275	2.97	1.151	4.64	83.117	4.82	115	4937	160	4500	48	4310	13
MH09-P-2.27	190	1255	6.62	210	0.362	0.5259	0.82	0.1226	2.73	0.774	3.83	56.124	4.02	86	3695	108	4107	40	4315	12
MH09-10.7	194	130	0.67	277	0.129	0.5268	0.19	0.1708	0.45	0.973	1.06	70.664	1.10	101	4380	34	4338	11	4318	3
MH09-P-1.1*	477	3268	6.85	492	0.507	0.5269	0.34	0.1611	1.09	0.698	2.46	50.682	2.52	79	3412	65	4006	25	4318	5
MH09-P-2.33	159	1052	6.61	185	0.359	0.5273	1.06	0.1245	3.90	0.811	4.63	58.981	4.88	89	3829	134	4157	49	4319	16
MH09-P-2.24	171	1212	7.08	203	0.658	0.5276	0.91	0.1246	4.28	0.817	3.91	59.450	4.12	89	3851	113	4165	41	4320	13
MH09-10.29	285	134	0.47	300	-0.011	0.5278	0.34	0.1250	0.84	0.739	4.01	53.759	4.07	83	3566	110	4065	41	4321	5
MH09-P-2.7	134	967	7.24	169	0.194	0.5295	0.45	0.1462	1.19	0.872	2.80	63.670	2.90	93	4042	84	4233	29	4325	7
MH09-10.13	95	54	0.57	122	0.104	0.5296	0.38	0.1476	0.91	0.884	1.09	64.583	1.20	94	4085	33	4248	12	4326	6
MH09-10.27	246	147	0.60	275	0.020	0.5296	0.41	0.1622	0.83	0.768	4.03	56.047	4.10	85	3672	113	4106	41	4326	6
MH09-10.26	154	73	0.47	176	-0.048	0.5302	0.45	0.1168	1.19	0.809	4.03	59.155	4.11	88	3822	116	4160	41	4327	7
MH09-10.8	178	70	0.39	197	0.201	0.5303	0.23	0.1173	0.76	0.779	1.05	56.931	1.10	86	3712	30	4122	11	4328	3
MH09-P-1.33	290	1920	6.63	294	0.743	0.5309	0.69	0.1475	2.93	0.688	3.18	50.389	3.33	78	3376	83	4000	33	4329	10
MH09-P-2.10	116	812	7.01	141	0.163	0.5308	0.57	0.1384	1.52	0.843	3.12	61.674	3.24	91	3940	92	4202	32	4329	8
MH09-P-2.32	163	1036	6.36	221	0.220	0.5307	0.98	0.1287	3.85	0.942	4.60	68.923	4.82	99	4278	144	4313	48	4329	14
MH09-P-2.9	116	832	7.16	150	0.105	0.5309	0.55	0.1415	1.40	0.896	3.12	65.607	3.24	95	4125	95	4263	32	4329	8
MH09-10.16	150	89	0.60	206	0.147	0.5311	0.34	0.1466	0.88	0.946	1.12	69.288	1.21	99	4293	35	4318	12	4330	5
MH09-10.25	172	104	0.61	205	0.008	0.5314	0.48	0.1463	0.99	0.824	4.04	60.406	4.13	90	3876	118	4181	41	4331	7
MH09-P-2.14	126	881	6.97	149	0.227	0.5317	0.66	0.1332	2.04	0.815	3.35	59.766	3.49	89	3844	97	4170	35	4331	10
MH09-P-2.29	202	1244	6.16	208	0.139	0.5315	0.86	0.1320	2.15	0.718	3.99	52.602	4.18	81	3488	107	4043	42	4331	13
MH09-P-2.35	181	1171	6.48	171	0.405	0.5317	1.12	0.1346	4.05	0.654	4.44	47.921	4.71	75	3242	113	3950	47	4332	16
MH09-P-1.15	227	1647	7.27	271	0.684	0.5323	0.53	0.1480	2.01	0.811	2.91	59.561	3.02	88	3830	84	4167	30	4333	8
MH09-P-2.19	142	995	7.01	161	0.190	0.5327	0.76	0.1364	2.44	0.785	3.62	57.634	3.79	86	3734	103	4134	38	4334	11
MH09-P-2.11	115	793	6.87	137	0.302	0.5329	0.62	0.1310	2.27	0.822	3.17	60.416	3.30	89	3868	92	4181	33	4335	9
MH09-P-1.35	303	2108	6.96	294	0.511	0.5333	0.67	0.1506	2.29	0.662	3.26	48.697	3.41	76	3276	84	3966	34	4336	10
MH09-P-1.36	303	2175	7.17	305	0.609	0.5332	0.70	0.1521	2.54	0.681	3.30	50.104	3.46	77	3350	86	3994	34	4336	10
MH09-P-2.26	172	1183	6.88	192	0.462	0.5332	0.91	0.1248	3.48	0.771	4.04	56.707	4.25	85	3686	113	4118	42	4336	13

Continued on Next Page...

Table 2.3 – Continued

Grain .spot	U ppm	Th ppm	Th/U	Pb ppm	$f206\%$	$^{207}Pb/^{206}Pb$ 204corr	$\pm1\sigma$ (%)	$^{208}Pb/^{206}Pb$ 204corr	$\pm1\sigma$ (%)	$^{206}Pb/^{238}U$ 204corr	$\pm1\sigma$ (%)	$^{207}Pb/^{235}U$ 204corr	$\pm1\sigma$ (%)	%c	$^{206}Pb/^{238}U$ date	$\pm1\sigma$ (Ma)	$^{207}Pb/^{235}U$ date	$\pm1\sigma$ (Ma)	$^{207}Pb/^{206}Pb$ date	$\pm1\sigma$ (Ma)
MH09-P-1.17	235	1745	7.43	280	0.704	0.5335	0.55	0.1491	2.11	0.809	2.95	59.548	3.07	88	3823	85	4167	31	4337	8
MH09-P-2.12	116	789	6.78	133	0.332	0.5336	0.64	0.1327	2.27	0.787	3.18	57.889	3.32	86	3742	90	4138	33	4337	9
MH09-P-1.10	201	1520	7.56	246	0.538	0.5340	0.44	0.1579	1.56	0.830	2.69	61.083	2.79	90	3894	79	4192	28	4338	7
MH09-P-2.18	134	917	6.82	155	0.441	0.5339	0.78	0.1281	3.24	0.797	3.54	58.654	3.72	87	3778	101	4151	37	4338	11
MH09-P-1.4	260	1997	7.67	388	0.314	0.5344	0.34	0.1597	0.95	1.012	2.61	74.548	2.67	104	4506	85	4391	27	4339	5
MH09-10.19	133	74	0.56	151	0.065	0.5346	0.42	0.1375	1.03	0.786	1.14	57.957	1.27	86	3740	32	4140	13	4340	6
MH09-10.22	143	81	0.57	162	-0.029	0.5348	0.41	0.1307	1.04	0.791	4.05	58.299	4.12	87	3756	115	4145	41	4340	6
MH09-P-1.12	207	1554	7.49	253	0.348	0.5348	0.45	0.1571	1.30	0.829	2.79	61.162	2.88	90	3894	82	4193	29	4340	7
MH09-10.23	246	100	0.40	236	-0.037	0.5352	0.57	0.1049	1.87	0.678	4.03	50.063	4.14	77	3338	105	3994	41	4341	8
MH09-P-2.22	166	1147	6.89	183	0.424	0.5351	0.83	0.1301	3.34	0.760	3.74	56.048	3.93	84	3643	104	4106	39	4341	12
MH09-P-1.11	206	1569	7.61	257	0.370	0.5354	0.45	0.1566	1.42	0.847	2.76	62.541	2.86	91	3956	82	4216	29	4342	7
MH09-P-1.40	283	2081	7.35	282	0.893	0.5356	0.80	0.1461	3.40	0.673	3.47	49.718	3.66	76	3318	90	3987	36	4342	12
MH09-P-2.5	155	1173	7.58	212	0.136	0.5357	0.38	0.1582	0.93	0.934	2.68	68.992	2.75	98	4252	83	4314	28	4342	6
MH09-P-2.8	127	889	7.03	152	0.280	0.5356	0.49	0.1412	1.42	0.826	2.87	61.014	2.97	89	3882	84	4191	30	4342	7
MH09-P-2.28	200	1346	6.74	214	0.428	0.5358	0.86	0.1304	3.03	0.737	3.87	54.432	4.07	82	3558	106	4077	41	4343	13
MH09-P-2.4	168	1284	7.63	239	0.149	0.5359	0.36	0.1587	0.92	0.967	2.63	71.486	2.70	100	4363	83	4349	27	4343	5
MH09-P-1.19	251	1927	7.68	344	0.506	0.5361	0.56	0.1486	2.07	0.932	3.15	68.882	3.26	98	4245	98	4312	33	4344	8
MH09-P-1.27	309	2228	7.21	339	0.681	0.5362	0.62	0.1527	2.30	0.742	3.13	54.831	3.26	82	3577	86	4084	33	4344	9
MH09-P-2.17	131	886	6.78	146	0.336	0.5364	0.76	0.1281	3.16	0.775	3.50	57.293	3.67	85	3698	98	4128	37	4344	11
MH09-10.15	117	65	0.56	158	0.023	0.5365	0.37	0.1415	0.83	0.935	1.12	69.185	1.22	98	4256	35	4317	12	4345	5
MH09-10.20	303	201	0.66	373	0.018	0.5368	0.34	0.1820	0.65	0.830	4.02	61.435	4.08	90	3896	118	4198	41	4345	5
MH09-10.4	137	73	0.54	188	0.083	0.5367	0.26	0.1337	0.67	0.951	1.13	70.392	1.19	99	4309	35	4334	12	4345	4
MH09-P-1.28	308	2257	7.32	363	0.797	0.5365	0.65	0.1494	2.70	0.795	3.19	58.815	3.34	87	3772	91	4154	33	4345	9
MH09-P-1.9	194	1460	7.54	240	0.373	0.5364	0.42	0.1591	1.27	0.839	2.67	62.046	2.76	90	3927	79	4208	28	4345	6
MH09-P-2.6	142	1074	7.58	189	0.082	0.5366	0.41	0.1545	1.08	0.914	2.74	67.659	2.82	96	4186	84	4294	28	4345	6
MH09-10.21	200	129	0.65	260	0.028	0.5369	0.39	0.1620	0.92	0.887	4.03	65.671	4.10	94	4094	122	4264	41	4346	6
MH09-P-1.13	215	1619	7.54	261	0.546	0.5370	0.49	0.1543	1.69	0.824	2.83	60.984	2.93	89	3873	82	4190	29	4346	7
MH09-P-1.6	219	1671	7.62	304	0.373	0.5368	0.37	0.1609	1.11	0.940	2.62	69.570	2.69	98	4272	82	4322	27	4346	5
MH09-10.24	227	171	0.75	233	-0.002	0.5375	0.42	0.1838	0.76	0.694	4.04	51.431	4.11	78	3398	107	4020	41	4347	6
MH09-P-1.7	216	1622	7.50	281	0.307	0.5373	0.37	0.1617	1.01	0.881	2.60	65.291	2.67	94	4074	79	4259	27	4347	5
MH09-P-1.8	207	1551	7.49	253	0.498	0.5372	0.41	0.1591	1.35	0.826	2.64	61.168	2.72	89	3881	77	4193	27	4347	6
MH09-P-2.2	191	1466	7.67	297	0.476	0.5378	0.34	0.1565	1.08	1.053	2.59	78.056	2.65	107	4636	86	4437	27	4348	5
MH09-P-1.21	281	2133	7.59	353	0.693	0.5382	0.56	0.1493	2.16	0.849	3.09	63.005	3.21	91	3962	91	4223	32	4349	8
MH09-10.2	257	195	0.76	357	0.070	0.5385	0.18	0.1958	0.37	0.928	1.05	68.928	1.09	97	4233	33	4313	11	4350	3
MH09-10.6	174	115	0.66	254	0.051	0.5385	0.20	0.1675	0.44	0.989	1.06	73.435	1.11	102	4433	34	4376	11	4350	3
MH09-P-1.22	287	2241	7.80	374	0.582	0.5385	0.55	0.1510	1.94	0.883	3.13	65.529	3.25	94	4078	95	4262	32	4350	8
MH09-P-1.30	322	2230	6.92	333	0.634	0.5384	0.62	0.1482	2.28	0.701	3.13	52.016	3.27	79	3423	83	4032	33	4350	9
MH09-P-1.34	313	2155	6.89	313	0.526	0.5385	0.67	0.1514	2.28	0.678	3.28	50.366	3.43	77	3338	85	4000	34	4350	10
MH09-P-1.14	241	1755	7.28	271	0.472	0.5388	0.50	0.1613	1.72	0.757	2.80	56.273	2.90	84	3635	78	4110	29	4351	7
MH09-P-1.32	327	2183	6.67	316	0.630	0.5387	0.67	0.1542	2.42	0.652	3.20	48.411	3.35	74	3235	82	3960	33	4351	10

Continued on Next Page...

Table 2.3 – Continued

Grain .spot	U ppm	Th ppm	Th/U	Pb ppm	f206%	$^{207}Pb/^{206}Pb$ 204corr	±1σ (%)	$^{208}Pb/^{206}Pb$ 204corr	±1σ (%)	$^{206}Pb/^{238}U$ 204corr	±1σ (%)	$^{207}Pb/^{235}U$ 204corr	±1σ (%)	%c	$^{206}Pb/^{238}U$ date	±1σ (Ma)	$^{207}Pb/^{235}U$ date	±1σ (Ma)	$^{207}Pb/^{206}Pb$ date	±1σ (Ma)
MH09-P-1.25	313	2283	7.29	363	0.757	0.5391	0.60	0.1489	2.29	0.783	3.14	58.178	3.26	86	3727	89	4143	33	4352	9
MH09-P-1.38	293	2041	6.97	311	0.393	0.5392	0.66	0.1592	1.93	0.718	3.35	53.390	3.49	80	3489	90	4058	35	4352	10
MH09-10.10	157	81	0.52	198	0.045	0.5394	0.33	0.1272	0.95	0.877	1.10	65.243	1.19	93	4060	33	4258	12	4353	5
MH09-P-1.18	260	1895	7.30	313	0.389	0.5395	0.52	0.1564	1.59	0.818	2.99	60.836	3.10	89	3853	87	4188	31	4353	8
MH09-P-1.2	320	2440	7.62	482	0.373	0.5396	0.33	0.1599	0.99	1.018	2.60	75.714	2.66	104	4525	85	4407	27	4353	5
MH09-P-1.24	304	2279	7.49	379	0.375	0.5397	0.56	0.1556	1.89	0.847	3.13	63.006	3.25	91	3954	93	4223	33	4353	8
MH09-P-1.26	312	2280	7.30	363	0.434	0.5397	0.56	0.1540	1.72	0.788	3.10	58.600	3.22	86	3744	88	4151	32	4353	8
MH09-P-2.13	120	796	6.65	135	0.334	0.5397	0.67	0.1337	2.40	0.776	3.29	57.722	3.44	85	3702	93	4135	34	4353	10
MH09-P-1.20	266	2024	7.61	340	0.478	0.5400	0.53	0.1508	1.71	0.868	3.09	64.598	3.20	92	4027	93	4248	32	4354	8
MH09-P-2.15	133	913	6.86	149	0.288	0.5400	0.69	0.1356	2.28	0.772	3.40	57.507	3.55	85	3690	96	4132	35	4354	10
MH09-P-2.21	166	1149	6.91	181	0.270	0.5400	0.84	0.1375	3.62	0.748	3.58	55.709	3.78	83	3601	99	4100	38	4354	12
MH09-P-2.25	177	1234	6.97	205	0.271	0.5398	0.86	0.1329	2.98	0.800	4.01	59.513	4.20	87	3788	115	4166	42	4354	13
MH09-P-2.20	157	1105	7.04	175	0.088	0.5403	0.79	0.1407	2.85	0.769	3.62	57.317	3.81	84	3678	102	4128	38	4355	12
MH09-P-1.16	228	1641	7.19	275	0.610	0.5406	0.52	0.1512	1.89	0.814	2.91	60.688	3.02	88	3840	84	4185	30	4356	8
MH09-P-1.29	324	2255	6.97	340	0.545	0.5408	0.60	0.1562	2.01	0.710	3.12	52.914	3.25	79	3457	83	4049	32	4356	9
MH09-P-1.37	294	2019	6.86	309	0.774	0.5408	0.70	0.1481	2.73	0.707	3.32	52.738	3.48	79	3448	89	4045	35	4356	10
MH09-10.5	108	62	0.57	150	0.078	0.5410	0.24	0.1421	0.67	0.957	1.09	71.418	1.15	99	4329	34	4348	11	4357	4
MH09-P-1.31	313	2148	6.87	320	0.788	0.5411	0.65	0.1503	2.58	0.689	3.17	51.401	3.32	78	3379	83	4020	33	4357	10
MH09-P-2.3	180	1390	7.74	266	0.162	0.5408	0.34	0.1617	0.84	1.006	2.62	75.034	2.68	103	4488	85	4398	27	4357	5
MH09-P-1.5	242	1839	7.59	338	0.430	0.5415	0.36	0.1592	1.14	0.941	2.60	70.277	2.66	98	4276	81	4332	27	4358	5
MH09-P-2.1*	215	1641	7.62	346	0.497	0.5413	0.33	0.1623	1.14	1.077	2.56	80.349	2.63	108	4710	86	4466	26	4358	5
MH09-P-1.39	283	2011	7.11	297	0.403	0.5418	0.68	0.1549	2.07	0.710	3.40	53.071	3.55	79	3460	91	4052	35	4359	10
MH09-P-2.16	131	894	6.84	149	0.168	0.5416	0.70	0.1375	2.02	0.786	3.48	58.685	3.64	86	3738	99	4152	36	4359	10
MH09-P-1.23	303	2315	7.65	359	0.461	0.5421	0.57	0.1540	1.88	0.802	3.15	59.934	3.27	87	3796	90	4173	33	4360	8
MH09-P-2.23	184	1263	6.86	201	0.211	0.5423	0.85	0.1308	2.81	0.752	3.89	56.213	4.09	83	3614	108	4109	41	4360	12
MH09-P-1.3	286	2196	7.68	442	0.287	0.5432	0.33	0.1617	0.91	1.044	2.61	78.157	2.67	106	4607	86	4439	27	4363	5
MH09-10.3	143	80	0.56	199	0.091	0.5436	0.25	0.1417	0.67	0.955	1.11	71.590	1.17	99	4322	35	4351	12	4364	4
MH09-P-2.30	195	1282	6.59	205	0.261	0.5468	0.90	0.1332	2.78	0.723	4.05	54.474	4.26	80	3506	110	4078	42	4372	13
Sample MA64 zircon grain 41 (17 analyses)																				
MA64-41.8-2	1035	3969	3.83	191	7.443	0.2958	1.13	0.1616	4.32	0.116	5.07	4.716	5.34	20	705	34	1770	45	3448	18
MA64-41.12	983	4340	4.41	210	8.320	0.3224	1.06	0.1873	3.84	0.126	5.07	5.615	5.31	21	767	37	1918	46	3581	16
MA64-41.8	1091	3966	3.64	224	0.016	0.3335	0.36	0.3373	0.47	0.143	5.07	6.567	5.13	24	861	41	2055	45	3633	5
MA64-41.9-2	775	2517	3.25	215	5.250	0.3733	0.72	0.1506	3.56	0.179	5.07	9.195	5.21	28	1060	50	2358	48	3805	11
MA64-41.3	634	2807	4.43	252	4.662	0.4091	0.40	0.1167	2.68	0.260	1.10	14.688	1.21	38	1492	15	2795	12	3943	6
MA64-41.9	754	2343	3.11	244	0.035	0.4315	0.33	0.2464	0.52	0.223	5.07	13.279	5.12	32	1299	60	2700	48	4023	5
MA64-41.7-2	672	1968	2.93	281	1.674	0.4628	0.47	0.2075	1.65	0.276	5.07	17.594	5.15	38	1570	71	2968	50	4127	7
MA64-41.7	581	1832	3.15	313	-0.010	0.4758	0.34	0.2667	0.56	0.359	5.08	23.563	5.13	47	1978	86	3250	50	4168	5
MA64-41.11	476	1159	2.44	300	1.650	0.4868	0.45	0.1843	1.82	0.416	5.08	27.897	5.16	53	2241	96	3415	51	4202	7
MA64-41.4	290	732	2.52	219	0.702	0.5029	0.27	0.1829	0.91	0.508	1.12	35.251	1.18	62	2650	24	3646	12	4250	4
MA64-41.5	261	505	1.93	255	0.982	0.5035	0.43	0.1866	1.54	0.649	2.76	45.063	2.85	76	3225	70	3889	28	4251	6

Continued on Next Page...

Table 2.3 – Continued

Grain .spot	U ppm	Th ppm	Th/U	Pb ppm	$f206\%$	$^{207}Pb/^{206}Pb$ 204corr	$\pm1\sigma$ (%)	$^{208}Pb/^{206}Pb$ 204corr	$\pm1\sigma$ (%)	$^{206}Pb/^{238}U$ 204corr	$\pm1\sigma$ (%)	$^{207}Pb/^{235}U$ 204corr	$\pm1\sigma$ (%)	%c	$^{206}Pb/^{238}U$ date	$\pm1\sigma$ (Ma)	$^{207}Pb/^{235}U$ date	$\pm1\sigma$ (Ma)	$^{207}Pb/^{206}Pb$ date	$\pm1\sigma$ (Ma)
MA64-41.6-2	475	992	2.09	327	0.706	0.5039	0.38	0.1951	1.19	0.460	5.08	31.957	5.14	57	2439	103	3549	51	4253	6
MA64-41.6	548	1242	2.27	377	-0.014	0.5073	0.32	0.2149	0.56	0.465	5.08	32.511	5.13	58	2461	104	3566	51	4263	5
MA64-41.1	237	399	1.68	241	0.595	0.5112	0.24	0.1872	0.75	0.681	1.13	48.025	1.18	78	3349	29	3952	12	4274	3
MA64-41.10	285	365	1.28	241	0.302	0.5249	0.42	0.1481	1.27	0.581	5.09	42.035	5.16	68	2952	121	3820	51	4313	6
MA64-41.10	246	161	0.65	316	0.232	0.5325	0.38	0.1538	1.06	0.881	5.09	64.658	5.16	94	4072	154	4249	52	4334	6
MA64-41.2	178	130	0.73	225	0.204	0.5328	0.24	0.1596	0.66	0.863	1.15	63.426	1.20	93	4012	34	4230	12	4335	3
Sample MA03 zircon grain 72 (18 analyses)																				
MA03-72.T.7	452	3101	6.86	122	0.000	0.3135	1.14	0.2478	2.15	0.201	1.48	8.670	1.98	33	1178	16	2304	18	3538	18
MA03-72.4	161	787	4.90	88	0.790	0.3281	0.49	0.1015	2.24	0.431	1.57	19.496	1.71	64	2310	31	3067	16	3608	8
MA03-72.T.8	87	21	0.25	79	-0.055	0.3505	1.38	0.0514	6.79	0.760	3.37	36.716	3.80	98	3643	94	3686	38	3709	21
MA03-72.T.1	262	727	2.77	131	0.000	0.3506	1.16	0.0725	6.35	0.407	2.16	19.681	2.58	59	2202	40	3076	25	3710	18
MA03-72.T.6	1471	7816	5.31	326	0.083	0.3540	0.68	0.2812	1.27	0.157	1.29	7.655	1.54	25	939	11	2191	14	3724	10
MA03-72.T.12	291	2127	7.32	125	0.248	0.3945	1.12	0.2438	2.93	0.303	1.72	16.478	2.17	44	1706	26	2905	21	3888	17
MA03-72.T.11	211	1360	6.43	120	1.036	0.3972	1.50	0.1596	6.53	0.413	1.96	22.633	2.61	57	2230	37	3211	25	3899	23
MA03-72.T.2	303	1950	6.44	164	0.203	0.4017	1.04	0.1696	3.44	0.398	1.86	22.027	2.25	55	2158	34	3185	22	3915	16
MA03-72.T.9	306	3314	10.83	171	0.014	0.4726	0.75	0.2272	1.66	0.383	1.90	24.931	2.13	50	2088	34	3306	21	4158	11
MA03-72.T.10	191	1358	7.10	127	0.000	0.4744	0.83	0.1939	1.96	0.463	1.97	30.307	2.23	59	2454	40	3497	22	4164	12
MA03-72-T.5	216	980	4.54	197	0.183	0.4850	0.91	0.1804	3.02	0.632	2.25	42.279	2.53	75	3158	56	3826	25	4196	13
MA03-72.1	196	694	3.55	211	0.463	0.5104	0.45	0.1718	1.54	0.734	2.17	51.633	2.27	83	3547	59	4024	23	4272	7
MA03-72.2	195	667	3.42	206	0.577	0.5107	0.46	0.1682	1.70	0.716	2.17	50.449	2.27	82	3482	58	4001	23	4273	7
MA03-72.T.13	116	348	3.01	106	0.030	0.5159	0.91	0.1703	2.36	0.629	2.20	44.714	2.48	73	3144	55	3881	25	4287	13
MA03-72-T.4	113	398	3.51	113	0.098	0.5210	0.95	0.1780	2.47	0.679	2.48	48.783	2.76	78	3341	65	3968	27	4302	14
MA03-72.3	173	511	2.95	188	0.348	0.5225	0.25	0.1706	0.75	0.737	1.57	53.063	1.63	83	3558	43	4052	16	4306	4
MA03-72.T.14	115	130	1.14	143	-0.039	0.5232	0.80	0.1718	2.07	0.855	2.29	61.687	2.52	92	3984	68	4202	25	4308	12
MA03-72.T.3	124	88	0.71	150	0.202	0.5465	0.92	0.1791	3.28	0.811	2.38	61.138	2.66	88	3830	69	4193	27	4372	13
Sample MA64 zircon grain 48 (10 analyses)																				
MA64-48.7	82	37	0.45	73	0.111	0.3637	0.50	0.1149	1.40	0.696	5.09	34.882	5.18	90	3404	135	3635	51	3765	8
MA64-48.3	98	33	0.33	94	0.019	0.3639	0.40	0.0889	0.97	0.763	5.09	38.304	5.16	97	3656	142	3728	51	3766	6
MA64-48.8	108	53	0.49	93	0.017	0.3651	0.42	0.1313	0.88	0.670	5.08	33.709	5.15	88	3305	131	3602	51	3771	6
MA64-48.6	67	26	0.39	59	-0.012	0.3659	0.51	0.0998	1.47	0.702	5.10	35.429	5.19	91	3429	136	3651	51	3775	8
MA64-48.4	112	44	0.39	112	-0.007	0.3667	0.38	0.1092	0.82	0.789	5.09	39.906	5.15	99	3751	145	3768	51	3778	6
MA64-48.10	100	35	0.35	74	-0.085	0.3670	1.01	0.0926	7.95	0.596	5.09	30.138	5.32	80	3012	123	3491	52	3779	15
MA64-48.9	95	80	0.83	71	0.056	0.3670	0.44	0.0898	1.35	0.596	5.09	30.176	5.16	80	3015	122	3493	51	3779	7
MA64-48.11	110	38	0.35	93	0.057	0.3674	0.37	0.0890	1.06	0.674	5.08	34.116	5.14	88	3320	132	3613	51	3781	6
MA64-48.1	89	37	0.42	89	-0.009	0.3687	0.38	0.1078	0.81	0.788	1.22	40.046	1.32	99	3745	35	3772	13	3786	6

Continued on Next Page...

Table 2.3 – Continued

Grain .spot	U ppm	Th ppm	Th/U	Pb ppm	$f206\%$	$^{207}Pb/^{206}Pb$ 204corr	$\pm1\sigma$ (%)	$^{208}Pb/^{206}Pb$ 204corr	$\pm1\sigma$ (%)	$^{206}Pb/^{238}U$ 204corr	$\pm1\sigma$ (%)	$^{207}Pb/^{235}U$ 204corr	$\pm1\sigma$ (%)	%c	$^{206}Pb/^{238}U$ date	$\pm1\sigma$ (Ma)	$^{207}Pb/^{235}U$ date	$\pm1\sigma$ (Ma)	$^{207}Pb/^{206}Pb$ date	$\pm1\sigma$ (Ma)
MA64-48.5	98	36	0.37	94	0.088	0.3693	0.42	0.0994	1.37	0.761	5.09	38.728	5.16	96	3646	142	3739	51	3788	6

$f206\%$ = 100 x (common ^{206}Pb/total ^{206}Pb)
$^{207}Pb/^{206}Pb$ 204corr = ^{204}Pb-corrected $^{207}Pb/^{206}Pb$ ratio
$^{206}Pb/^{238}U$ 204corr = ^{204}Pb-corrected $^{206}Pb/^{238}U$ ratio
$^{207}Pb/^{235}U$ 204corr = ^{204}Pb-corrected $^{207}Pb/^{235}U$ ratio
%c = % Concordance = $(^{206}Pb^*/^{238}U date)/(^{207}Pb^*/^{206}Pb^* date) \times 100$
$^{206}Pb/^{238}U$ date = ^{204}Pb-corrected $^{206}Pb/^{238}U$ date
$^{207}Pb/^{235}U$ date = ^{204}Pb-corrected $^{207}Pb/^{235}U$ date
$^{207}Pb/^{206}Pb$ date = ^{204}Pb-corrected $^{207}Pb/^{206}Pb$ date

2.6.2 Zircon MH09-10

SHRIMP analyses on grain MH09-10 were measured during four SHRIMP sessions. Zircon MH09-10 SHRIMP analysis spots are labelled on the CL image shown in Figure 2.3. Sessions 1 through 3 are summarized in Nelson (2002b, 2005), and sessions 3, 4 and the depth profile session were carried out during this study, and their CONCH-reduced data are shown in Table 2.3. The 30 analysis points, and 74 depth profile 3-scan analyses on grain MH09-10 form multiple statistical groups based on their $^{207}Pb/^{206}Pb$ dates between 4084±6 to 4372±13 Ma (95% confidence). Depth profile analyses are denoted with a"-P" in the analysis number. Analyses which consist of >90% concordant $^{207}Pb/^{206}Pb$ data yield dates which range between 4281±4 and 4364±4 Ma, and analyses from the 'core' of the grain only (not near an edge or on a crack) with >95% concordant $^{207}Pb/^{206}Pb$ data show a range of dates between 4318±3 and 4364±4 Ma.

SHRIMP results for grain MH09-10 are plotted on a Wetherill concordia diagram shown in Figure 2.3-A. The bulk of the analyses plot close to concordia or along a chord towards the origin that indicates recent radiogenic-Pb loss. A small group of younger and more discordant analyses are from sites located within the right-most section of the crystal (see CL in Figure 2.2) implying that this may be a younger rim component. Since these analyses are discordant and indicate the presence of a separate growth or alteration event on this crystal, they have not been used when calculating the concordant range in $^{207}Pb/^{206}Pb$ dates obtained on this grain.

SHRIMP 7-scan analyses from the core of the grain, that plot directly on concordia are shown in a Wetherill plot inset in Figure 2.3-A. There is a clear range of $^{207}Pb/^{206}Pb$ dates that plot along concordia from 4318±3 to 4364±4 Ma and that form four distinct groups. Initial studies on zircon grain MH09-10 (Nelson, 2002b; Wyche et al., 2004) have not been able to explain the processes behind the range of $^{207}Pb/^{206}Pb$ dates also observed here. The range of concordant $^{207}Pb/^{206}Pb$ dates between 4318±3 Ma and 4364±4 Ma lie on what should be isochemical CL zones on the core of this zircon, yet the $^{207}Pb/^{206}Pb$ ratios are not within uncertainty of a single mean value.

The Pb/U ratio determined using SHRIMP is based on that assumed on the CZ3 standard during the analysis session. The presence of other high-U minerals at the analysis site may result in an asymmetrical and incorrect Pb/U ratio, and possible reverse discordance of an analysis.

In order to assess the possibility of inclusions within zircon MH09-10, the QEMSCAN was used to map the surface of the grain to look for phosphates and other mineral inclusions that might be host to extra Pb or U. The resulting image in Figure 2.4 shows

Table 2.4: Summary of EPMA traverse A on zircon grain MH09-10. Table [A] shows that the average element concentration (ppm) along this traverse are above detection limits for all elements except for Sm.

El.	DL	SD	Ave. ppm
Y Lα	98	32	2879
U Mα	74	24	386
Yb Lα	53	17	510
Pb Mβ	53	17	173
Pb Mα	65	21	268
Dy Lα	47	15	168
U Mβ	57	19	369
Th Mα	36	12	126

that no inclusions were detected within the area of the grain surface exposed. The black pixels represent phosphates and other inclusion materials, and the red and pink pixels represent typical zircon. The lack of inclusions within this grain implies that the variation obtained in $^{207}Pb/^{206}Pb$ dates on SHRIMP analysis sites are not related to micro-inclusions that had differing $^{207}Pb/^{206}Pb$ ratios.

To further elucidate the chemical structure of grain MH09-10, EPMA traverses were obtained to look at chemical gradients across CL zones. The EPMA lines measured and the average ppm and detection limits are summarized in Table 2.4. Of the three traverses obtained, the first traverse (a 35μm traverse cutting obliquely across the CL zones, shown in Figure 2.5-a) had the best results. This traverse was acquired to detect whether elemental transport on a μm scale could be observed along a traverse that included sites having a range of $^{207}Pb/^{206}Pb$ dates. The EPMA traverse on grain MH09-10 spans from the 4364±4 Ma SHRIMP date location (analysis MH09-10.3) to the 4318±3 Ma date location (analysis MH09-10.7).

The results of the EPMA lines Dy Lα, Pb Mβ, Pb Mα, Th Mα, Th Mα, Yb Lα and Y Lα across traverse 1 are shown in Figure 2.5. Data collected for Sm Lα was not included as this was below detection limits. All plots follow roughly similar trends, with the final 5 points of each traverse being adversely impacted by the EPMA analysis sites nearing the edge of the grain. Although there are visible matching peaks and troughs along the plots, they were not far enough outside analytical uncertainties to confirm that the differences observed were caused by some diffusional process. The peaks appear to be in similar locations for Pb, U and Th, as well as Y, Yb and Dy.

To improve the analytical precision and to measure the isotopic makeup across zircon MH09-10, a SHRIMP traverse was obtained, measuring the elements in a full SHRIMP U-Th-Pb standard runtable. Each traverse is a series of 45 SHRIMP analysis steps, counting 1 second per analysis point, where each step along the traverse is approximately 3.3 μm. While the SHRIMP spot was about 25μm in size, differences were still detectable, the results were impacted by overlapping analysis areas. The plots in Figure

2.5-c show raw counts from the SHRIMP traverse across zircon MH09-10 (location of traverse in Figure 2.5-b) measuring: $^{196}Zr_2O^+$ (1 s), $^{206}Pb^+$ (1 s), $^{207}Pb^+$ (1 s), $^{208}Pb^+$ (1 s), $^{238}U^+$ (1 s), $^{232}Th^{16}O^+$ (1 s), $^{238}U^{16}O^+$ (1 s). There is a good correlation in the raw count rates shown in Figure 2.5-c between all the Pb peaks as well as the U and Th (E, F and G). However the Zr peak (A) shows variations due to SHRIMP spot locations on the grain that are partially correlated to an increase in ^{238}U, which may be due to different yields of these species due to surface topology.

In processing the results, the first four traverses were corrected for motor stage misalignment so they match with the location of each analysis spot on the other traverses, and were processed to calculate $^{207}Pb/^{206}Pb$ dates as if each spot was a single 4-scan analysis, with their standard deviation shown as the uncertainties on Figure 2.5-a. The analytical uncertainties on calculated $^{207}Pb/^{206}Pb$ dates are large because the peaks at each analysis point were measured for only one second. However, the overall results match closely with previously obtained 7 and 4-scan standard SHRIMP analysis points. The mean age across the center of the grain was calculated using all the results for this traverse as 4357 ±38 Ma. This calculated mean age's uncertainty fits within the range of dates previously obtained by single SHRIMP spots for this grain, and supports the inferred presence of geological sources of uncertainty in the core of this grain.

2.6.3 Zircon MA64-41

The SHRIMP results for grain MA64-41 have been plotted on a Wetherill concordia diagram shown in Figure 2.3-B and data on Table 2.3. The 17 analyses form 13 groups that generally lie along a recent radiogenic-Pb loss chord. Group 2 is comprised of the two most concordant analyses (93% concordant) and has a $^{207}Pb/^{206}Pb$ date of 4334±3 Ma.

The core of grain MA64-41 shows a similar range of $^{207}Pb/^{206}Pb$ dates to that of grain MH09-10. However the extra scatter in grain MA64-41 may be due to the existence of large cracks, possible inclusions, and recent radiogenic-Pb loss. There is a strong correlation between concordance, and U and Th concentration. The $^{207}Pb/^{206}Pb$ date with the most concordant analysis (93%) yielded the oldest $^{207}Pb/^{206}Pb$ date (4335±6 Ma) and had the lowest U (178ppm) and Th (130ppm) concentration. In contrast, the youngest $^{207}Pb/^{206}Pb$ date obtained, from the rim of the grain, was the least concordant (20%) had the lowest $^{207}Pb/^{206}Pb$ date (3448±18 Ma) and the second highest U (1030ppm) and Th (3950ppm) concentrations.

These extreme variations made grain MA64-41 difficult to compare with grain MH09-10, because grain MH09-10 has consistent Th and U and concordance patterns throughout the 'core' of that zircon crystal.

2.6.4 Zircon MA03-72

A Wetherill plot summary for SHRIMP results on grain MA03-72 are presented in Figure 2.3-C and data on Table 2.3. The data plot along a recent Pb-loss trend, similar to results from MA64-41. The first session data, shown in Figure 2.2, yielded a few ca. 20% discordant analyses close to ca. 4300 Ma. The second session used a much smaller spot during a 'traverse' of the grain (labelled with a "T" appended to their analysis number). This session yielded the oldest near-concordant (88% concordant) analysis, MA03-72.T.3, with a date of 4372±13 Ma on the core, and a 98% concordant rim analysis of 3708±21 Ma. These results suggest that the smaller spot size may have missed cracks and other metamict components on this very small zircon, resulting in more concordant, and older ages. The oldest age obtained on this zircon is the same as the oldest age obtained from a single analysis during a depth profile of grain MH09-10 of 4372±13 Ma.

2.6.5 Zircon MA64-48

The SHRIMP results for grain MA64-48 have been plotted on a Wetherill concordia diagram shown in Figure 2.3-D and data on Table 2.3. All analyses belong within one group which yields a date of 3778±6 Ma, providing a very simple population. There is no detectable variation within the $^{207}Pb/^{206}Pb$ dates on grain MA64-48 even with closely spaced SHRIMP analysis sites. This grain is useful to compare to other Hadean grain cores, as it indicates a younger geologic history which does not show any range, outside of analytical uncertainty, of $^{207}Pb/^{206}Pb$ dates.

2.6.6 Zircon REE analyses

SHRIMP REE analyses were obtained on zircons MH09-10, MA64-41 and MA64-48, and are summarized in Table 2.5. Analysis locations are shown in Figure 2.2 and their plots are summarized in Figure 2.6.

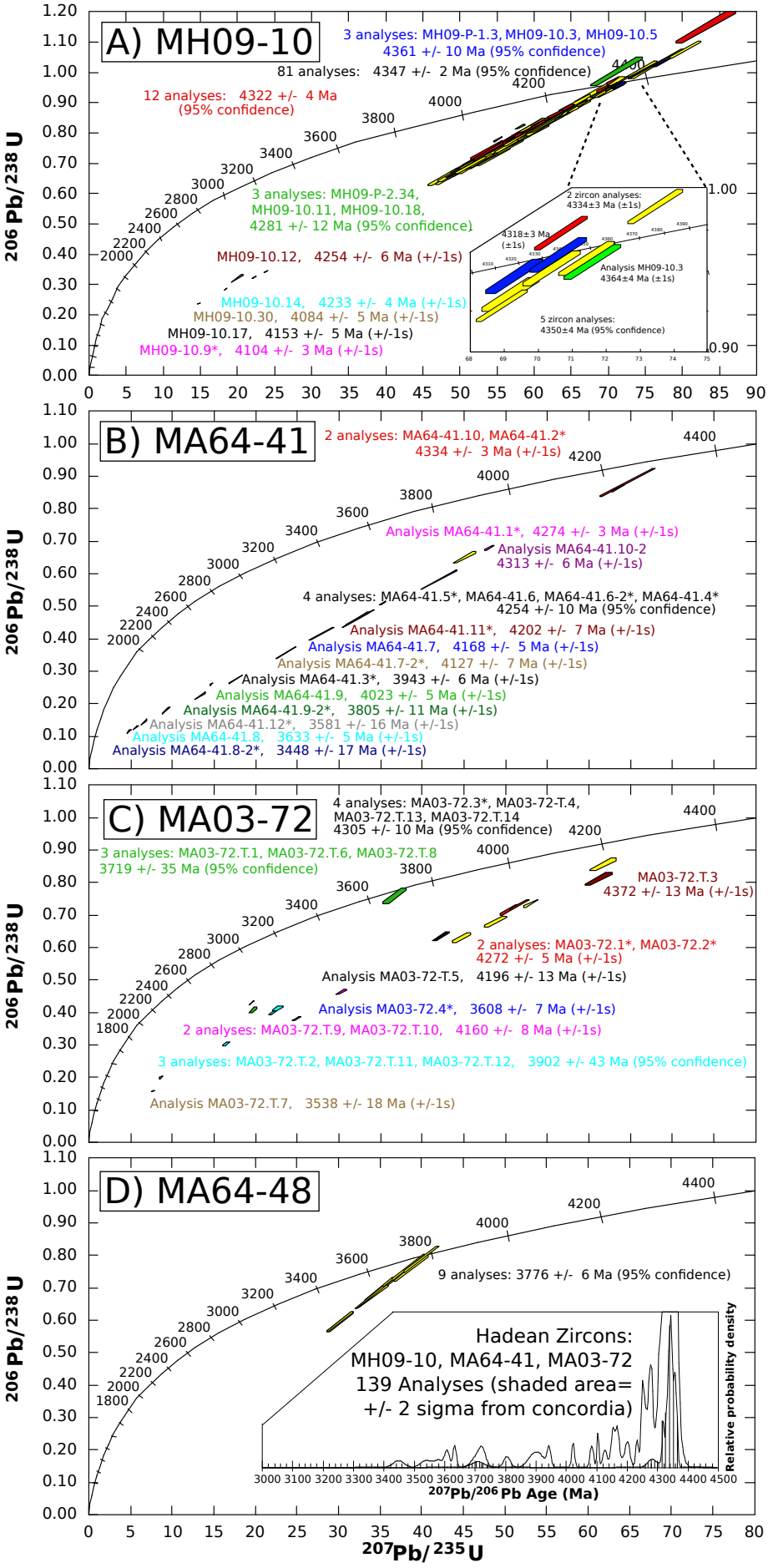

Figure 2.3: see next page for full description

Figure 2.3: Wetherill concordia diagrams with SHRIMP data showing zero-age Pb-loss trends for zircons (A) MH09-10, (B) MA64-41, (C) MA03-72 and (D) MA64-48. Inset (bottom of MA64-48 Wetherill diagram) probability summation plot for three Hadean zircons (139 analyses, zircons MH09-10, MA64-41 and MA03-72).

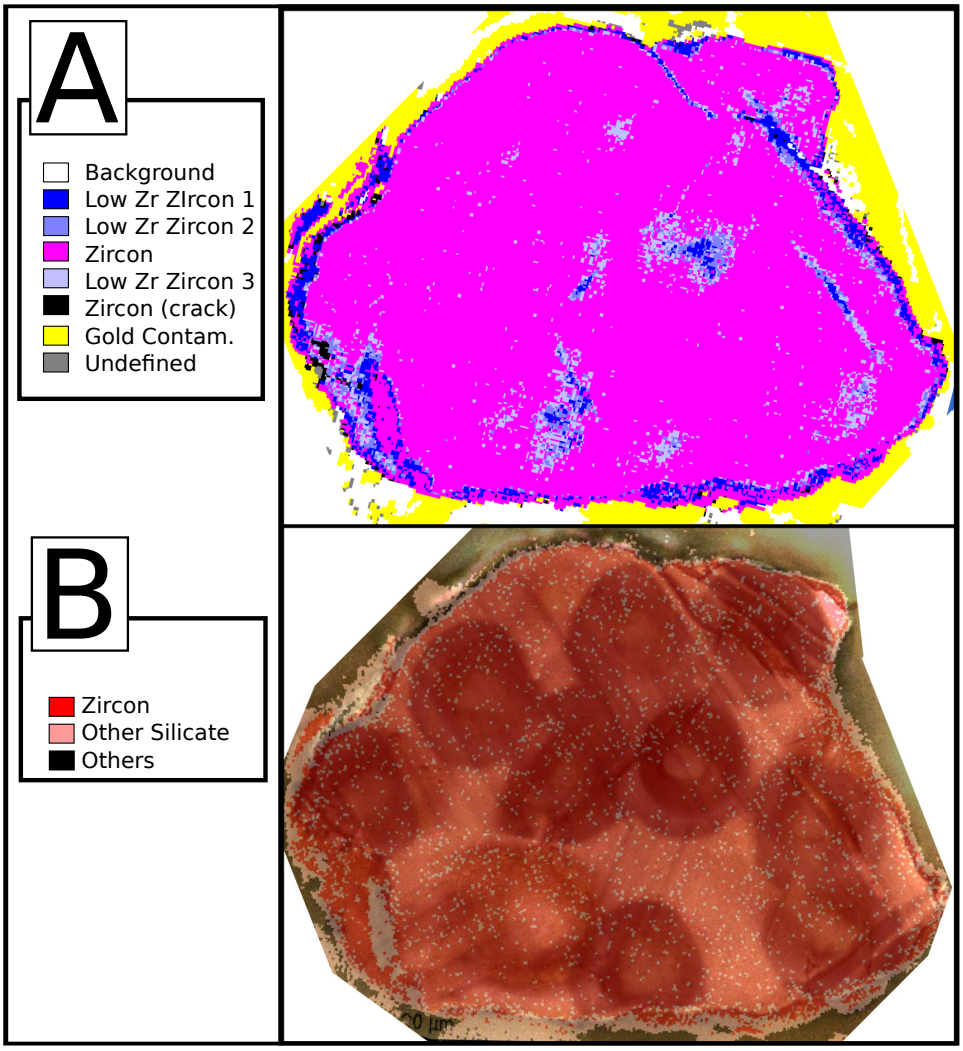

Figure 2.4: Zircon MH09-10 QEMSCAN images (A) showing concentration map (B) overlay of concentration map on a CL image. No phosphates or other inclusions were detected. Variation in Zr contents is attributable to excess gold coat from multiple SHRIMP sessions.

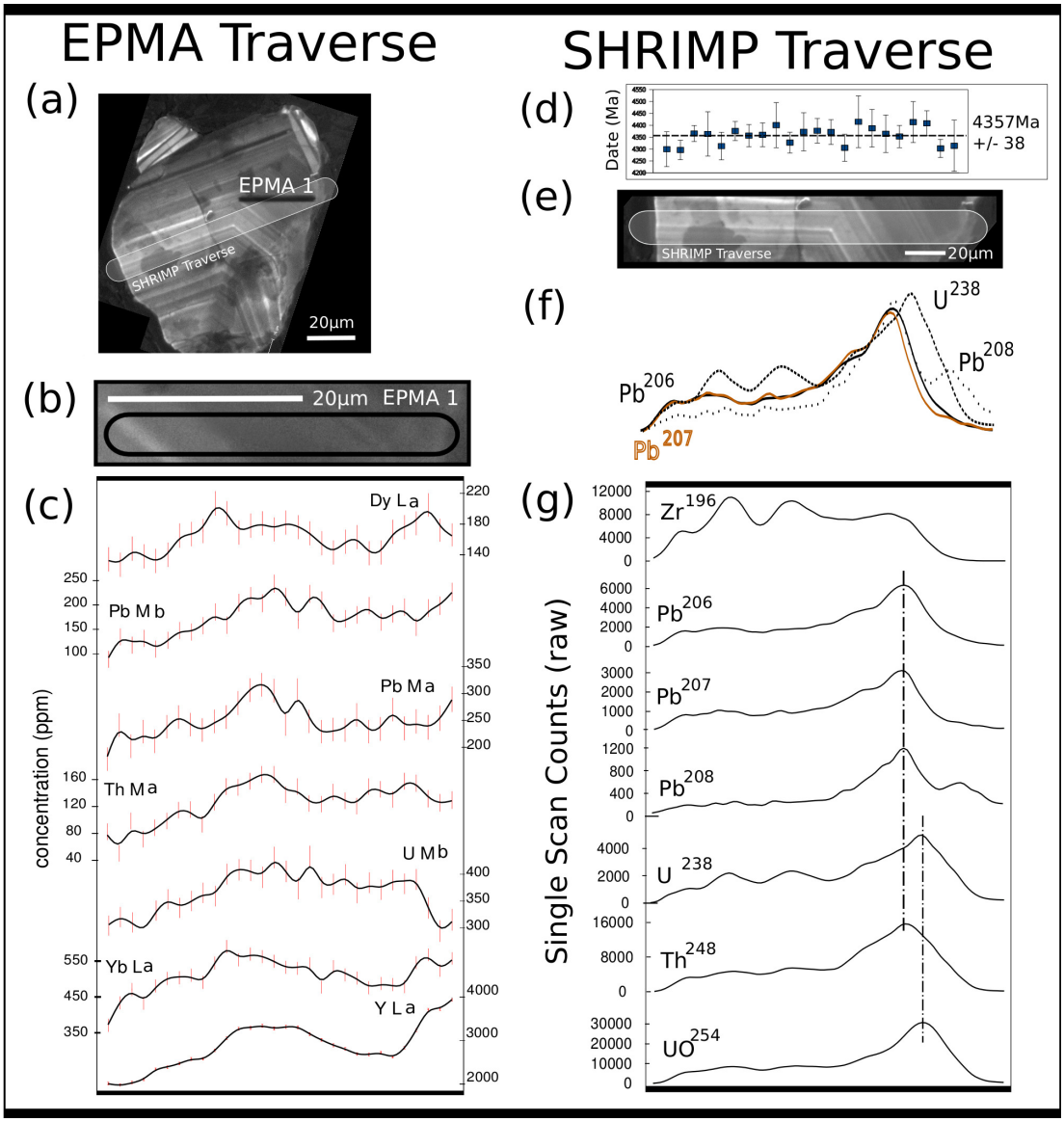

Figure 2.5: Zircon MH09-10 EPMA and SHRIMP traverses. EPMA traverse shows a) an overview of grain MH09-10 with location of this traverse, b) close-up CL image of the traverse location on grain MH09-10 and c) ppm concentration traverse plots across this CL zone. SHRIMP traverse shows d) calculated $^{207}Pb/^{206}Pb$ dates along the traverse (see text), e) close-up CL image of the traverse location on grain MH09-10 and f) combination of U and Pb showing 'skew' of U peak and the three Pb peaks, and g) traverse results for $^{196}Zr_2O^+$, $^{206}Pb^+$, $^{207}Pb^+$, $^{208}Pb^+$, $^{238}U^+$, $^{232}Th^{16}O^+$ and $^{238}U^{16}O^+$.

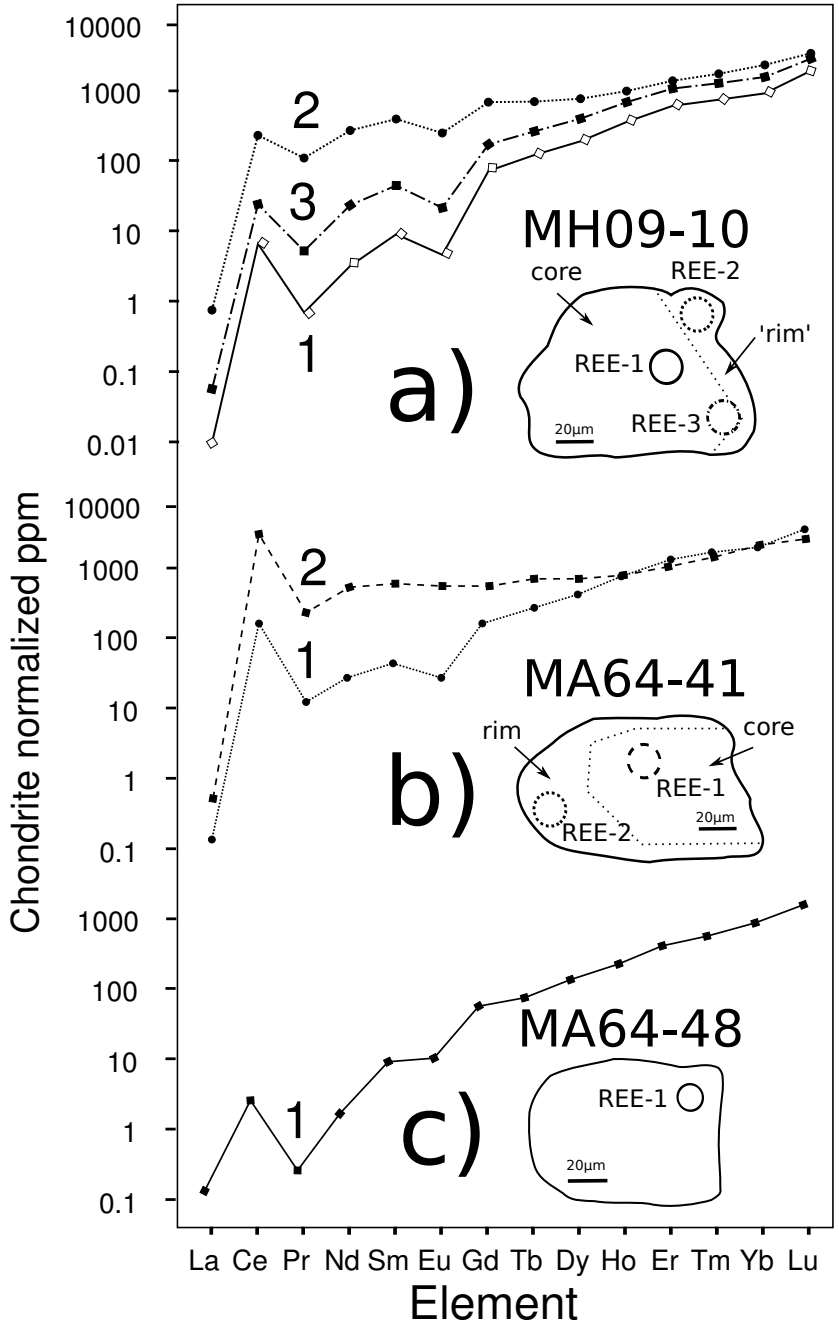

Figure 2.6: SHRIMP REE results for the a) zircon MH09-10, b) zircon MA64-41 and (c) zircon MA64-48. Schematic sketches of each grain, including core and rim components are also shown.

Table 2.5: SHRIMP REE results for zircon grains MH09-10, MA64-41, MA03-72 and MA64-48

label .spot	La ppm	Ce ppm	Pr ppm	Nd ppm	Sm ppm	Eu ppm	Gd ppm	Tb ppm	Dy ppm	Ho ppm	Er ppm	Tm ppm	Yb ppm	Lu ppm
SHRIMP REE Results														
MH09-10.1c	0.00	7.07	0.10	2.54	2.32	0.44	24.29	7.78	79.83	33.49	166.28	29.36	248.33	79.63
MH09-10.2r	0.31	244.51	16.62	212.23	100.28	23.87	230.19	44.34	320.41	91.94	376.47	68.25	629.34	140.66
MH09-10.3c	0.02	25.72	0.80	18.54	11.46	2.07	57.84	16.81	167.34	64.00	291.50	50.30	424.24	118.10
MA64-41.1c	0.04	135.04	1.60	18.02	9.87	2.41	50.11	16.75	176.15	68.86	315.47	59.36	531.29	125.12
MA64-41.2r	0.18	2769.47	33.13	366.42	137.38	46.65	183.22	39.75	262.29	66.09	268.01	51.89	506.14	105.00
MA64-48.1c	0.04	2.53	0.04	1.45	2.39	1.07	19.26	5.34	56.41	20.99	106.87	22.34	231.26	60.35
$_A$	0.054	23.10	0.179	2.770	4.230	0.201	21.64	6.716	72.25	29.27	155.4	35.89	404.0	100.3
$_B$	0.007	0.340	0.010	0.107	0.195	0.060	1.03	0.319	4.600	1.730	7.900	1.825	13.62	2.920
$_C$	0.088	0.812	0.023	0.133	0.338	0.100	1.085	0.421	4.980	1.798	8.636	1.834	23.467	3.543

Sample labels appended with c and r: "c" = core; "r" = rim

All values in ppm based on the zircon REE standard (P.Kinny)

$_A$ REE zircon standard ppm based on TIMS data from P.D. Kinny (personal communication)

$_B$ CZ3 zircon ppm based on ICPMS data from A. Kennedy (personal communication) $*$ Default dataset used

$_C$ CZ3 zircon ppm based on Cameca IMS3f data from A. Möller (personal communication)

Grain MH09-10 (Figure 2.6-a) has three REE analysis points which show different levels of increasing concentrations. These differences are mainly present in the variability of the LREE from analytical spots 1 through 3. This increase is on the "rim" component of grain MH09-10, and may be due to this zone being formed within a melt with different LREEs, or enrichment due to late interaction with low temperature fluids (Hoskin, 2005). In comparison, zircon MA64-41 (Figure 2.6-b) shows a similar trend in the core being lower in LREE than the rim. Zircon MA64-48 (Figure 2.6-c), with only one analysis site, shows relatively low LREE, similar to the best core analyses on grains MA64-41 and MH09-10. This data is consistent with relatively undisturbed core zones on these zircons, with rim overgrowths that are partially metamict and have suffered some form of later stage disturbance.

2.7 Discussion

The range of concordant $^{207}Pb/^{206}Pb$ dates obtained on the cores of grains MH09-10, MA03-72 and MA64-41 are not strongly correlated with (1) Th or U concentrations, (2) ^{204}Pb counts, (3) common-Pb correction method (^{204}Pb or ^{208}Pb), (4) variations observed within the $^{207}Pb/^{235}U$, $^{206}Pb/^{238}U$ and $^{208}Pb/^{232}Th$ dating systems or (5) micro-inclusions of phosphates or other minerals with differing $^{207}Pb/^{206}Pb$ ratios within the crystalline lattice. The $^{207}Pb/^{206}Pb$ dates obtained are also outside the range attributable to analytical uncertainty and constitute unique groups based on χ^2 grouping methods. The observed variation of over 50 M.y. on the core components of these Hadean grains is a function of some process which is not easily correlateable with aspects of crystal chemistry measured via the SHRIMP, Electron Microprobe or the QEMSCAN. To further our understanding of these ancient zircons, their early isotopic chemistry, crystal integrity and potential Hadean thermal drivers must be assessed.

Different 'simple' models of diffusional processes such as fast-transport diffusion, radon-loss, recoil-loss, first-order kinetic loss and modification processes such as recrystallization cannot easily account for the observed range in $^{207}Pb/^{206}Pb$ dates observed within these >4300 Ma zircons. If the range of $^{207}Pb/^{206}Pb$ dates on grain MH09-10 were due to loss or redistribution of radiogenic Pb early in the zircon history, the current range of concordant $^{207}Pb/^{206}Pb$ dates may be explained. Current models of Pb-loss in zircons include "younging" of grains towards grain boundaries, which is not observed in grain MH09-10, as the range of dates obtained are all within the 'core' of the zircon.

Observing the effects of diffusion through differences in concentration gradients of trace elements within grain MH09-10 as detected by EPMA traverses has been unable to show large discrepancies between the U and Pb concentrations. This is primarily due to the relatively low detection limits of the EPMA versus the concentration of the species analyzed. It may also be that the EPMA technique does not have adequate

spatial resolution nor detection limits to detect the effects arising from diffusional processes on sub-ppm and sub-μm scales. Further, if the early event or events causing Pb to be redistributed was slightly patchy, or only occurred on very small scales, it would be difficult to detect by this technique.

The SHRIMP traverse has detected variation in peak heights of all the Pb isotopes when compared to U, which suggests a redistribution of the more incompatible element Pb versus U. As the area this shows up in is near a grain edge, and not near the most concordant SHRIMP $^{238}U/^{206}Pb$ and $^{207}Pb/^{206}Pb$ dates, it may be caused by a lowered sensitivity due to distortion of the secondary-ion extraction field by the edge of the mineral. There is also evidence of late alteration near this analysis area, as recorded by enrichment of LREE of an adjacent area to this on the grain surface.

Without finding any inclusions within zircon MH09-10, and having assessed the robustness of the obtained $^{207}Pb/^{206}Pb$ dates by SHRIMP single spot analyses and calculations from a SHRIMP traverse, questions remain as to the source of the $^{207}Pb/^{206}Pb$ date variability.

2.7.1 Metamictization

The accumulation of radiation damage within the zircon crystalline lattice is largely a result of radioactive decay of ^{238}U to ^{206}Pb (8 α decay events), ^{235}U to ^{207}Pb (7 α decay events) and ^{232}Th to ^{208}Pb (6 α decay events). There are a large number of alpha decay events taking place for each of the U and Th atoms within the zircon lattice. Each α (helium nucleus) recoil atom that decays from U and Th is emitted into the crystalline lattice with an energy of approximately 70 to 100 keV and generates approximately 700 to 2,000 displaced atoms (Meldrum et al., 1998; Ewing et al., 2000; Ewing et al., 2003). As opposed to the β recoils, which only generate 0.1 displaced atoms (Ewing et al., 2003), the α decay events are a major source of structural damage to the crystalline lattice.

To decipher the amount of radiation damage a particular zircon has undergone, it is possible to calculate the number of α-decays/g of a particular sample as long as the age of the sample and the amount of ^{238}U, ^{235}U and ^{232}Th is known. Shown in Figure 2.7, the displacement dose for U and Th can be calculated where $D\alpha$ is the dose in units of α-decays/g, N_{238}, N_{235} and N_{232} are the measured number of atoms/g of ^{238}U, ^{235}U, and ^{232}Th, and $\tau_{(235)}$, $\tau_{(235)}$, and $\tau_{(235)}$ are their respective half-lives and t is the geologic age (Ewing et al., 2003).

Calculations of α-decay dose for the 4404 Ma zircon (Wilde et al., 2001; Peck et al., 2001) showed that after 585 M.y. the α-events/mg (dose) was $3.0x10^{15}$, which would

$$D\alpha = 8N_{238}[exp(t/\tau_{238}) - 1] + 7N_{235}[exp(t/\tau_{235}) - 1] + 6N_{232}[exp(t/\tau_{232}) - 1]$$

Figure 2.7: Equation to calculate α-decay dose for U and Th ($D\alpha$) (Ewing et al. 2003)

distort the crystalline lattice by introducing amorphous regions from the accumulation of radiation damage (Hoskin, 2005). This study further suggested that after 125 M.y. the zones in a ca. 4400 Ma crystal that had high U and Th would have received enough radiation damage to significantly alter them differentially from zones of lower U and Th content.

Zircons that have undergone a substantial amount of radiation damage throughout their life can become "metamict". That is, they lose their crystal structure and become amorphous over time (McLaren et al., 1994; Meldrum et al., 1998; Nasdala et al., 1998, 1996; Hanchar and Miller, 1993; Deliens et al., 1977). Although radiation damage can cause a portion of the structural damage of a zircon, it is not the only factor. Diffusional and hydrothermal processes also take part in expediting the metamictization process. It has been shown that hydrothermal processes can leach or enrich the zircon structure with Pb, U, Th and other typically incompatible elements such as Ca and Ba (Geisler and Pidgeon, 2002; Thorsten Geisler et al., 2001).

2.7.2 Hadean Isotopic Systematics and Radiation Damage

At approximately 4350 Ma, during a time where the oldest zircon dates are recorded (4300-4404 Ma), there was a higher abundance of ^{235}U versus ^{238}U, as well as approximately 15% of the initial short-lived radionuclide ^{244}Pu left to decay. ^{244}Pu has an ionic radius similar to ^{238}U, ^{235}U, and ^{232}Th, and is compatible with the Zr atomic location in a zircon lattice. This ^{244}Pu, along with very radioactively active ^{235}U would have been incorporated into zircons formed at this time. The higher abundance of ^{235}U versus ^{238}U during Earth's early history caused increased radiation damage within these Hadean zircons, and a larger proportion of ^{207}Pb generation in their first 100 Ma.

Microstructural damage to the lattice of >4000 Ma zircon (and in particular, >4300 Ma zircon) arising from fission of actinides including the extinct nuclide ^{244}Pu, may have facilitated radiogenic-Pb redistribution within these grains. These characteristics would have increased the chances that an early Archean thermal event would cause Pb-redistribution within these ancient zircons. Extra heat from short lived radionuclides may have caused zircons to accrue radiation damage quickly, forming amorphized zones which would enable faster Pb transport (Hoskin, 2005). These early conditions could have enhanced the occurrence of double-cascade impacts during radioactive decay (Schuster et al., 2009; Glasmacher et al., 2006). This damage from decay events would

result in up to 13μm long alpha fission tracks (Nasdala et al., 1999; Rahn et al., 2004) and ca. 5.5nm Pb ion tracks. The accumulation of these decay events has been shown to facilitate concentration of radiogenic Pb into these alpha radiation damage channels (Utsunomiya et al., 2004) that would result in eventual increased mobility of Pb and potentially U throughout the crystal structure.

At 3900 Ma, nearly 36% of the initial solar system abundance of ^{235}U will have decayed to ^{207}Pb, whereas only 7% of ^{238}U would have decayed to ^{206}Pb. Thermal events at ca. 4150 or 3900 Ma impacting these ancient zircons could account for a 25 to 40 Ma age range in ^{207}Pb/^{206}Pb ratios if they resulted in Pb-redistribution of at least 10% of the radiogenic Pb component at either of these ages.

2.7.3 Thermal Events

The U, Th and isotopic makeup of these zircons would have played a role in how fast these zircons accumulated radiation damage. The timing of early thermal events, and their subsequent impact on annealing radiation damaged zones within these ancient zircons have implications for the early Pb-redistribution described in this study.

Two methods of early Pb redistribution within these Hadean zircons are constant redistribution, and periodic redistribution. Constant redistribution refers to the re-distribution of ^{206}Pb and ^{207}Pb based on (mainly) volume diffusion, with some fast-track diffusion through small radiation damaged areas, and constant re-annealing of these radiation damaged areas. The extra decays and resulting radiation damage may have had a larger impact on the early history of these zircons, where they would have accumulated highly metamict zones if the crystals existed at lower temperatures than 850−950°C (near closure and self-annealing temperatures), and perhaps 600°C over longer (tens to hundreds of millions of years) periods of time.

The second method of early Pb redistribution is based on periodic redistribution, where the zircons were in a stable temperature environment from time to time (perhaps below 200−400°C), which allowed a slightly greater amount of radiation damage which was not instantly re-annealed. Periodic events of 800−1200°C may have caused redistribution of Pb (with more redistribution of ^{207}Pb than ^{206}Pb, due to its higher abundance) and potentially some redistribution of U and Th. With a 10% redistribution event at 3900 Ma (postulated 'late heavy bombardment era') and with an initial zircon crystallization age of 4341 Ma, this method would have created a range of concordant ^{207}Pb/^{206}Pb dates between 4297 Ma and 4382 Ma. A similar 10% redistribution at 4100 Ma on a 4341 Ma zircon would result in a range of 4313 Ma to 4367 Ma. These results are very similar to the range of dates that we see on the 90% concordant data on grain MH09-10, and on other Jack Hills and Narryer >4300 Ma zircons.

A timeline of early Hadean events is summarized in Figure 2.8-(A), showing the complex early history that these zircons would have undergone. Figure 2.8-B through G show multiple lines of evidence and stages of our preferred interpretation of age variation within these Hadean zircons. A brief summary of the steps involved in this interpretation of age variation as observed in these Hadean zircons is as follows: (1) Crystallization of a Hadean zircon at ca. 4350 Ma with oscillatory zoning of alternating high (zone '1') and low (zone '2') uranium contents. (2) Radiation damage accumulation, metamictization, and Pb-redistribution and accumulation within damaged areas of zone '1'. (3) First thermal event causing annealing of more metamict zones (zone '1') and driving thermally activated Pb-redistribution or loss, locking in isotopic 'change' to these areas into a new, highly ordered crystalline structure. (4) The originally high-U zones (zone '1') are now more stable than the originally low-U zones (zone '2') of the crystal. (5) A Second period of radiation damage accrual, mostly within the originally low-U zones (zone '2'), now having the least-ordered crystalline structure, resulting in radiation damage accumulation, metamictization, and Pb-redistribution and accumulation within damaged areas of zone '2'. (6) Second thermal event causing annealing of more metamict zones (zone '2') throughout the crystal, driving thermally activated Pb-redistribution or loss, and now locking in this new isotopic signature. (7) Further early thermal events could provide more Pb-redistribution and annealed overprinting within the crystal structure. (8) Late stage thermal, hydrothermal and over 3 Ga residence time within the host metasedimentary rocks would have caused enhanced metamictization within any high-U or structurally damaged zones of these zircons, resulting in Pb-loss and enrichment of LREE and Th. (9) Analyses within this single grain core could now be transposed in two directions on the Wetherill diagram, above and below the original crystallization age of the zircon crystal. (10) Any reversely-discordant analyses, as caused by Pb-gain to specific damaged zones prior to annealing, would likely be moved towards concordia during multiple protracted thermal events and late stage zero-age Pb-loss. (11) This process may explain many old zircons that exhibit multiple $^{207}Pb/^{206}Pb$ dates within their core.

2.8 Summary

1) Well preserved igneous zircons >4300 Ma show a >50 M.y. range of $^{207}Pb/^{206}Pb$ dates within interior 'cores' which indicate some form of early Pb-redistribution is occurring within these zircons. This suggests that individual $^{207}Pb/^{206}Pb$ dates (and their analytical uncertainties of ±5 Ma) on these ancient zircons are unreliable, as it is unlikely that these oscillatory zoned zircon cores have formed over time periods of ca. 50 M.y.

2) The existence of a range of $^{207}Pb/^{206}Pb$ dates within well preserved >4300 Ma

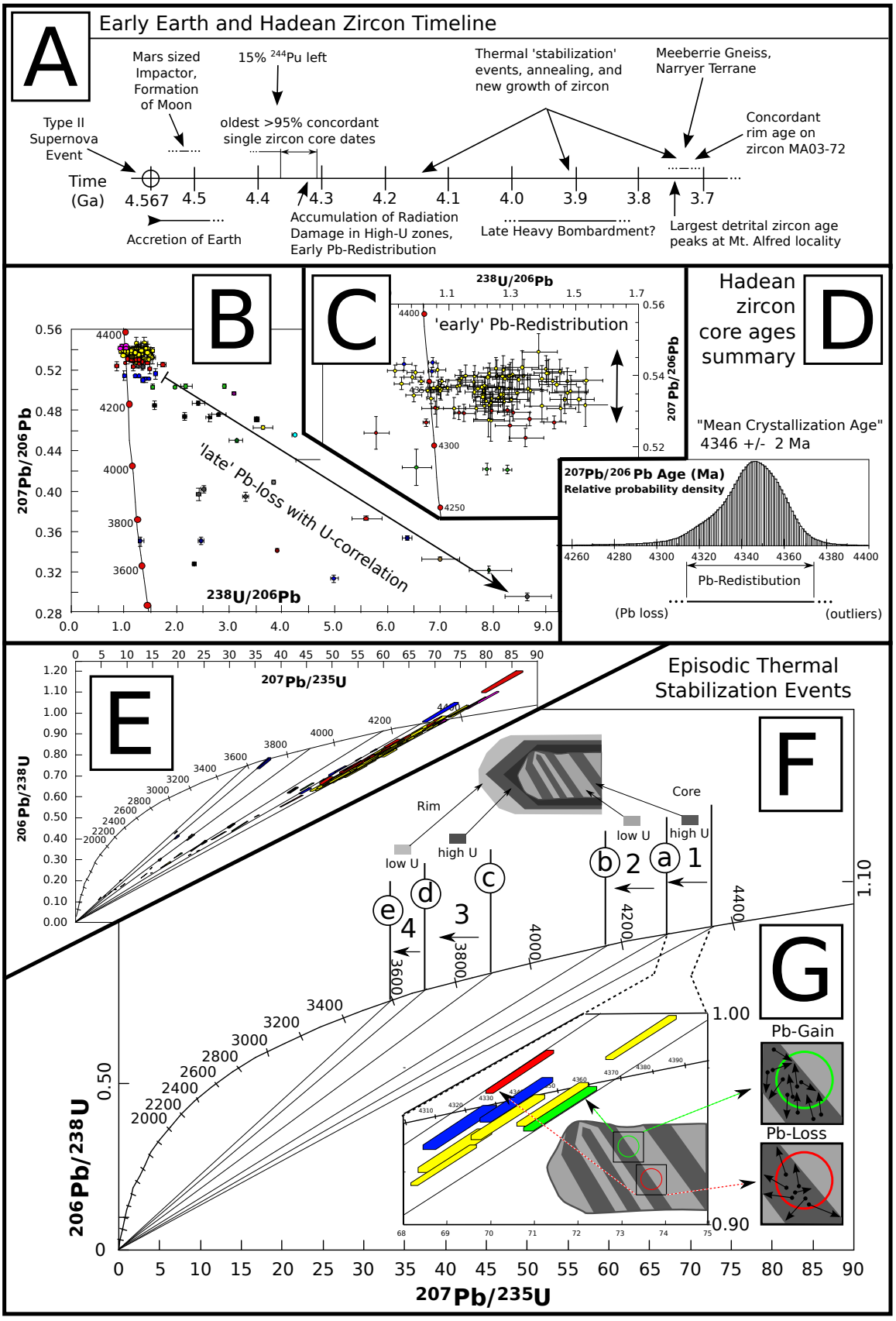

Figure 2.8: see next page for full description

Figure 2.8: Summary figure of Hadean zircon data showing (A) timeline of early Earth events. (B) Tera-Wasserburg concordia diagram showing late-stage Pb-loss trends with a uranium concentration correlation, and (C) 'early' Pb-redistribution with no uranium concentration correlation. (D) Hadean zircon age summary with calculated 'mean crystallization age' of 4346 ±2 Ma, showing spread of ages in a relative probability density plot with Pb-redistribution zone outlined below. (E) Wetherill plot with all Hadean zircon age data, including both core and rim components, and trend-lines towards the origin representing zero-age Pb-loss of different zones of each zircon. (F) Wetherill plot with Pb-loss trends intersecting concordia at possible thermal 'stabilization' event ages (labelled 'a' through 'e') which relate to either an annealing event (within the core) or new growth of zircon (rim) at ca. 4280, 4150, 3900, 3700 and 3600 Ma; numbered events (1-4, right to left) define a possible timing for annealing and stabilization events within each zircon, re-ordering the crystal lattice within more metamict high-U domains first (displayed in event 1) then the lower-U, second-to-become metamict domains second (displayed in event 2). Later possible events form metamorphic or igneous growth zones (3 and 4) may have undergone similar processes. All processes show advanced overprint by zero-age Pb-loss events, and multiple analyses plot within each trend-line. The inset figure (G) shows the most concordant analyses from the core of zircon grain MA09-10 within a Pb-redistribution field. A cartoon sketch of a detrital zircon core with possible SHRIMP analysis site locations is shown with igneous growth zones of higher (dark) and lower (bright) uranium concentrations. One possible way to obtain these results from a zircon crystallized at ca. 4346 Ma is for zones to have net gain and net loss of Pb early in their history. The oldest (green) analysis site links to a SHRIMP spot (circled) that shows a net gain of Pb during an early redistribution event. The youngest (red) analysis site links to a zone in the crystal that shows a net loss of Pb. This early redistribution would have heterogeneously distributed Pb throughout the crystal structure within radiation damaged zones, and would impart a skew on their $^{207}Pb/^{206}Pb$ ratios which would not reflect their original crystallization age. Later stage thermal events have left extra overprint on this early Pb-redistribution, and impart extra zero-age Pb-loss complexity as displayed in (E) and (F). These late stage thermal events and zero-age Pb-loss, present in these Hadean zircons, would have pulled any reversely discordant (due to Pb-gain) analyses back towards concordia.

igneous zircons is not consistent with the operation of simple chemical redistribution mechanisms, as the $^{207}Pb/^{206}Pb$ ratios do not correspond with U concentrations, and is best explained by the heterogeneous redistribution of Pb^*.

3) The robustness of zircon $^{207}Pb/^{206}Pb$ dates are often heavily relied upon to make geological interpretations. The use of geological shorthand in quoting these dates as single crystallization 'ages' must be assessed, as zircon grains exhibiting large ranges of dates within single growth zones may cast doubt on obtained results.

4) Further research into the post-Hadean history (<3800 Ma) of these detrital zircons will help elucidate the difference of the earlier Pb-redistribution events and the later stage metamorphic, tectonic and hydrothermal events which have overprinted many grains. Even accounting for this, however, it is likely insufficient when assigning 'ages' to these grains - as the 'pristine' core ages often show distinct spreads of ages, adding to the currently unrealized geological uncertainties inherent in Hadean zircons.

CHAPTER 3
3.0 GA YILGARN METASEDIMENTARY ROCKS

This chapter works to resolve the detrital zircon age complexities seen within ca. 3.0 Ga metasedimentary rocks throughout the Yilgarn Craton by statistically assessing all detrital zircon age data from these metasedimentary rocks in a publication which is published in the journal Precambrian Research. The study was a collaboration with Dr. David Nelson, and uses statistical analysis to decipher the potential makeup of the provenance of these zircons from the Illaara and Maynard Hills granite greenstone belts using data collected during this thesis, as well as assessing the overall age structures found within these samples when compared to other ca. 3000 Ma metasedimentary rocks throughout the Yilgarn Craton. Additional scripts and output data are presented in Appendix A. The contribution further elucidates Hadean age gaps in the data when comparing Mt. Alfred data to Jack Hills and Mt. Narryer, which leads to a discussion on pre-3800 Ma land masses, and evidence that the source of these zircons was a composite Hadean terrane.

3.1 Paper 1: Detrital zircon age structure within ca. 3 Ga metasedimentary rocks, Yilgarn Craton: Elucidation of Hadean source terranes by principal component analysis

Thern, E. R., Nelson, D. R., (2012). Detrital zircon age structure within ca. 3 Ga metasedimentary rocks, Yilgarn Craton: elucidation of Hadean source terranes by principal component analysis. Precambrian Research; v.214215; p. 2843

E.R. Thern[a*] and D.R. Nelson[b]

[a] Department of Imaging and Applied Physics, Curtin University of Technology, GPO Box U1987, Perth, WA 6001, Australia (*eric@thern.org)

[b] School of Natural Sciences, University of Western Sydney, Locked Bag 1797, Penrith, NSW 2751, Australia

Precambrian Research 214–215 (2012) 28–43

Contents lists available at SciVerse ScienceDirect

Precambrian Research

journal homepage: www.elsevier.com/locate/precamres

Detrital zircon age structure within ca. 3 Ga metasedimentary rocks, Yilgarn Craton: Elucidation of Hadean source terranes by principal component analysis

Eric R. Thern[a,*], David R. Nelson[b]

[a] Department of Imaging and Applied Physics, Curtin University of Technology, GPO Box U1987, Perth, WA 6001, Australia
[b] School of Natural Sciences, University of Western Sydney, Locked Bag 1797, Penrith, NSW 2751, Australia

ARTICLE INFO

Article history:
Received 8 July 2011
Received in revised form 19 October 2011
Accepted 20 October 2011
Available online 30 October 2011

Keywords:
Multivariate
Detrital zircon
Yilgarn
Hadean
Geochronology

ABSTRACT

A multivariate approach using a similarity matrix derived from >5500 U–Pb zircon analyses was used to investigate the complex and overlapping detrital zircon age structure within ca. 3 Ga metasedimentary rocks from the Yilgarn Craton, Western Australia. Detrital zircon analyses were grouped by their $^{207}Pb/^{206}Pb$ dates using a robust Chi-square grouping method which produced 74 Yilgarn-wide age groups from a pool of >3500 analyses and that were correlated between different metasedimentary rocks. Principal component analysis (PCA) was then used on a calculated similarity matrix of >65 samples which contained these age groups. PCA indicates that the main age populations of the detrital zircons in the ca. 3 Ga metasedimentary rocks were derived in varying portions from the Narryer and Yarlarweelor Gneiss Complexes. Differences between the age structure of >3.9 Ga zircon populations within the Mt. Alfred metasedimentary rocks with those from Mt. Narryer, Jack Hills and Maynard Hills localities is best explained by their derivation from two Hadean terranes which were joined by ca. 3.7 Ga.

1. Introduction

The oldest materials that survive on Earth, >4000 Ma zircons, are found within ca. 3 Ga metasedimentary rocks throughout the Yilgarn Craton. These zircons, with ages up to ca. 4350 Ma, have been found within the metasedimentary rocks of Mt. Narryer (Froude et al., 1983; Kinny et al., 1990; Crowley et al., 2005; Pidgeon and Nemchin, 2006), Jack Hills (Compston et al., 1985; Wilde et al., 2001; Peck et al., 2001; Cavosie et al., 2004, 2006; Crowley et al., 2005), Maynard Hills (Nelson, 2002; Wyche et al., 2004) and the Mt. Alfred locality of the Illaara Greenstone Belt (Nelson, 2005; Wyche, 2007). These ancient zircons are of unknown provenance, and their distribution throughout multiple disparate metasedimentary rocks >400 km apart within granite greenstone terranes and high grade Gneiss Complexes makes their relation to one another at time of deposition difficult to assess.

Whereas much thought and study has gone into these Hadean zircons from the Jack Hills and Mt. Narryer, the source terranes of these detrital grains is still unknown. There are hints of source rock diversity from the age structures within the detrital zircon data of the Jack Hills, Mt. Narryer and Toodyay Lake Grace zircon populations (Cavosie et al., 2004; Spaggiari et al., 2007; Dunn et al., 2005; Crowley et al., 2005; Pidgeon and Nemchin, 2006; Pidgeon et al., 2010), and some similarities between the metasedimentary rocks and the Narryer gneisses have been discussed (Kinny et al., 1988; Pidgeon et al., 2010). Adding to the complexity is the metamorphosed and deformed nature of the metasedimentary rocks which has obliterated much of their original sedimentary character.

To address these issues, new detrital zircon U–Pb analyses from the ca. 3 Ga Maynard Hills and Illaara Greenstone Belt metasedimentary rocks (Thern and Nelson, submitted for publication) are combined with existing data from ca. 3 Ga metasedimentary rocks from the Yilgarn Craton in order to investigate the age structures of their detrital zircon populations. Detrital zircon studies have used many techniques to assess and match age structures within datasets—some recent examples include the use of probability density plots (for example Pidgeon et al., 2010); discussion of histograms and binning[1] of age data (Vermeesch, 2005); usage of binning or fractions separated by predefined age limits (Andersen, 2005); hierarchical dendograms and cluster trees of mostly igneous samples (Condie et al., 2009) and on detrital samples (Weislogel et al., 2010); principal component analysis (PCA) (Sircombe, 1999, 2000); and kernel functional estimation of ages prior to clustering (Sircombe and Hazelton, 2004).

* Corresponding author. Tel.: +61 4 22529477.
E-mail address: eric@thern.org (E.R. Thern).

[1] Where pre-determined intervals of certain ages or values, 'bins', are defined that consist of the original data which falls into these intervals.

0301-9268/$ – see front matter © 2011 Elsevier B.V. All rights reserved.
doi:10.1016/j.precamres.2011.10.015

This paper offers a synthesis of >3 Ga detrital zircon data from the Yilgarn Craton in order to investigate sources of the Hadean zircons and the makeup of the pre-Yilgarn Craton source terranes. A multivariate statistical approach using robust age grouping of all sample data is used to produce a similarity matrix from the age groups in each sample. Principal component analysis (PCA) has then been applied to the resulting matrix, producing PCA-derived hierarchical clusters which are interpreted to define distinct provenances.

2. Geological setting

The Yilgarn Craton primarily consists of >3000 Ma gneisses (Narryer Gneiss Complex), >2900 Ma, ca. 2800 Ma and 2730–2680 Ma greenstones, and 2730–2630 Ma granites (Fig. 1). The greenstone belts are generally N–S trending 'rafts' within younger granites throughout the Yilgarn Craton. The ca. >2900 Ma greenstones are commonly associated with ca. 3 Ga clastic metasedimentary rocks,

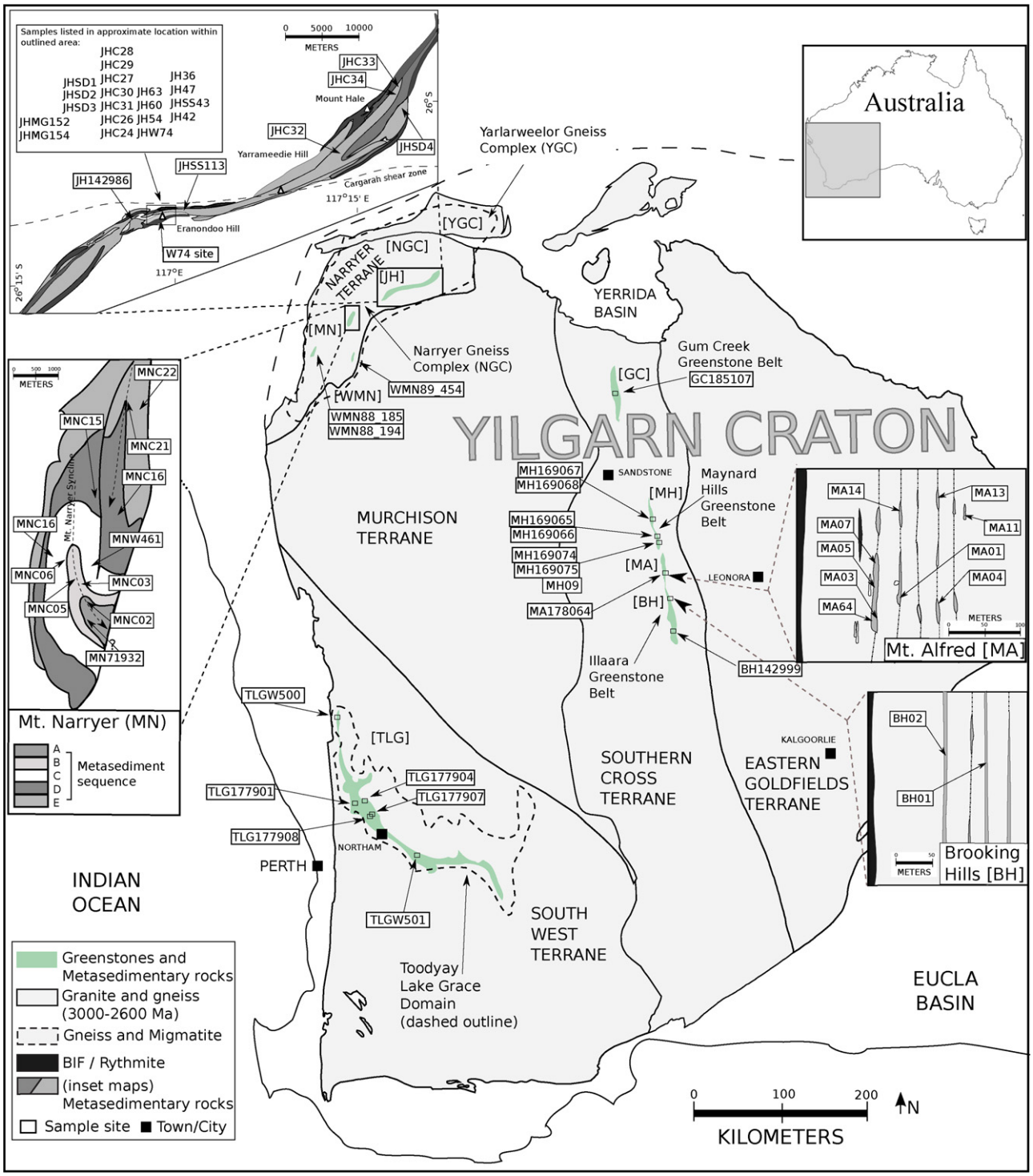

Fig. 1. Map of the Yilgarn Craton, Western Australia, showing locations of ca. 3 Ga metasedimentary rocks and of gneisses examined in this study. Inset maps are of Mt. Narryer (after Crowley et al., 2005), Jack Hills (after Spaggiari et al., 2007), Mt. Alfred and Brooking Hills. Samples used in this study have been prefixed with locality information: [JH] Jack Hills, [MN] Mt. Narryer, [WMN] West of Mt. Narryer, [TLG] Toodyay Lake Grace, [BH] Brooking Hills, [MA] Mt. Alfred, [MH] Maynard Hills and [GC] Gum Creek. See Table 1 for full reference list.

which can contain abundant early Archean and Hadean zircons. The current distribution of these metasedimentary rocks throughout the Yilgarn Craton is complex, and their relation to one another is difficult to establish as they are currently separated by up to 400 km (Wyche, 2007).

2.1. Yilgarn metasedimentary rocks: Narryer and South West terranes

Archean (ca. 3 Ga) metasedimentary rocks are found throughout the Yilgarn Craton (see Fig. 1). These occurrences are separated by ca. 2930–2650 Ma granite–greenstone terranes (Maynard Hills, Illaara [Mt. Alfred / Brooking Hills], Gum Creek), and ca. 2650–3730 Ma gneisses and granites (Mt. Narryer, Jack Hills, Toodyay Lake Grace Domain). The metasedimentary rocks at the Jack Hills and Mt. Narryer have been extensively studied due to their >3900 Ma detrital zircon populations. The Mt. Narryer metasedimentary belt, which contains sedimentary rocks hosting ca. 3120–4350 Ma detrital zircons, is a ca. 2 km thick sequence composed of five mostly intact lithostratigraphic units surrounded by Narryer gneisses (Fig. 1, inset Mt. Narryer map). The geology of this belt is described in detail within Crowley et al. (2005) and Pidgeon and Nemchin (2006). A number of samples collected west and east of Mt. Narryer (see Fig. 1, label 'WMN') were analyzed by Nutman et al. (1991) and mostly define detrital zircon ages between ca. 3050 Ma and 3750 Ma. The Jack Hills, composed of multiply-deformed and tectonically disrupted metasedimentary units containing 3060–4400 Ma detrital zircons (with some as-of-yet unresolved younger components at ca. 2650 Ma and ca. 1800–2000 Ma), is surrounded by ca. 2650 Ma granites and >3000 Ma gneisses as described from a structural viewpoint by Spaggiari et al. (2007), a detrital zircon viewpoint by Cavosie et al. (2004), Crowley et al. (2005), paleoenvironmentally by Eriksson and Wilde (2010) and with an overview of younger components within the belt by Wilde (2010). Metasedimentary rocks from the Toodyay Lake Grace Domain, with detrital zircon ages between ca. 3060 and 3750 Ma (along with one ca. 3850 Ma grain), are surrounded by gneisses of the Jimperding belt in the South West Terrane[2] of the Yilgarn Craton (Pidgeon et al., 2010).

2.2. Yilgarn metasedimentary rocks: Southern Cross Terrane

The ca. 3 Ga metasedimentary rocks of the Southern Cross Terrane are found in the Illaara, Maynard Hills and Gum Creek greenstone belts. These metasedimentary rocks are the oldest rocks identified within the Southern Cross Terrane, with no granites or gneisses older than their youngest detrital zircons. The Gum Creek greenstone belt metasedimentary rock occurrence is the most north-easterly ca. 3 Ga sediment occurrence yet identified in the Yilgarn, and includes mostly 3250–3500 Ma detrital zircons (Wingate and Bodorkos, 2007). The Maynard Hills, Mt. Alfred, and Brooking Hills metasedimentary rocks lie within the Maynard Hills and Illaara greenstone belts, respectively, in the central area of the Yilgarn Craton. Recent finds of >4000 Ma zircons, previously constrained to the Mt. Narryer and Jack Hills localities of the Narryer Terrane, within the Maynard Hills (Nelson, 2002; Wyche et al., 2004) and Mt. Alfred metasedimentary rocks (Nelson, 2005; Wyche, 2007) has allowed for further study into the provenance of these ancient grains. The Maynard Hills metasedimentary rocks include primarily ca. 3120–3700 Ma detrital zircons, with one grain >4300 Ma in age, and a number of grains >3800 Ma (Thern and Nelson, submitted for publication). The Mt. Alfred metasedimentary rock locality of the Illaara greenstone belt principally contains ca. 3300–3770 Ma detrital zircons, with a high proportion of 3800–3900 Ma and 4150–4350 Ma grains (>5–10%). Similarly, the two northern-most Brooking Hills samples (BH01 and BH02) have age structures in common with the Mt. Alfred samples, whereas the age structures of the detrital zircons in the southern-most Brooking Hills sample (BH142999) is similar to the Maynard Hills metasedimentary rocks.

2.3. Narryer Gneiss Complex (NGC)

The granites and gneisses from the Narryer Terrane represent potential original source rocks for the ca. 3 Ga metasedimentary rocks of the Yilgarn Craton. These rocks, collectively known as the Narryer Gneiss Complex (NGC), contain some of the oldest rocks identified within the Yilgarn Craton. The oldest component of the NGC, dismembered layered mafic intrusions of meta-anorthosite and deformed leucogabbro known as the Manfred Complex, forms the oldest part of the Meeberrie Gneiss at ca. 3730 Ma (Myers and Williams, 1985; Myers, 1988; Kinny et al., 1988; Kinny and Nutman, 1996). The Meeberrie Gneiss is a complex migmatite containing ca. 3300–3750 Ma zircons, (Kinny et al., 1988; Nutman et al., 1991; Kinny and Nutman, 1996; Pidgeon and Wilde, 1998), whose upper limit is defined by only a single 3757 ± 7 Ma zircon analysis (Pidgeon and Wilde, 1998). The Meeberrie Gneiss has been intruded by both the Eurada Gneiss (ca. 3440–3490 Ma; Nutman et al., 1991), and the Dugel Gneiss (ca. 3350–3380 Ma; Kinny et al., 1988; Nutman et al., 1991).

Early metamorphic events, as evidenced by anatexis and growth of new zircon within the Meeberrie Gneiss, suggest a possible granulite facies metamorphism event between 3730 Ma and 3600 Ma, with another event at ca. 3300 Ma (Kinny and Nutman, 1996). This later event may be coeval with the porphyritic granitic intrusions within the NGC between ca. 3250 and 3330 Ma (Myers and Williams, 1985; Kinny et al., 1990). The NGC was then deformed during prograde amphibolite to granulite facies metamorphism at ca. 2680 Ma, and retrograde amphibolite facies at ca. 2620 Ma that was coeval with granite intrusions throughout the Yilgarn (Myers, 1997).

2.4. Yarlarweelor Gneiss Complex (YGC)

A younger Gneiss Complex just north of the Narryer Terrane, the Yarlarweelor Gneiss Complex (YGC) consists of ca. 3300–1800 Ma granites, granitic gneiss and supracrustal rocks of the Narryer Terrane (Occhipinti et al., 2004). Rifting of the northwest portion of the Yilgarn Craton at ca. 2000 Ma may explain the occurrence of the YGC with younger Paleoproterozoic fault slices within the Errabiddy shear zone (Occhipinti et al., 2004). Zircons with ages >3000 Ma within the YGC may have been derived from the Narryer Gneiss Complex, as these dates correspond with the intrusion of late stage granites throughout the complex.

3. Samples

Data selected for this study were compiled from >55 previously published sample datasets from the metasedimentary rocks of the Toodyay Lake Grace Domain, Mt. Narryer, Jack Hills, Maynard Hills, and Brooking Hills, as well as 12 new samples from the Maynard Hills and Illaara greenstone belts (Thern and Nelson, submitted for publication). Most samples are metasedimentary rocks (metasandstones, metaconglomerates and quartzites) although a number of gneiss and granite samples were also included in order to compare the detrital populations in the metasedimentary rocks to known granitic and gneissic zircon populations from the Narryer

[2] In this paper, the term "Terrane" is used descriptively and is not intended to imply that the geological unit may not share parts of its geological history with that of adjacent terranes.

Table 1
Yilgarn detrital zircon data with labels used in this study and their original label, number of detrital zircons, number of used detrital zircons, youngest zircon age (maximum depositional age), oldest age of used analyses, and references. Dates are calculated from only the used portion of the data, that are ±10% of concordia and have been processed through CONCH χ^2 age grouping. These ages represent grouped $^{207}Pb/^{206}Pb$ dates that can be correlated between samples. Dates in parentheses or with (?) may represent contaminants or post-depositional disturbance.

Sample[§]	Original label	Number[†]	Used[‡]	Youngest[§§]	Oldest	Notes	Reference
Narryer Terrane							
Jack Hills [JH] – Jack Hills Greenstone Belt – Youngest zircon age: 3065 Ma							
JHW74	W74	254	212	3074 Ma	4175 Ma	[a]	(see table footnote)
JH142986	142986	58	46	3065 Ma	4129 Ma		(Nelson, 2000, 2004)
JH36	01JH36	205	192	3149 Ma	4281 Ma		Cavosie et al. (2004)
JH42	01JH42	75	71	3065 Ma	3914 Ma		Cavosie et al. (2004)
JH47	01JH47	37	33	3214 Ma	3855 Ma		Cavosie et al. (2004)
JH54	01JH54	129	102	3074 Ma	4350 Ma		Cavosie et al. (2004)
JH60	01JH60	47	41	3281 Ma	4175 Ma		Cavosie et al. (2004)
JH63	01JH63	18	5	3250 Ma	3746 Ma	[c,g]	Cavosie et al. (2004)
JHC24	24	103	93	3281 Ma	4113 Ma	[e]	Crowley et al. (2005)
JHC26	26	105	102	3074 Ma	3982 Ma	[e]	Crowley et al. (2005)
JHC27	27	29	24	3250 Ma	3855 Ma	[e]	Crowley et al. (2005)
JHC28	28	48	47	3281 Ma	3982 Ma	[e]	Crowley et al. (2005)
JHC29	29	53	49	3281 Ma	3644 Ma	[e]	Crowley et al. (2005)
JHC30	30	112	98	3074 Ma	4113 Ma	[e]	Crowley et al. (2005)
JHC31	31	19	19	3381 Ma	4113 Ma	[e]	Crowley et al. (2005)
JHC32	32	19	19	3281 Ma	3746 Ma	[e]	Crowley et al. (2005)
JHC33	33	15	13	3281 Ma	3604 Ma	[e]	Crowley et al. (2005)
JHC34	34	15	14	3281 Ma	3604 Ma	[e]	Crowley et al. (2005)
JHMG152	152	213	73	3074 Ma[**]	3982 Ma	[d,f]	Grange et al. (2010)
JHMG154	154	129	111	3188 Ma	3982 Ma	[f]	Grange et al. (2010)
JHSD1	JH1	78	59	3065 Ma	4255 Ma		Dunn et al. (2005)
JHSD2	JH2	80	62	3127 Ma	4150 Ma		Dunn et al. (2005)
JHSD3	JH3	92	18	3025 Ma[**]	4114 Ma	[d]	Dunn et al. (2005)
JHSD4	JH4	79	22	3025 Ma[**]	3746 Ma	[d]	Dunn et al. (2005)
JHSS113	01JH113	13	13	3318 Ma	3644 Ma	[b]	Cavosie et al. (2004)
JHSS43	01JH43	48	46	3127 Ma	3855 Ma	[b]	Cavosie et al. (2004)
Mt. Narryer [MN] – Narryer Terrane – Mt. Narryer – Youngest zircon age: 3074 Ma (3127 Ma, 3281 Ma?)							
MN71932	71932	20	10	3127 Ma	3318 Ma	[g]	Kinny et al. (1990)
MNC02	2	46	43	3074 Ma	4175 Ma	[e]	Crowley et al. (2005)
MNC03	3	49	49	3281 Ma	4113 Ma	[e]	Crowley et al. (2005)
MNC05	5	50	50	3281 Ma	4175 Ma	[e]	Crowley et al. (2005)
MNC06	6	52	51	3281 Ma	3746 Ma	[e]	Crowley et al. (2005)
MNC13	13	41	40	3381 Ma	4113 Ma	[e]	Crowley et al. (2005)
MNC15	15	41	38	3281 Ma	4175 Ma	[e]	Crowley et al. (2005)
MNC16	16	41	39	3281 Ma	4113 Ma	[e]	Crowley et al. (2005)
MNC21	21	35	31	3381 Ma	3746 Ma	[e]	Crowley et al. (2005)
MNC22	22	40	31	3281 Ma	3746 Ma	[e]	Crowley et al. (2005)
MNW461	W461	194	81	3281 Ma	4326 Ma		Pidgeon and Nemchin (2006)
West and East of Mt. Narryer [WMN] – West of Mt. Narryer and Mt. Murchison – Youngest zircon age: 3065 Ma (3025 Ma?)							
WMN88185	88J85	24	9	3025 Ma	3676 Ma		Nutman et al. (1991)
WMN88194	88194	52	43	3065 Ma	3855 Ma		Nutman et al. (1991)
WMN89454	89454	32	20	3281 Ma	3722 Ma		Nutman et al. (1991)
South West Terrane							
Toodyay Lake Grace [TLG] – Toodyay Lake Grace Domain – Youngest zircon age: 3065 Ma (2939 Ma?)							
TLG177901	177901	69	68	3149 Ma	3686 Ma		(Wingate et al., 2008a)
TLG177904	177904	155	153	3065 Ma	3686 Ma		(Wingate et al., 2008b)
TLG177907	177907	101	99	3065 Ma	3622 Ma		(Wingate et al., 2008c)
TLG177908	177908	47	34	3065 Ma	3491 Ma		(Wingate et al., 2008d)
TLGW500	W500	57	52	3188 Ma	3686 Ma		Pidgeon et al. (2010)
TLGW501	W501	103	83	2939 Ma	3855 Ma		Pidgeon et al. (2010)
Southern Cross Terrane							
Maynard Hills [MH] – Maynard Hills Granite Greenstone Belt – Youngest zircon age: 3052 Ma							
MH169074	169074	25	15	3125 Ma	3715 Ma	[g]	Nelson (2002)
MH169075	169075	45	37	3281 Ma	4364 Ma		Nelson (2002)
MH178065	178065	39	36	3250 Ma	3686 Ma		Nelson (2002)
MH178066	178066	35	30	3266 Ma	3452 Ma		Nelson (2002)
MH178067	178067	39	34	3281 Ma	3855 Ma		Nelson (2002)
MH178068	178068	26	21	3281 Ma	3817 Ma		Nelson (2002)
MH09	169075	178	64	3052 Ma	3855 Ma	[h]	Thern and Nelson (submitted for publication)
Gum Creek [GC] – Gum Creek Granite Greenstone Belt – Youngest zircon age: 3214 Ma							
GC184107	184107	55	52	3214 Ma	3491 Ma		(Wingate and Bodorkos, 2007)
Brooking Hills [BH] – Illaara Granite Greenstone Belt – Youngest zircon age: 3188 Ma							
BH142999	142999	33	22	3250 Ma	3715 Ma		(Nelson, 2000)
BH01	BH01	57	27	3188 Ma	3746 Ma		Thern and Nelson (submitted for publication)
BH02	BH02	77	43	3381 Ma	3770 Ma		Thern and Nelson (submitted for publication)
Mt. Alfred [MA] – Illaara Granite Greenstone Belt – Youngest zircon age 3251 Ma							
MA178064	178064	35	19	3491 Ma	4174 Ma		Nelson (2005)
MA64	178064	70	18	3491 Ma	4335 Ma	[i]	Thern and Nelson (submitted for publication)
MA01	MA01	73	39	3491 Ma	3770 Ma		Thern and Nelson (submitted for publication)
MA03	MA03	148	43	3591 Ma	4326 Ma		Thern and Nelson (submitted for publication)

Table 1 (*Continued*)

Sample[§]	Original label	Number[†]	Used[‡]	Youngest[§§]	Oldest	Notes	Reference
MA04	MA04	52	23	3604 Ma	3770 Ma		Thern and Nelson (submitted for publication)
MA05	MA05	85	47	3251 Ma	3770 Ma		Thern and Nelson (submitted for publication)
MA07	MA07	89	37	3591 Ma	4228 Ma		Thern and Nelson (submitted for publication)
MA11	MA11	73	27	3318 Ma	3770 Ma		Thern and Nelson (submitted for publication)
MA13	MA13	64	39	3437 Ma	3770 Ma		Thern and Nelson (submitted for publication)
MA14	MA14	69	41	3381 Ma	3770 Ma		Thern and Nelson (submitted for publication)

§ Sample label prefixed with locality abbreviation (2–3 letters): JH, MN, WMN, TLG, MH, GC, BH, MA.
† Number of zircons analyzed.
‡ Number of zircons used in this study which are >10% of concordia and >3000 Ma in age.
§§ Youngest zircon age in the >10% of concordia age-grouped data, representing the maximum depositional age.
** Youngest dates which are above 3000 Ma, not including possible late Archean and Paleoproterozoic analyses.
[a] Combined to a single "W74" sample where authors specifically define the sample is from the "W74" locality – data from samples 89–144 (Maas et al., 1992) and W74 Wilde et al. (2001); Cavosie et al. (2004); Pidgeon and Nemchin (2006).
[b] Single scan SHRIMP data: pre-processed such that analyses with more than 10 counts of ^{204}Pb on this first scan. (a) (no rastering) were removed, leaving only the most robust single scan analyses. (b) Analytical uncertainties of ±40 were assigned to all single scan analyses, as to not intentionally bias the χ^2 grouping.
[c] Has some component of single scan data included within 7-scan dataset.
[d] May be Paleoproterozoic in age (with large populations of ca. 2650 Ma and some 1700–2200 Ma ages).
[e] LAM-ICPMS data of Crowley et al. (2005).
[f] Composed of multiple different quartzite cobbles from two outcrops combined into two 'outcrop-wide' composite samples – (outcrop 152: cobbles A–C, F, H, I and L; outcrop 154: cobbles A, B, 4).
[g] Sample unused – <10 analyses.
[h] From the same aliquot of heavy mineral separates as MA169075, but different SHRIMP mount and analytical conditions.
[i] Same SHRIMP mount as MA178064, but post-polish differential numbering between sessions.

and Yarlarweelor Gneiss Complexes. The ca. 3 Ga metasedimentary rock samples are summarized in Table 1, where they are subdivided by locality with abbreviations used in this study.

All data presented have been obtained by sensitive high resolution ion microprobe (SHRIMP), with the exception of Crowley et al. (2005), where they were obtained using Laser Ablation Microprobe Inductively-Coupled Plasma Mass Spectrometry (LAM-ICPMS). The larger uncertainties of the LAM-ICPMS data (ca. 15–25 Ma) compared to that of SHRIMP data (ca. 5–10 Ma) introduces age-peak broadening within Gaussian summation probability plots, but are not problematic when using robust χ^2 grouping of data to make comparisons.

Data for the Narryer Gneiss Complex (NGC) (including Narryer Gneiss Complex and Jack Hills granites and gneisses) and Yarlarweelor Gneiss Complex (YGC) [with abbreviations used in this study in brackets] was compiled from the following sources, and combined to form two 'composite' samples for use in source provenance analysis: (1) Narryer Gneiss Complex [NGC]: Meeberrie gneiss GSWA 60735, Dugel gneiss GSWA 77218, leucogabbro GSWA 77239, anorthosite GSWA 77242 (Kinny et al., 1990), Meeberrie gneiss MN45, Meeberrie gneiss MN26 (Kinny et al., 1990), Meeberrie tonalitic gneiss 88–173, pale schlieric gneiss 88–180, Meeberrie granodioritic gneiss 88–191, Eurada gneiss 88–197, Eurada gneiss 88–175, Eurada gneiss 88–176 (Nutman et al., 1991); tonalitic gneiss W29, granodiorite W35, porphyritic granite W61, monzogranite W62, trondhjemite gniess W63, porphyritic granodiorite W65, (Pidgeon and Wilde, 1998); (2) Yarlarweelor Gneiss Complex [YGC]: GSWA Samples 142847, 142848, 142853, 142896, 142897 and 142902 (Nelson, 1997).

Further, the NGC composite terrane was split into component gneisses of Dugel (Dugel Gneiss Component "DGC"; samples: 77218 and MN45), Eurada (Eurada Gneiss Component "EGC"; samples: 88_176, 88_197, 105014, 105012, 10510, 105009, 105002 and W35), Meeberrie (Meeberrie Gneiss Component "MGC"; samples: 88_191, 88_180, 88_173, 60735, W65, W63 and W29), and Manfred Complex (MFC; samples: 77239, 77236 and 77242) based on their classification in the literature. Further samples (MN26, 105011 and W61) composed of mostly younger late-stage granitic ages of >3000 Ma Yarlarweelor Gneiss Complex affinity were added to this group. These were used in order to assess the individual "granitic" components of the Narryer Terrane within the detrital zircon data. These splits are mostly representative but they do not define pristine end-members of these components, as many samples contain some older and younger components. In particular, the Dugel Gneiss Component (DGC) includes many younger zircon ages from later stage events.

3.1. Selection of 3000 Ma as a lower age cutoff for samples in this study

When considering the depositional ages of these metasedimentary rocks, there is a need to take into account the multiple finds of younger (<3000 Ma) zircons from the Jack Hills (Cavosie et al., 2004; Dunn et al., 2005; Grange et al., 2010) and Toodyay Lake Grace metasedimentary rocks (Pidgeon et al., 2010). As mentioned in Pidgeon et al. (2010), most anomalous ca. 3000–2650 Ma zircons found in the TLG are analyses of either rim overgrowths during sillimanite metamorphism at ca. 2650 Ma, or are highly disturbed zones of the crystal which are characterized by high concentrations of U and lower Th/U ratios. In contrast, ca. 1600–2000 Ma grains found in the Jack Hills within samples JH3 and JH4 of Dunn et al. (2005) and a ca. 1580 Ma zircon in Cavosie et al. (2004), define even younger events than their large ca. 2650 Ma zircon age populations. Some metasedimentary rocks in these associations show deformation structures which appear to be coeval with late stage ca. 1760–1740 Ma tectonism (supported by ^{40}Ar/^{39}Ar cooling ages in micas; Spaggiari et al., 2004, 2008), and support tectonic interleaving of younger components into this section of the Jack Hills (Spaggiari et al., 2007). Samples JH3 and JH4 of Dunn et al. (2005) also contain different proportions of <3000 Ma zircons, which could support the proposal that they were deposited between ca. 2660 and 1800 Ma and contain components of older sequences (Dunn et al., 2005). Further young grains have been found in quartzite cobbles within a metaconglomerate (sample JHMG152) that exhibits a single young zircon at ca. 1200 Ma, a major peak at ca. 1600–1800 Ma and a spread of ages between ca. 2600 and 3000 Ma as documented by Grange et al. (2010). This is in contrast to another group of quartzite cobbles from sample JHMG154 which did not yield any zircons <3000 Ma.

By contrast, evidence for >3000 Ma depositional ages for the metasedimentary rocks of the Jack Hills belt are found in an authigenic xenotime age of 3080 ± 20 Ma, constraining depositional age to ca. 3080 Ma. Evidence of metamorphic monazite growth at 2653 ± 5 Ma within sample W74 constrains its deposition ages to >2650 Ma. The vast majority of the Jack Hills can be described as having a maximum depositional age of ca. 3060 Ma, similar to the

TLG samples, and zircons below this cutoff are tentatively interpreted here as either contaminants, having suffered Pb-loss, or in the case of JH3, JH4, and JHMG152, from tectonically interleaved younger sequences.

Throughout the Illaara and Maynard Hills greenstone belts, the metasedimentary rocks have yielded only a small number of zircons with commonly discordant $^{207}Pb/^{206}Pb$ dates that are younger than ca. 3100 Ma. Of these, most have characteristics, such as high uranium concentrations and low concordance, which are consistent with disturbance. Further constraining the Mt. Alfred metasedimentary rocks, a cross-cutting quartz-tourmaline hydrothermal vein has been dated via $^{40}Ar/^{39}Ar$ on tourmalines with well-defined plateau ages of 2940 ± 20 Ma (Thern et al., 2011), which constrains the minimum depositional age for the metamorphosed sedimentary rocks of this locality.

Since many zircon analyses between ca. 2650 Ma and 3000 Ma from the metasedimentary rocks studied here show varying degrees of high U concentrations, low Th/U ratios, convoluted CL zoning (relating to hydrothermal disturbance), high discordancy, or may be metamorphically grown components during peak regional metamorphic events between ca. 2730–2620 Ma, these analyses are interpreted to have been disturbed. Data below 3000 Ma have therefore not been included in this investigation.

The sample dataset consisting of 79 metasedimentary rock and 29 gneiss samples was combined giving a total of 5590 U–Pb analyses for the principal component analysis (PCA) investigation.

4. Methods

Concordant and discordant detrital zircon $^{207}Pb/^{206}Pb$ data of variable quality were collated. In order to assess these data, procedures were developed to identify all analyses which could be assigned to age groups consisting of ≥3 analyses. All data which was highly discordant or that could not be assigned to a group consisting of ≥3 analyses have been discarded. The resulting dataset, consisting of only the most robust $^{207}Pb/^{206}Pb$ age groups, was then processed into a similarity matrix for principal component and hierarchical clustering.

4.1. Concordant data cutoff: removing discordant analyses

Detrital zircon data have been assessed using different discordant cutoffs to determine whether discordant zircon data would negatively impact grouping outcomes. In this paper, percent concordance is expressed as in Eq. (1),

$$\%\ \text{concordance} = \frac{^{206}Pb^*/^{238}U\text{date}}{^{207}Pb^*/^{206}Pb^*\text{date}} \times 100 \quad (1)$$

where Pb^* is the radiogenic Pb component only. The detrital zircon analytical data were processed using concordia cutoff within CONCH (Nelson, 2006) of ±2%, ±5%, ±10%, and ±20% (as summarized in Table 2). Of the age groups within each concordia cutoff, the principal χ^2-calculated age groups found in each processed concordance group are similar, typically on the order of ±1 to 2 Ma. The larger cutoff of ±20% discordance produces the most "invalid" age groups of less than 3 analyses (45 groups), mostly comprised of discordant analyses.

The approximately 25 main age groups (which account for more than 85% of the analyses) appear in all concordance cutoffs, and yield less than 2 Ma age differences between ±2%, ±5% and ±10%. The ±20% analyses tend to skew the grouped ages slightly (greater than 2 Ma age differences), due to a contribution of discordant and commonly younger analyses. The value of ±10% of concordia, used for subsequent processing of all data in this paper, yields the best tradeoff by minimizing the more discordant analyses which produce spurious age groups, whilst providing the largest number of analyses.

Table 2
Age groups processed from zircon data at different concordance cutoff values. Shows how many analyses are within each concordia cutoff, the age groups of each concordia cutoff (as a total) and the age groups which are used (which have more than 3 analyses). The values ±10% of concordia yield the best tradeoff by minimizing the more discordant analyses which produce spurious age groups while utilizing the most individual zircon analyses to produce more robust χ^2 groups. For similarity analysis purposes, more zircon data points are preferred as they define more robust normalized abundances of each age group per sample, as well as more distinct age groups with more than 3 analyses. By utilizing ±2% of concordia analyses only, the utilized zircon age data points is nearly halved, which decreases the resolution of the structures within the detrital zircon data.

Concordia	Analyses	Groups (total)	Groups (used)
Total analyses: 5590			
±2%	2121	70	52
±5%	3116	104	62
±10%	3780	108	74
±20%	4320	127	82

4.1.1. χ^2 grouping of $^{207}Pb/^{206}Pb$ dates

Detrital zircon $^{207}Pb/^{206}Pb$ dates from all samples were grouped together using the Chi-square (χ^2) method of CONCH. This method produces Yilgarn-wide $^{207}Pb/^{206}Pb$ dates which are correlateable between different samples. χ^2 tests whether the observed frequencies differ significantly from the expected frequencies. A χ^2 value of about 1.0 indicates that these data are consistent within counting statistics and there are no additional sources of uncertainty, whereas a χ^2 value of greater than 1.0 indicates that there are additional sources of uncertainty amongst grouped analyses. Values of χ^2 significantly less than 1.0 for grouped analyses indicates that the analytical uncertainties have been over-estimated. The data presented in this study has been parsed using CONCH, which uses a default χ^2 grouping limit value of 1.75. This will identify the minimum number of clearly resolvable dates based on the uncertainty limits assigned to each individual analysis.

The CONCH grouping method has used ^{204}Pb-corrected $^{207}Pb/^{206}Pb$ ratios which were weighted according to the inverse square of the individual analytical uncertainty to determine a weighted mean ratio for all pooled analyses obtained for the sample. Analyses were then rejected from the group using two criteria. First, a χ^2 value was calculated for the grouped analyses using Eq. (2) (see Nelson, 2006). If the χ^2 value was greater than 1.75, geological sources of uncertainty were assumed to be present within the group and the analysis whose ratio with assigned uncertainty is most different from the weighted mean value was excluded from the group.

$$\chi^2 = \frac{1}{(n-1)} \times \sum_{i=1}^{n} \frac{(x_i - \mu_n)^2}{\sigma_n^2 + \sigma_i^2} \quad (2)$$

Second, a measure of the difference (D value) between each analysis and the population weighted mean is calculated using equation 3 (see Nelson, 2006) where any $^{207}Pb/^{206}Pb$ ratio whose calculated D value is greater than ±2.5 from the group weighted mean will also be excluded from the group.

$$D = \frac{\chi_i - \mu_n}{\sqrt{\sigma_{pop}^2 + \sigma_i^2}} \quad (3)$$

The weighted mean value of the remaining analyses are then recalculated. This process was repeated until all remaining analyses were within both parameter thresholds. Analyses that belong within a valid group were then excluded from the pool and the process repeated until all remaining analyses have been grouped. This grouping method is statistically conservative, in that only the

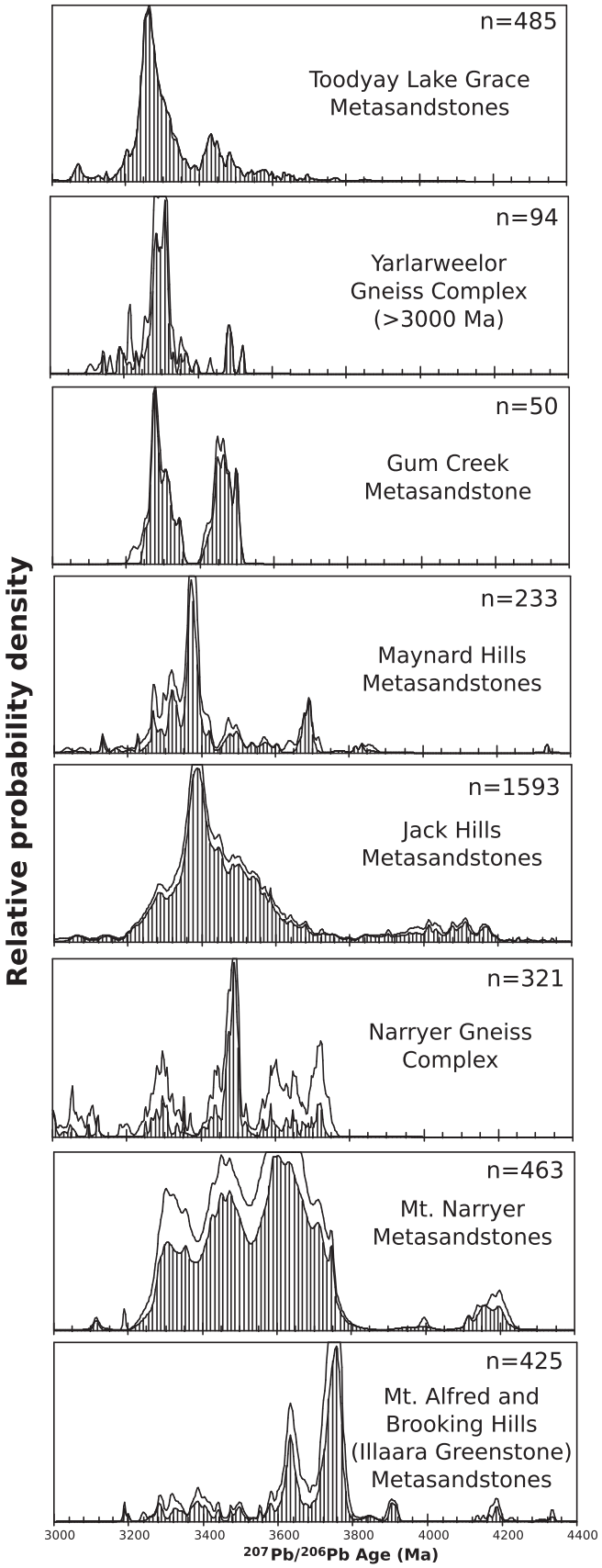

Fig. 2. Gaussian summation probability plots of ±10% of concordia detrital zircon data from the Toodyay Lake Grace metasedimentary rocks, Yarlarweelor Gneiss Complex (>3000 Ma component), Gum Creek metasedimentary rock, Maynard Hills metasedimentary rocks, Jack Hills metasedimentary rocks, Narryer Gneiss Complex, Mt. Narryer metasedimentary rocks, and the Illaara greenstone belt (Mt. Alfred and Brooking Hills) metasedimentary rocks. Non-shaded areas consist of analyses that fall outside of ±2σ of concordia, whereas shaded areas are of analyses within ±2σ of concordia. Major age population differences can be seen on these area-overview probability plots, but individual samples that might yield different age information are easily lost. The Gaussian summation probability plots have been sorted from a "mostly younger ages" (TLG, top) to "mostly older ages" (Mt. Alfred, bottom).

minimum number of clearly resolvable dates based on the uncertainty limits assigned to each individual analysis will be identified. Analyses with assigned uncertainties overlapping more than one age group will be assigned to the larger group (i.e. group containing more analyses), as larger groups are usually identified earlier during the grouping procedure.

Data was processed through CONCH in the following manner: (1) removal of duplicate, discordant and imprecise data from the dataset (many similar ages on one zircon, analyses with extremely high uncertainties, analyses with very high ^{204}Pb), (2) filtering using CONCH to include only data which falls within ±10% of concordia, (3) age cutoffs of more than 2900 Ma and less than 4500 Ma to remove disturbed and non-relevant age groups from the dataset, (4) application of "date summary" option on CONCH to only produce a summary of age groups as output, and (5) removal of any outlier groups younger than 3000 Ma and groups consisting of less than 3 analyses.

4.1.2. Production of a similarity matrix

The calculation of a similarity (variance-covariance) matrix for use in principal component analysis and hierarchical clustering was produced by using the χ^2 age groups output from CONCH. The similarity matrix was calculated as follows: (1) normalization of each samples analysis age groups by summing the number of analyses in each age group and ratioing them as a percentage of all analyses in the total sample, (2) normalization of each age group across all samples, (3) calculation of an age group percentage in each sample using normalized sample group data to normalized total group data, (4) comparing these differences per sample to produce a similarity matrix which defines how similar each sample is to every other sample.

4.2. Multivariate statistical analysis

A multivariate approach using a similarity matrix for pooled zircon analyses was used to group each sample via principal component analysis (PCA) hierarchical clustering with samples of similar zircon provenance components. The approach used the statistical software package FactoMineR (Lł et al., 2008) to produce principal components and hierarchical group output. Principal component analysis is used to simplify the observed variables within the 65 samples, which consist of more than 75 age groups and over 3500 individual analyses, to a smaller number of variables (principal components) which best describe the variance observed within the original variables. These variables are defined by eigenvectors which simplify a multidimensional array into vectors composed of three dimensions. Groups of PCA variables are matched to produce principal component clusters, which are three-dimensional ellipsoids best describing each set of vectors. These have been plotted with their principal component clusters which define principally-similar samples on hierarchical dendograms and factor maps. A hierarchical dendogram shows a 'height' or 'inertia' (Z axis) vector value along with the hierarchical clusters, whereas a principal component factor map retains the length and width (X and Y axis) spatial distributions of each vector. For further discussion on principal component analysis and an overview and application of the technique using detrital zircons, see Sircombe (1999), and references therein.

Herein, age groups as calculated via the χ^2 method are referred to as "groups" or "age groups", and principal component hierarchical clusters as "clusters". When singular dates are quoted, they are specifically referred to as dates. Clusters generally include multiple samples but may relate to some measure of locality information (Jack Hills, Mt. Narryer, etc.) and may be described in terms of both cluster, locality, or either depending on context.

5. Results

5.1. Age spectra of detrital zircon data

Gaussian summation probability plots of $^{207}Pb/^{206}Pb$ dates from the metasedimentary rock localities presented in this study are given in Fig. 2. The Toodyay Lake Grace (TLG) metasedimentary rocks have a major peak between ca. 3250 and 3350 Ma and one minor peak at ca. 3450 Ma. The Yarlarweelor Gneiss Complex (YGC) >3000 Ma component has a major peak around ca. 3280 Ma. The Gum Creek metasedimentary rock has peaks at ca. 3250–3350 Ma and ca. 3450–3500 Ma. The Maynard Hills metasedimentary rocks have a broad peak between 3280 Ma and 3400 Ma and minor peaks at ca. 3480 Ma and ca. 3680 Ma. The Jack Hills metasedimentary rocks are primarily composed of a major peak at ca. 3420 Ma, with a broad peak between 3300 Ma and 3600 Ma. The Narryer Gneiss Complex (NGC) consists mostly of age peaks that broadly correspond to 3700–3740 Ma (similar to Manfred Complex), 3600–3700 Ma (Similar to Meeberrie), 3420–3520 Ma (Similar to Eurada), and 3250–3350 Ma (Similar to Dugel, late granitic intrusions, and YGC). Mt. Narryer metasedimentary rocks have peaks at ca. 3300 Ma, ca. 3600 Ma, and minor peaks at ca. 3680 and ca. 3730 Ma. The Illaara Greenstone Belt (Mt. Alfred and Brooking Hills) consists of primarily of ca. 3600–3650 Ma and ca. 3700–3780 Ma age peaks. These probability plots show that each locality has different amounts of certain age components that allow for visual identification of broadly constrained provenance information.

5.2. Similarity matrix for comparing detrital samples

Binning data and standard Gaussian summation plots commonly skew data in ways that do not allow for easy comparisons across multiple data sets. First, when datasets are merged in a large detrital study, data may be blended together, blurring the age information. Second, the bin width is often larger than the analytical uncertainties of each analysis, blurring the results with potentially unrelated data. Comparisons being drawn from such binned data or from counting overall peak heights on Gaussian summation plots between samples is useful for detrital studies that involve simple (and different) age populations, but cannot easily deconvolve large datasets with complex overlapping age groups. The approach presented here, which involves use of analytical uncertainties applying to individual analyses to identify age groups within many overlapping detrital datasets, avoids some of these shortcomings by using a χ^2 age grouping method across all data. The correlateable age groups are then presented in hierarchical dendograms and clustering on a factor map based on principal component analysis using a computed similarity matrix. This quantitative method enables the age structures within these data to be statistically assessed.

5.2.1. Hierarchical clustering and principal component analysis (PCA) factor maps

The results of hierarchical clustering on a factor map using principal component analysis is shown in Fig. 3. This figure shows clusters of similar samples forming distinct groups. Hierarchical clustering shows the product of principal component group-splitting based on eigenvector inertia gain (ie. largest eigenvector differences are split first). The 'height' axis corresponds to the inertia gain (see inset 'inertia gain' plot in Fig. 3) which is a principal component vector value.

A principal component factor map (Fig. 4A) is shown as a projection of the hierarchical clustering dendogram in Fig. 3. Axes *X* and *Y* define principal component scores which relate to the similarity of each sample to all other samples. A score of zero defines samples which best reflect the overall percentages of age group abundances in all combined samples. Individual samples are shown as points (small circles) which form PCA-derived hierarchical clusters (large ellipses drawn around each) which are centered on the average cluster 'score' which relates to their age composition (open square points within each large ellipse). The PCA factor map in Fig. 4B shows hierarchical cluster ellipses, their 'trends' (shown as vectors), and approximate χ^2 grouped age locations. These ages relate to rough locations on the factor map where they become major components of nearby plotted samples.

6. Discussion

Data presented on the principal component factor map (see Fig. 4) shows individual samples divided into clusters composed primarily of about 15 major age groups, where each age group consists of more than 100 analyses, that gives each cluster a unique makeup. The elongate PCA-derived hierarchical cluster ellipses around each cluster's center defines proportional mixing of certain components of these major (and to a lesser extent, the approximately 25 minor) age groups between the samples within that cluster. This grouping method allows not only for the establishment of correlated age data between samples, but also allows for the observation of distinct age group trends within clusters of samples.

6.1. Hierarchical and principal component clusters

Major structures within these data can be seen readily when plotted within a hierarchical dendogram on a factor map (Fig. 3). These differences are shown as hierarchical splits, the first of which (inertia gain >6, largest split height) delineates nearly all of the Mt. Alfred samples (as well as the Manfred Complex Gneiss and a single Jack Hills sample, JHSD4) from the rest of the Yilgarn data. This first split (to the right, towards clusters 1 and 2) is primarily determined by the presence or absence of 3747 Ma and 3770 Ma age groups, which are a high proportion of analyses at the Mt. Alfred locality, and which occur in the Manfred Complex Gneiss component of the NGC. This split is also related to the presence of a smaller component of the 3645 Ma and 3687 Ma age groups. The other side of this first major split (towards clusters 3, 4, 5, 6, 7, 8 and 9) is composed of the rest of the samples from Jack Hills, Mt. Narryer, Toodyay Lake Grace, Maynard Hills, most of the NGC components (Dugel, Eurada, Meeberrie) as well as the YGC, and consist principally of 3381 Ma, 3282 Ma, 3437 Ma, 3319 Ma, 3251 Ma, 3473 Ma, 3551 Ma and 3350 Ma age groups. The third major split (at an inertia gain of ca. 3) separates the Toodyay Lake Grace samples (cluster 7; principal age groups of 3282 Ma and 3251 Ma; also includes YGC and DGC gneiss components) and the MGC and EGC gneiss components (clusters 8 and 9, respectively) from the Mt. Narryer, Jack Hills and Maynard Hills (clusters 3, 4, 5, 6; principal age groups of 3381 Ma, 3491 Ma, 3437 Ma, 3604 Ma, 3551 Ma and 3350 Ma).

Individual principal component clusters of samples consist of specific proportions of shared age groups and help define structure within the detrital zircon data when plotted on a PCA factor map (Fig. 4). The points in Fig. 4 represent each samples' deviation from all pooled analyses, such that their deviation from the center

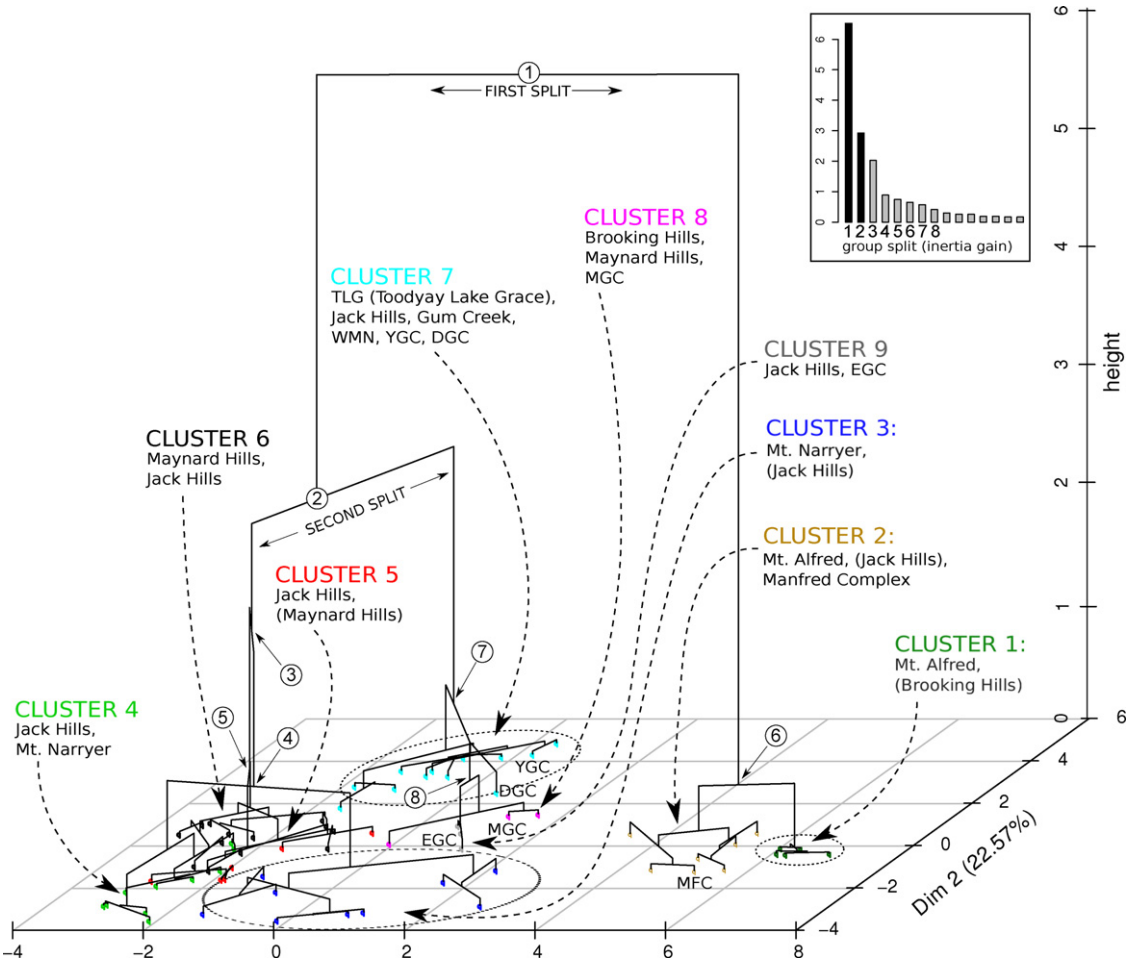

Fig. 3. Hierarchical clustering on a factor map using principal component analysis from similarity matrix data showing similar metasedimentary rock samples forming distinct clusters. Also marked are the igneous component samples; MFC (Manfred Complex), MGC (Meeberrie Gneiss Component), DGC (Dugel Gneiss Component), EGC (Eurada Gneiss Component) and YGC (Yarlarweelor Gneiss Complex). Hierarchical splits labeled as circled numbers and refer to the inset group split inertia gain plot. The first major hierarchical split (inertia gain >6, largest split height) separates nearly all of the Mt. Alfred samples from the rest of the ca. 3 Ga Yilgarn metasedimentary rocks. The second major split separates clusters 3, 4, 5 and 6 (Mt. Narryer, Jack Hills, Maynard Hills and Brooking Hills) with clusters 7, 8 and 9 (mostly Toodyay Lake Grace, with some samples of Gum Creek, Maynard Hills, Brooking Hills, Jack Hills and the Narryer Terrane granites and gneisses). The third split (left hand side under the second split) differentiates clusters 3 and 4 from clusters 5 and 6 (mostly Mt. Narryer with some Jack Hills and mostly Jack Hills with some Maynard Hills, Brooking Hills and Mt. Narryer, respectively). Of similar inertia gain height, splits 4 through 8 are the final splits which define each cluster. Split 6 separates Mt. Alfred cluster 2 (with samples consisting of zircons older than 3900 Ma) with cluster 1 (with some samples consisting of greater than 80% zircon populations with ages between ca. 3740 and 3770 Ma).

point (0, 0) defines age group structures not found in samples plotting further away. The Narryer Gneiss Complex, which mostly plots towards the center, is split into components of Meeberrie (MGC, cluster 8), Eurada (EGC, cluster 9), and Dugel (DGC, cluster 7) with the Yarlarweelor Gneiss Complex (>3000 Ma age groups, cluster 7) plotting near the top. The Dugel Gneiss Component (DGC) plots more towards the top (and is in cluster 7). This is consistent with the observation that some of the Dugel gneisses consist of mostly of Dugel-type ages (ca. 3381 Ma) but are 'contaminated' with various components of late stage granitic intrusions which are mostly similar to the YGC components in age (ca. 3282 Ma and 3251 Ma). In contrast, the Manfred Complex (MFC) of the Meeberrie Gneiss Component (MGC) plots far to the right (in cluster 2, and near cluster 1), which reflects that this component alone is not a major constituent of any other metasedimentary rock samples.

Metasedimentary rock samples plotted in Fig. 4 follow a generalized clockwise "age group younging" trend from cluster 1 to cluster 7. This reflects the major age groups present in these hierarchical clusters, where each cluster is principally composed of older to younger age groups. These clusters form elongate ellipses, the direction of which can be interpreted as multi-component mixing of end-member age groups and is shown as "trends" in Fig. 4B.

6.1.1. Principally oldest: clusters 1, 2 and 3

The most distinguishably different clusters in Fig. 4 are those of the Mt. Alfred samples, clusters 1 and 2. Cluster 1 (MA04, MA01, MA13, MA14 and BH02) primarily consists of 3747 Ma and 3770 Ma age groups, with most samples in this cluster being composed of more than 60% zircons older than 3700 Ma. The elongate pattern of the ellipse defining this cluster corresponds to increasing concentrations of age groups 3770 Ma, 3491 Ma and 3380 Ma, and decreasing 3747 Ma from E → W (denoting direction of trend on the diagram only). The N → S trend defines greater abundance of 3747 Ma, 3645 Ma, 3604 Ma, and a decrease in 3770 Ma and 3716 Ma age groups. These trends show the interrelation of suggested age group locations (marked in squares in Fig. 4) to each samples' abundance of that age group within their principal component clusters. The Brooking Hills sample (BH02) is also part of this cluster, which suggests that the metasedimentary rocks at Mt. Alfred are interrelated with the metasedimentary rocks from ca. 10 km south at Brooking Hills.

Related to cluster 1 (Mt. Alfred, Brooking Hills) is cluster 2, composed primarily of Mt. Alfred samples MA03, MA07, MA11, MA64 and MA178064, with one Jack Hills sample JHSD4, and the MFC gneiss component. The age characteristics of cluster 2 are similar

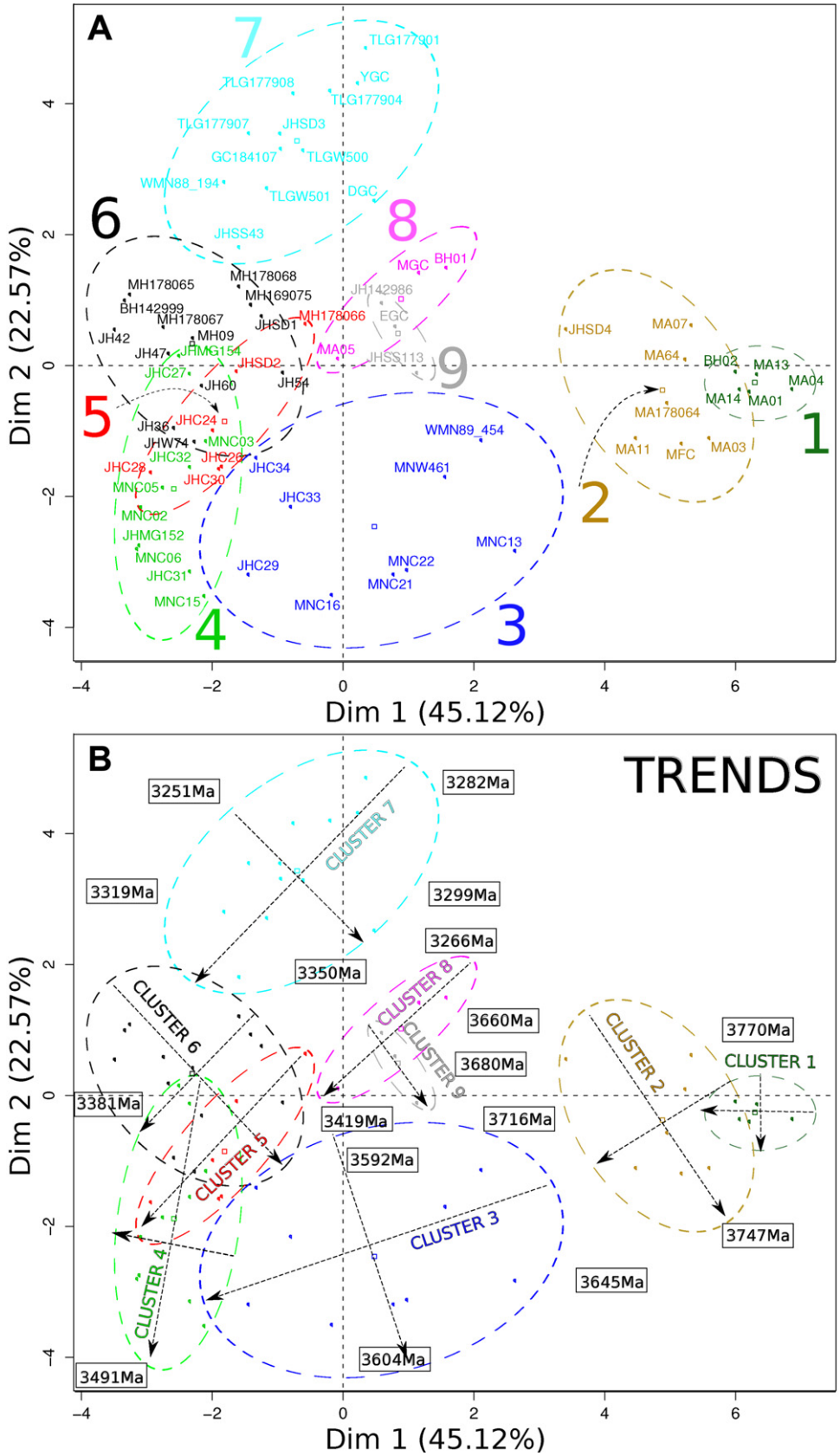

Fig. 4. (A) Principal component analysis (PCA) factor map showing individual metasedimentary rock samples graphed on principal component scores of the first two principal components (axes *X* and *Y*). (B) PCA factor map showing hierarchical group ellipses, their 'trends' shown as vectors (discussed in text) and approximate grouped age locations. The PCA technique uses the principal component eigenvectors calculated per sample to plot the most similar samples together. Individual samples are shown as points (small circles) which form principal component hierarchical groups (large circles drawn around each) which are centered on the average group composition (open square points within each large circle). These groups are calculated based on the percentage of age group abundances in each sample from a similarity matrix. Also marked are the igneous component samples; MFC (Manfred Complex), MGC (Meeberrie Gneiss Component), DGC (Dugel Gneiss Component), EGC (Eurada Gneiss Component) and YGC (Yarlarweelor Gneiss Complex).

to cluster 1, but also contain abundant zircons older than 3800 Ma. Trends from NE → SW, which are pointing towards the Mt. Narryer cluster 3, show increasing 3491 Ma and younger (groups less than 3600 Ma) zircon populations, and decreasing 3770 Ma and older (>3800 Ma) age groups. The NW → SE trend shows increases in age groups 3747 Ma and 3592 Ma, and decreases in 3720 Ma, 3660 Ma and 3680 Ma. This is consistent with their interrelation with cluster 1, and that Mt. Alfred is composed of primarily older zircon populations, with a sub-cluster (cluster 2) which contains some younger material as well as zircons older than 3800 Ma.

Composed of slightly younger age group populations, but with a component of >3800 Ma ages, Mt. Narryer (cluster 3) shows a dominant 3604 Ma age group, along with pronounced 3645 Ma, 3747 Ma, 3491 Ma and 3381 Ma ages. The trends in cluster 3 define increasing representation of 3381 Ma and 3491 Ma ages, and decreasing 3474 Ma, 3716 Ma, 3645 Ma, 3604 Ma and ages older than 3800 Ma in the NE → SW direction. An increase in older age groups (>3800 Ma, including the 4114 Ma age group) as well as the age groups 3644 Ma and 3747 Ma, is seen in the NW → SE trend, where decreasing 3719 Ma, 3445 Ma and 3280 Ma age groups cause the widening of the cluster in this direction. The cluster is principally composed of Mt. Narryer samples, with three Jack Hills samples (JHC29, JHC34 and JHC33) forming the left-most area within the cluster 3 ellipse (Fig. 4). The inclusion of these Jack Hills samples within this cluster shows that the source terranes of Mt. Narryer and Jack Hills, while different in some areas (the right-most samples of cluster 3), overlap the left-most samples in cluster 3, close to clusters 4, 5 and 6.

6.1.2. Principally younger: clusters 4, 5 and 6

This source-terrane age group overlap is seen in clusters 4, 5 and 6 (primarily Mt. Narryer, Jack Hills and Maynard Hills, respectively). These consist of different proportions of ages, but all share common age groups. Cluster 4 is distinguished by an evenly large distribution of age groups 3491 Ma and 3381 Ma (on an almost 1:1 ratio), a sub-population of 3281 Ma, 3437 Ma and 3604 Ma, and smaller heterogeneous distributions of 3319 Ma and 3551 Ma. The N → S elongated trend is defined by an increase in the 3604 Ma age group, and a weakly defined decrease in younger components, primarily the 3282 Ma and 3437 Ma age groups. Similar to cluster 4, cluster 5 (mostly Jack Hills, with a single Maynard Hills sample MH178066) shows shared age groups of 3381 Ma and 3491 Ma, but where the 3381 Ma group dominates the age distribution structure. Smaller age groups help define the elongation from NE → SW within the cluster 5 ellipse by the general decrease of 3319 Ma and 3350 Ma ages, and the increase of 3491 Ma, 3604 Ma and ages older than 3800 Ma, principally the 3983 Ma age group. Similarly, cluster 6 is composed of most of the Maynard Hills samples, with many Jack Hills samples (including Jack Hills W74), and a single Brooking Hills sample, and is defined by large age groups of 3381 Ma, 3282 Ma and 3319 Ma, and minor components of 3437 Ma and 3492 Ma. The abundance of age group 3319 Ma (and ratio of this group to the 3381 Ma and 3282 Ma groups) in this cluster is considered the main differentiator in this cluster between clusters 4 and 5, and the decrease in abundance of this age group along the NE → SW trend also follows decreases of the 3282 Ma and 3214 Ma age groups. Along this same trend, there is increasing representation of certain age groups, including 3551 Ma, a minor increase in 3747 Ma, and increases in the old (>3800) zircon component, primarily the 4080 Ma, 4120 Ma and 4180 Ma age groups. The interrelation of these three clusters (4, 5 and 6) which all have some samples with zircons older than 3800 Ma, shows that there are at least four major age groups (3319 Ma, 3282 Ma, 3381 Ma and 3491 Ma) contributing to all the samples within these clusters, with these major and the minor components of 3350 Ma, 3551 Ma, 3604 Ma, 3719 Ma and 3745 Ma defining the elongation and width of the PCA-derived hierarchical cluster ellipses.

6.1.3. Principally youngest: cluster 7

Forming the top-most cluster in Fig. 4, cluster 7 is primarily composed of Toodyay Lake Grace (TLG) samples, with one West Narryer metasedimentary rock, two Jack Hills metasedimentary rocks, the Gum Creek greenstone belt metasedimentary rock, and the YGC and DGC gneiss components. Defined by their large proportion of age groups 3282 Ma and 3251 Ma, cluster 7 is most similar to the late stage granitic intrusions and gneisses of the NGC and the older components of the YGC (>3000 Ma), which has been interpreted to have formed the northernmost extension of the Narryer Terrane (and NGC) prior to rifting at ca. 2000 Ma (Occhipinti et al., 2004). The noticeably elongated SW → NE direction of the cluster ellipse defines a general increase of 3282 Ma, 3251 Ma and 3219 Ma age groups (more similar to YGC), a general decrease of the 3381 Ma age group (DGC, Dugel Gneiss Component) and older components (age groups older than 3600 Ma), and less well defined decreases of 3747 Ma and 3855 Ma (based on only two samples). The elongation towards the center of the graph, NW → SE, shows a general increase in 3381 Ma, 3350 Ma, 3319 Ma, 3491 Ma and younger (<3180 Ma) age groups, and a decrease in the 3282 Ma and 3251 Ma age components, which are mostly diagnostic for this cluster. The occurrence of the Dugel Gneiss Component (DGC) within this sample may be due to contamination of "Dugel-like" gneiss samples with later stage granitic pegmatitic intrusions of YGC affinity, with distinct ages of 3282 Ma and 3251 Ma, as mentioned earlier. The Jack Hills, West Narryer and Gum Creek samples that are similar to the TLG samples occupy vastly different areas of the Yilgarn Craton (see map in Fig. 1). The Jack Hills samples are from a central part of the Jack Hills metasedimentary belt, close to the sampling site W74. Sample JHSD3, plotting in the center of the cluster, may be a younger metasedimentary rock (as mentioned earlier), and cannot be reliably assessed as this may incorporate later reworking at ca. 2650 Ma or ca. 1700 Ma. The West Narryer sample WMN88_194 is from ca. 50 km west of Mt. Narryer and is from a site next to a sample (WMN88_185) that had too few concordant analyses to be properly assessed. Gum Creek sample GC184107 is unique as it is the only sample from the northeast Yilgarn Craton (within the Southern Cross Terrane) from this dataset, and is the furthest away from the Toodyay Lake Grace samples. This samples' similarity to the TLG samples suggests that the source terrane for the TLG metasedimentary rocks were widespread. Pidgeon et al. (2010) suggested that the TLG metasedimentary rocks could have been derived from a missing part of the proto-Yilgarn which contained abundant ca. 3290 Ma granites. These results show that this missing piece of the proto-Yilgarn may be related to the Yarlarweelor Gneiss Complex (YGC).

6.1.4. Principally mixed: clusters 8 and 9

The central clusters 8 and 9 are the most 'mixed' and least 'distinctive' clusters. Cluster 8 is composed of a Mt. Alfred sample (MA05), and Brooking Hills sample (BH01), as well as the Meeberrie Gneiss Component. The samples in cluster 8 consists of equal proportions of most age groups, with the major groups being 3381 Ma and 3282 Ma, with an array of 3491 Ma, 3437 Ma, 3604 Ma, 3319 Ma, 3747 Ma, 3251 Ma, 3645 Ma, 3551 Ma, 3716 Ma, 3591 Ma, 3350 Ma, 3687 Ma and 3412 Ma age groups present. An elongation trend along the hierarchical cluster ellipse from NW → SE defines a general increase in the 3381 Ma age group and a decrease within the 3551 Ma age group. The clustering of these two samples along with the Meeberrie Gneiss Component (with a complex age spectra ranging between 3730 Ma and 3300 Ma; (Kinny and Nutman, 1996)) of the NGC defines the most mixed sample and suggests that certain source terranes were composed primarily of MGC-type

rocks. Similarly, cluster 9 is composed of two samples (both from the Jack Hills) and the Eurada Gneiss component, with broadly similar ages to cluster 8, but with a higher proportion of Eurada-type age groups of 3491 Ma and 3437 Ma. A weakly defined NE → SW trend shows a general increase in the 3447 Ma component. These samples show a high Eurada Gneiss Component affinity that may suggest their provenance was comprised principally of Eurada Gneiss.

6.1.5. Conceptualizing a provenance

All of the detrital zircon populations found within each metasedimentary rock sample so far described could be thought of as containing varying proportions of the 9 hierarchical clusters shown in Fig. 4. The unique percentages of age groups within these 9 clusters, visualized with Guassian summation probability plots in Fig. 5, may relate directly to source terranes of similar composition. Each cluster could be considered as sampling particular components perhaps related to topographic highs of an originally heterogeneous source terrane, in which topographic highs consisting of different age components have contributed to each sample. If these sediments were all deposited at the same time (ca. 3 Ga) and had similar depositional environments, then the major differentiation between these sediments may relate to their spatial distribution. Evidence for a shallow marine depositional environment for the metasedimentary rocks of ca. 3 Ga age across the Yilgarn Craton is found in the either fan or braid-delta style (as discussed for the Jack Hills metasedimentary rocks in Eriksson and Wilde (2010)), a fluvialite or braided stream environment (as discussed for the Mt. Narryer metasedimentary rocks in Williams and Myers (1987)), or within a shallow-marine shelf environment (as discussed for the Toodyay Lake Grace 'Jimperding Metamorphic Belt' metasedimentary rocks in Bosch et al. (1996); and the Maynard Hills metasedimentary rocks in Wyche et al. (2004)). This spatial component could relate to each sample being composed of zircons sourced from proximal highlands consisting of unique source rock compositions with distinct drainage patterns. The younging profile from clusters 1 through 7, as seen in the factor map within Fig. 4 and in the group Gaussian summation probability plots in Fig. 5, could have been produced by these clusters having a similar spatial configuration to these dominant aged source localities during the time of their deposition. Intermixing seen in some clusters, and that some clusters consist of samples from multiple localities could be explained by coalescing fan deltas which have mixed margins containing zircons from multiple provenance point-sources.

It is difficult to explain samples such as JHSD4 (within cluster 2 of the Mt. Alfred samples), and JHSD3 (within cluster 7 of the TLG samples) as they form parts of clusters which are spatially distant on the factor map from the bulk of the Jack Hills samples. Further confusing matters, samples MA05 and BH01 (within cluster 8) are distinctly different from MA and BH samples in clusters 1 and 2, even though they are spatially only about 50 m from samples that have been assigned to clusters 1 and 2, respectively. There are a number of explanations which might account for this arrangement of samples. First, the two Jack Hills samples JHSD4 and JHSD3 are potentially younger sediments, as they have ca. 2650 Ma and ca. 1700–2000 Ma detrital zircons within them. If correct, they represent later stage events and are not directly related to the ca. 3 Ga sedimentation. Another explanation would require a change in drainage patterns, possibly by denudation and opening of the topographic highs which would allow for the sampling of different sources (such as those similar to Mt. Alfred and one similar to TLG, although not necessarily the same rocks) and the deposition of these into the same fan delta. It is also possible that processes such as tidal reworking of the sediments, destroying and mixing vast quantities of these sediments prior to their diagenesis into sandstones, or braided river channels which led to the deposition of zones with distinctly different detrital zircon age populations

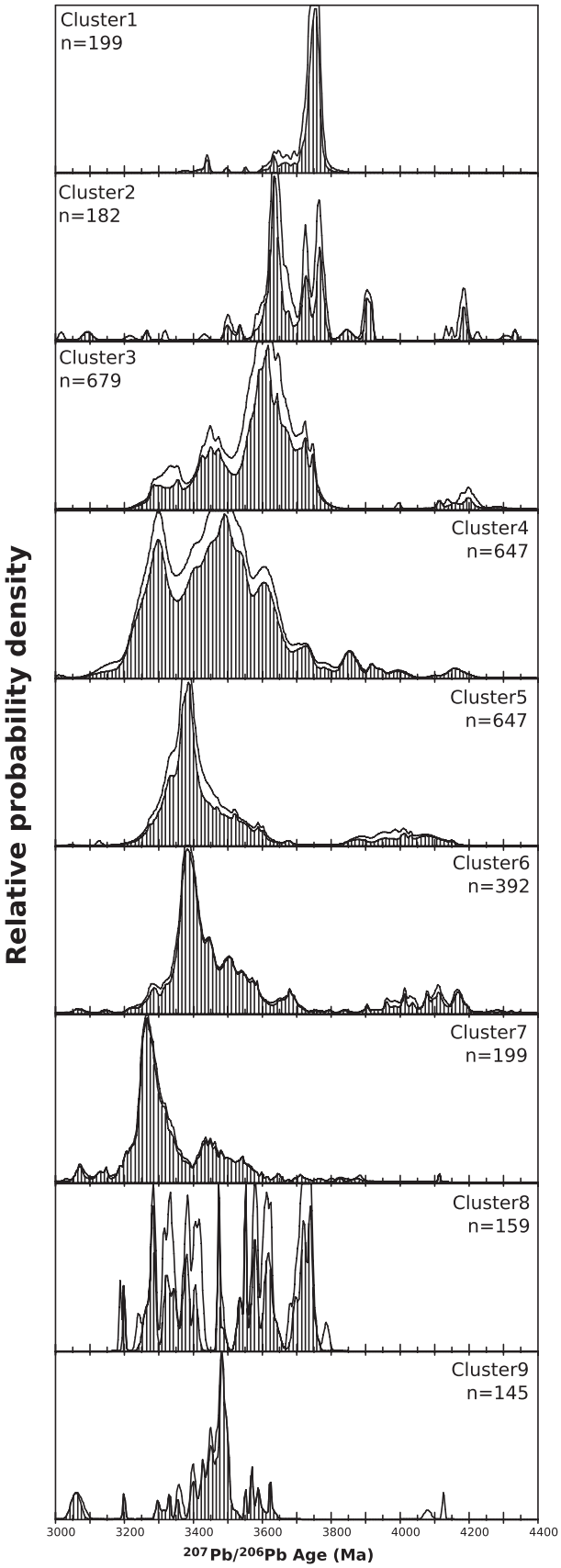

Fig. 5. Gaussian summation probability plots of ±10% of concordia detrital zircon data from the principal component hierarchical clusters. Plots show a "younging" from clusters 1 through 7, and "mixing" in clusters 8 and 9. Labels include the cluster number and number of analyses within the group. Non-shaded areas consist of analyses which fall outside of $\pm 2\sigma$ of concordia, whereas shaded areas are those analyses within $\pm 2\sigma$ of concordia.

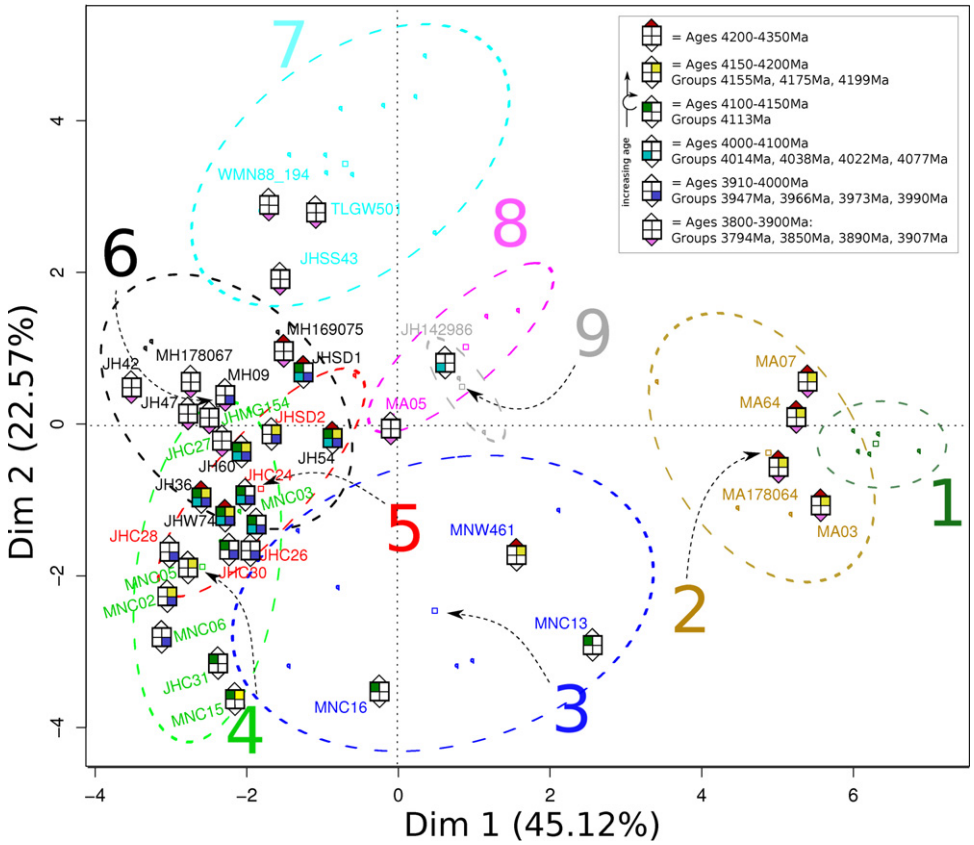

Fig. 6. Principal component analysis (PCA) factor map showing individual samples, principal component hierarchical clusters, and an overlay of samples containing Hadean zircons with these ages subdivided into 6 sub-groups of 50–100 Ma durations. Arrows point to center of cluster ellipses. Age components greater than 3800 Ma are denoted by filled in squares on each sample marker which relates to the age groups within the key, the filled in symbols denote younger ages (bottom) to older ages (top) in a clockwise fashion. Cluster 2 (Mt. Alfred) contains a simpler old component than do most of the Jack Hills. Some Mt. Narryer samples in cluster 3 show similar old components to cluster 2.

has influenced the detrital zircon composition of some samples. The impact of these alternatives would be to mix and homogenize (which may be the case for samples MA05, BH01, JH142986 and JHSS113) rather than impart another location's zircon age group structure on a particular sample. Alternatively, unrelated samples may have been fortuitously spatially juxtaposed by later tectonic processes. This explanation may be of primary relevance, as samples from the Jack Hills and throughout the Maynard Hills and Illaara greenstone belts (including MA and BH localities) are found within shear zones.

Further complicating interpretations, it is possible that some of these metasedimentary rocks have not only sampled distinct basement rocks (granites, gneisses) but may also have derived some zircons from a previous sediment deposited within a transitory basin. This earlier basin could have formed directly after the granites of the pre-NGC were formed. If this was the case, it would be difficult to ascertain whether detrital zircons were derived directly from constrained igneous sources, or from a provenance also containing earlier sediments with unique age components.

6.2. Hadean distributions and source terrane synthesis

Hadean (older than 3900 Ma) zircons occur within clusters 2, 3, 4, 5, and 6 (shown in Fig. 4). Samples containing these old zircon groups have been subdivided into 6 sub-groups, based on their >3800 Ma age structures, of 50–100 Ma durations and plotted on a factor map (Fig. 6). This diagram reveals the heterogeneity in >3800 Ma detrital zircon age structure that exists between Mt. Alfred cluster 2, Mt. Narryer cluster 3, and the Jack Hills clusters 4, 5 and 6. Mt. Narryer (cluster 3) shows some similar structures to both Mt. Alfred (cluster 2) with age groups between 4150 Ma and 4200 Ma, and Jack Hills (clusters 4, 5 and 6) with age groups between 4100 Ma and 4150 Ma. Many Mt. Narryer samples do not contain large amounts of 4200–4350 Ma ages, and lack most of the common Jack Hills ages between 3900 and 4100 Ma. Further unpublished data from the Jack Hills described by Holden et al. (2009) of about 7000 Jack Hills zircons older than 3800 Ma, shows a distinct age maximum between 3950 Ma and 4100 Ma. The Mt. Alfred samples of cluster 2 consist of detrital zircon age groups of 3800–3900 Ma and 4150–4350 Ma. The >4000 Ma ages at Mt. Alfred (cluster 2) are less complex, and older (containing no zircon ages younger than 4150 Ma), than those found at both Mt. Narryer and the Jack Hills. With the zircons older than 3800 Ma at Mt. Alfred consisting of more than 25 single grain analyses, and the main age peaks at Jack Hills being between ca. 3910 Ma and 4150 Ma, it is unlikely that the largest age groups of the Jack Hills Hadean zircon population have been missed at Mt. Alfred. The age gap in the Mt. Alfred data between 3910 Ma and 4150 Ma implies that at least two sources for these old zircons existed at the time of deposition of the host metasedimentary rocks.

To deconvolve the younger and Hadean zircon data, the younger age groups of samples containing Hadean zircons were matched to assess which age groups were shared. Age groups of 3491 Ma, 3604 Ma, 3645 Ma, 3687 Ma, 3716 Ma and 3747 Ma were all present in samples containing Hadean zircons, with the contribution of these ages to each sample following a similar (clockwise) overall age-group younging profile shown in the clusters presented on the factor map (Fig. 4B, clusters 1 through 7). The oldest shared component (other than the Hadean component) of all Hadean-zircon-bearing samples is the 3747 Ma age

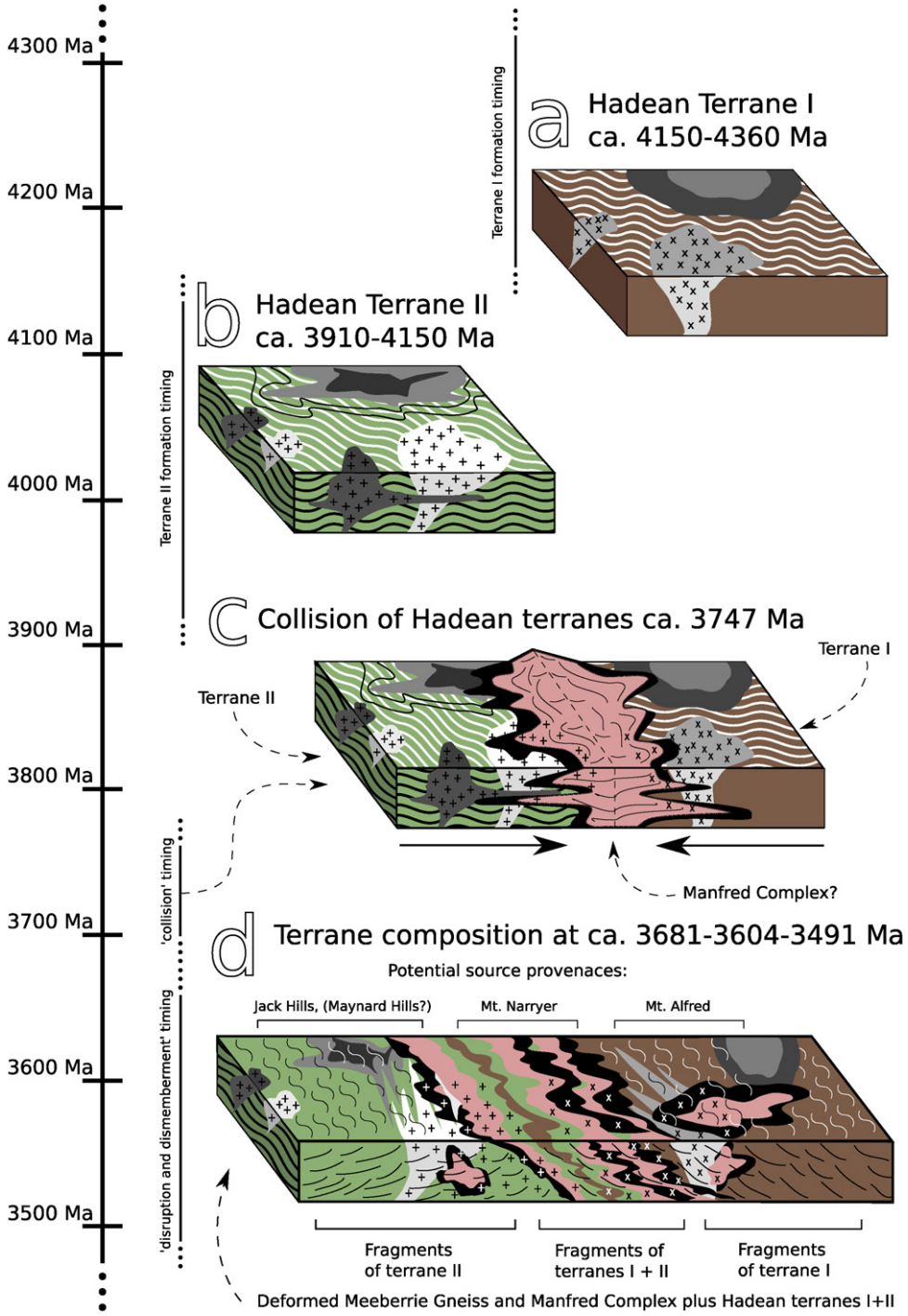

Fig. 7. Possible scenario for interpretation of >3491 Ma detrital age structure from >3 Ga metasedimentary rocks of the Yilgarn Craton. (A) A complex Hadean terrane formed at ca. 4150 Ma. (B) A second complex Hadean terrane formed by ca. 3900 Ma. (C) These two terranes begin to share a common history at ca. 3750 Ma. This common history could be accounted for by collision of two Hadean terranes and their intrusion by igneous rocks that could have included the Manfred Complex at 3747 Ma. (D) Disruption and dismemberment of the composite terrane with separation of the two Hadean components between 3747 Ma and 3491 Ma. This may have been coeval with intrusion and deformation of the Meeberrie Gneiss Complex at ca. 3600 Ma. This terrane was later intruded by the Eurada, Dugel, and younger granites to form the Narryer Gneiss Complex, that was later exhumed to provide the sources for the >3 Ga metasedimentary rocks of the Yilgarn Craton.

group, although it is in very low abundance within the Jack Hills samples. This age group of 3747 Ma occurs at Mt. Alfred in very high abundance, and within the same cluster that contains the Manfred Complex. The correlation between the 3747 Ma ages in the Manfred Complex and the youngest most-common ages for >4300 Ma Hadean zircon overgrowth rims of ca. 3676 ± 7 Ma, 3711 ± 10 Ma (Cavosie et al., 2004) and ca. 3720 ± 4 Ma (Thern and Nelson, submitted for publication) suggests this as a possible time when two Hadean fragments may have been integrated heterogeneously into one (or more) pre-Yilgarn (or pre-NGC) crustal components. Further evidence of this event is suggested in depth profiles yielding ages of ca. 3750 Ma in ca. 2 μm zones within two

>4100 Ma zircons from the Jack Hills and Mt. Narryer (Trail et al., 2007).

The combination of two crustal fragments of Hadean composition (seen in Fig. 7) between 3750 Ma and 3680 Ma may have been synchronous with the intrusion of the Manfred Complex and the oldest ages within the Meeberrie gneiss. If the combination of differing composite Hadean terranes at ca. 3750–3680 Ma was synchronous with the intrusion of the Manfred Complex, a layered intrusive of gabbro-anorthosite, age groups between 3770 Ma and 3907 Ma may have formed part of the terranes that included a Hadean zircon component. The distinctive structure and scarcity of the 3855 Ma age group (clusters 2, 6 and 7) and the high occurrence of the 3770 Ma age group at Mt. Alfred (cluster 1) hints at further age structure within these Hadean proto-terranes. Whether these Hadean crustal fragments were two distinctly different proto-'continents' of igneous character (gneisses), or whether they formed heterogeneous sedimentary or paragneiss assemblages is unknown. Whereas a layered sedimentary assemblage may more easily account for distinct Hadean zircon age groups, the formation of such a sedimentary package would require a previous heterogeneity within the zircon populations in this pre-3800 Ma sediment, and is difficult to assess. In either scenario, the combination of these fragments between ca. 3750 Ma and 3680 Ma did not homogenize their character fully, leaving distinct Hadean signatures within the detrital populations of the ca. 3 Ga host metasedimentary rocks.

The Hadean and younger zircon age populations within the Mt. Alfred metasedimentary rocks (cluster 2) may have been spatially separated from, and shared limited or no pre-3 Ga history with the detrital zircon populations occurring within the other Yilgarn >3 Ga metasedimentary rocks. Highlighting this difference, the abundances of 3747 Ma and 3770 Ma age groups at Mt. Alfred (clusters 1 and 2) are distinct when compared to other samples and clusters. Further, the maximum depositional age of the Mt. Alfred metasedimentary rocks are not well constrained (ca. 2940–3250 Ma), which could be interpreted as meaning these samples are older than other ca. 3 Ga Yilgarn metasedimentary rocks. However, there is evidence that these metasedimentary rocks from cluster 2 have shared some depositional sources, and thus may have been deposited spatially close to the other metasedimentary rock localities. First, the samples from Mt. Alfred share similar detrital zircon age groups with other Yilgarn ca. 3.0 Ga metasedimentary rocks, principally the 3491–3747 Ma age groups. Furthermore, the Mt. Alfred samples of cluster 2 are lithologically similar to the Mt. Narryer metasedimentary rocks in character and detrital zircon age distributions, albeit Mt. Alfred samples contain principally older <3800 Ma components, and lack the younger ca. 3300–3600 Ma age components found within Mt. Narryer. In addition, Mt. Alfred (clusters 1 and 2) are only ca. 30 km south of the Maynard Hills, and ca. 30 km north of Brooking Hills sample BH142999 which are both similar to the Jack Hills, within cluster 6. Finally, horizons of the Mt. Alfred (sample MA05) and northern Brooking Hills ca. 10 km south of Mt. Alfred (Sample BH01) resemble the Jack Hills metasedimentary rocks (without an old component, however), plotting centrally in cluster 8, and containing the youngest detrital zircons within the Mt. Alfred locality. All these lines of evidence suggest the ca. 3.0 Ga Yilgarn metasedimentary rocks were formed in one or possibly two closely spaced and/or converging basins of heterogeneous lithological associations.

Interpretation of the age of the youngest detrital zircon found within each sample as a maximum depositional age (see Table 1) shows a correlation between the maximum depositional age and the age trends found in clusters 1 through 7 in Fig. 4. If the ca. 3.0 Ga metasedimentary rocks of the Yilgarn were deposited between ca. 3250 and 2940 Ma, this could account for a general widening of provenance between clusters 1 (Mt. Alfred, primarily 3700–3770 Ma) to cluster 7 (Toodyay, primarily 3250–3330 Ma); blurring of cluster boundaries due to mixing of source terranes (between clusters 3 and 4; 4, 5, and 6; 6 and 7); depletion, mixing, or unavailability of certain source terranes (depletion of 3747 Ma and 3770 Ma ages from clusters 1 and 2 [Mt. Alfred] to cluster 7 [TLG]; and the depletion of age components older than 3600 Ma in Toodyay cluster 7, with the youngest components in highest percentages); as well as some potentially later mixtures of multiple sediments due to tidal reworking, braided river channels, or late (<3000 Ma) tectonic juxtaposition and mixing of sediments (clusters 8 and 9). If this is the case, the Mt. Alfred metasedimentary rocks could have sampled a potentially older early Archean terrane than those sampled by the metasedimentary rocks of the Jack Hills and Mt. Narryer. While it is likely this ancient Hadean source terrane is extant, it is considered likely that detrital zircon investigations of Mt. Alfred-like metasedimentary rocks may yield more information into the structure of the early Earth via sampling of unique Hadean components.

7. Conclusions

1 Principal component analysis (PCA) and hierarchical clustering of >3500 detrital zircon analyses has enabled grouping similar samples together and the deconvolution of constituent proto-source terranes of ca. 3 Ga metasedimentary rocks from the Yilgarn Craton. Age correlation biases were resolved by grouping all analyses together using a robust χ^2 grouping method, which produced Yilgarn-wide age groups suitable for PCA analysis.
2 Hierarchical clusters of the Yilgarn Archean metasedimentary rocks consist of differential mixing arrays of compositions similar to those of the Narryer Gneiss and components older than 3000 Ma within the Yarlarweelor Gneiss Complex. The clusters follow generalized younging trends (from clusters 1 through 7) on a factor map which facilitates investigation of their spatial distribution at time of deposition, and may be evidence for topographic highs with multiple river systems depositing into coalescing fan deltas. Alternatively, a literal interpretation of the youngest detrital zircons within each metasedimentary rock yields a general maximum depositional age younging profile of ca. 3250–3050 Ma which matches an overall PCA-derived hierarchical clustering younging profile, suggesting not only that the Mt. Narryer and Mt. Alfred sediments are older than those at Jack Hills, but that Mt. Alfred in particular has sampled a potentially older and chronologically simpler Archean terrane.
3 Samples of mixed age components which appear in contrastingly different hierarchical clusters may be explained in a number of ways. These include the sampling or mixing of different source terranes via coalescing fan delta margins, late-stage braided river systems which cross-cut multiple sediment horizons and tidal reworking of sediments. Alternatively, unrelated samples may have been fortuitously spatially juxtaposed by later tectonic processes.
4 Differences between the age structure of >3900 Ma zircon populations within the Mt. Alfred metasedimentary rocks with those from Mt. Narryer, Jack Hills and Maynard Hills localities is best explained by their derivation from two Hadean terranes.

Acknowledgements

We would like to both acknowledge and dedicate this contribution to Wulf Mueller, who spent time in the field at a number of these localities with both authors, and whose contribution to field interpretations and discussion of metasedimentary sequences will be missed. This manuscript has benefited from thorough and critical but constructive reviews by Jeff Chiarenzelli and Pat Eriksson.

References

Andersen, T., 2005. Detrital zircons as tracers of sedimentary provenance: limiting conditions from statistics and numerical simulation. Chemical Geology 216 (3–4), 249–270.

Bosch, D., Bruguier, O., Pidgeon, R., 1996. Evolution of an Archean metamorphic belt: a conventional and SHRIMP U–Pb study of accessory minerals from the Jimperding metamorphic belt, Yilgarn Craton, West Australia. Journal of Geology 104, 695–711.

Cavosie, A.J., Valley, J.W., Wilde, S.A., 2006. Correlated microanalysis of zircon: trace element, δ18O, and U–Th–Pb isotopic constraints on the igneous origin of complex >3900 Ma detrital grains. Geochimica et Cosmochimica Acta 70 (22), 5601–5616.

Cavosie, A.J., Wilde, S.A., Liu, D., Weiblen, P.W., Valley, J.W., 2004. Internal zoning and U–Th–Pb chemistry of Jack Hills detrital zircons: a mineral record of early Archean to Mesoproterozoic (4348–1576 Ma) magmatism. Precambrian Research 135 (4), 251–279.

Compston, W., Froude, D.O., Ireland, T.R., Kinny, P.D., Williams, I.S., Williams, I.R., Myers, J.S., 1985. The age of (a tiny part of) the Australian continent. Nature 317 (6037), 559–560.

Condie, K.C., Belousova, E., Griffin, W., Sircombe, K.N., 2009. Granitoid events in space and time: constraints from igneous and detrital zircon age spectra. Gondwana Research 15 (3–4), 228–242.

Crowley, J.L., Myers, J.S., Sylvester, P.J., Cox, R.A., 2005. Detrital zircon from the Jack Hills and Mount Narryer, Western Australia; evidence for diverse >4.0 Ga source rocks. Journal of Geology 113 (3), 239–263.

Dunn, S.J., Nemchin, A.A., Cawood, P.A., Pidgeon, R.T., 2005. Provenance record of the Jack Hills metasedimentary belt: source of the Earth's oldest zircons. Precambrian Research 138 (3–4), 235–254.

Eriksson, K.A., Wilde, S.A., 2010. Palaeoenvironmental analysis of Archaean siliciclastic sedimentary rocks in the west-central Jack Hills belt, Western Australia with new constraints on ages and correlations. Journal of the Geological Society 167, 827–840.

Froude, D.O., Ireland, T.R., Kinny, P.D., Williams, I.S., Compston, W., Williams, I.R., Myers, J.S., 1983. Ion microprobe identification of 4100–4200 Myr-old terrestrial zircons. Nature 304, 616–618.

Grange, M.L., Wilde, S.A., Nemchin, A.A., Pidgeon, R.T., 2010. Proterozoic events recorded in quartzite cobbles at Jack Hills, Western Australia: New constraints on sedimentation and source of >4 Ga zircons. Earth and Planetary Science Letters 292 (1–2), 158–169.

Holden, P., Lanc, P., Ireland, T.R., Harrison, T.M., Foster, J.J., Bruce, Z., 2009. Mass-spectrometric mining of Hadean zircons by automated SHRIMP multi-collector and single-collector U/Pb zircon age dating: the first 100,000 grains. International Journal of Mass Spectrometry 286 (2–3), 53–63.

Kinny, P.D., Nutman, A.P., 1996. Zirconology of the Meeberrie gneiss, Yilgarn Craton, Western Australia: an early Archaean migmatite. Precambrian Research 78 (1–3), 165–178.

Kinny, P.D., Wijbrans, J.R., Froude, D.O., Williams, I.S., Compston, W., 1990. Age constraints on the geological evolution of the Narryer Gneiss Complex, Western Australia. Australian Journal of Earth Sciences 37 (1), 51–69.

Kinny, P.D., Williams, I.S., Froude, D.O., Ireland, T.R., Compston, W., 1988. Early archaean zircon ages from orthogneisses and anorthosites at Mount Narryer, Western Australia. Precambrian Research 38 (4), 325–341.

Ł, S., Josse, J., Husson, F., 2008. FactoMineR: an R package for multivariate analysis. Journal of Statistical Software 25 (1), 1–18.

Maas, R., Kinny, P.D., Williams, I.S., Froude, D.O., Compston, W., 1992. The Earth's oldest known crust: A geochronological and geochemical study of 3900-4200 Ma old detrital zircons from Mt. Narryer and Jack Hills. Western Australia. Geochimica et Cosmochimica Acta 56 (3), 1281–1300.

Myers, J.S., 1988. Early Archaean Narryer Gneiss Complex, Yilgarn Craton, Western Australia. Precambrian Research 38 (4), 297–307.

Myers, J.S., 1997. Preface: Archaean geology of the eastern goldfields of Western Australia—regional overview. Precambrian Research 83 (1–3), 1–10.

Myers, J.S., Williams, I.R., 1985. Early Precambrian crustal evolution at Mount Narryer, Western Australia. Precambrian Research 27 (1–3), 153–163.

Nelson, D.R., 1997. Evolution of the Archaean granite–greenstone terranes of the eastern goldfields, Western Australia: SHRIMP U–Pb zircon constraints. Precambrian Research 83 (1–3), 57–81.

Nelson, D.R., 2000. 142986: metasandstone, Eranondoo Hill; in Compilation of geochronology data, 1999. No. Record 2000/2 in 1. Western Australia Geological Survey.

Nelson, D.R., 2002. Compilation of Geochronology Data, 2001. No. 2002/2 in 1. Western Australia Geological Survey.

Nelson, D.R., 2004. 142986: metasandstone, Eranondoo Hill; Data released: 2004 Geochronology dataset 290; in Compilation of geochronology data, June 2006 update. Western Australia Geological Survey.

Nelson, D.R., 2005. Compilation of Geochronology Data, 2003. No. 2005/2 in 1. Western Australia Geological Survey.

Nelson, D.R., 2006. CONCH: a visual basic program for interactive processing of ion-microprobe analytical data. Computers and Geosciences 32 (9), 1479–1498.

Nutman, A.P., Kinny, P.D., Compston, W., Williams, I.S., 1991. SHRIMP U–Pb zircon geochronology of the Narryer Gneiss Complex, Western Australia. Precambrian Research 52 (3–4), 275–300.

Occhipinti, S.A., Sheppard, S., Passchier, C., Tyler, I.M., Nelson, D.R., 2004. Palaeoproterozoic crustal accretion and collision in the southern Capricorn Orogen: the Glenburgh Orogeny. Precambrian Research 128 (3–4), 237–255.

Peck, W.H., Valley, J.W., Wilde, S.A., Graham, C.M., 2001. Oxygen isotope ratios and rare earth elements in 3.3–4.4 Ga zircons: ion microprobe evidence for high [delta]18O continental crust and oceans in the Early Archean. Geochimica et Cosmochimica Acta 65 (22), 4215–4229.

Pidgeon, R., Nemchin, A., 2006. High abundance of early Archaean grains and the age distribution of detrital zircons in a sillimanite-bearing quartzite from Mt. Narryer, Western Australia. Precambrian Research 150 (3–4), 201–220.

Pidgeon, R.T., Wilde, S.A., 1998. The interpretation of complex zircon U–Pb systems in Archaean granitoids and gneisses from the Jack Hills, Narryer Gneiss Terrane, Western Australia. Precambrian Research 91 (3–4), 309–332.

Pidgeon, R.T., Wingate, M.T.D., Bodorkos, S., Nelson, D.R., 2010. The age distribution of detrital zircons in quartzites from the Toodyay-Lake Grace Domain, Western Australia: implications for the early evolution of the Yilgarn Craton. American Journal of Science 310 (9), 1115–1135.

Sircombe, K., Hazelton, M., 2004. Comparison of detrital zircon age distributions by kernel functional estimation. Sedimentary Geology 171 (1–4), 91–111.

Sircombe, K.N., 1999. Tracing provenance through the isotope ages of littoral and sedimentary detrital zircon, eastern Australia. Sedimentary Geology 124 (1–4), 47–67.

Sircombe, K.N., 2000. Quantitative comparison of large sets of geochronological data using multivariate analysis: a provenance study example from Australia. Geochimica et Cosmochimica Acta 64 (9), 1593–1616.

Spaggiari, C.V., Pidgeon, R.T., Wilde, S.A., Anonymous, Grimes, C., John, B., Kelemen, P., Mazdab, F., Wooden, J., Cheadle, M., Hanghoj, K., Schwartz, J., 2004. Trace element chemistry of zircons from oceanic crust: A method for distinguishing detrital zircon provenance. Geological Society of America, 2004 annual meeting 36 (5), 207.

Spaggiari, C.V., Pidgeon, R.T., Wilde, S.A., 2007. The Jack Hills greenstone belt, Western Australia; Part 2, Lithological relationships and implications for the deposition of $\geq$4.0 Ga detrital zircons. Precambrian Research 155 (3–4), 261–286.

Spaggiari, C.V., Wartho, J.-A., Wilde, S.A., 2008. Proterozoic deformation in the northwest of the Archean Yilgarn Craton. Western Australia. Precambrian Research 162 (3–4), 354–384.

Thern, E., Jourdan, F., Evans, N., Mcdonald, B., Danisik, M., Frew, R., Nelson D.R., 2011. Post-depositional thermal history of the 4364–3060 Ma zircon-bearing metasandstones of the Illaara and Maynard Hills granite greenstone belts, Western Australia. Mineralogical Magazine Goldschmidt Conference Abstracts, p. 2003.

Thern, E., Nelson, D., Submitted for Publication. The early Archean Illaara and Maynard Hills Greenstone Belt siliciclastic metasedimentary rocks, Western Australia: age structures from detrital ca. 3000–4372 Ma zircons.

Trail, D., Mojzsis, S.J., Harrison, T.M., 2007. Thermal events documented in Hadean zircons by ion microprobe depth profiles. Geochimica et Cosmochimica Acta 71 (16), 4044–4065.

Vermeesch, P., 2005. Statistical uncertainty associated with histograms in the Earth science. Journal of Geophysical Research 110, 15p.

Weislogel, A., Graham, S., Chang, E., Wooden, J., Gehrels, G., 2010. Detrital zircon provenance from three turbidite depocenters of the Middle–Upper Triassic Songpan–Ganzi complex, central China: record of collisional tectonics, erosional exhumation, and sediment production. Geological Society of America Bulletin 122 (11–12), 2041–2062.

Wilde, S.A., 2010. Proterozoic volcanism in the Jack Hills Belt, Western Australia: some implications and consequences for the World's oldest zircon population. Precambrian Research 183 (1), 9–24.

Wilde, S.A., Valley, J.W., Peck, W.H., Graham, C.M., 2001. Evidence from detrital zircons for the existence of continental crust and oceans on the Earth 4.4 Gyr ago. Nature 409, 175–178.

Williams, I., Myers, J., 1987. Archaean Geology of the Mount Narryer Region Western Australia. West Australian Geological Survey Report 22 (32).

Wingate, M.T.D., Bodorkos, S., 2007. 184107: metamorphosed quartz sandstone, Christmas Bore. Vol. Geochronology dataset 678. Western Australia Geological Survey.

Wingate, M., Bodorkos, S., Kirkland, C., 2008a. 177901: quartzite, Kowalyou. Geochronology Record 739: Geological Survey of Western Australia, 5p.

Wingate, M., Bodorkos, S., Kirkland, C., 2008b. 177904: quartzite, Windmill Hill. Geochronology Record 739: Geological Survey of Western Australia, 7p.

Wingate, M., Bodorkos, S., Kirkland, C., 2008c. 177907: quartzite, Noondeening Hill. Geochronology Record 739: Geological Survey of Western Australia, 7p.

Wingate, M., Bodorkos, S., Kirkland, C., 2008d. 177908: quartzite, Baillie farm Geochronology Record 739: Geological Survey of Western Australia, 7p.

Wyche, S., 2007. Chapter 2.6 evidence of pre-3100 Ma crust in the Youanmi and South West Terranes, and Eastern Goldfields Superterrane, of the Yilgarn Craton. In: Martin, J., van Kranendonk, R.H.S., Bennett, V.C. (Eds.), Earth's Oldest Rocks. vol. 15. Elsevier, pp. 113–123.

Wyche, S., Nelson, D.R., Riganti, A., 2004. 4350–3130 Ma detrital zircons in the Southern Cross GraniteGreenstone Terrane, Western Australia: implications for the early evolution of the Yilgarn Craton. Australian Journal of Earth Sciences 51 (1), 31–45.

CHAPTER 4
DETRITAL ZIRCON PROVENANCE

This chapter is comprised of a paper submitted to Precambrian Research in June, 2012 (in review), which discusses the results of over 1000 zircon ages obtained throughout this study. Supplemental data, provided in the appendix, show some SEM photos of select grains from sample MA07 in Figure B.1, thin sections of select samples in Figure C.1, and an overview of most samples collected during this study, but not all processed for zircon geochronology in Figure C.2. The main focus of the study is to consider their provenance, and the relationship of these samples to those of the Narryer Terrane (Jack Hills, Mt. Narryer). This leads to new questions, and new potential answers, about how the Yilgarn Craton may have evolved between time of sandstone deposition at ca. 3000 Ma and final 'cratonization' of the Yilgarn at ca. 2660 Ma.

4.1 Paper 2: Provenance of ca. 4372−3000 Ma detrital zircons within Early Archean siliciclastic metasedimentary rocks from the Illaara and Maynard Hills Greenstone Belts, Western Australia

Thern, E. R., Nelson, D. R., (2012). Provenance of ca. 4372−3000 Ma detrital zircons within Early Archean siliciclastic metasedimentary rocks from the Illaara and Maynard Hills Greenstone Belts, Western Australia, submitted to Precambrian Research

E.R. Thern[a*] and D.R. Nelson[b]

[a] Department of Imaging and Applied Physics, Curtin University of Technology, GPO Box U1987, Perth, WA 6001, Australia (*eric@thern.org)

[b] School of Natural Sciences, University of Western Sydney, Locked Bag 1797, Penrith, NSW 2751, Australia

4.2 Abstract

The Illaara and Maynard Hills Greenstone Belts of the Southern Cross Terrane within the Yilgarn Craton contain ca. 3000 Ma siliciclastic metasedimentary rocks hosting detrital zircons with ages up to 4372 Ma. As granites and gneisses older than the youngest detrital zircons within these metasedimentary rocks have not been identified within the Southern Cross Terrane, the metasedimentary rocks of the Maynard Hills, Illaara and Gum Creek greenstone belts may be the oldest rocks within the Southern Cross Terrane. Well-preserved sedimentary structures are rare and upper-greenschist to middle-amphibolite facies metamorphism and shearing has obscured primary relationships between these greenstone-hosted metasedimentary rock occurrences. More than 1000 detrital zircons from twelve samples within these belts were analyzed to determine the age and composition of their provenance sources and to better constrain their stratigraphic relationships.

Depositional ages are currently constrained by the youngest zircons from Mt. Alfred's eastern (3318±6 Ma) and western (3264±7 Ma) horizons, and Maynard Hills ca. 3060 to 2960 Ma analyses; and a minimum depositional age of ca. 2940 Ma by $^{40}Ar/^{39}Ar$ plateau ages from tourmalines from stratiform quartz-tourmaline veins within the outcrops. Increasing age complexity and maximum depositional age 'younging' are recorded across the Mt. Alfred locality from East (almost exclusively 3700-3780 Ma) to West (3300-3700 Ma and >3800 Ma). The western-most horizon at Mt. Alfred contains abundant >3800 Ma zircons, but lack the prominent 3500 to 3300 Ma ages common to Jack Hills Hadean-zircon bearing metasedimentary rocks. This horizon at Mt. Alfred is most similar in detrital zircon age characteristics to the metasedimentary rocks at Mt. Narryer but without the younger zircon ages (of Eurada and Dugel gneiss affinity; 3480-3300 Ma) found in abundance at Mt. Narryer. This makes Mt. Alfred a unique source for detrital Hadean zircons.

The detrital zircon age similarities within greenstone-hosted metasedimentary rocks throughout the Yilgarn Craton, including the Illaara, Maynard Hills and Gum Creek Greenstone Belts of the Southern Cross Terrane, the Jack Hills and Mt. Narryer of the Narryer Terrane, and the Toodyay Lake Grace Domain within the South West Terrane, strongly suggest a shared provenance of these ca. >2940 Ma metasedimentary rocks. It is likely they were deposited contemporaneously between ca. 3300 and 2940 Ma, later separated by multiple younger ca. 2950 to 2630 Ma granite-greenstone formations during rifting and collision episodes, and occur today as 'rafts' within younger ca. 2730-2640 Ma granite-greenstones.

4.3 Introduction

The oldest rocks within the Yilgarn Craton, Western Australia, are currently exposed in the Narryer Gneiss Complex (NGC) of the Narryer Terrane (Figure 4.1). Ages of the younger components of the NGC, at ca. 3200 Ma, are older than any other rocks throughout the Yilgarn Craton, and this antiquity of the NGC has garnered much attention and study (de Laeter et al., 1981; Kinny et al., 1988). The principal tectonic components of the NGC are the Manfred Complex (up to ca. 3750 Ma) and the Meeberrie (3750 to 3300 Ma), Eurada (3490 to 3440 Ma) and Dugel Gneisses (3380 to 3350 Ma) as well as some younger (3330 to 3250 Ma) granites (Kinny et al., 1988; Nutman et al., 1991; Kinny and Nutman, 1996; Pidgeon et al., 1998). Following the discovery of detrital zircons with ages up to ca. 4200 Ma from the Mt. Narryer metasedimentary rocks (Froude et al., 1983; Compston et al., 1985; Kinny et al., 1990; Crowley et al., 2005; Pidgeon and Nemchin, 2006), detrital zircons as old as 4400 Ma were found in a metasedimentary rock sample from the Jack Hills Greenstone Belt (Compston et al., 1986b; Wilde et al., 2001; Peck et al., 2001; Cavosie et al., 2004; Crowley et al., 2005; Cavosie et al., 2006). The metasedimentary rocks at Jack Hills are among the most-studied on Earth with sample site W74 having well over 100,000 zircons analyzed thus far (Holden et al., 2009). More recently, zircons with ages older than 4000 Ma have been found within ca. 3000 Ma Southern Cross metasedimentary rocks within the Illaara (Nelson, 2005; Wyche, 2007) and Maynard Hills (Nelson, 2002b; Wyche et al., 2004) greenstone belts, over 400 km south-east of the Mt. Narryer and Jack Hills metasedimentary rocks. Further studies of ca. 3000 Ma metasedimentary rocks within the Toodyay Lake Grace Domain within the South West Terrane have yielded few zircons with ca. 3850 Ma ages, with most (>90%) ages below 3500 Ma (Pidgeon et al., 2010).

Throughout the Southern Cross, Murchison, and South West Terranes (see Fig. 4.1), ca. 3000 Ma metasedimentary rocks occur within ca. 2730 to 2600 Ma granites and gneisses, and greenstones of >2900 Ma, ca. 2800 Ma and ca. 2730 Ma ages. Similar metasedimentary rocks within the Narryer Terrane at Mt. Narryer and Jack Hills occur within >3000 Ma granites and gneisses as well as >2900 Ma greenstones, granites and gneisses, respectively. These greenstones are distributed along N–S trending elongate belts throughout the Yilgarn Craton (see Fig. 4.1). These >3000 Ma metasedimentary rocks commonly contain abundant zircons with ages older than 3250 Ma, older than any known rocks within the Yilgarn Craton outside of the Narryer Gneiss Complex within the Narryer Terrane. With the exception of those at Mt. Narryer, the metasedimentary rocks are located on the margins or within greenstone 'rafts' throughout the Yilgarn (Figure 4.1) and their relationship to one another and to the Narryer Gneiss Complex has remained problematic.

The aims of this study are to: (1) Obtain SHRIMP U-Pb zircon dates on detrital

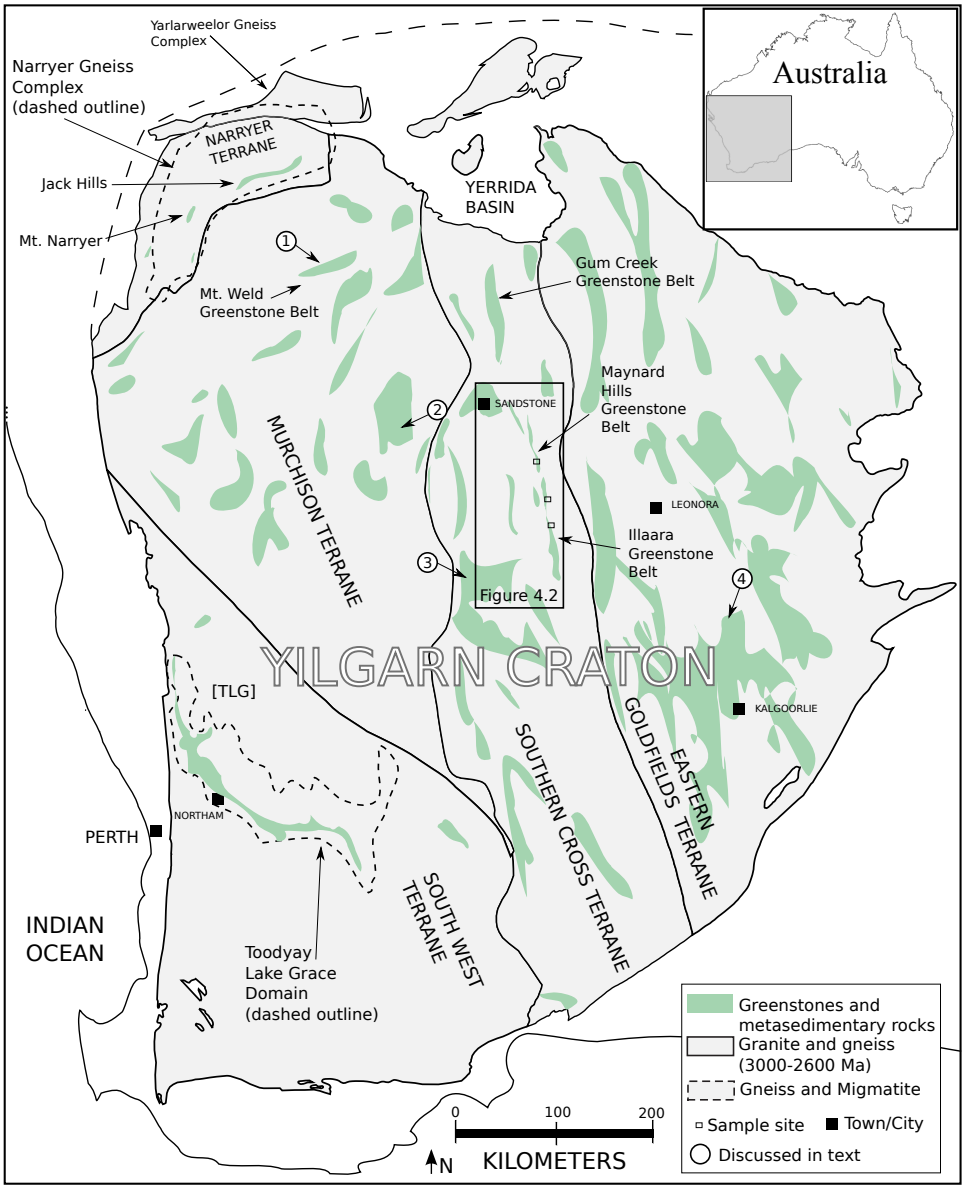

Figure 4.1: see next page for full description

Figure 4.1: Map of the Yilgarn Craton, Western Australia, showing locations of ca. 3000 Ma metasedimentary rocks (Toodyay Lake Grace Domain, Jack Hills, Mt. Narryer, Gum Creek, Maynard Hills, Illaara), greenstone belts, granites and gneisses. Also labelled are the greenstones at Mt. Weld (and the Mt. Weld ca. 2940-2960 Ma metasedimentary rocks) which is also the first of four numbered greenstone belts. These numbered greenstone belts are used as examples for typical greenstone associations close to their locality on the map. Label 1, the Mt. Weld greenstone belt from the Western Murchison Terrane, is composed of a lower >2900 Ma Luke Creek greenstone succession and an upper ca. 2800 Ma Mt. Farmer succession (Wiedenbeck and Watkins, 1993; Pidgeon et al., 1996). Label 2, the Windimurra Complex (a mafic-ultramafic intrusive complex) from the Eastern Murchison Terrane, is mostly composed of ca. 2850-2800 Ma ages (Mathison and Ahmat, 1996; Ivanic et al., 2010), and references therein. Label 3, the Marda-Diemals Greenstone Belt from the Central Southern Cross Terrane, is a ca. 2735 Ma upper greenstone overlying a >2900 Ma lower greenstone (Morris, 2007; and references therein). Label 4, from the 'Gindalbie Terrane' of the central Eastern Goldfields Terrane, is composed of ca. 2700-2680 Ma ages (Nelson, 1997). The area covered by Fig. 4.2 is also shown.

zircons from within the ca. 3000 Ma metasedimentary rock horizons from the Maynard Hills and Illaara Greenstone Belts; (2) Use this data and their Th-U/Pb chemistry and isotope systematics to investigate discordance trends and maximum depositional ages based on their youngest detrital zircons; (3) Discuss the post-depositional granite-greenstone, metamorphic and tectonic events to constrain their stratigraphy and depositional environment; (4) Investigate the geographical distribution of these metasedimentary rock occurrences throughout the Yilgarn Craton to ascertain the provenance sources of their Hadean detrital zircon populations; and (5) Draw inferences about possible relationships between these lithologically similar but dispersed metasedimentary rock occurrences and implications for the mechanisms of formation of the Yilgarn Craton.

4.4 Geological Background

The Maynard Hills, Mt. Alfred, and Brooking Hills metasedimentary rocks lie along the eastern margins of the Maynard Hills and Illaara Greenstone Belts, respectively (inset maps in Fig. 4.2), within the Southern Cross Terrane[1] in the central area of the Yilgarn Craton (Riganti, 2003; Wyche et al., 2004). As there are no granites or gneisses yet identified that are older than the youngest detrital zircons within these metasedimentary rocks (Wyche, 2007), the metasedimentary rocks of the Maynard Hills, Illaara and Gum Creek greenstone belts may be the oldest rocks yet identified within the Southern Cross Terrane. The metasedimentary rocks of the Illaara Greenstone Belt may

[1]In this paper, the term "Terrane" is used descriptively and is not intended to imply that the geological unit may not share parts of its geological history with that of adjacent terranes.

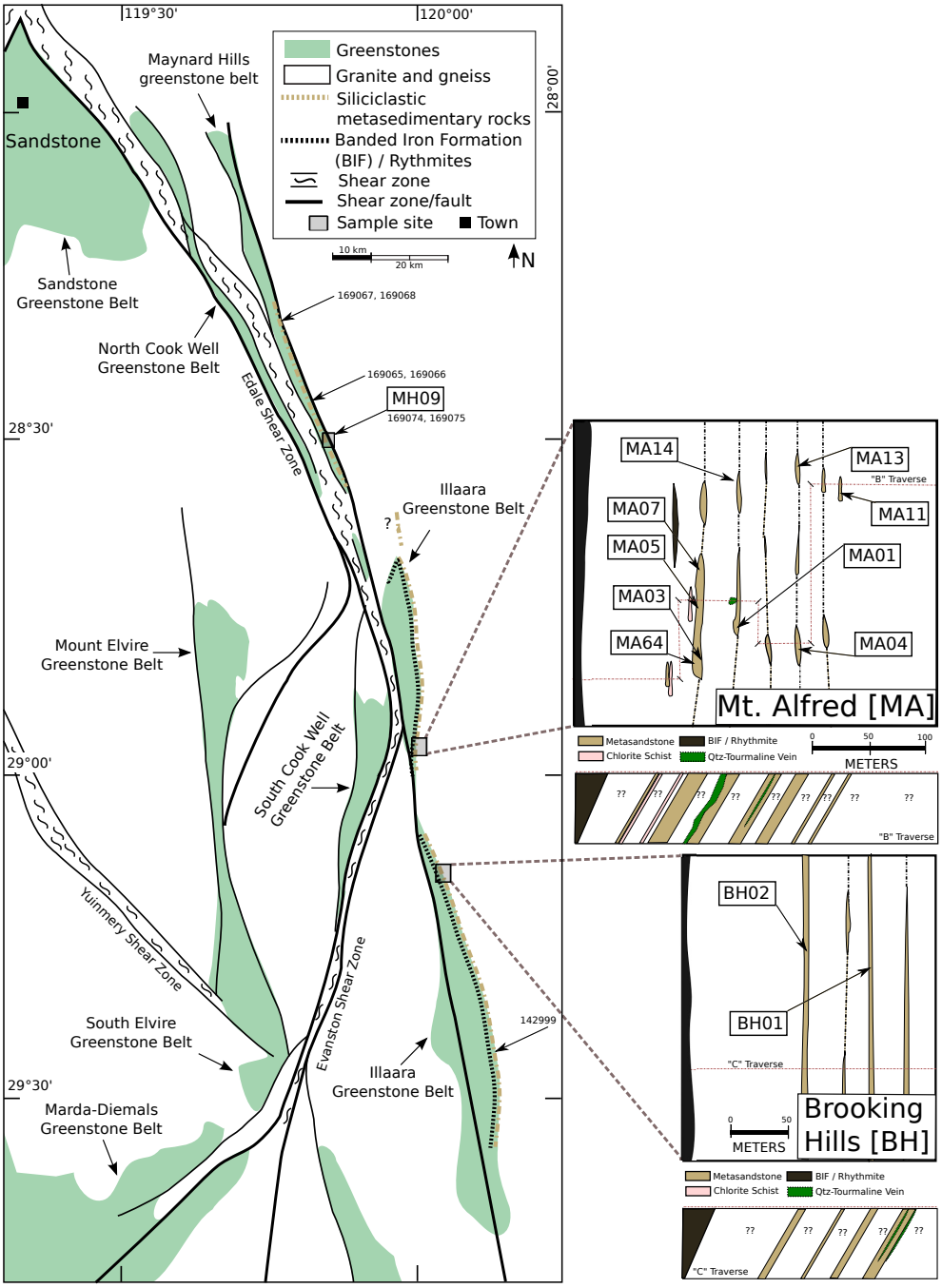

Figure 4.2: The Southern Cross Terrane Maynard Hills and Illaara Greenstone Belts with inset maps of the Mt. Alfred and Brooking Hills sampling localities. Numbered labels outside of boxes are previous GSWA sampling numbers and locations.

represent the southern extension of the lowest preserved sedimentary unit to those of the Maynard Hills Greenstone Belt (Wyche, 2007). The northernmost metasedimentary rocks of ca. 3000 Ma age identified within the Southern Cross Terrane, the Gum Creek Greenstone Belt metasedimentary rocks lie along the western boundary and structural base of the greenstone belt (Chen et al., 2006). Rare sedimentary structures, such as cross bedding, are found within the Maynard Hills metasedimentary rocks, and indicate that this unit youngs towards the west (Chen et al., 2004a). This, and the quartz-arenite affinity of the metasedimentary rocks of the Maynard Hills and Illaara greenstone belts suggest they were deposited on a broad continental shelf in a shallow marine environment (Wyche et al., 2004; Wyche, 2007). However, the obscuring of primary structures due to post-depositional metamorphic overprinting makes further sedimentological interpretations uncertain.

The Illaara and Maynard Hills greenstone belts have undergone multiple stages of deformation and granitic intrusion. Deposition of the oldest greenstones in this area is poorly constrained but are likely pre-2900 Ma in age, with episodes of granitic intrusions occurring between ca. 3000 and 2640 Ma (Pidgeon and Wilde, 1990; Wiedenbeck and Watkins, 1993; Yeats et al., 1996; Schiotte and Campbell, 1996; Mueller and McNaughton, 2000). Evidence of multiple ductile shearing, folding and shortening events are shown within the rocks of the central Southern Cross Terrane, with metamorphic events prior to ca. 2800 Ma being overprinted or obliterated by shearing and granitic intrusions between 2730 and 2660 Ma (Chen et al., 2004b; Chen et al., 2003). Late or post-kinematic granitic intrusions and late-stage shearing (Chen et al., 2004b; Chen et al., 2003), possibly related to (re)activation of the Edale and Evanston Shear Zones (see Fig. 4.2) between 2630 and 2600 Ma formed or reactivated the planar-foliation fabrics within the metasedimentary rocks, that contain aligned muscovite and fuchsite laths (Thern et al.; in prep).

Abundant banded iron formations (BIF) and cherts occur on the eastern margin of the Maynard Hills and Illaara greenstone belts. This is a common association within the older (>2900 Ma) greenstone belts throughout the Southern Cross Terrane (Riganti, 2003; Wyche et al., 2004), Murchison Terrane (Wiedenbeck and Watkins, 1993; Pidgeon et al., 1996) and Narryer Terrane (Eriksson and Wilde, 2010). These greenstone belts are commonly associated with clastic metasedimentary rocks that have been found to contain >3000 Ma detrital zircons (Nelson, 2002b, 2005). The distribution of the granite-greenstone belts throughout the Yilgarn Craton follow roughly N–S trending elongate patterns (see Fig. 4.1). The greenstones were formed during multiple events at >2900 Ma, ca. 2850 to 2800 Ma, and between 2730 and 2680 Ma (Wiedenbeck and Watkins, 1993; Pidgeon et al., 1996; Nelson, 1997).

Some examples of these greenstones, are the Mt. Weld greenstone belt from the

north-west part of the Murchison Terrane (label 1 on Fig. 4.1); composed of the >2900 Ma Luke Creek Group succession and the ca. 2850-2800 Ma Mt. Farmer Group succession (Wiedenbeck and Watkins, 1993; Pidgeon et al., 1996). Of similar age to the Mt. Farmer Group, the Windimurra Complex from the eastern Murchison Terrane (label 2 on Fig. 4.1) is mostly composed of ca. 2800 Ma age mafic-ultramafic intrusive rocks (Mathison and Ahmat 1996; Ivanic et al. 2010; and references therein). The Marda-Diemals greenstone belt from the Central Southern Cross Terrane (label 3 on Fig. 4.1) is a ca. 2735 Ma upper greenstone overlying a >2900 Ma lower greenstone sequence (Morris, 2007; and references therein). The 'Gindalbie Terrane' of the central Eastern Goldfields Terrane (label 4 on Fig. 4.1) is composed of ca. 2700-2680 Ma age mafic, basaltic and volcaniclastic rocks (Nelson, 1997). These examples from the Yilgarn Craton show a complex history of igneous events over the course of >300 Ma.

4.5 Sample selection

Sample sites at the Brooking Hills, Mt. Alfred and the Maynard Hills are composed of metamorphosed sedimentary rocks, including banded iron formations (BIFs) and rhythmites, metasandstones, quartz arenites, metapelites and greenschists. These metasedimentary rocks outcrop parallel to the Edale and Evanston Shear zones, and have planar foliation fabrics aligning N–S with these shears. Sample sites are shown on the simplified geological sketch maps of the Mt. Alfred and Brooking Hills (Figure 4.2, inset Mt. Alfred and Brooking Hills maps) with additional sampling information in Table 4.1.

Detrital zircons were separated from twelve samples collected near Mt. Alfred and the Brooking Hills. Samples MA01, MA03, MA04, MA05, MA07, MA11, MA13, MA14 and MA64 were all collected east of Mt. Alfred (sample label "MA") within the central northern Illaara Greenstone Belt. Samples BH01 and BH02 were collected from near the Brooking Hills (sample labels "BH") in the central part of the Illaara Greenstone Belt. Maynard Hills sample MH09 (sample label "MH") was picked from the same aliquot of zircon separates as sample 169075 (Nelson, 2002b), that were collected from the Maynard Hills Greenstone Belt. Mt. Alfred sample MA64 is from the same aliquot as sample 178064 (Nelson, 2005), from ca. 2 meters west of sample site MA03.

Samples are discussed as 'metasedimentary rocks', but nearly all original sedimentary features have been lost due to shearing and late stage metamorphic recrystallization. The loss of these original sedimentological features are compounded by growth of metamorphic minerals such as muscovite and fuchsite.

Table 4.1: List of sample localities and brief descriptions

Sample	South	East	Lithology and Description
Mt. Alfred [MA] – Southern area of the Northern Illaara Granite Greenstone Belt			
MA01	S 28° 50.637'	E 120° 00.024'	metasandstone; a clearish-green, recrystallized, fine to medium-grained, with fuchsite aligned with 5 cm-thick bedding-parallel foliation from a 2 m-thick, bedded quartzite unit.
MA03	S 28° 50.694'	E 119° 59.977'	metasandstone; a pale greenish-white, medium- to coarse-grained, quartzite from the western margin of a 20 m-thick, bedded quartzite unit; 2 m-east of GSWA sample 178064.
MA04	S 28° 50.636'	E 120° 00.127'	metasandstone; a clearish-green, reddish tinged, recrystallized, fine to medium-grained, with fuchsite and muscovite aligned with 5 cm-thick bedding-parallel foliation from a 10 m-thick, bedded quartzite unit.
MA05	S 28° 50.678'	E 119° 59.965'	metasandstone; a pale greenish-white, recrystallized, fine to medium-grained quartzite, with minor fuchsite / muscovite lathes aligned to 4 cm-thick bedding-parallel foliation on the eastern margin of this 20 m-thick outcrop.
MA07	S 28° 50.636'	E 119° 59.975'	metasandstone; a pale greenish-white, recrystallized, fine to medium-grained, with minor fuchsite/muscovite lathes aligned to 5-8 bedding-parallel foliation from a 20 m-thick, bedded quartzite unit.
MA11	S 28° 50.442'	E 120° 00.165'	metasandstone; a bright-clear-green, recrystallized, medium to coarse-grained, with large 1-2 cm-long fuchsite lathes aligned with 4 cm-thick bedding-parallel foliation from a 2 m-thick, bedded quartzite unit.
MA13	S 28° 50.441'	E 120° 00.107'	metasandstone; a moderately weathered, pale-white, yellowish, recrystallized, fine to medium-grained quartzite with 1-2 cm thick bedding-parallel foliation.
MA14	S 28° 50.432'	E 120° 00.048'	metasandstone; a clearish-green, recrystallized, fine to medium-grained, with fuchsite and muscovite aligned with 5 cm-thick bedding-parallel foliation from a 20 m-thick, bedded quartzite unit.
MA64	S 28° 50.694'	E 119° 59.971'	coarse sandstone; a pale pinkish-white, medium- to coarse- and even-grained, well-sorted quartz sandstone from a 20 m-thick, bedded quartzite unit; GSWA sample 178064.
Brooking Hills [BH] – Northern area of the Southern Illaara Granite Greenstone Belt			
BH01	S 28° 56.681'	E 120° 00.040'	metasandstone; a pale greenish-white, recrystallized, fine to medium-grained, with fuchsitic lathes aligned to 2-4 cm thick layer-parallel folioation from a 1 m-thick, bedded quartzite unit.
BH02	S 28° 56.699'	E 120° 00.021'	metasandstone; a pale greenish-white, recrystallized, medium-grained, with fuchsitic lathes aligned to 5-8 cm thick layer-parallel foliation from a 1 m-thick, bedded quartzite unit.
Maynard Hills [MH] – Southern section of the Maynard Hills Granite Greenstone Belt			
MH09	S 28° 29.316'	E 119° 49.050'	quartzite; a pale pinkish-grey, coarse grained massively recrystallized quartzite with thin (<1 mm thick) reddish-yellow clay-rich layers; zircons separated from GSWA sample 169075 (Nelson, 2002) aliquot.

1. All samples were free of any obvious veins or dykes.
2. Samples referred to as 'metasedimentary rocks' within text, as their primary sedimentalogical structures are obscured

4.6 Analytical Procedures

Zircons were separated from each ca. 5 kg of sample via crushing, milling, Wilfley table and heavy liquid separation. They were then put through a Frantz magnetic separator and then hand-picked from three magnetic fractions with no preference to size or shape of zircon crystals. The non-magnetic and mid-magnetic fractions were preferred as they yielded the highest abundance of non-metamict grains suitable for zircon geochronology.

Zircon grains and fragments of standards were mounted in epoxy resin and polished approximately a third to half way through to expose a surface suitable for in-situ U-Th-Pb data acquisition. Analysis of these zircons utilized the Sensitive High Resolution Ion Microprobe (SHRIMP) at the John de Laeter Centre of Mass Spectrometry, Curtin University of Technology, Perth, Australia using procedures similar to those described in Nelson (1997). Each analysis was comprised of six cycles measuring each of ten masses: $^{196}Zr_2{}^{16}O^+$ (2 s), $^{204}Pb^+$ (10 s), Background at mass 204.045 (10 s), $^{206}Pb^+$ (10 s), $^{207}Pb^+$ (20 s), $^{208}Pb^+$ (10 s), $^{238}U^+$ (5 s), $^{232}Th^{16}O^+$ (2 s), $^{238}U^{16}O^+$ (2 s), $^{238}U^{16}O_2{}^+$ (2 s). Average operating conditions across all sessions include a ca. 2.8nA O_2^- primary beam, ca. 30μm spot size and a mass resolution of >4500 R (1% peak height).

The Sri Lankan standard zircons M257 ($^{206}Pb/^{238}U$ age=561.3±0.3 Ma, 840 ug/g^{-1} U (Th/U approximately 0.27); Nasdala et al. (2008)) and CZ3 ($^{206}Pb/^{238}U$ age=564 ±0.3 Ma; Nelson, 1997) were used for U/Pb calibration and calculation of U and Th concentrations. During the SHRIMP sessions, 55 analyses of M257 indicated an average Pb*/U calibration uncertainty of ±1.54% (1σ), and 242 CZ3 analyses indicated an average Pb*/U calibration uncertainty of ±1.82% (1σ).

To monitor the $^{207}Pb/^{206}Pb$ ratios, analyses of the OGC-1 standard (TIMS reference value $^{207}Pb/^{206}Pb$ = 3465.4 ±0.6 Ma, $^{207}Pb^*$ = 30 ug/g^{-1}; Stern et al. (2009)) were measured during the analytical sessions. These analyses confirm the quality of the $^{207}Pb/^{206}Pb$ age data as they yielded a single group with a $^{207}Pb/^{206}Pb$ age of 3462 ±8 Ma, within uncertainty of the accepted $^{207}Pb/^{206}Pb$ age.

SHRIMP zircon analyses were reduced using CONCH software of Nelson (2006). Common Pb corrections were applied to all data using the ^{204}Pb correction method as described in Compston et al. (1984). Common Pb measured in standard analyses is considered to be on the mount surface and assumed to have an isotopic composition equivalent to Broken Hill common Pb ($^{204}Pb/^{206}Pb$=0.0625, $^{204}Pb/^{207}Pb$=0.9618, $^{204}Pb/^{208}Pb$=2.2285 Cumming and Richards 1975). All zircon dates obtained have been grouped by CONCH using the Chi-Square (χ^2) reduction method, with a χ^2 value less

than 1.75 used where age groups are quoted. Zircon dates and χ^2 age groups with 1–2 analyses are quoted to 1σ uncertainties, and χ^2 groups with more than 2 analyses are quoted at the 95% confidence level.

4.7 Results

Isotopic and chemical data from 1119 SHRIMP analyses on 958 zircons from twelve metasedimentary rock samples obtained from the Illaara and Maynard Hills greenstone belts are presented in Table 4.2. Of these, nearly 50% of the analyses are <90% concordant, mostly due to highly metamict analysis sites and zero-age Pb-loss (see the trends in the Wetherill diagrams of Figures 3 and 4). Data is summarized in Gaussian summation probability density plots in Fig. 4.5. Only analyses within 10% of concordia have been used for geological interpretations. Plots in Figures 3, 4, and 5 only show data ±20% of concordia and excludes data below ca. 3000 Ma. Interpretations based on zircons with ages younger than 3000 Ma, not shown on Figures 3, 4 or 5 uses Table 4.2 for reference.

Table 4.2: SHRIMP analytical results for detrital zircons

						Ratios									Dates (Ma)					
Grain .spot	U ppm	Th ppm	Th/U	Pb ppm	f206%	^{207}Pb/^{206}Pb 204corr	±1σ (%)	^{208}Pb/^{206}Pb 204corr	±1σ (%)	^{206}Pb/^{238}U 204corr	±1σ (%)	^{207}Pb/^{235}U 204corr	±1σ (%)	%c	^{206}Pb/^{238}U date	±1σ (Ma)	^{207}Pb/^{235}U date	±1σ (Ma)	^{207}Pb/^{206}Pb date	±1σ (Ma)
BH01 Zircons (73 analyses from 3 sessions)																				
BH01-15.2	126	40	0.31	41	0.218	0.1531	1.79	0.1056	3.68	0.299	1.51	6.309	2.48	71	1685	22	2020	22	2381	30
BH01-15.1	498	363	0.73	264	-0.019	0.1714	0.46	0.1983	0.64	0.450	2.19	10.630	2.29	93	2395	44	2491	21	2571	8
BH01-15.2	429	288	0.67	231	-0.026	0.1730	0.41	0.1938	0.58	0.457	1.84	10.907	1.93	94	2427	37	2515	18	2587	7
BH01-34.1	1557	562	0.36	694	-0.006	0.1918	0.22	0.0988	0.41	0.401	2.16	10.615	2.19	79	2175	40	2490	20	2758	4
BH01-43.1	852	242	0.28	322	2.008	0.1925	1.15	0.0432	9.83	0.331	1.86	8.778	2.31	67	1842	30	2315	21	2764	19
BH01-43.1	918	87	0.09	243	2.647	0.1952	0.86	0.0508	6.46	0.224	1.83	6.031	2.12	47	1303	22	1980	18	2786	14
BH01-50.1	1852	959	0.52	1057	0.083	0.2235	0.16	0.1315	0.31	0.488	1.82	15.038	1.85	85	2562	39	2818	18	3006	3
BH01-50.1	1173	446	0.38	690	0.135	0.2328	0.34	0.1016	0.84	0.509	1.36	16.353	1.45	86	2654	30	2898	14	3072	6
BH01-39.1	2098	114	0.05	988	0.014	0.2369	0.15	0.0191	0.89	0.436	1.82	14.228	1.85	75	2331	36	2765	18	3099	2
BH01-44.1	721	742	1.03	642	0.387	0.2460	0.23	0.2647	0.35	0.676	1.83	22.926	1.87	105	3329	48	3224	18	3159	4
BH01-22.1	702	457	0.65	495	0.007	0.2464	0.27	0.2608	0.35	0.543	2.17	18.446	2.22	88	2796	49	3013	21	3162	4
BH01-33.1	1024	608	0.59	745	0.013	0.2505	0.19	0.1714	0.31	0.594	2.16	20.530	2.19	94	3007	52	3117	21	3188	3
BH01-41.1	2068	877	0.42	1274	0.013	0.2509	0.13	0.1106	0.25	0.526	1.82	18.183	1.84	85	2723	40	2999	18	3190	2
BH01-28.1	683	678	0.99	595	-0.005	0.2522	0.21	0.2828	0.26	0.658	2.16	22.894	2.20	102	3260	55	3222	21	3199	3
BH01-44.1	561	503	0.90	544	0.105	0.2526	0.39	0.2477	0.56	0.747	1.39	26.033	1.49	112	3598	38	3348	15	3201	6
BH01-39.1	1649	94	0.06	951	0.075	0.2542	0.15	0.0211	1.31	0.524	1.82	18.380	1.85	85	2718	40	3010	18	3211	2
BH01-7.1	1140	488	0.43	450	0.049	0.2572	0.25	0.1745	0.42	0.320	2.16	11.337	2.20	55	1788	34	2551	21	3230	4
BH01-40.1	592	386	0.65	371	0.613	0.2590	0.31	0.1711	0.73	0.499	1.83	17.829	1.90	81	2611	39	2981	18	3241	5
BH01-36.1	260	278	1.07	215	0.029	0.2656	0.43	0.1846	0.76	0.663	2.19	24.302	2.29	100	3281	56	3281	22	3281	7
BH01-40.1	394	270	0.69	283	0.210	0.2658	0.32	0.1914	0.58	0.569	1.84	20.854	1.90	88	2904	43	3132	18	3281	5
BH01-20.1	425	502	1.18	379	0.024	0.2661	0.32	0.3077	0.41	0.657	2.19	24.113	2.25	99	3256	56	3273	22	3283	5
BH01-19.1	780	68	0.09	549	-0.002	0.2670	0.31	0.0242	1.19	0.633	2.18	23.313	2.24	96	3162	55	3240	22	3289	5
BH01-21.1	879	364	0.41	311	0.078	0.2671	0.34	0.3573	0.42	0.252	2.17	9.289	2.24	44	1450	28	2367	21	3289	5
BH01-27.1	203	253	1.25	169	0.018	0.2709	0.48	0.3234	0.60	0.606	2.23	22.643	2.34	92	3055	54	3212	23	3311	8
BH01-41.1	1850	696	0.38	1259	0.039	0.2713	0.13	0.1005	0.30	0.576	1.82	21.532	1.84	88	2931	43	3163	18	3313	2
BH01-25.2	683	736	1.08	586	0.054	0.2734	0.22	0.2792	0.29	0.641	1.83	24.165	1.87	96	3193	46	3275	18	3326	3
BH01-8.1	266	290	1.09	176	0.091	0.2743	0.42	0.2348	0.64	0.507	2.20	19.166	2.29	79	2642	48	3050	22	3331	7
BH01-25.1	390	837	2.14	373	-0.007	0.2746	0.34	0.5865	0.34	0.595	2.20	22.545	2.26	90	3012	53	3208	22	3332	5
BH01-25.2	613	628	1.02	512	0.092	0.2759	0.41	0.2882	0.54	0.618	1.39	23.524	1.49	93	3104	34	3249	15	3340	6
BH01-24.1	756	326	0.43	444	-0.006	0.2763	0.27	0.0992	0.63	0.497	2.17	18.927	2.22	78	2600	47	3038	21	3342	4
BH01-6.1	514	127	0.25	327	0.056	0.2772	0.31	0.0774	0.93	0.544	2.18	20.802	2.24	84	2802	50	3129	22	3347	5
BH01-18.1	1116	682	0.61	363	0.168	0.2822	0.37	0.3204	0.52	0.235	2.17	9.125	2.24	40	1358	27	2351	21	3375	6
BH01-2.1	340	63	0.18	260	-0.030	0.2904	0.34	0.0583	1.81	0.659	2.19	26.367	2.26	95	3262	56	3360	22	3420	5
BH01-3.1	465	283	0.61	182	0.040	0.2946	0.46	0.2493	0.82	0.295	2.17	11.970	2.28	48	1665	32	2602	21	3442	7
BH01-42.1	545	120	0.22	318	3.035	0.2983	0.51	0.1047	2.74	0.436	1.84	17.935	1.97	67	2333	36	2986	19	3462	8
BH01-29.2	824	287	0.35	606	0.030	0.3007	0.18	0.0920	0.45	0.614	1.83	25.440	1.86	89	3085	45	3325	18	3474	3

Continued on Next Page...

Table 4.2 – Continued

Grain .spot	U ppm	Th ppm	Th/U	Pb ppm	$f206\%$	^{207}Pb / ^{206}Pb 204corr	$\pm1\sigma$ (%)	^{208}Pb / ^{206}Pb 204corr	$\pm1\sigma$ (%)	^{206}Pb / ^{238}U 204corr	$\pm1\sigma$ (%)	^{207}Pb / ^{235}U 204corr	$\pm1\sigma$ (%)	%c	^{206}Pb / ^{238}U date	$\pm1\sigma$ (Ma)	^{207}Pb / ^{235}U date	$\pm1\sigma$ (Ma)	^{207}Pb / ^{206}Pb date	$\pm1\sigma$ (Ma)
BH01-23.1	166	218	1.31	74	0.126	0.3014	0.69	0.1447	1.50	0.355	2.25	14.750	2.43	56	1958	38	2799	23	3478	11
BH01-9.1	360	547	1.52	196	0.065	0.3022	0.36	0.1081	0.91	0.447	2.18	18.637	2.25	68	2383	43	3023	22	3482	6
BH01-32.1	914	348	0.38	314	0.130	0.3057	0.33	0.4061	0.40	0.232	2.16	9.773	2.22	38	1344	26	2414	20	3500	5
BH01-14.1	239	71	0.30	148	-0.040	0.3079	0.45	0.0653	1.48	0.524	2.22	22.257	2.32	77	2718	49	3195	23	3510	7
BH01-29.2	681	228	0.34	549	0.022	0.3112	0.20	0.0884	0.52	0.668	1.83	28.675	1.86	94	3299	47	3442	18	3527	3
BH01-13.1	960	1124	1.17	228	0.028	0.3116	0.38	0.2527	0.55	0.176	2.16	7.554	2.24	30	1044	21	2179	20	3529	6
BH01-10.1	175	125	0.72	168	0.043	0.3129	0.53	0.1702	1.44	0.751	2.26	32.398	2.38	102	3611	62	3562	23	3535	8
BH01-29.1	756	191	0.25	662	0.007	0.3162	0.19	0.0732	0.49	0.732	2.16	31.898	2.20	100	3539	59	3547	22	3552	3
BH01-48.1	357	255	0.71	160	1.371	0.3180	0.48	0.1322	1.88	0.342	1.84	14.974	1.96	53	1894	30	2814	19	3560	7
BH01-17.1	239	40	0.17	152	-0.011	0.3202	0.45	0.0633	1.25	0.535	2.22	23.608	2.33	77	2761	50	3252	23	3571	7
BH01-53.1	201	30	0.15	177	0.058	0.3207	0.65	0.0399	3.54	0.751	1.50	33.186	1.71	101	3609	41	3586	17	3573	10
BH01-12.1	70	27	0.39	60	-0.120	0.3214	0.74	0.1060	2.25	0.706	2.40	31.294	2.60	96	3444	64	3528	26	3576	11
BH01-16.1	343	559	1.63	219	0.076	0.3214	0.41	0.1226	1.02	0.512	2.21	22.666	2.29	74	2663	48	3213	22	3576	6
BH01-42.1	334	227	0.68	249	0.971	0.3221	0.38	0.0659	2.74	0.604	1.85	26.810	1.93	85	3044	45	3377	19	3580	6
BH01-51.1	228	74	0.32	140	0.241	0.3220	0.70	0.0522	3.95	0.515	1.47	22.854	1.70	75	2677	32	3221	17	3580	11
BH01-35.2	342	90	0.26	303	0.003	0.3244	0.28	0.0654	0.75	0.740	1.85	33.109	1.90	99	3572	51	3584	19	3591	4
BH01-48.1	314	228	0.73	128	1.082	0.3249	0.88	0.1690	2.70	0.305	1.40	13.657	1.75	48	1716	21	2726	17	3593	14
BH01-52.2	64	30	0.47	35	1.073	0.3256	1.69	0.1887	4.36	0.404	1.70	18.138	2.54	61	2187	31	2997	24	3597	26
BH01-35.1	327	82	0.25	326	-0.038	0.3266	0.28	0.0662	0.80	0.833	2.19	37.521	2.24	108	3907	64	3707	22	3601	4
BH01-35.2	339	88	0.26	305	0.028	0.3266	0.30	0.0666	0.93	0.750	1.86	33.760	1.92	100	3606	51	3603	19	3601	5
BH01-52.1	54	51	0.94	57	0.144	0.3278	1.40	0.2539	2.76	0.768	1.87	34.713	2.47	102	3673	52	3631	24	3607	22
BH01-45.1	436	99	0.23	374	0.076	0.3286	0.42	0.0671	1.39	0.713	1.40	32.320	1.51	96	3471	38	3560	15	3610	6
BH01-45.1	421	88	0.21	336	0.123	0.3290	0.26	0.0664	1.11	0.660	1.84	29.946	1.89	90	3268	47	3485	19	3612	4
BH01-12.2	114	110	0.96	106	0.537	0.3311	1.00	0.1205	3.69	0.729	1.61	33.264	2.00	97	3528	44	3588	20	3622	15
BH01-5.1	190	150	0.79	195	0.001	0.3310	0.38	0.2033	0.58	0.779	2.23	35.551	2.31	103	3713	63	3654	23	3622	6
BH01-10.2	171	120	0.70	172	0.247	0.3352	0.73	0.1742	1.56	0.766	1.53	35.399	1.78	101	3666	43	3650	18	3641	11
BH01-31.1	271	100	0.37	164	0.028	0.3366	0.40	0.1859	0.77	0.461	2.19	21.400	2.28	67	2444	45	3157	22	3647	6
BH01-26.1	288	73	0.25	106	0.011	0.3450	0.53	0.2367	0.78	0.271	2.21	12.872	2.33	42	1544	30	2670	22	3685	8
BH01-11.2	186	123	0.66	187	0.111	0.3474	0.70	0.1642	1.59	0.770	1.50	36.876	1.73	100	3680	42	3690	17	3696	11
BH01-11.1	187	156	0.84	194	0.022	0.3477	0.43	0.2151	0.80	0.768	2.25	36.807	2.35	99	3673	63	3688	23	3697	7
BH01-38.1	145	115	0.79	141	0.091	0.3515	0.41	0.1667	0.86	0.744	1.88	36.066	1.98	97	3586	52	3668	20	3714	6
BH01-47.1	147	99	0.67	148	0.074	0.3515	0.39	0.1689	0.82	0.769	1.88	37.289	1.97	99	3678	53	3701	19	3714	6
BH01-30.2	117	69	0.59	118	-0.020	0.3543	0.47	0.1517	1.25	0.782	1.90	38.196	2.02	100	3724	54	3725	20	3725	7
BH01-47.1	118	73	0.62	125	0.024	0.3542	0.74	0.1627	1.29	0.814	1.59	39.728	1.83	103	3837	46	3764	18	3725	11
BH01-30.2	99	57	0.57	99	0.075	0.3552	0.49	0.1398	1.14	0.775	1.92	37.941	2.04	99	3698	54	3718	20	3729	7
BH01-38.1	136	88	0.65	142	0.008	0.3552	0.40	0.1585	0.78	0.803	1.89	39.300	1.98	102	3798	54	3753	20	3729	6
BH01-30.1	111	58	0.52	121	0.063	0.3562	0.51	0.1322	1.56	0.852	2.28	41.853	2.40	106	3973	68	3816	24	3734	8

BH02 Zircons (107 analyses from 2 sessions)

Continued on Next Page. . .

Table 4.2 – Continued

Grain .spot	U ppm	Th ppm	Th/U	Pb ppm	$f206\%$	$^{207}Pb/^{206}Pb$ 204corr	$\pm1\sigma$ (%)	$^{208}Pb/^{206}Pb$ 204corr	$\pm1\sigma$ (%)	$^{206}Pb/^{238}U$ 204corr	$\pm1\sigma$ (%)	$^{207}Pb/^{235}U$ 204corr	$\pm1\sigma$ (%)	%c	$^{206}Pb/^{238}U$ date	$\pm1\sigma$ (Ma)	$^{207}Pb/^{235}U$ date	$\pm1\sigma$ (Ma)	$^{207}Pb/^{206}Pb$ date	$\pm1\sigma$ (Ma)
BH02-53.1	2225	747	0.34	1270	0.001	0.1703	0.18	0.1651	0.24	0.497	2.16	11.660	2.19	102	2600	46	2578	20	2560	3
BH02-53.1	2225	747	0.34	1270	0.001	0.1703	0.18	0.1651	0.24	0.497	2.16	11.660	2.19	102	2600	46	2578	20	2560	3
BH02-7.1	1530	397	0.26	776	0.007	0.1980	0.19	0.0778	0.40	0.462	1.29	12.605	1.32	87	2447	26	2651	12	2810	3
BH02-37.1	1253	1095	0.87	363	-0.022	0.2168	0.35	0.3905	0.38	0.209	1.29	6.262	1.38	41	1226	14	2013	12	2957	6
BH02-16.1	1035	2593	2.50	370	0.038	0.2369	0.29	0.3851	0.31	0.256	1.29	8.353	1.36	47	1468	17	2270	12	3099	5
BH02-29.1	348	180	0.52	246	0.032	0.2728	0.34	0.1365	0.72	0.582	1.34	21.895	1.42	89	2957	32	3179	14	3322	5
BH02-69.1	391	211	0.54	270	0.019	0.2761	0.35	0.1193	0.72	0.574	2.19	21.863	2.26	88	2925	51	3178	22	3341	5
BH02-69.1	391	211	0.54	270	0.019	0.2761	0.35	0.1193	0.72	0.574	2.19	21.863	2.26	88	2925	51	3178	22	3341	5
BH02-56.1	954	217	0.23	217	0.208	0.2787	0.42	0.2648	0.67	0.170	2.16	6.525	2.25	30	1011	20	2049	20	3356	7
BH02-56.1	954	217	0.23	217	0.208	0.2787	0.42	0.2648	0.67	0.170	2.16	6.525	2.25	30	1011	20	2049	20	3356	7
BH02-12.1	245	154	0.63	209	-0.006	0.2811	0.35	0.1633	0.58	0.688	1.36	26.659	1.44	100	3375	36	3371	14	3369	5
BH02-52.1	373	176	0.47	272	0.017	0.2943	0.33	0.0516	1.85	0.628	2.19	25.496	2.25	91	3143	54	3327	22	3440	5
BH02-52.1	373	176	0.47	272	0.017	0.2943	0.33	0.0516	1.85	0.628	2.19	25.496	2.25	91	3143	54	3327	22	3440	5
BH02-19.1	570	709	1.24	158	0.075	0.2981	0.39	0.3104	0.54	0.200	1.30	8.210	1.40	34	1174	14	2254	13	3460	6
BH02-23.1	283	97	0.34	250	-0.023	0.3162	0.31	0.1333	0.62	0.710	1.35	30.954	1.42	97	3458	36	3518	14	3552	5
BH02-15.1	270	157	0.58	180	-0.005	0.3170	0.37	0.2950	0.49	0.482	1.35	21.048	1.45	71	2534	28	3141	14	3555	6
BH02-3.1	237	311	1.31	111	0.012	0.3224	0.42	0.2925	0.57	0.336	1.34	14.959	1.45	52	1870	22	2813	14	3581	6
BH02-70.1	453	287	0.63	189	0.105	0.3228	0.40	0.3951	0.51	0.280	2.18	12.478	2.26	44	1593	31	2641	21	3583	6
BH02-70.1	453	287	0.63	189	0.105	0.3228	0.40	0.3951	0.51	0.280	2.18	12.478	2.26	44	1593	31	2641	21	3583	6
BH02-76.1	267	140	0.52	205	-0.023	0.3261	0.36	0.1715	0.63	0.597	2.20	26.824	2.28	84	3016	53	3377	22	3599	6
BH02-76.1	267	140	0.52	205	-0.023	0.3261	0.36	0.1715	0.63	0.597	2.20	26.824	2.28	84	3016	53	3377	22	3599	6
BH02-63.1	249	59	0.24	147	0.014	0.3296	0.39	0.1391	0.73	0.466	2.20	21.187	2.29	68	2467	45	3147	22	3615	6
BH02-63.1	249	59	0.24	147	0.014	0.3296	0.39	0.1391	0.73	0.466	2.20	21.187	2.29	68	2467	45	3147	22	3615	6
BH02-46.1	301	254	0.84	266	-0.025	0.3329	0.31	0.2307	0.47	0.657	1.35	30.175	1.43	90	3257	35	3493	14	3630	5
BH02-11.1	309	154	0.50	306	0.014	0.3333	0.29	0.2253	0.51	0.739	1.34	33.954	1.41	98	3566	37	3609	14	3632	4
BH02-33.1	226	90	0.40	209	-0.016	0.3341	0.37	0.1052	1.03	0.748	1.38	34.437	1.47	99	3599	38	3623	15	3636	6
BH02-2.1	571	357	0.63	218	0.045	0.3347	0.30	0.3410	0.39	0.264	1.31	12.186	1.38	42	1511	18	2619	13	3639	5
BH02-79.1	367	751	2.05	341	-0.025	0.3369	0.28	0.2835	0.40	0.666	2.19	30.933	2.24	90	3290	56	3517	22	3649	4
BH02-79.1	367	751	2.05	341	-0.025	0.3369	0.28	0.2835	0.40	0.666	2.19	30.933	2.24	90	3290	56	3517	22	3649	4
BH02-50.1	141	357	2.54	122	0.033	0.3398	0.57	0.1914	1.47	0.660	1.46	30.942	1.63	89	3269	37	3517	16	3662	9
BH02-40.1	356	367	1.03	224	-0.051	0.3401	0.37	0.3101	0.51	0.443	1.35	20.797	1.44	65	2366	27	3129	14	3663	6
BH02-72.1	163	169	1.04	125	-0.015	0.3414	0.47	0.2026	0.83	0.576	2.23	27.102	2.34	80	2931	53	3387	23	3669	7
BH02-72.1	163	169	1.04	125	-0.015	0.3414	0.47	0.2026	0.83	0.576	2.23	27.102	2.34	80	2931	53	3387	23	3669	7
BH02-18.1	212	387	1.82	182	-0.005	0.3416	0.37	0.2114	0.57	0.641	1.38	30.214	1.47	87	3195	35	3494	14	3670	6
BH02-64.1	305	190	0.62	190	0.083	0.3424	0.38	0.2623	0.64	0.450	2.19	21.249	2.27	65	2395	44	3150	22	3674	6
BH02-64.1	305	190	0.62	190	0.083	0.3424	0.38	0.2623	0.64	0.450	2.19	21.249	2.27	65	2395	44	3150	22	3674	6
BH02-62.1	99	47	0.48	96	-0.065	0.3432	0.57	0.1356	1.45	0.760	2.32	35.975	2.46	99	3645	65	3666	24	3677	9
BH02-62.1	99	47	0.48	96	-0.065	0.3432	0.57	0.1356	1.45	0.760	2.32	35.975	2.46	99	3645	65	3666	24	3677	9
BH02-17.1	284	426	1.50	262	0.011	0.3434	0.34	0.3103	0.46	0.648	1.37	30.685	1.45	88	3220	35	3509	14	3678	5
BH02-55.1	278	456	1.64	171	0.034	0.3461	0.41	0.2195	0.66	0.457	2.20	21.803	2.29	66	2426	45	3175	22	3690	6

Continued on Next Page...

Table 4.2 – Continued

Grain .spot	U ppm	Th ppm	Th/U	Pb ppm	$f206\%$	^{207}Pb / ^{206}Pb 204corr	$\pm1\sigma$ (%)	^{208}Pb / ^{206}Pb 204corr	$\pm1\sigma$ (%)	^{206}Pb / ^{238}U 204corr	$\pm1\sigma$ (%)	^{207}Pb / ^{235}U 204corr	$\pm1\sigma$ (%)	%c	^{206}Pb / ^{238}U date	$\pm1\sigma$ (Ma)	^{207}Pb / ^{235}U date	$\pm1\sigma$ (Ma)	^{207}Pb / ^{206}Pb date	$\pm1\sigma$ (Ma)
BH02-55.1	278	456	1.64	171	0.034	0.3461	0.41	0.2195	0.66	0.457	2.20	21.803	2.29	66	2426	45	3175	22	3690	6
BH02-36.1	266	302	1.13	253	-0.013	0.3463	0.33	0.2207	0.57	0.703	1.36	33.561	1.44	93	3432	36	3597	14	3691	5
BH02-66.1	230	219	0.95	244	-0.008	0.3469	0.34	0.2572	0.50	0.770	2.21	36.829	2.28	100	3681	62	3689	22	3693	5
BH02-66.1	230	219	0.95	244	-0.008	0.3469	0.34	0.2572	0.50	0.770	2.21	36.829	2.28	100	3681	62	3689	22	3693	5
BH02-75.1	176	161	0.91	162	-0.026	0.3472	0.39	0.1974	0.65	0.694	2.23	33.214	2.31	92	3397	59	3587	23	3695	6
BH02-75.1	176	161	0.91	162	-0.026	0.3472	0.39	0.1974	0.65	0.694	2.23	33.214	2.31	92	3397	59	3587	23	3695	6
BH02-32.1	217	191	0.88	127	-0.024	0.3476	0.46	0.1640	1.04	0.451	1.38	21.620	1.51	65	2400	28	3167	15	3697	7
BH02-42.1	221	113	0.51	172	-0.031	0.3478	0.38	0.1594	0.77	0.601	1.37	28.838	1.47	82	3035	33	3448	14	3697	6
BH02-74.1	206	130	0.63	214	-0.023	0.3514	0.36	0.1613	0.69	0.799	2.23	38.733	2.30	102	3787	64	3739	23	3713	5
BH02-74.1	206	130	0.63	214	-0.023	0.3514	0.36	0.1613	0.69	0.799	2.23	38.733	2.30	102	3787	64	3739	23	3713	5
BH02-14.1	154	321	2.09	128	-0.003	0.3524	0.40	0.1373	0.74	0.650	1.40	31.587	1.50	87	3229	36	3538	15	3717	6
BH02-78.1	268	241	0.90	244	-0.002	0.3522	0.36	0.2767	0.50	0.649	2.21	31.517	2.28	87	3224	56	3535	22	3717	5
BH02-78.1	268	241	0.90	244	-0.002	0.3522	0.36	0.2767	0.50	0.649	2.21	31.517	2.28	87	3224	56	3535	22	3717	5
BH02-68.1	180	175	0.97	178	-0.017	0.3525	0.40	0.2143	0.71	0.735	2.23	35.739	2.31	96	3553	61	3659	23	3718	6
BH02-68.1	180	175	0.97	178	-0.017	0.3525	0.40	0.2143	0.71	0.735	2.23	35.739	2.31	96	3553	61	3659	23	3718	6
BH02-31.1	274	188	0.69	156	0.020	0.3532	0.40	0.2466	0.58	0.414	1.36	20.164	1.47	60	2233	26	3099	14	3721	6
BH02-28.1	288	193	0.67	283	0.008	0.3536	0.29	0.1823	0.51	0.741	1.36	36.145	1.42	96	3576	37	3670	14	3722	4
BH02-49.1	371	265	0.72	302	-0.008	0.3534	0.30	0.2159	0.46	0.604	1.34	29.426	1.41	82	3046	33	3468	14	3722	5
BH02-45.1	164	76	0.46	161	-0.017	0.3549	0.40	0.1180	0.88	0.777	1.43	38.044	1.53	99	3708	40	3721	15	3728	6
BH02-54.1	209	127	0.61	172	0.019	0.3549	0.43	0.1924	0.83	0.618	2.23	30.252	2.33	83	3103	55	3495	23	3728	7
BH02-54.1	209	127	0.61	172	0.019	0.3549	0.43	0.1924	0.83	0.618	2.23	30.252	2.33	83	3103	55	3495	23	3728	7
BH02-30.1	120	66	0.55	118	-0.012	0.3552	0.47	0.1405	0.89	0.762	1.47	37.311	1.60	98	3651	41	3702	16	3729	7
BH02-60.1	211	106	0.50	209	0.000	0.3558	0.41	0.1282	0.79	0.776	2.23	38.089	2.31	99	3704	63	3722	23	3732	6
BH02-60.1	211	106	0.50	209	0.000	0.3558	0.41	0.1282	0.79	0.776	2.23	38.089	2.31	99	3704	63	3722	23	3732	6
BH02-4.1	188	91	0.48	166	0.019	0.3562	0.37	0.1495	0.89	0.680	1.39	33.401	1.48	90	3345	36	3593	15	3734	6
BH02-57.1	205	143	0.70	225	-0.015	0.3564	0.37	0.1822	0.64	0.830	2.23	40.778	2.30	104	3895	65	3790	23	3734	6
BH02-57.1	205	143	0.70	225	-0.015	0.3564	0.37	0.1822	0.64	0.830	2.23	40.778	2.30	104	3895	65	3790	23	3734	6
BH02-61.1	126	116	0.92	105	-0.017	0.3562	0.48	0.1516	0.91	0.640	2.26	31.419	2.37	85	3188	57	3532	23	3734	7
BH02-61.1	126	116	0.92	105	-0.017	0.3562	0.48	0.1516	0.91	0.640	2.26	31.419	2.37	85	3188	57	3532	23	3734	7
BH02-27.1	187	332	1.77	146	-0.013	0.3565	0.42	0.1886	0.76	0.588	1.39	28.920	1.50	80	2983	33	3451	15	3735	6
BH02-71.1	293	452	1.54	356	0.012	0.3568	0.29	0.3967	0.36	0.802	2.20	39.473	2.25	102	3797	63	3758	22	3736	4
BH02-71.1	293	452	1.54	356	0.012	0.3568	0.29	0.3967	0.36	0.802	2.20	39.473	2.25	102	3797	63	3758	22	3736	4
BH02-21.1	144	77	0.54	150	-0.016	0.3571	0.42	0.1429	0.98	0.810	1.42	39.853	1.53	102	3823	41	3767	15	3737	6
BH02-39.1	195	65	0.33	168	0.031	0.3571	0.43	0.0976	1.06	0.684	1.42	33.672	1.54	90	3359	37	3600	15	3737	7
BH02-51.1	147	90	0.61	159	-0.030	0.3570	0.42	0.1580	0.76	0.831	2.26	40.915	2.35	104	3900	66	3793	23	3737	6
BH02-51.1	147	90	0.61	159	-0.030	0.3570	0.42	0.1580	0.76	0.831	2.26	40.915	2.35	104	3900	66	3793	23	3737	6
BH02-9.1	231	187	0.81	244	-0.002	0.3573	0.31	0.2137	0.48	0.780	1.37	38.446	1.44	99	3719	39	3731	14	3738	5
BH02-43.1	147	119	0.81	151	-0.023	0.3575	0.42	0.2049	0.72	0.763	1.46	37.635	1.57	98	3657	41	3710	16	3739	6
BH02-22.1	241	198	0.82	249	-0.026	0.3578	0.32	0.2000	0.52	0.770	1.37	37.983	1.45	98	3680	38	3719	14	3741	5
BH02-73.1	196	93	0.48	198	-0.035	0.3579	0.36	0.1208	0.76	0.796	2.22	39.288	2.30	101	3775	64	3753	23	3741	6

Continued on Next Page. . .

Table 4.2 – Continued

Grain .spot	U ppm	Th ppm	Th/U	Pb ppm	$f206\%$	$^{207}Pb/^{206}Pb$ 204corr	$\pm1\sigma$ (%)	$^{208}Pb/^{206}Pb$ 204corr	$\pm1\sigma$ (%)	$^{206}Pb/^{238}U$ 204corr	$\pm1\sigma$ (%)	$^{207}Pb/^{235}U$ 204corr	$\pm1\sigma$ (%)	%c	$^{206}Pb/^{238}U$ date	$\pm1\sigma$ (Ma)	$^{207}Pb/^{235}U$ date	$\pm1\sigma$ (Ma)	$^{207}Pb/^{206}Pb$ date	$\pm1\sigma$ (Ma)
BH02-73.1	196	93	0.48	198	-0.035	0.3579	0.36	0.1208	0.76	0.796	2.22	39.288	2.30	101	3775	64	3753	23	3741	6
BH02-67.1	207	121	0.58	213	-0.064	0.3581	0.35	0.1484	0.72	0.792	2.22	39.118	2.29	101	3761	63	3749	23	3742	5
BH02-67.1	207	121	0.58	213	-0.064	0.3581	0.35	0.1484	0.72	0.792	2.22	39.118	2.29	101	3761	63	3749	23	3742	5
BH02-59.1	279	220	0.79	311	0.005	0.3585	0.29	0.1995	0.46	0.832	2.21	41.105	2.26	104	3901	65	3798	22	3744	4
BH02-59.1	279	220	0.79	311	0.005	0.3585	0.29	0.1995	0.46	0.832	2.21	41.105	2.26	104	3901	65	3798	22	3744	4
BH02-77.1	125	130	1.04	131	-0.038	0.3587	0.51	0.2217	0.99	0.773	2.28	38.243	2.40	99	3692	64	3726	24	3745	8
BH02-77.1	125	130	1.04	131	-0.038	0.3587	0.51	0.2217	0.99	0.773	2.28	38.243	2.40	99	3692	64	3726	24	3745	8
BH02-35.1	209	159	0.76	204	-0.019	0.3592	0.37	0.1961	0.61	0.727	1.39	36.021	1.49	94	3523	38	3667	15	3746	6
BH02-1.1	42	17	0.39	43	0.073	0.3592	0.83	0.0997	3.94	0.806	1.73	39.907	2.01	102	3810	50	3768	20	3747	13
BH02-44.1	170	115	0.68	168	-0.014	0.3595	0.40	0.1744	0.77	0.749	1.42	37.140	1.52	96	3605	39	3697	15	3748	6
BH02-48.1	122	85	0.69	115	-0.051	0.3595	0.49	0.1933	0.95	0.701	1.46	34.743	1.60	91	3424	39	3631	16	3748	7
BH02-41.1	128	58	0.45	127	-0.027	0.3599	0.48	0.1159	1.46	0.782	1.47	38.794	1.60	99	3724	41	3740	16	3749	7
BH02-80.1	278	156	0.56	283	-0.007	0.3601	0.31	0.1484	0.62	0.782	2.21	38.810	2.27	99	3723	62	3741	22	3750	5
BH02-80.1	278	156	0.56	283	-0.007	0.3601	0.31	0.1484	0.62	0.782	2.21	38.810	2.27	99	3723	62	3741	22	3750	5
BH02-65.1	118	66	0.56	128	0.000	0.3606	0.47	0.1468	1.00	0.839	2.29	41.713	2.39	105	3928	67	3812	24	3752	7
BH02-65.1	118	66	0.56	128	0.000	0.3606	0.47	0.1468	1.00	0.839	2.29	41.713	2.39	105	3928	67	3812	24	3752	7
BH02-25.1	118	150	1.28	118	0.045	0.3606	0.47	0.2384	0.72	0.727	1.47	36.154	1.60	94	3523	40	3671	16	3753	7
BH02-8.1	72	45	0.62	74	0.028	0.3608	0.56	0.1556	1.18	0.787	1.57	39.149	1.73	100	3743	45	3749	17	3753	8
BH02-6.1	197	127	0.64	196	-0.023	0.3615	0.35	0.1790	0.64	0.752	1.39	37.462	1.47	96	3613	38	3706	15	3756	5
BH02-13.1	153	103	0.67	156	-0.019	0.3617	0.38	0.1731	0.70	0.769	1.41	38.332	1.50	98	3676	39	3729	15	3757	6
BH02-5.1	220	235	1.07	239	-0.031	0.3619	0.31	0.2641	0.47	0.773	1.36	38.581	1.44	98	3693	38	3735	14	3758	5
BH02-10.1	183	86	0.47	187	-0.029	0.3627	0.36	0.1223	0.79	0.799	1.40	39.966	1.49	101	3786	40	3770	15	3761	5
BH02-26.1	135	109	0.81	135	-0.008	0.3628	0.45	0.2030	0.74	0.743	1.46	37.168	1.58	95	3582	40	3698	16	3762	7
BH02-34.1	119	60	0.50	110	-0.047	0.3635	0.55	0.1399	1.60	0.713	1.48	35.753	1.64	92	3471	40	3660	16	3764	8
BH02-58.1	133	153	1.15	113	0.026	0.3641	0.48	0.1852	0.81	0.637	2.26	31.970	2.37	84	3176	57	3549	23	3767	7
BH02-58.1	133	153	1.15	113	0.026	0.3641	0.48	0.1852	0.81	0.637	2.26	31.970	2.37	84	3176	57	3549	23	3767	7
BH02-47.1	68	43	0.62	70	-0.063	0.3652	0.72	0.1598	2.22	0.787	1.62	39.634	1.86	99	3743	46	3762	18	3771	11
MA01 Zircons (72 analyses from 3 sessions)																				
MA01-38.3	2123	244	0.11	913	0.050	0.1695	0.13	0.0299	0.61	0.416	1.53	9.729	1.55	88	2244	29	2409	14	2552	2
MA01-38.2	3380	600	0.18	1300	0.058	0.1755	0.21	0.0487	0.83	0.364	2.07	8.818	2.11	77	2003	36	2319	19	2611	4
MA01-38.1	1528	281	0.18	958	0.107	0.2113	0.16	0.0561	0.68	0.573	1.45	16.683	1.48	100	2919	34	2917	14	2916	3
MA01-5.1	603	1887	3.13	191	3.573	0.2995	0.65	0.2909	1.42	0.208	1.46	8.583	1.67	35	1217	16	2295	15	3468	10
MA01-20.1	680	5358	7.87	181	4.062	0.3098	0.70	0.2888	1.60	0.171	1.46	7.315	1.70	29	1019	14	2151	15	3520	11
MA01-35.1	431	795	1.84	151	2.417	0.3123	0.60	0.1575	2.28	0.255	1.47	10.993	1.65	41	1466	19	2523	15	3533	9
MA01-40.1	566	2060	3.64	168	2.864	0.3284	0.59	0.2225	1.73	0.203	1.46	9.181	1.64	33	1190	16	2356	15	3609	9
MA01-26.1	374	1136	3.04	222	1.815	0.3306	0.49	0.2132	1.45	0.421	1.48	19.179	1.62	63	2264	28	3051	16	3620	8
MA01-30.1	124	380	3.06	51	0.567	0.3409	0.68	0.2725	1.48	0.290	1.51	13.624	1.73	45	1641	22	2724	16	3667	10
MA01-7.1	325	660	2.03	185	1.295	0.3434	0.45	0.2326	1.23	0.402	1.47	19.014	1.60	59	2176	27	3043	15	3678	7

Continued on Next Page. . .

Table 4.2 – Continued

Grain .spot	U ppm	Th ppm	Th/U	Pb ppm	$f206\%$	^{207}Pb / ^{206}Pb 204corr	$\pm1\sigma$ (%)	^{208}Pb / ^{206}Pb 204corr	$\pm1\sigma$ (%)	^{206}Pb / ^{238}U 204corr	$\pm1\sigma$ (%)	^{207}Pb / ^{235}U 204corr	$\pm1\sigma$ (%)	%c	^{206}Pb / ^{238}U date	$\pm1\sigma$ (Ma)	^{207}Pb / ^{235}U date	$\pm1\sigma$ (Ma)	^{207}Pb / ^{206}Pb date	$\pm1\sigma$ (Ma)
MA01-54.1	379	3827	10.10	228	1.871	0.3453	0.48	0.4210	0.83	0.375	1.48	17.853	1.61	56	2053	26	2982	15	3687	7
MA01-42.1	416	4113	9.88	119	2.900	0.3459	0.67	0.2803	1.68	0.187	1.47	8.906	1.69	30	1104	15	2328	15	3689	10
MA01-62.1	59	30	0.51	52	2.020	0.3459	5.71	0.0861	47.94	0.683	3.18	32.592	6.87	91	3357	83	3568	68	3689	87
MA01-15.1	471	2904	6.16	171	4.064	0.3462	0.64	0.2582	1.79	0.231	1.47	11.034	1.67	36	1341	18	2526	16	3690	10
MA01-2.1	166	349	2.10	97	0.529	0.3483	0.50	0.1519	1.72	0.447	1.51	21.474	1.65	64	2383	30	3160	16	3700	8
MA01-68.1	304	551	1.82	104	2.064	0.3497	2.25	0.1851	8.47	0.246	1.86	11.846	3.09	38	1416	24	2592	29	3706	34
MA01-67.1	79	34	0.43	83	1.230	0.3499	3.29	0.0866	25.22	0.822	2.82	39.658	4.59	104	3867	82	3762	46	3707	50
MA01-33.1	70	219	3.12	63	0.420	0.3509	0.69	0.1621	2.29	0.684	1.60	33.080	1.82	91	3359	42	3583	18	3711	11
MA01-70.2	31	19	0.62	29	2.488	0.3511	3.95	0.0437	53.84	0.721	3.49	34.911	5.59	94	3500	94	3636	55	3712	60
MA01-13.1	91	331	3.61	72	0.438	0.3514	0.60	0.1328	2.19	0.605	1.57	29.322	1.74	82	3051	38	3464	17	3713	9
MA01-24.1	482	1491	3.10	214	2.961	0.3517	0.52	0.2698	1.37	0.290	1.47	14.068	1.62	44	1642	21	2754	15	3714	8
MA01-57.1	108	129	1.19	124	0.327	0.3524	1.71	0.2869	4.03	0.804	2.33	39.084	3.06	102	3804	67	3748	30	3718	26
MA01-65.1	41	20	0.48	42	0.162	0.3526	2.29	0.1304	7.66	0.788	3.01	38.304	4.01	101	3746	86	3728	40	3718	35
MA01-70.1	31	10	0.31	29	1.281	0.3534	4.73	0.0626	48.70	0.717	3.78	34.961	6.41	94	3486	102	3638	63	3722	72
MA01-53.1	184	390	2.12	104	0.483	0.3542	0.50	0.2154	1.27	0.413	1.50	20.173	1.64	60	2229	28	3100	16	3725	8
MA01-22.1	124	161	1.30	103	0.275	0.3552	0.48	0.2929	0.96	0.579	1.53	28.335	1.66	79	2943	36	3431	16	3729	7
MA01-44.1	34	19	0.56	35	0.020	0.3552	0.78	0.1464	1.94	0.809	1.77	39.621	2.02	102	3821	51	3761	20	3730	12
MA01-48.1	161	315	1.96	130	0.240	0.3552	0.44	0.3161	0.83	0.557	1.51	27.271	1.63	77	2853	35	3393	16	3730	7
MA01-18.1	109	201	1.85	61	0.313	0.3555	0.63	0.1384	2.07	0.430	1.53	21.070	1.72	62	2305	30	3142	17	3731	10
MA01-19.1	76	53	0.70	34	1.453	0.3556	1.00	0.1018	5.93	0.340	1.57	16.689	1.96	51	1888	26	2917	19	3731	15
MA01-47.1	198	60	0.30	181	0.116	0.3557	0.35	0.0732	1.72	0.741	1.50	36.333	1.59	96	3573	41	3676	16	3732	5
MA01-61.1	123	68	0.55	121	0.260	0.3558	1.97	0.1401	8.55	0.764	2.35	37.475	3.25	98	3658	66	3706	32	3732	30
MA01-17.1	31	8	0.26	32	0.101	0.3566	0.88	0.0681	5.34	0.832	1.78	40.908	2.08	104	3903	52	3793	21	3735	13
MA01-25.1	226	293	1.30	230	0.125	0.3569	0.31	0.1658	0.83	0.773	1.49	38.029	1.56	99	3691	42	3721	15	3737	5
MA01-23.1	47	49	1.06	50	0.042	0.3573	0.66	0.2406	1.34	0.784	1.67	38.642	1.87	100	3733	47	3736	19	3738	10
MA01-49.1	347	578	1.66	189	1.148	0.3572	0.42	0.2087	1.24	0.389	1.47	19.143	1.58	57	2117	27	3049	15	3738	6
MA01-8.1	236	278	1.18	199	0.186	0.3574	0.34	0.1722	0.92	0.637	1.49	31.376	1.57	85	3176	37	3531	15	3739	5
MA01-12.1	146	138	0.95	128	0.212	0.3576	0.42	0.1164	1.50	0.689	1.52	33.984	1.63	90	3379	40	3610	16	3740	6
MA01-29.1	106	143	1.35	81	0.272	0.3579	0.56	0.2633	1.22	0.541	1.55	26.710	1.71	75	2789	35	3373	17	3741	9
MA01-14.1	135	252	1.86	114	0.239	0.3585	0.46	0.1934	1.20	0.625	1.52	30.900	1.64	84	3130	38	3516	16	3743	7
MA01-16.1	171	223	1.30	119	0.212	0.3583	0.42	0.1417	1.31	0.532	1.50	26.282	1.61	73	2750	34	3357	16	3743	6
MA01-36.1	41	20	0.48	43	0.002	0.3588	0.68	0.1218	1.84	0.825	1.71	40.843	1.92	104	3880	50	3791	19	3745	10
MA01-27.1	195	394	2.02	113	0.775	0.3592	0.91	0.1550	3.27	0.433	1.56	21.464	1.90	62	2321	30	3160	18	3746	14
MA01-37.1	63	36	0.57	66	0.214	0.3591	0.62	0.1450	1.83	0.810	1.63	40.118	1.81	102	3826	47	3774	18	3746	9
MA01-6.1	143	572	4.00	130	0.542	0.3591	0.46	0.2042	1.25	0.665	1.52	32.938	1.65	88	3287	39	3579	16	3746	7
MA01-32.1	204	133	0.65	205	0.120	0.3592	0.32	0.1630	0.84	0.766	1.50	37.926	1.57	98	3665	42	3718	16	3747	5
MA01-52.1	17	7	0.41	17	0.331	0.3592	1.27	0.1033	5.81	0.797	2.04	39.490	2.54	101	3779	58	3758	25	3747	19
MA01-64.1	123	70	0.57	119	0.263	0.3595	1.41	0.1445	5.48	0.741	2.12	36.747	2.69	95	3576	58	3687	27	3748	21
MA01-60.1	92	38	0.42	83	0.349	0.3599	1.76	0.1032	9.25	0.707	2.36	35.060	3.11	92	3445	63	3640	31	3749	27
MA01-45.1	175	201	1.15	156	0.316	0.3601	0.40	0.2018	1.03	0.654	1.51	32.475	1.61	86	3244	38	3565	16	3750	6

Continued on Next Page. . .

Table 4.2 – Continued

Grain .spot	U ppm	Th ppm	Th/U	Pb ppm	f206%	$^{207}Pb/^{206}Pb$ 204corr	±1σ (%)	$^{208}Pb/^{206}Pb$ 204corr	±1σ (%)	$^{206}Pb/^{238}U$ 204corr	±1σ (%)	$^{207}Pb/^{235}U$ 204corr	±1σ (%)	%c	$^{206}Pb/^{238}U$ date	±1σ (Ma)	$^{207}Pb/^{235}U$ date	±1σ (Ma)	$^{207}Pb/^{206}Pb$ date	±1σ (Ma)
MA01-46.1	107	70	0.65	108	0.077	0.3603	0.46	0.1598	1.18	0.766	1.55	38.068	1.67	98	3667	43	3722	17	3751	7
MA01-9.1	219	595	2.71	175	0.330	0.3602	0.37	0.1536	1.14	0.605	1.49	30.065	1.58	81	3051	36	3489	16	3751	6
MA01-10.1	77	85	1.10	86	0.199	0.3607	0.54	0.2660	1.10	0.789	1.59	39.240	1.74	100	3749	45	3752	17	3753	8
MA01-3.1	101	103	1.01	105	0.049	0.3610	0.46	0.1903	1.09	0.775	1.56	38.586	1.68	99	3700	44	3735	17	3754	7
MA01-39.1	95	53	0.56	98	0.140	0.3610	0.49	0.1428	1.47	0.792	1.57	39.405	1.70	100	3759	45	3756	17	3754	7
MA01-41.1	67	43	0.64	71	0.148	0.3610	0.59	0.1639	1.66	0.799	1.61	39.785	1.78	101	3787	46	3765	18	3754	9
MA01-51.1	78	40	0.51	80	0.057	0.3609	0.58	0.1293	2.08	0.796	1.59	39.613	1.76	101	3775	46	3761	17	3754	9
MA01-59.1	92	69	0.75	91	0.808	0.3609	2.28	0.1838	8.28	0.726	2.44	36.114	3.54	94	3517	66	3670	35	3754	35
MA01-21.1	49	16	0.33	51	0.058	0.3613	0.64	0.0864	2.23	0.838	1.67	41.742	1.86	104	3923	49	3813	18	3755	10
MA01-31.1	143	111	0.78	149	0.173	0.3611	0.39	0.1933	0.98	0.774	1.52	38.552	1.61	98	3696	43	3734	16	3755	6
MA01-43.1	118	79	0.67	112	0.103	0.3616	0.45	0.1187	1.46	0.740	1.54	36.888	1.66	95	3570	42	3691	16	3757	7
MA01-58.1	57	21	0.37	52	0.052	0.3621	1.89	0.1015	7.03	0.717	2.68	35.803	3.47	93	3485	72	3661	34	3759	29
MA01-1.1	77	36	0.47	82	-0.003	0.3625	0.51	0.1261	1.36	0.839	1.59	41.961	1.73	104	3929	47	3818	17	3760	8
MA01-69.1	58	48	0.82	58	0.000	0.3625	2.55	0.2361	7.34	0.725	2.76	36.230	3.98	93	3514	75	3673	39	3760	39
MA01-50.1	76	42	0.55	79	-0.014	0.3627	0.53	0.1475	1.36	0.800	1.59	39.991	1.74	101	3788	46	3770	17	3761	8
MA01-56.1	209	185	0.88	182	0.226	0.3627	1.05	0.1312	3.88	0.671	1.91	33.575	2.29	88	3311	49	3598	23	3761	16
MA01-11.1	124	116	0.93	136	-0.006	0.3630	0.40	0.2438	0.80	0.789	1.54	39.477	1.64	100	3749	44	3758	16	3762	6
MA01-34.1	93	62	0.66	99	0.051	0.3629	0.48	0.1702	1.18	0.805	1.57	40.260	1.69	101	3806	45	3777	17	3762	7
MA01-4.1	144	136	0.95	161	0.014	0.3628	0.38	0.2441	0.75	0.811	1.52	40.559	1.61	102	3828	44	3784	16	3762	6
MA01-63.1	262	138	0.53	249	0.159	0.3633	0.95	0.1405	3.30	0.731	1.86	36.637	2.19	94	3538	51	3684	22	3764	14
MA01-28.1	57	29	0.51	94	4.181	0.3665	17.71	-0.0059	-1747.80	1.223	5.91	61.802	19.36	136	5150	210	4204	196	3777	272
MA01-66.1	104	51	0.49	96	-0.031	0.3701	1.48	0.1346	4.72	0.709	2.29	36.172	2.88	91	3454	61	3671	28	3792	22
MA03 Zircons (147 analyses from 5 sessions)																				
MA03-52.2	121	61	0.51	11	0.062	0.0574	4.30	0.1524	4.80	0.088	2.10	0.693	5.01	107	542	11	535	21	506	95
MA03-52.1	97	56	0.57	9	-1.002	0.0677	7.83	0.1989	6.52	0.088	1.55	0.817	8.17	63	541	8	606	37	859	163
MA03-71.1	296	95	0.32	54	0.343	0.0845	2.05	0.1041	3.73	0.177	2.10	2.063	3.12	80	1050	20	1137	21	1305	40
MA03-71.2	322	164	0.51	71	0.256	0.0854	1.57	0.1573	2.13	0.206	2.10	2.420	2.78	91	1205	23	1249	20	1324	30
MA03-32.2	212	97	0.46	121	0.081	0.1772	0.80	0.1279	1.88	0.508	2.15	12.408	2.39	101	2648	47	2636	22	2627	13
MA03-32.1	225	98	0.43	127	0.005	0.1776	0.48	0.1214	1.06	0.505	1.49	12.367	1.62	100	2635	32	2633	15	2631	8
MA03-40.2	294	102	0.35	138	0.110	0.1845	0.47	0.0547	2.04	0.439	1.47	11.163	1.60	87	2346	29	2537	15	2694	8
MA03-40.1	189	127	0.68	99	0.147	0.1895	0.59	0.1427	1.32	0.454	1.49	11.866	1.67	88	2414	30	2594	16	2738	10
MA03-100.1	1703	7899	4.64	506	8.663	0.2198	3.06	0.4424	3.57	0.163	1.67	4.948	3.66	33	975	15	1811	31	2980	49
MA03-20.1	1229	7417	6.03	333	5.974	0.2440	0.80	0.2396	1.78	0.176	1.46	5.917	1.75	33	1044	14	1964	15	3146	13
MA03-59.1	891	5365	6.02	158	4.452	0.2639	1.42	0.3090	2.66	0.114	2.10	4.165	2.68	21	698	14	1667	22	3270	22
MA03-89.1	815	4108	5.04	262	6.226	0.2682	3.21	0.1948	9.81	0.209	1.76	7.725	3.85	37	1223	20	2200	35	3296	50
MA03-78.1	678	2769	4.08	205	5.559	0.2716	2.42	0.1849	7.84	0.202	1.68	7.557	3.11	36	1185	18	2180	28	3315	38
MA03-67.1	218	1112	5.10	132	1.061	0.2726	0.88	0.3132	1.59	0.430	2.16	16.170	2.43	69	2307	42	2887	23	3321	14
MA03-95.1	736	3357	4.56	231	5.216	0.2802	2.35	0.1787	8.07	0.211	1.69	8.145	3.06	37	1233	19	2247	28	3364	37

Continued on Next Page. . .

Table 4.2 – Continued

Grain .spot	U ppm	Th ppm	Th/U	Pb ppm	$f206\%$	^{207}Pb / ^{206}Pb 204corr	$\pm1\sigma$ (%)	^{208}Pb / ^{206}Pb 204corr	$\pm1\sigma$ (%)	^{206}Pb / ^{238}U 204corr	$\pm1\sigma$ (%)	^{207}Pb / ^{235}U 204corr	$\pm1\sigma$ (%)	%c	^{206}Pb / ^{238}U date	$\pm1\sigma$ (Ma)	^{207}Pb / ^{235}U date	$\pm1\sigma$ (Ma)	^{207}Pb / ^{206}Pb date	$\pm1\sigma$ (Ma)
MA03-85.1	1013	7086	7.00	286	10.370	0.2842	3.85	0.3453	7.24	0.149	1.82	5.844	4.46	26	896	15	1953	39	3386	60
MA03-17.2	1165	6856	5.89	297	12.715	0.2852	1.75	0.4681	2.44	0.120	2.11	4.723	2.91	22	731	15	1771	24	3391	27
MA03-93.1	687	4321	6.29	244	4.637	0.2865	2.40	0.1809	8.31	0.242	1.70	9.558	3.11	41	1397	21	2393	29	3399	37
MA03-88.1	631	3299	5.23	216	4.819	0.2899	3.09	0.1797	10.92	0.231	1.80	9.249	3.77	39	1342	22	2363	35	3417	48
MA03-43.1	762	7374	9.68	198	6.529	0.2958	0.90	0.2762	2.10	0.157	1.47	6.420	1.81	27	942	13	2035	16	3449	14
MA03-2.1	867	4496	5.19	295	8.514	0.2977	0.90	0.2847	2.08	0.194	1.47	7.965	1.82	33	1143	15	2227	16	3458	14
MA03-96.1	127	464	3.66	63	2.676	0.3010	3.45	0.0947	21.96	0.380	2.18	15.769	4.30	60	2076	39	2863	41	3475	53
MA03-99.1	453	1594	3.52	135	2.311	0.3012	1.89	0.2071	5.78	0.216	1.70	8.949	2.70	36	1258	19	2333	25	3476	29
MA03-54.1	557	2482	4.45	238	5.260	0.3023	0.75	0.1953	2.44	0.280	1.47	11.678	1.73	46	1592	21	2579	16	3482	12
MA03-26.1	685	3870	5.65	261	4.909	0.3031	0.65	0.2185	1.90	0.249	1.46	10.405	1.67	41	1433	19	2471	16	3486	10
MA03-53.1	231	254	1.10	157	1.051	0.3032	0.51	0.1629	1.68	0.521	1.49	21.777	1.64	78	2703	33	3174	16	3487	8
MA03-84.1	752	8476	11.26	184	5.965	0.3033	3.24	0.2090	10.39	0.156	1.77	6.523	3.88	27	934	15	2049	34	3487	50
MA03-83.1	463	1926	4.16	219	3.114	0.3043	1.83	0.1875	6.38	0.333	1.71	13.958	2.66	53	1851	27	2747	25	3492	28
MA03-4.1	841	9069	10.79	151	5.336	0.3046	0.90	0.2309	2.52	0.115	1.46	4.834	1.81	20	702	10	1791	15	3494	14
MA03-6.1	370	768	2.07	164	1.884	0.3047	0.55	0.1727	1.84	0.326	1.47	13.708	1.63	52	1820	23	2730	15	3494	8
MA03-87.1	1008	5202	5.16	257	8.160	0.3052	2.58	0.1884	9.27	0.153	1.71	6.446	3.27	26	919	15	2038	29	3497	40
MA03-82.1	591	2273	3.85	281	5.432	0.3100	2.38	0.1890	8.54	0.310	1.76	13.243	3.13	49	1740	27	2697	30	3521	37
MA03-75.1	247	662	2.68	168	1.058	0.3113	0.69	0.1039	3.20	0.537	1.48	23.045	1.71	79	2770	33	3229	17	3528	11
MA03-81.1	726	1986	2.74	150	2.145	0.3122	1.71	0.1173	9.03	0.156	1.62	6.706	2.50	26	933	14	2073	22	3532	26
MA03-72.T.7	452	3101	6.86	122	0.000	0.3135	1.14	0.2478	2.15	0.201	1.48	8.670	1.98	33	1178	16	2304	18	3538	18
MA03-30.1	933	6630	7.10	267	8.261	0.3149	0.88	0.3146	1.94	0.160	1.47	6.960	1.80	27	958	13	2106	16	3545	14
MA03-11.2	424	3831	9.03	207	3.297	0.3207	0.88	0.1636	3.45	0.342	2.12	15.121	2.39	53	1896	35	2823	23	3573	13
MA03-46.1	213	837	3.92	108	1.674	0.3206	0.65	0.1352	2.80	0.381	1.49	16.846	1.70	58	2082	27	2926	16	3573	10
MA03-21.1	230	832	3.62	130	1.217	0.3213	0.55	0.2495	1.33	0.402	1.49	17.821	1.65	61	2180	28	2980	16	3576	9
MA03-103.1	340	174	0.51	299	0.067	0.3226	0.29	0.1317	0.60	0.701	1.57	31.189	1.63	96	3425	42	3525	16	3582	4
MA03-80.1	95	56	0.59	88	0.420	0.3225	1.78	0.0943	9.04	0.751	2.28	33.397	3.06	101	3612	63	3592	30	3582	27
MA03-64.1	692	5490	7.93	270	4.636	0.3244	0.88	0.2881	2.11	0.244	2.10	10.909	2.38	39	1407	27	2515	22	3591	14
MA03-42.1	812	3373	4.15	195	3.968	0.3252	0.64	0.1675	2.50	0.164	1.46	7.361	1.66	27	980	13	2156	15	3594	10
MA03-101.1	176	146	0.83	145	0.306	0.3253	0.45	0.0811	1.93	0.674	1.62	30.236	1.74	92	3322	42	3494	17	3595	7
MA03-104.1	193	83	0.43	161	0.103	0.3259	0.40	0.0796	1.25	0.687	1.61	30.880	1.71	94	3372	42	3515	17	3598	6
MA03-15.1	213	500	2.35	139	1.551	0.3262	0.56	0.0950	3.30	0.504	1.50	22.683	1.67	73	2632	32	3213	16	3599	9
MA03-72.4	161	787	4.90	88	0.790	0.3281	0.49	0.1015	2.24	0.431	1.57	19.496	1.71	64	2310	31	3067	16	3608	8
MA03-10.1	188	300	1.60	161	0.594	0.3298	0.45	0.2115	1.14	0.634	1.51	28.815	1.63	88	3164	38	3447	16	3616	7
MA03-45.1	92	187	2.02	78	0.170	0.3304	0.60	0.2297	1.35	0.622	1.56	28.338	1.74	86	3118	39	3431	17	3619	9
MA03-48.1	118	106	0.90	96	0.284	0.3309	0.52	0.0695	2.86	0.664	1.54	30.271	1.69	91	3281	40	3496	17	3621	8
MA03-73.1	252	414	1.64	174	0.649	0.3309	0.62	0.1698	1.86	0.522	2.15	23.820	2.31	75	2708	48	3261	23	3621	10
MA03-37.1	107	73	0.68	105	-0.023	0.3312	0.50	0.1782	1.32	0.753	1.55	34.392	1.68	100	3619	43	3621	17	3623	8
MA03-79.1	1500	13670	9.11	211	6.475	0.3312	2.55	0.3607	5.35	0.080	1.67	3.654	3.22	14	496	8	1561	26	3623	39
MA03-33.1	202	491	2.43	135	0.927	0.3316	0.48	0.1008	2.47	0.525	1.50	24.016	1.63	75	2722	33	3269	16	3624	7
MA03-11.1	257	787	3.06	176	1.194	0.3317	0.47	0.1267	2.06	0.524	1.49	23.958	1.61	75	2716	33	3267	16	3625	7

Continued on Next Page. . .

Table 4.2 – Continued

Grain .spot	U ppm	Th ppm	Th/U	Pb ppm	$f206\%$	$^{207}Pb/^{206}Pb$ 204corr	$\pm1\sigma$ (%)	$^{208}Pb/^{206}Pb$ 204corr	$\pm1\sigma$ (%)	$^{206}Pb/^{238}U$ 204corr	$\pm1\sigma$ (%)	$^{207}Pb/^{235}U$ 204corr	$\pm1\sigma$ (%)	%c	$^{206}Pb/^{238}U$ date	$\pm1\sigma$ (Ma)	$^{207}Pb/^{235}U$ date	$\pm1\sigma$ (Ma)	$^{207}Pb/^{206}Pb$ date	$\pm1\sigma$ (Ma)
MA03-102.1	82	64	0.78	76	0.041	0.3323	0.58	0.1217	1.51	0.731	1.72	33.489	1.88	97	3537	47	3595	19	3628	9
MA03-12.1	153	67	0.44	134	0.114	0.3324	0.43	0.0380	3.83	0.739	1.52	33.874	1.63	98	3567	42	3606	16	3628	7
MA03-19.1	93	90	0.97	88	0.059	0.3323	0.51	0.1823	1.21	0.731	1.56	33.473	1.70	97	3536	42	3595	17	3628	8
MA03-62.1	260	420	1.61	217	0.832	0.3329	0.56	0.1036	2.76	0.656	2.15	30.103	2.28	90	3251	55	3490	22	3630	9
MA03-97.1	162	318	1.96	116	2.551	0.3329	2.15	0.1406	10.04	0.526	2.00	24.134	3.12	75	2724	45	3274	30	3630	33
MA03-29.1	645	2187	3.39	244	6.085	0.3330	0.71	0.2370	2.12	0.232	1.47	10.649	1.71	37	1345	18	2493	16	3631	11
MA03-34.1	492	2398	4.88	197	4.903	0.3333	0.68	0.1316	3.50	0.271	1.47	12.452	1.69	43	1546	20	2639	16	3632	10
MA03-68.1	216	330	1.53	164	0.349	0.3335	0.55	0.1394	1.78	0.592	2.16	27.198	2.29	82	2996	52	3391	22	3633	8
MA03-86.1	376	4061	10.79	131	5.126	0.3337	2.66	0.1949	9.95	0.224	1.79	10.308	3.39	36	1303	21	2463	31	3634	41
MA03-39.1	163	99	0.61	155	0.012	0.3341	0.37	0.1547	0.91	0.744	1.51	34.293	1.60	99	3587	41	3618	16	3636	6
MA03-108.1	126	61	0.48	121	0.059	0.3348	0.45	0.1235	0.98	0.763	1.66	35.227	1.77	100	3656	46	3645	17	3639	7
MA03-49.1	128	129	1.01	122	0.068	0.3347	0.43	0.1565	1.08	0.739	1.54	34.109	1.65	98	3568	42	3613	16	3639	7
MA03-36.1	293	744	2.54	219	1.602	0.3353	0.46	0.2061	1.38	0.535	1.48	24.730	1.61	76	2762	33	3298	16	3641	7
MA03-57.1	137	206	1.50	99	0.314	0.3353	0.51	0.0657	3.07	0.588	1.53	27.184	1.67	82	2981	36	3390	16	3642	8
MA03-90.1	196	152	0.78	172	0.649	0.3364	1.55	0.1372	7.11	0.681	1.92	31.597	2.61	92	3349	50	3538	26	3646	24
MA03-56.1	97	82	0.84	96	-0.007	0.3372	0.49	0.2225	1.00	0.739	1.57	34.374	1.70	98	3568	43	3621	17	3650	8
MA03-1.1	269	278	1.03	194	0.719	0.3373	0.39	0.0814	2.26	0.575	1.48	26.744	1.58	80	2928	35	3374	15	3651	6
MA03-41.1	725	5512	7.61	193	5.231	0.3377	0.75	0.1701	3.08	0.173	1.46	8.061	1.72	28	1029	14	2238	16	3652	11
MA03-74.1	121	121	1.00	112	0.043	0.3387	0.73	0.1601	2.31	0.714	2.24	33.359	2.44	95	3475	60	3591	24	3657	11
MA03-24.1	36	18	0.50	36	0.028	0.3409	0.83	0.1302	2.73	0.773	1.74	36.334	2.02	101	3692	49	3676	20	3667	13
MA03-55.1	101	65	0.64	96	0.099	0.3412	0.51	0.1620	1.31	0.736	1.56	34.604	1.70	97	3554	43	3627	17	3668	8
MA03-25.1	309	2131	6.90	136	2.492	0.3414	0.61	0.0883	4.38	0.329	1.48	15.495	1.67	50	1834	24	2846	16	3669	9
MA03-3.1	405	1770	4.37	215	3.131	0.3456	0.54	0.1460	2.47	0.374	1.47	17.820	1.63	56	2048	26	2980	16	3688	8
MA03-91.1	261	439	1.68	201	0.719	0.3457	1.19	0.0815	7.92	0.612	1.81	29.172	2.29	83	3078	44	3459	22	3688	18
MA03-76.1	252	716	2.84	162	1.239	0.3491	0.67	0.1115	3.21	0.489	1.47	23.521	1.69	69	2565	31	3249	16	3703	10
MA03-72.T.8	87	21	0.25	79	-0.055	0.3505	1.38	0.0514	6.79	0.760	3.37	36.716	3.80	98	3643	94	3686	38	3709	21
MA03-72.T.1	262	727	2.77	131	0.000	0.3506	1.16	0.0725	6.35	0.407	2.16	19.681	2.58	59	2202	40	3076	25	3710	18
MA03-27.1	101	47	0.47	102	0.034	0.3517	0.45	0.1211	1.30	0.790	1.55	38.286	1.67	101	3752	44	3727	17	3714	7
MA03-66.1	351	1028	2.93	247	2.614	0.3529	0.71	0.2003	2.42	0.485	2.13	23.582	2.32	68	2547	45	3251	23	3720	11
MA03-31.1	98	95	0.98	106	0.044	0.3533	0.47	0.2479	0.93	0.786	1.56	38.275	1.68	100	3738	44	3727	17	3721	7
MA03-72.T.6	1471	7816	5.31	326	0.083	0.3540	0.68	0.2812	1.27	0.157	1.29	7.655	1.54	25	939	11	2191	14	3724	10
MA03-35.1	114	219	1.91	87	0.232	0.3549	0.49	0.1098	1.78	0.600	1.53	29.375	1.67	81	3031	37	3466	16	3728	7
MA03-69.1	121	151	1.25	122	0.043	0.3548	0.65	0.1878	1.52	0.755	2.24	36.941	2.41	97	3627	62	3692	24	3728	10
MA03-7.1	247	497	2.01	190	0.937	0.3569	0.40	0.1761	1.31	0.567	1.49	27.904	1.59	78	2896	35	3416	16	3737	6
MA03-8.1	219	539	2.46	158	0.712	0.3574	0.41	0.1175	1.84	0.554	1.49	27.276	1.60	76	2840	34	3393	16	3739	6
MA03-13.1	183	157	0.86	186	0.129	0.3597	0.37	0.1606	1.04	0.772	1.51	38.269	1.60	98	3686	42	3727	16	3749	6
MA03-66.2	235	425	1.81	223	0.351	0.3606	0.51	0.1785	1.44	0.708	2.16	35.200	2.28	92	3451	58	3644	22	3752	8
MA03-16.1	110	133	1.21	104	0.285	0.3629	0.48	0.1121	1.82	0.738	1.56	36.932	1.68	95	3563	43	3692	17	3762	7
MA03-22.1	53	19	0.37	52	0.063	0.3631	0.64	0.0975	2.15	0.791	1.65	39.611	1.85	100	3758	47	3761	18	3763	10
MA03-94.1	378	920	2.44	246	2.480	0.3636	1.56	0.2627	4.62	0.431	1.77	21.582	2.50	61	2308	34	3165	24	3765	24

Continued on Next Page...

Table 4.2 – Continued

Grain .spot	U ppm	Th ppm	Th/U	Pb ppm	$f206\%$	^{207}Pb / ^{206}Pb 204corr	$\pm1\sigma$ (%)	^{208}Pb / ^{206}Pb 204corr	$\pm1\sigma$ (%)	^{206}Pb / ^{238}U 204corr	$\pm1\sigma$ (%)	^{207}Pb / ^{235}U 204corr	$\pm1\sigma$ (%)	%c	^{206}Pb / ^{238}U date	$\pm1\sigma$ (Ma)	^{207}Pb / ^{235}U date	$\pm1\sigma$ (Ma)	^{207}Pb / ^{206}Pb date	$\pm1\sigma$ (Ma)
MA03-23.1	216	250	1.16	238	0.134	0.3639	0.32	0.2949	0.62	0.771	1.50	38.664	1.57	98	3683	42	3737	16	3766	5
MA03-51.1	64	88	1.38	54	0.238	0.3638	0.66	0.1051	2.56	0.662	1.63	33.187	1.83	87	3273	42	3586	18	3766	10
MA03-65.1	101	68	0.67	99	0.100	0.3638	0.69	0.1528	1.84	0.750	2.27	37.634	2.45	96	3608	63	3710	24	3766	10
MA03-9.1	85	92	1.09	83	0.035	0.3643	0.61	0.1608	2.03	0.751	1.59	37.707	1.78	96	3610	44	3712	18	3768	9
MA03-106.1	86	45	0.53	88	0.018	0.3646	0.48	0.1359	1.16	0.791	1.68	39.776	1.80	100	3758	48	3765	18	3769	7
MA03-50.1	124	35	0.28	121	0.062	0.3655	0.42	0.0706	1.75	0.789	1.54	39.785	1.64	99	3751	44	3765	16	3773	6
MA03-70.1	143	373	2.60	134	0.389	0.3681	0.67	0.1167	2.62	0.722	2.23	36.655	2.40	93	3504	60	3684	24	3784	10
MA03-92.1	178	521	2.93	156	1.351	0.3718	1.47	0.1848	5.44	0.631	1.93	32.331	2.57	83	3152	48	3560	25	3799	22
MA03-5.1	213	932	4.38	166	0.664	0.3857	0.42	0.2724	0.99	0.533	1.50	28.346	1.61	71	2754	34	3431	16	3854	6
MA03-61.1	271	1912	7.06	188	1.875	0.3919	0.70	0.2542	1.99	0.461	2.16	24.892	2.35	63	2443	44	3304	23	3878	11
MA03-72.T.12	291	2127	7.32	125	0.248	0.3945	1.12	0.2438	2.93	0.303	1.72	16.478	2.17	44	1706	26	2905	21	3888	17
MA03-17.1	104	79	0.76	103	0.126	0.3957	0.47	0.0849	2.06	0.776	1.56	42.337	1.68	95	3703	44	3827	17	3893	7
MA03-98.2	192	228	1.19	184	0.372	0.3962	0.30	0.0831	1.48	0.744	1.57	40.654	1.64	92	3586	43	3787	16	3895	4
MA03-72.T.11	211	1360	6.43	120	1.036	0.3972	1.50	0.1596	6.53	0.413	1.96	22.633	2.61	57	2230	37	3211	25	3899	23
MA03-58.1	117	96	0.82	133	0.060	0.3980	0.41	0.2076	0.95	0.821	1.55	45.073	1.65	99	3866	45	3889	16	3901	6
MA03-58.2	116	92	0.80	133	0.063	0.3978	0.32	0.2021	0.59	0.832	1.61	45.632	1.68	100	3902	47	3901	17	3901	5
MA03-38.2	514	1821	3.54	228	3.357	0.3992	0.52	0.1884	2.15	0.292	1.47	16.088	1.62	42	1653	21	2882	15	3906	8
MA03-17.3	102	160	1.57	84	0.081	0.4004	0.40	0.0858	1.35	0.639	1.61	35.275	1.71	81	3185	41	3646	17	3910	6
MA03-72.T.2	303	1950	6.44	164	0.203	0.4017	1.04	0.1696	3.44	0.398	1.86	22.027	2.25	55	2158	34	3185	22	3915	16
MA03-98.1	209	372	1.78	182	0.669	0.4084	1.08	0.0588	10.51	0.674	1.85	37.950	2.25	84	3321	48	3719	22	3940	16
MA03-14.1	129	452	3.49	101	0.582	0.4088	0.50	0.0973	2.74	0.592	1.53	33.361	1.67	76	2997	37	3591	16	3942	8
MA03-14.2	124	445	3.59	95	0.530	0.4108	0.41	0.1123	1.76	0.577	1.60	32.671	1.70	74	2936	38	3571	17	3949	6
MA03-38.3	308	662	2.15	208	1.625	0.4133	0.40	0.0707	3.75	0.501	1.48	28.523	1.58	66	2616	32	3437	16	3958	6
MA03-60.1	435	2589	5.95	190	3.052	0.4139	0.68	0.1909	2.76	0.287	2.11	16.359	2.30	41	1625	30	2898	22	3960	10
MA03-18.2	153	455	2.96	106	0.572	0.4396	0.45	0.1282	1.98	0.500	1.51	30.319	1.62	65	2615	32	3497	16	4050	7
MA03-47.1	247	1725	6.99	164	1.826	0.4487	0.45	0.1527	2.24	0.456	1.49	28.187	1.61	59	2420	30	3426	16	4081	7
MA03-44.2	188	476	2.53	139	0.859	0.4515	0.66	0.1990	2.25	0.506	2.19	31.504	2.37	65	2640	48	3535	23	4090	10
MA03-44.1	213	822	3.86	118	0.674	0.4535	0.42	0.1844	1.43	0.383	1.49	23.977	1.60	51	2092	27	3267	16	4097	6
MA03-105.1	147	111	0.75	179	0.024	0.4650	0.28	0.1797	0.55	0.857	1.59	54.935	1.65	97	3989	47	4086	16	4134	4
MA03-63.1	118	218	1.85	112	0.249	0.4652	0.60	0.1570	1.87	0.673	2.25	43.158	2.39	80	3317	58	3846	24	4134	9
MA03-38.5	211	235	1.11	204	0.248	0.4655	0.25	0.0378	2.33	0.741	1.57	47.542	1.62	86	3573	43	3942	16	4136	4
MA03-72.T.9	306	3314	10.83	171	0.014	0.4726	0.75	0.2272	1.66	0.383	1.90	24.931	2.13	50	2088	34	3306	21	4158	11
MA03-72.T.10	191	1358	7.10	127	0.000	0.4744	0.83	0.1939	1.96	0.463	1.97	30.307	2.23	59	2454	40	3497	22	4164	12
MA03-18.3	139	85	0.61	176	0.034	0.4753	0.27	0.1519	0.60	0.902	1.59	59.122	1.65	99	4145	49	4159	16	4166	4
MA03-107.1	139	134	0.96	162	0.116	0.4774	0.29	0.1610	0.67	0.823	1.60	54.191	1.66	93	3872	46	4072	17	4173	4
MA03-18.1	138	156	1.13	160	0.042	0.4799	0.36	0.1452	1.01	0.828	1.53	54.764	1.62	93	3887	45	4083	16	4181	5
MA03-47.2	221	543	2.46	178	0.884	0.4799	0.55	0.1421	2.64	0.561	2.15	37.136	2.29	69	2872	50	3697	23	4181	8
MA03-63.3	82	49	0.59	104	0.026	0.4803	0.35	0.1437	0.85	0.909	1.64	60.195	1.72	100	4168	50	4177	17	4182	5
MA03-47.3	209	517	2.47	169	0.714	0.4809	0.55	0.1435	2.43	0.563	2.15	37.307	2.28	69	2877	50	3702	23	4184	8
MA03-44.3	96	69	0.72	124	0.036	0.4827	0.32	0.1709	0.74	0.911	1.62	60.660	1.69	100	4176	50	4185	17	4189	5

Continued on Next Page. . .

Table 4.2 – Continued

Grain .spot	U ppm	Th ppm	Th/U	Pb ppm	$f206\%$	$^{207}Pb/^{206}Pb$ 204corr	$\pm1\sigma$ (%)	$^{208}Pb/^{206}Pb$ 204corr	$\pm1\sigma$ (%)	$^{206}Pb/^{238}U$ 204corr	$\pm1\sigma$ (%)	$^{207}Pb/^{235}U$ 204corr	$\pm1\sigma$ (%)	%c	$^{206}Pb/^{238}U$ date	$\pm1\sigma$ (Ma)	$^{207}Pb/^{235}U$ date	$\pm1\sigma$ (Ma)	$^{207}Pb/^{206}Pb$ date	$\pm1\sigma$ (Ma)
MA03-47.4	213	1018	4.78	164	0.866	0.4833	0.29	0.1557	1.14	0.530	1.56	35.325	1.63	65	2742	35	3648	16	4191	4
MA03-63.2	81	59	0.73	104	0.494	0.4834	0.65	0.1447	2.42	0.903	2.32	60.179	2.48	99	4147	71	4177	25	4191	10
MA03-38.4	210	284	1.35	230	0.674	0.4844	0.47	0.1268	2.28	0.774	2.17	51.706	2.28	88	3696	61	4026	23	4195	7
MA03-72-T.5	216	980	4.54	197	0.183	0.4850	0.91	0.1804	3.02	0.632	2.25	42.279	2.53	75	3158	56	3826	25	4196	13
MA03-38.1	227	224	0.99	245	0.417	0.4863	0.30	0.1135	1.38	0.775	1.49	51.957	1.56	88	3698	42	4031	16	4200	4
MA03-72.1	196	694	3.55	211	0.463	0.5104	0.45	0.1718	1.54	0.734	2.17	51.633	2.27	83	3547	59	4024	23	4272	7
MA03-72.2	195	667	3.42	206	0.577	0.5107	0.46	0.1682	1.70	0.716	2.17	50.449	2.27	82	3482	58	4001	23	4273	7
MA03-72.T.13	116	348	3.01	106	0.030	0.5159	0.91	0.1703	2.36	0.629	2.20	44.714	2.48	73	3144	55	3881	25	4287	13
MA03-72-T.4	113	398	3.51	113	0.098	0.5210	0.95	0.1780	2.47	0.679	2.48	48.783	2.76	78	3341	65	3968	27	4302	14
MA03-72.3	173	511	2.95	188	0.348	0.5225	0.25	0.1706	0.75	0.737	1.57	53.063	1.63	83	3558	43	4052	16	4306	4
MA03-72.T.14	115	130	1.14	143	-0.039	0.5232	0.80	0.1718	2.07	0.855	2.29	61.687	2.52	92	3984	68	4202	25	4308	12
MA03-72.T.3	124	88	0.71	150	0.202	0.5465	0.92	0.1791	3.28	0.811	2.38	61.138	2.66	88	3830	69	4193	27	4372	13
MA04 Zircons (52 analyses from 4 sessions)																				
MA04-13.1	323	238	0.74	34	0.153	0.0579	3.39	0.2251	2.33	0.095	1.46	0.760	3.85	111	586	8	574	17	526	74
MA04-13.2	318	244	0.77	33	-0.034	0.0605	2.29	0.2354	1.79	0.094	1.45	0.787	2.86	93	581	8	590	13	622	49
MA04-17.1	62	38	0.61	19	0.649	0.1006	2.45	0.1635	3.56	0.285	1.56	3.948	3.07	99	1614	22	1624	25	1635	46
MA04-17.2	66	51	0.76	24	-0.075	0.1081	1.64	0.2256	2.06	0.316	1.57	4.709	2.41	100	1770	24	1769	20	1767	30
MA04-2.1	965	1645	1.71	395	23.300	0.2421	1.95	0.2329	4.53	0.162	1.50	5.420	2.61	31	970	14	1888	22	3134	31
MA04-9.1	876	7913	9.03	541	18.863	0.2520	1.34	0.2663	2.83	0.272	1.48	9.457	2.12	49	1552	20	2383	19	3197	21
MA04-21.1	463	2793	6.04	186	11.223	0.2997	1.21	0.1723	4.59	0.223	1.49	9.228	2.03	37	1299	18	2361	19	3469	19
MA04-12.1	160	508	3.18	104	1.321	0.3217	0.60	0.1499	2.28	0.493	1.51	21.858	1.69	72	2583	32	3177	16	3578	9
MA04-42.1	311	1381	4.44	313	8.026	0.3236	1.23	0.4107	2.10	0.538	1.49	24.005	2.04	77	2775	34	3269	20	3587	19
MA04-3.1	133	444	3.33	62	1.622	0.3265	0.82	0.1991	2.53	0.335	1.51	15.097	1.81	52	1864	25	2821	17	3601	13
MA04-19.1	88	79	0.90	83	1.444	0.3280	0.68	0.1076	3.44	0.727	1.57	32.896	1.79	98	3524	43	3577	18	3608	10
MA04-29.1	212	560	2.64	160	0.985	0.3301	0.66	0.0906	3.82	0.597	2.17	27.157	2.34	83	3017	52	3389	23	3617	10
MA04-6.1	207	789	3.80	149	3.704	0.3303	0.69	0.1405	3.25	0.500	1.49	22.784	1.72	72	2615	32	3218	17	3619	11
MA04-15.1	230	250	1.09	207	0.814	0.3307	0.39	0.1423	1.45	0.691	1.49	31.519	1.59	94	3387	39	3535	16	3620	6
MA04-18.1	270	1164	4.31	164	5.772	0.3309	0.83	0.1673	3.41	0.393	1.49	17.915	1.79	59	2135	27	2985	17	3621	13
MA04-38.1	341	3661	10.72	199	10.780	0.3309	1.70	0.3492	3.50	0.297	1.49	13.533	2.40	46	1675	22	2718	23	3621	26
MA04-5.1	281	946	3.37	171	4.449	0.3336	0.70	0.1578	3.03	0.410	1.49	18.858	1.72	61	2215	28	3035	17	3634	11
MA04-23.1	160	287	1.79	137	0.571	0.3343	0.66	0.1657	2.02	0.651	2.20	29.994	2.38	89	3231	56	3487	23	3637	10
MA04-14.1	150	113	0.76	139	0.335	0.3353	0.41	0.1211	1.47	0.732	1.52	33.821	1.62	97	3539	41	3605	16	3641	6
MA04-1.1	190	600	3.16	146	4.948	0.3362	0.81	0.1721	3.27	0.505	1.51	23.417	1.80	72	2636	33	3244	18	3645	12
MA04-47.1	594	115	0.19	511	0.049	0.3368	0.56	0.0534	2.84	0.718	1.66	33.348	1.82	96	3489	45	3591	18	3648	9
MA04-27.1	198	1069	5.41	129	4.612	0.3377	1.22	0.1876	4.53	0.429	2.18	19.970	2.63	63	2301	42	3090	25	3652	19
MA04-35.1	76	301	3.98	39	4.753	0.3380	2.41	0.1935	8.55	0.333	1.79	15.524	3.18	51	1853	29	2848	30	3654	37
MA04-33.1	213	461	2.16	168	4.101	0.3422	1.08	0.2270	3.26	0.513	1.51	24.231	1.97	73	2671	33	3278	19	3673	17
MA04-45.1	56	542	9.74	33	1.867	0.3461	1.64	0.1013	9.42	0.443	1.85	21.127	2.62	64	2363	37	3144	25	3690	25

Continued on Next Page. . .

Table 4.2 – Continued

Grain .spot	U ppm	Th ppm	Th/U	Pb ppm	$f206\%$	$^{207}Pb/^{206}Pb$ 204corr	$\pm1\sigma$ (%)	$^{208}Pb/^{206}Pb$ 204corr	$\pm1\sigma$ (%)	$^{206}Pb/^{238}U$ 204corr	$\pm1\sigma$ (%)	$^{207}Pb/^{235}U$ 204corr	$\pm1\sigma$ (%)	%c	$^{206}Pb/^{238}U$ date	$\pm1\sigma$ (Ma)	$^{207}Pb/^{235}U$ date	$\pm1\sigma$ (Ma)	$^{207}Pb/^{206}Pb$ date	$\pm1\sigma$ (Ma)
MA04-7.1	256	742	2.90	181	3.278	0.3477	0.59	0.2121	1.92	0.475	1.49	22.755	1.67	68	2504	31	3217	16	3697	9
MA04-31.1	311	770	2.48	269	4.784	0.3480	0.88	0.1969	3.22	0.559	2.15	26.801	2.42	77	2861	50	3376	24	3698	13
MA04-37.1	215	582	2.71	182	1.263	0.3531	0.69	0.1877	2.12	0.613	1.51	29.844	1.73	83	3082	37	3482	17	3720	10
MA04-44.1	41	73	1.77	39	1.160	0.3530	1.52	0.1443	6.14	0.699	2.03	34.037	2.68	92	3418	54	3611	26	3720	23
MA04-4.1	182	812	4.46	152	1.619	0.3544	0.53	0.1984	1.75	0.592	1.50	28.948	1.66	80	2999	36	3452	16	3726	8
MA04-22.1	189	387	2.05	166	1.628	0.3550	0.77	0.2253	2.26	0.614	2.19	30.060	2.40	83	3087	54	3489	24	3729	12
MA04-32.1	60	33	0.55	61	0.295	0.3558	1.00	0.1317	3.55	0.785	2.44	38.517	2.75	100	3735	69	3733	27	3732	15
MA04-8.1	122	157	1.28	102	1.357	0.3560	0.57	0.1355	2.53	0.621	1.53	30.494	1.70	83	3115	38	3503	17	3733	9
MA04-28.1	116	68	0.58	119	0.357	0.3585	0.69	0.1380	2.41	0.787	2.26	38.902	2.44	100	3742	64	3743	24	3744	10
MA04-40.1	216	1258	5.83	109	2.043	0.3590	0.90	0.1546	3.57	0.361	1.50	17.875	1.84	53	1988	26	2983	18	3746	14
MA04-26.1	80	23	0.29	77	0.218	0.3593	0.78	0.0715	3.80	0.775	2.33	38.377	2.55	99	3697	66	3730	25	3747	12
MA04-20.1	109	67	0.61	114	0.097	0.3597	0.43	0.1033	1.52	0.826	1.54	40.965	1.65	104	3882	45	3794	16	3748	7
MA04-43.1	26	7	0.29	24	0.055	0.3599	1.42	0.0716	6.56	0.775	2.33	38.471	2.88	99	3700	65	3732	28	3749	22
MA04-11.1	40	15	0.39	41	-0.019	0.3599	0.70	0.0994	2.32	0.815	1.71	40.461	1.93	103	3844	49	3782	19	3750	11
MA04-16.1	97	80	0.82	99	0.263	0.3601	0.48	0.1458	1.49	0.776	1.56	38.518	1.68	99	3702	44	3733	17	3750	7
MA04-49.1	81	115	1.42	74	0.515	0.3600	1.93	0.1440	7.60	0.689	2.41	34.202	3.27	90	3379	63	3616	32	3750	29
MA04-50.1	76	47	0.62	78	0.864	0.3606	2.95	0.1229	16.77	0.785	2.60	39.011	4.17	100	3734	74	3746	41	3752	45
MA04-34.1	56	20	0.35	53	0.248	0.3609	0.95	0.0865	3.38	0.742	1.87	36.907	2.20	95	3577	51	3691	22	3754	14
MA04-10.1	134	260	1.94	140	0.148	0.3612	0.41	0.3173	0.76	0.723	1.52	35.995	1.63	93	3506	41	3666	16	3755	6
MA04-41.1	43	17	0.41	43	-0.058	0.3614	1.10	0.1038	3.53	0.794	2.01	39.585	2.40	100	3769	57	3760	24	3756	17
MA04-48.1	114	27	0.24	93	-0.028	0.3619	1.43	0.0598	7.10	0.669	2.24	33.394	2.81	88	3303	58	3592	28	3758	22
MA04-24.1	164	112	0.68	170	0.002	0.3622	0.52	0.1394	1.32	0.800	2.20	39.930	2.32	101	3788	63	3769	23	3759	8
MA04-30.1	64	31	0.49	67	0.173	0.3623	0.88	0.1232	2.96	0.811	2.41	40.527	2.66	102	3829	69	3784	26	3760	13
MA04-36.1	83	34	0.41	80	0.114	0.3643	0.77	0.1021	2.08	0.765	1.72	38.412	1.97	97	3661	48	3731	19	3768	12
MA04-39.1	147	328	2.22	153	0.345	0.3648	0.65	0.2922	1.13	0.718	1.57	36.139	1.77	93	3490	42	3670	18	3770	10
MA04-46.1	163	103	0.63	163	0.096	0.3660	0.56	0.1613	1.32	0.755	1.54	38.099	1.70	96	3626	43	3722	17	3775	9
MA04-25.1	8	3	0.35	8	0.853	0.3745	2.89	0.0687	22.75	0.726	4.00	37.470	5.22	92	3517	108	3706	52	3810	44
MA05 Zircons (85 analyses from 1 session)																				
MA05-16.2	657	63	0.10	363	0.039	0.2451	0.27	0.0270	1.38	0.505	1.33	17.060	1.39	84	2634	29	2938	13	3154	4
MA05-16.1	702	68	0.10	379	0.025	0.2458	0.24	0.0271	1.20	0.493	1.33	16.707	1.38	82	2583	28	2918	13	3158	4
MA05-72.1	810	773	0.95	341	4.481	0.2500	0.68	0.3071	1.17	0.274	1.33	9.460	1.57	49	1563	18	2384	14	3185	11
MA05-66.1	520	700	1.35	209	2.913	0.2510	0.69	0.2872	1.24	0.277	1.33	9.583	1.58	49	1576	19	2396	15	3191	11
MA05-19.1	268	427	1.59	141	1.965	0.2560	0.70	0.1491	2.24	0.408	1.35	14.389	1.60	68	2204	25	2776	15	3222	11
MA05-54.1	662	1356	2.05	190	4.616	0.2560	0.87	0.3431	1.39	0.182	1.33	6.413	1.68	33	1076	13	2034	15	3222	14
MA05-53.1	240	313	1.30	108	0.949	0.2580	0.64	0.2253	1.27	0.342	1.35	12.161	1.56	59	1895	22	2617	15	3235	10
MA05-39.1	1186	1214	1.02	288	9.544	0.2584	1.10	0.3850	1.61	0.131	1.34	4.669	1.83	25	794	10	1762	15	3237	17
MA05-81.1	882	996	1.13	306	8.821	0.2588	1.10	0.3711	1.67	0.192	1.34	6.863	1.84	35	1134	14	2094	16	3239	17
MA05-56.1	242	257	1.06	187	0.199	0.2590	0.41	0.2520	0.63	0.590	1.36	21.053	1.46	92	2988	32	3141	14	3241	6

Continued on Next Page...

Table 4.2 – Continued

Grain .spot	U ppm	Th ppm	Th/U	Pb ppm	f206%	$^{207}Pb/^{206}Pb$ 204corr	±1σ (%)	$^{208}Pb/^{206}Pb$ 204corr	±1σ (%)	$^{206}Pb/^{238}U$ 204corr	±1σ (%)	$^{207}Pb/^{235}U$ 204corr	±1σ (%)	%c	$^{206}Pb/^{238}U$ date	±1σ (Ma)	$^{207}Pb/^{235}U$ date	±1σ (Ma)	$^{207}Pb/^{206}Pb$ date	±1σ (Ma)
MA05-69.1	266	186	0.70	128	1.016	0.2603	0.59	0.1337	1.94	0.387	1.35	13.906	1.55	65	2111	24	2743	15	3248	9
MA05-67.1	231	329	1.42	134	2.985	0.2617	0.86	0.3024	1.52	0.391	1.37	14.115	1.71	65	2128	25	2757	16	3257	14
MA05-40.1	69	63	0.92	60	-0.220	0.2625	0.72	0.2488	1.15	0.671	1.47	24.281	1.71	101	3309	38	3280	17	3262	11
MA05-17.1	134	10	0.07	97	-0.050	0.2632	0.56	0.0208	9.48	0.658	1.40	23.881	1.57	100	3260	36	3264	15	3266	9
MA05-68.1	204	436	2.13	114	1.340	0.2660	0.72	0.3508	1.07	0.383	1.37	14.062	1.62	64	2092	24	2754	15	3283	11
MA05-63.1	352	433	1.23	169	1.651	0.2665	0.58	0.1430	1.94	0.373	1.35	13.716	1.53	62	2045	24	2730	14	3286	9
MA05-50.1	184	218	1.19	162	0.043	0.2669	0.42	0.3052	0.54	0.650	1.37	23.914	1.48	98	3228	35	3265	14	3288	7
MA05-61.1	365	215	0.59	285	0.031	0.2715	0.30	0.1531	0.51	0.636	1.35	23.796	1.42	96	3172	34	3260	14	3314	5
MA05-11.1	135	173	1.28	129	0.048	0.2723	0.47	0.3361	0.60	0.692	1.39	25.968	1.52	102	3389	37	3345	15	3320	7
MA05-65.1	245	374	1.53	109	2.441	0.2724	0.86	0.2272	2.01	0.319	1.36	11.981	1.70	54	1785	21	2603	16	3320	13
MA05-74.1	100	55	0.55	80	0.104	0.2730	0.57	0.1407	1.11	0.659	1.44	24.800	1.62	98	3263	37	3300	16	3323	9
MA05-24.1	162	142	0.88	92	0.293	0.2731	0.54	0.1893	1.11	0.445	1.37	16.755	1.54	71	2373	27	2921	15	3324	8
MA05-28.1	117	73	0.62	99	-0.062	0.2736	0.53	0.1620	1.14	0.680	1.40	25.662	1.56	101	3345	37	3334	15	3327	8
MA05-35.1	331	461	1.39	220	2.270	0.2755	0.59	0.3180	1.02	0.452	1.35	17.167	1.53	72	2404	27	2944	15	3338	9
MA05-44.1	104	60	0.58	89	-0.021	0.2762	0.55	0.1526	1.24	0.694	1.41	26.442	1.57	102	3399	37	3363	15	3342	9
MA05-60.1	210	130	0.62	78	0.543	0.2762	0.60	0.1623	1.49	0.293	1.36	11.168	1.56	50	1658	20	2537	15	3342	9
MA05-32.1	181	181	1.00	165	0.059	0.2770	0.40	0.2612	0.59	0.688	1.37	26.278	1.48	101	3375	36	3357	14	3346	6
MA05-3.1	310	210	0.68	211	1.265	0.2777	0.49	0.1738	1.37	0.522	1.35	20.004	1.49	81	2709	30	3092	14	3350	8
MA05-75.1	142	65	0.46	90	0.188	0.2802	0.57	0.1540	1.24	0.513	1.39	19.824	1.57	79	2670	30	3083	15	3364	9
MA05-41.1	122	117	0.96	82	0.194	0.2807	0.58	0.1106	1.87	0.556	1.40	21.512	1.58	85	2849	32	3162	15	3367	9
MA05-29.1	54	30	0.56	45	-0.031	0.2819	0.81	0.1473	2.18	0.682	1.51	26.506	1.80	99	3352	40	3365	18	3373	13
MA05-58.1	116	168	1.45	109	0.077	0.2822	0.53	0.3780	0.63	0.658	1.42	25.594	1.58	97	3258	36	3331	15	3375	8
MA05-78.1	932	1900	2.04	237	5.449	0.2823	0.84	0.2465	1.99	0.163	1.33	6.344	1.66	29	973	12	2025	15	3376	13
MA05-9.1	116	45	0.39	92	0.020	0.2826	0.52	0.1006	1.62	0.670	1.41	26.115	1.57	98	3307	37	3351	15	3377	8
MA05-51.1	96	38	0.40	78	-0.042	0.2827	0.59	0.1043	1.85	0.685	1.43	26.710	1.61	100	3365	37	3373	16	3378	9
MA05-43.1	110	284	2.57	493	22.628	0.2835	1.46	0.5063	1.84	1.610	1.46	62.925	2.19	183	6184	58	4222	22	3382	23
MA05-30.1	236	78	0.33	193	0.040	0.2837	0.35	0.0856	1.04	0.694	1.36	27.140	1.44	100	3397	36	3389	14	3383	5
MA05-76.1	364	117	0.32	285	0.045	0.2842	0.29	0.0859	0.71	0.663	1.35	25.978	1.41	97	3278	35	3346	14	3386	5
MA05-1.1	123	48	0.39	103	-0.061	0.2863	0.48	0.1020	1.27	0.702	1.41	27.731	1.54	101	3430	37	3410	15	3398	8
MA05-38.1	111	62	0.56	88	0.359	0.2864	0.60	0.1353	1.77	0.640	1.41	25.274	1.60	94	3189	35	3319	16	3398	9
MA05-10.1	296	273	0.92	157	1.587	0.2865	0.55	0.1609	1.73	0.403	1.34	15.931	1.51	64	2184	25	2873	14	3399	9
MA05-79.1	166	193	1.16	151	0.117	0.2868	0.45	0.3053	0.61	0.658	1.39	26.032	1.51	96	3260	35	3348	15	3400	7
MA05-33.1	258	240	0.93	174	0.677	0.2871	0.45	0.1603	1.27	0.530	1.35	20.973	1.48	81	2741	30	3137	14	3402	7
MA05-36.1	255	83	0.32	206	0.029	0.2875	0.33	0.0855	0.88	0.682	1.36	27.036	1.43	98	3352	35	3385	14	3404	5
MA05-25.1	117	59	0.50	99	-0.014	0.2886	0.47	0.1313	0.89	0.695	1.40	27.659	1.54	100	3402	37	3407	15	3410	7
MA05-55.1	341	484	1.42	176	3.842	0.2889	0.74	0.3116	1.41	0.333	1.35	13.275	1.61	54	1854	22	2699	15	3412	11
MA05-45.1	145	64	0.44	119	0.361	0.2893	0.48	0.1268	1.38	0.663	1.38	26.450	1.52	96	3279	36	3363	15	3414	7
MA05-49.1	251	231	0.92	182	0.667	0.2898	0.44	0.1973	1.00	0.554	1.35	22.124	1.47	83	2840	31	3189	14	3417	7
MA05-21.1	178	158	0.89	125	0.808	0.2903	0.53	0.1301	1.81	0.556	1.37	22.251	1.53	83	2850	32	3195	15	3419	8
MA05-82.1	168	199	1.19	142	0.595	0.2909	0.52	0.2555	0.93	0.622	1.39	24.942	1.54	91	3117	34	3306	15	3423	8

Continued on Next Page...

Table 4.2 – Continued

Grain .spot	U ppm	Th ppm	Th/U	Pb ppm	$f206\%$	$^{207}Pb/^{206}Pb$ 204corr	$\pm1\sigma$ (%)	$^{208}Pb/^{206}Pb$ 204corr	$\pm1\sigma$ (%)	$^{206}Pb/^{238}U$ 204corr	$\pm1\sigma$ (%)	$^{207}Pb/^{235}U$ 204corr	$\pm1\sigma$ (%)	%c	$^{206}Pb/^{238}U$ date	$\pm1\sigma$ (Ma)	$^{207}Pb/^{235}U$ date	$\pm1\sigma$ (Ma)	$^{207}Pb/^{206}Pb$ date	$\pm1\sigma$ (Ma)
MA05-6.1	210	219	1.04	132	1.636	0.2936	0.61	0.2502	1.34	0.448	1.36	18.121	1.56	69	2385	27	2996	15	3437	10
MA05-46.1	146	158	1.09	94	1.319	0.2966	0.70	0.2033	1.78	0.476	1.38	19.482	1.62	73	2511	29	3066	16	3453	11
MA05-8.1	225	314	1.40	208	0.427	0.3020	0.40	0.3771	0.55	0.630	1.36	26.223	1.47	90	3148	34	3355	14	3481	6
MA05-64.1	80	66	0.83	74	0.109	0.3028	0.60	0.2137	0.97	0.708	1.47	29.542	1.65	99	3449	39	3472	16	3485	9
MA05-34.1	294	725	2.47	133	5.061	0.3081	0.91	0.4774	1.26	0.257	1.36	10.928	1.72	42	1476	18	2517	16	3512	14
MA05-42.1	187	399	2.14	143	0.349	0.3161	0.43	0.1548	1.12	0.597	1.36	26.019	1.48	85	3018	33	3347	14	3551	7
MA05-73.1	496	437	0.88	268	3.294	0.3192	0.55	0.1406	2.37	0.386	1.34	16.975	1.51	59	2103	24	2933	14	3566	8
MA05-62.1	56	40	0.70	54	0.048	0.3205	0.69	0.1772	1.25	0.736	1.53	32.527	1.76	100	3556	42	3566	17	3572	11
MA05-4.1	169	119	0.70	161	0.020	0.3223	0.38	0.1789	0.79	0.734	1.38	32.612	1.47	99	3548	38	3569	14	3581	6
MA05-20.1	232	204	0.88	192	0.573	0.3227	0.39	0.1240	1.36	0.652	1.36	29.024	1.46	90	3237	35	3454	14	3583	6
MA05-48.1	160	119	0.74	138	0.078	0.3290	0.39	0.1140	0.99	0.692	1.38	31.375	1.48	94	3389	36	3531	15	3612	6
MA05-7.1	92	44	0.47	87	0.012	0.3290	0.48	0.1196	0.98	0.759	1.43	34.442	1.56	101	3642	40	3623	15	3612	7
MA05-37.1	84	26	0.31	78	0.087	0.3291	0.52	0.0813	1.70	0.762	1.44	34.588	1.59	101	3652	40	3627	16	3613	8
MA05-77.1	199	135	0.68	163	0.169	0.3291	0.40	0.1139	1.13	0.654	1.38	29.655	1.48	90	3242	35	3475	15	3613	6
MA05-47.1	460	384	0.83	443	0.005	0.3318	0.22	0.2174	0.35	0.720	1.33	32.955	1.38	96	3497	36	3579	14	3625	3
MA05-23.1	228	150	0.66	70	0.732	0.3380	0.58	0.1262	2.22	0.238	1.35	11.112	1.53	38	1379	17	2533	14	3654	9
MA05-57.1	226	299	1.32	49	1.013	0.3401	0.88	0.2565	1.97	0.154	1.34	7.209	1.69	25	922	11	2138	15	3663	14
MA05-5.2	274	326	1.19	187	1.140	0.3430	0.41	0.1397	1.59	0.513	1.35	24.265	1.46	73	2670	30	3279	14	3676	6
MA05-71.1	206	302	1.47	220	0.202	0.3439	0.37	0.3507	0.51	0.725	1.38	34.375	1.47	96	3515	37	3621	15	3680	6
MA05-31.1	324	245	0.76	195	0.944	0.3453	0.39	0.1510	1.34	0.451	1.34	21.484	1.44	65	2401	27	3161	14	3686	6
MA05-80.1	103	67	0.65	98	0.018	0.3499	0.51	0.1405	1.23	0.739	1.44	35.635	1.58	96	3565	39	3656	16	3707	8
MA05-2.1	135	62	0.46	134	0.018	0.3514	0.40	0.1166	0.95	0.783	1.40	37.948	1.51	100	3728	40	3719	15	3713	6
MA05-52.1	131	61	0.46	129	0.105	0.3523	0.43	0.1165	1.34	0.775	1.39	37.672	1.51	100	3701	39	3711	15	3717	7
MA05-18.1	183	113	0.62	165	0.346	0.3532	0.39	0.1302	1.29	0.699	1.37	34.040	1.47	92	3417	36	3611	15	3721	6
MA05-83.1	164	90	0.55	160	0.002	0.3534	0.37	0.1351	0.69	0.761	1.40	37.098	1.49	98	3649	39	3696	15	3722	6
MA05-59.1	181	164	0.91	171	0.235	0.3538	0.39	0.2060	0.79	0.701	1.38	34.209	1.48	92	3425	37	3616	15	3724	6
MA05-15.1	101	97	0.96	109	0.026	0.3562	0.45	0.2431	0.72	0.785	1.42	38.551	1.54	100	3735	40	3734	15	3734	7
MA05-5.1	188	156	0.83	189	0.048	0.3565	0.33	0.2042	0.61	0.746	1.37	36.680	1.45	96	3594	38	3685	14	3735	5
MA05-14.1	207	225	1.09	226	-0.031	0.3575	0.32	0.2781	0.51	0.774	1.37	38.157	1.44	99	3696	38	3724	14	3739	5
MA05-12.1	56	45	0.79	59	-0.021	0.3577	0.60	0.2047	0.97	0.777	1.51	38.347	1.69	99	3708	42	3729	17	3740	9
MA05-26.1	193	221	1.15	213	0.014	0.3577	0.33	0.2923	0.45	0.775	1.37	38.234	1.45	99	3700	39	3726	14	3740	5
MA05-22.1	88	73	0.83	89	-0.049	0.3579	0.51	0.1750	1.06	0.761	1.43	37.573	1.58	98	3650	40	3709	16	3741	8
MA05-70.1	53	39	0.73	55	0.031	0.3603	0.66	0.1907	1.13	0.777	1.55	38.613	1.76	99	3707	44	3736	17	3751	10
MA05-27.2	104	102	0.98	108	0.098	0.3687	0.50	0.2430	0.89	0.745	1.43	37.900	1.57	95	3591	39	3717	16	3786	8
MA05-27.1	187	186	1.00	182	0.285	0.3718	0.36	0.2615	0.67	0.687	1.37	35.212	1.46	89	3371	36	3645	14	3799	5
MA07 Zircons (89 analyses from 1 session)																				
MA07-8.1	1690	3208	1.90	191	4.850	0.2651	0.97	0.4915	1.15	0.065	1.33	2.388	1.74	12	408	5	1239	12	3277	15
MA07-61.1	243	2690	11.08	112	0.921	0.2701	0.60	0.2184	1.27	0.350	1.35	13.021	1.55	58	1933	23	2681	15	3307	9

Continued on Next Page. . .

Table 4.2 – Continued

Grain .spot	U ppm	Th ppm	Th/U	Pb ppm	$f206\%$	$^{207}Pb/^{206}Pb$ 204corr	$\pm1\sigma$ (%)	$^{208}Pb/^{206}Pb$ 204corr	$\pm1\sigma$ (%)	$^{206}Pb/^{238}U$ 204corr	$\pm1\sigma$ (%)	$^{207}Pb/^{235}U$ 204corr	$\pm1\sigma$ (%)	%c	$^{206}Pb/^{238}U$ date	$\pm1\sigma$ (Ma)	$^{207}Pb/^{235}U$ date	$\pm1\sigma$ (Ma)	$^{207}Pb/^{206}Pb$ date	$\pm1\sigma$ (Ma)
MA07-79.1	472	2375	5.03	152	1.249	0.2794	0.58	0.2956	1.01	0.228	1.33	8.791	1.52	39	1325	16	2317	14	3359	9
MA07-30.1	248	1052	4.25	181	0.625	0.2802	0.45	0.1558	1.19	0.580	1.36	22.408	1.48	88	2949	32	3202	14	3364	7
MA07-72.1	588	1316	2.24	198	1.960	0.2830	0.58	0.3513	0.93	0.225	1.33	8.792	1.52	39	1310	16	2317	14	3379	9
MA07-38.1	370	1597	4.31	222	1.674	0.2855	0.52	0.2243	1.20	0.437	1.35	17.193	1.50	69	2336	26	2946	14	3393	8
MA07-74.1	215	440	2.04	109	0.365	0.2886	0.49	0.0649	2.60	0.431	1.37	17.163	1.51	68	2311	27	2944	15	3410	8
MA07-60.1	764	2800	3.67	171	2.871	0.3020	0.71	0.2736	1.53	0.151	1.33	6.299	1.58	26	908	11	2018	14	3480	11
MA07-21.1	235	1079	4.58	144	0.826	0.3041	0.49	0.2326	1.04	0.451	1.36	18.906	1.51	69	2399	27	3037	15	3491	8
MA07-39.1	665	3491	5.25	185	2.121	0.3100	0.56	0.1982	1.62	0.200	1.33	8.540	1.51	33	1174	14	2290	14	3521	9
MA07-32.1	250	837	3.35	138	0.485	0.3173	0.44	0.0991	1.83	0.444	1.36	19.428	1.48	67	2369	27	3063	14	3557	7
MA07-34.1	306	1417	4.63	217	1.004	0.3190	0.42	0.1064	1.89	0.558	1.35	24.551	1.46	80	2859	31	3291	14	3565	6
MA07-73.1	497	1819	3.66	177	1.192	0.3207	0.46	0.1838	1.33	0.265	1.33	11.711	1.46	42	1514	18	2582	14	3573	7
MA07-27.1	99	138	1.40	98	0.197	0.3226	0.53	0.2695	0.83	0.723	1.44	32.150	1.59	98	3506	39	3555	16	3582	8
MA07-14.1	205	282	1.37	164	0.190	0.3239	0.38	0.1146	1.15	0.641	1.37	28.645	1.46	89	3194	34	3441	14	3589	6
MA07-40.1	705	1248	1.77	158	2.821	0.3248	0.67	0.2782	1.52	0.149	1.33	6.667	1.56	25	895	11	2068	14	3593	10
MA07-37.1	167	28	0.17	150	-0.014	0.3259	0.42	0.0431	2.96	0.763	1.39	34.267	1.50	102	3654	39	3618	15	3598	6
MA07-44.1	167	766	4.59	109	0.324	0.3267	0.51	0.2874	0.84	0.464	1.38	20.895	1.53	68	2457	28	3134	15	3602	8
MA07-19.1	512	3596	7.02	190	1.979	0.3277	0.51	0.1736	1.72	0.270	1.33	12.176	1.49	43	1538	18	2618	14	3606	8
MA07-64.1	127	554	4.38	80	0.406	0.3288	0.57	0.1477	1.56	0.494	1.40	22.381	1.58	72	2587	30	3200	15	3611	9
MA07-46.1	142	248	1.75	92	0.324	0.3292	0.51	0.1317	1.43	0.511	1.40	23.193	1.55	74	2661	30	3235	15	3613	8
MA07-5.1	71	494	6.96	41	0.558	0.3292	0.87	0.1831	2.33	0.437	1.45	19.848	1.78	65	2338	28	3084	17	3613	13
MA07-63.1	292	1074	3.68	185	0.881	0.3293	0.43	0.2011	1.08	0.469	1.36	21.302	1.47	69	2480	28	3152	14	3614	7
MA07-58.1	20	11	0.52	20	0.297	0.3301	1.20	0.1304	3.40	0.758	1.90	34.508	2.37	101	3638	53	3625	23	3618	18
MA07-10.1	580	3623	6.24	210	2.118	0.3317	0.49	0.2295	1.31	0.252	1.33	11.512	1.48	40	1447	17	2566	14	3625	8
MA07-71.1	259	138	0.53	148	0.569	0.3317	0.45	0.0922	2.13	0.456	1.36	20.871	1.48	67	2423	27	3133	14	3625	7
MA07-23.1	80	67	0.83	82	0.155	0.3320	0.57	0.2154	1.02	0.765	1.47	35.000	1.64	101	3661	41	3639	16	3626	9
MA07-11.1	110	970	8.83	50	0.786	0.3323	0.77	0.1432	2.65	0.350	1.40	16.038	1.68	53	1935	23	2879	16	3628	12
MA07-17.1	239	219	0.91	198	0.114	0.3325	0.33	0.0689	1.36	0.684	1.36	31.350	1.44	93	3359	36	3530	14	3628	5
MA07-50.1	365	825	2.26	99	1.274	0.3323	0.61	0.1486	2.24	0.204	1.34	9.349	1.54	33	1197	15	2373	14	3628	9
MA07-18.1	159	142	0.89	132	0.073	0.3325	0.48	0.0864	2.46	0.676	1.39	31.017	1.53	92	3331	36	3520	15	3629	7
MA07-59.1	68	40	0.59	65	-0.001	0.3325	0.59	0.1510	1.03	0.755	1.51	34.596	1.68	100	3624	42	3627	17	3629	9
MA07-33.1	123	337	2.73	84	0.099	0.3327	0.49	0.0317	3.50	0.577	1.41	26.482	1.55	81	2937	33	3364	15	3630	8
MA07-7.1	423	3520	8.32	243	1.617	0.3331	0.42	0.1881	1.29	0.417	1.34	19.137	1.45	62	2246	25	3049	14	3631	6
MA07-1.1	77	60	0.78	79	0.000	0.3335	0.55	0.2028	0.99	0.777	1.47	35.721	1.63	102	3706	41	3659	16	3633	8
MA07-43.1	201	101	0.50	184	0.055	0.3333	0.35	0.0989	0.94	0.740	1.38	34.023	1.46	98	3572	38	3611	14	3633	5
MA07-45.1	86	35	0.40	81	0.004	0.3334	0.52	0.1042	1.07	0.756	1.46	34.729	1.61	100	3628	41	3631	16	3633	8
MA07-55.1	148	192	1.30	161	0.052	0.3335	0.41	0.3286	0.57	0.762	1.40	35.038	1.51	100	3651	39	3640	15	3633	6
MA07-20.1	179	191	1.07	155	0.026	0.3337	0.37	0.0615	1.22	0.723	1.38	33.254	1.47	96	3507	37	3588	14	3634	6
MA07-22.1	156	134	0.86	157	-0.005	0.3338	0.39	0.2228	0.59	0.751	1.39	34.585	1.49	99	3613	38	3627	15	3635	6
MA07-28.1	136	399	2.94	111	0.162	0.3342	0.45	0.1110	1.30	0.652	1.40	30.057	1.52	89	3237	36	3489	15	3636	7
MA07-42.1	191	39	0.20	172	-0.000	0.3341	0.35	0.0522	1.00	0.753	1.38	34.703	1.47	100	3620	38	3630	14	3636	5

Continued on Next Page...

Table 4.2 – Continued

Grain .spot	U ppm	Th ppm	Th/U	Pb ppm	$f206\%$	$^{207}Pb/^{206}Pb$ 204corr	$\pm1\sigma$ (%)	$^{208}Pb/^{206}Pb$ 204corr	$\pm1\sigma$ (%)	$^{206}Pb/^{238}U$ 204corr	$\pm1\sigma$ (%)	$^{207}Pb/^{235}U$ 204corr	$\pm1\sigma$ (%)	%c	$^{206}Pb/^{238}U$ date	$\pm1\sigma$ (Ma)	$^{207}Pb/^{235}U$ date	$\pm1\sigma$ (Ma)	$^{207}Pb/^{206}Pb$ date	$\pm1\sigma$ (Ma)
MA07-77.1	247	269	1.09	154	0.251	0.3341	0.40	0.0924	1.45	0.503	1.37	23.157	1.47	72	2626	29	3234	14	3636	6
MA07-12.1	95	195	2.05	90	0.041	0.3345	0.51	0.2957	0.71	0.677	1.43	31.209	1.58	92	3331	37	3526	16	3638	8
MA07-66.1	348	639	1.84	188	0.624	0.3346	0.41	0.1144	1.60	0.425	1.34	19.602	1.45	63	2282	26	3072	14	3638	6
MA07-35.1	112	95	0.85	117	-0.008	0.3351	0.46	0.2197	0.72	0.780	1.42	36.017	1.55	102	3716	40	3667	15	3640	7
MA07-78.1	214	565	2.63	147	0.320	0.3349	0.43	0.1207	1.33	0.540	1.38	24.944	1.49	76	2784	31	3306	15	3640	7
MA07-69.1	195	445	2.29	161	0.193	0.3351	0.42	0.2376	0.74	0.609	1.37	28.159	1.48	84	3068	34	3425	15	3641	6
MA07-3.1	135	225	1.67	83	0.254	0.3354	0.50	0.1142	1.61	0.486	1.39	22.494	1.54	70	2555	29	3205	15	3642	8
MA07-9.1	240	197	0.82	196	0.127	0.3355	0.34	0.1193	0.91	0.651	1.36	30.115	1.44	89	3232	35	3491	14	3642	5
MA07-81.1	211	487	2.31	161	0.277	0.3356	0.40	0.0767	1.73	0.620	1.37	28.707	1.47	85	3112	34	3444	14	3643	6
MA07-36.1	79	48	0.61	77	0.000	0.3365	0.56	0.1584	0.95	0.762	1.47	35.357	1.64	100	3652	41	3649	16	3647	9
MA07-62.1	190	76	0.40	152	0.096	0.3366	0.40	0.1021	1.07	0.646	1.37	29.960	1.48	88	3211	35	3486	15	3647	6
MA07-6.1	181	96	0.53	177	0.042	0.3368	0.35	0.1372	0.72	0.767	1.38	35.609	1.46	101	3669	39	3656	14	3648	5
MA07-13.1	232	169	0.73	203	0.248	0.3370	0.35	0.1105	1.11	0.695	1.36	32.310	1.45	93	3403	36	3560	14	3649	5
MA07-4.1	200	96	0.48	189	0.089	0.3369	0.35	0.1178	0.89	0.753	1.37	34.962	1.46	99	3617	38	3638	14	3649	5
MA07-29.1	87	327	3.75	81	0.151	0.3372	0.57	0.2386	0.99	0.685	1.45	31.866	1.62	92	3365	38	3546	16	3650	9
MA07-49.1	126	216	1.71	75	0.205	0.3371	0.56	0.1286	1.55	0.469	1.41	21.788	1.58	68	2478	29	3174	15	3650	9
MA07-80.1	264	1437	5.44	124	0.864	0.3381	0.50	0.2109	1.24	0.344	1.35	16.017	1.50	52	1904	22	2878	14	3654	8
MA07-25.1	157	61	0.39	149	-0.025	0.3383	0.47	0.1009	2.11	0.767	1.39	35.783	1.52	100	3670	39	3660	15	3655	7
MA07-41.1	64	43	0.67	64	-0.058	0.3382	0.77	0.1734	2.22	0.773	1.51	36.030	1.78	101	3690	42	3667	18	3655	12
MA07-24.1	59	29	0.49	57	-0.140	0.3395	0.85	0.1262	3.59	0.764	1.53	35.784	1.84	100	3660	43	3661	18	3661	13
MA07-31.1	92	110	1.20	82	0.024	0.3396	0.55	0.0919	2.07	0.726	1.45	33.977	1.61	96	3517	39	3609	16	3661	8
MA07-2.1	84	47	0.57	74	0.084	0.3415	0.55	0.1041	1.70	0.710	1.45	33.411	1.62	94	3457	39	3593	16	3669	8
MA07-26.1	190	91	0.48	181	0.064	0.3431	0.36	0.0762	1.23	0.779	1.38	36.833	1.46	101	3712	39	3689	14	3677	5
MA07-70.1	113	361	3.19	82	0.260	0.3438	0.56	0.0871	2.43	0.585	1.43	27.730	1.60	81	2969	34	3410	16	3680	9
MA07-51.1	94	52	0.55	86	0.057	0.3444	0.63	0.0806	3.71	0.744	1.45	35.317	1.65	97	3585	40	3648	16	3682	10
MA07-68.1	234	654	2.79	127	0.604	0.3458	0.47	0.1830	1.24	0.403	1.37	19.233	1.50	59	2185	25	3054	14	3689	7
MA07-57.1	201	237	1.18	165	0.202	0.3482	0.40	0.1553	0.97	0.627	1.38	30.095	1.48	85	3137	34	3490	15	3699	6
MA07-75.1	136	247	1.81	123	0.137	0.3589	0.45	0.1886	0.92	0.677	1.41	33.499	1.53	89	3333	37	3595	15	3745	7
MA07-56.1	102	79	0.78	102	0.231	0.3636	0.50	0.1547	1.22	0.755	1.44	37.871	1.58	96	3628	40	3717	16	3765	8
MA07-67.1	91	47	0.52	92	0.005	0.3641	0.49	0.1200	1.00	0.792	1.45	39.767	1.59	100	3761	41	3765	16	3767	7
MA07-16.1	117	81	0.69	125	0.052	0.3654	0.45	0.1746	1.06	0.806	1.42	40.591	1.54	101	3809	41	3785	15	3773	7
MA07-15.1	217	282	1.30	253	-0.031	0.3667	0.31	0.3268	0.44	0.797	1.37	40.281	1.44	100	3777	39	3778	14	3778	5
MA07-47.1	702	1180	1.68	188	1.757	0.3675	0.46	0.1256	2.24	0.196	1.33	9.953	1.46	31	1156	14	2430	13	3781	7
MA07-65.2	28	27	0.96	32	0.566	0.3810	1.25	0.2405	3.26	0.795	1.79	41.749	2.31	98	3770	51	3813	23	3836	19
MA07-65.1	26	28	1.08	30	0.434	0.3867	1.04	0.2712	2.04	0.806	1.77	42.980	2.17	99	3811	51	3842	21	3858	16
MA07-54.1	213	643	3.01	117	0.395	0.3886	0.43	0.1265	1.46	0.415	1.37	22.214	1.48	58	2236	26	3193	14	3866	7
MA07-47.2	271	535	1.97	183	0.434	0.3939	0.36	0.0954	1.67	0.519	1.36	28.208	1.44	69	2696	30	3426	14	3886	5
MA07-53.1	74	80	1.09	88	0.107	0.3992	0.54	0.2358	0.96	0.844	1.49	46.487	1.64	101	3947	44	3920	16	3906	8
MA07-54.2	185	613	3.32	105	0.372	0.4020	0.48	0.1801	1.29	0.411	1.38	22.778	1.52	57	2219	26	3217	15	3917	7
MA07-76.2	248	965	3.89	184	0.635	0.4057	0.40	0.1892	1.15	0.529	1.36	29.583	1.46	70	2736	30	3473	14	3930	6

Continued on Next Page. . .

Table 4.2 – Continued

Grain .spot	U ppm	Th ppm	Th/U	Pb ppm	f206%	$^{207}Pb/^{206}Pb$ 204corr	±1σ (%)	$^{208}Pb/^{206}Pb$ 204corr	±1σ (%)	$^{206}Pb/^{238}U$ 204corr	±1σ (%)	$^{207}Pb/^{235}U$ 204corr	±1σ (%)	%c	$^{206}Pb/^{238}U$ date	±1σ (Ma)	$^{207}Pb/^{235}U$ date	±1σ (Ma)	$^{207}Pb/^{206}Pb$ date	±1σ (Ma)
MA07-48.4	424	1282	3.02	275	0.757	0.4112	0.33	0.0902	1.86	0.489	1.35	27.745	1.42	65	2568	28	3410	14	3951	5
MA07-76.1	164	463	2.83	145	0.252	0.4228	0.40	0.1565	1.12	0.644	1.39	37.551	1.49	80	3206	35	3708	15	3992	6
MA07-48.2	209	671	3.21	145	0.200	0.4440	0.39	0.0811	1.77	0.525	1.37	32.134	1.47	67	2720	30	3554	14	4065	6
MA07-52.1	171	302	1.76	171	0.101	0.4790	0.35	0.1862	0.75	0.696	1.38	45.940	1.47	81	3404	37	3908	15	4178	5
MA07-52.2	162	186	1.15	207	0.049	0.4839	0.34	0.2022	0.63	0.879	1.40	58.631	1.48	97	4065	42	4151	15	4193	5
MA07-48.1	86	68	0.79	104	0.039	0.4945	0.46	0.1317	1.47	0.859	1.46	58.586	1.59	95	3998	44	4150	16	4225	7
MA07-48.3	112	310	2.78	105	0.220	0.5058	0.46	0.1285	1.45	0.666	1.43	46.474	1.55	77	3292	37	3920	15	4258	7
MA11 Zircons (73 analyses from 1 session)																				
MA11-59.2	2214	4870	2.20	270	20.383	0.2158	2.88	0.4114	3.38	0.050	1.30	1.485	3.30	11	314	4	924	20	2950	46
MA11-59.1	2195	4110	1.87	281	20.452	0.2188	2.74	0.4213	3.19	0.052	1.30	1.570	3.18	11	327	4	958	20	2972	44
MA11-69.2	1923	2270	1.18	335	15.870	0.2243	2.06	0.3392	3.01	0.082	1.25	2.543	2.54	17	509	6	1284	19	3012	33
MA11-69.1	2216	534	0.24	350	16.138	0.2352	1.86	0.3303	2.92	0.074	1.25	2.396	2.36	15	459	6	1241	17	3088	30
MA11-31.1	1027	1383	1.35	322	10.702	0.2360	1.32	0.5255	1.34	0.156	1.23	5.084	1.91	30	936	11	1833	16	3093	21
MA11-13.1	448	2363	5.27	177	4.703	0.2696	0.88	0.2290	2.14	0.263	1.24	9.790	1.61	46	1507	17	2415	15	3304	14
MA11-3.1	343	455	1.33	276	0.620	0.2721	0.37	0.1967	0.77	0.622	1.24	23.350	1.33	94	3119	31	3242	13	3318	6
MA11-21.1	525	860	1.64	295	3.990	0.2771	0.69	0.3775	1.06	0.352	1.22	13.433	1.48	58	1942	21	2711	14	3346	11
MA11-13.2	251	1091	4.35	147	0.521	0.2867	0.48	0.0996	1.88	0.484	1.26	19.128	1.40	75	2544	27	3048	14	3400	7
MA11-44.2	226	577	2.56	148	0.533	0.2892	0.49	0.0832	2.20	0.544	1.26	21.677	1.41	82	2799	29	3169	14	3413	8
MA11-63.1	555	3026	5.45	281	4.049	0.2894	0.67	0.2262	1.73	0.341	1.23	13.611	1.47	55	1892	20	2723	14	3415	10
MA11-44.1	110	145	1.32	88	0.216	0.2928	0.60	0.1079	1.80	0.660	1.33	26.633	1.53	95	3266	34	3370	15	3432	9
MA11-56.1	497	2628	5.29	267	3.531	0.2954	0.68	0.1396	2.87	0.386	1.23	15.731	1.48	61	2106	22	2861	14	3446	11
MA11-40.2	568	1476	2.60	222	6.976	0.3031	1.03	0.3256	2.04	0.227	1.24	9.484	1.71	38	1319	15	2386	16	3486	16
MA11-55.1	176	105	0.60	152	0.148	0.3051	0.45	0.1076	1.45	0.705	1.28	29.661	1.41	98	3440	34	3476	14	3496	7
MA11-55.2	135	101	0.75	114	0.093	0.3063	0.52	0.1011	1.48	0.692	1.32	29.237	1.48	97	3391	35	3462	15	3503	8
MA11-41.1	368	438	1.19	228	2.946	0.3095	0.63	0.3197	1.21	0.404	1.24	17.223	1.46	62	2186	23	2947	14	3518	10
MA11-23.1	364	1868	5.14	128	1.928	0.3115	0.65	0.1759	2.07	0.257	1.23	11.037	1.46	42	1474	16	2526	14	3528	10
MA11-57.1	54	705	13.00	17	2.321	0.3157	2.00	0.1722	7.07	0.230	1.47	10.028	2.63	38	1337	18	2437	24	3549	31
MA11-34.1	313	3136	10.02	129	4.243	0.3169	0.92	0.1814	3.18	0.279	1.25	12.206	1.64	45	1588	18	2620	15	3555	14
MA11-16.1	85	95	1.11	67	0.915	0.3228	0.77	0.1159	3.42	0.617	1.38	27.456	1.66	86	3098	34	3400	16	3583	12
MA11-14.1	106	397	3.73	75	0.502	0.3240	0.67	0.1541	1.93	0.543	1.32	24.238	1.56	78	2794	30	3278	15	3589	10
MA11-22.1	122	381	3.14	67	0.884	0.3260	0.75	0.1915	1.96	0.411	1.31	18.481	1.59	62	2220	25	3015	15	3598	11
MA11-12.1	332	740	2.23	175	2.733	0.3262	0.63	0.1817	2.15	0.370	1.24	16.647	1.46	56	2030	22	2915	14	3599	10
MA11-73.1	43	260	6.10	16	1.377	0.3277	1.89	0.1485	7.10	0.277	1.51	12.528	2.56	44	1578	21	2645	24	3606	29
MA11-47.1	279	1466	5.26	164	3.466	0.3280	0.72	0.2249	2.03	0.394	1.26	17.830	1.52	59	2142	23	2981	15	3608	11
MA11-18.1	129	776	6.00	90	0.914	0.3285	0.67	0.3246	1.19	0.478	1.31	21.645	1.54	70	2518	27	3168	15	3610	10
MA11-70.1	32	283	8.75	18	1.120	0.3285	1.63	0.1363	6.37	0.433	1.61	19.600	2.43	64	2318	31	3072	23	3610	25
MA11-48.1	103	91	0.88	106	0.026	0.3304	0.49	0.2220	0.76	0.769	1.35	35.019	1.50	102	3676	38	3639	15	3619	8
MA11-43.1	50	27	0.54	50	0.163	0.3306	0.78	0.1567	1.90	0.775	1.50	35.323	1.77	102	3699	42	3648	18	3620	12

Continued on Next Page. . .

Table 4.2 – Continued

Grain .spot	U ppm	Th ppm	Th/U	Pb ppm	$f206\%$	^{207}Pb / ^{206}Pb 204corr	$\pm1\sigma$ (%)	^{208}Pb / ^{206}Pb 204corr	$\pm1\sigma$ (%)	^{206}Pb / ^{238}U 204corr	$\pm1\sigma$ (%)	^{207}Pb / ^{235}U 204corr	$\pm1\sigma$ (%)	%c	^{206}Pb / ^{238}U date	$\pm1\sigma$ (Ma)	^{207}Pb / ^{235}U date	$\pm1\sigma$ (Ma)	^{207}Pb / ^{206}Pb date	$\pm1\sigma$ (Ma)
MA11-20.1	137	259	1.89	131	0.056	0.3311	0.46	0.2019	0.82	0.722	1.31	32.942	1.44	97	3502	35	3579	14	3622	7
MA11-62.1	144	110	0.77	143	0.050	0.3329	0.44	0.1942	0.78	0.756	1.31	34.721	1.43	100	3631	36	3631	14	3630	7
MA11-37.1	301	1960	6.52	158	2.670	0.3337	0.65	0.1934	2.10	0.367	1.25	16.877	1.48	55	2014	22	2928	14	3634	10
MA11-5.1	288	1310	4.55	214	1.884	0.3338	0.52	0.2004	1.55	0.531	1.25	24.423	1.42	76	2744	28	3285	14	3635	8
MA11-58.1	148	139	0.93	150	0.086	0.3339	0.43	0.2174	0.72	0.758	1.30	34.900	1.42	100	3637	36	3636	14	3635	7
MA11-26.1	314	1169	3.72	217	1.774	0.3357	0.51	0.2137	1.40	0.490	1.25	22.673	1.41	71	2570	26	3213	14	3643	8
MA11-61.1	117	436	3.74	102	0.350	0.3356	0.56	0.2788	0.97	0.624	1.31	28.850	1.49	86	3124	32	3448	15	3643	9
MA11-36.1	85	172	2.03	73	0.178	0.3358	0.60	0.1527	1.35	0.668	1.38	30.933	1.57	91	3299	36	3517	15	3644	9
MA11-74.1	314	1610	5.12	200	2.401	0.3365	0.58	0.2819	1.32	0.424	1.25	19.696	1.44	63	2281	24	3077	14	3647	9
MA11-29.1	184	1117	6.08	103	0.702	0.3368	0.57	0.1673	1.66	0.424	1.27	19.678	1.46	62	2277	24	3076	14	3648	9
MA11-75.1	79	37	0.48	75	-0.049	0.3367	0.65	0.1237	2.08	0.757	1.39	35.150	1.60	100	3634	39	3643	16	3648	10
MA11-51.1	325	1637	5.04	270	1.343	0.3416	0.44	0.3034	0.87	0.564	1.24	26.554	1.37	79	2882	29	3367	13	3670	7
MA11-9.1	262	777	2.96	180	1.324	0.3422	0.48	0.1676	1.61	0.506	1.25	23.882	1.40	72	2640	27	3264	14	3672	7
MA11-38.1	231	669	2.90	167	1.057	0.3440	0.50	0.2111	1.28	0.523	1.26	24.819	1.41	74	2713	28	3301	14	3681	8
MA11-53.1	77	275	3.56	64	0.419	0.3445	0.69	0.1117	2.54	0.651	1.38	30.920	1.62	88	3232	35	3516	16	3683	10
MA11-40.1	317	1121	3.53	290	0.603	0.3448	0.35	0.2967	0.62	0.634	1.24	30.144	1.33	86	3166	31	3492	13	3684	5
MA11-30.1	102	249	2.44	78	0.291	0.3474	0.62	0.1127	2.39	0.605	1.34	28.974	1.55	83	3049	33	3453	15	3696	9
MA11-33.1	199	593	2.98	156	0.277	0.3478	0.41	0.0879	1.68	0.629	1.27	30.173	1.38	85	3146	32	3492	14	3698	6
MA11-4.1	90	36	0.40	87	0.024	0.3489	0.53	0.0764	1.68	0.784	1.37	37.708	1.53	101	3731	39	3712	15	3702	8
MA11-2.1	191	106	0.55	153	0.854	0.3500	0.47	0.1122	2.05	0.619	1.28	29.871	1.42	84	3106	32	3483	14	3707	7
MA11-50.1	151	632	4.19	83	0.580	0.3509	0.59	0.1945	1.44	0.407	1.29	19.708	1.48	59	2203	24	3077	14	3711	9
MA11-54.1	202	592	2.93	159	0.645	0.3518	0.45	0.1304	1.64	0.605	1.27	29.325	1.40	82	3048	31	3464	14	3715	7
MA11-53.2	103	77	0.75	104	0.000	0.3535	0.52	0.1818	1.10	0.767	1.36	37.390	1.51	99	3670	38	3704	15	3722	8
MA11-24.1	182	184	1.01	187	0.098	0.3538	0.37	0.2073	0.66	0.762	1.28	37.160	1.38	98	3651	36	3698	14	3723	6
MA11-38.2	85	486	5.73	61	0.619	0.3540	0.74	0.1635	2.15	0.541	1.38	26.427	1.64	75	2789	31	3362	16	3724	11
MA11-52.1	105	68	0.64	107	0.181	0.3541	0.52	0.1536	1.36	0.783	1.35	38.239	1.51	100	3729	38	3726	15	3725	8
MA11-27.1	156	311	1.99	147	0.210	0.3545	0.43	0.1497	1.10	0.722	1.29	35.311	1.41	94	3505	35	3647	14	3726	7
MA11-30.2	102	388	3.80	85	0.286	0.3545	0.60	0.1903	1.38	0.620	1.34	30.324	1.53	83	3112	33	3497	15	3726	9
MA11-46.1	106	71	0.67	109	0.063	0.3546	0.48	0.1380	1.05	0.799	1.34	39.081	1.48	102	3787	38	3748	15	3727	7
MA11-71.1	110	71	0.65	111	0.042	0.3552	0.48	0.1666	0.94	0.769	1.34	37.682	1.48	99	3678	37	3712	15	3730	7
MA11-10.1	159	120	0.76	168	0.022	0.3557	0.46	0.1886	1.27	0.792	1.31	38.850	1.44	101	3761	37	3742	14	3732	7
MA11-45.1	122	82	0.67	125	0.018	0.3557	0.47	0.1708	1.03	0.778	1.33	38.162	1.46	99	3710	37	3724	14	3732	7
MA11-66.1	160	649	4.06	131	0.512	0.3572	0.49	0.1708	1.33	0.610	1.29	30.050	1.43	82	3071	31	3488	14	3738	8
MA11-60.1	137	163	1.19	137	0.076	0.3575	0.44	0.1728	0.85	0.755	1.31	37.189	1.44	97	3624	36	3699	14	3739	7
MA11-68.1	99	49	0.50	87	0.558	0.3580	0.61	0.1300	2.19	0.682	1.35	33.658	1.55	90	3352	35	3600	15	3741	9
MA11-32.1	127	438	3.46	110	0.317	0.3587	0.50	0.1831	1.16	0.646	1.32	31.958	1.47	86	3214	33	3549	14	3744	8
MA11-49.1	143	130	0.91	152	-0.024	0.3615	0.42	0.1577	0.92	0.814	1.30	40.548	1.42	102	3837	38	3784	14	3756	6
MA11-1.1	224	435	1.94	183	0.316	0.3616	0.39	0.1947	0.85	0.603	1.27	30.083	1.37	81	3043	31	3490	14	3757	6
MA11-42.1	64	102	1.60	69	0.028	0.3619	0.69	0.2197	1.55	0.791	1.44	39.475	1.67	100	3757	41	3758	17	3758	11
MA11-19.1	159	397	2.50	172	0.133	0.3621	0.41	0.3089	0.61	0.752	1.30	37.521	1.41	96	3613	36	3707	14	3759	6

Continued on Next Page. . .

Table 4.2 – Continued

Grain .spot	U ppm	Th ppm	Th/U	Pb ppm	f206%	$^{207}Pb/^{206}Pb$ 204corr	±1σ (%)	$^{208}Pb/^{206}Pb$ 204corr	±1σ (%)	$^{206}Pb/^{238}U$ 204corr	±1σ (%)	$^{207}Pb/^{235}U$ 204corr	±1σ (%)	%c	$^{206}Pb/^{238}U$ date	±1σ (Ma)	$^{207}Pb/^{235}U$ date	±1σ (Ma)	$^{207}Pb/^{206}Pb$ date	±1σ (Ma)
MA11-6.1	101	120	1.19	99	0.047	0.3624	0.49	0.1490	1.05	0.755	1.35	37.698	1.49	96	3624	37	3712	15	3760	7
MA11-35.1	126	36	0.28	125	0.052	0.3627	0.46	0.0712	2.24	0.801	1.32	40.071	1.45	101	3794	38	3772	14	3761	7
MA11-28.1	95	86	0.90	100	-0.100	0.3657	0.54	0.1932	1.15	0.787	1.36	39.658	1.52	99	3741	39	3762	15	3774	8
MA13 Zircons (64 analyses from 1 session)																				
MA13-64.1	341	834	2.45	48	0.766	0.0730	2.75	0.1867	2.48	0.127	1.81	1.277	3.47	76	770	13	836	20	1014	56
MA13-59.1	333	1587	4.77	154	3.395	0.2758	0.84	0.1242	3.66	0.341	1.83	12.979	2.11	57	1893	30	2678	20	3339	13
MA13-58.1	332	1177	3.54	206	2.621	0.2872	0.65	0.1529	2.31	0.458	1.83	18.145	2.02	71	2432	37	2997	19	3403	10
MA13-31.1	138	201	1.46	128	4.959	0.2913	1.06	0.0088	68.20	0.692	1.90	27.804	2.29	99	3391	50	3412	22	3425	17
MA13-12.1	205	108	0.53	181	0.129	0.3052	0.38	0.1223	0.95	0.716	1.84	30.122	1.93	100	3480	50	3491	19	3497	6
MA13-61.1	360	2196	6.11	168	5.517	0.3212	0.91	0.2515	2.40	0.290	1.83	12.861	2.14	46	1643	27	2670	20	3576	14
MA13-50.1	249	2099	8.42	110	5.497	0.3246	1.32	0.3546	2.54	0.261	1.86	11.674	2.41	42	1494	25	2579	23	3592	20
MA13-35.1	220	1270	5.76	158	2.877	0.3308	0.72	0.2143	2.12	0.492	1.85	22.417	2.06	71	2577	39	3202	20	3621	11
MA13-57.1	337	790	2.34	216	3.176	0.3308	0.62	0.1562	2.52	0.450	1.83	20.545	2.00	66	2397	37	3117	19	3621	10
MA13-4.1	233	1776	7.62	166	2.898	0.3361	0.66	0.1686	2.47	0.500	1.84	23.176	2.03	72	2615	40	3234	20	3645	10
MA13-36.1	216	1031	4.78	136	2.819	0.3376	0.74	0.1624	2.88	0.444	1.84	20.671	2.07	65	2369	37	3123	20	3652	11
MA13-9.1	45	19	0.41	43	-0.087	0.3386	1.27	0.1119	6.90	0.766	2.06	35.752	2.55	100	3665	58	3660	25	3657	19
MA13-32.1	98	160	1.63	97	0.471	0.3389	0.58	0.1639	1.55	0.756	1.92	35.317	2.07	99	3629	53	3648	20	3658	9
MA13-40.1	95	236	2.50	74	1.085	0.3395	0.77	0.2042	2.09	0.572	1.91	26.779	2.15	80	2917	45	3375	21	3660	12
MA13-26.1	231	1500	6.50	147	2.440	0.3401	0.67	0.2144	1.95	0.440	1.84	20.631	2.03	64	2350	36	3121	20	3663	10
MA13-62.1	130	44	0.34	118	0.064	0.3420	0.48	0.0835	1.91	0.735	1.89	34.675	2.01	97	3553	52	3629	20	3672	7
MA13-22.1	94	43	0.45	91	0.004	0.3423	0.51	0.1180	1.03	0.768	1.90	36.259	2.03	100	3675	53	3674	20	3673	8
MA13-63.1	163	1011	6.21	107	1.328	0.3459	0.69	0.1830	2.16	0.479	1.86	22.843	2.06	68	2523	39	3220	20	3689	11
MA13-46.1	184	726	3.95	130	1.465	0.3469	0.59	0.1801	1.87	0.514	1.85	24.600	2.01	72	2675	41	3292	20	3693	9
MA13-37.1	170	616	3.62	60	0.718	0.3471	0.74	0.1354	2.56	0.270	1.84	12.909	2.06	42	1540	25	2673	19	3694	11
MA13-56.1	175	988	5.63	109	2.283	0.3475	0.81	0.1801	2.83	0.438	1.86	20.999	2.12	63	2343	37	3139	21	3696	12
MA13-15.1	206	900	4.38	169	0.900	0.3510	0.45	0.1373	1.67	0.622	1.84	30.099	1.95	84	3117	46	3490	19	3711	7
MA13-10.1	145	590	4.06	94	1.057	0.3517	0.63	0.1848	1.90	0.471	1.86	22.851	2.04	67	2489	38	3221	20	3714	10
MA13-48.1	146	9	0.06	129	0.081	0.3519	0.43	0.0048	18.37	0.759	1.87	36.814	1.98	98	3640	52	3689	20	3715	7
MA13-54.1	77	120	1.56	62	0.556	0.3521	0.73	0.1573	2.14	0.613	1.94	29.782	2.15	83	3084	48	3480	21	3716	11
MA13-1.1	76	47	0.62	78	0.011	0.3532	0.54	0.1578	0.97	0.793	1.94	38.634	2.08	101	3765	55	3736	21	3721	8
MA13-13.1	181	253	1.40	182	0.230	0.3533	0.39	0.1903	0.84	0.750	1.85	36.541	1.94	97	3608	51	3681	19	3721	6
MA13-30.1	231	1140	4.95	163	0.822	0.3537	0.49	0.1908	1.34	0.517	1.84	25.219	1.96	72	2687	40	3317	19	3723	7
MA13-51.1	183	406	2.22	159	1.118	0.3541	0.51	0.1514	1.85	0.646	1.85	31.517	1.98	86	3211	47	3535	20	3725	8
MA13-11.1	148	208	1.40	141	0.371	0.3544	0.45	0.1521	1.21	0.722	1.86	35.289	1.97	94	3504	50	3647	19	3726	7
MA13-23.1	49	22	0.45	49	0.096	0.3546	0.74	0.1107	2.01	0.793	2.02	38.786	2.23	101	3765	58	3740	22	3727	11
MA13-16.1	153	1466	9.61	129	0.828	0.3562	0.53	0.1554	1.73	0.630	1.86	30.958	2.00	84	3151	46	3518	20	3734	8
MA13-3.1	159	359	2.26	147	0.509	0.3570	0.47	0.1711	1.32	0.690	1.86	33.958	1.97	90	3382	49	3609	19	3737	7
MA13-47.1	55	34	0.62	57	0.126	0.3572	0.72	0.1379	1.97	0.799	1.99	39.338	2.20	101	3785	57	3754	22	3738	11

Continued on Next Page...

Table 4.2 – Continued

Grain .spot	U ppm	Th ppm	Th/U	Pb ppm	$f206\%$	$^{207}Pb/^{206}Pb$ 204corr	$\pm1\sigma$ (%)	$^{208}Pb/^{206}Pb$ 204corr	$\pm1\sigma$ (%)	$^{206}Pb/^{238}U$ 204corr	$\pm1\sigma$ (%)	$^{207}Pb/^{235}U$ 204corr	$\pm1\sigma$ (%)	%c	$^{206}Pb/^{238}U$ date	$\pm1\sigma$ (Ma)	$^{207}Pb/^{235}U$ date	$\pm1\sigma$ (Ma)	$^{207}Pb/^{206}Pb$ date	$\pm1\sigma$ (Ma)
MA13-19.1	139	60	0.43	137	0.080	0.3574	0.41	0.1041	1.10	0.777	1.87	38.273	1.96	99	3705	53	3727	19	3739	6
MA13-39.1	63	58	0.92	66	0.098	0.3578	0.83	0.2346	2.00	0.766	1.98	37.765	2.24	98	3665	55	3714	22	3740	13
MA13-8.1	54	33	0.61	58	0.101	0.3580	0.66	0.1548	1.34	0.824	1.99	40.686	2.17	104	3875	58	3788	21	3742	10
MA13-5.1	129	515	3.99	112	1.142	0.3587	0.57	0.1596	2.00	0.639	1.88	31.592	2.03	85	3184	47	3538	20	3744	9
MA13-6.1	251	262	1.04	252	0.437	0.3585	0.34	0.2046	0.79	0.736	1.83	36.394	1.91	95	3557	50	3677	19	3744	5
MA13-52.1	60	91	1.51	61	0.081	0.3589	0.70	0.2372	1.28	0.742	1.98	36.723	2.18	96	3579	54	3686	22	3745	11
MA13-45.1	80	98	1.23	78	0.066	0.3591	0.67	0.1370	2.28	0.760	1.93	37.627	2.12	97	3644	54	3710	21	3746	10
MA13-60.1	136	112	0.82	144	0.024	0.3590	0.43	0.2078	0.69	0.779	1.88	38.574	1.98	99	3714	53	3735	20	3746	7
MA13-41.1	210	279	1.33	198	0.221	0.3593	0.37	0.1762	0.83	0.708	1.85	35.076	1.93	92	3451	49	3641	19	3747	6
MA13-43.1	165	1155	7.00	137	0.587	0.3595	0.49	0.1222	1.91	0.640	1.86	31.698	1.99	85	3187	47	3541	20	3748	7
MA13-17.1	73	74	1.01	69	0.225	0.3598	0.62	0.1202	1.93	0.730	1.94	36.196	2.11	94	3532	53	3672	21	3749	9
MA13-53.1	80	52	0.65	80	0.040	0.3598	0.56	0.1111	1.38	0.789	1.93	39.113	2.07	100	3748	55	3748	21	3749	8
MA13-38.1	127	203	1.60	124	0.082	0.3604	0.46	0.1438	1.08	0.752	1.89	37.366	2.00	96	3615	52	3703	20	3751	7
MA13-44.1	140	173	1.24	156	0.083	0.3603	0.48	0.3104	0.79	0.771	1.88	38.310	1.99	98	3685	53	3728	20	3751	7
MA13-28.1	96	63	0.66	99	0.097	0.3604	0.52	0.1648	1.02	0.782	1.91	38.842	2.04	99	3723	54	3742	20	3752	8
MA13-49.1	65	198	3.03	53	0.124	0.3604	0.87	0.2236	2.17	0.588	1.96	29.227	2.25	79	2982	47	3461	22	3752	13
MA13-24.1	85	87	1.02	87	0.102	0.3607	0.57	0.1875	1.23	0.764	1.93	38.025	2.08	98	3661	54	3721	21	3753	9
MA13-2.1	91	181	1.98	77	0.267	0.3610	0.58	0.0796	2.83	0.678	1.91	33.760	2.07	89	3338	50	3603	20	3754	9
MA13-34.1	132	163	1.23	127	0.108	0.3609	0.45	0.1383	1.02	0.741	1.88	36.868	1.99	95	3574	52	3690	20	3754	7
MA13-27.1	42	42	1.00	45	0.088	0.3615	0.95	0.2550	2.06	0.767	2.06	38.249	2.37	98	3671	58	3726	23	3756	14
MA13-21.1	108	61	0.57	112	0.031	0.3623	0.46	0.1447	0.91	0.799	1.89	39.919	2.00	101	3786	54	3769	20	3760	7
MA13-29.1	93	38	0.40	92	-0.034	0.3626	0.51	0.0749	1.59	0.794	1.92	39.698	2.04	100	3768	55	3763	20	3761	8
MA13-42.1	36	15	0.42	36	-0.146	0.3627	0.87	0.1122	2.44	0.789	2.10	39.442	2.37	100	3748	60	3757	23	3761	13
MA13-55.1	109	80	0.74	112	0.073	0.3626	0.49	0.1861	0.93	0.772	1.89	38.581	2.01	98	3687	53	3735	20	3761	7
MA13-20.1	181	216	1.20	202	0.035	0.3633	0.37	0.2875	0.56	0.785	1.85	39.331	1.93	99	3736	52	3754	19	3764	6
MA13-25.1	93	263	2.82	88	0.356	0.3635	0.60	0.1590	1.65	0.717	1.92	35.914	2.08	93	3483	52	3664	21	3764	9
MA13-14.1	100	62	0.62	101	0.100	0.3637	0.49	0.1247	1.32	0.789	1.89	39.583	2.01	100	3751	54	3760	20	3765	7
MA13-33.1	110	130	1.18	110	0.047	0.3650	0.48	0.1696	0.86	0.755	1.91	38.014	2.02	96	3627	53	3720	20	3771	7
MA13-7.1	56	24	0.42	58	-0.001	0.3657	0.62	0.1090	1.29	0.811	1.98	40.884	2.15	101	3828	57	3792	21	3774	9
MA13-18.1	25	10	0.38	25	-0.134	0.3687	1.63	0.0971	11.24	0.801	2.25	40.741	2.94	100	3794	65	3789	29	3786	25
MA14 Zircons (67 analyses from 1 session)																				
MA14-67.1	1473	4220	2.86	409	10.854	0.2592	1.11	0.3431	1.83	0.147	1.81	5.267	2.24	27	886	15	1863	19	3242	17
MA14-53.1	128	544	4.26	56	1.201	0.2821	0.91	0.1503	2.88	0.342	1.86	13.318	2.17	56	1898	31	2702	20	3374	14
MA14-68.1	100	77	0.77	86	-0.107	0.2822	0.78	0.1762	2.07	0.687	1.91	26.730	2.15	100	3371	50	3374	21	3375	12
MA14-12.1	259	64	0.25	214	0.129	0.2943	0.36	0.0655	1.57	0.704	1.83	28.571	1.91	100	3436	49	3439	19	3440	6
MA14-28.1	357	254	0.71	312	0.082	0.2944	0.29	0.1467	0.61	0.702	1.82	28.506	1.88	100	3429	48	3437	18	3441	5
MA14-46.1	88	383	4.36	64	0.645	0.2950	0.77	0.1862	1.89	0.562	1.91	22.879	2.14	84	2877	44	3222	21	3444	12
MA14-30.1	286	997	3.49	151	4.492	0.3217	0.91	0.2657	2.24	0.337	1.83	14.926	2.14	52	1870	30	2811	20	3578	14

Continued on Next Page...

Table 4.2 – Continued

Grain .spot	U ppm	Th ppm	Th/U	Pb ppm	$f206\%$	$^{207}Pb/^{206}Pb$ 204corr	$\pm1\sigma$ (%)	$^{208}Pb/^{206}Pb$ 204corr	$\pm1\sigma$ (%)	$^{206}Pb/^{238}U$ 204corr	$\pm1\sigma$ (%)	$^{207}Pb/^{235}U$ 204corr	$\pm1\sigma$ (%)	%c	$^{206}Pb/^{238}U$ date	$\pm1\sigma$ (Ma)	$^{207}Pb/^{235}U$ date	$\pm1\sigma$ (Ma)	$^{207}Pb/^{206}Pb$ date	$\pm1\sigma$ (Ma)
MA14-62.1	190	968	5.10	122	1.080	0.3251	0.59	0.1975	1.58	0.472	1.85	21.143	2.01	69	2491	38	3145	20	3594	9
MA14-44.1	176	638	3.62	112	1.144	0.3263	0.65	0.4376	0.90	0.407	1.84	18.296	2.03	61	2200	34	3005	20	3600	10
MA14-17.1	109	121	1.11	98	0.546	0.3277	0.58	0.1436	1.80	0.694	1.89	31.375	2.04	94	3399	50	3531	20	3607	9
MA14-43.1	88	63	0.72	90	0.029	0.3326	0.55	0.1859	1.04	0.780	1.91	35.789	2.05	102	3719	54	3661	20	3629	8
MA14-38.1	145	1056	7.30	124	1.915	0.3329	0.66	0.2648	1.53	0.588	1.87	26.978	2.06	82	2980	45	3383	20	3630	10
MA14-66.1	97	84	0.86	95	0.248	0.3337	0.57	0.1584	1.38	0.757	1.90	34.809	2.05	100	3632	53	3633	20	3634	9
MA14-60.1	143	212	1.48	122	0.273	0.3372	0.49	0.0397	3.93	0.711	1.87	33.066	1.99	95	3463	50	3583	20	3650	8
MA14-54.1	174	2072	11.93	105	2.391	0.3391	0.74	0.2294	2.02	0.413	1.84	19.327	2.07	61	2230	35	3058	20	3659	11
MA14-54.1	189	2178	11.55	112	2.287	0.3410	0.72	0.2232	2.03	0.408	1.85	19.201	2.07	60	2208	35	3052	20	3667	11
MA14-15.1	258	87	0.34	151	4.717	0.3463	0.83	0.2154	2.68	0.376	1.84	17.943	2.11	56	2057	32	2987	20	3691	13
MA14-11.1	253	1079	4.27	186	2.866	0.3483	0.60	0.2488	1.61	0.490	1.83	23.508	2.00	69	2569	39	3248	20	3699	9
MA14-40.1	41	20	0.47	42	-0.071	0.3518	1.05	0.1218	4.93	0.799	2.05	38.749	2.42	102	3785	59	3739	24	3715	16
MA14-45.1	40	18	0.45	41	0.178	0.3526	0.87	0.1133	3.41	0.802	2.05	38.991	2.33	102	3797	59	3745	23	3718	13
MA14-42.1	55	21	0.38	57	0.121	0.3533	0.67	0.0926	2.21	0.828	1.98	40.356	2.16	105	3890	58	3779	21	3721	10
MA14-14.1	186	380	2.04	136	0.228	0.3544	0.44	0.0903	1.69	0.585	1.84	28.599	1.95	80	2971	44	3440	19	3726	7
MA14-20.1	200	1336	6.68	159	1.276	0.3544	0.51	0.1466	1.94	0.589	1.85	28.801	1.98	80	2987	44	3447	19	3726	8
MA14-69.1	36	37	1.02	40	-0.032	0.3558	0.92	0.2542	1.51	0.806	2.10	39.523	2.39	102	3809	60	3759	24	3732	14
MA14-64.1	70	262	3.75	59	0.486	0.3560	0.78	0.2157	1.84	0.621	1.95	30.477	2.19	83	3113	48	3502	22	3733	12
MA14-58.1	139	363	2.61	127	0.903	0.3569	0.59	0.1631	1.97	0.678	1.87	33.350	2.04	89	3336	49	3591	20	3737	9
MA14-16.1	142	74	0.52	145	0.121	0.3573	0.43	0.1272	1.23	0.797	1.86	39.285	1.96	101	3780	53	3753	19	3738	7
MA14-37.1	39	22	0.56	42	0.275	0.3574	0.91	0.1355	3.34	0.839	2.06	41.342	2.35	105	3927	60	3803	23	3739	14
MA14-32.1	81	109	1.34	50	0.167	0.3583	0.77	0.1846	1.99	0.459	1.91	22.675	2.15	65	2435	39	3213	21	3743	12
MA14-4.1	96	89	0.93	105	0.060	0.3583	0.51	0.2321	0.92	0.791	1.91	39.060	2.03	100	3756	54	3747	20	3743	8
MA14-34.1	106	149	1.41	104	0.110	0.3593	0.52	0.1281	1.57	0.763	1.89	37.797	2.02	98	3655	53	3715	20	3747	8
MA14-59.1	96	320	3.33	77	0.344	0.3593	0.65	0.1351	2.07	0.613	1.91	30.375	2.10	82	3082	47	3499	21	3747	10
MA14-21.1	161	751	4.68	114	0.407	0.3595	0.49	0.1942	1.15	0.524	1.85	25.961	1.98	72	2715	41	3345	19	3748	7
MA14-41.1	95	251	2.64	101	0.167	0.3595	0.54	0.3068	0.85	0.734	1.90	36.400	2.04	95	3550	52	3677	20	3748	8
MA14-47.1	79	101	1.28	81	0.172	0.3594	0.58	0.1448	1.54	0.790	1.92	39.160	2.08	100	3754	55	3750	21	3748	9
MA14-50.1	31	16	0.54	33	0.126	0.3596	0.91	0.1343	2.33	0.833	2.13	41.316	2.42	104	3907	62	3803	24	3748	14
MA14-52.1	173	416	2.40	152	0.525	0.3596	0.46	0.1505	1.46	0.664	1.85	32.924	1.96	88	3283	48	3578	19	3748	7
MA14-55.1	163	278	1.71	135	0.279	0.3595	0.43	0.1520	1.11	0.634	1.86	31.437	1.96	84	3166	46	3533	19	3748	7
MA14-18.1	119	328	2.76	96	0.281	0.3599	0.53	0.1787	1.28	0.606	1.88	30.076	2.02	81	3055	46	3489	20	3749	8
MA14-6.1	142	573	4.04	116	0.283	0.3597	0.48	0.2141	1.00	0.598	1.86	29.672	1.98	81	3023	45	3476	19	3749	7
MA14-24.1	51	41	0.81	56	0.402	0.3601	0.84	0.1981	2.31	0.814	2.00	40.410	2.26	102	3839	58	3781	22	3750	13
MA14-61.1	74	49	0.65	78	0.139	0.3600	0.64	0.1622	1.54	0.799	1.95	39.662	2.12	101	3786	56	3762	21	3750	10
MA14-7.1	162	109	0.68	166	0.035	0.3601	0.38	0.1669	0.75	0.781	1.86	38.792	1.95	99	3722	53	3740	19	3750	6
MA14-19.1	279	1271	4.55	241	0.281	0.3606	0.36	0.3739	0.51	0.572	1.82	28.455	1.90	78	2917	43	3435	19	3752	5
MA14-13.1	87	70	0.80	85	0.014	0.3606	0.52	0.1398	1.04	0.753	1.91	37.456	2.04	96	3620	53	3706	20	3753	8
MA14-27.1	135	318	2.35	112	0.300	0.3606	0.50	0.1930	1.17	0.615	1.86	30.587	1.99	82	3091	46	3506	20	3753	8
MA14-48.1	98	59	0.60	96	0.188	0.3607	0.51	0.0868	1.94	0.781	1.89	38.861	2.02	99	3722	54	3742	20	3753	8

Continued on Next Page...

Table 4.2 – Continued

Grain .spot	U ppm	Th ppm	Th/U	Pb ppm	$f206\%$	$^{207}Pb/^{206}Pb$ 204corr	$\pm1\sigma$ (%)	$^{208}Pb/^{206}Pb$ 204corr	$\pm1\sigma$ (%)	$^{206}Pb/^{238}U$ 204corr	$\pm1\sigma$ (%)	$^{207}Pb/^{235}U$ 204corr	$\pm1\sigma$ (%)	%c	$^{206}Pb/^{238}U$ date	$\pm1\sigma$ (Ma)	$^{207}Pb/^{235}U$ date	$\pm1\sigma$ (Ma)	$^{207}Pb/^{206}Pb$ date	$\pm1\sigma$ (Ma)
MA14-49.1	52	36	0.70	56	0.108	0.3608	0.71	0.1787	1.61	0.811	1.99	40.326	2.20	102	3827	58	3779	22	3753	11
MA14-10.1	102	73	0.71	105	0.100	0.3609	0.54	0.1551	1.56	0.786	1.90	39.122	2.04	100	3740	54	3749	20	3754	8
MA14-57.1	138	77	0.55	144	-0.029	0.3611	0.44	0.1419	0.89	0.806	1.88	40.139	1.98	102	3811	54	3774	20	3755	7
MA14-22.1	121	75	0.62	127	0.042	0.3615	0.44	0.1589	0.85	0.805	1.88	40.103	1.98	101	3805	54	3773	20	3756	7
MA14-29.1	77	71	0.92	86	0.116	0.3615	0.62	0.2305	1.33	0.810	1.93	40.353	2.10	102	3824	56	3779	21	3756	9
MA14-2.1	74	289	3.90	49	0.551	0.3617	0.81	0.1742	2.37	0.488	1.92	24.357	2.18	68	2564	41	3283	21	3757	12
MA14-56.1	56	36	0.64	59	0.168	0.3617	0.68	0.1617	1.64	0.796	1.97	39.693	2.16	100	3774	56	3763	21	3757	10
MA14-8.1	182	317	1.74	162	0.182	0.3616	0.40	0.2296	0.70	0.645	1.85	32.158	1.94	85	3209	47	3555	19	3757	6
MA14-9.1	193	156	0.81	206	0.006	0.3617	0.35	0.2007	0.59	0.792	1.85	39.505	1.92	100	3761	53	3758	19	3757	5
MA14-26.1	60	66	1.10	62	0.133	0.3621	0.87	0.1232	4.06	0.810	1.98	40.459	2.26	102	3826	57	3782	22	3759	13
MA14-25.1	127	187	1.47	118	0.083	0.3626	0.46	0.1626	1.06	0.703	1.88	35.134	1.99	91	3431	50	3642	20	3761	7
MA14-51.1	248	303	1.22	287	0.030	0.3626	0.32	0.3048	0.49	0.804	1.84	40.221	1.90	101	3805	53	3776	19	3761	5
MA14-33.1	88	102	1.15	102	0.068	0.3629	1.05	0.2886	2.64	0.810	1.94	40.543	2.32	102	3826	56	3784	23	3762	16
MA14-39.1	182	154	0.85	192	0.074	0.3633	0.36	0.1957	0.65	0.785	1.85	39.305	1.93	99	3734	52	3753	19	3764	5
MA14-5.1	71	66	0.93	79	0.135	0.3633	0.59	0.2387	1.04	0.805	1.94	40.339	2.10	101	3808	56	3779	21	3764	9
MA14-65.1	150	134	0.89	142	0.134	0.3633	0.43	0.0653	1.67	0.766	1.86	38.365	1.97	97	3666	52	3729	19	3764	7
MA14-23.1	134	468	3.50	138	0.137	0.3641	0.44	0.2763	0.72	0.728	1.87	36.565	1.97	94	3528	51	3682	19	3767	7
MA14-36.1	77	55	0.71	83	-0.006	0.3641	0.53	0.1829	0.89	0.802	1.93	40.248	2.06	101	3795	55	3777	20	3767	8
MA14-35.1	108	135	1.25	108	0.062	0.3643	0.49	0.1700	1.06	0.756	1.89	37.978	2.01	96	3630	52	3719	20	3768	7
MA14-31.1	93	56	0.60	97	0.028	0.3646	0.51	0.1518	1.06	0.798	1.90	40.097	2.03	100	3781	54	3773	20	3769	8
MA64 Zircons (78 analyses from 3 sessions)																				
MA64-49.1	1568	5946	3.79	335	9.763	0.2529	1.59	0.2435	3.55	0.123	1.15	4.293	2.07	23	748	8	1692	17	3203	25
MA64-43.1	1236	5282	4.27	357	6.690	0.2628	1.17	0.3556	1.87	0.170	1.14	6.177	1.73	31	1014	11	2001	15	3264	18
MA64-62.1	338	1080	3.20	150	0.986	0.2748	0.85	0.3083	1.37	0.317	1.22	11.995	1.57	53	1773	19	2604	15	3333	13
MA64-41.8-2	1035	3969	3.83	191	7.443	0.2958	1.13	0.1616	4.32	0.116	5.07	4.716	5.34	20	705	34	1770	45	3448	18
MA64-56.1	348	1333	3.84	159	1.390	0.3022	0.81	0.1681	2.49	0.346	1.20	14.397	1.53	55	1913	20	2776	14	3481	12
MA64-58.1	371	168	0.45	276	0.044	0.3023	0.23	0.1363	0.50	0.599	1.11	24.960	1.16	87	3025	27	3307	11	3482	4
MA64-59.1	108	136	1.26	61	0.492	0.3039	0.57	0.1410	1.71	0.443	1.18	18.584	1.37	68	2366	23	3020	13	3490	9
MA64-70.1	86	57	0.67	76	-0.086	0.3070	0.95	0.1698	1.85	0.692	1.61	29.309	1.97	97	3392	42	3464	19	3506	15
MA64-53.1	843	1482	1.76	221	4.479	0.3220	0.99	0.2403	2.67	0.169	1.14	7.523	1.60	28	1009	11	2176	14	3579	15
MA64-41.12	983	4340	4.41	210	8.320	0.3224	1.06	0.1873	3.84	0.126	5.07	5.615	5.31	21	767	37	1918	46	3581	16
MA64-72.1	246	416	1.69	158	0.809	0.3229	0.69	0.1719	1.94	0.486	1.28	21.630	1.52	71	2553	27	3167	15	3584	11
MA64-46.1	99	80	0.80	67	0.300	0.3262	0.94	0.0958	4.02	0.547	1.50	24.620	1.86	78	2815	34	3293	18	3599	14
MA64-55.1	430	283	0.66	310	0.218	0.3265	0.41	0.1502	0.99	0.563	1.17	25.366	1.29	80	2881	27	3322	13	3601	6
MA64-42.1	449	1421	3.17	167	2.346	0.3270	0.86	0.1772	2.94	0.266	1.18	11.981	1.54	42	1519	16	2603	14	3603	13
MA64-50.1	85	113	1.33	50	-0.107	0.3306	0.93	0.1498	1.78	0.465	1.57	21.194	1.92	68	2462	32	3148	19	3620	14
MA64-71.1	180	196	1.09	116	0.609	0.3311	0.78	0.0813	3.93	0.518	1.32	23.651	1.62	74	2691	29	3254	16	3622	12
MA64-42.2	180	112	0.62	139	0.137	0.3328	0.59	0.1089	1.56	0.622	1.30	28.546	1.49	86	3118	32	3438	15	3630	9

Continued on Next Page...

Table 4.2 – Continued

Grain .spot	U ppm	Th ppm	Th/U	Pb ppm	$f206\%$	$^{207}Pb/^{206}Pb$ 204corr	$\pm1\sigma$ (%)	$^{208}Pb/^{206}Pb$ 204corr	$\pm1\sigma$ (%)	$^{206}Pb/^{238}U$ 204corr	$\pm1\sigma$ (%)	$^{207}Pb/^{235}U$ 204corr	$\pm1\sigma$ (%)	%c	$^{206}Pb/^{238}U$ date	$\pm1\sigma$ (Ma)	$^{207}Pb/^{235}U$ date	$\pm1\sigma$ (Ma)	$^{207}Pb/^{206}Pb$ date	$\pm1\sigma$ (Ma)
MA64-68.1	486	832	1.71	264	2.595	0.3330	0.74	0.1324	3.45	0.395	1.19	18.128	1.48	59	2145	22	2997	14	3631	11
MA64-73.1	158	159	1.01	143	0.139	0.3332	0.63	0.1578	1.32	0.704	1.37	32.361	1.58	95	3437	37	3561	16	3632	10
MA64-41.8	1091	3966	3.64	224	0.016	0.3335	0.36	0.3373	0.47	0.143	5.07	6.567	5.13	24	861	41	2055	45	3633	5
MA64-46.2	265	244	0.92	210	0.571	0.3338	0.58	0.1659	1.63	0.600	1.26	27.628	1.45	83	3031	31	3406	14	3635	9
MA64-74.1	194	129	0.66	175	0.286	0.3410	0.59	0.1046	2.00	0.718	1.32	33.734	1.51	95	3487	36	3602	15	3667	9
MA64-44.1	420	1003	2.39	185	2.278	0.3467	0.75	0.1337	3.44	0.321	1.20	15.348	1.49	49	1795	19	2837	14	3693	11
MA64-51.1	149	224	1.50	98	0.271	0.3519	0.73	0.1258	1.88	0.515	1.37	24.998	1.63	72	2679	30	3308	16	3715	11
MA64-64.1	190	266	1.40	78	0.592	0.3528	0.87	0.1519	2.59	0.311	1.28	15.149	1.63	47	1748	20	2825	16	3719	13
MA64-57.1	181	354	1.95	124	0.544	0.3547	0.36	0.0462	3.34	0.555	1.14	27.144	1.24	76	2846	26	3389	12	3727	6
MA64-66.1	76	43	0.56	73	-0.038	0.3570	0.84	0.1318	1.64	0.751	1.63	36.987	1.92	97	3612	45	3693	19	3737	13
MA64-63.2	329	864	2.63	171	1.134	0.3591	0.73	0.1146	3.64	0.394	1.22	19.489	1.50	57	2140	22	3066	14	3746	11
MA64-48.7	82	37	0.45	73	0.111	0.3637	0.50	0.1149	1.40	0.696	5.09	34.882	5.18	90	3404	135	3635	51	3765	8
MA64-48.3	98	33	0.33	94	0.019	0.3639	0.40	0.0889	0.97	0.763	5.09	38.304	5.16	97	3656	142	3728	51	3766	6
MA64-48.8	108	53	0.49	93	0.017	0.3651	0.42	0.1313	0.88	0.670	5.08	33.709	5.15	88	3305	131	3602	51	3771	6
MA64-48.6	67	26	0.39	59	-0.012	0.3659	0.51	0.0998	1.47	0.702	5.10	35.429	5.19	91	3429	136	3651	51	3775	8
MA64-48.4	112	44	0.39	112	-0.007	0.3667	0.38	0.1092	0.82	0.789	5.09	39.906	5.15	99	3751	145	3768	51	3778	6
MA64-48.10	100	35	0.35	74	-0.085	0.3670	1.01	0.0926	7.95	0.596	5.09	30.138	5.32	80	3012	123	3491	52	3779	15
MA64-48.9	95	80	0.83	71	0.056	0.3670	0.44	0.0898	1.35	0.596	5.09	30.176	5.16	80	3015	122	3493	51	3779	7
MA64-75.1	162	70	0.44	121	0.115	0.3669	0.36	0.1361	0.88	0.575	2.73	29.093	2.80	78	2929	64	3457	27	3779	5
MA64-48.11	110	38	0.35	93	0.057	0.3674	0.37	0.0890	1.06	0.674	5.08	34.116	5.14	88	3320	132	3613	51	3781	6
MA64-48.1	89	37	0.42	89	-0.009	0.3687	0.38	0.1078	0.81	0.788	1.22	40.046	1.32	99	3745	35	3772	13	3786	6
MA64-48.5	98	36	0.37	94	0.088	0.3693	0.42	0.0994	1.37	0.761	5.09	38.728	5.16	96	3646	142	3739	51	3788	6
MA64-41.9-2	775	2517	3.25	215	5.250	0.3733	0.72	0.1506	3.56	0.179	5.07	9.195	5.21	28	1060	50	2358	48	3805	11
MA64-63.1	200	285	1.43	178	0.440	0.3733	0.64	0.3501	1.03	0.594	1.29	30.555	1.51	79	3004	31	3505	15	3805	10
MA64-54.1	405	706	1.74	159	1.102	0.3920	0.62	0.1502	2.36	0.286	1.18	15.437	1.40	42	1619	17	2843	13	3879	9
MA64-65.3	155	135	0.87	178	0.057	0.3991	0.29	0.2245	0.52	0.817	1.16	44.941	1.23	99	3849	34	3886	12	3906	4
MA64-65.1	106	88	0.83	122	0.052	0.4013	0.40	0.2113	1.03	0.821	1.20	45.443	1.32	99	3865	35	3897	13	3914	6
MA64-65.2	133	18	0.13	135	0.003	0.4018	0.30	0.0349	1.38	0.822	1.17	45.569	1.25	99	3869	34	3900	12	3916	5
MA64-41.3	634	2807	4.43	252	4.662	0.4091	0.40	0.1167	2.68	0.260	1.10	14.688	1.21	38	1492	15	2795	12	3943	6
MA64-40.2	185	194	1.05	143	0.803	0.4156	0.34	0.0484	3.71	0.598	1.15	34.283	1.24	76	3023	28	3618	12	3966	5
MA64-41.9	754	2343	3.11	244	0.035	0.4315	0.33	0.2464	0.52	0.223	5.07	13.279	5.12	32	1299	60	2700	48	4023	5
MA64-54.2	270	507	1.88	181	0.769	0.4481	0.30	0.2191	0.82	0.456	1.12	28.180	1.19	59	2422	23	3425	12	4079	4
MA64-40.3	268	821	3.06	152	1.335	0.4626	0.33	0.1563	1.43	0.389	1.12	24.843	1.20	51	2120	20	3302	12	4126	5
MA64-45.2	153	356	2.32	93	0.239	0.4626	0.34	0.0870	1.58	0.451	1.15	28.777	1.24	58	2401	23	3446	12	4126	5
MA64-41.7-2	672	1968	2.93	281	1.674	0.4628	0.47	0.2075	1.65	0.276	5.07	17.594	5.15	38	1570	71	2968	50	4127	7
MA64-60.1	396	531	1.34	206	1.531	0.4630	0.31	0.2270	1.00	0.340	1.11	21.703	1.19	46	1886	18	3171	12	4128	5
MA64-45.3	195	318	1.63	165	0.105	0.4666	0.30	0.1624	0.71	0.601	2.73	38.688	2.78	73	3035	66	3738	28	4139	4
MA64-47.1	175	163	0.93	157	0.219	0.4683	0.29	0.1781	0.68	0.628	1.15	40.568	1.22	76	3143	28	3785	12	4145	4
MA64-47.2	131	102	0.78	159	0.077	0.4699	0.29	0.1636	0.64	0.860	1.18	55.710	1.25	96	4000	35	4100	12	4150	4
MA64-67.1	226	404	1.79	112	0.256	0.4706	0.32	0.1618	0.87	0.350	1.13	22.719	1.21	47	1935	19	3215	12	4152	5

Continued on Next Page...

Table 4.2 – Continued

Grain .spot	U ppm	Th ppm	Th/U	Pb ppm	$f206\%$	$^{207}Pb/^{206}Pb$ 204corr	$\pm1\sigma$ (%)	$^{208}Pb/^{206}Pb$ 204corr	$\pm1\sigma$ (%)	$^{206}Pb/^{238}U$ 204corr	$\pm1\sigma$ (%)	$^{207}Pb/^{235}U$ 204corr	$\pm1\sigma$ (%)	%c	$^{206}Pb/^{238}U$ date	$\pm1\sigma$ (Ma)	$^{207}Pb/^{235}U$ date	$\pm1\sigma$ (Ma)	$^{207}Pb/^{206}Pb$ date	$\pm1\sigma$ (Ma)
MA64-61.1	223	240	1.08	208	0.127	0.4710	0.24	0.1838	0.53	0.654	1.13	42.444	1.19	78	3242	29	3829	12	4153	4
MA64-40.4	138	267	1.94	102	0.341	0.4760	0.35	0.1562	1.09	0.519	1.16	34.062	1.25	65	2695	25	3612	12	4168	5
MA64-41.7	581	1832	3.15	313	-0.010	0.4758	0.34	0.2667	0.56	0.359	5.08	23.563	5.13	47	1978	86	3250	50	4168	5
MA64-61.2	206	213	1.03	205	0.106	0.4793	0.27	0.1820	0.64	0.694	1.15	45.887	1.21	81	3399	30	3907	12	4179	4
MA64-40.1	98	52	0.53	124	0.332	0.4807	0.33	0.1340	1.15	0.896	1.21	59.384	1.29	99	4124	37	4164	13	4183	5
MA64-61.3	205	214	1.04	202	0.101	0.4824	0.26	0.1823	0.53	0.684	2.72	45.515	2.77	80	3361	71	3899	27	4188	4
MA64-40.5	132	189	1.43	128	0.212	0.4828	0.32	0.1384	0.96	0.688	2.74	45.825	2.80	81	3377	72	3906	28	4189	5
MA64-45.1	81	56	0.69	99	0.000	0.4826	0.50	0.1451	2.47	0.872	1.25	58.056	1.40	97	4043	38	4141	14	4189	7
MA64-41.11	476	1159	2.44	300	1.650	0.4868	0.45	0.1843	1.82	0.416	5.08	27.897	5.16	53	2241	96	3415	51	4202	7
MA64-69.1	118	140	1.19	131	0.116	0.4881	0.34	0.1520	0.89	0.786	1.19	52.890	1.28	89	3739	34	4048	13	4206	5
MA64-52.3	260	336	1.30	240	0.717	0.4969	0.42	0.2033	1.26	0.618	2.76	42.366	2.85	73	3103	68	3828	28	4232	6
MA64-41.4	290	732	2.52	219	0.702	0.5029	0.27	0.1829	0.91	0.508	1.12	35.251	1.18	62	2650	24	3646	12	4250	4
MA64-41.5	261	505	1.93	255	0.982	0.5035	0.43	0.1866	1.54	0.649	2.76	45.063	2.85	76	3225	70	3889	28	4251	6
MA64-41.6-2	475	992	2.09	327	0.706	0.5039	0.38	0.1951	1.19	0.460	5.08	31.957	5.14	57	2439	103	3549	51	4253	6
MA64-41.6	548	1242	2.27	377	-0.014	0.5073	0.32	0.2149	0.56	0.465	5.08	32.511	5.13	58	2461	104	3566	51	4263	5
MA64-52.2	164	232	1.42	178	0.358	0.5101	0.35	0.1803	1.01	0.736	1.20	51.734	1.29	83	3554	33	4026	13	4271	5
MA64-41.1	237	399	1.68	241	0.595	0.5112	0.24	0.1872	0.75	0.681	1.13	48.025	1.18	78	3349	29	3952	12	4274	3
MA64-52.1	182	252	1.39	194	0.349	0.5175	0.35	0.1826	0.97	0.721	1.21	51.420	1.30	82	3498	33	4020	13	4292	5
MA64-41.10	285	365	1.28	241	0.302	0.5249	0.42	0.1481	1.27	0.581	5.09	42.035	5.16	68	2952	121	3820	51	4313	6
MA64-41.10	246	161	0.65	316	0.232	0.5325	0.38	0.1538	1.06	0.881	5.09	64.658	5.16	94	4072	154	4249	52	4334	6
MA64-41.2	178	130	0.73	225	0.204	0.5328	0.24	0.1596	0.66	0.863	1.15	63.426	1.20	93	4012	34	4230	12	4335	3
MH09 Zircons (193 analyses from 1 session)																				
MH09-184.1	1214	398	0.33	452	0.821	0.1940	0.60	0.1091	1.84	0.323	1.37	8.629	1.57	65	1802	22	2300	14	2777	10
MH09-74.1	954	919	0.96	284	0.298	0.2022	0.61	0.1780	1.10	0.248	1.38	6.910	1.57	50	1427	18	2100	14	2844	10
MH09-150.1	1272	986	0.77	313	0.118	0.2107	0.52	0.2180	0.73	0.199	1.37	5.786	1.52	40	1171	15	1944	13	2911	8
MH09-174.1	1064	573	0.54	708	0.323	0.2174	0.41	0.1456	0.90	0.561	1.38	16.807	1.49	97	2870	32	2924	14	2961	7
MH09-81.1	114	19	0.17	51	0.936	0.2178	1.78	0.0660	9.95	0.391	1.67	11.741	2.59	72	2128	30	2584	24	2964	29
MH09-152.1	191	46	0.24	162	0.510	0.2179	0.80	0.1124	2.23	0.727	1.54	21.847	1.82	119	3523	42	3177	18	2965	13
MH09-175.1	564	291	0.52	312	0.065	0.2276	0.53	0.1389	0.96	0.469	1.41	14.713	1.56	82	2479	29	2797	15	3035	8
MH09-96.1	147	108	0.74	100	1.170	0.2306	1.40	0.2330	2.64	0.520	1.61	16.522	2.26	88	2697	35	2908	22	3056	22
MH09-146.1	604	202	0.33	263	0.613	0.2307	0.69	0.1378	1.83	0.361	1.40	11.495	1.64	65	1989	24	2564	15	3057	11
MH09-25.1	670	893	1.33	193	6.714	0.2319	2.08	0.2440	4.23	0.184	1.44	5.898	2.68	36	1091	14	1961	23	3065	33
MH09-43.1	777	545	0.70	289	0.644	0.2330	0.66	0.2143	1.20	0.292	1.39	9.398	1.61	54	1654	20	2378	15	3073	11
MH09-169.1	573	501	0.87	355	0.171	0.2333	0.52	0.2716	0.72	0.475	1.41	15.294	1.56	82	2507	29	2834	15	3075	8
MH09-102.1	1507	134	0.09	332	7.206	0.2352	1.56	0.1271	6.07	0.148	1.39	4.797	2.22	29	889	12	1784	19	3088	25
MH09-176.1	562	259	0.46	295	0.027	0.2354	0.54	0.1221	1.18	0.448	1.40	14.549	1.57	77	2387	28	2786	15	3089	9
MH09-159.1	919	85	0.09	316	2.326	0.2359	0.88	0.0417	9.24	0.287	1.38	9.346	1.73	53	1628	20	2373	16	3092	14
MH09-185.1	831	512	0.62	815	0.169	0.2359	0.35	0.1949	0.60	0.791	1.39	25.737	1.48	122	3758	40	3337	14	3092	6

Continued on Next Page...

Table 4.2 – Continued

Grain .spot	U ppm	Th ppm	Th/U	Pb ppm	$f206\%$	$^{207}Pb/^{206}Pb$ 204corr	$\pm1\sigma$ (%)	$^{208}Pb/^{206}Pb$ 204corr	$\pm1\sigma$ (%)	$^{206}Pb/^{238}U$ 204corr	$\pm1\sigma$ (%)	$^{207}Pb/^{235}U$ 204corr	$\pm1\sigma$ (%)	%c	$^{206}Pb/^{238}U$ date	$\pm1\sigma$ (Ma)	$^{207}Pb/^{235}U$ date	$\pm1\sigma$ (Ma)	$^{207}Pb/^{206}Pb$ date	$\pm1\sigma$ (Ma)
MH09-47.1	778	386	0.50	210	0.389	0.2366	0.69	0.1946	1.27	0.216	1.38	7.053	1.62	41	1262	16	2118	14	3097	11
MH09-170.1	485	255	0.53	638	10.060	0.2377	1.40	0.3125	2.32	0.733	1.45	24.012	2.14	114	3544	40	3269	21	3104	22
MH09-168.1	497	186	0.37	238	0.413	0.2416	0.64	0.1083	2.00	0.406	1.41	13.523	1.62	70	2197	26	2717	15	3130	10
MH09-87.1	692	228	0.33	432	0.981	0.2422	0.58	0.1132	2.07	0.517	1.40	17.259	1.58	86	2686	31	2949	15	3134	9
MH09-2.1	727	591	0.81	501	0.025	0.2426	0.39	0.2103	0.54	0.551	1.39	18.421	1.49	90	2828	32	3012	14	3137	6
MH09-178.1	542	173	0.32	245	8.943	0.2448	2.47	0.2798	4.66	0.263	1.49	8.862	3.04	48	1503	20	2324	28	3151	39
MH09-37.1	566	359	0.63	276	0.847	0.2450	0.73	0.2333	1.38	0.373	1.41	12.589	1.67	65	2042	25	2649	16	3153	12
MH09-139.1	516	674	1.31	552	2.212	0.2452	0.75	0.3380	1.12	0.733	1.43	24.782	1.70	112	3545	39	3300	17	3154	12
MH09-99.1	671	104	0.16	276	2.358	0.2463	0.91	0.1147	3.71	0.324	1.40	10.988	1.77	57	1807	22	2522	16	3161	14
MH09-119.1	607	371	0.61	1444	23.941	0.2467	1.82	0.4945	2.05	0.849	1.47	28.887	2.48	125	3963	43	3450	24	3163	29
MH09-79.1	519	242	0.47	419	0.225	0.2472	0.48	0.1489	1.00	0.666	1.42	22.690	1.55	104	3289	37	3214	15	3167	8
MH09-126.1	491	521	1.06	359	0.016	0.2474	0.48	0.2934	0.58	0.551	1.42	18.787	1.55	89	2828	32	3031	15	3168	8
MH09-6.1	294	206	0.70	183	0.121	0.2485	0.70	0.1975	1.23	0.498	1.46	17.074	1.70	82	2606	31	2939	16	3175	11
MH09-98.1	565	401	0.71	397	0.044	0.2499	0.45	0.1847	0.68	0.568	1.42	19.573	1.54	91	2900	33	3071	15	3184	7
MH09-155.1	622	476	0.76	493	0.070	0.2520	0.41	0.2062	0.61	0.630	1.40	21.881	1.51	98	3149	35	3178	15	3197	7
MH09-165.1	420	143	0.34	297	10.851	0.2522	2.24	0.2202	5.53	0.399	1.49	13.888	2.84	68	2166	27	2742	27	3199	35
MH09-73.1	227	133	0.59	149	0.201	0.2534	0.78	0.1367	1.69	0.545	1.51	19.043	1.78	87	2805	34	3044	17	3206	12
MH09-34.1	348	175	0.50	183	6.252	0.2536	1.97	0.2492	4.25	0.335	1.49	11.716	2.62	58	1863	24	2582	25	3207	31
MH09-107.1	571	787	1.38	516	0.451	0.2542	0.49	0.3721	0.61	0.637	1.41	22.324	1.55	99	3177	35	3198	15	3211	8
MH09-77.1	880	1244	1.41	237	5.811	0.2545	1.55	0.0965	8.36	0.190	1.41	6.658	2.22	35	1120	14	2067	20	3213	24
MH09-15.1	438	349	0.80	376	4.279	0.2553	1.09	0.2073	2.76	0.595	1.44	20.961	1.92	94	3011	35	3137	19	3218	17
MH09-127.1	579	317	0.55	411	0.097	0.2589	0.45	0.1391	0.95	0.588	1.41	20.988	1.53	92	2981	34	3138	15	3240	7
MH09-161.1	281	323	1.15	256	0.132	0.2590	0.61	0.3023	0.79	0.674	1.47	24.074	1.67	103	3322	38	3271	16	3240	10
MH09-186.1	177	105	0.59	136	0.054	0.2593	0.80	0.1787	1.35	0.620	1.54	22.178	1.82	96	3112	38	3192	18	3242	13
MH09-4.1	545	257	0.47	173	2.896	0.2595	1.19	0.3004	2.08	0.217	1.41	7.751	1.96	39	1264	16	2203	18	3243	19
MH09-116.1	335	723	2.16	348	0.093	0.2600	0.57	0.5807	0.55	0.653	1.46	23.422	1.63	100	3241	37	3245	16	3247	9
MH09-140.1	335	383	1.14	201	0.114	0.2600	0.64	0.2684	0.89	0.455	1.45	16.301	1.66	74	2416	29	2895	16	3247	10
MH09-18.1	276	68	0.25	209	0.082	0.2612	0.60	0.0614	1.97	0.666	1.48	23.974	1.66	101	3289	38	3267	16	3254	10
MH09-113.1	816	438	0.54	195	7.071	0.2614	1.85	0.2154	4.73	0.151	1.42	5.438	2.47	28	906	12	1891	21	3255	29
MH09-121.1	405	1092	2.70	163	2.871	0.2618	1.30	0.1983	3.37	0.291	1.44	10.499	2.06	51	1646	21	2480	19	3258	20
MH09-117.1	506	100	0.20	333	0.227	0.2620	0.51	0.0558	2.56	0.576	1.42	20.813	1.57	90	2933	33	3130	15	3259	8
MH09-101.1	328	113	0.35	255	0.041	0.2631	0.53	0.0931	1.18	0.664	1.45	24.090	1.61	101	3283	37	3272	16	3266	8
MH09-95.1	440	355	0.81	389	3.029	0.2636	0.90	0.2130	2.22	0.631	1.45	22.931	1.80	96	3154	36	3224	18	3268	14
MH09-108.1	468	175	0.37	330	0.120	0.2638	0.49	0.1035	1.22	0.597	1.42	21.724	1.56	92	3019	34	3171	15	3269	8
MH09-53.1	634	342	0.54	494	0.042	0.2640	0.39	0.1423	0.71	0.643	1.40	23.403	1.50	98	3200	35	3244	15	3271	6
MH09-180.1	329	203	0.62	142	2.433	0.2644	1.27	0.1974	3.26	0.316	1.46	11.503	2.06	54	1768	23	2565	19	3273	20
MH09-9.1	516	155	0.30	156	3.997	0.2646	1.53	0.1430	5.69	0.218	1.43	7.963	2.22	39	1273	16	2227	20	3274	24
MH09-46.1	219	564	2.58	104	1.823	0.2652	1.48	0.2536	3.00	0.342	1.54	12.519	2.26	58	1898	25	2644	21	3278	23
MH09-136.1	73	78	1.07	67	0.120	0.2655	1.17	0.2823	1.52	0.685	1.82	25.088	2.28	103	3365	48	3312	22	3279	18
MH09-142.1	332	196	0.59	125	2.244	0.2663	1.34	0.2133	3.24	0.276	1.46	10.132	2.10	48	1571	20	2447	19	3284	21

Continued on Next Page...

Table 4.2 – Continued

Grain .spot	U ppm	Th ppm	Th/U	Pb ppm	$f206\%$	^{207}Pb / ^{206}Pb 204corr	$\pm1\sigma$ (%)	^{208}Pb / ^{206}Pb 204corr	$\pm1\sigma$ (%)	^{206}Pb / ^{238}U 204corr	$\pm1\sigma$ (%)	^{207}Pb / ^{235}U 204corr	$\pm1\sigma$ (%)	%c	^{206}Pb / ^{238}U date	$\pm1\sigma$ (Ma)	^{207}Pb / ^{235}U date	$\pm1\sigma$ (Ma)	^{207}Pb / ^{206}Pb date	$\pm1\sigma$ (Ma)
MH09-182.1	232	185	0.79	147	1.354	0.2662	1.15	0.2686	2.14	0.457	1.48	16.784	1.99	74	2428	30	2923	19	3284	18
MH09-137.1	608	186	0.31	455	0.042	0.2667	0.41	0.0823	0.98	0.644	1.41	23.675	1.51	97	3204	36	3255	15	3287	6
MH09-65.1	411	203	0.49	188	4.708	0.2669	1.51	0.1908	4.29	0.313	1.46	11.524	2.23	53	1756	22	2567	21	3288	24
MH09-129.1	272	220	0.81	150	1.899	0.2679	1.26	0.3229	2.08	0.379	1.49	13.998	2.07	63	2071	26	2750	20	3294	20
MH09-163.1	328	105	0.32	201	0.117	0.2681	0.62	0.1089	1.53	0.514	1.45	19.013	1.64	81	2675	32	3042	16	3295	10
MH09-149.1	277	205	0.74	198	0.204	0.2691	0.69	0.2363	1.09	0.548	1.48	20.322	1.71	85	2815	34	3107	17	3301	11
MH09-193.1	447	268	0.60	329	0.074	0.2694	0.49	0.1536	0.86	0.599	1.43	22.270	1.57	92	3028	35	3196	15	3303	8
MH09-147.1	687	158	0.23	461	0.025	0.2696	0.39	0.0615	1.04	0.585	1.40	21.740	1.50	90	2969	33	3172	15	3304	6
MH09-135.1	70	49	0.71	61	0.250	0.2700	1.23	0.1893	2.13	0.693	1.84	25.780	2.34	103	3393	49	3338	23	3306	19
MH09-177.1	472	568	1.20	417	0.080	0.2699	0.48	0.3424	0.59	0.635	1.42	23.615	1.56	96	3167	36	3253	15	3306	8
MH09-30.1	222	120	0.54	158	0.571	0.2699	0.82	0.1627	1.97	0.565	1.51	21.039	1.80	87	2888	35	3140	17	3306	13
MH09-16.1	316	202	0.64	193	0.119	0.2703	0.62	0.1584	1.18	0.495	1.46	18.442	1.65	78	2592	31	3013	16	3308	10
MH09-72.1	282	92	0.33	111	4.738	0.2704	2.07	0.1366	8.39	0.277	1.53	10.317	2.72	48	1575	21	2464	25	3308	33
MH09-35.1	382	228	0.60	349	0.045	0.2710	0.48	0.1877	0.76	0.725	1.44	27.077	1.57	106	3514	39	3386	15	3312	7
MH09-69.1	202	202	1.00	181	-0.009	0.2720	0.69	0.2604	0.91	0.681	1.54	25.524	1.76	101	3347	40	3328	17	3317	11
MH09-8.1	198	201	1.01	174	0.083	0.2720	0.68	0.2672	0.91	0.662	1.52	24.831	1.74	99	3275	39	3302	17	3318	11
MH09-97.1	480	308	0.64	392	0.134	0.2721	0.46	0.1747	0.87	0.653	1.43	24.495	1.55	98	3240	36	3288	15	3318	7
MH09-133.1	184	122	0.66	157	0.121	0.2726	0.72	0.1757	1.21	0.682	1.54	25.633	1.78	101	3352	40	3333	17	3321	11
MH09-83.1	160	85	0.53	129	6.452	0.2726	2.37	0.2055	6.63	0.517	1.69	19.434	3.08	81	2686	37	3064	30	3321	37
MH09-151.1	109	88	0.81	98	0.000	0.2730	1.09	0.2232	1.69	0.701	1.66	26.390	2.10	103	3425	44	3361	21	3323	17
MH09-61.1	289	84	0.29	222	0.068	0.2735	0.68	0.0768	3.09	0.662	1.47	24.953	1.69	98	3274	38	3306	17	3326	11
MH09-103.1	215	70	0.33	168	0.363	0.2736	0.77	0.0850	3.22	0.660	1.52	24.908	1.79	98	3269	39	3305	17	3327	12
MH09-31.1	238	196	0.82	121	1.265	0.2736	1.20	0.1373	4.14	0.401	1.50	15.121	2.04	65	2173	28	2823	19	3327	19
MH09-76.1	324	222	0.68	149	1.740	0.2739	1.08	0.2065	2.63	0.339	1.47	12.820	1.93	57	1884	24	2666	18	3328	17
MH09-64.1	182	99	0.54	135	4.800	0.2745	1.83	0.1909	5.40	0.503	1.60	19.045	2.58	79	2627	34	3044	25	3332	29
MH09-12.1	143	105	0.73	122	-0.039	0.2748	0.89	0.1989	1.56	0.672	1.59	25.462	1.91	99	3313	41	3326	19	3334	14
MH09-59.1	121	91	0.75	100	0.044	0.2749	0.91	0.2072	1.38	0.645	1.65	24.453	1.98	96	3209	42	3287	19	3334	14
MH09-88.1	288	243	0.84	238	0.990	0.2751	0.77	0.2425	1.54	0.613	1.49	23.250	1.76	92	3082	36	3237	17	3335	12
MH09-143.1	196	106	0.54	155	0.163	0.2752	0.72	0.1321	1.51	0.650	1.53	24.680	1.77	97	3230	39	3296	17	3336	11
MH09-172.1	167	106	0.63	151	0.071	0.2753	0.77	0.1682	1.42	0.727	1.56	27.601	1.82	106	3523	42	3405	18	3336	12
MH09-75.1	180	182	1.01	161	0.119	0.2754	0.92	0.2701	1.26	0.669	1.56	25.421	1.91	99	3304	40	3325	19	3337	14
MH09-162.1	40	16	0.39	33	0.505	0.2758	1.80	0.0991	6.82	0.681	2.15	25.913	2.97	100	3350	56	3343	29	3339	28
MH09-63.1	225	237	1.05	127	1.143	0.2757	1.08	0.1235	4.01	0.450	1.51	17.094	1.96	72	2394	30	2940	19	3339	17
MH09-32.1	149	133	0.89	129	0.284	0.2760	0.92	0.2293	1.53	0.661	1.60	25.154	1.94	98	3271	41	3314	19	3340	14
MH09-38.1	47	17	0.37	39	0.421	0.2760	1.97	0.0890	9.85	0.709	2.07	26.988	3.03	103	3455	55	3383	30	3341	31
MH09-57.1	249	91	0.37	135	0.787	0.2761	0.95	0.1353	3.00	0.436	1.51	16.608	1.88	70	2334	29	2912	18	3341	15
MH09-130.1	206	150	0.73	185	0.032	0.2765	0.66	0.1916	0.99	0.710	1.52	27.053	1.73	103	3457	41	3385	17	3343	10
MH09-86.1	276	70	0.25	223	0.157	0.2766	0.60	0.0641	2.49	0.695	1.47	26.514	1.66	102	3402	39	3366	16	3344	9
MH09-109.1	214	114	0.53	174	0.048	0.2768	0.71	0.1402	1.72	0.667	1.52	25.454	1.76	98	3294	39	3326	17	3345	11
MH09-190.1	112	60	0.53	95	-0.168	0.2768	1.08	0.1442	2.99	0.701	1.68	26.762	2.10	102	3425	45	3375	21	3345	17

Continued on Next Page. . .

Table 4.2 – Continued

Grain .spot	U ppm	Th ppm	Th/U	Pb ppm	$f206\%$	$^{207}Pb/^{206}Pb$ 204corr	$\pm1\sigma$ (%)	$^{208}Pb/^{206}Pb$ 204corr	$\pm1\sigma$ (%)	$^{206}Pb/^{238}U$ 204corr	$\pm1\sigma$ (%)	$^{207}Pb/^{235}U$ 204corr	$\pm1\sigma$ (%)	%c	$^{206}Pb/^{238}U$ date	$\pm1\sigma$ (Ma)	$^{207}Pb/^{235}U$ date	$\pm1\sigma$ (Ma)	$^{207}Pb/^{206}Pb$ date	$\pm1\sigma$ (Ma)
MH09-28.1	425	371	0.87	330	0.126	0.2770	0.50	0.1803	0.86	0.616	1.44	23.523	1.58	92	3094	35	3249	15	3346	8
MH09-110.1	65	41	0.63	57	0.619	0.2776	1.42	0.1612	3.63	0.690	1.89	26.428	2.51	101	3384	50	3362	25	3350	22
MH09-160.1	174	58	0.33	143	0.058	0.2777	0.76	0.0892	2.34	0.697	1.56	26.696	1.82	102	3410	41	3372	18	3350	12
MH09-52.1	263	214	0.81	190	0.190	0.2777	0.71	0.2506	1.14	0.545	1.48	20.857	1.72	84	2804	34	3132	17	3350	11
MH09-89.1	142	92	0.64	107	0.298	0.2778	1.35	0.1584	3.14	0.604	1.59	23.128	2.21	91	3045	39	3232	22	3351	21
MH09-134.1	93	58	0.63	78	0.198	0.2781	1.04	0.1692	1.99	0.674	1.73	25.842	2.12	99	3321	45	3341	21	3352	16
MH09-78.1	69	62	0.89	64	0.619	0.2781	1.34	0.2361	2.45	0.695	1.84	26.638	2.41	101	3401	49	3370	24	3352	21
MH09-141.1	161	92	0.57	124	0.305	0.2782	0.91	0.1667	2.10	0.614	1.58	23.560	1.92	92	3087	39	3250	19	3353	14
MH09-56.1	92	53	0.58	77	0.170	0.2782	1.04	0.1528	2.00	0.681	1.76	26.116	2.15	100	3347	46	3351	21	3353	16
MH09-112.1	208	116	0.56	191	0.255	0.2784	0.72	0.1403	1.88	0.745	1.53	28.617	1.77	107	3591	42	3440	17	3354	11
MH09-23.1	144	88	0.61	99	0.375	0.2784	0.95	0.1834	1.94	0.536	1.59	20.584	1.94	83	2767	36	3119	19	3354	15
MH09-29.1	125	94	0.75	100	0.565	0.2784	1.06	0.2061	2.17	0.614	1.65	23.572	2.07	92	3086	40	3251	20	3354	17
MH09-27.1	83	35	0.42	69	0.000	0.2786	1.18	0.1142	3.49	0.686	1.77	26.350	2.24	100	3367	46	3360	22	3355	18
MH09-33.1	108	101	0.93	96	0.269	0.2786	0.98	0.2496	1.48	0.667	1.68	25.631	2.04	98	3295	43	3333	20	3355	15
MH09-189.1	245	283	1.16	229	0.085	0.2789	0.62	0.3083	0.79	0.683	1.50	26.285	1.69	100	3358	39	3357	17	3357	10
MH09-104.1	133	105	0.79	99	0.073	0.2793	0.90	0.1500	1.69	0.600	1.61	23.125	1.94	90	3032	39	3232	19	3359	14
MH09-105.1	181	101	0.56	143	0.888	0.2794	0.99	0.1566	2.95	0.623	1.56	23.996	1.95	93	3121	39	3268	19	3360	15
MH09-195.1	119	50	0.42	102	0.234	0.2797	0.93	0.1090	2.72	0.717	1.65	27.635	2.00	104	3483	44	3406	20	3361	15
MH09-54.1	343	365	1.06	307	0.130	0.2796	0.54	0.2845	0.76	0.660	1.45	25.468	1.61	97	3269	37	3326	16	3361	8
MH09-194.1	168	193	1.15	160	0.239	0.2802	0.79	0.3061	1.11	0.690	1.56	26.658	1.84	101	3383	41	3371	18	3364	12
MH09-41.1	80	49	0.62	67	0.217	0.2805	1.26	0.1623	2.45	0.671	1.82	25.969	2.34	98	3311	47	3345	23	3366	20
MH09-36.1	239	134	0.56	186	0.139	0.2808	0.66	0.1498	1.43	0.631	1.50	24.432	1.72	94	3154	38	3286	17	3367	10
MH09-40.1	139	117	0.84	124	0.288	0.2810	0.91	0.2173	1.71	0.684	1.61	26.515	1.95	100	3362	42	3366	19	3368	14
MH09-111.1	79	35	0.45	65	0.308	0.2810	1.17	0.1141	3.23	0.682	1.81	26.416	2.27	99	3351	47	3362	22	3369	18
MH09-50.1	296	96	0.33	154	1.477	0.2811	1.11	0.1245	4.47	0.409	1.48	15.866	1.96	66	2212	28	2869	19	3369	17
MH09-5.1	81	43	0.53	73	0.114	0.2811	1.47	0.1417	5.07	0.733	1.75	28.406	2.42	105	3544	48	3433	24	3369	23
MH09-183.1	99	87	0.88	90	0.157	0.2812	1.02	0.2385	1.60	0.686	1.69	26.607	2.08	100	3368	44	3369	20	3370	16
MH09-14.1	209	130	0.62	110	0.950	0.2815	1.03	0.1675	2.70	0.409	1.52	15.888	1.94	66	2212	28	2870	18	3371	16
MH09-125.1	156	102	0.65	135	0.468	0.2816	0.90	0.1805	2.05	0.677	1.57	26.288	1.91	99	3333	41	3357	19	3372	14
MH09-82.1	80	39	0.48	67	0.191	0.2816	1.26	0.1207	3.02	0.690	1.79	26.778	2.32	100	3381	47	3375	23	3372	20
MH09-85.1	235	103	0.44	164	1.544	0.2817	1.02	0.1241	4.01	0.546	1.52	21.196	1.93	83	2808	35	3148	19	3372	16
MH09-131.1	242	121	0.50	197	0.284	0.2819	0.68	0.1370	1.71	0.662	1.50	25.715	1.72	97	3273	38	3336	17	3373	11
MH09-90.1	139	46	0.33	114	0.034	0.2821	0.78	0.0862	1.74	0.694	1.62	26.994	1.88	101	3398	43	3383	18	3374	12
MH09-93.1	194	182	0.94	168	1.122	0.2820	0.97	0.2367	2.04	0.641	1.54	24.912	1.92	95	3192	39	3305	19	3374	15
MH09-10.1	197	106	0.54	165	0.049	0.2823	0.69	0.1392	1.49	0.684	1.53	26.637	1.76	100	3361	40	3370	17	3376	11
MH09-164.1	228	125	0.55	204	0.007	0.2824	0.62	0.1486	1.04	0.726	1.51	28.284	1.70	104	3520	41	3429	17	3376	10
MH09-20.1	117	41	0.35	95	0.099	0.2825	0.93	0.0920	3.00	0.686	1.66	26.716	2.00	100	3367	43	3373	20	3377	14
MH09-3.1	201	132	0.66	170	0.088	0.2827	0.70	0.1792	1.39	0.671	1.51	26.170	1.75	98	3312	39	3353	17	3378	11
MH09-21.1	139	53	0.38	113	0.330	0.2832	0.93	0.1157	2.70	0.666	1.60	26.013	1.95	97	3291	41	3347	19	3381	14
MH09-39.1	171	75	0.44	143	0.154	0.2834	0.87	0.1123	2.25	0.694	1.55	27.095	1.87	100	3396	41	3387	18	3382	14

Continued on Next Page...

Table 4.2 – Continued

Grain .spot	U ppm	Th ppm	Th/U	Pb ppm	$f206\%$	$^{207}Pb/^{206}Pb$ 204corr	$\pm1\sigma$ (%)	$^{208}Pb/^{206}Pb$ 204corr	$\pm1\sigma$ (%)	$^{206}Pb/^{238}U$ 204corr	$\pm1\sigma$ (%)	$^{207}Pb/^{235}U$ 204corr	$\pm1\sigma$ (%)	%c	$^{206}Pb/^{238}U$ date	$\pm1\sigma$ (Ma)	$^{207}Pb/^{235}U$ date	$\pm1\sigma$ (Ma)	$^{207}Pb/^{206}Pb$ date	$\pm1\sigma$ (Ma)
MH09-145.1	149	60	0.40	106	0.313	0.2836	0.94	0.1216	2.44	0.586	1.59	22.899	1.94	88	2971	38	3223	19	3383	15
MH09-84.1	174	113	0.65	85	4.516	0.2837	1.96	0.2323	4.83	0.326	1.58	12.760	2.67	54	1820	25	2662	25	3383	31
MH09-44.1	74	34	0.45	62	0.046	0.2854	1.13	0.1222	2.42	0.693	1.82	27.256	2.26	100	3393	48	3393	22	3393	18
MH09-153.1	114	134	1.17	116	0.332	0.2862	1.11	0.2284	2.05	0.773	1.64	30.515	2.09	109	3693	46	3504	21	3397	17
MH09-71.1	128	113	0.88	87	0.717	0.2867	1.15	0.1166	4.33	0.549	1.64	21.706	2.12	83	2822	38	3171	21	3400	18
MH09-1.1	56	24	0.43	47	-0.163	0.2896	1.24	0.1141	3.14	0.694	1.89	27.692	2.38	99	3396	50	3408	23	3415	19
MH09-118.1	45	38	0.84	42	-0.036	0.2897	1.37	0.2239	2.01	0.718	2.03	28.677	2.59	102	3488	55	3443	25	3416	21
MH09-158.1	413	242	0.59	303	0.140	0.2902	0.52	0.1570	1.07	0.586	1.43	23.435	1.59	87	2972	34	3245	15	3419	8
MH09-138.1	88	98	1.12	84	0.244	0.2906	1.11	0.2984	1.69	0.697	1.74	27.936	2.18	100	3410	46	3417	21	3421	17
MH09-120.1	89	76	0.85	82	0.108	0.2935	1.00	0.2238	1.57	0.702	1.73	28.423	2.10	100	3429	46	3434	21	3436	15
MH09-48.1	858	226	0.26	203	5.454	0.2941	1.46	0.2138	4.11	0.154	1.41	6.236	2.15	27	922	12	2010	19	3439	23
MH09-60.1	427	343	0.80	289	0.220	0.2985	0.73	0.1983	1.36	0.522	1.43	21.483	1.69	78	2707	32	3161	16	3463	11
MH09-19.1	145	116	0.81	134	0.260	0.2996	0.83	0.2106	1.54	0.709	1.60	29.300	1.89	100	3456	43	3464	19	3468	13
MH09-114.1	138	88	0.64	130	0.080	0.3005	0.77	0.1661	1.38	0.747	1.61	30.963	1.87	104	3597	44	3518	18	3473	12
MH09-55.1	120	190	1.58	102	0.666	0.3014	1.12	0.4008	1.54	0.573	1.65	23.803	2.11	84	2919	39	3260	21	3477	17
MH09-51.1	137	143	1.05	131	0.178	0.3029	0.84	0.2782	1.21	0.701	1.62	29.277	1.92	98	3424	43	3463	19	3485	13
MH09-22.1	47	49	1.05	43	1.416	0.3031	2.28	0.2600	5.05	0.662	2.11	27.643	3.29	94	3273	54	3407	32	3486	35
MH09-68.1	98	57	0.58	90	0.275	0.3034	0.99	0.1528	2.38	0.729	1.73	30.521	2.10	101	3532	47	3504	21	3488	15
MH09-45.1	59	65	1.11	57	0.027	0.3043	1.18	0.2991	1.58	0.708	1.91	29.698	2.37	99	3450	51	3477	23	3492	18
MH09-70.1	123	72	0.59	53	-0.075	0.3061	1.24	0.1962	2.55	0.332	1.63	14.029	2.17	53	1850	26	2752	21	3502	19
MH09-91.1	323	77	0.24	348	4.854	0.3128	1.00	0.1688	3.73	0.722	1.48	31.139	1.89	99	3503	40	3523	19	3535	15
MH09-132.1	382	216	0.56	212	0.159	0.3168	0.56	0.1441	1.22	0.440	1.44	19.223	1.61	66	2351	28	3053	16	3554	9
MH09-13.1	44	31	0.71	42	0.000	0.3171	1.34	0.1859	2.32	0.740	2.09	32.374	2.62	100	3572	57	3562	26	3556	21
MH09-128.1	110	68	0.62	109	0.164	0.3195	0.85	0.1607	1.79	0.771	1.65	33.982	1.95	103	3686	46	3610	19	3567	13
MH09-115.1	514	375	0.73	256	1.049	0.3256	0.67	0.2360	1.51	0.359	1.42	16.119	1.65	55	1978	24	2884	16	3597	10
MH09-62.1	190	81	0.43	171	0.024	0.3283	0.63	0.1104	1.43	0.725	1.54	32.814	1.73	97	3515	42	3575	17	3609	10
MH09-66.1	94	30	0.31	83	0.056	0.3296	1.16	0.0783	2.94	0.727	1.74	33.020	2.21	97	3520	47	3581	22	3615	18
MH09-100.1	154	81	0.52	146	0.182	0.3326	0.70	0.1497	1.40	0.738	1.58	33.853	1.81	98	3564	43	3606	18	3629	11
MH09-156.1	110	86	0.79	85	1.505	0.3328	1.20	0.2061	3.15	0.556	1.67	25.520	2.17	79	2851	38	3328	21	3630	18
MH09-166.1	335	99	0.30	295	0.110	0.3337	0.49	0.0817	1.43	0.721	1.46	33.184	1.60	96	3500	39	3586	16	3634	7
MH09-179.1	339	96	0.28	214	1.247	0.3344	0.72	0.1195	3.10	0.483	1.45	22.278	1.70	70	2541	30	3196	17	3637	11
MH09-192.1	226	168	0.74	217	0.101	0.3351	0.57	0.2088	0.92	0.721	1.48	33.302	1.66	96	3499	40	3590	16	3640	9
MH09-181.1	89	33	0.37	89	0.069	0.3361	0.91	0.0945	2.12	0.805	1.77	37.300	2.09	104	3807	51	3702	21	3645	14
MH09-173.1	297	96	0.32	267	0.188	0.3366	0.52	0.0889	1.71	0.727	1.47	33.718	1.62	97	3521	40	3602	16	3647	8
MH09-7.1	124	266	2.14	91	0.743	0.3367	1.02	0.1970	2.54	0.540	1.62	25.086	2.02	76	2785	37	3312	20	3648	16
MH09-58.1	254	91	0.36	154	0.189	0.3370	0.68	0.0807	2.87	0.494	1.50	22.960	1.72	71	2588	32	3225	17	3649	10
MH09-123.1	184	180	0.98	126	0.618	0.3404	0.84	0.3467	1.32	0.461	1.55	21.661	1.85	67	2446	31	3169	18	3665	13
MH09-124.1	86	83	0.96	90	0.070	0.3414	0.91	0.2507	1.33	0.759	1.75	35.749	2.07	99	3642	49	3660	20	3669	14
MH09-92.1	82	80	0.97	90	0.155	0.3415	0.92	0.2443	1.46	0.798	1.77	37.585	2.10	103	3783	51	3709	21	3669	14
MH09-171.1	266	147	0.55	227	0.349	0.3415	0.61	0.1607	1.58	0.651	1.48	30.635	1.67	88	3231	38	3507	16	3670	9

Continued on Next Page...

Table 4.2 – Continued

Grain .spot	U ppm	Th ppm	Th/U	Pb ppm	$f206\%$	$^{207}Pb/^{206}Pb$ 204corr	$\pm1\sigma$ (%)	$^{208}Pb/^{206}Pb$ 204corr	$\pm1\sigma$ (%)	$^{206}Pb/^{238}U$ 204corr	$\pm1\sigma$ (%)	$^{207}Pb/^{235}U$ 204corr	$\pm1\sigma$ (%)	%c	$^{206}Pb/^{238}U$ date	$\pm1\sigma$ (Ma)	$^{207}Pb/^{235}U$ date	$\pm1\sigma$ (Ma)	$^{207}Pb/^{206}Pb$ date	$\pm1\sigma$ (Ma)
MH09-67.1	103	65	0.62	105	0.647	0.3415	1.01	0.1499	3.20	0.778	1.72	36.643	2.10	101	3711	49	3684	21	3670	15
MH09-122.1	136	164	1.20	156	0.252	0.3441	0.75	0.3073	1.13	0.801	1.60	37.990	1.85	103	3792	46	3720	18	3681	11
MH09-157.1	274	105	0.38	265	0.106	0.3464	0.52	0.1016	1.42	0.771	1.48	36.847	1.63	100	3686	41	3689	16	3691	8
MH09-187.1	122	103	0.84	106	0.405	0.3465	0.91	0.2478	1.70	0.627	1.65	29.975	1.98	85	3139	41	3486	19	3692	14
MH09-42.1	200	142	0.71	220	1.830	0.3468	0.87	0.1867	2.87	0.785	1.53	37.544	1.85	101	3736	43	3708	18	3693	13
MH09-49.1	125	60	0.48	122	0.137	0.3482	0.79	0.1232	2.12	0.768	1.65	36.890	1.92	99	3675	46	3691	19	3699	12
MH09-167.1	71	151	2.13	89	-0.085	0.3484	1.18	0.5569	1.40	0.765	1.87	36.768	2.34	99	3664	52	3687	23	3700	18
MH09-24.1	220	108	0.49	166	0.191	0.3541	0.63	0.1594	1.36	0.576	1.50	28.111	1.70	79	2931	35	3423	17	3725	10
MH09-11.1	80	59	0.74	83	0.197	0.3658	1.02	0.1954	2.47	0.771	1.78	38.901	2.16	98	3685	50	3743	21	3774	15
MH09-17.1	76	61	0.80	84	0.212	0.3862	0.97	0.2018	2.02	0.806	1.83	42.919	2.18	99	3810	53	3841	22	3856	15
MH09-188.1	60	41	0.69	67	0.236	0.3887	1.04	0.1827	2.09	0.813	1.91	43.573	2.29	99	3835	55	3856	23	3866	16
MH09-191.1	125	50	0.40	133	0.078	0.3894	0.70	0.1022	1.80	0.828	1.65	44.444	1.87	100	3888	48	3875	19	3869	11
MH09-144.1	302	185	0.61	360	0.031	0.4246	0.43	0.1588	0.83	0.875	1.48	51.240	1.59	101	4053	44	4017	16	3999	6

$f206\%$ = 100 x (common ^{206}Pb/total ^{206}Pb)
$^{207}Pb/^{206}Pb$ 204corr = ^{204}Pb-corrected $^{207}Pb/^{206}Pb$ ratio
$^{206}Pb/^{238}U$ 204corr = ^{204}Pb-corrected $^{206}Pb/^{238}U$ ratio
$^{207}Pb/^{235}U$ 204corr = ^{204}Pb-corrected $^{207}Pb/^{235}U$ ratio
%c = % Concordance
$^{206}Pb/^{238}U$ date = ^{204}Pb-corrected $^{206}Pb/^{238}U$ date
$^{207}Pb/^{235}U$ date = ^{204}Pb-corrected $^{207}Pb/^{235}U$ date
$^{207}Pb/^{206}Pb$ date = ^{204}Pb-corrected $^{207}Pb/^{206}Pb$ date

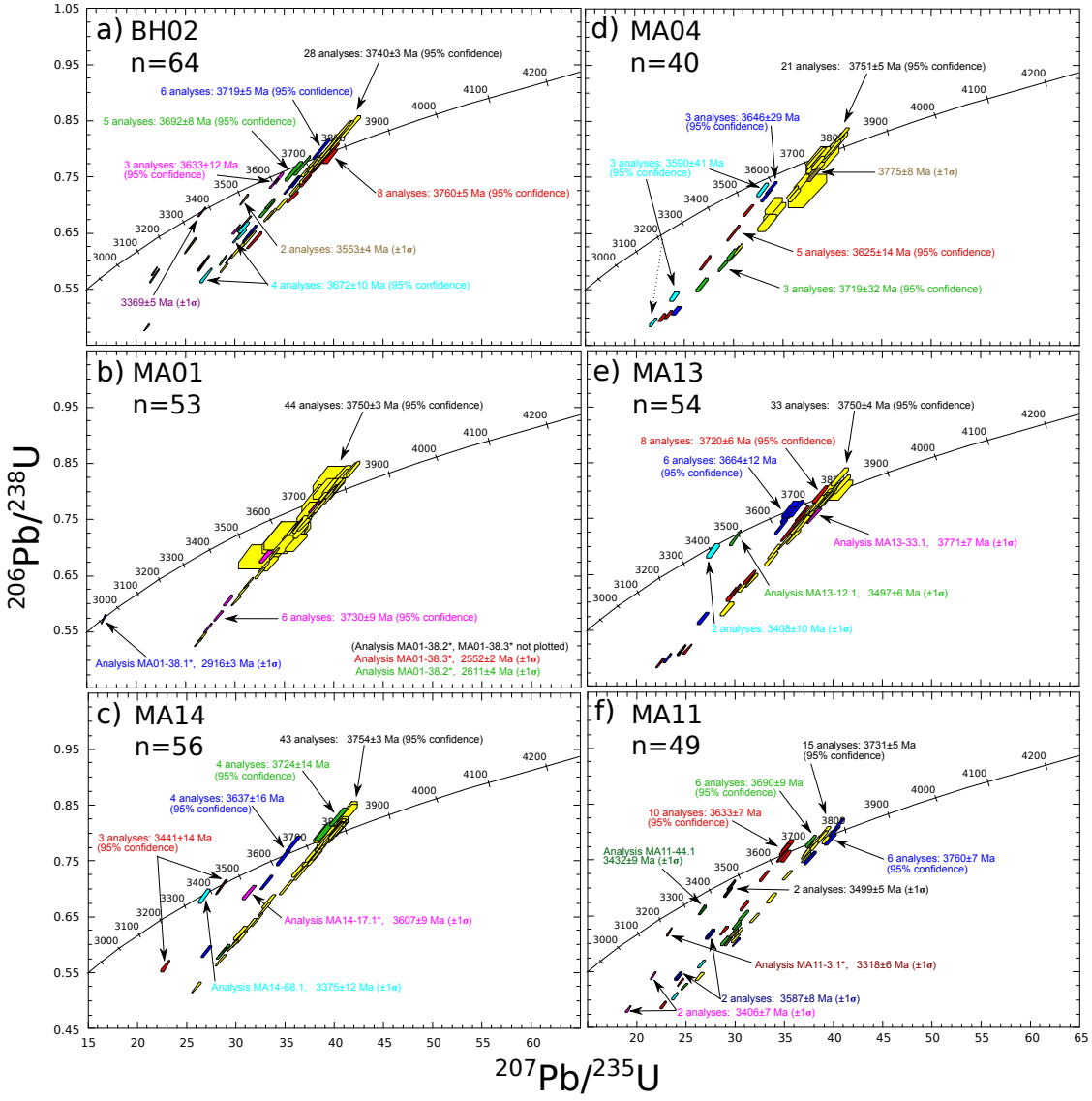

Figure 4.3: Wetherill concordia plots for zircon samples (a) BH02 (Brooking Hills), (b) MA01, (c) MA14, (d) MA04, (e) MA13, and (f) MA11 (Mt. Alfred) with major groups and grains of interest labelled. Discordance trends indicate zero-age Pb-loss. Data that are outside ±30% of concordia have not been plotted.

4.8 Discussion

4.8.1 Discordance patterns

Analyses that indicate a high concentration of uranium are commonly highly metamict and thus, readily disturbed during later stage metamorphic and fluid-fluxing events. Zircon analyses plotted by discordance percentage, age and uranium concentration reveal trends that reflect the degree of discordance as a function of their uranium concentration and $^{207}Pb/^{206}Pb$ age (Figure 4.6). Analyses that are both highly discordant and have uranium concentrations greater than ca. 300 ppm tend to indicate generally lower, and more scattered $^{207}Pb/^{206}Pb$ dates (shown in Fig. 4.6-B). This is

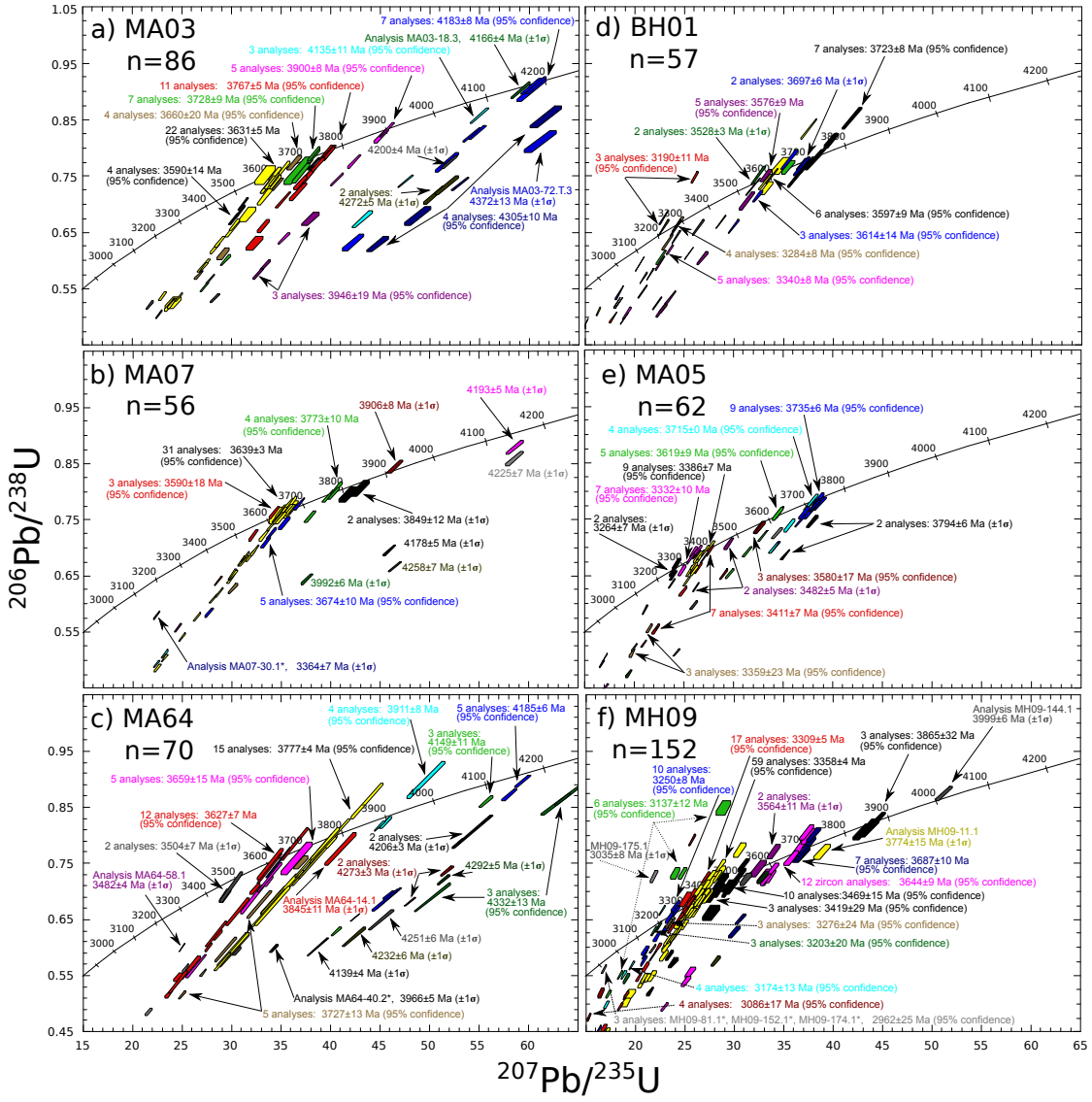

Figure 4.4: Wetherill concordia plots for zircon samples (a) MA03, (b) MA07, (c) MA64, (e) MA05 (Mt. Alfred), (d) BH01 (Brooking Hills), and (f) MH09 (Maynard Hills) with major groups and grains of interest labelled. Discordance trends indicate zero-age Pb-loss. Data that are outside ±30% of concordia have not been plotted.

consistent with higher uranium analysis sites being more readily disturbed and more likely to exhibit older (non zero age) discordance trends (non-vertical dotted lines in Fig. 4.6). Uranium concentration cutoffs at possible metamorphic events these detrital zircons would have experienced (Thern and Nelson, 2012b), marked at '(i)' and '(ii)' (Figure 4.6, A and B, dashed lines for <25% and <50% concordant analyses) define high-temperature 'stabilization' events. The slope of the dotted-line discordance trends below these metamorphic events on Fig. 4.6 results from preferential early disturbance of higher uranium analysis sites, producing more complex, non-vertical discordance trends. These events may have annealed some zircons, stabilizing their structure, while disturbing, or destroying, a certain proportion of grains with elevated uranium concentrations.

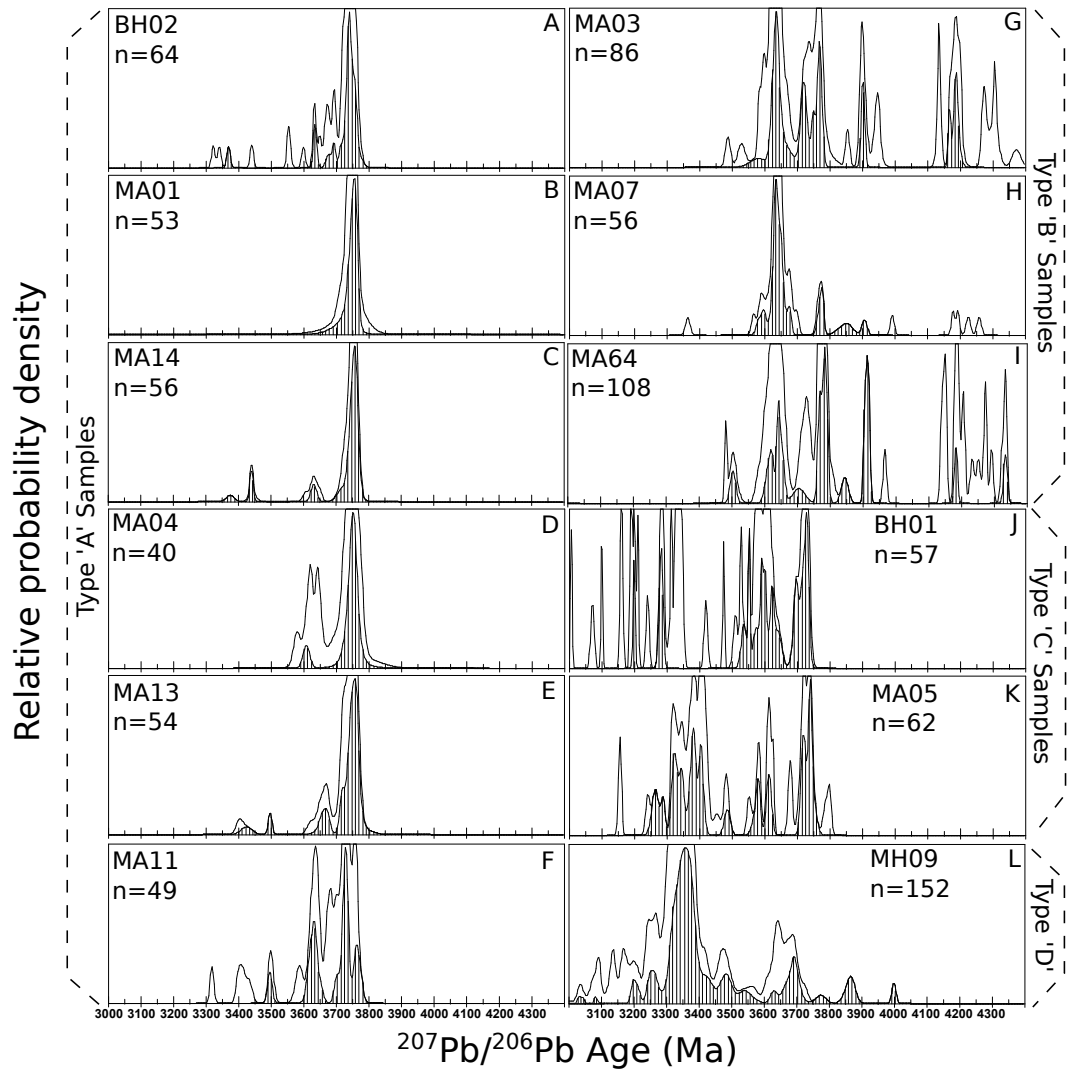

Figure 4.5: Gaussian summation probability density plots for zircon samples BH01 and BH02 (Brooking Hills), MA01, MA03, MA04, MA05, MA07, MA11, MA13, MA14, MA64 (Mt. Alfred), and MH09 (Maynard Hills). Data outside ±20% of concordia have not been plotted. Filled plots denote data within $\pm 2\sigma$ of concordia whereas open outlines is data that plots outside $\pm 2\sigma$ of concordia but above the ±20% of concordia cutoff used in the Wetherill plots.

At ages prior to these metamorphic events, disturbance trends are generally more vertical, with less scattering of $^{207}Pb/^{206}Pb$ dates, that relates to zero-age Pb-loss of moderately U-rich 'stabilized' zircons. The later trends (below events 'i' and 'ii') are most

likely a product of variable disturbance of high-U (> 300 ppm) zircons at non zero time and overprinting of zero-age Pb-loss, forming more complex disturbance trends. Due to the complexity of the discordant analyses, an overall uranium concentration cutoff of >300 ppm has been used to discount disturbed analysis sites from interpretations, where analyses with uranium contents above this level are typically highly discordant (see Fig. 4.6). A thorium concentration cutoff of approximately 400 ppm has also been used, although this seems less diagnostic of disturbed grains, and is only used in conjunction with the uranium cutoff to assess zero-age Pb-loss and Th enrichment in highly metamict zones.

4.8.2 Detrital Zircon Geochronology

The age structures of the detrital zircons from the samples in this study have been grouped into four types. Type "A" (samples MA01, MA04, MA11, MA13, MA14 and BH02) consist mostly of analyses older than 3680 Ma with lesser numbers of analyses down to the youngest zircon analysis within this group of ca. 3318 Ma. Type "B" (samples MA03, MA07 and MA64) consist of analyses mostly older than 3590 Ma with lesser amounts of ca. 10% discordant zircon analyses with ages as young as ca. 3360 Ma, and a 5-15% proportion of Hadean zircons greater than 3800 Ma in age. Type "C" (samples MA05 and possibly BH01) consist of many age groups between ca. 3300 Ma and 3750 Ma. Type "D" (sample MH09 and other Maynard Hills samples from other studies, see Nelson 2002b, 2005) consists of analyses mostly older than 3200 Ma, with a dominant peak at ca. 3350 Ma plus some analyses between 3060 and 2960 Ma.

Age groups consisting of 2 or more concordant analyses are herein interpreted as robust max depositional ages, whereas dates based on a single concordant analysis are interpreted as providing "tentative" or estimates of max depositional ages.

4.8.2.1 Type "A" samples

4.8.2.2 Brooking Hills Sample BH02 (Illaara G.B.)

Sample BH02 is from the western-most metasedimentary rock horizon exposed at Brooking Hills (Fig. 4.1, inset Brooking Hills map). A total of 77 analyses (Table 4.2) were obtained, 64 of these within ±20% of concordia (Fig. 4.3-A). Dates from this sample span from ca. 3370 Ma to ca. 3760 Ma (Fig. 4.5-A). Sample BH02 lacks many of the mixed age groups found in Brooking Hills sample BH01 (see section 6.2.13, below) and consists primarily of >3700 Ma age groups. The oldest group of 3760±5 Ma consists of eight analyses, whereas 28 analyses comprise the largest group at 3740±3 Ma, six analyses at 3719±5 Ma, five analyses at 3692±8 Ma and a number of smaller groups

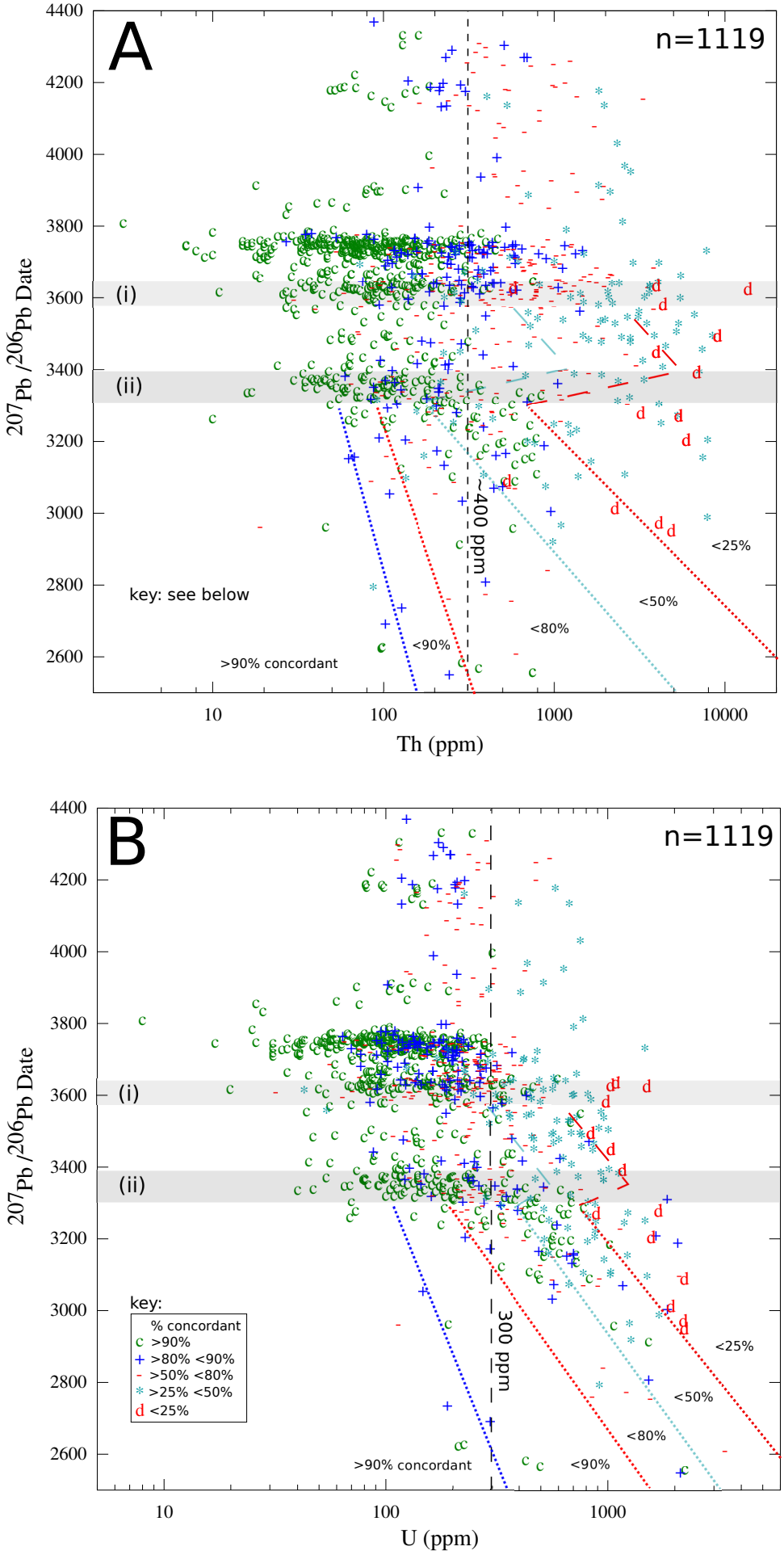

Figure 4.6: see next page for full description

Figure 4.6: Plots of $^{207}Pb/^{206}Pb$ date vs. U ppm (A) and Th ppm (B) for all data within this study. Data marked with "c" (green) are >90% concordant (including reversely discordant up to 110%), "+" (blue) are between 80-89% concordant, "-" (red) are between 50-79% concordant,"*" (light blue) are between 25-49% concordant and "d" (red) are between 0-24% concordant. Trend lines of the same color define concordance fields where most analyses within that trend have the same level of discordance. Higher U and Th concentrations relates directly to the degree of concordance. Shaded areas (i) and (ii) denote two major metamorphic events that may relate to early metamorphic events of the Narryer Terrane as recorded within the Narryer Gneiss Complex, from which these zircons are likely sourced. Dashed trend lines tentatively relate the earlier 3600 Ma event with disturbance trends within the eastern Mt. Alfred >3590 Ma populations.

composed of 2 to 3 analyses between 3690 to 3553 Ma. Of the four analyses with dates below 3100 Ma, all contain >1000 ppm U and are highly discordant, and most probably reflect disturbance during post-depositional events. The most concordant youngest single analysis at 3369±5 Ma (100% concordant) provides a maximum depositional age for this sample.

4.8.2.3 Mt. Alfred Sample MA01 (Illaara G.B.)

Sample MA01 is from a central-west metasedimentary rock horizon exposed at Mt. Alfred (Figure 4.1, inset Mt. Alfred map). A total of 73 analyses (Table 4.2) were obtained, 53 of these within ±20% of concordia (Fig. 4.3-B). Dates from this sample span from ca. 3730 Ma to 3750 Ma (Fig. 4.5-B). The simplest metasedimentary rock sample presented here, the main age group of 3750±3 Ma consists of 44 zircon analyses with a minor group of 6 analyses yielding an age of 3730±9 Ma. One variably disturbed analysis (MA01-38) is of a high-U zircon (>1000-3000 ppm) which yields discordant dates between 2552±2 Ma to 2916±3 Ma and has clearly been disturbed. With high uranium concentrations above 300 ppm and discordance of up to 70%, analyses with ages between 3468±10 Ma (MA01-5.1) and ca. 3700 Ma cannot be used to determine the maximum depositional age. The youngest concordant age group of 3730±9 Ma (6 analyses) therefore provides the most robust maximum depositional age for this sample.

4.8.2.4 Mt. Alfred Sample MA14 (Illaara G.B.)

Sample MA14 is from a central-west metasedimentary rock horizon exposed at Mt. Alfred (Figure 4.1, inset Mt. Alfred map). A total of 69 analyses (Table 4.2) were obtained, 59 of these within ±20% of concordia (Fig. 4.3-C). Dates from this sample span from ca. 3375 Ma to 3755 Ma (Fig. 4.5-C). Of similar detrital zircon age spectra to samples MA13 and MA04, analyses from sample MA14 consist primarily of a major

age group at 3754±3 Ma (43 analyses) with other age groups at 3724±14 Ma (4 analyses), 3637±16 Ma (4 analyses) and 3441±14 Ma (4 analyses). The youngest concordant analysis of 3375±12 Ma provides a maximum depositional age for this sample.

4.8.2.5 Mt. Alfred Sample MA04 (Illaara G.B.)

Sample MA04 is from a central-east metasedimentary rock horizon exposed at Mt. Alfred (Figure 4.1, inset Mt. Alfred map). A total of 52 analyses (Table 4.2) were obtained, 40 of these within ±20% of concordia (Fig. 4.3-D). Dates from this sample span from ca. 3590 Ma to 3775 Ma (Fig. 4.5-D). The largest age group is 3751±5 Ma (21 analyses), with smaller groups of 5 analyses at 2625±14 Ma and groups of 3 analyses each at 3719±32 Ma, 3646±29 Ma and 3625±14 Ma composed of slightly (5–10%) discordant analyses. A single analysis at 3775±8 Ma is the oldest analysis in this sample, and is just slightly outside of analytical uncertainty of the main 3751±5 Ma group. Dates younger than 2940 Ma (two analyses; MA04-13 and MA04-17; see Table 4.2) are viewed as being contaminants. Dates between 3134±31 Ma and 3469±19 Ma (3 zircon analyses) are highly discordant and contain >400 ppm U and >1500 ppm Th. The maximum depositional age is therefore provided by the youngest age group of 3590±41 Ma (3 analyses).

4.8.2.6 Mt. Alfred Sample MA13 (Illaara G.B.)

Sample MA13 is from a central-east metasedimentary rock horizon exposed at Mt. Alfred (Figure 4.1, inset Mt. Alfred map). A total of 64 analyses (Table 4.2) were obtained, 54 of these within ±20% of concordia (Fig. 4.3-E). Dates from this sample span from ca. 3400 Ma to 3771 Ma (Fig. 4.5-E). Within the same metasedimentary rock horizon as sample MA04, analyses from sample MA13 contain similar ca. 3700-3775 Ma dates with large groups at 3750±4 Ma (33 analyses) and 3720±6 Ma (8 analyses), a slightly smaller group at 3664±12 Ma (6 analyses) and a small number of younger analyses at 3497±6 Ma (1 analysis) and 3408±10 Ma (2 analyses). A single analysis at 3771±7 Ma is the oldest analysis in this sample, and is just outside of analytical uncertainty of the main 3750±4 Ma group. A single grain (MA13-64) with a date of 1014±56 Ma (76% concordant, >300 ppm U; refer to Table 4.2) has been isotopically disturbed. The youngest age group of 3408±10 Ma provides a maximum depositional age for this sample.

4.8.2.7 Mt. Alfred Sample MA11 (Illaara G.B.)

Sample MA11 is from the western-most metasedimentary rock exposed at Mt. Alfred (Figure 4.1, inset Mt. Alfred map). A total of 73 analyses (Table 4.2) were obtained, 49 of these within ±20% of concordia (Fig. 4.3-F). Dates from this sample

span from ca. 3318 Ma to 3760 Ma (Fig. 4.5-F). Sample MA11 is primarily composed of analyses between 3630 and 3760 Ma, with the largest age groups at 3731±5 Ma (15 analyses), 3760±7 Ma (6 analyses), 3690±9 Ma (6 analyses) and 3633±7 Ma (10 analyses). Smaller groups at 2587±8 Ma (2 analyses), 3499±5 Ma (2 analyses) and 3406±7 Ma (2 analyses) are made up of a number of concordant to slightly discordant analyses. Dates that fall below ca. 3300 Ma are marked by a high level of discordance (up to 89%), high U (1027-2216 ppm) and Th (534-4870 ppm) concentrations. The youngest near-concordant (only 6% discordant) analysis of 3318±6 Ma provides a maximum depositional age for this sample.

4.8.2.8 Type "B" samples

4.8.2.9 Mt. Alfred Sample MA03 (Illaara G.B.)

Sample MA03 is from the eastern-most metasedimentary rock horizon exposed at Mt. Alfred (Figure 4.1, inset Mt. Alfred map). A total of 146 analyses (Table 4.2) were obtained, 86 of these within ±20% of concordia (Fig. 4.4-A). Dates from this sample span from ca. 3590 Ma to 4372 Ma (Fig. 4.5-A). The largest age groups are 3631±5 Ma (22 analyses), 3767±5 Ma (11 analyses) and 3728±9 Ma (7 analyses). Analyses older than 3900 Ma make up approximately 15% of the total sample, and are made up of a group of 5 analyses at 3900±8 Ma, a slightly discordant group of analyses at 3946±19 Ma, and a number of groups composed of 2 to 3 analyses indicating dates of 4135±11 Ma (slightly discordant) to 4372±13 Ma (MA03-72.T.3; see Table 4.2). Ages younger than 2940 Ma (four zircons; MA03-52, MA03-71, MA03-32 and MA03-40; see Table 4.2) are viewed as being contaminants (see section 6.3, below). Analyses between the ages of 2950 and 3590 Ma are highly discordant, with uranium contents of up to 1703 ppm, indicating disturbance. The youngest age group of 3590±14 Ma (4 analyses) provides a robust maximum depositional age for this sample.

4.8.2.10 Mt. Alfred Sample MA07 (Illaara G.B.)

Sample MA07 is from the eastern-most metasedimentary rock horizon exposed at Mt. Alfred (Figure 4.1, inset Mt. Alfred map). A total of 89 analyses (Table 4.2) were obtained, 56 of these within ±20% of concordia (Fig. 4.4-B). Dates from this sample span from ca. 3360 Ma (slightly discordant) to 4258 Ma (slightly discordant) shown in Fig. 4.5-B. From the same metasedimentary horizon as sample MA03, MA07 contains the ca. 3600-3700 Ma dates with a large group similar to that found in MA03 at 3639±3 Ma (31 analyses) and populations older than 3800 Ma, but lacks the zircon age group at ca. 3730 Ma. Other age groups present in this sample are at 3674±10 Ma (5 analyses), 3773±10 Ma (4 analyses), 3590±18 Ma (3 analyses), 3849±12 Ma (2 analyses) and a

number of single analyses indicating dates of 3900 to 4258 Ma. The oldest analyses obtained include a single slightly discordant analysis at 4258±7 Ma (MA07-48.3) and a few less discordant analyses of 4225±7 Ma (MA07-48.1) and 4193±5 Ma (MA07-52.2). Analyses with dates older than 3750 Ma fall between ca. 3775-3910 Ma and ca. 4175-4258 Ma, with a gap between 3910-4175 Ma if the discordant analysis at 3992±6 Ma (MA07-76.1) is excluded. The youngest analysis of 3364±7 Ma (MA07-30.1; 12% discordant), or robust group of 3 analyses at 3590±18 Ma, provide maximum depositional age estimates for this sample.

4.8.2.11 Mt. Alfred Sample MA64 (Illaara G.B.)

Sample MA64 is from the eastern horizon exposed at Mt. Alfred (Figure 4.1, inset Mt. Alfred map; 2 meters west of sample MA03). A total of 108 analyses (Table 4.2) were obtained, 70 of these within ±20% of concordia (Fig. 4.4-C). Dates from this sample span from ca. 3500 Ma to 4335 Ma (Fig. 4.5-C). The largest age groups at 3777±4 Ma (15 analyses; 5 on individual zircons since a single grain has 10 analyses), 3627±7 Ma (12 analyses), 3727±9 Ma (5 analyses) and 3659±15 Ma (5 analyses), plus a large percentage of >3900 Ma zircon analyses. These older analyses include groups at 4185±6 Ma (5 analyses), 3911±8 Ma (4 analyses), 4149±11 Ma (3 analyses) and 4332±13 Ma (3 analyses on a single zircon; MA64-41) and a number of analyses that are between 2 to 20% discordant at 3845±11 Ma, 3966±5 Ma, 4139±4 Ma, 4232±6 Ma, 4251±6 Ma, 4273±3 Ma and 4292±5 Ma. The youngest concordant age group at 3504±7 Ma (2 analyses) provides a maximum depositional age for this sample.

4.8.2.12 Type "C" samples

4.8.2.13 Brooking Hills sample BH01 (Illaara G.B.)

Sample BH01 is from the Brooking Hills within the Illaara Greenstone Belt (Fig. 4.2, inset Brooking Hills map). A total of 57 analyses (Table 4.2) were obtained, all within ±20% of concordia (Fig. 4.4-D). Dates from this sample span from ca. 3190 Ma to ca. 3725 Ma (Fig. 4.5-D). Sample BH01 is a variably mixed sample with many small (<2 to 3 analyses) $^{207}Pb/^{206}Pb$ age groups. Most analyses lie between the youngest and oldest groups of 3190±11 Ma and 3723±8 Ma, with a number of discordant analyses below 3190 Ma. Major groups at 3723±8 Ma (7 analyses), 3597±9 Ma (6 analyses), 3576±9 Ma (5 analyses) and 3340±8 Ma (5 analyses) are mixed with smaller groups comprised of 2 to 3 analyses each (Fig. 4.4-D). Of the four dates below 3000 Ma, all are either highly discordant or contain >300 ppm U. Two 13% discordant analyses with ages of 3073±6 Ma and 3099±2 Ma may provide an estimate of maximum depositional age for this sample, however their U contents >1000 ppm and discordance >10% indicates

that these dates have been disturbed. The youngest concordant age group of 3 analyses at 3190±11 Ma thus provides the most robust maximum depositional age for this sample.

4.8.2.14 Mt. Alfred Sample MA05 (Illaara G.B.)

Sample MA05 is from the eastern margin of the eastern-most metasedimentary rock horizon exposed at Mt. Alfred (Figure 4.1, inset Mt. Alfred map). This sample is from the same metasedimentary rock horizon as samples MA03, MA07 and MA64, but contains a distinctly different zircon age spectra (see Fig. 4.5-E). A total of 85 analyses (Table 4.2) were obtained, 62 of these within ±20% of concordia (Fig. 4.4-E). The distribution of dates obtained on zircons from this sample spans from ca. 3260 Ma to ca. 3800 Ma (Fig. 4.5-E). The analyses in this sample form many smaller concordant groups with no major groups of more than 10 analyses. Age groups with >5 analyses are 3735±6 Ma (9 analyses), 3386±7 Ma (9 analyses), 3411±7 Ma (7 analyses) and 3332±10 Ma (7 analyses) whereas groups composed of 2 to 5 analyses include 3794±6 Ma (2 analyses), 3715±10 Ma (4 analyses), 3619±9 Ma (5 analyses), 3580±17 Ma (3 analyses), 3482±5 Ma (2 analyses), 3359±23 Ma (3 analyses) and 3264±7 Ma (2 analyses). This sample lacks any analyses older than ca. 3800 Ma, in contrast to other samples from this same metasedimentary horizon (MA03, MA07, MA64). The youngest concordant age group of 3264±7 Ma (2 analyses) provides a maximum depositional age for this sample.

4.8.2.15 Type "D"

4.8.2.16 Maynard Hills Sample MH09 (Maynard Hills G.B.)

Sample MH09 is from the Maynard Hills Greenstone Belt. The heavy mineral fraction analyzed is from the same aliquot of sample 169075 (Nelson, 2002b). A total of 178 analyses (Table 4.2) were obtained, 152 of these within ±20% of concordia (Fig. 4.4-F). Dates from this sample span from ca. 2960 Ma to 4000 Ma (Fig. 4.5-F). Analyses from sample MH09 are distinctly different from the Mt. Alfred samples, with the notable absence of large groups of analyses between 3400 and 3300 Ma (with the possible exceptions of type 'C' samples MA05 and BH01). The largest groups within sample MH09 are those of 3358±4 Ma (59 analyses), 3309±5 Ma (17 analyses), 3644±9 Ma (12 analyses) and 3250±8 Ma (10 analyses). There are many smaller groups (Fig. 4.4-F) that add to the complexity of the zircon analyses younger than 3800 Ma. A lack of 3800 to 3700 Ma analyses is apparent, with only a single date of 3774±15 Ma within this range. Ages above 3800 Ma include a group of 3 analyses at 3865±32 Ma and a single analysis at 3999±6 Ma (MH09-144.1); adding to the ca. 4350 Ma grain found in the previous aliquot of sample 169075 (Nelson, 2002b; Wyche et al., 2004). The

youngest (slightly discordant and including a single analysis with >1000 ppm U; refer to Table 4.2) age group of 2962±25 Ma (3 analyses on 3 zircons) provides a tentative maximum depositional age for this sample. A more conservative, and robust maximum depositional age is constrained by the age group at 3137±12 Ma (6 analyses).

4.8.2.17 Hadean zircons and sample heterogeneity

Zircons older than 3800 Ma have been found in four samples, (type 'B' samples MA03, MA07, MA64 (178064; Nelson, 2002) and type 'D' sample MH09 (169075; Nelson, 2005). Sample MH09, from the Maynard Hills, has previously been analyzed (as sample 169075) and contained a single zircon with one analysis at 4364 Ma (Nelson, 2002b). The aliquot used in this study yielded numerous analyses at ca. 3850 Ma, one at 3900 Ma and a single zircon with an age of nearly 4000 Ma (MH09-144). Of the 190 zircon analyses of sample MH09 obtained during this study, no additional >4000 Ma zircons were found, highlighting the scarcity of these ancient zircons and the fortuitous nature of their discovery within sample 169075.

In contrast to the single Maynard Hills sample that has yielded only a few zircon analyses older than 3800 Ma, the Mt. Alfred locality within the Illaara Greenstone Belt has yielded many >3800 Ma zircon analyses, two of which have dates greater than 4300 Ma. Mt. Alfred sample 178064 (Nelson, 2002) contained a number of >3800 Ma zircons, with one approaching 4300 Ma. Additional work on the same aliquot of zircons (MA64, see Fig. 4.4 and Table 4.2) resulted in numerous analyses with ages greater than 4000 Ma, with the oldest being 4334 Ma. Additional sampling at site MA03 along this outcrop, from a few meters east of sample 178064 (Nelson, 2002), and an additional sample from about 150 meters along the metasedimentary rock horizon (MA07) yielded more >3800 Ma analyses. A sample from between these two sites (MA05) resulted in large groups of analyses with ages less than 3590 Ma, not found within samples MA03 or MA07 but no analyses greater than 3800 Ma. Additionally, all of the metasedimentary rock horizons at Mt. Alfred to the east of these Hadean zircon-bearing samples contain abundant 3780 to 3700 Ma age groups, but nothing greater than 3800 Ma, even though the sampling sites are 50 to 100 meters apart. This difference in Hadean zircon abundance within the metasedimentary rocks indicates that it would be easy to sample the metasedimentary rock horizon and not detect Hadean zircons. In the case of the Mt. Alfred type 'B' samples (MA64, MA03 and MA07), where >3800 Ma zircons can be in excess of 15% of the total sample, it would be hard to miss this more abundant component. However, if one were to analyze only Mt. Alfred type 'A' samples (MA01, MA04, MA11, MA13 or MA14), the Hadean zircons present only 50-100 meters away would have been missed, and the overall age structure of the metasedimentary rocks at this locality would have emphasized mostly 3600-3780 Ma ages.

Further south in the Illaara Greenstone Belt at the two Brooking Hills sample sites (BH01 and BH02) as well as sample site 142999 (Nelson, 2000b), no zircon analyses with ages older than 3800 Ma have been found. No other samples from the Maynard Hills Greenstone Belt have yielded zircons with ages older than 3800 Ma except for sample 169075/MH09 (Nelson, 2002; Wyche et al., 2004; Wyche et al., 2007; this study). Further north in the Southern Cross Terrane, the Gum Tree Greenstone Belt, a metasedimentary rock (GSWA sample 184107) with a presumed >3000 Ma depositional age, and with lithological and detrital age characteristics similar to those of the Maynard Hills, did not yield analyses older than 3800 Ma (Wingate and Bodorkos, 2007). To the southwest within the South West Terrane, Hadean zircons have not been identified apart from a few ca. 3850 Ma zircons within the Toodyay Lake Grace Domain metasedimentary rocks. No other >3800 Ma zircons from the Yilgarn Craton have yet to be identified other than those from the Jack Hills, Mt. Narryer, Mt. Alfred and Maynard Hills metasedimentary rock localities and two >3800 Ma xenocrysts found within gneisses of the Narryer and Murchison Terranes (Nelson, 2000c). These >3800 to 4200 Ma zircon xenocrysts within the gneisses of the Narryer and Murchison terranes show that the Narryer Terrane and the northern Murchison Terrane formed in proximity to, or were contaminated by, crustal sources that included a Hadean component.

4.8.3 Depositional age constraints

The metasedimentary rocks documented herein were sampled over a 30 km distance spanning the Maynard Hills and Illaara greenstone belts. Results from the Mt. Alfred locality, from a ca. 250 sqm area, show that exposed metasedimentary rock horizons can contain different age populations. Samples from different groups of metasedimentary horizons at Mt. Alfred, grouped as types 'A', 'B' and 'C', reveal a general up-section younging (east type-'A' to west type-'C') based on the youngest detrital zircon in each type and the overall mean age of analyses within each type. The eastern to western metasedimentary rock horizons at this locality also show an increase in age complexity from types 'A' to 'B' to 'C', and horizons with abundant >3800 Ma analyses (type 'B'). The eastern-most horizons at Mt. Alfred are composed of mostly >3700 Ma analyses (type 'A') and represent a unique provenance of zircons that may be related to Manfred-Complex style gneisses (Thern and Nelson, 2012b). The western-most horizon sampled at Mt. Alfred contains many younger ca. 3700 to 3300 Ma analyses (types 'B' and 'C') as well as Hadean zircons (type 'B'). This Hadean component is absent in the eastern metasedimentary rock (type 'A') horizons only 50 to 100 meters away. These metasedimentary rock horizons have complex age characteristics that require multiple samples from multiple horizons to ascertain the character of their depositional environment and provenance. This heterogeneity indicates that more than one sample must be analyzed from any greenstone or metasedimentary belt in order to investigate the provenance of the metasedimentary rocks of that belt.

Using the youngest concordant detrital zircon analysis or group within each sample to provide the maximum depositional age for a sedimentary rock has been commonly used throughout studies involving detrital minerals. There are a number of limitations to this approach, outlined in Nelson (2001). First, it is not uncommon for the youngest detrital zircon to be significantly older than the time of sediment deposition. This can arise from a number of factors; the host rocks may not have components close to the age of sedimentation, the source region may not have contained younger rocks, or the youngest detrital zircons are present in very small abundance and may require a large amount of analytical time to identify. In samples that have 'complex' age structure (type 'C' samples from this study, for example) maximum depositional age estimates are more likely to be closer to the true depositional age than for 'simple' samples with few age groups (type 'A' samples from this study) (Nelson, 2001). Second, detrital zircon analyses may be reset due to Pb-loss events during late-stage metamorphism that could then post-date the real depositional age for the sediment, causing erroneously young maximum depositional ages. An example of this is found in the Toodyay Lake-Grace Domain metasedimentary rocks of the Jimperding Metamorphic Belt, where some detrital zircons have 'alteration' zones and rims that are ca. 2650 Ma in age (Pidgeon et al., 2010).

In discussing the first limitation, that the youngest detrital zircon may be significantly older than the time of sedimentation, a good example is found in the age structures within the Illaara Greenstone Belt metasedimentary rocks at Mt. Alfred. A number of the Mt. Alfred samples (types 'A' and 'B') have maximum depositional ages based on their youngest concordant zircon of nearly 3600 Ma (samples MA03 and MA04) and even up to 3730 Ma (sample MA01). When compared to the youngest zircons found within metasedimentary rock horizons 50 to 100 meters to the west and even further along the same N–S trending metasedimentary rock horizons, the youngest concordant zircon ages are closer to ca. 3250 Ma (type 'C'). Samples with type 'C' ages (MA05 and BH01) are the most complex, with numerous small groups of ages. These type 'C' samples yield the youngest detrital zircons yet identified at the Mt. Alfred and Brooking Hills localities. It is hard to imagine that the "older" samples were deposited at ca. 3600 Ma considering their proximity to the "younger" samples of ca. 3300-3250 Ma ages. This gap in younger zircons may be due to this minor source component being unavailable during deposition. With a paucity of ca. 3000-3200 Ma rocks throughout the Narryer Terrane (Kinny et al., 1988; Nutman et al., 1991; Kinny and Nutman, 1996; Pidgeon et al., 1998), the lack of detrital zircons found within this time period may be interpreted to indicate that these sediments were deposited at different times between 3300 and 2960 Ma, as constrained by the youngest detrital zircon from each of the four types of samples ('A', 'B', 'C' and 'D'). This is also consistent with the age of the youngest detrital zircons from many metasedimentary rock samples throughout [i] the

Jack Hills (ca. 3060 Ma) Cavosie et al. (2004); Crowley et al. (2005), [ii] the Toodyay Lake Grace Domain (ca. 3060 to 2940 Ma) Pidgeon et al. (2010), [iii] Mt. Narryer (ca. 3130 to 3075 Ma) Kinny et al. (1990); Crowley et al. (2005), [iv] the Maynard Hills (ca. 3125 to 2960 Ma.) Nelson (2002b), and [v] Gum Creek (ca. 3214 Ma) Wingate and Bodorkos (2007).

The second limitation, that many detrital zircons could be reset due to Pb-loss events, has been assessed by determining a uranium concentration cutoff for disturbed grains (Fig. 4.6) and applying this to grains younger than ca. 3000 Ma. With a small number of exceptions, there are few concordant analyses younger than ca. 3000 Ma found within the samples of this study. Of these, a few ca. 2960 Ma ca. 10% normally and reversely discordant ages from the Maynard Hills sample MH09 may indicate the maximum depositional age for this sample, but the most concordant analysis in this group has >1000 ppm uranium and makes this interpretation tenuous. Other analyses younger than 3000 Ma that are not discordant and do not have high U ppm values may be explained as contaminants, or reset during peak metamorphic events between ca. 2730-2630.

Samples with analyses younger than ca. 2940 Ma typically have high uranium concentrations >300 ppm and are interpreted to result from late stage Pb redistribution or disturbance. This is also the time of cross-cutting and stratiform quartz-tourmaline veins throughout the Mt. Alfred and Brooking Hills localities (at least for type 'A' samples) that place a minimum depositional age on these metasedimentary rocks of ca. 2940 Ma based on $^{40}Ar/^{39}Ar$ plateau ages (Thern et al.; in prep) obtained on the tourmalines from these veins (Thern et al., 2011). Further evidence of stratiform or cross-cutting tourmaline veins that have intruded other metasedimentary rocks throughout the Yilgarn Craton may help constrain their minimum depositional ages (Thern et al.; in prep). Although poorly constrained due to the scarcity of zircons less than 3300 Ma in age, it is most likely that the Illaara and Maynard Hills greenstone belt metasedimentary rocks were deposited between 3300 and 2940 Ma.

The depositional age of the metasedimentary rocks of the Illaara and Maynard Hills greenstone belts is best described by pooling the grouped samples and using the youngest detrital zircon within each 'type' of grouped sample to define the maximum depositional age for all samples within that type group. Since the sample groups occur in proximity to one another, and occur with similar detrital zircon ages, it is reasonable to assume that they sampled similar sources and were deposited coevally. Maximum depositional ages for each group type are listed as follows: type 'A': 3318 Ma; type 'B': 3364 Ma; type 'C': 3264 Ma (MA05) or 3180 Ma (BH01); and type 'D': ca. 2960 Ma to 3056 Ma. This timing, along with their detrital zircon age similarities, implies that these sediments were deposited coevally with those from the Gum Creek Greenstone

Belt, the Jack Hills, Mt. Narryer and Toodyay Lake Grace Domain and that they could have originally formed a single sedimentary succession that was deposited at some time between 3300 and 2940 Ma. If all metasedimentary occurrences sampled were deposited in the same sedimentary basin at approximately the same time, then the best estimate of this deposition time is provided by the maximum deposition age of the youngest population group; 3056 Ma to 2960 Ma.

4.8.4 Depositional environment

If all the ca. 3000 Ma metasedimentary rocks examined in this study were deposited coevally, those of the Narryer Terrane (Jack Hills and Mt. Narryer) may have formed coalescing fan deltas of which the metasedimentary rocks of the Southern Cross formed the eastern to south-eastern edge and the Toodyay Lake Grace Domain metasedimentary rocks may have formed the southern edge. Later stage rifting, folding, tectonic shearing and metamorphism may have then resulted in a complex juxtaposition of the metasedimentary rocks contained within horizons throughout the Southern Cross. The Mt. Narryer and Jack Hills sedimentary rocks may therefore have been deposited within the same sedimentary basin as the lithologically similar metasedimentary rocks of the Southern Cross. Metamorphic and tectonic events between 3000 and 2600 Ma have obscured most original sedimentary features (Chen et al., 2004a; Wyche et al., 2004). Numerous sedimentological features such as cross-bedding and graded bedding have been found within the Toodyay Lake Grace Domain (Bosch et al., 1996), Jack Hills (Eriksson and Wilde, 2010) and Mt. Narryer (Crowley et al., 2005) metasedimentary rocks, that have helped define younging directions and depositional environments (Eriksson and Wilde, 2010). In contrast, the Southern Cross metasedimentary rocks have only one documented occurrence of cross bedding within the Maynard Hills Greenstone Belt, that define a younging-upward direction to the west (Chen et al., 2004a).

The metasedimentary rocks of type ‘A’ show the simplest age populations with ages mostly between 3780 and 3700 Ma. These samples may be indicative of a constrained source, where the topographic highs of the provenance were composed almost entirely of these rock ages. The small amount of 3700 to 3590 Ma zircons could have been picked up from the less-exposed, more complex basement rocks that are found in abundance in sample types ‘B’ and ‘C’. If these more complex younger rocks became topographic highs after deposition of type ‘A’ samples, then types ‘B’ and ‘C’ samples deposited in the western Mt. Alfred locality with ages between ca. 3750 to 3200 Ma are easier to explain. Sample MA05, type ‘C’, is the western-most sample at Mt. Alfred from the same sedimentary ’horizon’ along with MA07, MA03 and MA64, and completes an ‘up-section’ younging and increase in complexity for the Mt. Alfred metasedimentary rocks from east to west. The Maynard Hills Greenstone Belt metasedimentary rocks (type ‘D’, sample MH09) may be further up-section to those within the Illaara Greenstone

Belt (Wyche et al., 2004) and the Mt. Alfred sample locality. The type 'D' sample at Maynard Hills may represent younger metasedimentary rocks with possible maximum depositional ages between ca. 3050 to 2960 Ma and a higher proportion of <3500 Ma detrital zircons than anywhere within the Mt. Alfred or Brooking Hills samples yet identified.

If the deposition of these metasedimentary rocks occurred between ca. 3300 and 2940 Ma, differences in the age structures of their detrital zircon populations may be related to the uplift and exposure of more complex source terranes over time. Examples of similar up-section younging and increase in complexity, displayed within samples from east to west within the Mt. Alfred locality (types 'A' to 'C'), has been documented in Robb and Meyer (1990, 1995). These authors explained this up-section younging and increase in complexity by the process of progressively younger granitoid unroofing during basin filling. Another study by Kositcin and Krapez (2004) explained the provenance for the detrital age spectra determined within the Central Rand Group (from the Witwatersrand Basin) as being consistent with a magmatic fold-thrust belt. This in turn was attributed to provenance-wide uplift and a general increase in structural complexity including unroofing of contemporaneous granitoids, similar to a study of Robb and Meyer (1990), supporting a retroarc basin as the depositional setting for the Central Rand Group (Kositcin and Krapez, 2004). Whereas the same may not be true for the provenance of the Mt. Alfred metasedimentary rocks, it is clear that their detrital zircons were derived from diverse sources, and one explanation is that their source changed from structurally simple to structurally complex between deposition of type 'A' sediments on the east to type 'B' and 'C' sediments to the west. Whether this indicates that there was a tectonic regime change between the deposition of these sediments, or that there was a constrained source is still unclear. If this reflects a tectonic regime change within the provenance, it could indicate a change in depositional setting from a passive margin/continental shelf (thermal-subsidence basin) to a foreland basin type setting. Whereas the provenance of the metasedimentary rocks at Mt. Alfred may have been similar to components within the Narryer Gneiss Complex (NGC) (Thern and Nelson, 2012b), a process such as the unroofing of granitoids would require that the NGC was not fully deformed at the time of deposition of these sediments, and that the proto-NGC was comprised of largely heterogeneous granitic components. Evidence that the currently exposed NGC may be much more homogenized and migmatized than a proto-NGC terrane at 3300 to 3000 Ma is two-fold. First, much of the currently exposed gneissic fabric (although may have been overprinted from older metamorphic events) is due to 2750–2600 Ma, and 3300 Ma metamorphic events (Kinny and Nutman, 1996). Second, denudation of at least 3 km of Yilgarn cover (Weber and Ricken, 2005) may have destroyed previous NGC components, and exposed deeper and more complex NGC components. Any models that show up-section increases in detrital zircon age complexity

when applied to sediments derived from a present day NGC-like provenance would require an earlier proto-NGC to be composed of less deformed and heterogeneously mixed granites and gneisses.

A further complication to this interpretation is shown in the west to east increase in complexity at the Brooking Hills, 15km south of Mt. Alfred. Here, the detrital zircon age characteristics between samples BH01 (type 'C') and BH02 (type 'A') show that the controls on what constitutes "up-section" are poorly constrained. Whereas the Brooking Hills results are from only two samples, the fact that the more complex sample is to the east presents a dilemma in terms of defining upward-younging or increasing complexity of source terranes. First, it is possible that the depositional environment, that may have consisted of coalescing fan deltas feeding a broad continental shelf, may have been fed by multiple sources in a cyclical fashion, based on storm surges or other events, resulting in sedimentary horizons with differing provenance characteristics. Second, some sediments may have been tidally reworked, adding complexity to their detrital zircon age spectra soon after original deposition. Third, the contrasting ages of type 'A' sediments between those of types 'B', 'C' and 'D' may be explained by sediments of type 'A' being sourced from an exotic terrane unrelated to that of types 'B', 'C' or 'D'. Shared zircon age groups between most of these >3000 Ma metasedimentary rocks with those of others from the Yilgarn Craton makes it unlikely that they did not share some similar provenance (Thern and Nelson, 2012b). Finally, of possibly primary importance, these metasedimentary rocks may be complexly interleaved due to late stage metamorphism, folding, and shearing along the Edale shear zone. The impact and complexity of these overprinting tectonic and metamorphic events make it difficult to assess any real sedimentological structures, and may be obscuring the detrital zircon geochronological record. Possible late stage tectonic interleaving and juxtaposition of what appear to be continuous stratigraphic horizons complicate interpretations based on detrital zircon age spectra from these metasedimentary 'packages'. These late stage processes may bring together originally geographically diverse sediments with different provenances, that now form what appears to be a single stratigraphic unit. The similar detrital zircon age groups found throughout the metasedimentary rocks of the Illaara and Maynard Hills Greenstone Belts, and the contrasting age characteristics of individual metasedimentary rock horizons would suggest that, at the Mt. Alfred locality at least, (i) these tectonic processes did not homogenize all the metasedimentary horizons together, and (ii) the metasedimentary rocks shared similar provenance components, but represent different depositional cycles.

If the provenance of these metasedimentary rocks included the Narryer Gneiss Complex (Thern and Nelson, 2012b), a source terrane composed of exposed Meeberrie and Manfred-style rocks, with few exposures of younger Eurada and Dugel-style rock ages, may account for the detrital zircon ages within type 'A' metasedimentary rocks.

Later tectonic thrusting and uplift of the NGC, during a possible continental collision coeval with the development of a rift basin, may have led to exposures of Eurada and Dugel style gneisses and younger (ca. 3300 to 2960 Ma) granitoids, and would have increased the complexity of the exposed provenance source rocks. Detrital zircons from the first exposures of these complex rocks, including mostly 3700 to 3350 Ma ages and a small Hadean component containing >3800 Ma zircons could then have been deposited in type 'B' sediments at Mt. Alfred (MA03, MA07 and MA64), perhaps stratigraphically above type 'A' sediments. Younger exposures including 3700 to 3250 Ma rocks are evidenced within the detrital zircon ages found within the western edge of the same metasedimentary rock horizon at Mt. Alfred in sample MA05 (type 'C'). Some younger ages between ca. 2960 and 3060 Ma, and large populations of 3360 to 3250 Ma zircons from sample MH09 (type 'D') within the Maynard Hills Greenstone Belt complete a 'younging sequence' that may reflect a greater complexity of their provenance and later stage deposition to the metasedimentary rocks at the Mt. Alfred locality (types 'A' through 'C'). The detrital zircon age structure of sample MH09 has similar detrital age characteristics when compared to sediments from the Jack Hills (Nelson, 2002b; Wyche et al., 2004; Wyche, 2007). Similarities between the metasedimentary rocks of the Yilgarn, summarized on Fig. 4.7, shows their shared zircon ages to the Narryer Gneiss Complex and Yarlarweelor Gneiss Complex (Fig. 4.7; A and B vs. C, D, E, F, G and H). Some tentative detrital zircon age similarities may be established further between the Mt. Narryer and the Mt. Alfred and Brooking Hills (Fig. 4.7, G and H), the Maynard Hills with the Jack Hills (Fig. 4.7, F and E), and Gum Creek with the Toodyay Lake Grace Domain (Fig. 4.7, D and C). These similarities, discussed further in Thern and Nelson (2012b), strongly suggest a similar provenance and imply a strong relationship between all these ca. 3000 Ma metasedimentary rocks throughout the Yilgarn Craton.

4.8.5 Relationships between metasedimentary rock occurrences within the Yilgarn Craton

The metasedimentary rocks from the Southern Cross have similar detrital zircon ages to those of the Mt. Narryer and Jack Hills within the Narryer Terrane (Nelson, 2002b; Wyche et al., 2004; Wyche, 2007), even though they are currently more than 400 km apart. Detrital zircon analysis reveals age populations from the Southern Cross metasedimentary rocks that imply they were derived from NGC-like gneiss components (Thern and Nelson, 2012b). A proto-source composed of NGC-like components is also likely for the other ca. 3000 Ma metasedimentary rocks throughout the Yilgarn Craton (Thern and Nelson, 2012b). Although the detrital zircon populations within the Southern Cross metasedimentary rocks have different proportions of Narryer-like age populations, there are a number of striking similarities between the Southern Cross, Narryer Terrane and Toodyay Lake Grace Domain metasedimentary rocks: (1) The

youngest detrital zircons in all samples (defining their max depositional ages) are not younger than ca. 2960 Ma; (2) Lithological similarities between these metasedimentary rocks show that they could have been deposited in a similar depositional environment; (3) The occurrence of detrital Hadean zircons within metasedimentary rocks from both the Narryer and Southern Cross Terranes is most easily explained by their sharing similar provenance with a distinct Hadean-bearing source locality; and (4) The only rocks within the Yilgarn Craton from which the detrital zircon age structures found within these ca. 3000 Ma metasedimentary rocks could have been derived are those from the Narryer Gneiss Complex within the Narryer Terrane.

These lines of evidence, based mostly on pre-3000 Ma geochronology, shows that the metasedimentary rocks, now separated by up to 400 km, may have shared a common provenance region. The ca. 3000 Ma deposition of sediments within the Narryer and Southern Cross Terranes of a proto-Yilgarn may have had a basement similar to the Narryer Gneiss Complex. This basement would have contained some proto-NGC type rocks that contained Hadean zircons, as evidenced by Hadean xenocrysts in ca. 2600 Ma gneisses (Nelson, 2000c). Alternatively, multiple distinct Hadean terranes of similar composition formed the basement rocks that were in close proximity to one another (or later accreted to one another to form a proto-Yilgarn terrane) and on which the different metasedimentary rocks of the Narryer and Southern Cross Terranes were deposited. The overall similarities of age structures within these metasedimentary rocks and the NGC strongly suggests that the sedimentary precursors were deposited approximately coevally (between 3300 and 2940 Ma) and were later disrupted to form as rafts within ca. 2950 to 2690 Ma greenstones and ca. 2640 to 2730 Ma granites.

The spatial separation of the metasedimentary rocks and their relation to greenstones throughout the Southern Cross Terrane may have been produced by processes similar to those described within the Eastern Goldfields Terrane where the formation of a N–S trending extensional rift basin was accompanied by the eruption of felsic volcanics and voluminous mafic and ultramafic flows between 2715 and 2670 Ma followed by compression at ca. 2660 Ma (Nelson, 1997). There is an expanding amount of evidence that all the ca. 3000 Ma metasedimentary rocks from the Southern Cross are rifted components from a Narryer nucleus (Wyche, 2007). First, since they are likely part of this post-depositional (<2960 Ma) rifting, the rocks between the Narryer Terrane and the Southern Cross Terrane are all younger than the age of the metasedimentary rocks (discussed in Wyche (2007)); with the exception of any small rifted components from the Narryer Terrane (of which there are none yet found). Second, Nd depleted mantle model ages and Hf isotopes of zircons from younger granites reflect some proportion of older crustal fragments (Narryer Gneiss Complex?) that may have been rifted from the Narryer Terrane and melted/reworked during 2750 to 2600 Ma plutonism throughout the Yilgarn Craton. Evidence for this is found within Nd studies (see Blewett et al. 2010,

and references therein) that show much of the Murchison and Southern Cross Terranes have >3000 Ma Nd depleted mantle model ages, suggesting their derivation from older crust. Further evidence from Hf data across the Yilgarn Craton from Griffin et al. (2004) suggests that the Hf model ages of ca. 2700 to 2600 Ma zircons from the central Southern Cross approach 3700 Ma, that could support their derivation from melts including a ca. >3700 Ma crustal component. Third, xenocrystic zircons older than 3000 Ma found within the ca. 2730 to 2640 Ma gneisses and granites of the Murchison and Southern Cross Terranes should show similar age characteristics to those from the Narryer Terrane. That there are many >3000 Ma zircon xenocrysts within the Murchison and Southern Cross Terranes (Nelson (2000c, 2002b, 2005); Wyche (2007); and references therein), shows that it is possible that fragments of a NGC-type basement were rifted from the Narryer Terrane and were reworked into younger (ca. 2750 to 2600 Ma) granites and gneisses. Finally, the detrital zircon age characteristics of all inferred ca. 3000 Ma metasedimentary rocks share detrital zircon age similarities, that has previously been mentioned in this paper (see Fig. 4.7) and in previous studies (Nelson, 2002b; Wyche et al., 2004; Wyche, 2007; Thern and Nelson, 2012b) and is one of the best methods to assess the provenance and similarity of these early Archean metasedimentary rocks.

Considering the current geochronological evidence, the Southern Cross metasedimentary rocks were probably deposited between ca. 3300 and 2940 Ma, contemporaneously with those of Mt. Narryer, Jack Hills, and the Toodyay Lake Grace Domain, on a continental shelf on the southeastern-most margin of a Narryer-style terrane (Fig. 4.8; A, B and C). This terrane may have been composed of >3000 Ma Narryer gneisses and granites as evidenced by the detrital zircon age similarities between these metasedimentary rocks and the igneous zircon structures of the Narryer Gneiss Complex (Thern and Nelson, 2012b). The same Narryer-style gneisses and granites may have formed the basement rocks of these sediments (Fig. 4.8; dashed outline around 'depositional fans'). It is postulated that initial rifting between 3060 to 2960 Ma may have started within the thinner basement rocks of these sediments along a continental shelf (Fig. 4.8; C). During this time, the Gum Creek sediments may have been deposited to the north, and the Toodyay Lake Grace Domain sediments to the south (bottom and top 'fans' in Fig. 4.8 C). Continued rifting and granite-greenstone formation along the southeast margin of the Narryer-type nucleus at ca. 2960 to 2900 Ma would have led to the separation of the sedimentary successions now found in the Illaara and Maynard Hills greenstone belts (Fig. 4.8; D). On the northwest of this rift, the Mt. Narryer and Jack Hills sediments may have retained their 'original' locations, with the Jack Hills being engulfed partially by the >2900 Ma granite-greenstone forming event. These events may be coeval with the ca. 3000 Ma Luke Creek Group sequence within the greenstones of the Murchison (Wiedenbeck and Watkins, 1993), and the lower ca. 3000 Ma greenstone formations throughout the Southern Cross. The deposition of these sediments within the >2900 Ma Mt. Weld Greenstone Belt (see Fig. 4.1; D) of the northern Murchison Terrane

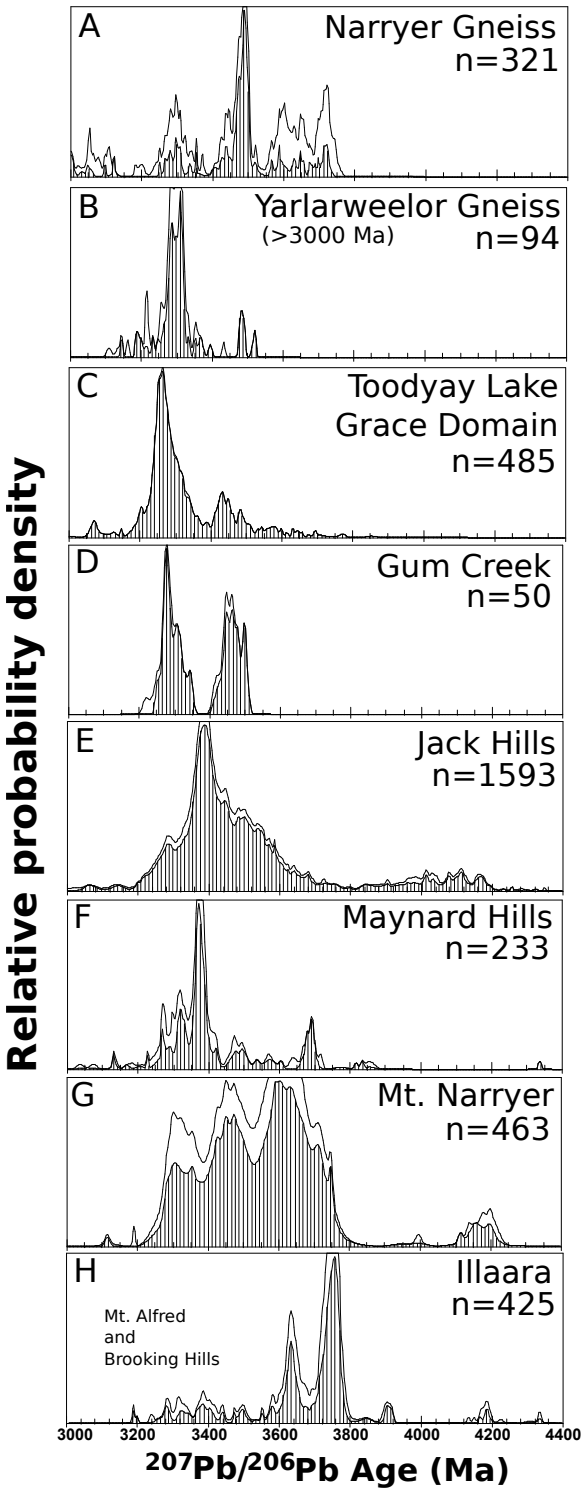

Figure 4.7: Gaussian summation probability density plots for the Mt. Alfred samples compared to all other >3000 Ma metasedimentary rocks from the Yilgarn Craton. Plots contain data that are ±10% of concordia. Mt. Alfred metasedimentary rocks are composed of significantly older zircon ages greater than 3700 Ma when compared to Mt. Narryer, Jack Hills, the Toodyay Lake Grace Domain and the Maynard Hills. Similarities between the metasedimentary rocks of the Yilgarn, summarized on Fig. 4.7, shows shared similarities between these rocks and the Narryer Gneiss and Yarlarweelor Gneiss Complexes (Fig. 4.7; A and B vs. C, D, E, F, G and H). Some tentative detrital age population similarities can be established further between the Mt. Narryer and the Mt. Alfred and Brooking Hills (Fig. 4.7, G and H), the Maynard Hills with the Jack Hills (Fig. 4.7, F and E), and Gum Creek with the Toodyay Lake Grace Domain (Fig. 4.7, D and C).

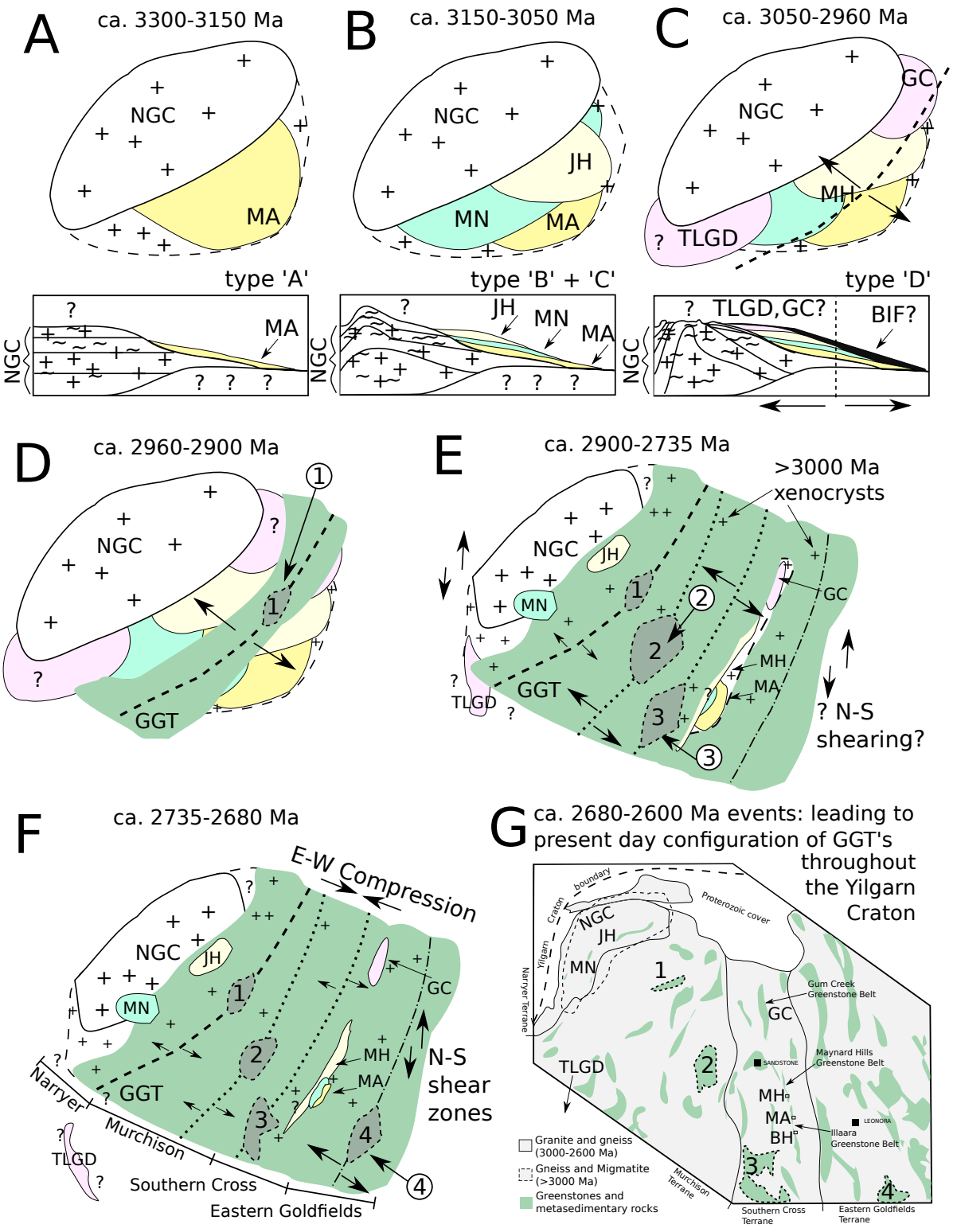

Figure 4.8: see next page for full description

Figure 4.8: Schematic history of the Yilgarn Craton summarized in time slices (A through G) to describe the impact that discrete deposition and rifting events have had on >2940 Ma metasedimentary rocks. (A) at 3300 Ma the NGC is formed and is exhumed and eroded, deposition of Mt. Alfred 'type A' sediments; (B) further erosion and increasing complexity of basement rocks, deposition of Mt. Alfred 'type B and C' sediments, Mt. Narryer, Jack Hills and tentatively Maynard Hills; (C) rifting of the south-eastern margin causes disruption of the clastic apron, sedimentation of youngest sequences including Maynard Hills, Toodyay Lake Grace Domain and Gum Creek sediments and later sedimentation of cherty rhythmites and banded iron formation (BIF); (D) rifting and volcanics forming within the rift zone, initial formation of ca. >2900 Ma granite greenstone terranes (GGT) similar to Luke Creek group greenstones (location 1), formation of the lower Marda-Diemals greenstone succession (location 3), and deposition of the Mt. Weld metasandstone (location 1); (E) further rifting events between 2900 and 2735 Ma, formation of Mt. Farmer group greenstones at 2850 to 2800 Ma (on top of Mt. Weld at location 1), the Windimurra intrusive complex (location 2), and ca. 2735 Ma greenstones overlying the >2900 Ma greenstones at the Marda-Diemals Greenstone Belt; (F) rifting and collision episodes between 2735 and 2660 Ma include E–W compression, folding and N−S shearing throughout the central Yilgarn, as evident in the central Southern Cross Terrane (Chen et al., 2004b), voluminous granite plutonism throughout the Yilgarn Craton, and ca. 2680 Ma GGT formation throughout the Eastern Goldfields Terrane of similar age to the Gindalbie Terrane greenstones (Nelson, 1997); (G) late stage granitic intrusions between 2660 and 2630 Ma (Chen et al., 2003; Chen et al., 2004b), and post to late-reactivation of N–S shear zones between 2630 and 2600 Ma complete the ca. 2600 Ma configuration of these metasedimentary rocks within the Southern Cross Terrane of the Yilgarn Craton.

between 2960 Ma and 2935 Ma (Wingate et al., 2008e) may be related to this rifting, and is a possible indication that this initial rift did not fully close. Later rifting at ca. 2800 Ma (failed rift?), 2735 Ma and 2690 Ma, collisions and granitic intrusions may have produced some stacked greenstone successions. Examples are the ca. 2800 Ma Mount Farmer Group greenstones, that overlie those of the Luke Creek Group (Wiedenbeck and Watkins, 1993), and the Marda Diemals ca. 3000 Ma lower greenstones that underlie the >2735 Ma upper greenstones (Nelson, 2001; Morris et al., 2007) (Fig. 4.8; E and F). Voluminous granite intrusions between 2760 to 2680 Ma and 2670 to 2630 Ma (Qiu et al., 1999; Nelson, 2001, 2002b), along with folding and shearing (Chen et al., 2003; Chen et al., 2004a) may have produced most of the current arrangement of greenstones throughout the Yilgarn Craton (Fig. 4.8; F). All of these factors combine to explain the current arrangement of the metasedimentary rocks hosted in greenstones older than 2900 Ma throughout the Southern Cross Terrane (Fig. 4.8; G, and also Fig. 4.1), and their relation to the ca. 3000 Ma metasedimentary rocks of the Narryer Terrane. The current evidence is thus in favor of a shared depositional history for the ca. 3000 Ma metasedimentary rocks of the Yilgarn Craton.

4.9 Conclusions

(1) Metasedimentary rock horizons of the Yilgarn Craton contain zircon age populations that reveal the evolution of their provenance source terranes. The >3000 Ma metasedimentary rocks at Mt. Alfred highlight that detrital zircon age differences found in closely spaced metasedimentary rock outcrop lenses require detailed geochronological studies on multiple samples to best correlate and assess their depositional age and environment. Complications to interpretations arise where post-depositional tectonic processes have produced juxtaposed 'sedimentary successions', although at the Mt. Alfred locality it is shown that (i) these tectonic processes did not homogenize all the metasedimentary horizons together, and (ii) the metasedimentary rocks share similar provenance components, whereas zircon age structure differences observed between samples from the same locality are more reasonably interpreted as resulting from their deposition during different depositional cycles.

(2) SHRIMP U-Pb detrital zircon analytical data from the Mt. Alfred locality (mostly from a ca. 250 sqm area) show that the eastern-most horizons (type 'A') are composed of mostly >3700 Ma zircons and represent a unique provenance that may be derived from Manfred-Complex style gneisses (Thern and Nelson, 2012b). The western-most horizon at Mt. Alfred (type 'B') contains many younger ca. 3300-3700 Ma zircons as well as Hadean zircons, that are absent in the eastern metasedimentary rock horizons only ca. 50 meters away. Detrital zircon age structures shown at Mt. Alfred (types 'A', 'B' and 'C') may reflect increased up-section complexity and possible younging, that

could be revealing an increase of provenance complexity over time. This up-section increase in zircon age group complexity and maximum depositional age younging from east to west in Mt. Alfred may be continued in the stratigraphically-higher Maynard Hills metasedimentary rocks (type 'D'; sample MH09), and further afield with the metasedimentary rocks of the Jack Hills in the Narryer Terrane, and those of the Gum Creek Greenstone Belt north of the Maynard Hills.

(3) The detrital zircon age similarities within the metasedimentary rocks of the Illaara, Maynard Hills and Gum Creek Greenstone Belts, the Jack Hills, Mt. Narryer and the Toodyay Lake Grace Domain, discussed further in Thern and Nelson 2012b, strongly suggest a similar provenance and imply a strong relationship between ca. 3000 Ma metasedimentary rocks that are found distributed over a wide area of the Yilgarn Craton. These metasedimentary rocks were likely deposited coevally (between ca. 3300 and 2940 Ma) and were later separated by multiple younger ca. 2950 to 2690 Ma greenstones, where they occur today as 'rafts' within younger ca. 2640 to 2730 Ma granites.

(4) The type 'B' metasedimentary rocks at Mt. Alfred contain abundant detrital zircons older than 3800 Ma, but with a higher proportion of younger (<3600 Ma) detrital zircon ages dissimilar to those found at Jack Hills. The Hadean zircon bearing metasedimentary rocks at Mt. Alfred are most similar to samples from Mt. Narryer, albeit lacking most of the younger zircon age structures (of Eurada and Dugel gneiss affinity; 3480 to 3300 Ma in age) found in abundance within some Mt. Narryer samples. This makes Mt. Alfred a unique source for Hadean zircons, where the youngest concordant detrital zircon may be on the order of ca. 3590 Ma.

(5) Hadean zircons are confined to particular metasedimentary rock horizons at the Mt. Alfred and Maynard Hills sampling sites. This is similar to evidence at Jack Hills and Mt. Narryer where particular metasedimentary rock horizons are Hadean-zircon rich, whereas others have a lower proportion or no grains older than 3800 Ma. This suggests that Hadean zircons are related to pulses of sedimentary deposition that are now recorded within particular metasedimentary rock lenses, and that the Hadean zircon source rocks were ephemeral.

Acknowledgements

Many thanks to Adam Frew, Adam Freeman, Stefan Klaric, Anna van der Helder and Renee Bingham for providing excellent support on multiple sampling trips to the Maynard Hills and Illaara Greenstone Belts. Ion microprobe (SHRIMP) analyses were conducted at the John de Laeter Centre for Isotope Research, in Perth, Australia.

CHAPTER 5
DEPOSITIONAL AGE AND ENVIRONMENT

Chapter five presents a manuscript which discusses tourmaline $^{40}Ar/^{39}Ar$ plateau ages and boron isotopic data to elucidate geological events from within the Mt. Alfred and Brooking Hills localities of the Illaara Greenstone Belt. These tourmalines occur as post-depositional, stratiform layers within the metasedimentary rocks, and may have grown during a period of diagenesis, or enhanced heating and hydrothermal fluid flow. The stratiform nature of the tourmalines, along with the association of barite in a parallel metasedimentary unit and B isotopes places constraints on a possible depositional environment of these metasedimentary rocks. This study also discusses the issue of Ar closure temperature in tourmaline. The tourmaline $^{40}Ar/^{39}Ar$ dates obtained can be used for assigning minimum depositional ages to these sedimentary units, constraining the timing of deposition. Supplemental data tables, provided in the Appendix, show full tourmaline $^{40}Ar/^{39}Ar$ results in Tables D.1 and D.2, and B isotopic results in Table E.1.

5.1 Manuscript 2: Minimum depositional age and environmental constraints of Hadean-zircon-bearing siliciclastic metasedimentary rocks of the Illaara Greenstone Belt inferred by tourmaline Ar-Ar geochronology and boron isotopes

5.2 Abstract

Tourmaline $^{40}Ar/^{39}Ar$ plateau ages and boron isotopic data are presented from stratiform vein tourmalines within the ca. 3.0 Ga siliciclastic metasedimentary rocks at the Mt. Alfred and Brooking Hills localities within the Illaara Greenstone Belt, Western Australia. These metasedimentary rocks host detrital zircons with ages between ca. 3200−3730 Ma, and are parallel to metasedimentary units containing detrital Hadean zircons at the Mt. Alfred locality. The tourmalines occur as post-depositional stratiform layers, and are inferred to have grown during a hydrothermal fluid circulation event. A minimum depositional age, that also constrains the end-stages of deposition of these early Archean metasedimentary rocks, has been determined at ca. 2939±15 Ma (95% confidence) via multiple robust $^{40}Ar/^{39}Ar$ plateau ages. An initial indication of Ar closure temperature in tourmaline was experimentally calculated to be >600 °C. The association of barite and rhythmites in parallel metasedimentary units, indications of relatively enriched $\delta^{11}B$ within tourmaline, and their 2939±15 M $^{40}Ar/^{39}Ar$ dates suggest the host sediments were deposited prior to 2939±15 M within a marine-intertidal-evaporitic environment. Younger stratiform tourmaline, crystallized on the margins of late-stage quartz veins, give an age of 2622±20 Ma, defining the timing of the quartz veining, and a second stage of tourmaline growth from B-rich fluids.

5.3 Introduction and Geological Setting

The Yilgarn Craton of Western Australia is host to numerous >3000 Ma metamorphosed sandstone occurrences, mostly as elongated lenses, with some yielding abundant detrital zircons showing ages in excess of ca. 4000 Ma (Mt. Narryer (Froude et al., 1983), Jack Hills (Compston et al., 1986a), Maynard Hills (Nelson, 2002b), and Mt. Alfred (Nelson, 2005, and this study, see Chapters 2, 3 and 4). The Mt. Alfred and Brooking Hills siliciclastic metasedimentary rocks lie within the Illaara Greenstone Belt, in the central area of the Yilgarn Craton (Figure 5.1) and have a maximum depositional age of ca. 3100 Ma (see Chapter 4). Geological field investigation at the Mt. Alfred locality of the Illaara Greenstone Belt resulted in the finding of stratiform tourmaline horizons and layers throughout these metasedimentary rocks. These tourmaline occurrences appear as stratiform veins, from millimeter to meter thickness, with extensional fabric overprinting due to multiple late-stage tectonic events and their proximity to the Edale Shear Zone. These tectonic and metamorphic events are primarily dated to being between ca. 2730−2630 Ma (Chen et al., 2003; Chen et al., 2004a).

Stratiform quartz-tourmaline layers are a common occurrence in sedimentary sequences (Marschall and Jiang, 2011). Archean tourmaline occurrences are relatively

understudied, however, with only a few published examples of tourmalines associated with quartz arenites (Donaldson and de Kemp, 1998), the ca. 3800 Ma Isua supracrustals (Chaussidon and Uitterdijk Appel, 1997), gold deposits at Big Bell mine, Western Australia (Jiang et al., 2002) and within the Abitibi Greenstone belt (King and Kerrich, 1989).

Stratiform tourmalines in metasedimentary rocks are often formed from post-depositional hydrothermal or metamorphic fluid flow (Marschall and Jiang, 2011). They can record information about depositional environment in their B isotopic signatures, with high δ^{11}B values, interpreted as indicating derivation within evaporitic or meta-evaporitic environments (Cook and Ashley, 1992; Harraz and El-Sharkawy, 2001). Evidence for evaporitic environmental depositional settings can also be constrained by the presence of barite (Cook and Ashley, 1992; Sugitani et al., 2003; Hesse and Schacht, 2011). Studies utilizing the ^{40}Ar/^{39}Ar dating technique on tourmaline are rare (Marschall and Jiang, 2011), with only one recent study within the past decade on young ca. 300 Ma tourmalines (Martínez-Martínez et al., 2010). As the ^{40}Ar/^{39}Ar geochronometer on tourmaline is so new, the Ar closure temperature is not well constrained.

By using boron isotopic systematics and ^{40}Ar/^{39}Ar geochronology on tourmalines from post-depositional stratiform quartz-tourmalines from within the siliciclastic metasedimentary rocks of the Illaara Greenstone Belt, the aims of this study are to: (1) Investigate the boron isotopic makeup of these tourmalines to elucidate the possible source of B-rich fluids; (2) Obtain ^{40}Ar/^{39}Ar ages on separated tourmalines; (3) Determine a closure temperature estimate for the ^{40}Ar/^{39}Ar system within natural tourmalines; (4) Assign a minimum depositional age to the metasedimentary rocks by using ^{40}Ar/^{39}Ar ages; and (5) Constrain the depositional environment of these early Archean metasedimentary rocks.

5.4 Sample selection

Sample sites at the Brooking Hills, Mt. Alfred and the Maynard Hills are composed of metamorphosed sedimentary rocks, including banded iron formations (BIFs) and rhythmites, metasandstones, metapelites and greenschists. These metasedimentary rocks outcrop parallel to the Edale and Evanston shear zones, and have planar foliation fabrics aligning N−S with these shears. Sample sites are shown on the simplified geological sketch maps of the Mt. Alfred and Brooking Hills (Figure 5.2, inset Mt. Alfred and Brooking Hills maps) with additional sampling information in Table 5.1.

Tourmalines were separated from four samples collected near Mt. Alfred and the Brooking Hills shown in Figure 5.2. Samples MA08 and MA24 were collected east of Mt. Alfred (sample label "MA") within the central northern Illaara Greenstone Belt.

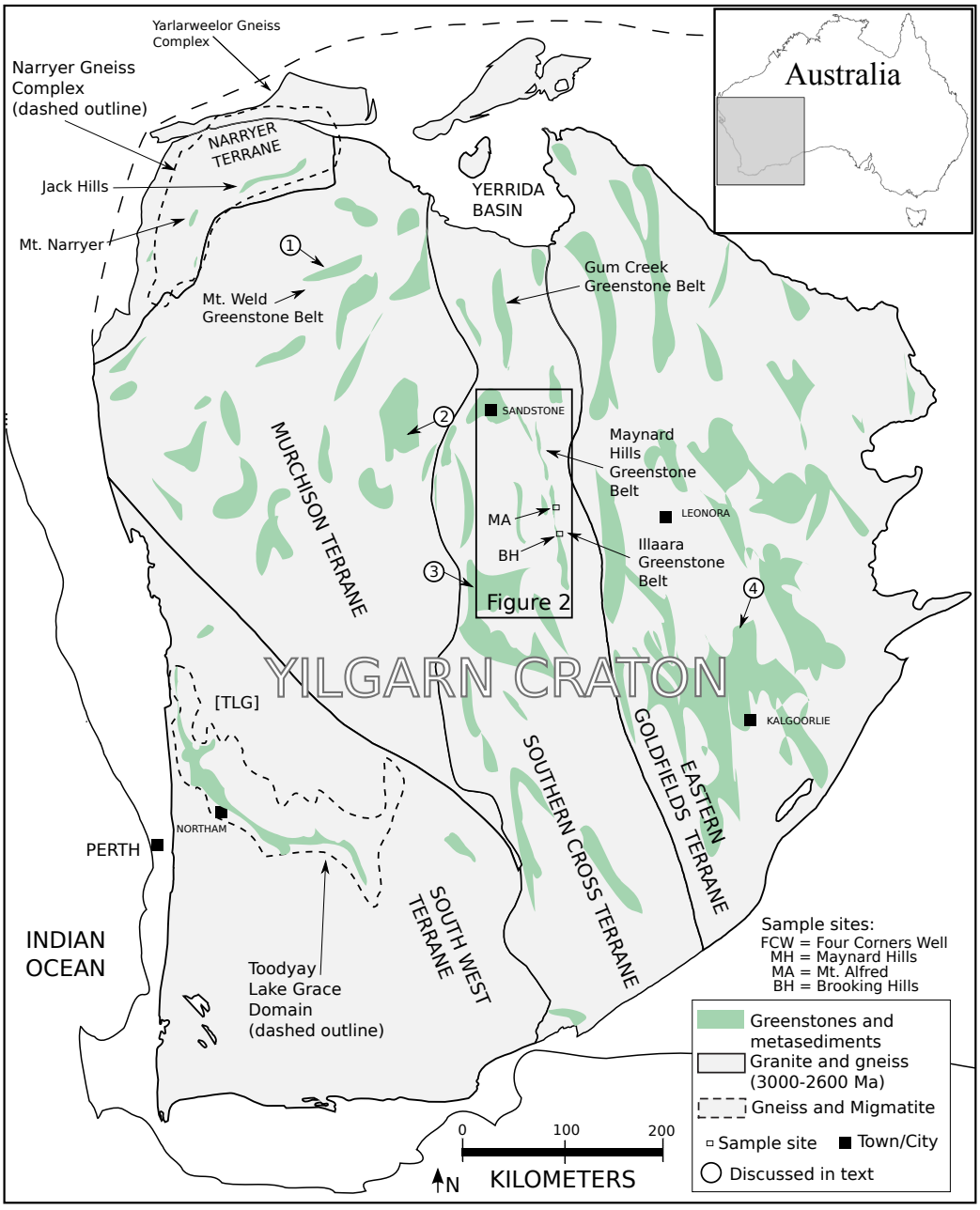

Figure 5.1: Map of the Yilgarn Craton, Western Australia, showing locations of ca. 3000 Ma metasedimentary rocks (Toodyay Lake Grace Domain, Jack Hills, Mt. Narryer, Gum Creek, Maynard Hills, Illaara), greenstone belts, granites and gneisses. The area covered by Figure 5.2 is also shown.

Sample site MA08 is a massive, 2 to 4m wide, quartz-tourmaline vein aligned parallel to possible original sedimentary layering and the foliation fabric. The largest (2 to 4m wide) part of the outcrop at site MA08 occurs along a 10 to 20 meter long layer, and continues along the foliation fabric of the siliciclastic metasedimentary rocks at the Mt. Alfred locality. These form small 2 to 4 cm wide boudinaged stratiform layers, with some having contents of >50% tourmaline. Tourmalines from sample site MA24 form a parallel outcrop about 75m to the south of the massive quartz-tourmaline vein at site MA08, and are composed primarily of mm to cm size stratiform tourmaline veins. Samples BH04 and BH05 were collected from near the Brooking Hills (sample labels "BH") in the central part of the Illaara Greenstone Belt from small, 1 to 2 cm wide stratiform quartz-tourmaline veins. Barites in thin section are shown from sample MA11, a parallel outcrop ca. 100 meters northeast of sample site MA08, discussed in detail in Chapter 4.

Samples are referred to herein as 'metasedimentary rocks', but all have undergone at least greenschist facies metamorphism and nearly all original sedimentary features have been lost due to shearing and late stage metamorphic recrystallization, and is compounded by growth of metamorphic minerals such as muscovite and fuchsite.

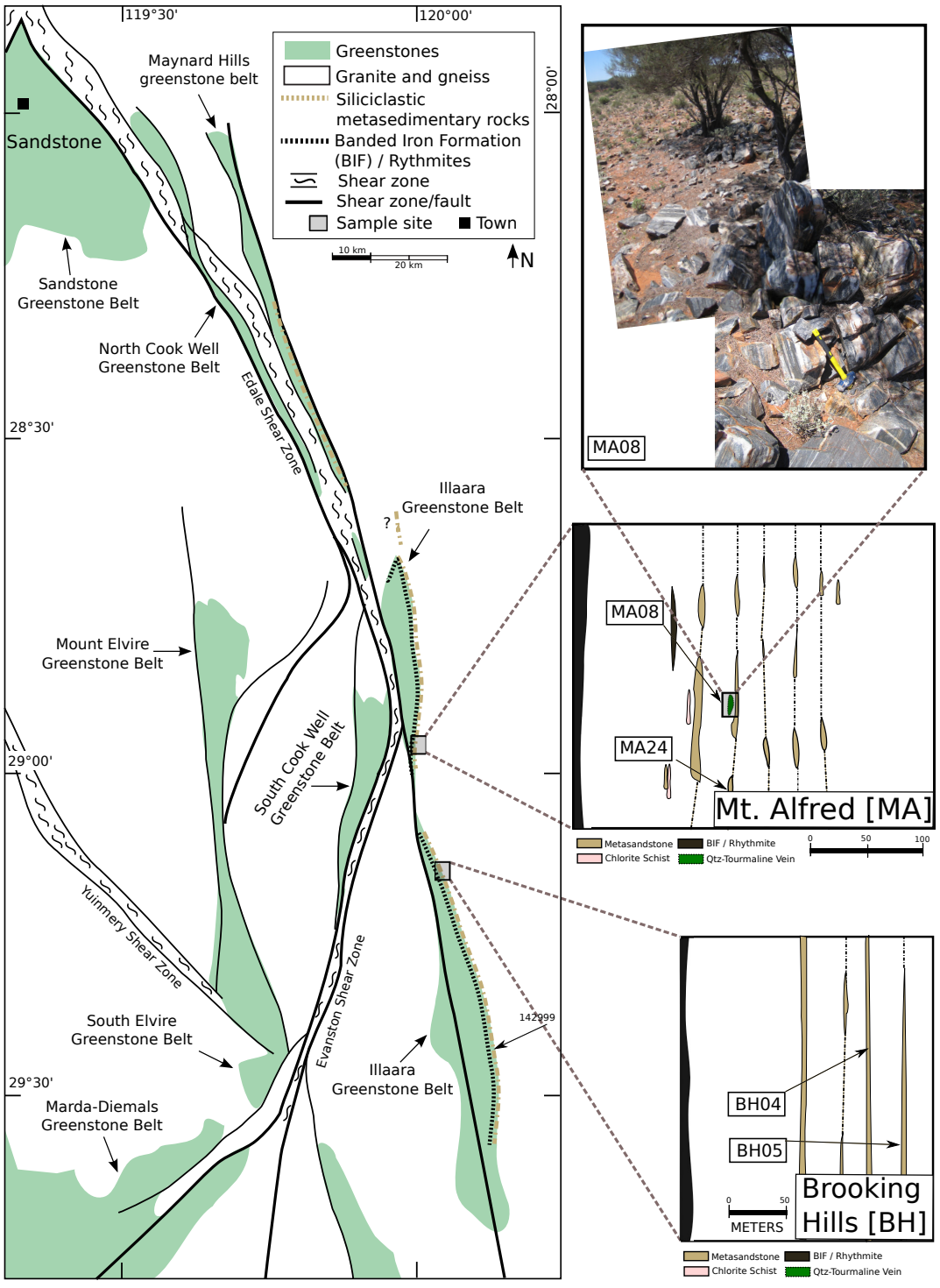

Figure 5.2: The Maynard Hills and Illaara greenstone belts of the Southern Cross Terrane with inset maps of the Mt. Alfred and Brooking Hills sampling localities, and field photos of sample site MA08, showing the massive quartz-tourmaline outcrop and quartz veining.

Table 5.1: List of sample localities and brief descriptions

Sample	South	East	Lithology and Description
Mt. Alfred [MA] – Illaara Greenstone Belt			
MA08	S 28° 50.590'	E 120° 00.020'	Quartz-tourmaline; Dark quartz-tourmaline vein of ca. 2-4 m thickness, bedding-parallel foliation fabrics present in some locations, large late-stage cross-cutting quartz veins throughout.
MA11	S 28° 50.442'	E 120° 00.165'	Metasandstone; bright-clear-green, recrystallized, medium to coarse-grained, with large 1-2 cm-long fuchsite lathes aligned with 4 cm-thick bedding-parallel foliation.
MA24	S 28° 50.395'	E 120° 00.042'	Metasandstone; banded-dark-green, recrystallized, medium to coarse-grained 2 cm-thick bedding-parallel foliation and mm-cm stratiform tourmaline-quartz layering.
Brooking Hills [BH] – Illaara Greenstone Belt			
BH04	S 28° 56.681'	E 120° 00.040'	Metasandstone; pale greenish-white, recrystallized, fine to medium-grained, with fuchsitic lathes aligned to 2-4 cm thick layer-parallel foliation with 1-2 cm stratiform quartz tourmaline layers.
BH05	S 28° 56.699'	E 120° 00.021'	Metasandstone; pale greenish-white, recrystallized, medium-grained, with fuchsitic lathes aligned to 5-8 cm thick layer-parallel foliation with 1-2 cm stratiform quartz tourmaline layers.

5.5 Analytical techniques

5.5.1 Sample preparation

Approximately 5kg of sample was crushed via a conventional jaw-crusher and disc mill to reduce fragment size, sieved through a 500μm mesh to standardize grain size, and processed over a Wilfley table to remove the bulk of the quartz and produce 250 grams of heavy mineral separates. The resulting material was processed through heavy liquid and magnetic separation to separate out the bulk of the zircons from other heavy minerals present in the samples. These were then sieved into size fractions of >200μm, >100μm, and <100μm, respectively, and tourmalines were picked from the largest fraction.

Tourmalines were separated for $^{40}Ar/^{39}Ar$ analysis by manually separating the cleanest sample into a ca. 20 mg aliquot. After hand picking the cleanest tourmaline crystals (without obvious inclusions, cracks, or core-rim zones) with an optical microscope, the selected tourmalines were leached in diluted HF for one minute and then thoroughly rinsed with distilled water in an ultrasonic cleaner. Tourmalines from the massive vein (sample MA08) and stratiform veins (samples MA24 and BH04) were mounted in epoxy resin discs and polished to about a third of the way through the surface of each grain for boron isotopic analysis on a Cameca IMS 5fE7 ion microprobe. After thorough cleaning, drying, and gold coating, the mount was imaged by reflected and transmitted optical light in order to discern the most obvious cracks, inclusions, cores, and other structures prior to analysis.

5.5.2 Ion Microprobe B isotopic analysis

Secondary ion mass spectrometry (SIMS) analyses were undertaken using a Cameca IMS 5fE7 ion microprobe located on the Hawkesbury Campus of the University of Western Sydney. Sample surfaces were conductively coated with a 35 nm thick layer of gold using a Leica EM SCD005 sputter coater unit. Boron isotopic analyses were performed using a O_2^- primary ion source operated at 10 keV and with a secondary-ion extraction potential of 5keV, providing a net primary ion impact energy of 15keV at an incidence angle of 24.6 degrees normal to the sample surface. The secondary ion mass spectrometer slits were set to obtain a mass resolving power to 500 (10% of peak height) and an energy window of 50 keV, with no sample energy offset. The magnetic field of the mass spectrometer was sequentially stepped to direct the species $^{10}B+$ and $^{11}B+$ into an electron multiplier to determine their count rates. The analytical data were processed using CONCH (Nelson, 2006) to obtain means and uncertainties.

5.5.3 $^{40}Ar/^{39}Ar$ tourmaline analysis

Samples were loaded into 5 large wells of one 1.9 cm diameter and 0.3 cm depth aluminum disc. These wells were bracketed by small wells that included GA1550 biotite used as a neutron fluence monitor for which an age of 99.77 ± 0.11 Ma was adopted and a good in-between grain reproducibility has been demonstrated (Renne et al., 1998, 2010). The discs were Cd-shielded (to minimize undesirable nuclear interference reactions) and irradiated for 25 hours in the Hamilton McMaster University nuclear reactor (Canada) in position 5C. The mean J-values computed from standard grains within the small pits range from 0.0026752 ± 0.0000040 (0.15%) to 0.0026644 ± 0.000054 (0.20%) determined as the average and standard deviation of J-values of the small wells for each irradiation disc. Mass discrimination was monitored using an automated air pipette and provided a mean value of 1.00646 ± 0.00238 per dalton (atomic mass unit). The correction factors for interfering isotopes were (39Ar/37Ar)Ca = 7.30x10-4 (± 11%), (36Ar/37Ar)Ca = 2.82x10-4 (± 1%) and (40Ar/39Ar)K = 6.76x10-4 (± 32%).

$^{40}Ar/^{39}Ar$ analyses were performed at the Western Australian Argon Isotope Facility at Curtin University, operated by a consortium consisting of Curtin University and the University of Western Australia. The samples were step-heated using a 110 W Spectron Laser System, with a continuous Nd-YAG (IR; 1064 nm) laser rastered over the sample during 1 minute to ensure homogeneously distributed temperature. The gas was purified in a stainless steel extraction line using a GP50 and two AP10 SAES getters and a liquid nitrogen condensation trap. Ar isotopes were measured in static mode using a MAP 215-50 mass spectrometer (resolution of ca. 500; sensitivity of $2x10^{-14}$ mol/V) with a Balzers SEV 217 electron multiplier mostly using 9 to 10 cycles of peak-hopping. The data acquisition was performed with the Argus program written by M.O. McWilliams and ran under a LabView environment. The raw data were processed using the ArArCALC software (Koppers, 2002) and the ages have been calculated using the decay constants recommended by Renne et al. (2010). Blanks were monitored every 3 to 4 steps and typical ^{40}Ar blanks range from $1x10^{-16}$ to $2x10^{-16}$ mol.

Our criteria for the determination of plateau are as follows: plateaus must include at least 70% of ^{39}Ar. The plateau should be distributed over a minimum of 3 consecutive steps agreeing at 95% confidence level and satisfying a probability of fit (P) of at least 0.05. Plateau ages are given at the 2σ level and are calculated using the mean of all the plateau steps, each weighted by the inverse variance of their individual analytical error. Mini-plateaus are defined similarly except that they include between 50% and 70% of ^{39}Ar. Integrated ages (2σ) are calculated using the total gas released for each Ar isotope. Inverse isochrons include the maximum number of steps with a probability of fit $\geq$0.05. The uncertainties on the $^{40}Ar^*/^{39}Ar$ ratios of the monitors are included in

the calculation of the integrated and plateau age uncertainties, but not the errors on the age of the monitor and on the decay constant (internal errors only, see discussion in Min et al. (2000)).

5.5.4 $^{40}Ar/^{39}Ar$ tourmaline diffusion

Tourmalines from sample MA08 were selected and placed in a copper foil package for the furnace run diffusion experiment. The sample was step-heated in a double vacuum high frequency Pond Engineering furnace. The gas was purified in a stainless steel extraction line using two AP10 and one GP50 SAES getters and a liquid nitrogen condensation trap. Ar isotopes were measured in static mode using a MAP 215-50 mass spectrometer (resolution of 400; sensitivity of 4x10-14 mol/V) with a Balzers SEV 217 electron multiplier mostly using 9 to 10 cycles of peak-hopping.

Data reduction procedures are the same as the tourmaline laser section (as above). The diffusion characteristics were calculated using only the age-plateau data, where a linear line could be fit to the data. Uncertainties cited on all dates given herein are at 95% confidence.

5.6 Results

5.6.1 Sample MA08 Tourmaline (Mt. Alfred)

Tourmalines from sample MA08, a massive 2-4 meter wide quartz-tourmaline vein, are shown in Figure 5.3 within an ion-probe mount (A) and as separate grains (B). Selected grains (labelled lower case 'a' in Figure 5.3-A) show terminations and crystal facets. Many grains show fluid inclusions in Figure 5.3-A, of both light, transparent inclusions and dark to black inclusions. At least one grain in Figure 5.3-A has an obvious core and rim, labelled with 'c' for core and 'r' for rim. Many grains did appear to have core components while hand-picking, however for Ar isotopic work, these grains were avoided. Tourmalines in Figure 5.3-B are shown as separate grains, showing surfaces of each grain. Selected grains from Figure 5.3-B (labelled lower case 'b') show the cross-section of a classic hexagonal-trigonal tourmaline shape. Many grains have been broken or are fragments due to, at least in part, the crushing and milling during heavy mineral separation.

Age data from the $^{40}Ar/^{39}Ar$ geochronology on these tourmalines is presented in Figure 5.4. This shows two well-defined plateau ages for sample MA08 laser packages 1 and 2, and the plateau for the diffusion run within the furnace. The two tourmaline multi-grain laser package $^{40}Ar/^{39}Ar$ plateaus show a consistency between the duplicate sample runs, where >75% of radiogenic ^{39}Ar is represented in the plateau, and gives ages

of 2936±21 Ma for the first run, and 2941±19 Ma for the second run, within uncertainty of an average age of 2939±15 Ma calculated for both analyses. Six single-grain tourmaline step-heating experiments show that, while the overall uncertainties are higher due to their small K contents, they correspond perfectly to the multi-grain packages (see Figure 5.6 for comparison, and Appendix Table D.1). The plateau in K/Ca in Figure 5.5 shows an internal consistency in K/Ca ratios and general agreement with the $^{40}Ar/^{39}Ar$ age plateau in figure 5.4. These results show that multi-grain tourmaline is a good candidate mineral for $^{40}Ar/^{39}Ar$ geochronology when proper care is taken to pick only the most inclusion-free samples.

The furnace sample run, for the diffusion experiment (shown in the final plateau of Figure 5.4), shows an age of 2928±14 within uncertainty of the 2939±15 Ma age obtained on the two laser packages. Only the data within the age plateau of the furnace run was used when calculating a closure temperature for Ar within tourmaline. As tourmaline is very hydrous, the breakdown from crystalline to amorphous structure happens within a very small window of incremental heating temperature. The amount of data obtained for line fitting was therefore not enough to calculate a precise closure temperature, and only constrains the temperature to between ca. 600°C and about 750°C. Further analytical runs are being planned to constrain this closure temperature further.

5.6.2 Sample MA08 Zircons

Zircons from sample MA08 are all detrital, with similar shapes and features to those found in all surrounding sample sites (see Chapter 4 for all sample sites). A summary of ages obtained on 19 zircons (see Table 5.2) are shown in the Wetherill diagram and Gaussian summation probability plots in Figure 5.7. Zircon analyses form a main concordant age group of 6 analyses at 3623±10 Ma, a semi-discordant group of 2 analyses at 3726±2 Ma, and have the youngest nearly-concordant analysis at 3272±2 Ma.

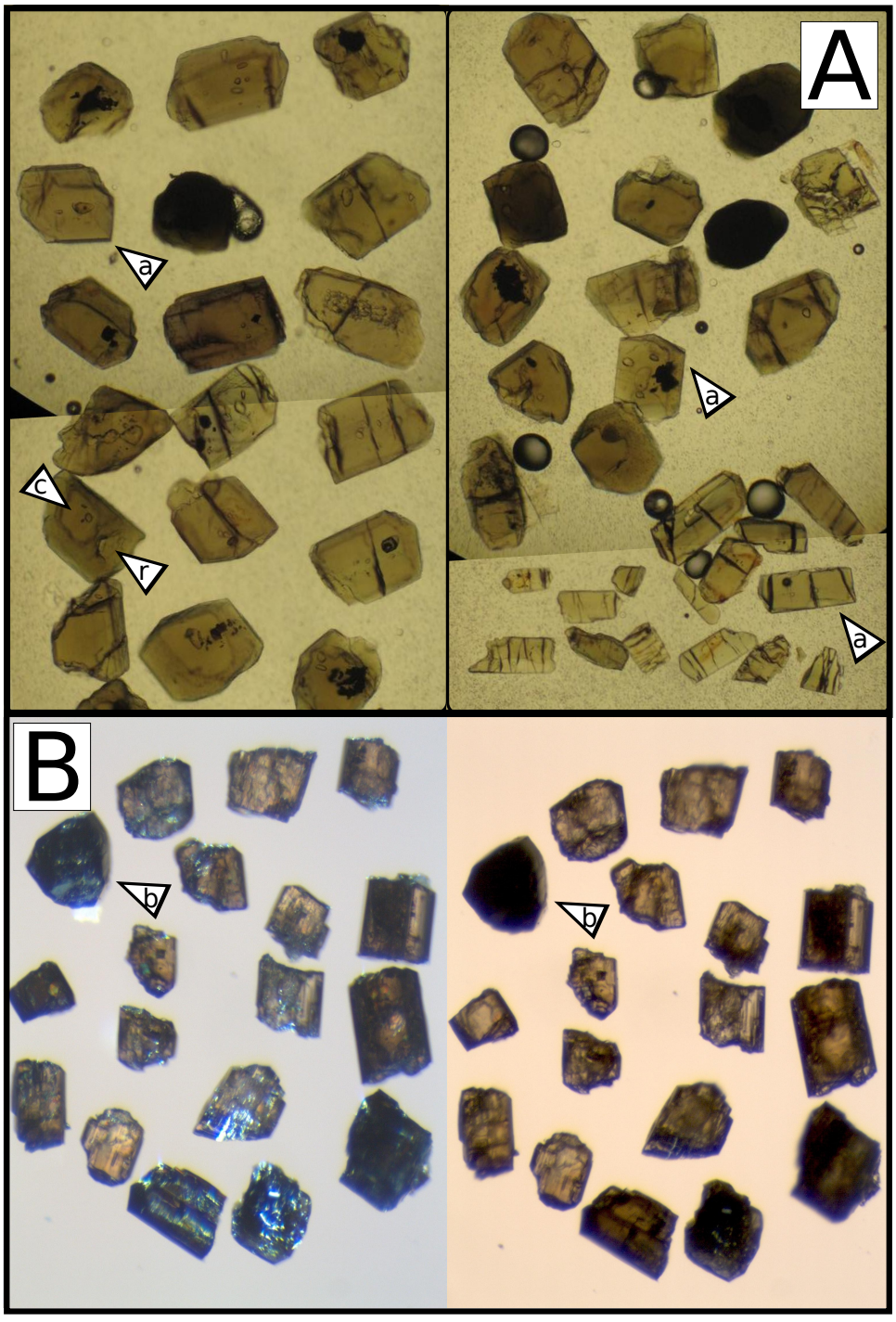

Figure 5.3: Tourmalines from sample MA08 in an ion-probe mount (A) and as separate grains (B). Selected grains (lower case a) show terminations and crystal facets. (A) Many grains show fluid inclusions, and some show core-rim features (lower case c 'core', r 'rim'). (B) tourmalines as separate grains, showing surfaces of each grain. Selected grains (lower case b) show cross-sections of a classic hexagonal-trigonal tourmaline shape. Many grains have been broken or are fragments due to, at least in part, the crushing and milling during heavy mineral separation.

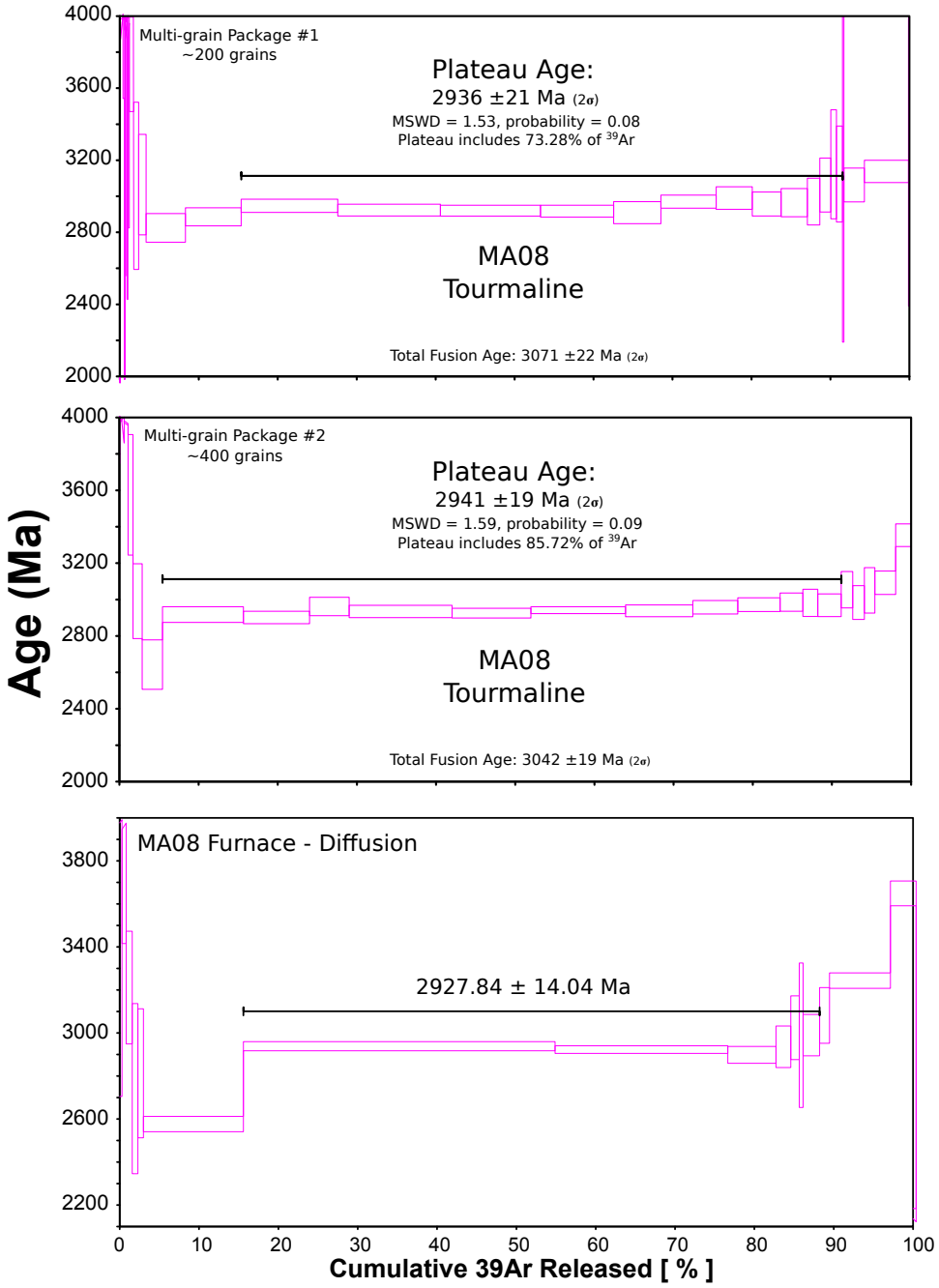

Figure 5.4: Argon age plateaus for tourmaline sample MA08 laser packages 1 and 2, and the plateau for the diffusion run within the furnace. Plateaus show a consistency between these duplicate sample runs, where >75% of radiogenic ^{39}Ar represents the plateau.

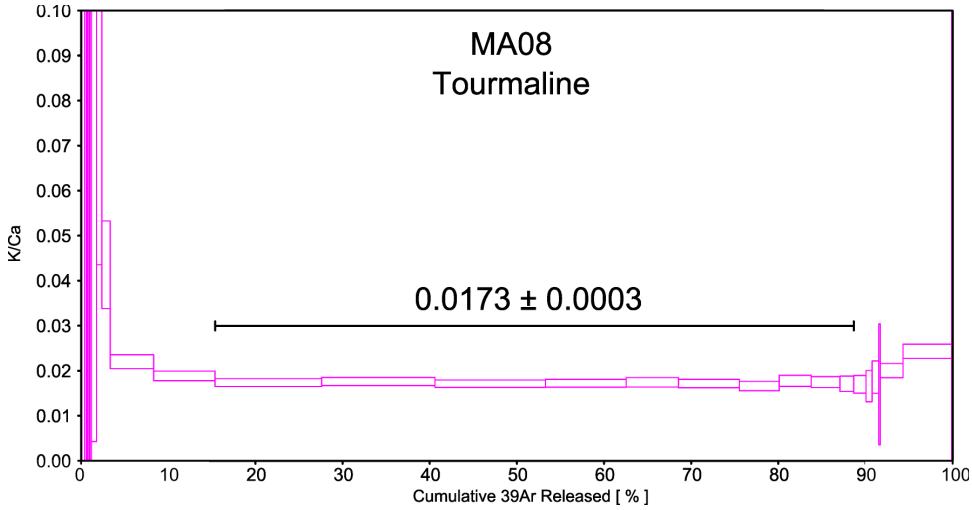

Figure 5.5: K/Ca plateau for tourmalines from sample MA08 laser package 1. The plateau in K/Ca shows an internal consistency in K/Ca ratios and general agreement with the ^{39}Ar age plateau in figure 5.4.

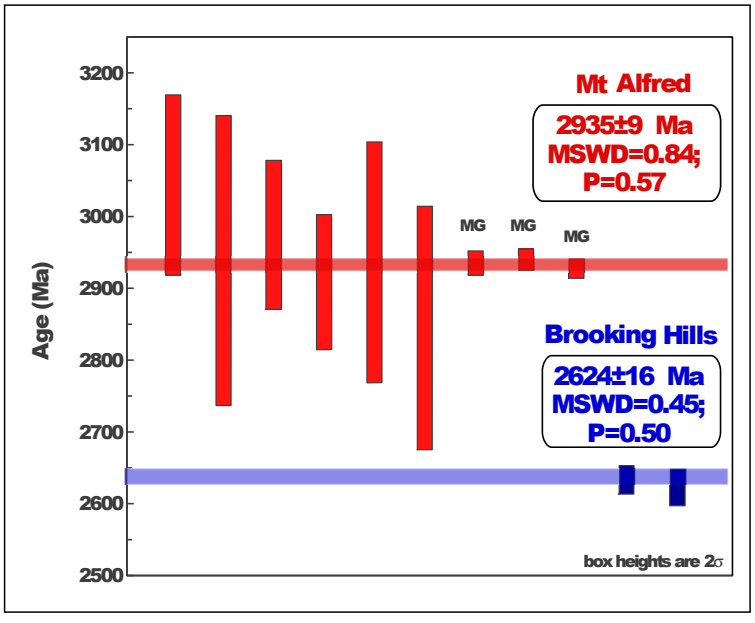

Figure 5.6: Single grain and multi-grain (labelled 'MG') data for sample MA08 (top) show the same dates. Single grain analyses on sample BH05 (bottom) shows the late-stage growth event of secondary tourmalines.

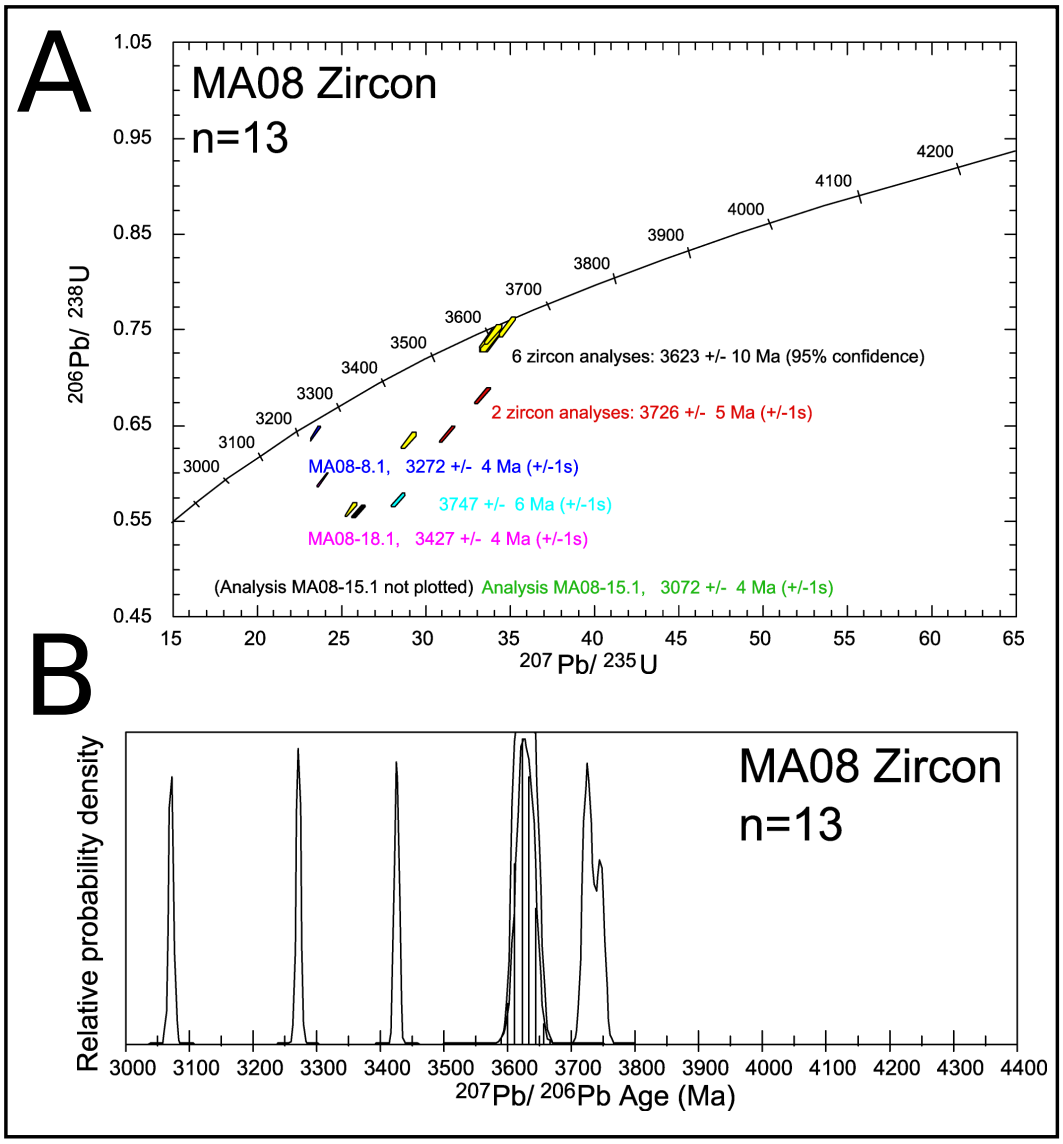

Figure 5.7: Zircon populations within sample MA08. (A) Wetherill diagram showing main concordant age group at 3623±10 Ma; (B) Gaussian probability plot.

Table 5.2: SHRIMP analytical results for sample MA08

						Ratios									Dates (Ma)					
						^{207}Pb		^{208}Pb		^{206}Pb		^{207}Pb			^{206}Pb		^{207}Pb		^{207}Pb	
Grain .spot	U ppm	Th ppm	Th/U	Pb ppm	f206%	^{206}Pb 204corr	$\pm1\sigma$ (%)	^{206}Pb 204corr	$\pm1\sigma$ (%)	^{238}U 204corr	$\pm1\sigma$ (%)	^{235}U 204corr	$\pm1\sigma$ (%)	%c	^{238}U date	$\pm1\sigma$ (Ma)	^{235}U date	$\pm1\sigma$ (Ma)	^{206}Pb date	$\pm1\sigma$ (Ma)
MA08 Zircons (19 analyses)																				
MA08-15.1	903	590	0.65	495	0.060	0.2329	0.25	0.1730	0.40	0.452	1.21	14.526	1.26	78	2406	24	2785	12	3072	4
MA08-8.1	664	585	0.88	565	0.101	0.2641	0.23	0.2703	0.32	0.642	1.22	23.398	1.27	98	3199	31	3244	12	3272	4
MA08-20.1*	335	230	0.69	158	0.777	0.2824	0.52	0.1688	1.37	0.368	1.24	14.320	1.40	60	2019	21	2771	13	3376	8
MA08-18.1	610	96	0.16	417	0.034	0.2917	0.24	0.0448	1.00	0.594	1.22	23.873	1.27	88	3004	29	3263	12	3427	4
MA08-9.1*	185	1800	9.72	86	1.154	0.3108	0.70	0.0739	4.55	0.374	1.27	16.022	1.52	58	2048	22	2878	15	3525	11
MA08-6.1	361	2689	7.45	76	0.317	0.3134	0.72	0.2115	1.44	0.158	1.22	6.841	1.49	27	947	11	2091	13	3538	11
MA08-2.1	131	109	0.83	82	0.085	0.3251	0.58	0.2547	0.90	0.457	1.31	20.480	1.50	67	2426	26	3114	14	3594	9
MA08-17.1*	219	367	1.68	174	0.463	0.3291	0.44	0.2838	0.76	0.562	1.27	25.517	1.39	80	2876	29	3328	14	3613	7
MA08-1.1	78	55	0.71	75	0.016	0.3306	0.56	0.1820	0.91	0.745	1.38	33.937	1.55	99	3588	38	3608	15	3620	9
MA08-14.1*	184	604	3.29	163	0.283	0.3312	0.43	0.2836	0.70	0.634	1.29	28.960	1.41	87	3166	32	3452	14	3623	7
MA08-11.1	1029	575	0.56	130	0.110	0.3318	0.43	0.1986	0.80	0.096	1.20	4.384	1.32	16	590	7	1709	11	3625	7
MA08-19.1	70	39	0.55	66	0.076	0.3318	0.99	0.1363	4.28	0.739	1.47	33.803	1.87	98	3566	40	3604	18	3625	15
MA08-23.1	75	70	0.93	75	-0.070	0.3322	0.62	0.2382	1.05	0.738	1.42	33.809	1.62	98	3563	39	3604	16	3627	10
MA08-5.1	98	86	0.87	99	0.000	0.3351	0.53	0.2233	0.90	0.754	1.35	34.811	1.51	99	3620	37	3633	15	3640	8
MA08-19.2	130	806	6.19	96	0.115	0.3360	0.55	0.1825	1.08	0.560	1.31	25.953	1.49	79	2867	30	3345	15	3645	8
MA08-21.1	205	365	1.78	92	0.520	0.3416	0.63	0.1995	1.57	0.334	1.26	15.753	1.48	51	1860	20	2862	14	3670	10
MA08-12.1	187	139	0.74	160	0.108	0.3535	0.40	0.1908	0.76	0.641	1.28	31.260	1.39	86	3194	32	3527	14	3722	6
MA08-13.1	120	138	1.15	110	0.008	0.3553	0.47	0.2082	0.74	0.681	1.33	33.350	1.46	90	3347	35	3591	14	3730	7
MA08-10.1	200	447	2.24	149	0.027	0.3592	0.41	0.1548	0.88	0.572	1.27	28.336	1.38	78	2916	30	3431	14	3747	6

f206% = 100 x (common ^{206}Pb/total ^{206}Pb)
$^{207}Pb/^{206}Pb$ 204corr = ^{204}Pb-corrected $^{207}Pb/^{206}Pb$ ratio
$^{206}Pb/^{238}U$ 204corr = ^{204}Pb-corrected $^{206}Pb/^{238}U$ ratio
$^{207}Pb/^{235}U$ 204corr = ^{204}Pb-corrected $^{207}Pb/^{235}U$ ratio
%c = % Concordance
$^{206}Pb/^{238}U$ date = ^{204}Pb-corrected $^{206}Pb/^{238}U$ date
$^{207}Pb/^{235}U$ date = ^{204}Pb-corrected $^{207}Pb/^{235}U$ date
$^{207}Pb/^{206}Pb$ date = ^{204}Pb-corrected $^{207}Pb/^{206}Pb$ date

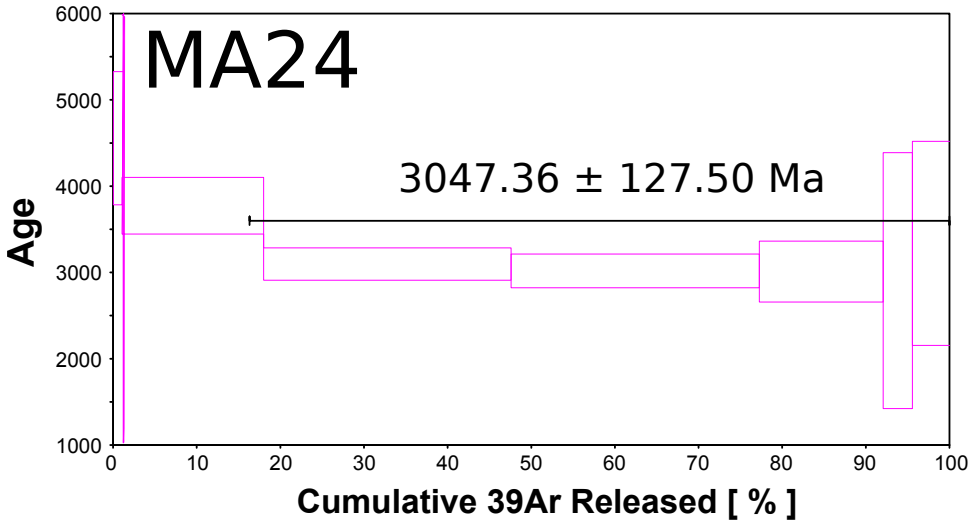

Figure 5.8: Argon age plateaus for tourmaline sample MA08 laser packages 1 and 2, and the plateau for the diffusion run within the furnace. Plateaus show a consistency between these duplicate sample runs, where >75% of radiogenic ^{39}Ar represents the plateau.

5.6.3 Sample MA24 Tourmaline (Mt. Alfred)

Tourmalines from sample site MA24 form a slightly parallel outcrop 75 meters to the south of the massive quartz-tourmaline vein at site MA08. A single-grain analysis of one of these MA24 stratiform tourmalines resulted in a plateau age of 3047±128 Ma (see Figure 5.8), which is within analytical uncertainty of the age of 2939±15 Ma obtained on sample MA08 tourmalines.

5.6.4 Sample BH05 Tourmaline (Brooking Hills)

Individual, large (ca. 500-1000μm) tourmalines from the Brooking Hills yielded younger ages than those of sample MA08. Three individual grains were analyzed by ^{40}Ar/^{39}Ar step-heating to produce plateaus, shown in Figure 5.9. The average result of these two analyses is an age of 2622±20 Ma. These results are compared to those of sample MA08 in Figure 5.6. These tourmalines are generally larger than those from sample MA08, and appear to be grown on the margins of late-stage quartz veins along shearing fabric. An example of this is shown in Figure 5.10, which shows an overview field photo with shearing fabric and a quartz-tourmaline stratiform vein (center). The inset close-up photo shows the quartz vein which lies parallel with the siliciclastic metasedimentary rock 'bedding' plane (label 'a') with growth of tourmalines on the margins of this quartz vein (labels 'b' and 'c'). Similar "edge" growth of tourmalines is also displayed along the margins of sample site MA08, where large (mm to cm), acicular crystal growths have

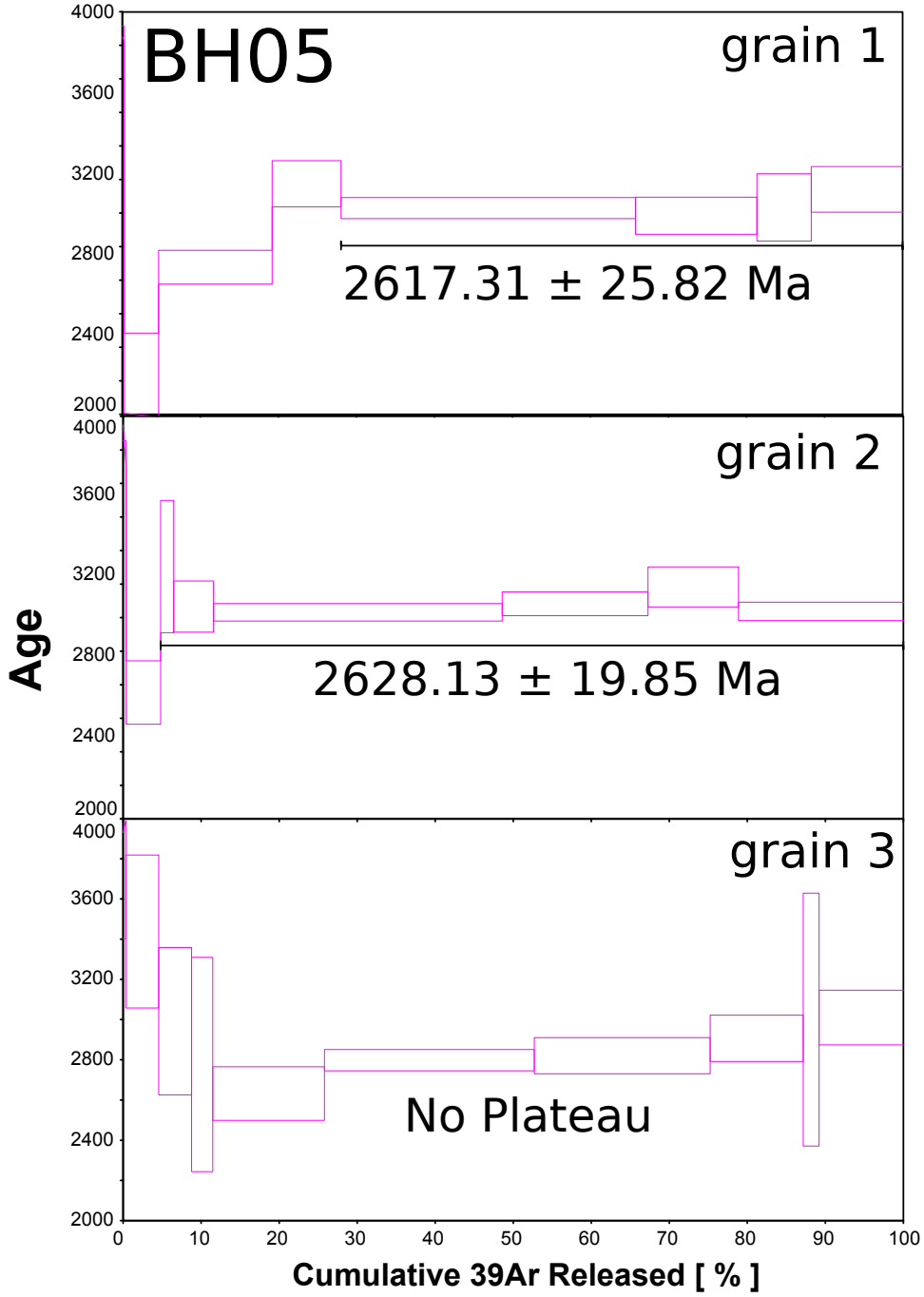

Figure 5.9: Argon age plateaus for tourmaline sample BH05 individual grains 1, 2 and 3. Plateaus 1 and 2 show a consistency between these duplicate sample runs, where >75% of radiogenic ^{39}Ar represents the plateau; whereas grain 3 did not yield a plateau.

formed within fresh quartz veining during later stage SiO_2 fluid circulation. These tourmaline growths are often aligned with, or perpendicular to, when formed as acicular 1-2 cm crystals, the foliation fabric and 'bedding' planes as seen in the siliciclastic metasedimentary rock units. This veining along pre-existing quartz-tourmaline stratiform veins suggests that fluid flow was enhanced along these, likely weaker foliation fabric planes.

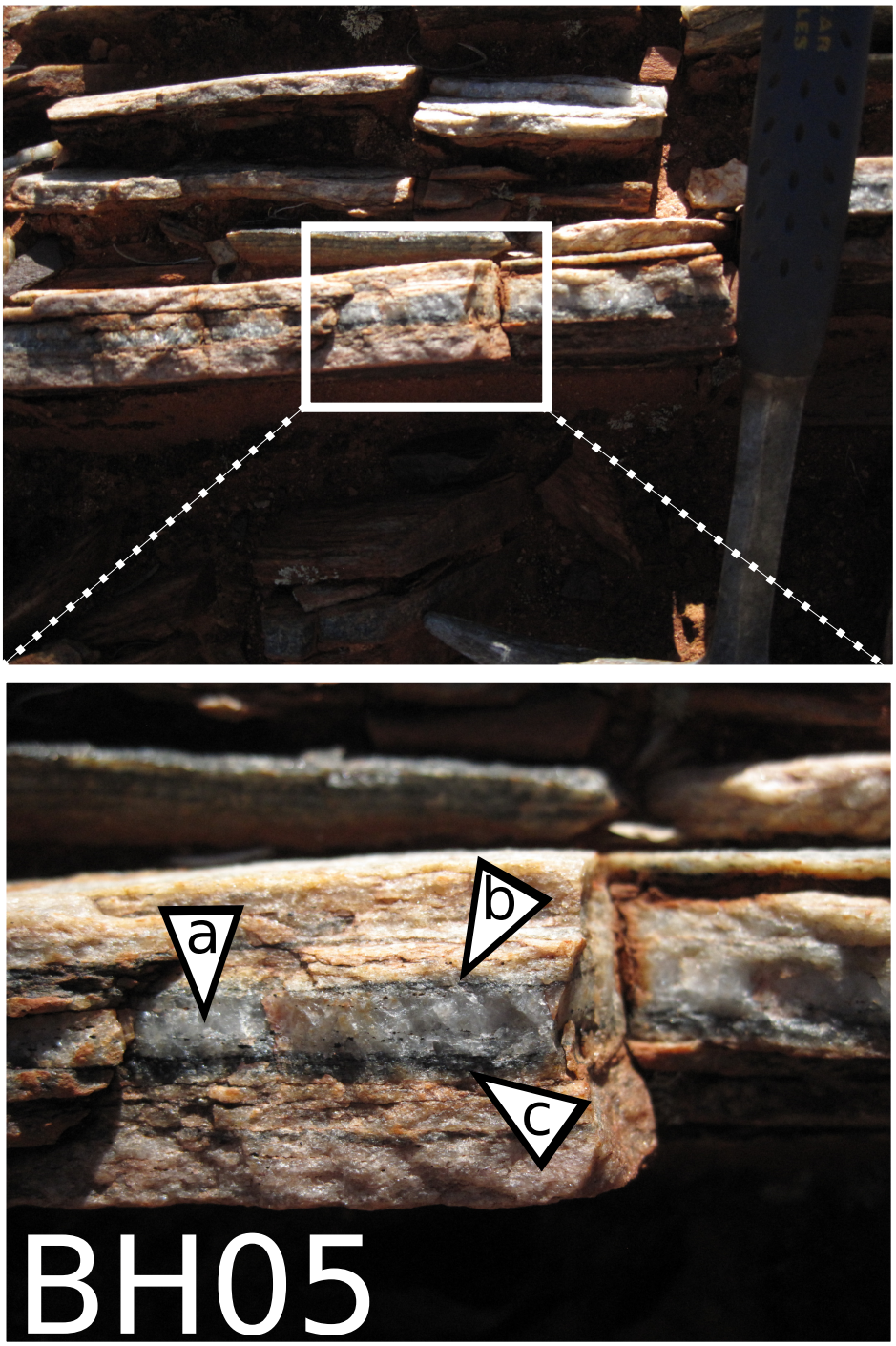

Figure 5.10: Field photo of sample site for tourmalines from sample BH05. Top photo shows a hammer for scale and associated quartzite units which show shear sense. Inset photo shows quartz vein which lies parallel with the siliciclastic metasedimentary rock 'bedding' plane (label 'a') with growth of tourmalines on the margins of this quartz vein (labels 'b' and 'c').

5.6.5 Boron isotopes

Boron isotopic results for samples MA24, MA08 and BH04 (sample BH05 was not analyzed) are shown in two graphs in Figure 5.11. The histogram in Figure 5.11-A shows most analyses have a δ^{11}B value of around -2.0. Sample MA24 has a broad peak and many analyses below -2.0, sample MA08 shows a bi-polar distribution above and below -4.0, and sample BH04 shows a simple population centering around -1.0. Stacked analyses are shown in Figure 5.11-B, outlining different fields for the formation of tourmaline. Most of the tourmalines fall within the carbonates and evaporites field, and the decompression and prograde field of tourmaline formation. All analyses are enriched in heavy boron ^{11}B relative to the continental crust. A bipolar distribution of δ^{11}B values is evident from sample MA08, which mostly relates to cores (enriched δ^{11}B) and rims (depleted δ^{11}B), outlined in Figure 5.11-B. Sample MA24 shows a broad spectrum of δ^{11}B values when compared to sample MA08. This may relate to sample MA08 tourmalines being from one large (meters across), consistent quartz-tourmaline vein structure, whereas sample MA24 is comprised of many small (1−100 mm) stratiform quartz tourmaline veins. Input from previous generations of tourmaline (detrital?) or breakdown of minerals with boron content not enriched in ^{11}B, may be the cause of smaller stratiform veins producing many values below -2.0 δ^{11}B.

5.6.6 Sample MA11 Barite (Mt. Alfred)

Barites, $BaSO_4$, are found in many samples throughout the Mt. Alfred locality. Some well preserved barites and barite veining occur in sample MA11, shown in detail in Figure 5.12. Figure 5.12-A shows EDS data spectrum plots and analysis sites, with larger versions of the EDS data plots shown in Figure 5.12. This figure shows a close-up of the barite veining (caused by late-stage tectonic shearing) and a central rounded barite grain shows the barite association with muscovite and andalusite. Also shown are EDS spectra of a zircon and monazite grain (lower left of inset SEM photo). Figure 5.12-B shows singular barite crystals (top) and barite veining (center). Whereas Figure 5.12-C shows elongated, stretched, and disaggregated barite veining (center) caused by ca. 2730−2630 Ma shearing.

5.7 Discussion

The pristine nature of many tourmalines, including pristine primary-growth terminations and lack of diagenetically-grown tourmaline features such as lamillae, suggests this tourmaline growth was thermally driven by B-enriched fluid flows at syn- or post-diagenetic times. The detrital zircons from within the quartz-tourmaline vein have ages of ca. 3270−3730 Ma, resembling those commonly found at the Mt. Alfred and Brooking Hills localities (see Chapter 4). These detrital zircons provide further evidence

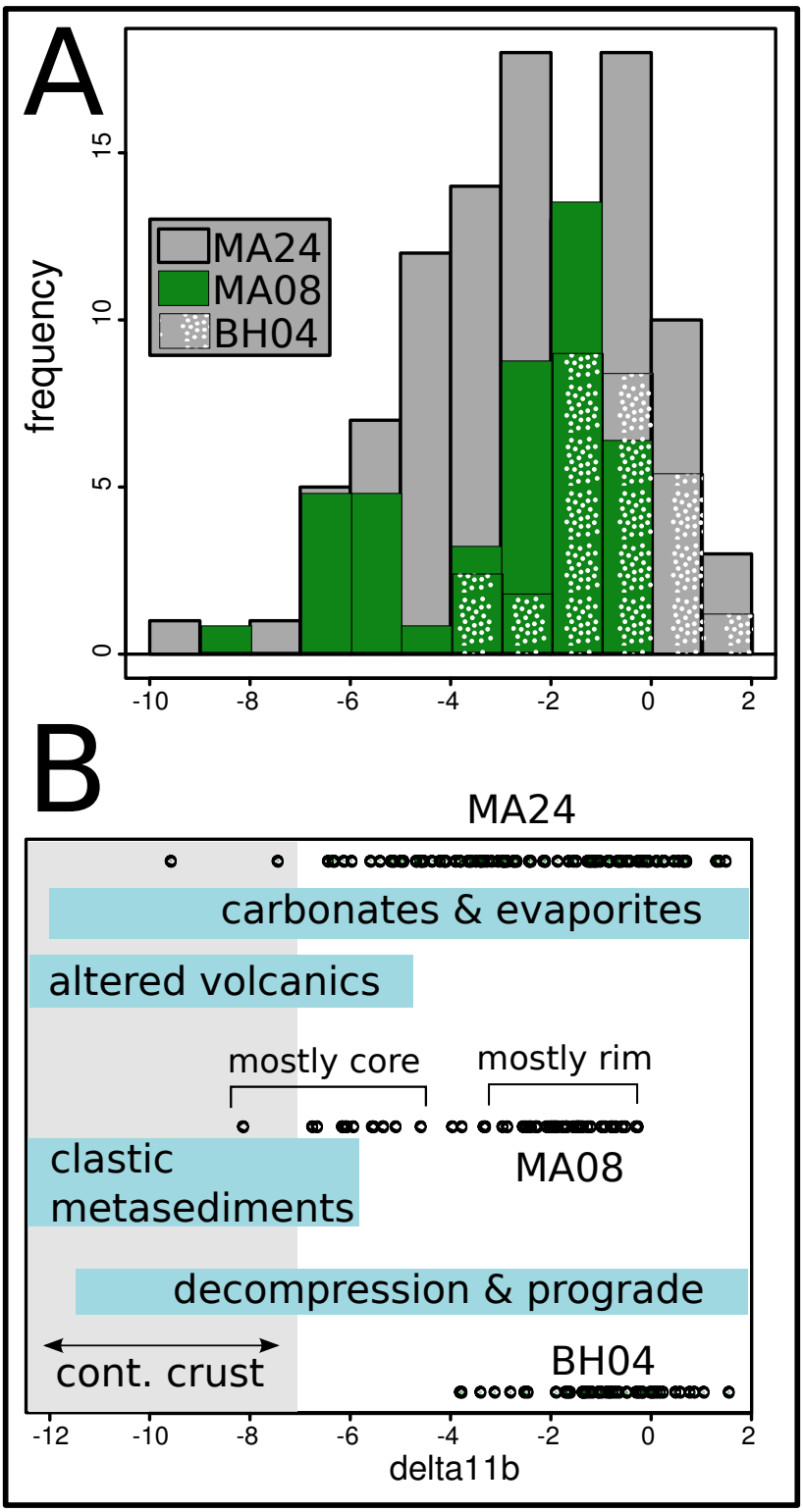

Figure 5.11: Graphs of boron isotopic results for samples MA24, MA08 and BH04. Histogram in (A) shows most analyses around δ^{11}B value of -2.0. Sample MA24 has a broad peak and many analyses below -2.0 δ^{11}B, sample MA08 shows a bi-polar distribution above and below -4.0 δ^{11}B, and sample BH04 shows a simple population centering around -1.0 δ^{11}B. Stacked analyses are shown in graph B, which shows different fields for the formation of tourmaline. Most of the tourmalines fall within the carbonates and evaporites field, or also the decompression and prograde field of tourmaline formation. All analyses are enriched in heavy boron versus the continental crust. Sample MA08 shows a bipolar distribution, which mostly relates to cores and rims (labelled).

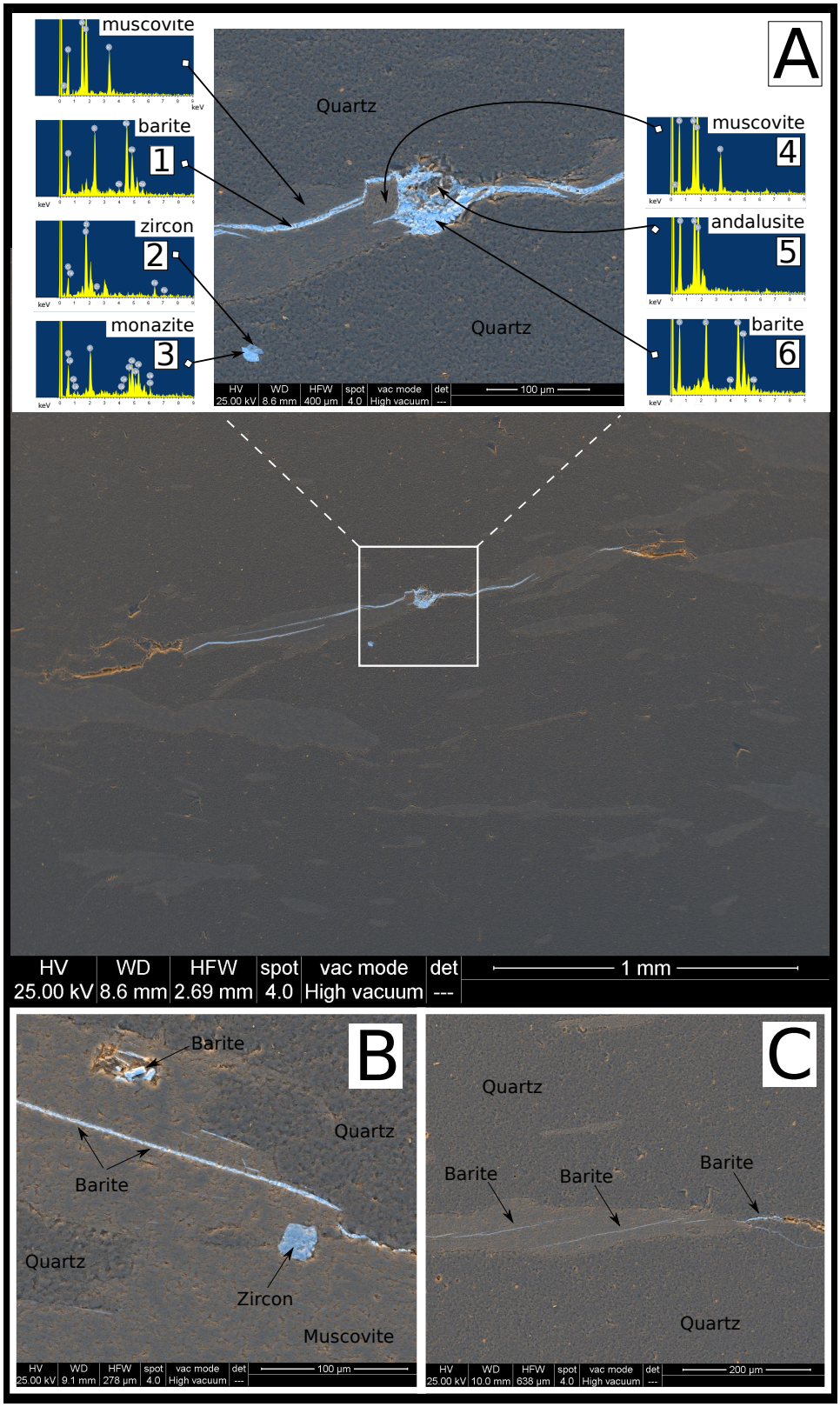

Figure 5.12: Sample MA11 thin section SEM combined BSE+SE images showing associated barite grains and veining. (A) Shows EDS data spectrum plots and analysis sites. A close-up of the barite veining (caused by late-stage tectonic shearing) and a central rounded barite grain shows the barite association with muscovite and andalusite. Also shown are EDS spectra of a zircon and monazite grain (lower left of inset SEM photo). (B) Shows singular barite crystals (top) and barite veining (center). (C) shows elongated, stretched, and disaggregated barite veining (center) caused by ca. 2730−2630 Ma shearing. Barite does not occur in any sample without some association with muscovite.

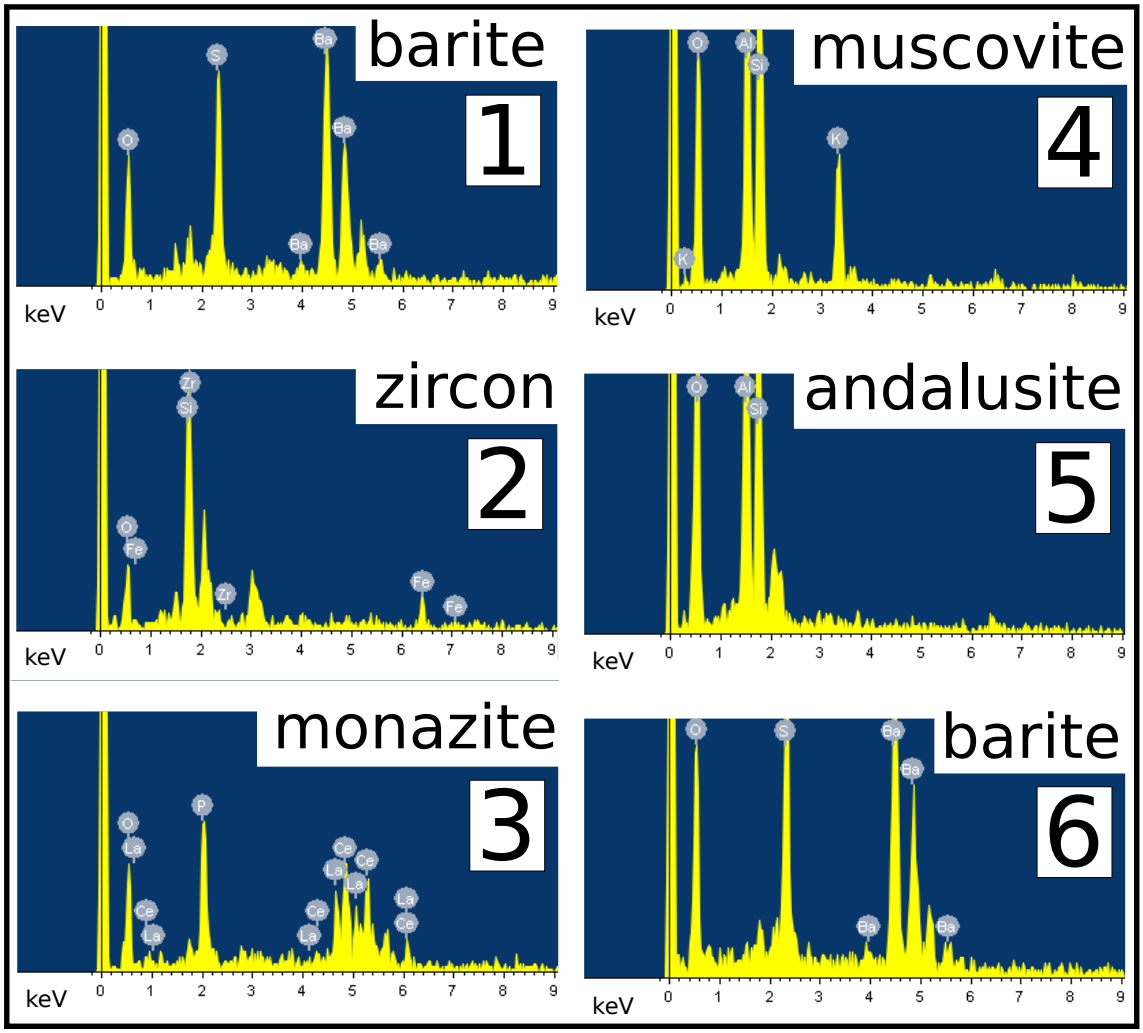

Figure 5.13: Sample MA11 thin section SEM EDS data spectrum plots showing blow-up x-ray spectrum for Figure 5.12-A. (1) barite, (2) zircon, (3) monazite, (4) muscovite, (5) andalusite, and (6) barite.

that post-depositional B-rich hydrothermal fluids fluxed through these sediments, mineralizing quartz and tourmaline in proximity to, or as a replacement of, these original sediments. The B-rich hydrothermal fluids may have been locally derived, or perhaps derived from another heat source but B-enriched by the breakdown of illite and clays within sedimentary layers.

Stratiform tourmalines occur as post-depositional stratiform layers within the metasedimentary rocks, and may have grown during a period of enhanced heating and hydrothermal fluid flow. The $^{40}Ar/^{39}Ar$ tourmaline age of 2939±15 Ma, the first Archean tourmaline ever directly dated, provides a minimum depositional age for the siliciclastic metasedimentary rocks of the Illaara Greenstone Belt. This age highly constrains deposition of the original sediments at Mt. Alfred, which also constrains the window of Hadean-zircon-bearing sedimentation and availability of Hadean grains to between 2939 Ma and ca. 3100 Ma. Further stratiform veining within sample MA24, and possibly all other stratiform veins throughout the Mt. Alfred locality, have produced ages within uncertainty of 2939±15 Ma. This age, when combined with similar $\delta^{11}B$ values and field relations, offers a co-genetic link between the 1 to 4m wide massive quartz-tourmaline vein (sample MA08) and those hosted in small stratiform layers (sample MA24) at Mt. Alfred. The existence of post-depositional tourmalines within these Archean metasedimentary rocks allows for their $^{40}Ar/^{39}Ar$ dates to be used for assigning minimum depositional ages to these sedimentary units.

The closure temperature of the tourmalines from sample MA08 has been calculated to be >600°C. This provides the first experimentally-calculated closure temperature estimate for natural tourmalines, and suggest tourmaline is highly robust and will retain a crystallization age even after upper greenschist to mid-amphibolite facies metamorphic events. The peak thermal events throughout the Illaara Greenstone Belt at ca. 2730 Ma (Nelson, 2001; Chen et al., 2003; Chen et al., 2004a) of upper-greenschist to mid-amphibolite grades have thus not reset these tourmaline ages.

The stratiform nature of the tourmalines, along with the association of barite in a parallel metasedimentary unit and B isotopes will put some constraints on possible depositional environment of these metasedimentary rocks.

5.7.1 Depositional Environment

Inferring a depositional environment from existing tourmaline and barite occurrences is difficult, given that the nature of fluid flow events and crystallization of both are still poorly resolved. However, some speculation is possible from the initial $\delta^{11}B$ values and the presence of barites within many metasedimentary samples.

Barite does not appear to occur in any sample without some association with muscovite, and/or andalusite, suggesting a detrital provenance which is linked to these more clay-rich layers. The presence of banded rhythmites around all siliciclastic metasedimentary rocks from the Mt. Alfred locality, abundant barites, and evidence from elevated δ^{11}B values within the tourmalines suggest the host sediments at Mt. Alfred were deposited within a marine-intertidal-evaporitic environment. Alternatively, sulphur-rich magmatic fluids interacted with briny seawater and circulated within these weaker clay-rich bedding planes, crystallizing tourmalines from the breakdown of ilmenite and other phases, producing enriched (above continental average) δ^{11}B values, and forming barites. Barite, however, is relatively insoluble and is likely to have been derived from pre-existing sedimentary minerals, such as halite, gypsum or other evaporitic-brine related marine sediments.

5.7.2 Late stage tourmalines

The tourmalines from the Brooking Hills sample site BH05, with an age of 2622±20 Ma, are significantly younger than those of sample MA08 and may require a different formation mechanism. Their formation along the margins of quartz veining, as displayed in Figure 5.10, suggest either that (i) late-stage quartz vein fluids were B-rich, or (ii) they became B-enriched by interacting with the margins of the siliciclastic metasedimentary rocks. This second hypothesis could be explained by the breakdown of local B-rich minerals, possibly smaller earlier tourmalines from the 2939 Ma event. Future δ^{11}B analyses on these samples, and δ^{18}O on the vein quartz and metasediment quartz may yield more information about their mineralization, and the character of their host fluids.

The ages of these tourmalines correspond to the timing of quartz veining throughout the Illaara Greenstone Belt during semi-ductile to brittle late-stage deformation. The age of this event is important, as most of the quartz veins cross-cut existing folding and shearing, which defines the end-stage of high-temperature (ca. $>350-400$°C) geodynamic events within this greenstone belt.

5.8 Conclusions

1) Dating stratiform tourmaline by the $^{40}Ar/^{39}Ar$ technique offers a unique approach to the resolution of complex geological relationships in Archean metasedimentary environments, previously closed to geochronological investigation.

2) Closure temperature estimates from a furnace run on multi-grain tourmalines resulted in estimates of Ar diffusion within tourmaline of >600°C. These results suggest

tourmaline is highly robust, and will retain a crystallization age even after upper greenschist to mid-amphibolite facies metamorphic events. Further studies, currently being undertaken, will constrain this temperature further.

3) $^{40}Ar/^{39}Ar$ tourmaline ages of 2939±15 Ma, the first Archean tourmaline ever directly dated, reveals the minimum depositional age for the siliciclastic metasedimentary rocks of the Illaara Greenstone Belt. This age constrains the deposition of the original sediments at Mt. Alfred, which places limits on Hadean-zircon-bearing source rock availability to weathering and deposition to 2939 Ma and ca. 3100 Ma.

4) Tourmaline boron isotopic analysis, field relations, and $^{40}Ar/^{39}Ar$ ages reveal coeval crystallization at 2939±15 Ma of tourmalines within the 1 to 4m wide massive quartz-tourmaline vein (sample MA08) and those hosted in small stratiform layers (sample MA24) at Mt. Alfred.

5) Evidence from elevated $\delta^{11}B$ values within the tourmalines, abundant barites within the metasedimentary rocks, and association with banded rhythmites suggest the host sediments at Mt. Alfred were deposited within a marine-intertidal-evaporitic environment. This evidence also suggest that these B-rich fluids were derived, at least in part, from the breakdown of locally-hosted clays and illite within sedimentary horizons. Alternatively, sulphur-rich magmatic fluids interacted with briny seawater and circulated within these weaker clay-rich bedding planes, crystallizing tourmalines from the breakdown of ilmenite and other phases, producing enriched (above continental average) $\delta^{11}B$ values, and forming barites. Barite, however, is relatively insoluble and is likely to have been derived from pre-existing sedimentary minerals, such as halite, gypsum or other evaporitic-brine related marine sediments.

6) A younger generation of tourmalines from the Brooking Hills, sample site BH05, shows that late stage hydrothermal quartz-vein fluids remobilized boron and crystallized new tourmalines at 2622±20 Ma on the margins of existing 2939±15 Ma stratiform tourmaline layers. Similar late-stage margin quartz-vein crystallization of tourmaline is also found on the edges of sample MA08 at Mt. Alfred, suggesting that the timing of quartz-veining throughout the Illaara Greenstone Belt metasedimentary rocks was coeval with this event at 2622±20 Ma. This age thus constrains the late stage quartz veining events which often cross-cut all tectono-metamorphic features such as folding and shearing recorded within the metasedimentary rocks.

CHAPTER 6
POST-DEPOSITIONAL THERMAL HISTORY

In Chapter 6, a manuscript is presented which discusses geochronological results on rutiles, muscovites, zircons and goethites, and reveals a broad and varied post-depositional history of the Illaara and Maynard Hills greenstone belt metasedimentary rocks. Rutile SHRIMP Pb-Pb age data constrain rutile growth episodes after deposition of the host sediments. Imaging and microstructural studies show metamorphic and detrital features in the rutiles, and what this reveals about the metamorphic history of the greenstone belts. The timing of late-stage tectonic shearing is revealed by muscovite-fuchsite $^{40}Ar/^{39}Ar$ geochronology, and younger events are determined through (U−Th)/He analyses on zircon and goethite. An overview of post-depositional events defines not only the thermal history of the metasedimentary rocks in the two greenstone belts, but advances the model of Yilgarn Craton formation as presented in Chapter Four. Supplementary data tables for muscovite-fuchsite $^{40}Ar/^{39}Ar$ results are shown in Appendix Table G.1.

6.1 Manuscript 3: Post-depositional thermal history of ca. 3.0 Ga metasedimentary rocks of the central Yilgarn Illaara and Maynard Hills Greenstone Belts, Western Australia

6.2 Abstract

The post-depositional thermal history of ca. 3.0 Ga Illaara and Maynard Hills greenstone belt siliciclastic metasedimentary rocks (peak metamorphism of upper- greenschist to mid- amphibolite facies) are characterized by a combination of SHRIMP U-Pb rutile, $^{40}Ar/^{39}Ar$ and (U-Th)/He geochronology. SHRIMP U-Pb rutile analyses from 8 metasandstone samples reveal a complex history of events between their deposition at ca. 3.0 Ga, and the subsequent intrusions of mafic-ultramafics at ca. 2.8 Ga, folding, thrusting and granitic intrusions (ca. 2730 to 2630 Ma, regional D1 to D3 events). Some individual rutile grains yield multiple U-Pb dates which span from before the maximum depositional age of the metasedimentary rocks at ca. 3060 Ma to the last major metamorphic and granitic event at ca. 2630 Ma. These rutiles exhibit weakly defined core-rim younging profiles which represent multiple stages of metamorphic growth and crystallization and a possible Pb-loss overprinting. Results suggest that under protracted upper greenschist to pulses of mid-amphibolite metamorphic conditions rutile can retain signatures of multiple thermal events and even retain some of their original detrital ages and characteristics. $^{40}Ar/^{39}Ar$ plateau ages on muscovites from metasandstones from both greenstone belts show that late to post-deformation, planar-foliation recrystalization at 2610±15 Ma (possibly coeval with the end of D3) marks the end of high-grade stabilizing tectono-thermal events and temperatures above 350−400°C. Zircon (U−Th)/He dates of 230±13 Ma define exhumation, with temperatures <180°C for the metasandstones, similar to fission track results from the northern Yilgarn. Goethite (U−Th)/He dates of 25±2 Ma are probably coeval with Fe-rich meteoric fluid influx and associated zero-age Pb-loss and Fe enrichment in metamict zones of both rutile and zircon within the metasandstones.

6.3 Introduction

The Yilgarn Craton of Western Australia is host to numerous >3000 Ma metasandstones, mostly occurring as elongated lenses, with some yielding abundant zircon ages in excess of ca. 4000 Ma (Mt. Narryer; Froude et al. (1983), Jack Hills; Compston et al. (1986a), Maynard Hills Nelson (2002b); and Mt. Alfred Nelson (2005); and Chapter 4 of this study). Zircons older than 4300 Ma have been identified from the Jack Hills (Narryer Terrane; Wilde et al. (2001); Peck et al. (2001); Cavosie et al. (2004), Mt. Narryer, Maynard Hills (Southern Cross Terrane); Nelson (2002b); Wyche et al. (2004) and Mt. Alfred (Illaara greenstone belt); Nelson (2005). Recent finds of >4300 Ma zircons (Nelson, 2002b; Wyche et al., 2004) in the central Yilgarn localities of the Maynard Hills and Illaara greenstone belts has prompted a broader investigation of these ancient zircons as well as their host siliciclastic metasedimentary rocks.

Throughout the Southern Cross, Murchison, and South West Terranes (see Figure 6.1), ca. 3.0 Ga metasedimentary rocks occur as rafts within ca. 2730 to 2600 Ma granites and gneisses, and >2900 Ma, ca. 2800 Ma and ca. 2730 Ma greenstones. Similar metasedimentary rocks within the Narryer Terrane at Mt. Narryer and Jack Hills occur within >3000 Ma granites and gneisses as well as >2900 Ma greenstones, granites and gneisses, respectively. The greenstones are distributed along N−S trending elongate belts throughout the Yilgarn Craton (see Figure 6.1). These >3000 Ma metasedimentary rocks commonly contain abundant zircons with ages older than 3250 Ma, older than any known rocks within the Yilgarn Craton outside of the Narryer Gneiss Complex within the Narryer Terrane. With the exception of those at Mt. Narryer, the metasedimentary rocks are located on the margins or within greenstone 'rafts' throughout the Yilgarn (Figure 6.1) and their relationship to one another and to the Narryer Gneiss Complex has remained problematic.

Post-depositional events can be assessed through research into metamorphic rutile, muscovite-fuchsites and (U−Th)/He dating of zircon and goethite. Rutile is a common accessory mineral in detrital sediments (Force, 1991; Meinhold, 2010) and is found in abundance in the Archean metasedimentary rocks of the Illaara and Mayanard Hills greenstone belts. Rutile from other ca. 3.0 Ga metasedimentary rocks at the Jack Hills yielded SHRIMP ages of ca. 2500 Ma which correspond to a regional metamorphic event (Harrison et al., 2007). This suggests rutile was either reset, or grew during this event, and that ages obtained on rutiles from ca. 3.0 Ga metasedimentary rocks throughout the Yilgarn may be difficult to assess due to their protracted histories. Metamorphic rutile growth in metasedimentary rocks can occur through the breakdown of ilmenite during greenschist facies or higher (Luvizotto and Zack, 2009; Meinhold, 2010). Higher grade events, amphibolite or granulite facies, can also cause considerable amounts of Pb diffusion within rutiles, causing measurable core-rim younging and impacting on the overall U-Pb and Pb-Pb ages determined on smaller grains (Mezger et al., 1989; Kooijman et al., 2010).

By using samples obtained from the siliciclastic metasedimentary rocks found within the Illaara and Maynard Hills greenstone belts, the aims of this study are to: (1) Obtain SHRIMP U-Pb dates on rutile samples to assess their age systematics in reference to Yilgarn-wide tectono-thermal events; (2) Use $^{40}Ar/^{39}Ar$ analyses on muscovite-fuchsite samples to determine cooling times of late stage shearing; (3) Investigate late stage thermal and hydrothermal events based on (U−Th)/He ages obtained on zircon and goethite; (4) Determine an overall post-depositional thermal history for the greenstone belts; and (5) Use this history to discuss the formation dynamics of greenstone belts throughout the Yilgarn Craton.

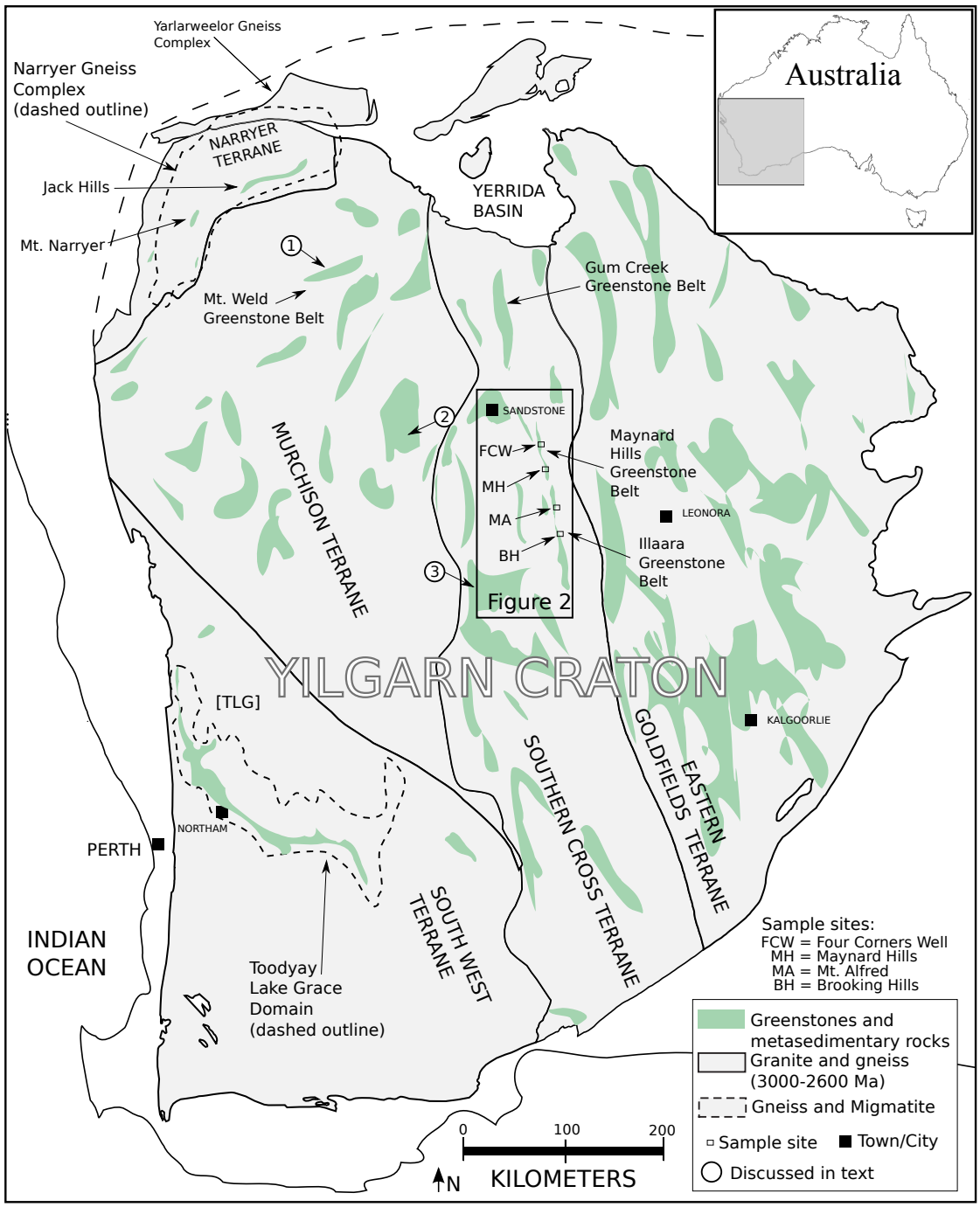

Figure 6.1: see next page for full description

Figure 6.1: Map of the Yilgarn Craton, Western Australia, showing locations of ca. 3000 Ma metasedimentary rocks (Toodyay Lake Grace Domain, Jack Hills, Mt. Narryer, Gum Creek, Maynard Hills, Illaara), greenstone belts, granites and gneisses. Also labelled are the greenstones at Mt. Weld (and the Mt. Weld ca. 2940-2960 Ma metasedimentary rocks) which is also the first of four numbered greenstone belts. These numbered greenstone belts are used as examples for typical greenstone associations close to their locality on the map. Label 1, the Mt. Weld greenstone belt from the Western Murchison Terrane, is composed of a lower >2900 Ma Luke Creek greenstone succession and an upper ca. 2800 Ma Mt. Farmer succession (Wiedenbeck and Watkins, 1993; Pidgeon et al., 1996). Label 2, the Windimurra Complex (a mafic-ultramafic intrusive complex) from the Eastern Murchison Terrane, is mostly composed of ca. 2850-2800 Ma ages (Mathison and Ahmat, 1996; Ivanic et al., 2010), and references therein. Label 3, the Marda-Diemals Greenstone Belt from the Central Southern Cross Terrane, is a ca. 2735 Ma upper greenstone overlying a >2900 Ma lower greenstone (Morris, 2007; and references therein). The area covered by Fig. 2 is also shown.

6.4 Geological setting

The Maynard Hills, Mt. Alfred and Brooking Hills metasandstones lie within the Maynard Hills and Illaara greenstone belts, respectively, in the central area of the Yilgarn Craton. The Maynard Hills metasandstones represent the northern extension of the lowermost metasedimentary unit of the Illaara greenstone belt (Wyche et al., 2004). Both the Maynard Hills and Mt. Alfred metasandstones have been impacted by the Edale Shear Zone, which has strongly deformed the greenstones and associated metasedimentary rocks.

The Illaara and Maynard Hills greenstone belts have undergone multiple stages of deformation and granitic intrusion. Deposition of the oldest greenstones from this area probably occurred before 2900 Ma and was accompanied by episodes of granitic intrusions between 3000 Ma to 2620 Ma (Pidgeon and Wilde, 1990; Wiedenbeck and Watkins, 1993; Wang et al., 1996, 1998b; Yeats et al., 1996; Mueller and McNaughton, 2000; Schiotte and Campbell, 1996; Wang et al., 1998a). Zircon xenocrysts within granitic rocks and porphyries with ages between 2900−3040 Ma have been found within the Southern Cross Terrane (eg. GSWA samples 142920, 169066). Dates from the Mt. Weld Greenstone Belt, within the northeastern part of the Murchison Terrane (see Figure 6.1 label '1') suggest timing of deposition and possible rifting-related tectonic events between 2940-2960 Ma, and may be related to an earlier shared history between the Jack Hills metasedimentary rocks and those of the Illaara and Maynard Hills greenstone belts (see Chapter 4, Figure 8 for discussion). To the northeast on the border of the Murchison Terrane, large mafic-ultramafic intrusions between 2800−2815 Ma are preserved at the Windimurra, Narndee and Youanmi igneous complexes (Ivanic et al., 2010) (see Figure 6.1, label '2'). Major tectonic events of the central Yilgarn, matching ages of many granitic intrusions, have been studied from the Marda-Diemals Greenstone Belt,

approximately 40km east-southeast of the Illaara Greenstone Belt (Chen et al., 2003; Chen et al., 2004a) (see Figure 6.1, label '3'). The first major event, at 2730 Ma, relates to intrusion of ca. 2730 Ma granites, and resulted in coaxial shortening, the earliest phase of folding and thrusting, and eruption of the Marda andesite-rhyolite (Chen et al., 2004a). The major folds throughout the Illaara and Maynard Hills greenstone belts were mostly formed at this time (Chen et al., 2003). This event is followed by an event at ca. 2660 Ma, during which voluminous granitic intrusions were emplaced, accompanied by E−W shortening and NW−NE ductile shearing (Chen et al., 2004a). Final post-kinematic granitic intrusions at ca. 2630 are found throughout the central Southern Cross Terrane, and have been dated near the Marda Diemals Greenstone Belt (Chen et al., 2003).

6.5 Sample selection

Sample sites are shown on the simplified geological sketch maps of the Mt. Alfred and Brooking Hills (Figure 6.2, inset Mt. Alfred and Brooking Hills maps) with additional sampling information in Table 1. Eight rutile samples were separated from multiple metasandstone units throughout the Illaara and Maynard Hills greenstone belts at (north to south) Maynard Hills (MH), Mt. Alfred (MA), and Brooking Hills (BH). Muscovites and fuchsites were concentrated from six samples, including one from further north in the Maynard Hills at the Four Corners Well location of the Maynard Hills Greenstone Belt (FCW), which is on the eastern-most edge of the belt and features mylonitic structures. Rutiles, zircons and goethite were all extracted for (U−Th)/He thermochronology from the single sample MA14. Tourmalines for (U−Th)/He thermochronology were isolated from sample MA08, described in detail in the Chapter 5. Full sample descriptions, locality, petrographic analysis and zircon geochronology is presented elsewhere (Thern and Nelson, 2012a) (See chapter 4), where sample names are the same as those presented here, except without the trailing "R". Samples collected include one from Maynard Hills (MH09), one from the Brooking Hills (BH01), and six from Mt. Alfred (MA03, MA04, MA05, MA07, MA11, and MA13). Sample labels, brief rock description and coordinates are listed in Table 6.1.

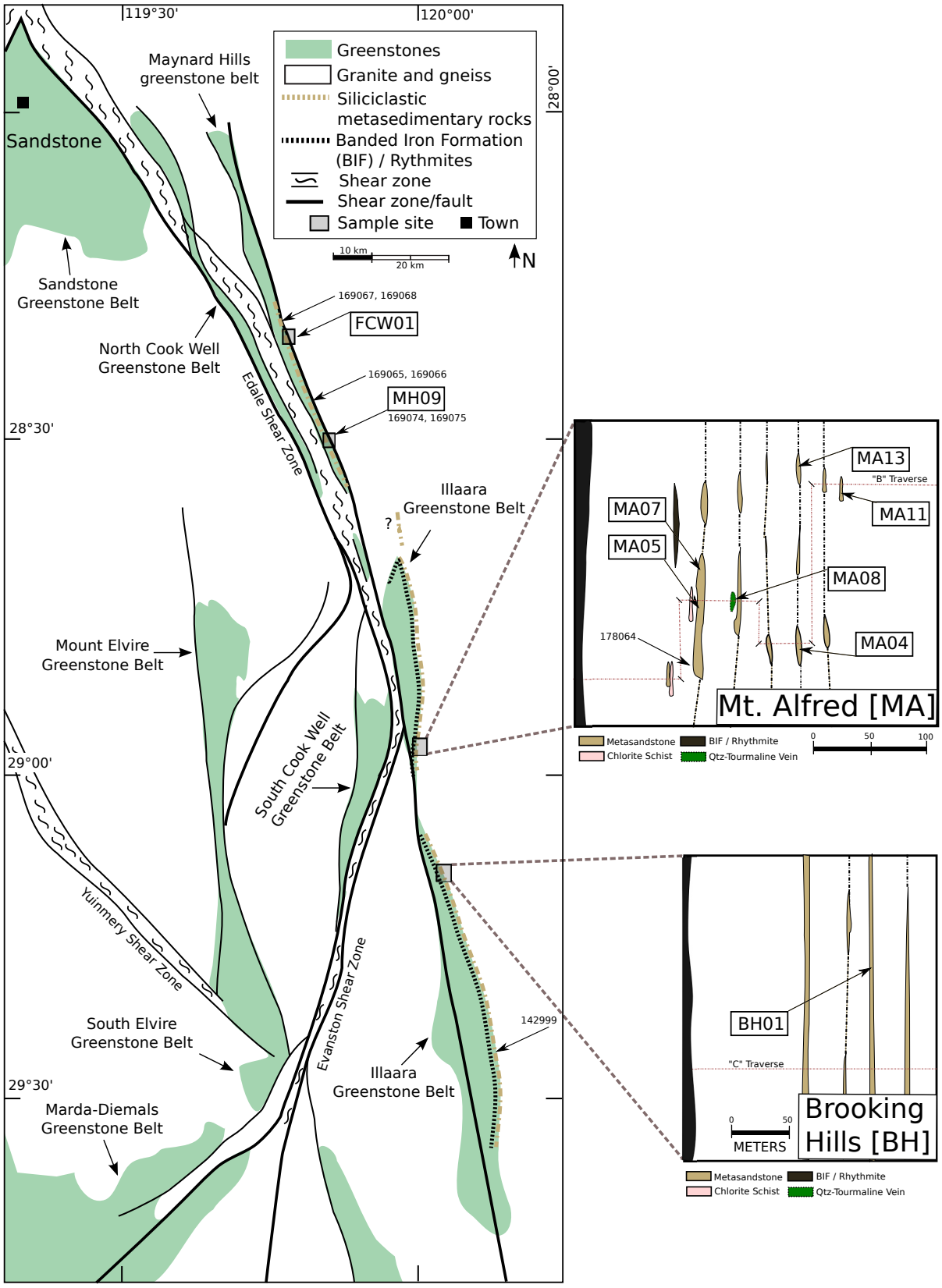

Figure 6.2: Maynard Hills and Illaara Greenstone Belts within the Southern Cross Terrane, with inset maps of the Mt. Alfred and Brooking Hills sampling localities. Numbered labels outside of boxes are previous GSWA sampling numbers and locations.

Table 6.1: List of sample localities and brief descriptions for rutiles, muscovites and goethite

Sample	South	East	Lithology and Description
Maynard Hills [MH] – Maynard Hills Greenstone Belt			
FCW01	S 28° 19.685'	E 119° 44.377'	schistose-quartzite; mylonitic quartzite with interleaved muscovite lathes (ca. 5 cm banding) highly strained textures.
MH09	S 28° 29.316'	E 119° 49.050'	quartzite; pale pinkish-grey, coarse grained massively recrystallized quartzite with reddish-yellow clay-rich layers; zircons separated from GSWA sample 169075 (Nelson, 2002) aliquot.
Mt. Alfred [MA] – Illaara Greenstone Belt			
MA03	S 28° 50.694'	E 119° 59.977'	metasandstone; pale greenish-white, medium- to coarse-grained, quartzite from the western margin of a 20 m-thick, bedded quartzite unit; 2 m-east of GSWA sample 178064.
MA04	S 28° 50.636'	E 120° 00.127'	metasandstone; clearish-green, reddish tinged, recrystallized, fine to medium-grained, with fuchsite and muscovite aligned with 5 cm-thick bedding-parallel foliation from a 10 m-thick, bedded quartzite unit.
MA05	S 28° 50.678'	E 119° 59.965'	metasandstone; pale greenish-white, recrystallized, fine to medium-grained quartzite, with minor fuchsite / muscovite lathes aligned to 4 cm-thick bedding-parallel foliation on the eastern margin of the 20 m-thick outcrop.
MA07	S 28° 50.636'	E 119° 59.975'	metasandstone; pale greenish-white, recrystallized, fine to medium-grained, with minor fuchsite/muscovite lathes aligned to 5-8 bedding-parallel foliation from a 20 m-thick, bedded quartzite unit.
MA11	S 28° 50.442'	E 120° 00.165'	metasandstone; bright-clear-green, recrystallized, medium to coarse-grained, with large 1-2 cm-long fuchsite lathes aligned with 4 cm-thick bedding-parallel foliation from a 2 m-thick, bedded quartzite unit.
MA13	S 28° 50.441'	E 120° 00.107'	metasandstone; moderately weathered, pale-white, yellowish, recrystallized, fine to medium-grained quartzite with 1-2 cm thick bedding-parallel foliation.
MA14	S 28° 50.432'	E 120° 00.048'	metasandstone; clearish-green, recrystallized, fine to medium-grained, with fuchsite and muscovite aligned with 5 cm-thick bedding-parallel foliation from a 20 m-thick, bedded quartzite unit.
Brooking Hills [BH] – Illaara Greenstone Belt			
BH01	S 28° 56.681'	E 120° 00.040'	metasandstone; pale greenish-white, recrystallized, fine to medium-grained, with fuchsitic lathes aligned to 2-4 cm thick layer-parallel foliation from a 1 m-thick, bedded quartzite unit.

1. All samples were free of any obvious veins or dykes.
2. Samples referred to as 'metasedimentary rocks' within text, as their primary sedimentalogical structures are obscured

6.6 Analytical procedures

6.6.1 Sample preparation

Zircons, rutiles and goethites were separated from ca. 5 kg of sample via crushing, milling, Wilfley table and heavy liquid separation. They were then put through a Frantz magnetic separator and then hand-picked from three magnetic fractions with no preference to size or shape of the grains. The non-magnetic and mid-magnetic fractions were preferred as they yielded the highest abundance of non-metamict grains suitable for geochronology.

Rutile grains and fragments of standards were mounted in epoxy resin and polished approximately a third to half way through to expose a surface suitable for in-situ U-Th-Pb data acquisition. Analysis of these zircons utilized the Sensitive High Resolution Ion Microprobe (SHRIMP) at the John de Laeter Centre of Mass Spectrometry, Curtin University of Technology, Perth.

Multiple fuchsite (Cr-rich muscovite) grains were also separated from the >500μm sieved fraction of selected metasandstone samples for $^{40}Ar/^{39}Ar$ analysis.

6.6.2 Ion Microprobe U−Th-Pb analyses of rutile

Rutile is known to display a matrix effect (similar to that of badeleyite) which effects the rutile $^{206}Pb/^{238}U$ ages based on grain orientation (Taylor et al., 2012). As this study involves rutiles with ages older than 2600 Ma, the $^{206}Pb/^{238}U$ ratio is most useful as a rough indication of concordance rather than for geologically meaningful dates, where $^{207}Pb/^{206}Pb$ dates produce a more precise measure of the age of the mineral.

The runtable used for rutile data in this study consisted of 8 masses to measure elements of interest and background: $^{208}Ti_2O^+$ (2 s), $^{204}Pb^+$ (10 s), $^{204.045}$Background (10 s), $^{206}Pb^+$ (20 s), $^{207}Pb^+$ (40 s), $^{208}Pb^+$ (10 s), $^{238}U^+$ (10 s), $^{238}U^{16}O^+$ (5 s), $^{238}U^{16}O_2{}^+$ (3 s).

The rutile standard used to calibrate the $^{206}Pb/^{238}U$ analyses is a multi-grain standard from the Windmill Hill metasandstone of the Jimperding metamorphic belt, Western Australia (Clark et al., 2000). To overcome the limitations of using a multi-grain standard, many analyses of the standard grains were done to improve the uncertainties – over 135 analyses over 9 sessions. The rutiles of this standard are slightly discordant (ca. 8%), and have a $^{206}Pb^*/^{238}U$ ratio of 0.5025 (based on TIMS analyses by L.M. Heaman), a mean $^{207}Pb/^{206}Pb$ date of 2642 Ma, and an average U content of 164 ppm

(P.D. Kinny, personal communication).

The Sri Lankan standard zircons M257 ($^{206}Pb/^{238}U$ age=561.3±0.3 Ma, 840 ug/g^{-1} U (Th/U approximately 0.27); Nasdala et al. (2008)) and CZ3 ($^{206}Pb/^{238}U$ age=564±0.3 Ma; Nelson, 1997) were used as an alternative for U/Pb calibration as well as U and Th concentration calculation. During the SHRIMP sessions, 55 analyses of M257 indicated an average Pb*/U calibration uncertainty of ±1.54% (1σ), and 242 CZ3 analyses indicated an average Pb*/U calibration uncertainty of ±1.82% (1σ).

All SHRIMP rutile analyses have been reduced using CONCH software (Nelson, 2006) and grouped by their $^{207}Pb/^{206}Pb$ dates using a χ^2 value of 1.75. The rutile analyses were normalized based on the linear covariation between $^{206}Pb^*/UO$ and UO_2/UO as analyzed on unknowns and standards. It was found that using the UO_2/UO calibration is better suited to rutile than using $^{206}Pb^*/UO$ vs. UO/U, as is commonly used for zircon.

All age calculations are based on ^{208}Pb-corrected $^{207}Pb/^{206}Pb$ dates on the rutiles, unless otherwise stated. Rutiles strongly exclude Th from their crystalline lattice sites, and commonly have either no detectable Th or only very small amounts. As thorium concentrations in most rutiles within this study were less than 1 ppm, the measured ^{208}Pb (52.4% of common Pb) was largely or entirely of common origin, and yields more precise $^{207}Pb/^{206}Pb$ dates than do corrections using ^{204}Pb (1.4% of common Pb). Where measured thorium concentrations are less than 10 ppm, the ^{208}Pb correction method becomes unreliable and can yield unrealistically old ages, and have in this study been superceded by the ^{204}Pb method (Cumming and Richards, 1975), which is less precise but more robust on slightly disturbed grains.

6.6.3 $^{40}Ar/^{39}Ar$ analyses of muscovite/fuchsite

Muscovite-fuchsite samples were loaded into 5 wells of one 1.9 cm diameter and 0.3 cm depth on an aluminum disc. These wells were bracketed by smaller wells that included GA1550 biotite used as a neutron fluence monitor, for which an age of 99.77 ± 0.11 Ma was adopted and for which a good in-between grain reproducibility has been demonstrated (Renne et al., 1998, 2010). The discs were Cd-shielded (to minimize undesirable nuclear interference reactions) and irradiated for 25 hours in the Hamilton McMaster University nuclear reactor (Canada) in position 5C. The mean J-values computed from standard grains within the small pits range from 0.0026752 ± 0.0000040 (0.15%) to 0.0026644 ± 0.000054 (0.20%) determined as the average and standard deviation of J-values of the small wells for each irradiation disc. Mass discrimination was monitored using an automated air pipette and provided a mean value of 1.00646 ± 0.00238 per dalton (atomic mass unit). The correction factors for interfering isotopes were $(^{39}Ar/^{37}Ar)Ca = 7.30x10^{-4}$ (±11%), $(^{36}Ar/^{37}Ar)Ca = 2.82x10^{-4}$ (±1%) and

(^{40}Ar/^{39}Ar)K = 6.76x10^{-4} (±32%).

^{40}Ar/^{39}Ar analyses were performed at the Western Australian Argon Isotope Facility at Curtin University. The samples were step-heated using a 110 W Spectron Laser System, with a continuous Nd-YAG (IR; 1064 nm) laser rastered over the sample during 1 minute to ensure homogeneously distributed temperature. The gas was purified in a stainless steel extraction line using a GP50 and two AP10 SAES getters and a liquid nitrogen condensation trap. Ar isotopes were measured in static mode using a MAP 215-50 mass spectrometer (mass resolution of ca. 500; sensitivity of 2x10^{-14} mol/V) with a Balzers SEV 217 electron multiplier mostly using 9 to 10 cycles of peak-hopping. The data acquisition was performed with the Argus program written by M.O. McWilliams and ran under a LabView environment. The raw data were processed using the ArArCALC software (Koppers, 2002) and the ages have been calculated using the decay constants recommended by Renne et al. (2010). Blanks were monitored every 3 to 4 steps and typical ^{40}Ar blanks range from 1x10^{-16} to 2x10^{-16} mol.

Our criteria for the determination of plateau are as follows: plateaus must include at least 70% of ^{39}Ar. The plateau should be distributed over a minimum of 3 consecutive steps agreeing at 95% confidence level and satisfying a probability of fit (P) of at least 0.05. Plateau ages are calculated using the mean of all the plateau steps, each weighted by the inverse variance of their individual analytical error. Mini-plateaus are defined similarly except that they include between 50% and 70% of ^{39}Ar. Integrated ages (2σ) are calculated using the total gas released for each Ar isotope. Inverse isochrons include the maximum number of steps with a probability of fit $\geq$0.05. The uncertainties on the ^{40}Ar*/^{39}Ar ratios of the monitors are included in the calculation of the integrated and plateau age uncertainties, but not the uncertainties on the age of the monitor and on the decay constant (internal uncertainties only, see discussion in Min et al. (2000).

6.6.4 (U−Th)/He analyses of zircon, goethite, rutile and tourmaline

For goethite analyses, goethites were hand-picked under a binocular microscope, ultrasonically cleaned in ethanol, left to dry and broken into smaller pieces. Care was taken to select shards of sufficient size (>150 μm), representing aggregates consisting of small (ca. 1 μm) crystals, in order to eliminate the effect of alpha ejection (Farley et al., 1996). ^{4}He, ^{238}U and ^{232}Th were measured using isotope-dilution mass spectrometry (quadrupole and ICP-MS, respectively). ^{4}He from the samples was extracted under high vacuum using Nd-YAG laser and analysed on the CSIRO Pfeiffer Prisma QMS-200 mass spectrometer Earth Science and Resource Engineering extraction line at the John de Laeter Centre for Isotope Research in Perth.

The goethite samples were then degassed at 500°C for 15 minutes. Released gas was purified using a cold finger cooled with liquid nitrogen and a hot (ca. 350°C) Ti-Zr getter, spiked with 99.9% pure ^{3}He and introduced into the mass spectrometer next to a cold Ti-Zr getter. ^{4}He/^{3}He ratios, corrected for HD and ^{3}H by monitoring mass 1, were measured by a Channeltron detector operated in static mode. A "re-extract" (Farley et al., 2002) was run after each sample to verify complete outgassing of the samples. The He gas results were blank-corrected by heating empty Nb tubes using the same procedure. Following the ^{4}He measurements, Nb tubes containing the samples were retrieved from the laser cell, spiked with ^{233}U and ^{230}Th and dissolved in 200 μl of 50% HCl in Parr bombs heated to 210°C for 60 hours. Each Parr bomb also contained blank and spiked standard solutions. All solutions were analysed for U and Th at TSW Analytical Ltd. (University of Western Australia, Perth) on an Agilent 7500 ICP-MS. For more details on analytical procedure, refer to Evans et al. (2005).

For zircon, rutile and tourmaline, minerals were selected under a binocular microscope in order to avoid grains with cracks or U- and Th-rich mineral/fluid/gas inclusions that may contribute excess helium to the analysis. Grain measurements were taken for the calculation of an alpha correction factor (Ft; Farley et al., 2002) and every effort was made to select grains with a diameter larger than 70 microns in order to maximum helium gas values and minimize the Ft correction. Images of selected grains were recorded digitally and grain measurements were taken. Measured and photographed grains were loaded in niobium microvials. Helium was thermally extracted from single crystals heated to >1200°C using a 1064 nm Nd-YAG laser. U and Th were also determined using isotope dilution inductively coupled mass spectrometry. Samples were removed from the laser chamber and transferred to Parr pressure dissolution vessels where they were spiked with ^{235}U and ^{230}Th (25μl of a solution containing 15ppb ^{235}U and 15ppb ^{230}Th for zircon and 25μl of a solution containing 15ppb ^{235}U and 5ppb ^{230}Th for rutile and tourmaline) and digested at 240°C for 40 hours in 350μl of HF. Standard solutions containing the same spike amounts as the unknown samples (as well as 25μl of a solution containing 81ppb ^{235}U and 82ppb ^{230}Th for zircon and 25μl of a solution containing 25ppb ^{235}U and 25ppb ^{230}Th for rutile and tourmaline) were treated the same as the samples, as were a series of unspiked reagent blanks (just 25μl of HF). After the 40 hour dissolution, samples were removed from the pressure vessels and allowed to dry for 2 days. 300μl of HCl was added to each vial and a second bombing for 24 hours at 200°C ensured dissolution of fluoride salts. Final solutions were diluted to 10% acidity for analysis on an Agilent 7500CS mass spectrometer (at the University of Western Australia, TSWTM Analytical). For single crystals digested in small volumes (0.3-0.5 ml), U and Th isotope ratios were measured to a precision of $< 2\%$. The zircon (U$-$Th)/He thermochronology method at CSIRO has an overall precision of <6% and more detailed description of U and Th analysis can be found in Evans et al. (2005).

6.7 Results

In order to properly assess whether the TiO_2 mineral separates were rutile, or some polymorph such as anatase or brookite, they were first analyzed by XRD. These results, as well as their crystal structure, as seen in Figure 6.5, show that the TiO_2 mineral separates from each sample are rutile.

6.7.1 Rutile Geochronology and Imaging

SHRIMP U-Pb and Pb-Pb rutile data from the eight metasandstones studied are presented in Table 6.2. Wetherill Concordia plots are shown in Figure 6.4 and probability plots in Figure 6.3 show that the bulk of all analyses fall within a single 2656.2±2.8 Ma group, very similar to the $^{207}Pb/^{206}Pb$ age of the rutile standard used in this study (multigrain rutile analyses shown in Appendix Table F.1). Rutiles which have >10ppm Th are not used in these interpretations, with the exception of those analyses which use the ^{204}Pb-correction method instead of ^{208}Pb (as noted previously). Reverse discordance, recorded in analyses within Figure 6.4, is mostly a function of the multi-grain rutile standard offering a poor U/Pb calibration. This is mostly an analytical artefact, and does not impact the obtained $^{207}Pb/^{206}Pb$ dates, which are used when discussing geological interpretations below.

Table 6.2: SHRIMP analytical results for rutile samples from the Maynard Hills (MH09), Brooking Hills (BH01), and Mt. Alfred (MA03, MA04, MA05, MA07, MA11, and MA13)

						Ratios							Dates (Ma)							
Grain .spot	U ppm	Th ppm	Th/U	Pb ppm	$f206\%$ ^{208}corr	$\frac{^{207}Pb}{^{206}Pb}$ ^{208}corr	$\pm1\sigma$ %	$\frac{^{206}Pb}{^{238}U}$ ^{208}corr	$\pm1\sigma$ %	$\frac{^{207}Pb}{^{235}U}$ ^{208}corr	$\pm1\sigma$	%conc. ^{208}corr	$\frac{^{206}Pb}{^{238}U}$ ^{208}corr	$\pm1\sigma$	$\frac{^{207}Pb}{^{235}U}$ ^{208}corr	$\pm1\sigma$	$\frac{^{207}Pb}{^{206}Pb}$ ^{204}corr	$\pm1\sigma$	$\frac{^{207}Pb}{^{206}Pb}$ ^{208}corr	$\pm1\sigma$
BH01 Rutiles (39 analyses)																				
BH01R2-5.1	24	0	0.02	3	7.604	0.1570	2.94	0.1073	7.85	2.323	8.72	27	657	49	1219	62	2516	134	2423	50
BH01R-2.1	13	0	-0.01	9	1.792	0.1719	2.31	0.6209	12.19	14.719	12.69	121	3113	301	2797	121	2751	170	2577	39
BH01R-4.1	15	0	0.00	10	1.756	0.1738	1.88	0.6303	10.33	15.106	10.73	121	3151	258	2822	103	2581	96	2595	31
BH01R2-7.2	3	0	0.02	1	-0.228	0.1752	1.79	0.5671	10.35	13.699	10.72	111	2896	242	2729	102	2632	53	2608	30
BH01R2-12.1	3	0	0.04	2	-0.454	0.1756	1.69	0.5799	9.36	14.040	9.72	113	2948	222	2752	92	2564	72	2612	28
BH01R2-2.2	13	0	0.00	8	1.103	0.1760	1.93	0.5791	10.19	14.053	10.61	113	2945	241	2753	101	2713	104	2615	32
BH01R2-4.1	26	0	0.01	5	0.764	0.1760	1.84	0.1707	10.39	4.143	10.78	39	1016	98	1663	88	2611	56	2615	31
BH01R2-9.1	14	0	0.01	4	0.375	0.1767	1.62	0.2470	9.34	6.017	9.67	54	1423	119	1978	84	2549	49	2622	27
BH01R2-9.2	47	1	0.01	23	0.296	0.1772	1.40	0.4757	9.32	11.620	9.59	96	2509	194	2574	90	2616	46	2626	23
BH01R-5.1	33	0	0.01	18	1.511	0.1774	1.73	0.5073	12.60	12.408	12.93	101	2645	273	2636	122	2715	116	2629	29
BH01R2-4.2	17	0	0.01	9	0.874	0.1783	1.60	0.5338	8.82	13.124	9.16	105	2757	198	2689	87	2738	210	2637	27
BH01R2-11.2	23	0	0.01	11	0.594	0.1787	1.51	0.4527	8.13	11.153	8.45	91	2407	163	2536	79	2530	85	2641	25
BH01R-6.1	13	0	0.02	7	1.649	0.1797	2.28	0.5370	12.51	13.307	12.99	105	2771	282	2702	123	2530	206	2650	38
BH01R2-8.1	7	0	0.01	2	1.473	0.1805	2.42	0.2259	9.70	5.622	10.28	49	1313	115	1919	89	2645	68	2658	40
BH01R2-13.1	13	0	0.02	7	-0.272	0.1806	1.35	0.4910	9.43	12.229	9.69	97	2575	200	2622	91	2623	48	2659	22
BH01R2-1.1	23	0	0.01	3	0.822	0.1808	1.85	0.1052	7.73	2.622	8.17	24	645	47	1307	60	2682	60	2660	31
BH01R-11.1	25	1	0.03	12	0.873	0.1809	1.67	0.4740	9.29	11.822	9.64	94	2501	193	2590	90	2664	82	2661	28
BH01R2-3.1	18	0	0.02	6	0.044	0.1813	1.57	0.3358	10.88	8.395	11.19	70	1867	176	2275	102	2637	34	2665	26
BH01R2-7.1	63	1	0.01	5	0.925	0.1820	2.00	0.0734	7.24	1.842	7.75	17	457	32	1061	51	2553	104	2671	33
BH01R-3.1	29	0	-0.00	17	1.349	0.1826	1.66	0.5618	12.85	14.146	13.16	107	2874	298	2760	125	2779	29	2677	27
BH01R2-2.1	9	0	0.02	2	0.893	0.1840	2.17	0.2301	10.87	5.837	11.35	50	1335	131	1952	99	2638	86	2689	36
BH01R2-3.2	44	1	0.02	24	0.449	0.1845	1.54	0.5215	10.71	13.266	11.01	100	2705	237	2699	104	2635	73	2694	25
BH01R2-6.1	23	0	0.01	3	1.088	0.1845	2.05	0.1297	9.81	3.299	10.27	29	786	73	1481	80	2697	88	2694	34
BH01R2-5.2	35	1	0.02	22	0.877	0.1848	1.61	0.5971	11.59	15.212	11.90	112	3018	280	2829	114	2696	47	2696	27
BH01R2-7.2	33	0	0.01	17	0.480	0.1848	1.39	0.4850	9.01	12.355	9.29	95	2549	190	2632	87	2685	39	2696	23
BH01R-9.1	33	1	0.04	16	0.893	0.1848	1.73	0.4645	11.01	11.837	11.35	91	2459	225	2592	107	2558	95	2697	28
BH01R2-10.1	4	0	0.04	2	0.552	0.1857	2.14	0.4614	12.22	11.814	12.67	90	2446	249	2590	119	2602	88	2704	35
BH01R2-6.2	17	0	0.01	9	0.548	0.1856	1.64	0.5080	9.70	13.003	10.03	98	2648	211	2680	95	2783	107	2704	27
BH01R2-6.2	3	0	0.02	2	-0.154	0.1858	1.66	0.5550	9.45	14.218	9.80	105	2846	217	2764	93	2726	90	2705	27
BH01R2-11.1	5	0	0.03	3	-0.412	0.1861	1.82	0.5009	11.74	12.854	12.10	97	2618	253	2669	115	2640	50	2708	30
BH01R-1.1	16	0	0.01	10	1.339	0.1878	2.14	0.5763	11.79	14.923	12.24	108	2934	278	2810	117	2512	148	2723	35
BH01R2-10.2	28	0	0.01	16	0.422	0.1882	1.44	0.5378	9.79	13.953	10.07	102	2774	221	2747	96	2746	34	2726	24
BH01R2-4.2	7	0	0.02	3	-0.146	0.1885	1.42	0.3943	9.15	10.246	9.44	79	2143	167	2457	88	2731	44	2729	23
BH01R-7.1	31	4	0.14	18	-0.775	0.1920	1.75	0.5691	10.20	15.063	10.56	105	2904	239	2819	101	2584	83	2759	29

Continued on Next Page...

Table 6.2 – Continued

Grain .spot	U ppm	Th ppm	Th/U	Pb ppm	$f206\%$ ^{208}corr	Ratios $\frac{^{207}Pb}{^{206}Pb}$ ^{208}corr	$\pm1\sigma$ %	$\frac{^{206}Pb}{^{238}U}$ ^{208}corr	$\pm1\sigma$ %	$\frac{^{207}Pb}{^{235}U}$ ^{208}corr	$\pm1\sigma$	%conc. ^{208}corr	Dates (Ma) $\frac{^{206}Pb}{^{238}U}$ ^{208}corr	$\pm1\sigma$	$\frac{^{207}Pb}{^{235}U}$ ^{208}corr	$\pm1\sigma$	$\frac{^{207}Pb}{^{206}Pb}$ ^{204}corr	$\pm1\sigma$	$\frac{^{207}Pb}{^{206}Pb}$ ^{208}corr	$\pm1\sigma$
BH01R2-8.2	19	0	0.02	10	1.545	0.1948	1.96	0.4848	11.84	13.021	12.24	92	2548	249	2681	116	2704	118	2783	32
BH01R2-1.2	14	0	-0.00	8	1.279	0.1985	1.79	0.5189	10.90	14.198	11.26	96	2694	240	2763	107	2901	34	2814	29
BH01R-8.1	13	0	0.01	9	3.290	0.2010	2.40	0.5765	15.16	15.980	15.64	104	2934	358	2876	151	2941	298	2835	39
BH01R-10.1	26	0	0.01	17	0.958	0.2125	1.45	0.6076	11.28	17.802	11.55	105	3060	275	2979	111	2951	41	2925	23
BH01R2-8.2	8	6	0.79	3	-12.082	0.2662	3.84	0.4437	9.44	16.283	10.62	72	2367	187	2894	102	2623	33	3284	60
MA03 Rutiles (7 analyses)																				
MA03R-1.4	16	1	0.05	11	16.310	0.1633	8.80	0.3978	31.50	8.954	33.75	87	2159	579	2333	318	2637	324	2490	149
MA03R-1.5	13	1	0.06	20	9.783	0.1835	5.83	1.0652	36.49	26.952	37.66	174	4675	1228	3382	386	2260	373	2685	97
MA03R-1.1	23	0	0.01	12	0.649	0.1893	1.65	0.5071	10.96	13.235	11.29	97	2644	238	2697	107	2566	165	2736	27
MA03R-3.4*	16	1	0.04	27	34.911	0.1966	10.12	0.5138	28.37	13.928	31.29	96	2673	623	2745	305	3206	281	2798	166
MA03R-3.1	6	1	0.20	5	5.877	0.2019	5.58	0.7076	23.47	19.700	24.80	121	3449	629	3077	244	2890	349	2842	91
MA03R-4.1	12	31	2.66	8	-57.930	0.4772	3.36	0.8940	9.77	58.817	10.72	99	4117	298	4154	107	2829	251	4172	50
MA03R-2.1	12	31	2.58	9	-48.598	0.4775	4.85	0.9229	11.99	60.760	13.49	101	4215	372	4187	136	2944	117	4173	72
MA04 Rutiles (80 analyses)																				
MA04R-7.3	70	0	0.01	59	2.200	0.1609	1.72	0.7776	11.39	17.250	11.73	150	3708	322	2949	113	2353	69	2465	29
MA04R-9.5	143	1	0.01	99	1.223	0.1747	1.31	0.6573	10.61	15.832	10.85	125	3257	271	2867	104	2539	39	2603	22
MA04R-9.6	185	1	0.00	89	0.279	0.1768	1.14	0.4734	8.92	11.538	9.14	95	2498	185	2568	86	2616	22	2623	19
MA04R2-4.2	175	1	0.01	88	-0.011	0.1775	0.49	0.4962	3.27	12.145	3.37	99	2598	70	2616	32	2622	10	2630	8
MA04R-10.4	314	1	0.00	194	0.942	0.1789	1.12	0.5900	9.62	14.556	9.82	113	2989	230	2787	94	2615	29	2643	19
MA04R2-4.1	107	1	0.01	60	0.050	0.1796	0.64	0.5484	5.53	13.579	5.65	106	2819	126	2721	53	2639	31	2649	11
MA04R-5.8	135	0	0.00	75	0.472	0.1799	1.09	0.5330	7.82	13.220	8.03	104	2754	175	2696	76	2652	22	2652	18
MA04R-9.7	192	1	0.00	105	0.348	0.1799	1.16	0.5302	9.19	13.149	9.41	103	2742	205	2690	89	2644	25	2652	19
MA04R2-5.2	80	0	0.00	48	0.608	0.1802	0.77	0.5825	5.72	14.476	5.87	111	2959	136	2781	56	2645	29	2655	13
MA04R2-3.1	297	0	0.00	146	0.092	0.1804	0.45	0.4824	4.94	11.998	5.02	96	2538	104	2604	47	2655	11	2656	7
MA04R2-5.1	114	0	0.00	62	0.225	0.1809	0.61	0.5301	5.24	13.223	5.35	103	2742	117	2696	51	2634	20	2661	10
MA04R-7.4	121	2	0.01	91	0.872	0.1809	1.21	0.7187	8.80	17.927	9.03	131	3491	237	2986	87	2630	33	2661	20
MA04R2-3.2	379	0	0.00	186	0.041	0.1812	0.40	0.4826	3.12	12.057	3.20	95	2538	66	2609	30	2664	7	2664	7
MA04R2-5.3	140	0	0.00	82	0.110	0.1812	0.52	0.5736	3.20	14.328	3.31	110	2922	75	2772	31	2662	12	2664	9
MA04R-1.4	189	1	0.00	108	0.473	0.1813	1.09	0.5557	8.45	13.891	8.66	107	2849	195	2742	82	2646	25	2665	18
MA04R-11.4	166	0	0.00	90	1.594	0.1815	1.28	0.5047	7.65	12.630	7.91	99	2634	165	2652	75	2676	32	2666	21
MA04R2-2.1	116	0	0.00	71	0.190	0.1816	0.60	0.5959	5.31	14.919	5.42	113	3013	128	2810	52	2674	15	2667	10
MA04R-6.3	364	2	0.00	229	0.827	0.1815	0.97	0.5995	9.74	15.005	9.91	114	3028	235	2816	95	2654	23	2667	16
MA04R-3.4	68	0	0.01	59	0.928	0.1821	1.56	0.8158	11.32	20.479	11.61	144	3845	328	3114	113	2633	46	2672	26
MA04R2-1.3	265	5	0.02	136	-0.145	0.1828	0.50	0.5035	3.92	12.688	4.01	98	2629	85	2657	38	2674	12	2678	8

Continued on Next Page...

Table 6.2 – Continued

						Ratios							Dates (Ma)								
Grain .spot	U ppm	Th ppm	Th/U	Pb ppm	$f206\%$ ^{208}corr	$\frac{^{207}Pb}{^{206}Pb}$ ^{208}corr	$\pm1\sigma$ %	$\frac{^{206}Pb}{^{238}U}$ ^{208}corr	$\pm1\sigma$ %	$\frac{^{207}Pb}{^{235}U}$ ^{208}corr	$\pm1\sigma$	%conc. ^{208}corr	$\frac{^{206}Pb}{^{238}U}$ ^{208}corr	$\pm1\sigma$	$\frac{^{207}Pb}{^{235}U}$ ^{208}corr	$\pm1\sigma$	$\frac{^{207}Pb}{^{206}Pb}$ ^{204}corr	$\pm1\sigma$	$\frac{^{207}Pb}{^{206}Pb}$ ^{208}corr	$\pm1\sigma$
MA04R-5.3	155	0	0.00	109	1.729	0.1827	1.15	0.6523	8.33	16.433	8.55	121	3237	212	2902	82	2646	34	2678	19
MA04R-10.9	207	1	0.00	115	0.148	0.1828	0.99	0.5433	8.76	13.694	8.94	104	2797	199	2729	85	2681	17	2679	16
MA04R-2.12	401	1	0.00	209	0.131	0.1830	0.73	0.5096	6.27	12.859	6.40	99	2655	136	2669	60	2676	13	2680	12
MA04R-6.5	491	4	0.01	258	0.181	0.1829	0.81	0.5122	7.94	12.919	8.08	99	2666	173	2674	76	2672	15	2680	13
MA04R2-1.1	342	0	-0.00	156	0.280	0.1831	0.46	0.4440	5.20	11.210	5.28	88	2368	103	2541	49	2686	11	2682	8
MA04R2-7.1	152	7	0.04	75	-0.382	0.1833	0.72	0.4863	5.96	12.292	6.09	95	2555	126	2627	57	2667	35	2683	12
MA04R-5.7	194	0	0.00	110	0.291	0.1833	0.86	0.5510	6.63	13.925	6.80	105	2829	152	2745	64	2664	19	2683	14
MA04R2-2.2	134	0	0.00	66	0.108	0.1835	0.55	0.4861	3.52	12.296	3.63	95	2554	74	2627	34	2679	13	2684	9
MA04R2-1.4	383	0	0.00	198	0.032	0.1841	0.40	0.5071	3.48	12.871	3.55	98	2644	76	2670	33	2697	8	2690	7
MA04R-10.8	251	1	0.00	128	0.192	0.1843	0.90	0.4961	8.05	12.605	8.21	96	2597	172	2651	77	2666	20	2692	15
MA04R-2.8	312	1	0.00	160	0.170	0.1865	0.76	0.4997	6.48	12.849	6.61	96	2612	139	2669	62	2706	15	2712	12
MA04R-8.8	271	1	0.00	138	0.212	0.1869	0.88	0.4935	7.46	12.718	7.62	95	2586	159	2659	72	2696	19	2715	15
MA04R-12.10	448	1	0.00	222	0.201	0.1872	0.77	0.4811	6.74	12.417	6.87	93	2532	141	2636	65	2715	14	2717	13
MA04R2-6.1	560	0	0.00	358	0.054	0.1873	0.39	0.6245	5.32	16.128	5.38	115	3128	132	2884	51	2717	10	2719	6
MA04R2-8.4	151	2	0.01	89	-0.149	0.1873	0.74	0.5801	4.99	14.982	5.14	108	2949	118	2814	49	2715	25	2719	12
MA04R-8.9	163	1	0.00	84	0.432	0.1874	1.16	0.4939	9.32	12.760	9.54	95	2588	199	2662	90	2697	28	2719	19
MA04R2-7.2	138	17	0.12	66	-1.512	0.1874	0.85	0.4754	4.76	12.283	4.94	92	2507	99	2626	46	2622	44	2720	14
MA04R2-8.1	195	0	0.00	92	0.083	0.1880	0.54	0.4607	5.30	11.942	5.39	90	2443	108	2600	51	2715	11	2725	9
MA04R-2.7	303	1	0.00	179	0.314	0.1893	0.79	0.5705	6.99	14.889	7.13	106	2910	164	2808	68	2721	17	2736	13
MA04R-2.11	341	1	0.00	187	0.091	0.1907	0.73	0.5348	6.49	14.059	6.62	100	2762	146	2754	63	2737	14	2748	12
MA04R-8.4	224	2	0.01	170	0.448	0.1907	0.89	0.7258	8.48	19.086	8.64	128	3518	230	3046	84	2744	17	2748	15
MA04R2-6.2	660	1	0.00	442	0.016	0.1908	0.32	0.6529	3.39	17.175	3.44	118	3239	86	2945	33	2752	6	2749	5
MA04R2-1.2	437	1	0.00	238	0.045	0.1918	0.36	0.5289	3.27	13.987	3.34	99	2737	73	2749	32	2748	7	2758	6
MA04R-11.3	93	0	0.00	61	1.764	0.1925	1.40	0.5968	9.13	15.842	9.41	109	3017	220	2867	90	2747	39	2764	23
MA04R-12.9	453	1	0.00	227	0.096	0.1925	0.73	0.4855	6.65	12.886	6.78	92	2551	140	2671	64	2751	14	2764	12
MA04R-4.4	218	1	0.00	141	0.995	0.1932	1.05	0.6094	8.46	16.232	8.66	111	3067	207	2891	83	2735	28	2770	17
MA04R-11.5	109	0	0.00	62	0.419	0.1935	1.17	0.5476	7.76	14.608	7.99	102	2815	177	2790	76	2741	28	2772	19
MA04R-12.4	373	1	0.00	296	0.726	0.1938	0.88	0.7535	8.72	20.138	8.87	130	3620	242	3098	86	2760	20	2775	14
MA04R-12.3	278	1	0.00	193	1.050	0.1943	0.90	0.6504	8.52	17.423	8.67	116	3230	216	2958	83	2761	22	2779	15
MA04R-8.5	251	1	0.00	149	0.366	0.1954	0.84	0.5704	7.76	15.369	7.91	104	2910	182	2838	76	2778	17	2788	14
MA04R2-9.3	185	0	0.00	118	0.090	0.1966	0.56	0.6177	3.78	16.743	3.89	111	3101	93	2920	37	2801	10	2798	9
MA04R-12.6	415	1	0.00	223	0.115	0.1980	0.66	0.5204	6.54	14.209	6.66	96	2701	144	2764	63	2802	12	2810	11
MA04R-2.9	402	1	0.00	226	0.123	0.1982	0.67	0.5432	6.16	14.841	6.28	99	2797	140	2805	60	2811	12	2811	11
MA04R-12.11	189	1	0.00	114	0.483	0.1985	1.02	0.5754	9.26	15.749	9.45	104	2930	218	2862	90	2802	21	2814	17
MA04R-5.6	244	0	0.00	139	0.309	0.1990	0.77	0.5475	6.22	15.021	6.36	100	2815	142	2817	61	2814	15	2818	13
MA04R-12.5	332	1	0.00	225	0.720	0.1995	0.81	0.6407	7.94	17.620	8.08	113	3192	200	2969	78	2802	18	2822	13
MA04R-12.8	434	1	0.00	231	0.123	0.1997	0.70	0.5138	6.63	14.148	6.75	95	2673	145	2760	64	2824	12	2824	11
MA04R-5.4	179	0	0.00	136	1.348	0.2000	0.94	0.7003	7.86	19.310	8.03	121	3422	209	3057	78	2794	25	2826	15
MA04R-7.5	193	0	0.00	119	0.265	0.2016	0.85	0.5913	6.32	16.437	6.48	105	2995	151	2903	62	2812	18	2839	14

Continued on Next Page...

Table 6.2 – Continued

Grain .spot	U ppm	Th ppm	Th/U	Pb ppm	$f206\%$ ^{208}corr	Ratios $\frac{^{207}Pb}{^{206}Pb}$ ^{208}corr	$\pm1\sigma$ %	$\frac{^{206}Pb}{^{238}U}$ ^{208}corr	$\pm1\sigma$ %	$\frac{^{207}Pb}{^{235}U}$ ^{208}corr	$\pm1\sigma$	%conc. ^{208}corr	Dates (Ma) $\frac{^{206}Pb}{^{238}U}$ ^{208}corr	$\pm1\sigma$	$\frac{^{207}Pb}{^{235}U}$ ^{208}corr	$\pm1\sigma$	$\frac{^{207}Pb}{^{206}Pb}$ ^{204}corr	$\pm1\sigma$	$\frac{^{207}Pb}{^{206}Pb}$ ^{208}corr	$\pm1\sigma$
MA04R-4.5	193	0	0.00	119	0.230	0.2024	0.80	0.5932	6.04	16.552	6.19	106	3002	145	2909	59	2834	16	2845	13
MA04R-4.3	276	1	0.00	218	0.450	0.2032	0.78	0.7511	7.16	21.045	7.30	127	3612	198	3141	71	2838	17	2852	13
MA04R-2.6	391	1	0.00	216	0.194	0.2037	0.72	0.5283	6.79	14.839	6.92	96	2734	151	2805	66	2843	14	2856	12
MA04R-3.7	196	0	0.00	126	0.214	0.2037	0.82	0.6163	6.29	17.313	6.44	108	3095	155	2952	62	2855	15	2856	13
MA04R-7.6	181	0	0.00	113	0.399	0.2039	0.98	0.5922	7.13	16.650	7.31	105	2998	171	2915	70	2860	18	2858	16
MA04R-2.10	372	1	0.00	201	0.113	0.2051	0.68	0.5177	6.30	14.644	6.42	94	2690	139	2792	61	2860	12	2867	11
MA04R-8.6	352	1	0.00	206	0.262	0.2053	0.78	0.5579	7.32	15.794	7.46	100	2858	169	2864	71	2859	15	2869	13
MA04R2-8.3	182	0	0.00	102	0.029	0.2056	0.43	0.5386	3.32	15.270	3.40	97	2778	75	2832	32	2867	9	2871	7
MA04R-8.7	419	1	0.00	217	0.165	0.2067	0.71	0.4967	6.40	14.154	6.53	90	2600	137	2760	62	2875	13	2880	12
MA04R-5.9	199	0	0.00	119	0.226	0.2077	0.79	0.5705	6.57	16.340	6.71	101	2910	154	2897	64	2891	14	2888	13
MA04R-10.6	320	1	0.00	247	0.744	0.2116	0.79	0.7197	8.08	20.998	8.21	120	3495	218	3139	80	2920	16	2918	13
MA04R-3.5	148	0	0.00	129	0.545	0.2154	0.94	0.8162	7.80	24.243	7.97	131	3847	226	3278	78	2912	23	2947	15
MA04R-10.10	429	1	0.00	269	0.132	0.2165	0.63	0.5950	6.61	17.760	6.72	102	3010	159	2977	65	2948	11	2955	10
MA04R2-8.2	250	0	0.00	161	0.026	0.2230	0.36	0.6093	3.24	18.732	3.31	102	3067	79	3028	32	3000	7	3002	6
MA04R-12.7	221	37	0.17	128	-2.174	0.2248	1.33	0.5643	8.95	17.493	9.21	96	2884	208	2962	89	2883	18	3016	21
MA04R-5.5	220	0	0.00	138	0.244	0.2256	0.79	0.5923	6.74	18.422	6.88	99	2999	162	3012	66	3017	15	3021	13
MA04R2-9.2	258	0	0.00	161	0.025	0.2293	0.34	0.5919	2.90	18.713	2.96	98	2997	69	3027	29	3044	7	3047	5
MA04R-10.5	186	1	0.00	154	1.182	0.2311	0.95	0.7509	9.83	23.923	10.00	118	3611	272	3265	98	3046	21	3059	15
MA04R-5.2	187	1	0.00	130	1.460	0.2320	0.92	0.6272	7.84	20.067	8.01	102	3138	195	3095	78	3062	22	3066	15
MA04R2-9.1	219	0	-0.00	177	0.095	0.2378	0.38	0.7546	4.88	24.742	4.94	117	3624	135	3298	48	3116	8	3105	6
MA04R-10.7	348	1	0.00	234	0.138	0.2452	0.63	0.6258	7.13	21.153	7.24	99	3133	177	3146	70	3153	10	3154	10
MA05 Rutiles (46 analyses)																				
MA05R-5.1	5	0	0.03	3	1.414	0.1724	2.31	0.4907	4.99	11.661	5.76	100	2574	106	2578	54	2698	55	2581	39
MA05R-6.1	8	1	0.07	5	2.553	0.1745	2.42	0.5359	5.82	12.890	6.58	106	2766	131	2672	62	2610	58	2601	40
MA05R-13.1	11	0	0.00	6	0.650	0.1750	1.51	0.4750	4.41	11.460	4.84	96	2505	92	2561	45	2603	36	2606	25
MA05R-14.2	17	0	0.00	10	1.714	0.1750	1.28	0.5251	4.63	12.669	4.96	104	2721	103	2655	47	2616	39	2606	21
MA05R-10.1	5	0	0.00	3	3.813	0.1753	2.20	0.4740	4.20	11.457	4.97	96	2501	87	2561	46	2812	43	2609	37
MA05R2-8.3	75	1	0.01	45	0.178	0.1754	1.04	0.5921	7.87	14.321	8.06	115	2998	189	2771	77	2597	39	2610	17
MA05R2-8.2	70	0	0.01	32	0.585	0.1759	1.15	0.4371	8.66	10.602	8.88	89	2338	170	2489	83	2602	51	2615	19
MA05R-2.1	32	0	0.00	17	0.207	0.1760	0.93	0.5346	4.32	12.978	4.53	106	2761	97	2678	43	2609	22	2616	16
MA05R2-8.1	66	0	0.00	40	0.350	0.1761	0.97	0.5864	8.07	14.239	8.25	114	2975	192	2766	78	2628	46	2617	16
MA05R2-11.1	79	0	-0.00	47	0.247	0.1767	0.84	0.5754	6.41	14.018	6.57	112	2930	151	2751	62	2648	22	2622	14
MA05R-9.1	7	0	0.02	4	2.969	0.1768	1.99	0.4988	4.64	12.157	5.27	99	2608	99	2617	49	2608	74	2623	33
MA05R-12.1	8	0	0.03	4	2.545	0.1768	2.03	0.4932	4.74	12.027	5.39	99	2585	101	2606	51	2621	73	2624	34
MA05R-11.1	21	1	0.04	13	1.309	0.1770	1.12	0.5913	3.31	14.429	3.63	114	2995	79	2778	34	2633	28	2625	19
MA05R-8.1	7	0	0.01	4	2.351	0.1770	2.10	0.4715	5.25	11.507	5.89	95	2490	108	2565	55	2565	93	2625	35

Continued on Next Page...

Table 6.2 – Continued

Grain .spot	U ppm	Th ppm	Th/U	Pb ppm	$f206\%$ ^{208}corr	Ratios $\frac{^{207}Pb}{^{206}Pb}$ ^{208}corr	$\pm1\sigma$ %	$\frac{^{206}Pb}{^{238}U}$ ^{208}corr	$\pm1\sigma$ %	$\frac{^{207}Pb}{^{235}U}$ ^{208}corr	$\pm1\sigma$	%conc. ^{208}corr	Dates (Ma) $\frac{^{206}Pb}{^{238}U}$ ^{208}corr	$\pm1\sigma$	$\frac{^{207}Pb}{^{235}U}$ ^{208}corr	$\pm1\sigma$	$\frac{^{207}Pb}{^{206}Pb}$ ^{204}corr	$\pm1\sigma$	$\frac{^{207}Pb}{^{206}Pb}$ ^{208}corr	$\pm1\sigma$
MA05R2-11.2	94	0	0.00	49	0.127	0.1776	0.68	0.5138	4.37	12.582	4.50	102	2673	96	2649	42	2635	13	2631	11
MA05R-7.1	24	0	0.00	14	1.827	0.1778	1.25	0.5335	5.31	13.082	5.61	105	2756	119	2686	53	2589	42	2633	21
MA05R2-10.1	62	0	0.00	31	0.441	0.1780	0.96	0.4770	7.26	11.709	7.44	95	2514	151	2581	70	2652	45	2635	16
MA05R-2.2	25	0	0.00	14	0.255	0.1782	1.06	0.5427	4.80	13.333	5.04	106	2795	109	2704	48	2641	22	2636	18
MA05R2-10.2	62	0	0.00	30	0.237	0.1784	1.00	0.4732	6.46	11.637	6.66	95	2497	134	2576	62	2640	35	2638	17
MA05R-1.2	11	0	0.00	6	0.339	0.1785	1.44	0.5241	5.38	12.900	5.74	103	2717	119	2672	54	2639	39	2639	24
MA05R2-1.1	31	0	0.00	18	0.513	0.1786	1.12	0.5603	7.87	13.800	8.09	109	2868	182	2736	77	2649	39	2640	19
MA05R2-5.2	48	0	0.00	27	0.183	0.1790	0.89	0.5498	4.87	13.567	5.06	107	2824	111	2720	48	2637	38	2643	15
MA05R-14.1	15	0	0.00	8	1.447	0.1790	1.39	0.5280	5.12	13.032	5.47	103	2733	114	2682	52	2574	51	2644	23
MA05R-4.1	18	0	0.00	9	0.332	0.1793	1.10	0.5130	3.94	12.681	4.22	101	2669	86	2656	40	2634	25	2646	18
MA05R2-8.4	94	1	0.01	61	0.144	0.1794	0.79	0.6357	6.37	15.729	6.52	120	3172	160	2860	62	2648	28	2648	13
MA05R2-1.2	56	0	0.00	32	0.043	0.1799	0.79	0.5631	4.77	13.965	4.93	109	2880	111	2747	47	2655	13	2651	13
MA05R-15.1	41	0	0.00	23	0.818	0.1799	0.79	0.5470	3.57	13.567	3.75	106	2813	81	2720	35	2649	20	2652	13
MA05R-1.1	14	0	0.00	7	0.174	0.1800	1.28	0.5077	4.97	12.603	5.29	100	2647	108	2650	50	2649	24	2653	21
MA05R2-9.2	48	0	0.00	25	0.264	0.1805	0.96	0.5179	5.56	12.893	5.76	101	2690	122	2672	54	2696	50	2658	16
MA05R-2.3	36	0	0.01	19	0.363	0.1806	0.94	0.5209	4.23	12.971	4.44	102	2703	93	2678	42	2669	19	2659	16
MA05R2-9.1	35	0	0.00	23	0.788	0.1817	1.26	0.6126	8.00	15.350	8.25	115	3081	196	2837	79	2705	115	2669	21
MA05R-11.2	19	9	0.51	14	2.173	0.1827	2.50	0.5996	3.47	15.103	4.52	113	3028	84	2822	43	2620	41	2677	41
MA05R2-2.1	37	0	0.00	21	0.262	0.1831	0.94	0.5567	6.64	14.057	6.82	106	2853	153	2754	65	2682	31	2681	16
MA05R2-5.1	37	0	0.00	20	0.326	0.1831	0.99	0.5283	6.32	13.336	6.52	102	2734	141	2704	62	2669	30	2681	16
MA05R2-7.1	27	1	0.05	15	0.302	0.1890	1.73	0.5488	11.44	14.299	11.78	103	2820	262	2770	112	2686	133	2733	28
MA05R2-6.2	72	8	0.11	39	-1.215	0.1905	1.10	0.5308	6.48	13.939	6.71	100	2745	145	2746	64	2629	22	2746	18
MA05R2-3.1	22	0	-0.01	8	2.454	0.1910	2.05	0.3360	11.19	8.849	11.62	68	1867	181	2323	106	2924	145	2751	34
MA05R2-6.1	76	9	0.12	41	-1.286	0.1910	1.18	0.5322	7.50	14.015	7.74	100	2751	168	2751	73	2675	20	2751	19
MA05R2-2.2	45	7	0.16	25	-2.005	0.1940	1.07	0.5553	5.71	14.858	5.94	103	2847	132	2806	57	2605	50	2777	18
MA05R-1.3	16	5	0.33	10	-2.345	0.2036	2.36	0.6127	4.44	17.203	5.28	108	3081	109	2946	51	2579	45	2855	38
MA05R2-7.2	27	14	0.50	13	-5.585	0.2380	3.06	0.4801	11.09	15.753	11.87	81	2528	232	2862	114	2780	41	3107	49
MA05R-3.1	4	13	2.96	5	0.092	0.2820	19.15	0.6105	8.37	23.737	21.84	91	3072	205	3258	216	2714	179	3374	303
MA05R2-4.3	16	1	0.08	13	-0.106	0.2918	2.25	0.7142	18.94	28.735	19.35	101	3474	510	3445	192	3347	67	3427	35
MA05R2-4.1	89	1	0.01	32	0.794	0.3339	1.09	0.3044	8.21	14.016	8.42	47	1713	124	2751	80	3613	42	3635	17
MA05R2-4.2	11	2	0.16	17	-0.904	0.3828	2.28	1.3162	21.44	69.472	21.85	141	5415	790	4321	222	3800	38	3843	34
MA05R2-4.4	27	1	0.03	46	-0.045	0.3855	0.89	1.4400	13.13	76.536	13.27	149	5750	500	4418	134	3854	18	3853	13
MA07 Rutiles (12 analyses)																				
MA07R2-5.1	17	10	0.59	26	-6.039	0.2435	5.57	1.4442	22.60	48.493	23.94	183	5761	866	3962	243	2891	216	3143	89
MA07R2-1.2	19	9	0.47	14	-5.487	0.2482	3.07	0.7038	14.22	24.081	14.92	108	3435	379	3272	146	2917	109	3173	49
MA07R2-7.2	23	10	0.41	16	-5.056	0.2606	2.69	0.6474	12.53	23.262	13.15	99	3218	318	3238	129	2979	58	3250	42

Continued on Next Page...

Table 6.2 – Continued

Grain .spot	U ppm	Th ppm	Th/U	Pb ppm	$f206\%$ ^{208}corr	Ratios $\frac{^{207}Pb}{^{206}Pb}$ ^{208}corr	$\pm1\sigma$ %	$\frac{^{206}Pb}{^{238}U}$ ^{208}corr	$\pm1\sigma$ %	$\frac{^{207}Pb}{^{235}U}$ ^{208}corr	$\pm1\sigma$	%conc. ^{208}corr	Dates (Ma) $\frac{^{206}Pb}{^{238}U}$ ^{208}corr	$\pm1\sigma$	$\frac{^{207}Pb}{^{235}U}$ ^{208}corr	$\pm1\sigma$	$\frac{^{207}Pb}{^{206}Pb}$ ^{204}corr	$\pm1\sigma$	$\frac{^{207}Pb}{^{206}Pb}$ ^{208}corr	$\pm1\sigma$
MA07R2-3.1	25	30	1.18	17	13.821	0.2940	6.08	0.3211	12.00	13.020	14.12	52	1795	188	2681	134	2889	355	3439	95
MA07R2-7.1	25	35	1.42	15	-23.925	0.3573	4.23	0.6658	13.05	32.807	14.22	88	3290	337	3575	141	2886	56	3739	64
MA07R2-1.4	36	42	1.17	24	-10.350	0.3595	2.72	0.5642	9.20	27.964	9.92	77	2884	214	3418	98	3262	64	3748	41
MA07R2-4.1	4	6	1.52	4	0.488	0.3859	6.59	0.6694	18.80	35.617	20.68	86	3304	487	3656	207	3387	253	3855	100
MA07R2-1.3	33	129	3.89	19	-123.518	0.6202	8.19	1.0753	11.85	91.954	15.22	103	4706	396	4602	154	2748	74	4556	84
MA07R2-1.1	22	116	5.17	24	-316.884	0.7933	20.89	3.5717	18.86	390.658	29.84	213	9798	957	6062	312	3163	56	4600	13
MA07R2-2.1	8	37	4.38	6	-174.045	0.6799	7.83	1.5788	12.76	148.019	15.78	133	6107	505	5081	161	2908	164	4600	14
MA07R2-3.1	21	104	4.92	18	-183.407	0.7426	20.00	1.4438	19.82	147.832	29.87	125	5760	758	5080	311	3241	166	4600	53
MA07R2-9.1	19	90	4.82	16	-223.292	0.7478	16.25	2.1422	17.68	220.867	25.46	160	7381	781	5485	263	3152	85	4600	15
MA11 Rutiles (38 analyses)																				
MA11R2-9.1	87	1	0.02	76	-0.213	0.1644	0.38	0.8670	3.65	19.658	3.71	161	4025	109	3075	36	2483	6	2502	6
MA11R2-1.2	28	0	0.00	31	0.159	0.1718	0.63	1.0923	8.28	25.877	8.38	185	4759	279	3342	82	2574	12	2575	11
MA11R2-10.1	31	1	0.02	18	0.542	0.1761	1.53	0.5650	9.24	13.715	9.55	110	2887	215	2730	91	2663	44	2616	25
MA11R2-5.2	7	0	0.01	4	-0.153	0.1774	1.19	0.6405	7.18	15.664	7.42	121	3191	181	2857	71	2625	25	2628	20
MA11R2-1.1	44	0	0.01	20	0.143	0.1780	0.78	0.4346	6.73	10.666	6.87	88	2326	131	2494	64	2626	15	2634	13
MA11R2-9.2	27	1	0.04	14	-0.475	0.1779	0.83	0.5019	5.37	12.313	5.54	100	2622	116	2629	52	2607	14	2634	14
MA11R2-4.1	8	0	0.03	4	-0.333	0.1782	1.42	0.5280	9.30	12.975	9.58	104	2733	207	2678	91	2609	23	2636	24
MA11R2-5.1	29	0	0.00	18	0.744	0.1787	1.21	0.5755	7.23	14.175	7.48	111	2930	170	2761	71	2642	57	2640	20
MA11R2-6.1	24	0	0.00	15	1.082	0.1791	1.51	0.5895	8.93	14.554	9.24	113	2987	214	2787	88	2636	73	2644	25
MA11R2-4.1	12	0	0.03	9	1.470	0.1793	2.02	0.6715	11.43	16.599	11.86	125	3312	296	2912	114	2829	124	2646	33
MA11R2-8.1	11	0	0.03	6	-0.403	0.1792	1.56	0.4963	9.90	12.265	10.21	98	2598	212	2625	96	2634	62	2646	26
MA11R2-7.2	20	0	0.01	11	0.311	0.1801	1.44	0.5246	7.60	13.029	7.92	102	2719	169	2682	75	2608	76	2654	24
MA11R2-6.2	169	6	0.04	80	-0.368	0.1808	0.46	0.4690	4.73	11.691	4.81	93	2479	97	2580	45	2624	9	2660	8
MA11R2-7.1	28	0	0.00	16	1.761	0.1811	1.52	0.5243	8.21	13.092	8.53	102	2717	182	2686	81	2692	86	2663	25
MA11R2-8.3	9	0	0.04	4	-0.515	0.1812	1.78	0.4685	10.99	11.706	11.35	93	2477	226	2581	107	2643	36	2664	29
MA11R2-3.1	10	0	0.01	5	-0.177	0.1818	1.31	0.5324	9.19	13.348	9.44	103	2752	206	2705	89	2649	37	2670	22
MA11R2-1.3	27	0	0.02	9	0.003	0.1823	1.20	0.3137	8.69	7.887	8.92	66	1759	134	2218	81	2661	21	2674	20
MA11R2-3.2	11	0	0.02	6	-0.182	0.1829	1.07	0.5059	7.04	12.758	7.26	98	2639	153	2662	68	2635	30	2679	18
MA11R2-7.2	5	0	0.02	2	-0.213	0.1828	1.43	0.4516	8.05	11.384	8.35	90	2402	161	2555	78	2658	25	2679	24
MA11R2-8.2	10	0	0.04	5	-0.490	0.1831	1.88	0.4935	11.52	12.458	11.90	96	2586	245	2640	112	2653	24	2681	31
MA11R2-8.1	82	0	0.00	43	0.375	0.1834	0.83	0.5079	6.33	12.843	6.48	99	2647	137	2668	61	2671	23	2684	14
MA11R2-10.1	10	0	0.01	5	-0.117	0.1843	1.06	0.4596	6.70	11.677	6.91	91	2438	136	2579	65	2700	77	2692	17
MA11R2-5.1	14	0	0.01	10	-0.100	0.1860	0.75	0.6927	5.22	17.768	5.36	125	3393	138	2977	52	2700	12	2707	12
MA11R2-2.1	190	0	-0.00	109	0.191	0.1868	0.59	0.5591	6.13	14.397	6.23	105	2863	142	2776	59	2718	12	2714	10
MA11R2-1.1	41	2	0.04	26	0.397	0.1873	1.67	0.6180	12.30	15.960	12.62	114	3102	303	2874	121	2594	72	2719	28
MA11R2-5.3	16	0	0.01	7	-0.077	0.1874	0.76	0.4485	4.80	11.587	4.95	88	2388	96	2572	46	2720	24	2719	12

Continued on Next Page...

Table 6.2 – Continued

Grain .spot	U ppm	Th ppm	Th/U	Pb ppm	$f206\%$ ^{208}corr	Ratios $\frac{^{207}Pb}{^{206}Pb}$ ^{208}corr	$\pm1\sigma$ %	$\frac{^{206}Pb}{^{238}U}$ ^{208}corr	$\pm1\sigma$ %	$\frac{^{207}Pb}{^{235}U}$ ^{208}corr	$\pm1\sigma$	%conc. ^{208}corr	Dates (Ma) $\frac{^{206}Pb}{^{238}U}$ ^{208}corr	$\pm1\sigma$	$\frac{^{207}Pb}{^{235}U}$ ^{208}corr	$\pm1\sigma$	$\frac{^{207}Pb}{^{206}Pb}$ ^{204}corr	$\pm1\sigma$	$\frac{^{207}Pb}{^{206}Pb}$ ^{208}corr	$\pm1\sigma$
MA11R2-6.1	31	0	0.01	17	-0.171	0.1876	0.67	0.5174	5.16	13.384	5.28	99	2688	113	2707	50	2699	19	2721	11
MA11R2-11.5	165	1	0.01	101	-0.011	0.1920	0.49	0.5973	4.07	15.814	4.16	109	3019	98	2866	40	2767	13	2759	8
MA11R2-2.1	20	0	0.01	12	-0.182	0.1941	1.01	0.5665	8.97	15.157	9.15	104	2893	209	2825	87	2759	19	2777	17
MA11R2-2.2	21	0	0.02	14	-0.235	0.1959	0.91	0.6452	7.41	17.428	7.58	115	3209	187	2959	73	2774	14	2792	15
MA11R2-11.1	94	0	0.00	49	0.109	0.1963	0.77	0.5037	6.55	13.634	6.69	94	2629	141	2725	63	2796	21	2796	13
MA11R2-11.6	81	2	0.02	41	0.821	0.1972	0.82	0.4782	5.43	12.999	5.59	90	2519	113	2680	53	2813	21	2803	13
MA11R2-11.2	45	0	0.00	25	0.133	0.2040	0.87	0.5386	6.94	15.148	7.10	97	2777	157	2825	68	2871	18	2858	14
MA11R2-9.1	110	1	0.01	70	0.272	0.2177	0.80	0.6016	7.86	18.057	7.99	102	3036	190	2993	77	2967	22	2964	13
MA11R2-11.3	108	0	0.00	61	0.052	0.2198	0.59	0.5386	4.87	16.322	4.98	93	2777	110	2896	48	2980	10	2979	9
MA11R2-7.1	4	2	0.46	2	-6.291	0.2286	2.22	0.5284	8.38	16.657	8.93	90	2735	187	2915	86	2648	65	3042	36
MA11R2-3.1	69	59	0.86	43	-12.415	0.2728	3.21	0.6626	10.59	24.921	11.44	99	3277	272	3305	112	2689	53	3322	50
MA11R2-3.2	43	38	0.87	28	-12.507	0.2735	3.46	0.6959	10.56	26.240	11.52	102	3405	280	3356	113	2695	42	3326	54
MA13 Rutiles (31 analyses)																				
MA13R2-5.1	22	0	0.01	13	-0.072	0.1778	0.63	0.6162	4.31	15.105	4.43	118	3095	106	2822	42	2625	12	2632	10
MA13R2-16.1	31	0	0.01	15	-0.141	0.1779	0.67	0.4835	4.71	11.861	4.84	97	2543	99	2594	45	2613	13	2633	11
MA13R2-9.1	35	0	0.01	17	-0.144	0.1780	0.72	0.4972	5.66	12.203	5.79	99	2602	121	2620	54	2605	14	2634	12
MA13R2-7.1	319	0	0.00	183	0.164	0.1783	0.54	0.5620	5.83	13.819	5.92	109	2875	135	2737	56	2634	12	2637	9
MA13R2-15.1	42	0	0.01	19	-0.081	0.1785	0.61	0.4343	4.88	10.688	5.00	88	2325	95	2496	46	2638	13	2639	10
MA13R2-4.3	87	1	0.01	49	0.079	0.1794	0.69	0.5515	3.96	13.644	4.10	107	2831	91	2725	39	2650	20	2648	11
MA13R2-17.1	32	0	0.00	17	-0.035	0.1796	0.56	0.5280	4.10	13.077	4.20	103	2733	91	2685	40	2649	10	2649	9
MA13R2-14.1	54	0	0.00	31	-0.045	0.1803	0.49	0.5547	3.92	13.793	4.01	107	2845	90	2736	38	2649	9	2656	8
MA13R2-4.1	92	0	-0.00	51	0.263	0.1806	0.72	0.5448	5.40	13.561	5.53	105	2803	123	2720	52	2681	34	2658	12
MA13R2-5.1	237	3	0.01	119	0.018	0.1811	0.56	0.4941	5.17	12.335	5.27	97	2588	110	2630	50	2656	13	2663	9
MA13R2-3.1	104	3	0.03	57	-0.218	0.1814	0.72	0.5384	5.38	13.464	5.51	104	2777	121	2713	52	2638	16	2665	12
MA13R2-10.1	52	1	0.02	24	-0.238	0.1814	0.59	0.4543	4.33	11.365	4.45	91	2415	87	2554	42	2646	15	2666	10
MA13R2-13.1	39	0	0.01	20	-0.071	0.1815	0.60	0.5070	4.68	12.687	4.79	99	2644	101	2657	45	2660	10	2666	10
MA13R2-4.2	106	0	0.00	58	0.130	0.1815	0.62	0.5394	3.70	13.495	3.83	104	2781	84	2715	36	2653	16	2666	10
MA13R2-6.1	68	0	0.01	43	0.112	0.1816	0.76	0.6202	5.74	15.528	5.88	117	3111	142	2848	56	2660	27	2667	13
MA13R2-7.1	89	0	0.00	48	-0.040	0.1816	0.43	0.5347	4.13	13.388	4.20	104	2761	93	2707	40	2663	8	2667	7
MA13R2-3.2	98	6	0.06	57	-0.691	0.1818	0.75	0.5743	5.52	14.395	5.66	110	2925	130	2776	54	2611	15	2669	12
MA13R2-1.1	221	8	0.04	111	-0.291	0.1820	0.62	0.4949	5.32	12.417	5.43	97	2592	114	2636	51	2652	10	2671	10
MA13R2-2.1	46	0	0.01	23	-0.072	0.1825	0.57	0.4991	4.55	12.561	4.66	98	2610	98	2647	44	2670	9	2676	9
MA13R2-11.1	55	0	0.00	25	-0.055	0.1827	0.50	0.4545	4.09	11.449	4.19	90	2415	82	2560	39	2671	8	2677	8
MA13R2-8.1	60	4	0.06	29	-0.837	0.1827	0.78	0.4785	4.65	12.055	4.81	94	2521	97	2609	45	2608	12	2678	13
MA13R2-1.1	61	0	0.01	29	-0.078	0.1830	0.53	0.4677	4.45	11.803	4.55	92	2473	91	2589	43	2672	11	2681	9
MA13R2-12.1	37	0	0.00	20	-0.046	0.1831	0.57	0.5246	4.26	13.246	4.37	101	2719	95	2697	41	2692	12	2681	9

Continued on Next Page...

Table 6.2 – Continued

Grain .spot	U ppm	Th ppm	Th/U	Pb ppm	$f206\%$ ^{208}corr	Ratios $\frac{^{207}Pb}{^{206}Pb}$ ^{208}corr	$\pm1\sigma$ %	$\frac{^{206}Pb}{^{238}U}$ ^{208}corr	$\pm1\sigma$ %	$\frac{^{207}Pb}{^{235}U}$ ^{208}corr	$\pm1\sigma$	%conc. ^{208}corr	Dates (Ma) $\frac{^{206}Pb}{^{238}U}$ ^{208}corr	$\pm1\sigma$	$\frac{^{207}Pb}{^{235}U}$ ^{208}corr	$\pm1\sigma$	$\frac{^{207}Pb}{^{206}Pb}$ ^{204}corr	$\pm1\sigma$	$\frac{^{207}Pb}{^{206}Pb}$ ^{208}corr	$\pm1\sigma$
MA13R2-2.2	109	0	0.00	63	0.080	0.1850	0.56	0.5661	3.48	14.442	3.60	107	2892	81	2779	34	2692	13	2699	9
MA13R2-4.2	52	0	0.00	25	-0.047	0.1854	0.51	0.4734	4.03	12.101	4.13	92	2498	84	2612	39	2700	9	2702	8
MA13R2-10.2	46	5	0.11	22	-1.504	0.1877	0.89	0.4801	4.60	12.422	4.79	93	2528	96	2637	45	2615	10	2722	15
MA13R2-4.1	50	0	0.00	25	-0.033	0.1885	0.49	0.4850	4.07	12.605	4.16	93	2549	86	2651	39	2737	15	2729	8
MA13R2-3.1	23	4	0.18	14	-2.592	0.1973	0.82	0.6194	4.34	16.852	4.52	111	3108	107	2926	43	2637	35	2804	13
MA13R2-8.1	122	41	0.34	70	-4.998	0.2185	0.75	0.5901	5.31	17.776	5.46	101	2990	127	2978	53	2655	17	2970	12
MA13R2-6.1	12	19	1.50	7	-26.741	0.3438	1.50	0.6847	5.08	32.461	5.47	91	3363	133	3564	54	2608	33	3680	23
MA13R2-2.1*	130	412	3.17	104	-41.079	0.4970	0.97	0.9246	5.04	63.365	5.25	100	4221	156	4229	53	3012	21	4232	14
MH09 Rutiles (30 analyses)																				
MH09R2-2.1	9	0	0.01	3	0.770	0.1722	1.66	0.3089	8.41	7.334	8.78	67	1735	128	2153	79	2576	64	2579	28
MH09R2-11.1	87	0	-0.00	56	1.592	0.1732	1.15	0.5989	9.02	14.300	9.24	117	3026	218	2770	88	2598	41	2589	19
MH09R2-8.1	59	1	0.01	7	0.744	0.1737	1.56	0.1136	6.96	2.720	7.33	27	693	46	1334	54	2559	62	2594	26
MH09R2-5.1	39	0	0.01	8	0.360	0.1758	1.10	0.2097	7.07	5.083	7.29	47	1227	79	1833	62	2581	30	2613	18
MH09R2-7.1	48	0	0.01	6	0.555	0.1763	1.35	0.1295	6.96	3.148	7.25	30	785	51	1444	56	2611	34	2618	22
MH09R2-12.1	81	0	0.00	51	0.673	0.1772	0.83	0.6007	5.89	14.677	6.05	115	3033	142	2795	58	2595	28	2627	14
MH09R2-6.1	132	0	0.00	58	0.471	0.1775	0.89	0.4289	6.63	10.498	6.80	87	2301	128	2480	63	2642	31	2630	15
MH09R2-13.1	31	0	0.01	19	2.486	0.1777	1.73	0.5557	9.96	13.611	10.33	108	2849	230	2723	98	2624	71	2631	29
MH09R2-1.1	27	0	0.00	14	2.766	0.1778	1.97	0.4768	11.15	11.687	11.57	95	2513	232	2580	109	2717	93	2632	33
MH09R2-5.1	108	0	0.00	50	0.390	0.1781	0.79	0.4465	6.24	10.968	6.39	90	2380	124	2520	60	2630	32	2636	13
MH09R2-14.1	8	0	0.01	4	-0.054	0.1785	1.12	0.4585	7.53	11.287	7.75	92	2433	153	2547	72	2662	29	2639	19
MH09R2-10.1	138	0	0.00	82	0.934	0.1787	0.98	0.5626	8.39	13.858	8.56	109	2877	195	2740	81	2621	41	2640	16
MH09R2-9.1	23	0	0.01	3	0.866	0.1787	1.71	0.1423	6.85	3.504	7.27	32	857	55	1528	57	2703	26	2640	28
MH09R2-11.1	5	0	0.01	3	-0.150	0.1787	1.27	0.5489	7.45	13.527	7.71	107	2821	170	2717	73	2633	23	2641	21
MH09R2-4.1	84	1	0.01	6	0.442	0.1791	1.39	0.0724	5.58	1.787	5.92	17	450	24	1041	39	2626	38	2645	23
MH09R2-12.1	34	0	0.00	13	-0.034	0.1792	0.64	0.3911	4.70	9.665	4.82	80	2128	85	2403	44	2646	13	2646	11
MH09R2-13.1	28	0	0.00	13	-0.035	0.1793	0.67	0.4569	4.92	11.292	5.04	92	2426	99	2548	47	2638	12	2646	11
MH09R2-17.1	31	0	0.00	13	-0.000	0.1794	0.62	0.3996	4.62	9.886	4.74	82	2167	85	2424	44	2664	22	2647	10
MH09R2-7.1	107	3	0.03	54	0.070	0.1794	0.85	0.4926	6.28	12.183	6.44	98	2582	134	2619	61	2639	17	2647	14
MH09R2-16.1	19	0	0.01	8	-0.063	0.1797	0.87	0.4092	6.37	10.138	6.54	83	2211	119	2447	61	2653	27	2650	15
MH09R2-4.1	196	6	0.03	112	-0.180	0.1801	0.69	0.5592	5.95	13.884	6.08	108	2863	138	2742	58	2611	18	2653	11
MH09R2-9.1	44	0	0.00	26	1.409	0.1801	1.18	0.5485	6.87	13.623	7.11	106	2819	157	2724	67	2629	46	2654	20
MH09R2-10.1	82	1	0.01	15	0.232	0.1802	0.97	0.1793	5.86	4.455	6.06	40	1063	57	1723	50	2641	22	2655	16
MH09R2-8.1	89	0	-0.00	48	0.498	0.1803	0.80	0.5272	5.62	13.108	5.78	103	2730	125	2687	55	2664	27	2656	13
MH09R2-6.1	6	0	0.03	9	-0.195	0.1807	1.10	1.6805	11.00	41.869	11.19	239	6356	445	3816	111	2614	19	2659	18
MH09R2-3.1	74	1	0.01	16	0.068	0.1808	0.75	0.2110	5.34	5.261	5.48	46	1234	60	1863	47	2646	15	2660	12
MH09R2-2.1	191	0	-0.00	103	0.541	0.1840	0.60	0.5194	5.23	13.174	5.34	100	2697	115	2692	50	2684	15	2689	10

Continued on Next Page...

Table 6.2 – Continued

Grain .spot	U ppm	Th ppm	Th/U	Pb ppm	$f206\%$ ^{208}corr	Ratios $\frac{^{207}Pb}{^{206}Pb}$ ^{208}corr	$\pm1\sigma$ %	$\frac{^{206}Pb}{^{238}U}$ ^{208}corr	$\pm1\sigma$ %	$\frac{^{207}Pb}{^{235}U}$ ^{208}corr	$\pm1\sigma$	%conc. ^{208}corr	Dates (Ma) $\frac{^{206}Pb}{^{238}U}$ ^{208}corr	$\pm1\sigma$	$\frac{^{207}Pb}{^{235}U}$ ^{208}corr	$\pm1\sigma$	$\frac{^{207}Pb}{^{206}Pb}$ ^{204}corr	$\pm1\sigma$	$\frac{^{207}Pb}{^{206}Pb}$ ^{208}corr	$\pm1\sigma$
MH09R2-1.1	4	0	-0.01	1	2.959	0.1993	5.73	0.2647	20.73	7.277	22.19	54	1514	280	2146	201	2820	410	2821	94
MH09R2-15.1	25	7	0.28	12	-4.047	0.2078	2.19	0.4953	7.27	14.193	7.85	90	2594	155	2763	75	2634	30	2889	36
MH09R2-1.2	23	8	0.35	13	-4.417	0.2154	2.12	0.5708	9.42	16.950	9.91	99	2911	221	2932	95	2626	62	2946	34

$f206\%$ = 100 x (common ^{206}Pb/total ^{206}Pb)
^{207}Pb/^{206}Pb 204corr = ^{204}Pb-corrected ^{207}Pb/^{206}Pb ratio
^{206}Pb/^{238}U 204corr = ^{204}Pb-corrected ^{206}Pb/^{238}U ratio
^{207}Pb/^{235}U 204corr = ^{204}Pb-corrected ^{207}Pb/^{235}U ratio
%c = % Concordance
^{206}Pb/^{238}U date = ^{208}Pb-corrected ^{206}Pb/^{238}U date
^{207}Pb/^{235}U date = ^{208}Pb-corrected ^{207}Pb/^{235}U date
^{207}Pb/^{206}Pb date = ^{208}Pb-corrected ^{207}Pb/^{206}Pb date

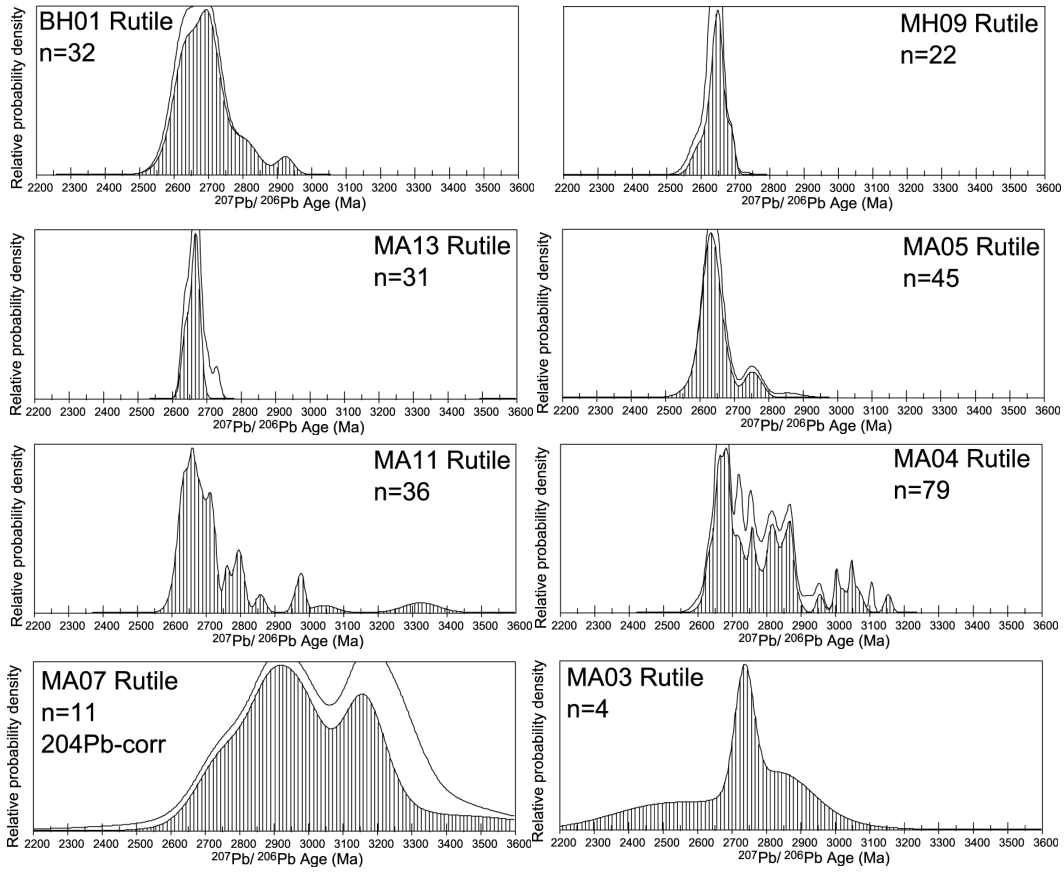

Figure 6.3: Gaussian summation probability density plots for rutile samples from the Maynard Hills (MH09), Brooking Hills (BH01), and Mt. Alfred (MA03, MA04, MA05, MA07, MA11, and MA13). Plots for MA07 are ^{204}Pb corrected, and sample MA03 only includes partial dataset (see text for discussion)

Rutile data summarized in Wetherill Concordia plots (Figure 6.4) shows data that is ±10% of concordia. Robust datasets were collected for samples BH01, MA04, MA05, MA11, MA13 and MH09 due to their high quality rutiles - whereas MA07 and MA03 yielded few pristine rutiles and few decent results.

A summary of rutile age groups (Table 6.3) shows that many samples have one or more age groups in common. The youngest groupings of ca. 2589±19 for sample MH09 is comprised of only three analyses, and may be due to Pb-loss or the presence of disturbed zones within the rutiles. The second youngest age groups of 2626±30, 2636±7, 2636±13 and 2643±7 Ma (Samples MA04, MA05, MA13 and MH09, respectively) are very close in age to the bulk of the rutile standard ages. Brooking Hills sample BH01 has a simple population of rutile ages comprised of a group of 23 analyses indicating the date of 2660±16 Ma, plus a group of 5 analyses indicating a date of 2754±45 Ma.

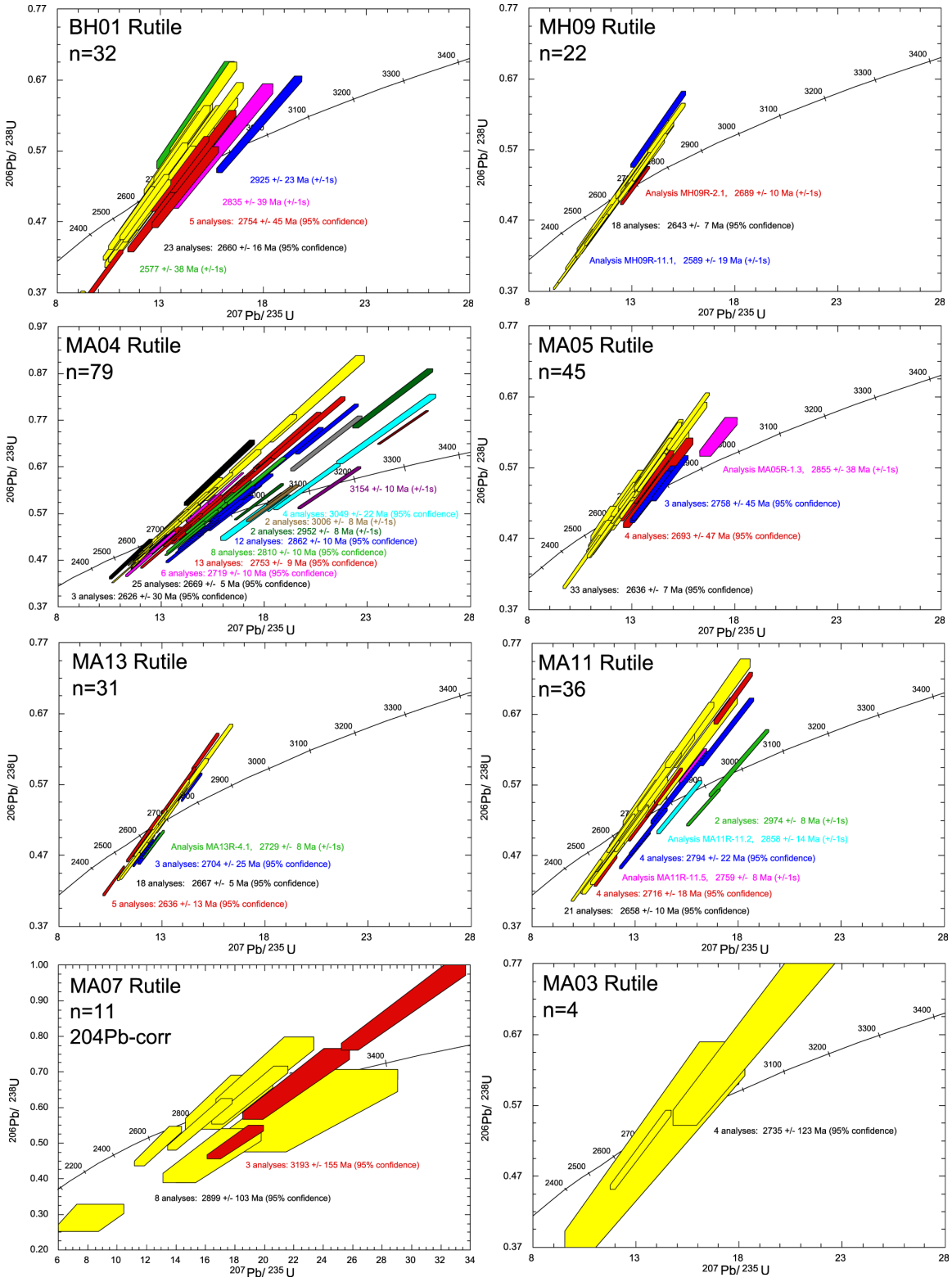

Figure 6.4: Wetherill plots for rutile samples from the Maynard Hills (MH09), Brooking Hills (BH01), and Mt. Alfred (MA03, MA04, MA05, MA07, MA11, and MA13). Plots for MA07 are ^{204}Pb-corrected, and sample MA03 only includes a partial dataset, see text for discussion.

Table 6.3: List of samples with ^{208}Pb-corrected ^{207}Pb/^{206}Pb age groups which have at least 3 analyses per group.

Sample	[Number of grains#] ^{207}Pb/^{206}Pb age of group (Ma)							
BH01			[23] 2660±16		[5] 2754±45			
MA03				[4] 2735±123				
MA04		[3] 2626±30	[25] 2669±5	[6] 2719±10	[13] 2753±9	[8] 2810±10	[12] 2862±10	[4] 3049±22
MA05		[33] 2636±7	[4] 2693±47		[3] 2758±45			
MA07**						[8] 2899±103		[3] 3193±155
MA11			[21] 2658±10	[4] 2716±18		[4] 2794±22		
MA13		[5] 2636±13	[18] 2667±5	[3] 2704±25				
MH09		[18] 2643±7						
RUT*	[4] 2604±17	[111] 2635±1	[10] 2661±7					
χ^2 groups of all unknowns (above) with >5 analyses in each group								
		[21] 2624±8	[112] 2656±3	[25] 2687±5	[21] 2730±7	[8] 2758±8	[17] 2804±8	[12] 2862±8	[6] 2965±13

#where at least 3 rutile grains per group, *rutile standard, **uses ^{204}Pb-corrected ^{207}Pb/^{206}Pb age groups

Table 6.4: All rutiles grouped using the χ^2 method of CONCH showing age groups shared between all analyses. Groups with >10 analyses are interpreted to include analyses of large (>30μm) thermally reset zones that are large enough to resolve on the scale of a single SHRIMP analysis spot.

Rutile Grains	Date (Ma)	Exp. $\pm$ 2σ	χ^2 value
21	2624	8	0.98
112	2656	3	0.99
25	2687	5	0.99
4	2713	14	0.95
21	2730	7	1.00
8	2758	7	0.93
17	2804	7	0.98
12	2862	8	0.88
6	2965	13	0.86
4	3007	16	0.84
3	3050	21	0.79
3	3106	26	0.89
2	3154	10	0.14

Some dates obtained on individual rutile grains were much older than expected, and may reflect the measurement of rutile that included small inclusions of zircon. One such example is MA05R grain 4 (Table 6.2) which exhibits ^{204}Pb-corrected dates between ca. 3347 Ma and 3854 Ma with $f_{206}\%$ <1, Th contents <2ppm, and unexpectedly large uncertainties on ^{206}Pb/^{238}U and ^{207}Pb/^{235}U ratios. These analyses are not assessed or used in geological interpretations due to these large analytical uncertainties.

A summary of all rutile analyses grouped using χ^2 is shown in Table 6.4. These results show common, statistically robust age groups shared across the different samples and is interpreted to reveal the timing of rutile growth, recrystallization, or Pb-loss events.

Optical characteristics, EDS analysis and SHRIMP analysis sites for sample MA04 are shown in Figure 6.5. The SHRIMP analysis sites are shown in sections a and b, with section c showing grouped ages superimposed onto the rutile grains. Grain number 5, numbered on Figure 6.5-(a through c), has what appears to be a core of >3000 Ma age, with multiple rim or overgrowth components, outlined in detail in Figure 6.5-d. Chemical characterization of this grain was undertaken by EDS analysis, analysis sites shown in Figure 6.5-d, which revealed little variation in the elements Ti, Zr, Cr, Fe, V, or Nb (displayed in the EDS plot within Figure 6.5-f).

Additional rutiles are shown in sections e, g, h, and i of Figure 6.5. Some grains show different metamorphic and possibly detrital characteristics. Rounding on many grains may indicate some are of detrital origin, even though the age of these grains indicates that they are post-depositional. Imaging alone, however, is not a very diagnostic tool to detect growth zones within rutile, and the EDS technique (discussed earlier) has also not detected obvious growth zones within these crystals. MA11 rutiles (section 'e')

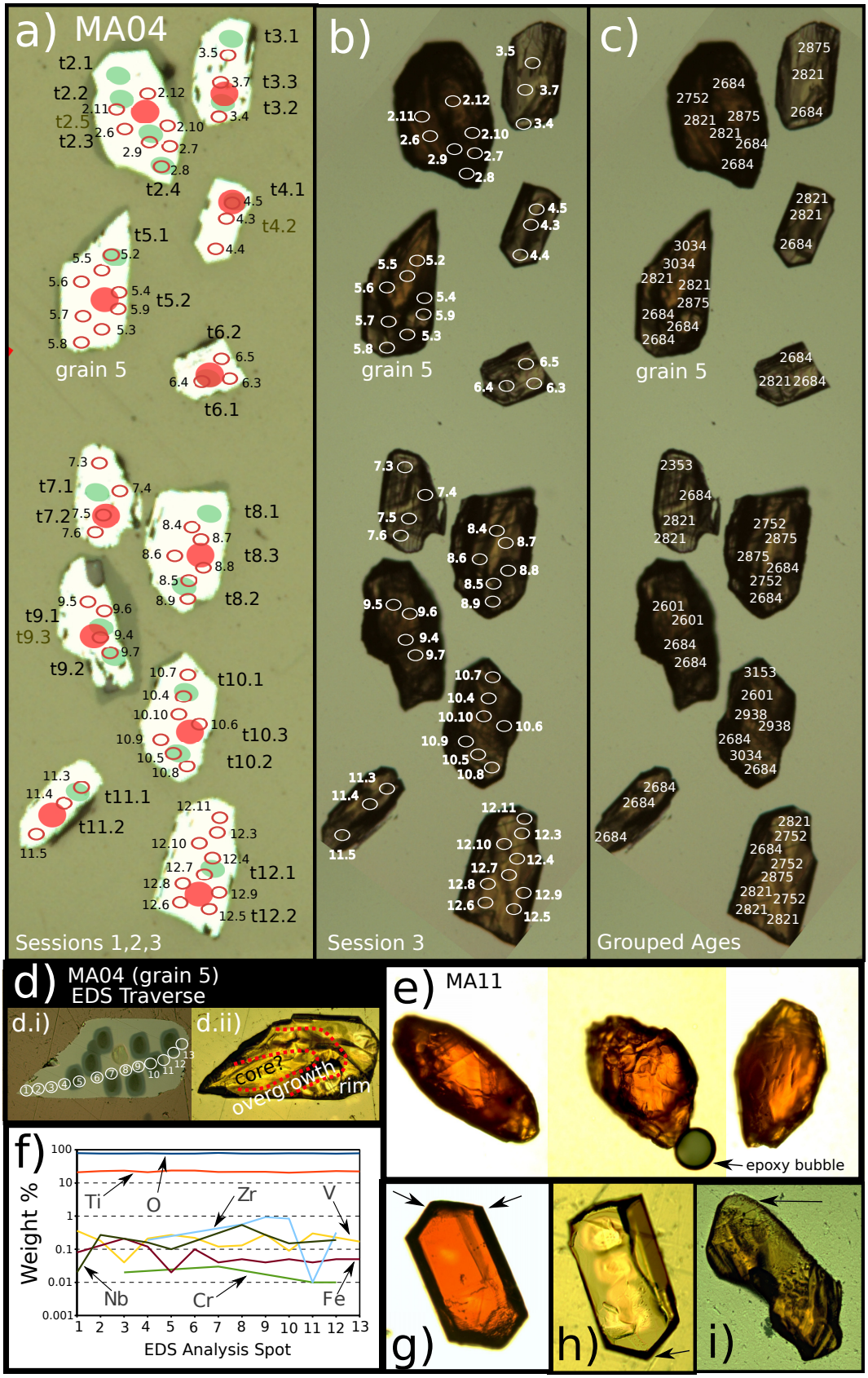

Figure 6.5: Transmitted light image of sample MA04 session 1 rutiles with assigned $^{207}Pb/^{206}Pb$ dates showing heterogeneous internal structure within individual zircons and 'core'-rim younging. The SHRIMP analysis sites are shown in sections a and b, with section c showing grouped ages superimposed onto the rutile grains. Grain number 5 (d) shows a core of >3000 Ma age, with multiple rim or overgrowth components. EDS analysis sites on this grain (f) reveal little variation in the elements Ti, Zr, Cr, Fe, V, or Nb. Additional rutiles (e, g, h and i) show crystal facets, and pitting and rounding which may be associated with detrital transport or metamorphic fluid interaction. See text for further discussion.

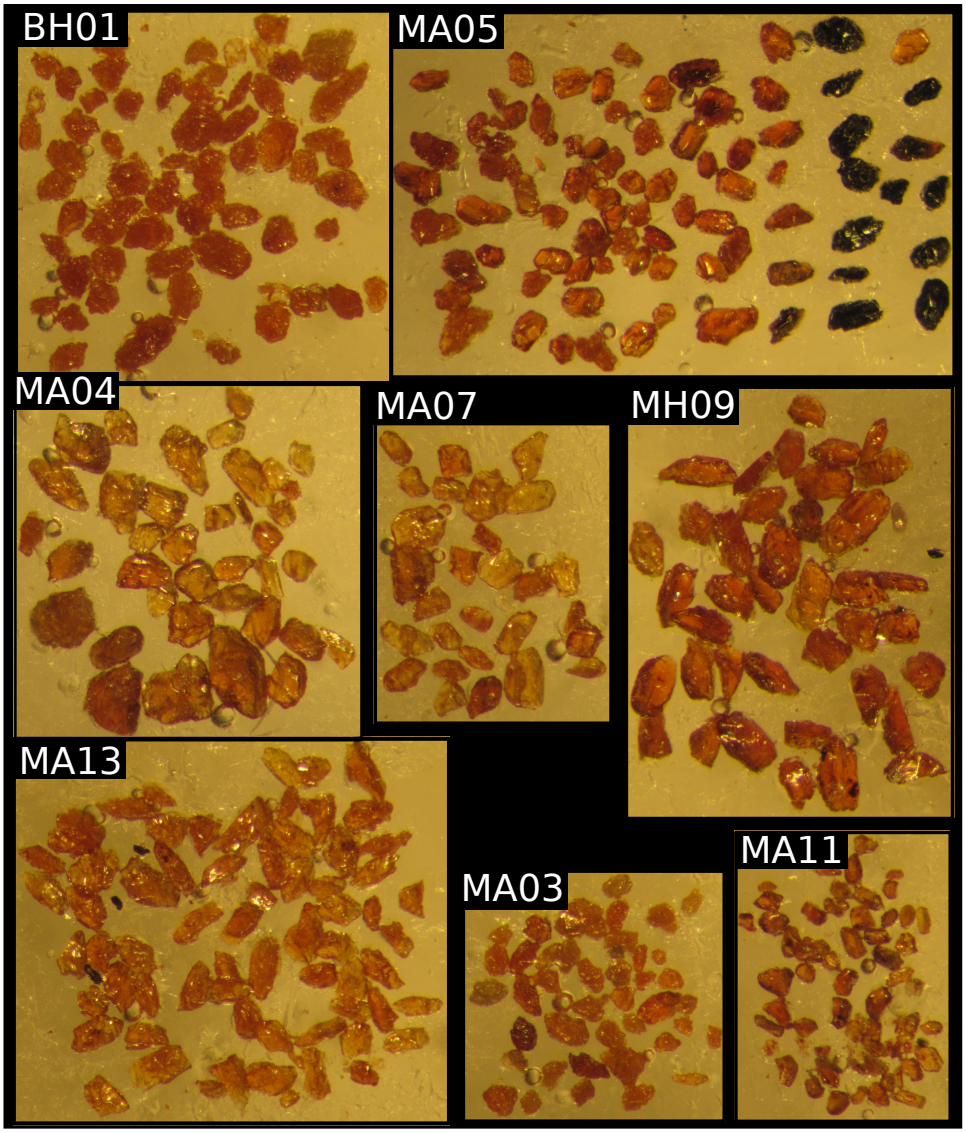

Figure 6.6: Rutile samples imaged on double sided tape prior to mounting in epoxy for SHRIMP analysis. Rutiles here analyzed samples from the Maynard Hills (MH09), Brooking Hills (BH01), and Mt. Alfred (MA03, MA04, MA05, MA07, MA11, and MA13).

are ca. 300−500μm grains that show elongation along the shear fabric, which suggests these grew, or were deformed and reset during metamorphic events. Rutiles in section 'g' and 'h' show well-terminated crystal facets (arrows), which suggests pristine post-depositional growth of these crystals, and shows that crystal growth was happening during metamorphic events. The rutile shown in section 'i' reveals what looks to be detrital transport features of pitting and rounding (arrow); however it is also possible that this atypical pitting may be related to metamorphic fluid interaction with this grain.

SEM images were taken on polished thin sections to determine the location of these grains within the matrix of their host rocks. In Figure 6.7, which is composed of

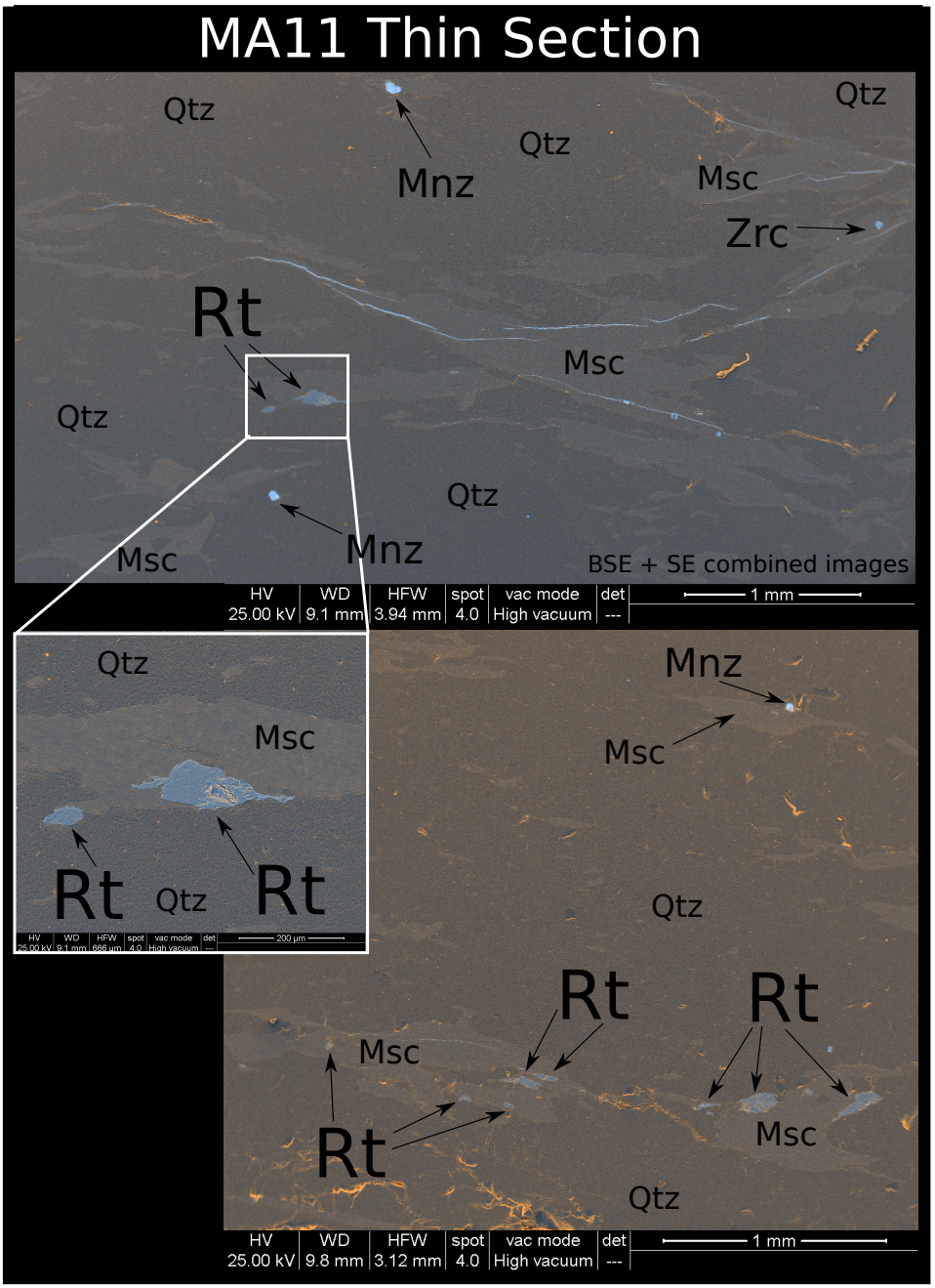

Figure 6.7: Sample MA11 thin section combined BSE and SE images showing rutiles (Rt), muscovites (Msc), Monazite (Mnz) and Zircon (Zrc) in a quartz matrix (Qtz). Occurrence of rutile within or next to muscovite lathes is commonly witnessed within samples analyzed in this study.

combined BSE and SE images, sample MA11 is shown in thin section, highlighting rutiles (Rt), muscovites (Msc), monazite (Mnz) and zircon (Zrc) in a quartz matrix (Qtz). Rutile is commonly seen within or next to muscovite lathes within samples analyzed in this study.

6.7.2 Fuchsite $^{40}Ar/^{39}Ar$ geochronology

$^{40}Ar/^{39}Ar$ plateau ages on muscovite and fuchsite from selected samples representing the most northern sample locality (FCW01) within the Maynard Hills Greenstone Belt, the central Illaara Greenstone Belt at the Mt. Alfred locality (MH05), and a sample from the most southern site at the Brooking Hills locality (BH01) of the Illaara Greenstone Belt are shown in Figure 6.8. Additional $^{40}Ar/^{39}Ar$ results, including all tables with processed data are shown in Appendix Table G.1. All $^{40}Ar/^{39}Ar$ results show extremely well behaved incremental heating plateaus, and are within uncertainty of an average age of ca. 2610 Ma.

6.7.3 (U−Th)/He Thermochronology

Rutiles, tourmalines, zircons and goethites were analyzed for (U−Th)/He dates. The results are summarized in the Appendix Table H.

The tourmaline results show a broad range of (U−Th)/He dates between ca. 348 Ma to >4000 Ma. These results suggest that the tourmalines may have had fluid inclusions, or were altered. This may have caused different yields of He, or enhanced U and Th contents which made the age calculations meaningless. These ages are thus not used to interpret geological events in this study. Further analyses of tourmaline by the (U−Th)/He technique will require detailed microstructural evaluation of each tourmaline picked.

The rutile results yielded (U−Th)/He ages from ca. 1400−3200 Ma, a spread of ages which is difficult to reconcile. The most likely explanation for these results is that these rutiles were either (i) inclusion rich, or (ii) metamict and/or hydrothermally altered. With a hard to interpret dataset, and no repeat data undertaken, it's impossible to interpret the results in a geological context, so these are not considered to reflect meaningful (U−Th)/He ages.

The zircon and goethite (U−Th)/He results show reproducable dates, with one outlier in each set of four analyses. The zircon (U−Th)/He ages of 238±14, 323±19, 217±13, and 236±14 Ma, excluding the 322 Ma age as an outlier are all within uncertainty of an average age at 230±13 Ma. The goethite (U−Th)/He ages of 22±1, 19±1, 35±2, and 23±1, excluding the 35 Ma age as an outlier, are all within uncertainty of an average age of 25±2.

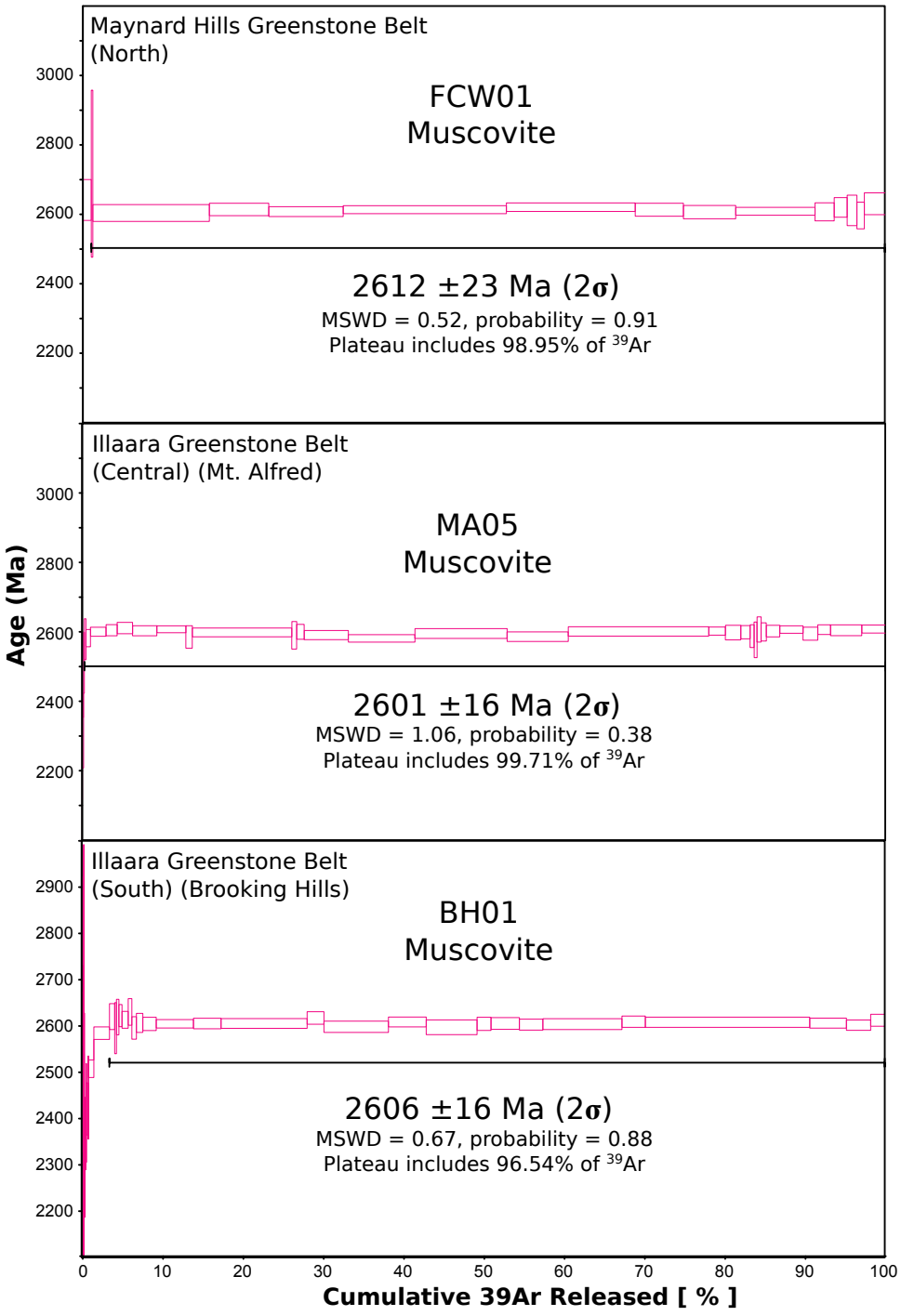

Figure 6.8: $^{40}Ar/^{39}Ar$ age spectra where individual steps are plotted as a function of the percent ^{39}Ar released. Well behaved plateau ages on three muscovite samples show ages within uncertainty of ca. 2610 Ma using greater than 95% of ^{39}Ar released by incremental heating. Uncertainties quoted are at 95% confidence.

6.8 Discussion

6.8.1 Fully and partially reset rutiles and their host rocks

The rutile analytical results presented in this study indicate that these rutiles have what appear to be detrital as well as metamorphic features. They also have a wide range of ages, with poorly defined core-rim younging which suggests a level of Pb-loss. Some rutiles with younger 'rim' components have well defined metamorphic overgrowths and poorly defined older cores. The closure temperature of rutile is significantly lower than zircon; between 400-450°C from geological samples (Mezger et al., 1989) to experimentally obtained results of 570-630°C (Cherniak, 2000; Kooijman et al., 2010). It therefore seems likely that the rutile Pb-isotopic system would be more readily reset than that in zircon, which has a closure temperature of ca. 900°C (Cherniak, 2000). The zircons in these upper-greenschist to mid-amphibolite grade metasedimentary rocks retain their original dates (see Chapter 4), but the rutiles retain only a small signature of their original detrital ages.

During the high-grade metamorphic events, the influx of water and the breakdown of certain mineral components, such as ilmenite might have resulted in Ti-bearing fluids flowing throughout porous zones within the metasedimentary rocks. Occurrence of rutile within or next to muscovite lathes is common (see Figure 6.7) and provides evidence for the breakdown of associated Ti-bearing minerals as a source of Ti for new rutile growth during thermal events. The thermal and/or hydrothermal events have had enough of an impact within the metasedimentary rocks to allow some of the rutiles within the samples to have their ages reset due to Pb-loss, or for new metamorphic growth of rutile to have occurred. A combination of these two events, including dissolution and reprecipitation of rutile, could account for the multiple age zones, and similarity of trace elements, observed within the rutiles.

6.8.2 Rutile Ages, Thermal Events and Depositional Constraints

To get an overall sense of rutile age groups throughout the greenstone belts studied herein, all analyses were grouped (see Table 6.4) using the χ^2 method of CONCH to resolve statistically shared age groups. Age groups consisting of more than 10 analyses may have formed due to the formation of large (>30μm) thermally reset, or new metamorphic growth zones large enough to resolve on the scale of a single SHRIMP analysis spot. Alternatively, these older ages may be mixtures of older, undisturbed components and more recent growth or fully reset components. The preferred interpretation is that these age groups result from growth or recrystallization in 'zones' within each rutile grain. These grouped ages match with known thermal events of the Yilgarn Craton, spanning >2900 Ma to ca. 2630 Ma (see Chapter 4, Figure 8, sections d through g for

overview of events).

This complex thermal history has resulted in the latest major thermal pulse, involving new metamorphic growth and Pb-loss, leaving the largest overprint on the rutile ages. This late thermal pulse appears to be 'over-represented' within the ages of these rutiles, with 112 rutile analyses grouping into a single 2656±3 Ma age. Due to the upper-greenschist to mid-amphibolite facies metamorphism of the central Yilgarn, older rutile dates are less well-preserved after so many younger thermal pulses, and are thus the least represented ages in these samples. Thermal events older than ca. 2660 Ma are still in evidence, albeit in smaller proportions (ie. 25 analyses at ca. 2687 Ma, 21 analyses at ca. 2730 Ma, 17 analyses at 2804 Ma, 12 analyses at 2862 Ma, and fewer older analyses at older age groups).

As the youngest detrital zircons from these metasandstones are ca. 2960 to 3300 Ma in age (Thern and Nelson, 2012b) (see also, Chapters 3 and 4), the oldest group of ages from the rutiles (6 analyses at 2965±13 Ma, 4 analyses at 3007±19, 3 analyses at 3050±24 Ma, 3 analyses at 3106±34 Ma and 2 analyses at 3154±15 Ma) are the closest match for a maximum depositional age. This is further constrained by $^{40}Ar/^{39}Ar$ plateau ages on tourmaline which have an age of 2939±15 Ma, offering a minimum depositional age for these metasedimentary rocks (discussed in Chapter 5). If a proportion of these rutile ages older than 2939 Ma are from detrital rutiles, they then likely represent the influx of detrital sedimentary material during deposition from eroded high-grade metamorphic terranes (Force, 1980). The oldest rutile ages have been obtained only on cores of grains, specifically the ca. 3050 Ma ages on grain MA04R-5, as seen in Figure 6.5-d, which may be the originally detrital component of this rutile grain. Rutile analyses between ca. 2950-3050 Ma may be either reflecting differential Pb-loss of original detrital components within these grains, or may reflect a more robust maximum depositional age for the original sediments. Dates older than 3154±15 Ma are typically disturbed, suffer from high Th contents, and have potential zircon inclusions or common-Pb correction problems that yield older than expected ages; and these dates are difficult to interpret geologically.

6.8.3 Post late-metamorphic events

The youngest rutile dates, at 2624±8 Ma, are within analytical uncertainty of $^{40}Ar/^{39}Ar$ dates on muscovite-fuchsites, and are the same as ages obtained on late-stage tourmalines (2622±20 Ma) from quartz veins (see discussion in Chapter 5). Individual $^{40}Ar/^{39}Ar$ plateau ages on muscovites from samples taken from throughout both greenstone belts, including sample FCW01 from a mylonite shear zone from the central part of the Maynard Hills Greenstone Belt (see Figure 6.2), all define ages within uncertainty of 2610±15 Ma. These results, with their extremely flat age plateaus, reveal that rapid

cooling to below ca. 400°C occurred during post-kinematic shearing or recrystallization at this time throughout the Illaara and Maynard Hills greenstone belts. This age defines the final thermal event recorded within these greenstone belts during the end-stages of 'cratonization' of the central Yilgarn. The only recorded tectonic events which post-date this have resulted in brittle deformation features such as kink-folds, and late-stage exhumation and meteoric fluid infiltration events.

Exhumation of the Mt. Alfred locality within the Illaara Greenstone Belt is recorded by the 230±13 Ma (U−Th)/He ages on detrital zircons from sample MA14. This cooling from ca. 400°C at 2610±15 Ma to below ca. 180°C (helium closure temperature in zircon) at 230±13 Ma was most likely due to the denudation of the central Yilgarn Craton. These results suggest enhanced denudation rates prior to ca. 230 Ma, in line with fission track estimates from the northern Yilgarn Craton (Weber et al., 2005). The lack of Archean detrital zircons within placer deposits throughout the Perth basin also suggests that the peneplanation of the Yilgarn Craton was complete prior to ca. 250 Ma (Sircombe and Freeman, 1999).

A low-relief, stable Yilgarn Craton after ca. 230 Ma would have left mainly a lateritized surface, exposed to near-surface fluid interaction at recent times. Iron-rich meteoric fluid fluxing through the outcrops of metasedimentary rocks likely led to the growth of goethite at 25±2 Ma as layers and rinds around detrital minerals. This final stage event, as measured by (U−Th)/He thermochronology, is also to have been likely coeval to Fe-enrichment within zircon cracks, and was a likely catalyst of zero-age Pb-loss shown within the detrital zircon populations (see Chapter 4, Figure 6).

6.9 Summary

The geodynamic history of the central Southern Cross Terrane Illaara and Maynard Hills Greenstone Belts from sandstone deposition at ca. 3.0 Ga to goethite (U−Th)/He retention at 25±2 Ma is summarized in Figure 6.9. Rutile data have been pooled and grouped by the χ^2 method of CONCH, which produces age groups that correspond to many of these thermal events as documented from zircon geochronology and field relations. Rutile groups (derived from all pooled data) also reflect individual sample groupings, and are therefore interpreted as meaningful dates even though many analyses have large uncertainties (which shows up as 'smoothing' of the peaks on the Gaussian probability plot). The oldest rutile ages, older than the $^{40}Ar/^{39}Ar$ tourmaline minimum depositional age at 2939±15 Ma, are potentially of detrital rutiles. The rest of the rutile age groups reflect the impact of thermal events on their siliciclastic host rocks during their rift-related migration and break-up from the Jack Hills Greenstone Belt and Narryer Terrane, as discussed in Chapter 4, Figure 8. The rutile age group 2862±8 Ma

is difficult to assess geologically. The group of 17 rutile analyses at 2804±8 Ma, however, may relate to the ca. 2800−2815 Ma mafic-ultramafic (possibly plume-derived) magmatism throughout the central Yilgarn at the Narndee, Youanmi and Windimurra complexes (Ivanic et al., 2010). Peaks of igneous zircon ages (Figure 6.9; right hand side Gaussian summation plot) and rutile ages (Figure 6.9; left hand side Gaussian summation plot and grouped ages) correspond with major structural events such as D_1 N−S shortening at ca. 2730 Ma, D_2 E−W shortening at ca. 2680 Ma, D_3 E−W shortening at ca. 2660 Ma (Qiu et al., 1999; Nelson, 2000c, 2001; Chen et al., 2001, 2003; Chen et al., 2004a), and minor peaks representing possible Au-timing (at least for the southern portion of the Southern Cross Terrane) at ca. 2630 Ma (Joly et al., 2010) and post-kinematic intrusions (Chen et al., 2004a). The youngest rutile ages, at ca. 2624±8 Ma and the late-stage tourmalines from quartz vein margins (2622±20 Ma) define the timing of post-deformation quartz veining throughout the Illaara Greenstone Belt (discussed in Chapter 5). Recrystallization and rapid cooling at ca. 2610±15 Ma as measured by $^{40}Ar/^{39}Ar$ on fuchsites, is the last time the Illaara and Maynard Hills greenstone belt siliciclastic metasedimentary rocks have been to temperatures between ca. 300-400°C. The lack of thermal events throughout the Proterozoic reveals a relatively quiescent late history of the central Southern Cross Terrane, when temperatures likely remained constrained between ca. 200-300°C. Late stage events are elucidated by using (U−Th)/He thermochronology, that may relate to exhumation due to denudation at 230±13 Ma (based on zircon data) and goethite crystallization due to Fe-rich meteoric fluid fluxing at 25±2 Ma, the timing of probable Fe-enrichment and Pb-loss within detrital zircons. This data reveals a complex thermal history of the siliciclastic metasedimentary rocks of the Illaara and Maynard Hills greenstone belts.

6.10 Conclusions

1. Rutiles from siliciclastic metasedimentary rocks throughout the Maynard Hills and Illaara greenstone belts exhibit dominant age groupings that coincide with major thermal and/or hydrothermal events known throughout the central Yilgarn Craton.

2. Single rutile grains with multiple dates between the maximum depositional age of the metasedimentary rocks (ca. 3.0 Ga) and the last major metamorphic event associated with granitic intrusions at ca. 2630 Ma, exhibit weakly defined core-rim younging profiles which suggests Pb-loss events within some of the rutiles during thermal events. Metamorphic rutiles, and metamorphic overgrowths which have pristine crystal facets and terminations, are most likely overgrowths formed during metamorphic fluid-fluxing within the metasedimentary rocks. A combination of these two events have left a complex overprint of thermal events recorded within the rutiles.

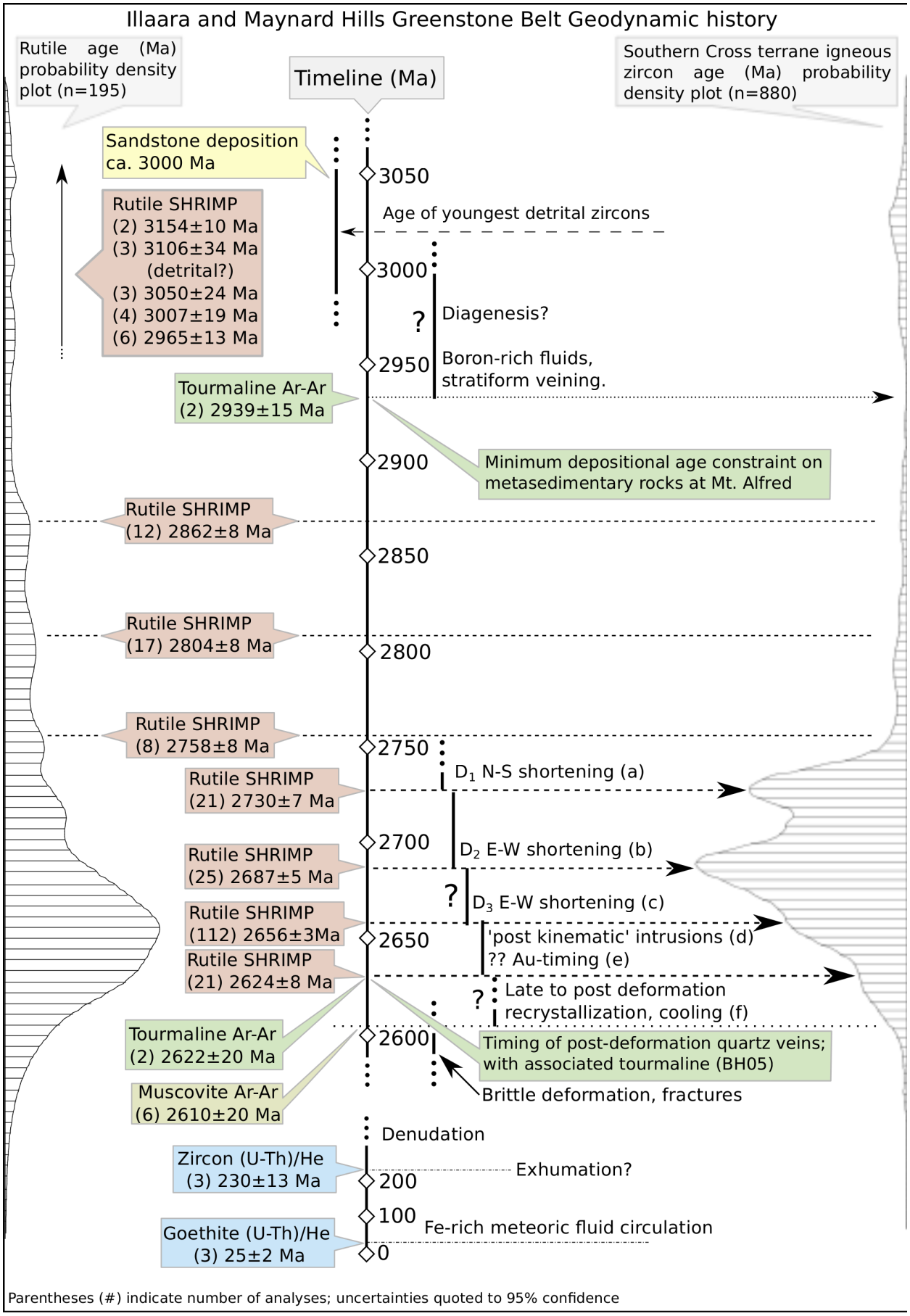

Figure 6.9: see next page for full description

Figure 6.9: Geodynamic history of the central Southern Cross Illaara and Maynard Hills granite-greenstone terranes from sandstone deposition at ca. 3060 Ma to goethite (U-Th)/He retention at 24.8±1.4 Ma. The diagram shows rutile age probability histogram on the left (this study) and igneous zircon probability histogram on the right (GSWA datasets) with a timeline of major events down the middle. Peaks of zircon ages correspond with major structural events such as N-S Shortening, E-W Shortening, with minor peaks representing late Au-timing, post-kinematic intrusions. Late stage recrystallization at 2610±15 Ma Ma as measured by $^{40}Ar/^{39}Ar$ on fuchsites is the last major thermal event recorded by these metasandstones. Late stage (U−Th)/He dates may relate to exhumation due to denudation at 230.2±13.4 Ma (based on zircon data) and goethite crystallization due to Fe-rich meteoric fluids at 24.8±1.4 Ma. See text for discussion.

3. Muscovite-fuchsite 2610±15 Ma $^{40}Ar/^{39}Ar$ plateau ages define late stage post-kinematic shearing and recrystallization throughout the Illaara and Maynard Hills greenstone belts. The reproducibility of individual fuchsite ages and their well-defined plateaus strongly suggest there were no further tectonic or metamorphic events with temperatures above ca. 300°C within the Illaara and Maynard Hills greenstone belts after this time.

4. Zircon (U−Th)/He data suggest that denudation of the central Yilgarn Craton brought the metasedimentary rocks of the Illaara Greenstone Belt closer to the surface, cooling below a thermal gradient of ca. 180°C at 230±13 Ma.

5. The age of goethite crystallization, as revealed by (U−Th)/He results show near-zero-age influx and circulation of fluid at 25±2. This may relate to the Fe-enrichment in cracks and outer zones, as well as fluid-enhanced zero-age Pb-loss, detected in detrital zircons from these metasedimentary rocks.

6. The results show that the early Archean to Hadean zircon-bearing metasedimentary rocks of the Illaara and Maynard Hills greenstone belts have a complex post-depositional history from their deposition at ca. 3.0 Ga until the last major tectonic events ending at ca. 2600 Ma (ca. >300°C). The timing of this final major metamorphic event is in contrast to the Archean and Hadean zircon-bearing metasedimentary rocks of the Jack Hills, on the north-east margin of the Yilgarn Craton, which have $^{40}Ar/^{39}Ar$ muscovite ages as young as 1600 Ma caused by overprinting of multiple thermal events during the Capricorn orogeny, and even younger evidence of xenotime ages at ca. 800 Ma (Rasmussen et al., 2010). The metasedimentary rocks throughout the Illaara and Maynard Hills greenstone belts, in contrast, have been shielded by their location in the center of the Yilgarn Craton, with an almost nonexistant Proterozoic thermal history above ca. 300°C, and thus offer a somewhat geologically less complex source for detrital

Hadean zircons.

CHAPTER 7
CONCLUSIONS

This study has presented an investigation of detrital, metamorphic and hydrothermal minerals from siliciclastic metasedimentary rocks of the Illaara and Maynard Hills greenstone belts. This research has shown that the minerals from these rocks contain information about a complex geodynamic history spanning 4372 Ma to 26 Ma, allowing reconstructions of the early Earth environment, including information about the pre-Yilgarn Craton and the Hadean components within it. The later 'cratonization' events (rifting, magmatism) leading to the current configuration of dispersed ca. 3.0 Ga metasedimentary rocks within the Yilgarn Craton have been revealed through this study.

7.1 Timeline of events: A synthesis

A brief synopsis of the events outlined in this study are shown in Figure 7.1. This figure refers to a timeline of events and matches these events with evidence presented in each chapter. Supplemental to this overview are the final figures in each chapter, in chronological order: Figure 2.8 from Chapter 2 (Hadean Zircons); Figure 7 from Chapter 3 (3.0 Ga Yilgarn metasedimentary rocks); Figure 8 from Chapter 4 (Detrital Zircon Provenance); and Figure 6.9 from Chapter 6 (Post-depositional Thermal History. The end of each chapter throughout this thesis contains full conclusions, and are not duplicated here in full.

7.2 Further Study and Future Directions

The following are a few concepts and ideas for future studies. Some of these have been planned, or are being discussed.

Future sampling of siliciclastic metasedimentary rocks throughout the Yilgarn, in particular units in association with 2900−3000 Ma greenstone belts, may reveal more structure of a pre-Yilgarn land mass, and potentially reveal more Hadean detrital zircons. For example, further investigations including traverses across the 'sedimentary horizons' throughout the Illaara and Maynard Hills is necessary to constrain the Hadean-zircon bearing units, and investigations into the Gum Creek Greenstone Belt may help put those detrital zircon ages into context. Intermediate metasedimentary rock units with depositional ages older than ca. 2900 Ma, such as those found at Mt. Weld, could be a key target as a primary zone of breakup or initial rift zone between the Jack Hills and Illaara-Maynard Hills greenstone belt metasedimentary rocks.

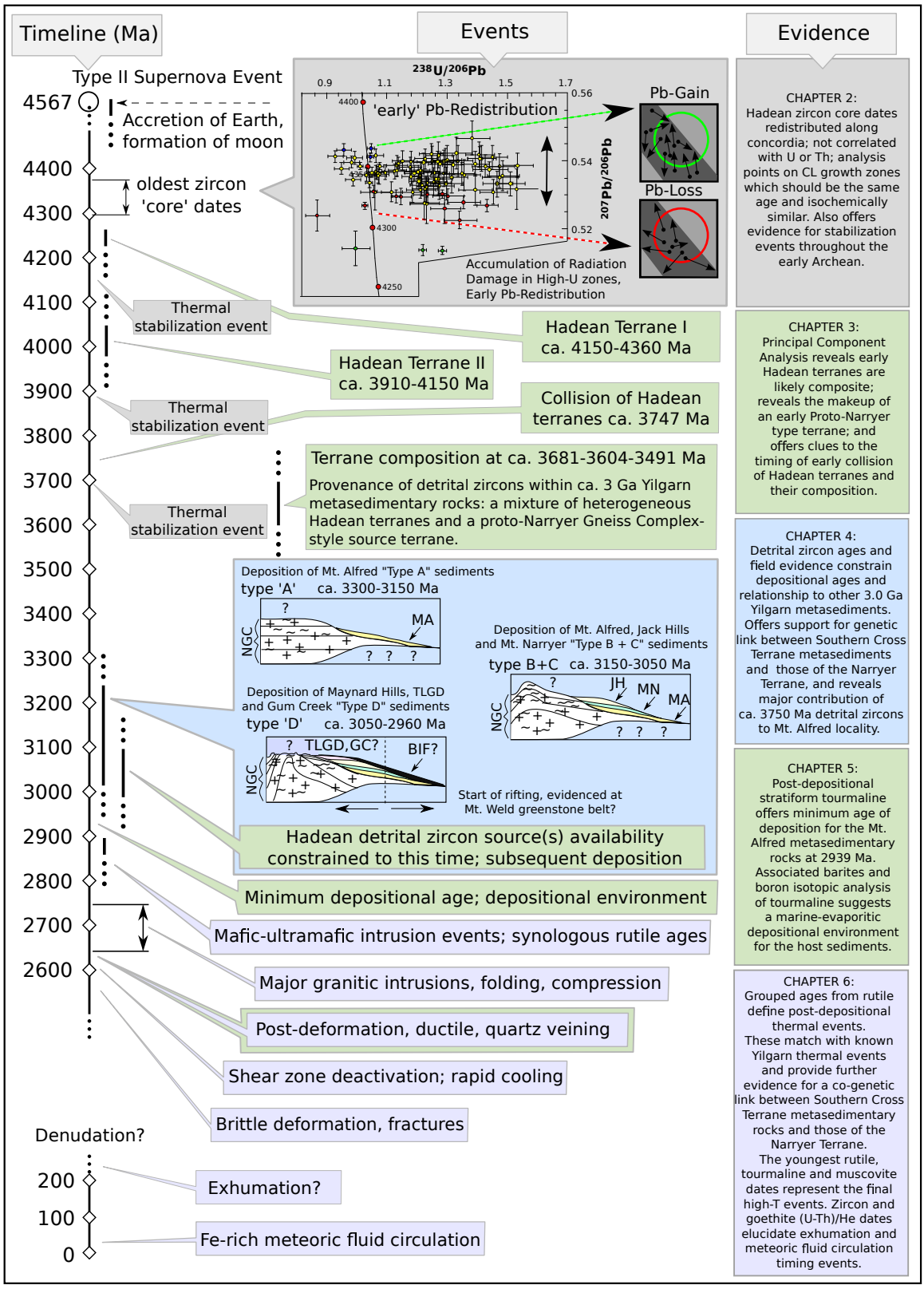

Figure 7.1: Timeline of events discussed throughout this study. Timeline (left), events and findings (middle) and evidence (right) which discusses some points from each chapter. Events (middle) are color coded to the evidence and each chapter (right).

Characterization of these detrital zircons may also benefit from Hf and δ^{18}O isotopic analysis of zircons with similar age groups throughout the ca. 3.0 Ga metasedimentary rocks of the Yilgarn Craton, which should reveal source melt characteristics, and further elucidating provenance. This may reveal further information about the makeup of the Hadean components that were likely part of the Narryer Terrane. Some of this work has been planned with samples presented within this thesis.

Extra sampling and further study of the Illaara and Maynard Hills greenstone belts has also been planned. During the course of this study, an extra 30 samples were collected throughout these greenstone belts in order to further elucidate the Hadean sources, and the provenance complexities that can be glimpsed through extensive detrital zircon dating. This may reveal more information about the diverse detrital zircon dates of the eastern and western Mt. Alfred localities, and to what extent late stage shearing has overprinted these results.

Tourmalines found within stratiform quartz-tourmaline veins throughout the Illaara Greenstone Belt siliciclastic metasedimentary rocks are currently being investigated further. In particular, to decipher the coeval nature of the B-rich fluids, investigations into the δ^{18}O values found within the vein quartz, detrital quartz, banded rhythmites and tourmalines is being undertaken. Along with the δ^{11}B analysis, which will be further refined, this will elucidate the source of fluids as either being derived from the sediments directly (early evidence suggests this) or from a magmatic source. Microstructural studies on individual tourmalines which have core-rim variations may yield information about the possible detrital sources of some tourmaline cores, which would help with a geological reconstruction of their provenance.

Future sampling of stratiform tourmalines from the central Yilgarn Craton, and in particular near Mt. Weld and Jack Hills is also being planned. If the tourmalines found at these localities share ages and isotopic ratios of those found at Mt. Alfred, they may reveal information about their co-genetic nature. This could advance some of the Yilgarn Craton formation evidence as discussed within this thesis, showing an early rift zone where the Illaara and Maynard Hills greenstone belt metasedimentary rocks were first disaggregated from a Narryer-type nucleus terrane, rifting from the early Jack Hills sediments.

Barites, often found as either individual grains or tectonically-stretched layers throughout the metasedimentary rocks offer some additional clues to the depositional settings of their precursor sediments. Distinguishing between barite from post-depositional hydrothermal fluid, or from diagenetic barites crystallized from sulphate-rich seawater interaction is an important constraint to assess, as it could yield information about seawater chemistry and depositional setting. The measurement of ^{87}Sr/^{86}Sr, δ^{34}S and δ^{18}O

will reveal information about whether these sediments were deposited near, or were later influenced by a rift environment due to volcanic activity, were deposited in an intertidal evaporitic environment and reflect a component of original seawater chemistry, or that their ratios have been disturbed by later meteoric water interaction.

Further analysis on the rutiles, especially microstructural studies on their 'detrital' cores, may reveal provenance characteristics. This may be enhanced by Hf isotopic and REE analysis, which could reveal information about their original, likely metamorphic, terrane. One question to assess may be whether these rutiles are linked to deformation and metamorphic events at ca. 3000-3300 Ma during granitic intrusion events throughout the Narryer Terrane, and where gneissic fabrics and metamorphic features are detected within the Narryer Gneiss Complex.

CHAPTER 8
SUPPORTING AND COLLABORATIVE PAPERS

A collection of in-press publications is presented in this chapter which collates work undertaken during candidature. Zircons of different ages which have undergone distinct metamorphic and thermal conditions were studied to further elucidate their U-Pb, Pb-Pb, and (U−Th)/He age responses. Whereas the overall studies represent distinctly different studies to the overall theme of this thesis, the in-depth zircon characteristics are only meaningful when presented within the geological context of each study.

8.1 Paper 3: Enriched Grenvillian lithospheric mantle as a consequence of long-lived subduction beneath Laurentia

The third paper (chapter 8) is first authored by J. Chiarenzelli and co-authored by M. Lupulescu, B. Cousens, E. Thern, L. Coffin and S. Regan. J. Chiarenzelli is the primary author. M. Lupulescu undertook the geochemistry analyses. B. Cousens analyzed the samples and obtained Nd results. The candidate collected U-Pb zircon SHRIMP data, processed, and interpreted these results. L. Coffin provided petrography for samples. S. Regan provided field assistance. All authors provided editorial support during the submission of the manuscript.

Chiarenzelli, J., Lupulescu, M., Cousens, B., Thern, E., Coffin, L., Regan, S. (2010) Enriched Grenvillian Lithospheric Mantle as a Consequence of Long-Lived Subduction Beneath Laurentia. Geology, February 2010; v.38; no. 2; p. 151-154.

8.2 Paper 4: Differentiating Shawinigan and Ottawan orogenesis in the Central Adirondacks

The fourth paper is first authored by J. Chiarenzelli and co-authored by D. Valentino, M. Lupulescu, E. Thern and S. Johnston. D. Valentino introduced the problem and collected the original samples. The first author processed separates for analysis, conducted the analyses. The candidate analyzed the zircons using the SEM (Cathodoluminescence imaging) as well as SHRIMP Pb-Pb and U-Pb dating, processed and interpreted the results within their geological context. D. Valentino and M. Lupulescu provided scientific advice throughout the manuscript process. LA-MC-ICPMS data was processed by S. Johnston, who also provided logistical support during the analyses. All authors provided editorial support during the submission of the manuscript.

J. Chiarenzelli, D. Valentino, M. Lupulescu, E. Thern, and S. Johnston (2011) Differentiating Shawinigan and Ottawan orogenesis in the Central Adirondacks. Geosphere, Feb 2011; 7: 222.

8.3 Paper 5: Tectonic implications of the discovery of a Shawinigan ophiolite (Pyrites Complex) in the Adirondack Lowlands

The fifth paper (chapter 8) is first authored by Jeff Chiarenzelli and co-authored by Marian Lupulescu, Eric Thern and Brian Cousens. The first author collected the samples, processed separates for analysis, and conducted analyses using LA-MC-ICPMS. The candidate analyzed the zircons using the SEM (Cathodoluminescence imaging) as well as SHRIMP Pb-Pb and U-Pb dating, processed and interpreted the results within their geological context. M. Lupulescu provided scientific advice throughout the manuscript process. Nd data was processed by Brian Cousens, who also provided logistical support during the analyses. All authors provided editorial support during the submission of the manuscript.

J. Chiarenzelli, M. Lupulescu, E. Thern, and B. Cousens (2011) Tectonic implications of the discovery of a Shawinigan ophiolite (Pyrites Complex) in the Adirondack Lowlands. Geosphere, April 1, 2011; 7(2): 333 356

8.4 Paper 6: Zircon response to high-grade metamorphism as revealed by U−Pb and cathodoluminescence studies

The sixth paper (chapter 8) is first authored by W. Siebel and co-authored by C. K. Shang, E. Thern, M. Daniŝík and J. Rohrmuller. The first author collected the samples, processed separates for analysis, and conducted U-Pb ID-TIMS analyses and obtained all SEM images on the zircons. The candidate analyzed the zircons, obtaining SHRIMP U-Pb and Pb-Pb ages, processed the data and helped with their geological interpretations. C. K. Shang, M. Daniŝík and J. Rohrmuller provided scientific advice and editorial support throughout the manuscript process.

W. Siebel, C. K. Shang, E. Thern, M. Danišík and J. Rohrmuller (2012) Zircon response to high-grade metamorphism as revealed by U−Pb and cathodoluminescence studies. Int J Earth Sci (Geol Rundsch), 22 April 2012; DOI 10.1007/s00531-012-0772-5

8.5 Paper 7: Emplacement age and thermal footprint of the diamondiferous Ellendale E9 lamproite pipe, Western Australia

The seventh paper (chapter 8) is first authored by Noreen J. Evans and co-authored by Brent I. A. McInnes, Brad McDonald, Martin Daniŝík, Fred Jourdan, Celia Mayers, Eric Thern and Dudley Corbett. Evans conducted the ICPMS analyses, and interpreted processed data from (U−Th)/He and SHRIMP analyses, along with B. McInnes. Samples were collected by Brent I. A. McInnes, Dudley Corbett and Brad McDonald. Brad McDonald conducted the (U−Th)/He analyses and provided technical support. Martin Daniŝík developed and performed the zircon etching protocols. Fred Jourdan analyzed the phlogopite and processed the data relating to the $^{40}Ar/^{39}Ar$ method. Celia Mayers performed all the microscopy and helped with the presentation of the (U−Th)/He results within the manuscript. The candidate provided support during the acquisition of zircon data on the SHRIMP, processed the data, produced plots and data tables and helped with interpretations. All authors provided editorial support during the submission of the manuscript.

Noreen J. Evans, Brent I. A. McInnes, Brad McDonald, Martin Danišík, Fred Jourdan, Celia Mayers, Eric Thern, Dudley Corbett. (2012) Emplacement age and thermal footprint of the diamondiferous Ellendale E9 lamproite pipe, Western Australia. Miner Deposita, 14 July 2012; DOI 10.1007/s00126-012-0430-7

Appendices

APPENDIX A
SIMILARITY MATRIX OF DETRITAL ZIRCON DATA AND ASSOCIATED SCRIPTS

A.1 CONCH χ^2 ^{207}Pb/^{206}Pb Yilgarn-wide detrital zircon groupings

Example data used for calculations and principal component analysis in Chapter 3.
This is output from CONCH's grouping software, and slightly edited for use in these similarity matrix scripts.

```
Group No,         n,207Pb/206Pb,Exp.    ,Obs.    ,Age (Ma),Exp.    ,Obs.    ,Unc. level ,   chi-sq,Analysis
    labels
    ,,,,,,,,,,,,,,,,,,,,,,,,,,,,,,,,,,,,,,,,,,,,,,,,,,,,,,,,,,,,,,,,,,,,,,,,,,,,,,,,,,,,,,,,,,,,,,,,,,,,,,,,,,,,
```

1,860,0.28274,0.00014,0.00017,3378.1,0.8,0.9,95% conf.,1.59,MH09_4000−64.1*,MH09_4000−71.1*,MH09_4000−83.1*,MH09_4000−85.1*,MH09_4000−89.1,MH09_4000−93.1*,MH09_4000−104.1*,MH09_4000−105.1*,MH09_4000−141.1,MH09_4000−145.1*,MA05_3800−9.1,MA05_3800−29.1,MA05_3800−30.1,MA05_3800−38.1,MA05_3800−51.1,MA05_3800−58.1,MA05_3800−76.1,MH09_4000−1.1,MH09_4000−3.1,MH09_4000−5.1,MH09_4000−10.1,MH09_4000−20.1,MH09_4000−21.1*,MH09_4000−27.1,MH09_4000−29.1*,MH09_4000−33.1,MH09_4000−36.1,MH09_4000−38.1,MH09_4000−39.1,MH09_4000−40.1,MH09_4000−41.1,MH09_4000−44.1,BH02−12.1,MA14−68.1,BH142999_3800−9.1,BH142999_3800−13.1,BH142999_3800−15.1,BH142999_3800−21.1,BH142999_3800−28.1,BH142999_3800−29.1,MH169074−9.1,MH169074−12.1,MH09_4000−9.1,MH09_4000−14.1,MH09_4000−33.1,MH09_4000−17.1,MH09_4000−20.1,MH09_4000−21.1,MH09_4000−22.1,MH09_4000−23.1,MH09_4000−24.1,MH09_4000−26.1,MH09_4000−29.1,MH09_4000−30.2,MH09_4000−30.3,MH09_4000−35.1,MH09_4000−36.1,MH09_4000−39.1,MH178065−1.1,MH178065−3.1,MH178065−5.1,MH178065−7.1,MH178065−10.1,MH178065−14.1,MH178065−17.1,MH178065−19.1,MH178065−26.1,MH178065−31.1,MH178065−33.1,MH178065−37.1,MH178065−39.1,MH178066−1.1,MH178066−3.1,MH178066−5.1,MH178066−6.1,MH178066−7.1,MH178066−8.1,MH178066−11.1,MH178066−13.1,MH178066−15.1,MH178066−16.1,MH178066−17.1,MH178066−18.1,MH178066−21.1,MH178066−22.1,MH178066−23.1,MH178066−24.1,MH178066−27.1,MH178066−29.1,MH178066−31.1,MH178066−35.1,MH178067_3800−1.1,MH178067_3800−3.1,MH178067_3800−8.1,MH178067_3800−13.1,MH178067_3800−15.1,MH178067_3800−16.1,MH178067_3800−19.1,MH178067_3800−23.1,MH178067_3800−25.1,MH178067_3800−27.1,MH178067_3800−36.1,MH178068_3800−2.1,MH178068_3800−12.1,MH178068_3800−15.1,MH178068_3800−17.1,MH178068_3800−24.1,JH986_4000−13.1,JH986_4000−26.1,JH986_4000−36.1,TLGDW500−12.1,TLGDW500−16.1,TLGDW500−33.1,TLGDW500−7.1,TLGDW500−32.1,TLGDW500−25.1,TLGDW501_3800−7.1,TLGDW501_3800−65.1,TLGDW501_3800−62.1,TLGDW501_3800−82.1,TLGDW501_3800−50.1,TLGDW501_3800−72.1,TLGDW501_3800−95.1,TLGDW501_3800−81.1,TLGD901−38.1,TLGD904−18.1,TLGD904−40.1,TLGD907−46.2,TLGD907−43.1,TLGD907−67.2,TLGD907−5.1,TLGD907−52.1,TLGD908−3.1,TLGD908−30.1,NNTX−142847.14.1,NNTX−142853.6.1,MNW461_4000−36−1,MNW461_4000−55−1,MNW461_4000−71−1,MNW461_4000−97−1,MNW461_4000−131−1,MNW461_4000−172,MNW461_4000−148,JHW74_4000−49,JHW74_4000−8,JHW74_4000−76,JHW74_4000−48,JHW74_4000−22,JHW74_4000−21,JHW74_4000−84,JHW74_4000−3,JHW74_4000−43,JHW74_4000−31,JHW74_4000−47,JHW74_4000−91,JHW74_4000−74,JHW74_4000−35,JHW74_4000−16,JHW74_4000−73,JHW74_4000−93,JHW74_4000−5,JHW74_4000−52,JHW74_4000−63,JHW74_4000−38,JHW74_4000−32,JHW74_4000−45,JHW74_4000−26,JHW74_4000−71,JHW74_4000−70,JHW74_4000−12,JHW74_4000−81,JHW74_4000−69,JHW74_4000−14,JHW74_4000−28,JHW74_4000−57,JHW74_4000−25,JHW74_4000−4,JHW74_4000−6,JHW74_4000−51,JHW74_4000−92,JHW74_4000−64,JH54_4000−78−3,JHMG152_4000−B7a,JHMG152_4000−B7b,JHMG152_4000−B8a,JHMG152_4000−B11,JHMG152_4000−B15,JHMG152_4000−B16,JHMG152_4000−B20,JHMG152_4000−B24,JHMG152_4000−B24b,JHMG152_4000−B27,JHMG152_4000−B2−1,JHMG152_4000−B4−1,JHMG152_4000−B5−1,JHMG152_4000−B6−1,JHMG152_4000−L1a,JHMG152_4000−L4−1,JHMG152_4000−L8−1,JHMG152_4000−L12−1,JHMG152_4000−L13−1,JHMG152_4000−L20−1,JHMG152_4000−L23−1,JHMG152_4000−L24−1,JHMG152_4000−L25−1,JHMG154_3900−B34,JHMG154_3900−B41,JHMG154_3900−B42,JHMG154_3900−B43,JHMG154_3900−B50,JHMG154_3900−B54,JHMG154_3900−B55,JHMG154_3900−B67,JHMG154_3900−B76,JHMG154_3900−B3−1,JHMG154_3900−B4−1,JHMG154_3900−B6−1,JHMG154_3900−B7−1,JHMG154_3900−B10−1,JHMG154_3900−B11−1,JHMG154_3900−B15−1,JHMG154_3900−B17−1,JHMG154_3900−B22−1,JHMG154_3900−B28−1,JHMG154_3900−4−7,JHMG154_3900−4−8,JHMG154_3900−A3−1,JHMG154_3900−A6−1,NT88_185−1,NT88_185−5,NT88_185−21,NT88_194_3900−12,NT88_194_3900−52,NT88_194_3900−20,NT88_194_3900−33,NT88_194_3900−4,NT88_194_3900−53,NT88_194_3900−16,NT88_194_3900−14,NT88_194_3900−11,NT88_194_3900−36,NT88_194_3900−19,NT88_194_3900−2,NT88_194_3900−25,NT88_194_3900−39,NT88_194_3900−45,NT88_194_3900−32,NT88_194_3900−3,NT88_194_3900−49,NT88_194_3900−29,NT88_194_3900−24,NT88_194_3900−55,NT88_194_3900−17,NT88_194_3900−1,NT88_194_3900−37,NT88_194_3900−27,NT88_194_3900−21,NT88_194_3900−51,NT88_194_3900−31,NT88_194_3900−43,NT88_194_3900−15,NT88_194_3900−5,NT88_194_3900−18,NT89_54−1,NT89_54−5,NT89_54−7,NT89_54−12,NT89_54−15,NT89_54−23,NT89_54−28,NT89_54−30,NT89_54−33,JHSD1_4000−3,JHSD1_4000−8,JHSD1_4000−17,JHSD1_4000−22,JHSD1_4000−25,JHSD1_4000−29,JHSD1_4000−33,JHSD1_4000−34,JHSD1_4000−38,JHSD1_4000−61,JHSD1_4000−72,JHSD1_4000−75,JHSD2_4000−1,JHSD2_4000−5,JHSD2_4000−8,JHSD2_4000−9,JHSD2_4000−12,JHSD2_4000−13,JHSD2_4000−14,JHSD2_4000−15,JHSD2_4000−17,JHSD2_4000−22,JHSD2_4000−23,JHSD2_4000−27,JHSD2_4000−28,JHSD2_4000−30,JHSD2_4000−31,JHSD2_4000−40,JHSD2_4000−41,JHSD2_4000−42,JHSD2_4000−44,JHSD2_4000−46,JHSD2_4000−49,JHSD2_4000−51,JHSD2_4000−52,JHSD2_4000−56,JHSD2_4000−57,JHSD2_4000−63,JHSD2_4000−64,JHSD2_4000−66,JHSD2_4000−68,JHSD2_4000−69,JHSD2_4000−75,JHSD2_4000−76,JHSD2_4000−77,JHSD2_4000−80,JHSD3_4000−33,JHSD3_4000−54,JHSD3_4000−84,JHIC−1,JHIC−3,JHIC−17,JHIC−77,JHIC−91,JHIC−104,MNIC−281,MNIC−323,MNIC−324,MNIC−327,JH60_4000−4,JH60_4000−6,JH60_4000−7,JH60_4000−9,JH60_4000−10,JH60_4000−12,JH60_4000−15,JH60_4000−17,JH60_4000−19,JH60_4000−21,JH60_4000−23,JH60_4000−27,JH60_4000−33,JH60_4000−34,JH54_4000−3,JH54_4000−10,JH54_4000−16,JH54_4000−24,JH54_4000−30,JH54_4000−34,JH54_4000−39,JH54_4000−42,JH54_4000−45,JH54_4000−48,JH54_4000−49,JH54_4000−52,JH54_4000−55,JH54_4000−56,JH54_4000−60,JH54_4000−63,JH54_4000−65,JHW74_4000−1,JHW74_4000−2,JHW74_4000−3,JHW74_4000−5,JHW74_4000−10,JHW74_4000−12,JHW74_4000−15,JHW74_4000−17,JHW74_4000−20,JHW74_4000−21,JHW74_4000−22,JHW74_4000−26,JHW74_4000−28,JHW74_4000−30,JHW74_4000−32,JHW74_4000−35,JHW74_4000−36,JHW74_4000−39,JHW74_4000−42,JHW74_4000−43,JHW74_4000−44,JHW74_4000−49,JHW74_4000−50,JHW74_4000−54,JHW74_4000−55,JHW74_4000−58,JHW74_4000−59,JHW74_4000−70,JHW74_4000−71,JHW74_4000−72,JHW74_4000−75,JHW74_4000−80,JHW74_4000−81,JHW74_4000−82,JHW74_4000−84,JHW74_4000−85,JHW74_4000−91,JHW74_4000−92,JHW74_4000−96,JHW74_4000−98,JHW74_4000−100,JHW74_4000−102,JHW74_4000−105,JHW74_4000−113,JHW74_4000−116,JHW74_4000−122,JHW74_4000−123,JHW74_4000−134,JH36_4000−3,JH36_4000−5,JH36_4000−11,JH36_4000−13,JH36_4000−15,JH36_4000−20,JH36_4000−26,JH36_4000−30,JH36_4000−32,JH36_4000−37,JH36_4000−38,JH36_4000−40,JH36_4000−42,JH36_4000−44,JH36_4000−50,JH36_4000−58,JH36_4000−59,JH36_4000−62,JH36_4000−63,JH36_4000−65,JH36_4000−66,JH36_4000−70,JH36_4000−71,JH36_4000−73,JH36_4000−83,JH36_4000−89,JH36_4000−95,JH36_4000−97,JH36_4000−101,JH36_4000−105,JH36_4000−106,JH36_4000−109,JH36_4000−123,JH36_4000−126,JH36_4000−133,JH36_4000−136,JH36_4000−147,JH36_4000−149,JH36_4000−152,JH36_4000−156,JH36_4000−157,JH36_4000−161,JH36_4000−162,JH36_4000−165,JH36_4000−166,JH36_4000−169,JH36_4000−171,JH36_4000−172,JH36_4000−178,JH36_4000−184,JH36_4000−188,JH47_3800−5,JH47_3800−7,JH47_3800−8,JH47_3800−9,JH47_3800−11,JH47_3800−12,JH47_3800−14,JH47_3800−15,JH47_3800−17,JH47_3800−18,JH43−11,JH43−16,JH43−33,JH42_3900−2,JH42_3900−3,JH42_3900−24,JH42_3900−26,JH42_3900−42,JH42_3900−43,JH42_3900−56,JH42_3900−62,JH42_3900−66,JH42_3900−68,JH42_3900−72

2,385,0.26556,0.00014,0.00019,3280,0.9,1.1,95% conf.,1.75,MH09_4000-108.1*,MH09_4000-149.1*,MH09_4000
-163.1*,MA05_3800-17.1,MA05_3800-40.1,MA05_3800-50.1,BH01-40.1*,BH01-19.1,BH01-20.1*,BH01-36.1*,
BH142999_3800-11.1,BH142999_3800-20.1,BH142999_3800-23.1,BH142999_3800-27.1,MH09_4000-6.1,
MH09_4000-1.2,MH178065-2.1,MH178065-4.1,MH178065-6.1,MH178065-9.1,MH178065-20.1,MH178065-22.1,
MH178065-29.1,MH178065-36.1,MH178066-28.1,MH178067_3800-11.1,MH178067_3800-24.1,MH178067_3800
-35.1,MH178067_3800-24.2,MH178068_3800-4.1,MH178068_3800-22.1,TLGDW500-15.1,TLGDW500-17.1,
TLGDW500-55.1,TLGDW500-47.1,TLGDW500-13.1,TLGDW500-59.1,TLGDW500-38.1,TLGDW501_3800-98.1,
TLGDW501_3800-89.1,TLGDW501_3800-86.1,TLGDW501_3800-75.1,TLGDW501_3800-26.1,TLGDW501_3800-91.1,
TLGDW501_3800-28.3,TLGDW501_3800-66.1,TLGDW501_3800-31.1,TLGDW501_3800-52.1,TLGDW501_3800-34.1,
TLGDW501_3800-15.1,TLGDW501_3800-10.1,TLGDW501_3800-49.1,TLGDW501_3800-74.1,TLGDW501_3800-57.1,
TLGDW501_3800-32.1,TLGDW501_3800-25.1,NMH107-20.1,NMH107-54.1,NMH107-43.1,NMH107-41.1,NMH107
-14.1,NMH107-53.1,NMH107-48.1,NMH107-39.1,NMH107-36.1,NMH107-47.1,NMH107-29.1,NMH107-31.1,NMH107
-1.1,NMH107-27.1,NMH107-35.1,NMH107-34.1,TLGD901-29.1,TLGD901-15.1,TLGD901-39.1,TLGD901-35.1,
TLGD901-58.1,TLGD901-6.1,TLGD901-36.1,TLGD901-12.1,TLGD901-66.1,TLGD901-10.1,TLGD901-17.1,TLGD901
-49.1,TLGD901-32.1,TLGD901-2.1,TLGD901-33.1,TLGD901-11.1,TLGD901-23.1,TLGD901-55.1,TLGD901-42.1,
TLGD901-22.1,TLGD901-4.1,TLGD901-16.1,TLGD901-45.1,TLGD901-69.1,TLGD901-40.1,TLGD904-16.1,TLGD904
-108.1,TLGD904-11.1,TLGD904-49.1,TLGD904-39.1,TLGD904-95.1,TLGD904-119.1,TLGD904-112.1,TLGD904
-80.1,TLGD904-96.1,TLGD904-63.2,TLGD904-82.3,TLGD904-23.1,TLGD904-82.2,TLGD904-94.1,TLGD904-70.1,
TLGD904-30.1,TLGD904-34.1,TLGD904-61.1,TLGD904-73.2,TLGD904-9.1,TLGD904-58.1,TLGD904-93.1,TLGD904
-17.1,TLGD904-82.1,TLGD904-84.1,TLGD904-110.1,TLGD904-50.1,TLGD904-6.1,TLGD904-26.1,TLGD904-22.1,
TLGD904-49.2,TLGD904-32.1,TLGD904-99.1,TLGD904-23.2,TLGD904-62.1,TLGD904-91.1,TLGD904-17.2,
TLGD904-85.2,TLGD907-27.1,TLGD907-33.1,TLGD907-18.1,TLGD907-51.2,TLGD907-83.1,TLGD907-31.1,
TLGD907-51.1,TLGD907-51.3,TLGD907-36.1,TLGD907-32.1,TLGD907-30.1,TLGD907-74.1,TLGD907-57.1,
TLGD907-15.1,TLGD907-55.1,TLGD907-65.1,TLGD907-14.1,TLGD907-63.1,TLGD908-11.1,TLGD908-12.1,
TLGD908-14.1,TLGD908-16.1,TLGD908-21.1,TLGD908-22.1,TLGD908-22.2,TLGD908-23.1,TLGD908-24.1,
TLGD908-27.1,TLGD908-30.2,TLGD908-31.1,TLGD908-32.1,NNTX-142847.13.1,NNTX-142847.16.1,NNTX
-142847.18.1,NNTX-142847.19.1,NNTX-142847.2.1,NNTX-142847.20.1,NNTX-142847.22.1,NNTX-142847.23.1,
NNTX-142847.3.1,NNTX-142847.4.1,NNTX-142847.5.1,NNTX-142847.7.1,NNTX-142897.1.1,MNW461_4000
-119-1,MNW461_4000-188,MNW461_4000-183,JHMG152_4000-F7a,JHMG152_4000-F7b,JHMG152_4000-F12,
JHMG152_4000-H2b,JHMG154_3900-B3a,JHMG154_3900-B3b,JHMG154_3900-B4,JHMG154_3900-B7,JHMG154_3900-
B7b,JHMG154_3900-B9,JHMG154_3900-B11,JHMG154_3900-B15,JHMG154_3900-B19,JHMG154_3900-B20,
JHMG154_3900-B21,JHMG154_3900-B26,JHMG154_3900-B30,JHMG154_3900-B31,JHMG154_3900-B32,JHMG154_3900
-B35,JHMG154_3900-B36,JHMG154_3900-B44,JHMG154_3900-B45,JHMG154_3900-B51,JHMG154_3900-B52,
JHMG154_3900-B58,JHMG154_3900-B60,JHMG154_3900-B64,JHMG154_3900-B68,JHMG154_3900-B69,JHMG154_3900
-B70,JHMG154_3900-B71,JHMG154_3900-B1-1,JHMG154_3900-B9-1,JHMG154_3900-B19-1,JHMG154_3900-B24-1,
JHMG154_3900-B26-1,JHMG154_3900-4-5,JHMG154_3900-A8-1,NT88_185-12,NT88_194_3900-47,NT88_194_3900
-23,JHSD1_4000-42,JHSD2_4000-21,JHSD3_4000-6,JHSD3_4000-51,JHSD3_4000-62,JHSD3_4000-72,JHSD3_4000
-76,JHSD4-38,JHIC-15 ,JHIC-24 ,JHIC-32 ,JHIC-36 ,JHIC-47 ,JHIC-52 ,JHIC-56 ,JHIC-57 ,JHIC-60 ,
JHIC-66 ,JHIC-67 ,JHIC-68 ,JHIC-69 ,JHIC-70 ,JHIC-71 ,JHIC-75 ,JHIC-79 ,JHIC-80 ,JHIC-81 ,JHIC-87
,JHIC-95 ,JHIC-106 ,JHIC-107 ,JHIC-118 ,JHIC-125 ,MNIC-172 ,MNIC-193 ,MNIC-194 ,MNIC-195 ,MNIC
-196 ,MNIC-197 ,MNIC-198 ,MNIC-199 ,MNIC-200 ,MNIC-202 ,MNIC-203 ,MNIC-204 ,MNIC-205 ,MNIC-206 ,
MNIC-244 ,MNIC-260 ,MNIC-276 ,MNIC-307 ,JH60_4000-11 ,JH60_4000-26 ,JH54_4000-4 ,JHW74_4000-64 ,
JHW74_4000-126 ,JHW74_4000-131 ,JH36_4000-34 ,JH36_4000-53 ,JH36_4000-114 ,JH36_4000-132 ,
JH36_4000-181 ,JH47_3800-1 ,JH47_3800-2 ,JH47_3800-20 ,JH43-12 ,JH43-15 ,JH43-17 ,JH43-26 ,JH43
-29 ,JH43-44 ,JH42_3900-6 ,JH42_3900-10 ,JH42_3900-28 ,JH42_3900-30 ,JH42_3900-31 ,JH42_3900-32 ,
JH42_3900-49 ,JH42_3900-59 ,JH42_3900-61 ,JH42_3900-63 ,JH42_3900-70
,,,

3,365,0.30345,0.00015,0.00021,3487.9,0.8,1.1,95% conf.,1.89,MA05_3800-8.1*,MA05_3800-64.1,MH09_4000
-19.1,MH09_4000-22.1,MH09_4000-45.1,MA11-55.1,MA11-55.2,MA13-12.1,BH142999_3800-6.1,BH142999_3800
-10.1,BH142999_3800-16.1,BH142999_3800-17.1,MH169074-13.1,MH09_4000-5.1,MA64_4000-33.1,MH178065
-15.1,MH178065-32.1,MH178065-34.1,MH178067_3800-10.1,MH178067_3800-14.1,MH178067_3800-21.1,
MH178068_3800-1.1,MH178068_3800-14.1,MH178068_3800-17.2,MA64_4000.70.1,JH986_4000-12.1,JH986_4000
-16.1,JH986_4000-21.1,JH986_4000-23.1,JH986_4000-28.1,JH986_4000-34.1,JH986_4000-38.1,JH986_4000
-39.1,JH986_4000-40.1,JH986_4000-46.1,JH986_4000-49.1,JH986_4000-5.1,JH986_4000-51.1,MA01-62.1,
TLGDW500-41.1,TLGDW500-6.1,TLGDW501_3800-59.1,TLGDW501_3800-56.1,TLGDW501_3800-9.1,NMH107-26.1,
NMH107-49.1,NMH107-19.1,NMH107-51.1,NMH107-55.1,NMH107-13.1,NMH107-30.1,NMH107-9.1,TLGD901-25.1,
TLGD904-43.1,TLGD904-60.1,TLGD904-3.1,TLGD904-106.1,TLGD907-22.1,TLGD907-38.1,TLGD907-56.1,
TLGD907-13.1,TLGD907-35.1,TLGD907-49.1,TLGD907-10.1,TLGD908-37.1,MNIC-105002.1.1,MNIC-105009.1.1,
MNIC-105009.15.1,MNIC-105009.16.1,MNIC-105009.2.1,MNIC-105009.3.1,MNIC-105009.4.1,MNIC
-105009.8.1,MNIC-105009.9.1,MNIC-105010.10.1,MNIC-105010.13.1,MNIC-105010.14.1,MNIC-105010.15.1,
MNIC-105010.16.1,MNIC-105010.17.1,MNIC-105010.18.1,MNIC-105010.19.1,MNIC-105010.20.1,MNIC
-105010.4.1,MNIC-105010.6.1,MNIC-105010.7.1,MNIC-105010.8.1,MNIC-105011.14.1,MNIC-105011.2.1,MNIC
-105011.4.1,MNIC-105012.12.1,MNIC-105012.2.1,MNIC-105012.6.1,MNIC-105012.8.1,MNIC-105012.9.1,MNIC
-105014.1.1,MNIC-105014.10.1,MNIC-105014.13.1,MNIC-105014.14.1,MNIC-105014.19.1,MNIC-105014.4.1,
MNIC-105014.7.1,NNTX-142896.2.1,MNW461_4000-39-1,MNW461_4000-95-1,JHW74_4000-62,JHW74_4000-90,
JHW74_4000-17,JHW74_4000-85,JHW74_4000-lb,JHW74_4000-la,JHMG152_4000-B3,JHMG152_4000-B6,
JHMG152_4000-B13,JHMG152_4000-B22,JHMG152_4000-B23,JHMG152_4000-B28,JHMG152_4000-F1,JHMG152_4000-
F5a,JHMG152_4000-F5b,JHMG152_4000-L1b,JHMG152_4000-L8,JHMG152_4000-L2-1,JHMG152_4000-L14-1,
JHMG152_4000-L19-1,JHMG154_3900-B10,JHMG154_3900-B14a,JHMG154_3900-B14b,JHMG154_3900-B22,
JHMG154_3900-B23a,JHMG154_3900-B23b,JHMG154_3900-B25,JHMG154_3900-B27,JHMG154_3900-B29,
JHMG154_3900-B47,JHMG154_3900-B62,JHMG154_3900-B2-1,JHMG154_3900-B5-1,JHMG154_3900-B16-1,
JHMG154_3900-B18-1,JHMG154_3900-B20-1,JHMG154_3900-B25-1,JHMG154_3900-4-4,JHMG154_3900-A4-1,
NT88_194_3900-38,NT88_194_3900-7,NT89_54-3,NT89_54-9,NT89_54-16,NT89_54-19,NT89_54-20,NT89_54-25,
JHSD1_4000-21,JHSD1_4000-32,JHSD2_4000-67,JHSD4-43C,JHIC-5 ,JHIC-38 ,JHIC-89 ,JHIC-94 ,JHIC-96 ,
JHIC-103 ,JHIC-136 ,MNIC-171 ,MNIC-243 ,MNIC-266 ,MNIC-270 ,MNIC-273 ,MNIC-282 ,MNIC-289 ,MNIC
-298 ,MNIC-301 ,MNIC-302 ,MNIC-303 ,MNIC-304 ,MNIC-305 ,MNIC-325 ,JH63-7 ,JH60_4000-3 ,JH60_4000
-30 ,JH54_4000-12 ,JH54_4000-28 ,JH54_4000-44 ,JH54_4000-46 ,JH54_4000-50 ,JH54_4000-59 ,
JH54_4000-61 ,JH54_4000-62 ,JHW74_4000-14 ,JHW74_4000-41 ,JHW74_4000-62 ,JHW74_4000-73 ,
JHW74_4000-97 ,JHW74_4000-114 ,JHW74_4000-132 ,JH36_4000-8 ,JH36_4000-14 ,JH36_4000-31 ,JH36_4000
-46 ,JH36_4000-48 ,JH36_4000-51 ,JH36_4000-55 ,JH36_4000-61 ,JH36_4000-64 ,JH36_4000-72 ,
JH36_4000-76 ,JH36_4000-87 ,JH36_4000-92 ,JH36_4000-99 ,JH36_4000-110 ,JH36_4000-117 ,JH36_4000
-121 ,JH36_4000-134 ,JH36_4000-137 ,JH36_4000-140 ,JH36_4000-141 ,JH36_4000-143 ,JH36_4000-154 ,
JH36_4000-159 ,JH36_4000-168 ,JH36_4000-174 ,JH36_4000-175 ,JH36_4000-179 ,JH36_4000-186 ,
JH36_4000-187 ,JH47_3800-10 ,JH47_3800-13 ,JH47_3800-24 ,JH47_3800-26 ,JH47_3800-27 ,JH43-8 ,JH43
-9 ,JH43-28 ,JH42_3900-8 ,JH42_3900-13 ,JH42_3900-19 ,JH42_3900-27 ,JH42_3900-38 ,JH42_3900-46 ,
JH42_3900-48 ,JH42_3900-67 ,JH113-3 ,JH113-10 ,JH113-11 ,JH113-13
,,,

4,185,0.27266,0.00018,0.00025,3321.4,1.1,1.5,95% conf.,1.9,MH09_4000-88.1*,MH09_4000-177.1*,MH09_4000
-193.1*,MA05_3800-11.1,MA05_3800-28.1,MA05_3800-44.1,MA05_3800-61.1,MA05_3800-74.1,MH09_4000-8.1,
MH09_4000-12.1,MH09_4000-32.1*,MH09_4000-35.1,BH01-25.1,BH01-27.1,MA11-3.1*,BH142999_3800-7.1,
BH142999_3800-8.1,BH142999_3800-30.1,BH142999_3800-32.1,MH169074-4.1,MH169074-15.1,MH09_4000-3.1,
MH09_4000-12.1,MH09_4000-13.1,MH09_4000-18.1,MH09_4000-38.1,MH178065-13.1,MH178065-16.1,MH178065
-28.1,MH178065-30.1,MH178066-10.1,MH178066-12.1,MH178066-33.1,MH178067_3800-6.1,MH178067_3800
-9.1,MH178067_3800-12.1,MH178067_3800-17.1,MH178067_3800-26.1,MH178068_3800-3.1,MH178068_3800
-18.1,MH178068_3800-21.1,JH986_4000-48.1,TLGDW500-8.1,TLGDW500-11.1,TLGDW501_3800-60.1,
TLGDW501_3800-21.1,TLGDW501_3800-97.1,TLGDW501_3800-51.1,NMH107-24.1,NMH107-8.1,NMH107-50.1,
NMH107-33.1,TLGD901-21.1,TLGD901-60.1,TLGD901-1.1,TLGD901-41.1,TLGD901-57.1,TLGD901-37.1,TLGD901
-7.1,TLGD901-53.1,TLGD901-44.1,TLGD904-92.1,TLGD904-62.2,TLGD904-72.1,TLGD904-31.1,TLGD904-69.1,
TLGD904-55.1,TLGD904-116.1,TLGD904-55.2,TLGD904-87.1,TLGD904-7.1,TLGD904-24.1,TLGD904-5.1,TLGD904
-79.1,TLGD907-16.1,TLGD907-59.1,TLGD907-47.1,TLGD907-1.1,TLGD907-48.1,TLGD907-53.1,TLGD907-53.2,
TLGD907-28.1,TLGD907-72.1,TLGD907-29.1,TLGD907-43.2,TLGD907-70.1,TLGD907-21.1,TLGD907-11.1,
TLGD908-4.1,TLGD908-7.1,TLGD908-29.1,TLGD908-30.3,MNIC-105002.10.1,MNIC-105002.20.1,MNIC
-105011.13.1,MNIC-105011.16.1,MNIC-105011.21.1,MNIC-105011.6.1,NNTX-142847.24.1,NNTX-142847.6.1,
NNTX-142847.9.1,NNTX-142853.16.1,MNW461_4000-77-1,MNW461_4000-79-1,MNW461_4000-99-1,MNW461_4000
-74-1,JHMG154_3900-B2,JHSD1_4000-4,JHSD1_4000-6,JHSD1_4000-49,JHSD1_4000-63,JHSD2_4000-65,
JHSD2_4000-71,JHSD3_4000-1,JHSD3_4000-31,JHIC-41 ,JHIC-45 ,JHIC-64 ,JHIC-84 ,JHIC-101 ,MNIC-191 ,
MNIC-192 ,MNIC-255 ,MNIC-262 ,JH60_4000-5 ,JH60_4000-20 ,JH54_4000-13 ,JH54_4000-33 ,JHW74_4000
-24 ,JHW74_4000-31 ,JHW74_4000-110 ,JHW74_4000-120 ,JHW74_4000-129 ,JH36_4000-22 ,JH36_4000-23 ,
JH36_4000-130 ,JH36_4000-142 ,JH36_4000-155 ,JH36_4000-180 ,JH47_3800-28 ,JH43-22 ,JH43-23 ,JH43
-24 ,JH43-36 ,JH42_3900-7 ,JH42_3900-11 ,JH42_3900-25 ,JH42_3900-37 ,JH42_3900-40 ,JH113-7
,,

5,220,0.2914,0.00021,0.00031,3425.1,1.1,1.7,95% conf.,2.14,MH09_4000-158.1*,MA05_3800-25.1,MA05_3800
-45.1*,MA05_3800-82.1*,BH01-2.1,MA11-44.1,MA13-31.1*,BH142999_3800-26.1,MH169074-7.1,MH178065
-25.1,MH178065-27.1,MH178067_3800-22.1,MH178067_3800-30.1,MH178067_3800-31.1,MH178067_3800-32.1,
JH986_4000-27.1,JH986_4000-43.1,JH986_4000-47.1,TLGDW500-20.1,TLGDW500-46.1,TLGDW500-40.1,
TLGDW500-60.1,TLGDW500-52.1,TLGDW500-34.1,TLGDW501_3800-19.3,TLGDW501_3800-11.1,TLGDW501_3800
-43.1,TLGDW501_3800-42.1,NMH107-44.1,NMH107-42.1,NMH107-22.1,NMH107-17.1,NMH107-25.1,TLGD901
-46.1,TLGD901-18.1,TLGD904-47.1,TLGD904-20.1,TLGD904-35.1,TLGD904-66.3,TLGD904-78.2,TLGD904-28.1,
TLGD904-97.1,TLGD904-120.1,TLGD907-34.1,TLGD907-26.1,TLGD907-67.1,TLGD907-50.1,TLGD907-60.1,
TLGD907-3.1,TLGD908-1.1,TLGD908-15.2,TLGD908-18.1,MNIC-105002.14.1,MNIC-105010.1.1,MNIC
-105010.2.1,MNIC-105010.21.1,MNIC-105011.15.1,MNW461_4000-169,MNW461_4000-156,JHMG152_4000-B4,
JHMG152_4000-B17,JHMG152_4000-H10,JHSD1_4000-7,JHSD1_4000-35,JHSD1_4000-39,JHSD1_4000-46,
JHSD1_4000-48,JHSD1_4000-51,JHSD1_4000-57,JHSD1_4000-62,JHSD1_4000-70,JHSD1_4000-74,JHSD2_4000
-20,JHSD2_4000-45,JHSD2_4000-48,JHSD2_4000-72,JHIC-4 ,JHIC-29 ,JHIC-93 ,JHIC-129 ,MNIC-280 ,MNIC
-284 ,MNIC-285 ,MNIC-287 ,MNIC-288 ,MNIC-291 ,MNIC-296 ,MNIC-300 ,MNIC-313 ,JH63-5 ,JH63-6 ,
JH60_4000-2 ,JH60_4000-14 ,JH60_4000-16 ,JH60_4000-18 ,JH60_4000-24 ,JH60_4000-32 ,JH54_4000-1 ,
JH54_4000-11 ,JH54_4000-19 ,JH54_4000-20 ,JH54_4000-21 ,JH54_4000-22 ,JH54_4000-23 ,JH54_4000-25
,JH54_4000-32 ,JH54_4000-35 ,JH54_4000-36 ,JHW74_4000-16 ,JHW74_4000-18 ,JHW74_4000-23 ,
JHW74_4000-25 ,JHW74_4000-29 ,JHW74_4000-33 ,JHW74_4000-34 ,JHW74_4000-47 ,JHW74_4000-56 ,
JHW74_4000-57 ,JHW74_4000-61 ,JHW74_4000-63 ,JHW74_4000-66 ,JHW74_4000-67 ,JHW74_4000-69 ,
JHW74_4000-77 ,JHW74_4000-79 ,JHW74_4000-83 ,JHW74_4000-90 ,JHW74_4000-99 ,JHW74_4000-101 ,
JHW74_4000-107 ,JHW74_4000-108 ,JHW74_4000-109 ,JHW74_4000-112 ,JHW74_4000-121 ,JHW74_4000-124 ,
JH36_4000-2 ,JH36_4000-4 ,JH36_4000-9 ,JH36_4000-17 ,JH36_4000-21 ,JH36_4000-25 ,JH36_4000-28 ,
JH36_4000-33 ,JH36_4000-35 ,JH36_4000-36 ,JH36_4000-39 ,JH36_4000-41 ,JH36_4000-45 ,JH36_4000-54
,JH36_4000-56 ,JH36_4000-57 ,JH36_4000-69 ,JH36_4000-79 ,JH36_4000-81 ,JH36_4000-84 ,JH36_4000-85
,JH36_4000-91 ,JH36_4000-100 ,JH36_4000-102 ,JH36_4000-103 ,JH36_4000-104 ,JH36_4000-113 ,
JH36_4000-116 ,JH36_4000-120 ,JH36_4000-122 ,JH36_4000-124 ,JH36_4000-129 ,JH36_4000-144 ,
JH36_4000-145 ,JH36_4000-148 ,JH36_4000-160 ,JH36_4000-164 ,JH36_4000-167 ,JH36_4000-176 ,
JH36_4000-185 ,JH47_3800-22 ,JH47_3800-29 ,JH43-5 ,JH43-10 ,JH43-34 ,JH43-37 ,JH42_3900-1 ,
JH42_3900-4 ,JH42_3900-9 ,JH42_3900-14 ,JH42_3900-18 ,JH42_3900-33 ,JH42_3900-36 ,JH42_3900-51 ,
JH42_3900-53 ,JH42_3900-60 ,JH42_3900-64 ,JH42_3900-69 ,JH113-1 ,JH113-4 ,JH113-6 ,JH113-12
,,

6,213,0.35922,0.00028,0.00038,3746.6,1.2,1.6,95% conf.,1.76,MA05_3800-5.1,MA05_3800-12.1,MA05_3800
-14.1,MA05_3800-15.1,MA05_3800-22.1,MA05_3800-26.1,MA07_4000-56.1,MA05_3800-70.1,BH01-47.1,
MH09_4000-11.1,BH02-1.1,BH02-8.1,BH02-9.1,BH02-13.1,BH02-21.1,BH02-22.1,BH02-25.1,BH02-26.1,BH02
-30.1,BH02-34.1,BH02-35.1,BH02-41.1,BH02-43.1,BH02-44.1,BH02-47.1,BH02-48.1,BH02-51.1,BH02-57.1,
BH02-60.1,BH02-65.1,BH02-67.1,BH02-71.1*,BH02-73.1,BH02-77.1,BH01-30.1,MA11-6.1,MA11-10.1,MA11
-19.1,MA11-35.1,MA11-42.1,MA11-45.1,MA11-49.1,MA11-60.1,MA11-71.1,MA14-4.1,MA14-5.1,MA14-7.1,MA14
-10.1,MA14-13.1,MA14-16.1,MA14-22.1,MA14-24.1,MA14-25.1,MA14-26.1,MA14-29.1,MA14-33.1,MA14-34.1,
MA14-37.1,MA14-40.1,MA14-41.1,MA14-42.1,MA14-45.1,MA14-47.1,MA14-48.1,MA14-49.1,MA14-50.1,MA13
-3.1*,MA13-6.1*,MA13-8.1,MA13-17.1,MA13-18.1,MA13-19.1,MA13-21.1,MA14-56.1,MA14-57.1,MA13-23.1,
MA13-24.1,MA13-25.1,MA13-27.1,MA13-28.1,MA13-29.1,MA13-34.1,MA13-38.1,MA13-39.1,MA13-41.1*,MA13
-42.1,MA13-44.1,MA13-45.1,MA13-47.1,MA13-52.1,MA13-53.1,MA13-55.1,MA13-60.1,MA14-61.1,MA14-69.1,
MA64_4000-15.1,MA64_4000-34.1,MA64_4000.66.1,MA01-57.1,MA01-58.1,MA01-59.1,MA01-60.1,MA01-61.1,
MA01-63.1,MA01-64.1,MA01-65.1,MA01-66.1,MA01-67.1,MA01-69.1,MA01-70.1,MA01-70.2,MA01-1.1,MA01
-3.1,MA01-10.1,MA01-12.1*,MA01-17.1,MA01-21.1,MA01-23.1,MA01-25.1*,MA01-31.1*,MA01-34.1,MA01
-36.1,MA01-37.1,MA01-39.1,MA01-41.1,MA01-43.1,MA01-44.1,MA01-46.1,MA01-50.1,MA01-51.1,MA01-52.1,
MA03_4000-72.T.8,MA03_4000-9.1,MA03_4000-13.1,MA03_4000-16.1*,MA03_4000-22.1,MA03_4000-65.1,
MA03_4000-66.2*,MA03_4000-69.1,MA04_3800-49.1,MA04_3800-50.1,MA04_3800-10.1*,MA04_3800-11.1,
MA04_3800-16.1*,MA04_3800-20.1,MA04_3800-34.1,MA04_3800-36.1,MA04_3800-39.1*,MA04_3800-41.1,
MA04_3800-43.1,MA04_3800-44.1*,MA04_3800-24.1,MA04_3800-25.1,MA04_3800-26.1,MA04_3800-28.1,
MA04_3800-30.1,MA04_3800-32.1,TLGDW501_3800-71.1,TLGDW501_3800-18.1,TLGDW501_3800-20.2,
MNW461_4000-106-1,MNW461_4000-84-1,MNW461_4000-17-1,MNW461_4000-12-1,MNW461_4000-89-1,MNW461_4000
-196,MNW461_4000-130-1,MNW461_4000-35-1,MNW461_4000-30-1,MNW461_4000-151,MNW461_4000-15-1,
MNW461_4000-127-1,MNW461_4000-25-1,JHW74_4000-61,JHW74_4000-40,JHMG152_4000-L17-1,JHMG152_4000-
L21-1,JHMG154_3900-B17,JHMG154_3900-B49,JHMG154_3900-B57,JHMG154_3900-B72,JHMG154_3900-B12-1,
JHMG154_3900-B14-1,JHMG154_3900-A2-1,JHMG154_3900-A10-1,NT88_194_3900-12,NT88_194_3900-46,
NT88_194_3900-46,NT88_194_3900-13,NT89_54-31,JHSD4-7,JHSD4-29,JHIC-121 ,MNIC-229 ,MNIC-238 ,MNIC
-241 ,JH63-8 ,JH60_4000-1 ,JH36_4000-6 ,JH43-1 ,JH43-42
,,

```
7,134,0.26007,0.0002,0.00026,3247.1,1.2,1.6,95% conf.,1.77,MH09_4000-117.1*,MH09_4000-127.1*,
    MH09_4000-186.1,MA05_3800-56.1*,MH09_4000-15.1*,MH09_4000-18.1,BH142999_3800-31.1,TLGDW500-14.1,
    TLGDW500-2.1,TLGDW500-36.1,TLGDW500-19.1,TLGDW500-57.1,TLGDW500-58.1,TLGDW500-43.1,TLGDW500-62.1,
    TLGDW500-50.1,TLGDW500-31.1,TLGDW500-45.1,TLGDW500-37.1,TLGDW500-22.1,TLGDW500-42.1,TLGDW501_3800
    -35.1,TLGDW501_3800-1.1,TLGDW501_3800-33.1,TLGDW501_3800-28.2,TLGDW501_3800-53.1,TLGDW501_3800
    -78.1,TLGDW501_3800-76.1,NMH107-5.1,NMH107-18.1,NMH107-46.1,NMH107-32.1,TLGD901-8.1,TLGD901-19.1,
    TLGD901-20.1,TLGD901-30.1,TLGD901-48.1,TLGD901-3.1,TLGD901-9.1,TLGD901-64.1,TLGD901-47.1,TLGD901
    -26.1,TLGD901-51.1,TLGD901-63.1,TLGD904-89.2,TLGD904-91.2,TLGD904-29.1,TLGD904-67.1,TLGD904-12.1,
    TLGD904-57.1,TLGD904-59.1,TLGD904-44.1,TLGD904-73.1,TLGD904-75.2,TLGD904-104.2,TLGD904-103.1,
    TLGD904-8.1,TLGD904-14.1,TLGD904-10.1,TLGD904-117.1,TLGD904-74.1,TLGD904-102.1,TLGD904-65.1,
    TLGD904-2.1,TLGD904-98.1,TLGD904-36.1,TLGD904-111.1,TLGD907-4.1,TLGD907-76.1,TLGD907-20.1,TLGD907
    -7.1,TLGD907-87.1,TLGD907-45.1,TLGD907-62.1,TLGD907-71.1,TLGD907-81.1,TLGD907-45.2,TLGD907-17.1,
    TLGD907-32.2,TLGD907-25.1,TLGD907-19.1,TLGD907-84.1,TLGD907-8.1,TLGD907-73.1,TLGD908-5.1,TLGD908
    -6.1,TLGD908-25.1,TLGD908-27.2,TLGD908-35.1,NNTX-142847.21.1,JHMG152_4000-H2a,JHMG154_3900-B37,
    JHMG154_3900-B75,NT88_194_3900-41,NT88_194_3900-6,JHSD3_4000-59,JHIC-19 ,JHIC-23 ,JHIC-31 ,JHIC
    -46 ,JHIC-74 ,JHIC-105 ,MNIC-207 ,MNIC-220 ,MNIC-259 ,MNIC-261 ,JH63-2 ,JH47_3800-6 ,JH47_3800-30
     ,JH47_3800-31 ,JH43-6 ,JH43-30 ,JH43-32 ,JH43-46 ,JH42_3900-5 ,JH42_3900-44 ,JH42_3900-47 ,
    JH42_3900-52
    ,,,,,,,,,,,,,,,,,,,,,,,,,,,,,,,,,,,,,,,,,,,,,,,,,,,,,,,,,,,,,,,,,,,,,,,,,,,,,,,,,,,,,,,,,,,,,,,,,,,,,,,,,,,,,,,,,,,

8,181,0.32395,0.00031,0.0004,3588.7,1.5,1.9,95% conf.,1.66,MH09_4000-156.1*,MA05_3800-4.1,MA05_3800
    -20.1*,MA07_4000-27.1,MA07_4000-37.1,MA07_4000-58.1,MA05_3800-62.1,BH01-42.1*,BH01-12.2*,BH01
    -52.1,BH01-53.1,MH09_4000-13.1,BH01-12.1,MA14-17.1*,MH169074-6.1,MA64_4000-12.1,MH178065-11.1,
    JH986_4000-37.1,MA03_4000-80.1,MA03_4000-90.1,MA03_4000-101.1*,MA03_4000-103.1,MA03_4000-104.1,
    MA04_3800-19.1*,TLGDW501_3800-85.1,TLGDW501_3800-99.1,TLGD904-13.2,TLGD904-86.1,TLGD904-15.1,
    TLGD904-15.2,TLGD904-101.1,MNW461_4000-14-1,MNW461_4000-104-1,MNW461_4000-163,MNW461_4000-51-1,
    MNW461_4000-72-1,MNW461_4000-194,MNW461_4000-122-1,MNW461_4000-128-1,MNW461_4000-173,MNW461_4000
    -113-1,MNW461_4000-107-1,MNW461_4000-168,MNW461_4000-165,MNW461_4000-179,JHW74_4000-86,JHW74_4000
    -39,JHW74_4000-68,JHW74_4000-79,JH36_4000-56-2,JHMG152_4000-B2,JHMG152_4000-B18,JHMG152_4000-F8,
    JHMG152_4000-L1-1,JHMG152_4000-L3-1,JHMG152_4000-L5-1,JHMG152_4000-L11-1,JHMG152_4000-L16-1,
    JHMG152_4000-L18-1,JHMG152_4000-L22-1,JHMG152_4000-L26-1,JHMG154_3900-B5,JHMG154_3900-B63,
    JHMG154_3900-4-6,NT89_54-2,NT89_54-10,NT89_54-14,NT89_54-27,JHSD1_4000-50,JHSD1_4000-68,
    JHSD2_4000-25,JHSD2_4000-78,JHIC-6 ,JHIC-7 ,JHIC-8 ,JHIC-9 ,JHIC-10 ,JHIC-13 ,JHIC-14 ,JHIC-16 ,
    JHIC-22 ,JHIC-48 ,JHIC-49 ,JHIC-50 ,JHIC-54 ,JHIC-62 ,JHIC-98 ,MNIC-226 ,MNIC-239 ,MNIC-252 ,MNIC
    -265 ,MNIC-267 ,MNIC-277 ,MNIC-278 ,JH60_4000-28 ,JH54_4000-2 ,JH54_4000-5 ,JH54_4000-14 ,
    JHW74_4000-13 ,JHW74_4000-37 ,JHW74_4000-40 ,JHW74_4000-51 ,JHW74_4000-53 ,JHW74_4000-88 ,
    JHW74_4000-89 ,JH36_4000-19 ,JH36_4000-67 ,JH36_4000-68 ,JH36_4000-86 ,JH36_4000-98 ,JH36_4000
    -139 ,JH36_4000-183 ,JH47_3800-25 ,JH43-2 ,JH43-4 ,JH113-8 ,JH113-9
    ,,,,,,,,,,,,,,,,,,,,,,,,,,,,,,,,,,,,,,,,,,,,,,,,,,,,,,,,,,,,,,,,,,,,,,,,,,,,,,,,,,,,,,,,,,,,,,,,,,,,,,,,,,,,,,,,,,,

9,118,0.3357,0.0003,0.00038,3643.3,1.4,1.7,95% conf.,1.55,MH09_4000-166.1*,MH09_4000-173.1*,MH09_4000
    -192.1*,MA07_4000-1.1,MA07_4000-4.1,MA07_4000-6.1,MA07_4000-12.1,MA07_4000-13.1*,MA07_4000-18.1,
    MA07_4000-20.1,MA07_4000-22.1,MA07_4000-23.1,MA07_4000-24.1,MA07_4000-25.1,MA07_4000-29.1,
    MA07_4000-31.1,MA07_4000-35.1,MA07_4000-36.1,MA07_4000-41.1,MA07_4000-42.1,MA07_4000-43.1,
    MA07_4000-45.1,MA07_4000-55.1,MA07_4000-59.1,BH01-10.2*,BH02-33.1,BH02-79.1,MA11-36.1,MA11-43.1,
    MA11-58.1,MA11-62.1,MA11-75.1,MA14-43.1,MA13-9.1,MA13-32.1,MA14-60.1,MA14-66.1,MA64_4000-2.1,
    MA64_4000-3.1,MA64_4000-18.1,MA64_4000-19.1,MA64_4000-20.1,MA64_4000-26.1,MA64_4000.73.1,
    MA03_4000-102.1,MA03_4000-108.1,MA03_4000-12.1,MA03_4000-19.1,MA03_4000-24.1,MA03_4000-39.1,
    MA03_4000-49.1,MA03_4000-56.1,MA03_4000-74.1,MA04_3800-47.1,MA04_3800-14.1*,TLGDW501_3800-58.1,
    TLGD904-118.1,TLGD904-45.1,TLGD904-101.2,MNW461_4000-152,MNW461_4000-80-1,MNW461_4000-92-1,
    MNW461_4000-93-1,MNW461_4000-81-1,MNW461_4000-96-1,MNW461_4000-141,MNW461_4000-117-1,MNW461_4000
    -166,MNW461_4000-146,MNW461_4000-40-1,MNW461_4000-73-1,JH36_4000-5-2,JHMG152_4000-A9,JHMG152_4000
    -L10-1,JHMG154_3900-B66,NT88_185-14,JHSD4-10,JHSD4-28,JHSD4-42,JHSD4-75,JHIC-39 ,JHIC-40 ,JHIC-51
     ,JHIC-110 ,JHIC-113 ,MNIC-218 ,MNIC-219 ,MNIC-249 ,JH54_4000-27 ,JHW74_4000-118 ,JH36_4000-1 ,
    JH36_4000-80 ,JH36_4000-88 ,JH36_4000-115 ,JH36_4000-125 ,JH36_4000-151 ,JH36_4000-170 ,JH36_4000
    -182 ,JH47_3800-19 ,JH42_3900-21 ,JH42_3900-58 ,JH113-5
    ,,,,,,,,,,,,,,,,,,,,,,,,,,,,,,,,,,,,,,,,,,,,,,,,,,,,,,,,,,,,,,,,,,,,,,,,,,,,,,,,,,,,,,,,,,,,,,,,,,,,,,,,,,,,,,,,,,,

10,77,0.29795,0.00025,0.00034,3459.6,1.3,1.8,95% conf.,1.79,MH169074-11.1,MH169074-14.1,MH178066-4.1,
    JH986_4000-19.1,JH986_4000-29.1,JH986_4000-33.1,JH986_4000-45.1,TLGDW500-5.1,TLGDW500-3.1,
    TLGDW501_3800-96.1,TLGDW501_3800-8.1,NMH107-28.1,NMH107-38.1,NMH107-16.1,NMH107-12.1,NMH107-3.1,
    NMH107-2.1,NMH107-7.1,NMH107-15.1,TLGD901-67.1,TLGD901-34.1,TLGD901-27.1,TLGD901-28.1,TLGD904
    -33.1,TLGD904-113.1,TLGD907-50.2,TLGD907-6.1,TLGD907-49.2,MNIC-105009.11.1,MNIC-105009.17.1,MNIC
    -105010.3.1,MNIC-105012.1.1,MNIC-105012.5.1,MNW461_4000-132,JHSD1_4000-2,JHSD2_4000-58,JHSD3_4000
    -92,JHIC-28 ,JHIC-30 ,JHIC-115 ,MNIC-279 ,MNIC-299 ,MNIC-309 ,MNIC-311 ,MNIC-316 ,MNIC-317 ,MNIC
    -320 ,MNIC-321 ,MNIC-329 ,JH54_4000-40 ,JH54_4000-47 ,JHW74_4000-38 ,JHW74_4000-76 ,JHW74_4000-95
     ,JH36_4000-16 ,JH36_4000-18 ,JH36_4000-60 ,JH36_4000-94 ,JH36_4000-118 ,JH36_4000-150 ,JH36_4000
    -173 ,JH47_3800-32
    ,,,,,,,,,,,,,,,,,,,,,,,,,,,,,,,,,,,,,,,,,,,,,,,,,,,,,,,,,,,,,,,,,,,,,,,,,,,,,,,,,,,,,,,,,,,,,,,,,,,,,,,,,,,,,,,,,,,

11,46,0.26894,0.00023,0.00021,3299.8,1.4,1.2,95% conf.,0.75,MH09_4000-147.1*,MH169074-10.1,MH09_4000
    -1.1,JH986_4000-1.1,TLGDW500-35.1,TLGDW500-49.1,TLGDW500-30.1,TLGDW501_3800-30.1,TLGDW501_3800
    -36.1,TLGDW501_3800-24.1,NMH107-6.1,NMH107-40.1,TLGD901-68.1,TLGD901-14.1,TLGD904-64.1,TLGD904
    -52.1,TLGD904-25.1,TLGD904-83.2,TLGD904-89.1,TLGD907-2.1,TLGD907-69.1,TLGD907-9.1,MNIC
    -105011.12.1,MNIC-105011.19.1,MNIC-105011.3.1,NNTX-142847.10.1,NNTX-142847.11.1,NNTX-142847.12.1,
    NNTX-142847.15.1,NNTX-142847.17.1,NNTX-142902.4.1,NNTX-142902.5.1,JHSD3_4000-8,JHIC-42 ,JHIC-72 ,
    JHIC-73 ,JHIC-92 ,JHIC-137 ,MNIC-258 ,MNIC-275
    ,,,,,,,,,,,,,,,,,,,,,,,,,,,,,,,,,,,,,,,,,,,,,,,,,,,,,,,,,,,,,,,,,,,,,,,,,,,,,,,,,,,,,,,,,,,,,,,,,,,,,,,,,,,,,,,,,,,

12,85,0.31458,0.00044,0.00055,3543.5,2.2,2.7,95% conf.,1.56,BH01-10.1,MH09_4000-11.1,MH178068_3800
    -6.1,MH178068_3800-8.1,TLGDW501_3800-83.1,TLGDW501_3800-37.1,TLGD904-13.3,JHW74_4000-89,
    JHMG152_4000-B19,JHMG152_4000-F6,JHMG154_3900-B12,JHMG154_3900-B28,JHMG154_3900-B40,JHMG154_3900-
    B61,JHMG154_3900-B73,JHMG154_3900-B74,JHMG154_3900-4-3,JHMG154_3900-4-9,JHSD1_4000-10,JHSD1_4000
    -24,JHSD1_4000-31,JHSD1_4000-37,JHSD2_4000-7,JHIC-35 ,MNIC-263 ,MNIC-274 ,JH60_4000-8 ,JH60_4000
    -31 ,JH54_4000-7 ,JH54_4000-8 ,JH54_4000-9 ,JH54_4000-17 ,JH54_4000-29 ,JH54_4000-53 ,JH54_4000
    -58 ,JHW74_4000-9 ,JHW74_4000-19 ,JHW74_4000-60 ,JHW74_4000-78 ,JHW74_4000-106 ,JHW74_4000-111 ,
    JHW74_4000-117 ,JHW74_4000-125 ,JHW74_4000-127 ,JH36_4000-7 ,JH36_4000-27 ,JH36_4000-49 ,
    JH36_4000-52 ,JH36_4000-82 ,JH36_4000-90 ,JH36_4000-96 ,JH36_4000-111 ,JH36_4000-112 ,JH36_4000
    -119 ,JH36_4000-131 ,JH36_4000-135 ,JH36_4000-138 ,JH36_4000-146 ,JH36_4000-153 ,JH36_4000-163 ,
    JH36_4000-189 ,JH47_3800-3 ,JH43-14 ,JH43-18 ,JH43-19 ,JH43-20 ,JH43-27 ,JH43-35 ,JH43-38 ,JH43
    -39 ,JH43-47 ,JH42_3900-15 ,JH42_3900-34 ,JH42_3900-39 ,JH42_3900-65 ,JH113-2
    ,,,,,,,,,,,,,,,,,,,,,,,,,,,,,,,,,,,,,,,,,,,,,,,,,,,,,,,,,,,,,,,,,,,,,,,,,,,,,,,,,,,,,,,,,,,,,,,,,,,,,,,,,,,,,,,,,,,
```

13,82,0.34526,0.00035,0.0005,3686.2,1.5,2.2,95% conf.,2.05,MH09_4000-171.1*,MH09_4000-187.1*,
MA07_4000-2.1,MA07_4000-26.1,MA07_4000-51.1,MA05_3800-71.1,BH01-11.2,MH09_4000-42.1*,BH02-36.1,
BH02-62.1,BH02-66.1,BH02-75.1,BH01-11.1,MA11-4.1,MA13-22.1,MA13-62.1,BH142999_3800-12.1,
BH142999_3800-22.1,MH09_4000-15.1,MH09_4000-16.1,MH09_4000-27.1,MH09_4000-32.1,MH09_4000-34.1,
MH09_4000-32.2,MH178065-24.1,MH178067_3800-7.1,MH178067_3800-18.1,MH178067_3800-29.1,
MH178067_3800-33.1,MH178068_3800-5.1,MH178068_3800-13.1,MH178068_3800-16.1,MH178068_3800-23.1,
MA64_4000.74.1,MA01-33.1*,MA03_4000-55.1,TLGDW500-1.1,TLGD901-54.1,MNW461_4000-67-1,MNW461_4000
-124-1,MNW461_4000-103-1,MNW461_4000-152-2,JH54_4000-77-2,JH54_4000-77-13,JHMG152_4000-L3,
JHSD2_4000-34,JHSD4-23,JHSD4-32,JHSD4-40,JHSD4-48,JHIC-37 ,JHW74_4000-45 ,JH36_4000-10 ,JH36_4000
-43 ,JH36_4000-74 ,JH36_4000-75 ,JH36_4000-77 ,JH36_4000-107 ,JH36_4000-108 ,JH42_3900-20 ,
JH42_3900-45
,,

14,56,0.25391,0.00037,0.00056,3209.3,2.3,3.5,95% conf.,2.22,MH09_4000-73.1*,TLGDW501_3800-84.1,
TLGDW501_3800-70.1,TLGDW501_3800-61.1,NMH107-4.1,TLGD901-31.1,TLGD901-5.1,TLGD901-62.1,TLGD904
-54.2,TLGD904-83.1,TLGD904-90.1,TLGD904-90.2,TLGD904-19.1,TLGD904-77.1,TLGD904-38.2,TLGD904-50.2,
TLGD904-37.1,TLGD904-76.1,TLGD907-86.1,NNTX-142847.8.1,NNTX-142853.4.1,JHMG152_4000-F3a,
JHMG154_3900-B13,JHMG154_3900-B53,NT88_185-20,NT88_185-15,JHSD3_4000-87,JHSD4-63,JHIC-12 ,JHIC-27
,JHIC-33 ,JHIC-134 ,MNIC-173 ,MNIC-174 ,MNIC-208 ,MNIC-209 ,MNIC-216 ,MNIC-254 ,MNIC-257 ,MNIC
-315 ,MNIC-328 ,JH47_3800-23 ,JH43-3 ,JH43-40 ,JH42_3900-35 ,JH42_3900-71
,,

15,29,0.28691,0.00038,0.00041,3401,2.1,2.2,95% conf.,1.09,MA05_3800-1.1,MA05_3800-36.1,MA05_3800
-79.1,JH986_4000-18.1,JH986_4000-20.1,JH986_4000-32.1,JH986_4000-4.1,TLGD904-81.1,TLGD904-66.1,
TLGD904-66.2,NNTX-142853.5.1,JHSD1_4000-55,JHSD2_4000-3,JHSD2_4000-4,JHSD2_4000-59,JHSD2_4000-60,
JHSD2_4000-73,JHIC-26 ,JHIC-90 ,MNIC-297
,,

16,41,0.35326,0.00044,0.00039,3721.1,1.9,1.7,95% conf.,0.78,MA05_3800-2.1,MA05_3800-18.1*,MA05_3800
-52.1,MA05_3800-59.1*,MA05_3800-80.1,MA05_3800-83.1,BH02-28.1,BH02-45.1,BH02-68.1,BH02-74.1,MA11
-24.1,MA11-27.1,MA11-46.1,MA11-52.1,MA11-53.2,MA13-1.1,MA13-11.1*,MA13-13.1,MA13-48.1,MH169074
-16.1,MA64_4000-16.1,MH178067_3800-34.1,MA01-47.1,MA03_4000-27.1,MA03_4000-31.1,TLGDW501_3800
-77.1,MNW461_4000-100-1,MNW461_4000-82-1,JHSD4-21,JHSD4-37,JHIC-120 ,MNIC-214 ,MNIC-215 ,MNIC-231
,MNIC-240 ,MNIC-245 ,MNIC-246 ,JH42_3900-55
,,

17,32,0.30843,0.00048,0.00046,3513.1,2.4,2.3,95% conf.,0.88,MH169074-3.1,TLGD904-68.1,TLGD904-51.2,
TLGD907-40.1,TLGD907-23.1,TLGD907-85.1,MNIC-105002.15.1,MNIC-105014.12.1,NNTX-142897.7.1,
JHSD2_4000-35,JHIC-109 ,MNIC-242 ,JH54_4000-43 ,JHW74_4000-68 ,JHW74_4000-104 ,JH36_4000-12 ,
JH36_4000-24 ,JH36_4000-47 ,JH36_4000-93 ,JH36_4000-128 ,JH47_3800-4 ,JH43-41 ,JH42_3900-17 ,
JH42_3900-23 ,JH42_3900-29 ,JH42_3900-57
,,

18,49,0.27803,0.00031,0.00037,3351.9,1.7,2.1,95% conf.,1.43,MA05_3800-32.1,BH01-25.2*,MH09_4000
-28.1*,MH09_4000-31.1,MH178065-21.1,MH178065-38.1,MH178066-2.1,MH178066-9.1,MH178066-20.1,
JH986_4000-9.1,NMH107-45.1,NMH107-37.1,TLGD904-79.2,TLGD904-79.3,TLGD904-115.1,TLGD907-12.1,
TLGD907-43.3,TLGD908-9.1,NNTX-142853.17.1,NNTX-142853.18.1,NNTX-142902.8.1,MNW461_4000-145,
JHSD1_4000-15,JHSD1_4000-45,JHSD1_4000-58,JHSD1_4000-78,JHSD2_4000-11,JHSD2_4000-50,JHIC-102 ,
MNIC-251 ,MNIC-326 ,JH54_4000-15 ,JH54_4000-41 ,JH36_4000-29 ,JH36_4000-127 ,JH47_3800-33 ,JH43
-31
,,

19,16,0.30071,0.00035,0.00032,3473.9,1.8,1.7,95% conf.,0.78,BH01-29.2*,MNIC-105009.5.1,MNIC
-105010.11.1,MNIC-105010.9.1,MNIC-105012.10.1,MNIC-105012.11.1,MNIC-105012.13.1,MNIC-105012.14.1,
MNIC-105014.16.1,NNTX-142897.19.1,MNW461_4000-195,MNIC-286 ,MNIC-306 ,MNIC-322
,,

20,24,0.2629,0.00033,0.00016,3264.2,2,0.9,95% conf.,0.22,TLGDW500-4.1,TLGD901-61.1,TLGD901-52.1,
TLGD901-65.1,TLGD904-104.1,TLGD904-75.1,TLGD904-56.1,TLGD904-38.1,TLGD904-63.3,TLGD904-8.2,
TLGD904-100.1,TLGD904-27.1,TLGD904-44.2,TLGD907-80.1,TLGD907-82.1,TLGD907-75.1,TLGD907-77.1,
TLGD908-26.1,NNTX-142897.8.1,JHSD4-62,JHIC-44 ,JHIC-83 ,JHIC-133
,,

21,70,0.4565,0.00075,0.001,4106.5,2.4,3.3,95% conf.,1.75,MNW461_4000-43-1,JHW74_4000-29,JHW74_4000
-66,JH54_4000-10-3,JH54_4000-81-2,JH54_4000-81-3,JH60_4000-51-2,JH60_4000-51-3,JH60_4000-68-3,
JHW74_4000-30-3,JHW74_4000-41-2,JHW74_4000-131-4,JHW74_4000-154-1,JHW74_4000-174-2,JHMG152_4000-
L15-1,JHSD1_4000-30,JH60_4000-25 ,JH60_4000-29 ,JH54_4000-6 ,JH54_4000-54 ,JH54_4000-64 ,
JHW74_4000-48 ,JHW74_4000-94 ,JH36_4000-78
,,

22,35,0.36411,0.00053,0.00066,3767.1,2.2,2.8,95% conf.,1.49,MA07_4000-15.1,MA07_4000-16.1,MA07_4000
-67.1,MA05_3800-27.2,BH02-5.1,BH02-6.1,BH02-10.1,MA11-28.1,MA14-9.1,MA14-23.1,MA14-31.1,MA14
-35.1,MA14-36.1,MA14-39.1,MA14-51.1,MA13-7.1,MA13-14.1,MA13-20.1,MA13-33.1,MA14-65.1,MA64_4000
-28.1,MA64_4000.48.3,MA64_4000.48.4,MA64_4000.48.6,MA64_4000.48.7,MA01-4.1,MA01-11.1,MA03_4000
-106.1,MA03_4000-23.1,MA03_4000-50.1,MA03_4000-70.1,MA04_3800-46.1,TLGDW501_3800
-69.1,,

23,26,0.32856,0.00052,0.00064,3610.4,2.5,3,95% conf.,1.44,MA05_3800-7.1,MA05_3800-37.1,MA05_3800
-48.1,BH01-45.1*,BH01-5.1,BH01-35.1,MA11-20.1,MA11-48.1,MA64_4000-17.1,MH178065-23.1,MA03_4000
-37.1,MA03_4000-48.1*,MA04_3800-15.1*,JHSD2_4000-70,JHSD4-26,JHSD4-46,JHIC-99 ,MNIC-237 ,MNIC-253
,MNIC-264 ,MNIC-269 ,JHW74_4000-86 ,JHW74_4000-119
,,

24,65,0.2323,0.00041,0.00053,3067.9,2.8,3.6,95% conf.,1.62,MH09_4000-96.1*,MH09_4000-169.1*,
JH986_4000-17.1,JH986_4000-17.2,JH986_4000-17.3,JH986_4000-17.4,JH986_4000-17.5,TLGDW501_3800
-88.1,TLGDW501_3800-94.1,TLGD904-1.1,TLGD904-78.1,TLGD907-88.1,TLGD907-42.1,TLGD907-39.1,TLGD907
-64.1,TLGD907-37.1,TLGD908-20.1,TLGD908-21.2,TLGD908-28.1,JHW74_4000-46,JHMG152_4000-F3b,NT88_185
-19,NT88_185-18,NT88_185-13,NT88_194_3900-40,JHSD1_4000-76,JHSD3_4000-40,JHSD4-78,JHIC-119 ,JHIC
-131 ,JHIC-143 ,MNIC-179 ,MNIC-180 ,MNIC-181 ,MNIC-182 ,MNIC-183 ,JH54_4000-18 ,JH54_4000-37
,,

25,56,0.42995,0.00068,0.00095,4017.3,2.4,3.3,95% conf.,1.86,JHW74_4000-2,JH60_4000-68-4,JHW74_4000
-13-2,JHW74_4000-15-2,JHW74_4000-30-2,JHW74_4000-114-2,JHW74_4000-152-2,JHMG154_3900-B13-1,
JHSD1_4000-73,JHSD2_4000-6,JHSD2_4000-32,JH60_4000-13 ,JHW74_4000-4 ,JHW74_4000-6 ,JHW74_4000-46
,JHW74_4000-65 ,JHW74_4000-103
,,

26,10,0.35202,0.00063,0.00112,3715.7,2.7,4.8,95% conf.,2.78,JHIC-34 ,MNIC-212 ,MNIC-217 ,MNIC-228 ,
MNIC-232 ,MNIC-234 ,MNIC-236 ,MNIC-248
,,

```
27,28,0.24157,0.00044,0.00065,3130.4,2.9,4.3,95% conf.,2.02,MH09_4000-87.1*,MH09_4000-2.1,
      TLGDW501_3800-16.1,TLGDW501_3800-54.1,TLGDW501_3800-27.1,TLGDW501_3800-55.1,MNIC-105002.12.1,NNTX
      -142896.1.1,JHMG154_3900-B6,JHSD2_4000-10,JHIC-11 ,JHIC-20 ,JHIC-21 ,JHIC-112 ,JHIC-117 ,JHIC-130
       ,JHIC-141 ,MNIC-175 ,MNIC-176 ,MNIC-177 ,MNIC-178 ,JH43-21 ,JH43-25 ,JH43-43 ,JH43-45 ,JH42_3900
      -22
      ,,,,,,,,,,,,,,,,,,,,,,,,,,,,,,,,,,,,,,,,,,,,,,,,,,,,,,,,,,,,,,,,,,,,,,,,,,,,,,,,,,,,,,,,,,

28,22,0.31853,0.00049,0.00074,3562.8,2.4,3.6,95% conf.,2.21,BH02-23.1,MH09_4000-2.1,JH986_4000-53.1,
      TLGD901-59.1,TLGD904-13.1,TLGD904-121.1,TLGD907-61.1,JHSD1_4000-26,JHSD1_4000-28,JHSD1_4000-40,
      JHSD1_4000-59,JHIC-97 ,JHIC-144 ,MNIC-268 ,MNIC-271 ,MNIC-272
      ,,,,,,,,,,,,,,,,,,,,,,,,,,,,,,,,,,,,,,,,,,,,,,,,,,,,,,,,,,,,,,,,,,,,,,,,,,,,,,,,,,,,,,,,,,

29,50,0.47701,0.00086,0.00114,4171.7,2.7,3.6,95% conf.,1.72,MA64_4000.45.1,MA03_4000-63.2,MNW461_4000
      -121-2,MNW461_4000-19-2,MNW461_4000-118-1,MNW461_4000-83-1,MNW461_4000-63-1,JHW74_4000-88,
      JH54_4000-17-2,JH54_4000-66-4,JH54_4000-66-R2,JH54_4000-77-1,JH54_4000-77-11,JH60_4000-39-2,
      JHW74_4000-143-2,JHSD1_4000-12,JHSD1_4000-23,JH60_4000-22 ,JH54_4000-38 ,JH54_4000-51 ,JHW74_4000
      -52 ,JHW74_4000-74
      ,,,,,,,,,,,,,,,,,,,,,,,,,,,,,,,,,,,,,,,,,,,,,,,,,,,,,,,,,,,,,,,,,,,,,,,,,,,,,,,,,,,,,,,,,,

30,18,0.25122,0.00035,0.00057,3192.5,2.2,3.6,95% conf.,2.52,MH09_4000-98.1*,BH01-28.1,BH01-33.1,
      JH986_4000-44.1,TLGDW500-53.1,TLGDW501_3800-79.1,TLGD901-24.1,TLGD904-4.1,TLGD904-54.1,TLGD904
      -114.1,TLGD908-33.1,NNTX-142848.19.1,NNTX-142853.13.1,NNTX-142897.15.1,JHIC-2 ,JHIC-86
      ,,,,,,,,,,,,,,,,,,,,,,,,,,,,,,,,,,,,,,,,,,,,,,,,,,,,,,,,,,,,,,,,,,,,,,,,,,,,,,,,,,,,,,,,,,

31,35,0.40026,0.00076,0.00119,3910.1,2.8,4.5,95% conf.,2.34,MA07_4000-53.1,MA64_4000-9.1,MA64_4000
      -25.1,MA64_4000.65.1,MA64_4000.65.2,MA64_4000.65.3,MA03_4000-58.2,MA03_4000-17.1,MA03_4000-58.1,
      JH54_4000-77-8,JH60_4000-39-3,JHMG152_4000-L12,JHMG152_4000-L7-1,JHMG154_3900-B18b,JHMG154_3900-
      B46,JH54_4000-26 ,JHW74_4000-128 ,JH42_3900-12 ,JH42_3900-16 ,JH42_3900-50
      ,,,,,,,,,,,,,,,,,,,,,,,,,,,,,,,,,,,,,,,,,,,,,,,,,,,,,,,,,,,,,,,,,,,,,,,,,,,,,,,,,,,,,,,,,,

34,18,0.29522,0.00036,0.00036,3445.3,1.9,1.9,95% conf.,0.93,BH02-52.1,MA14-12.1,MA14-28.1,JH986_4000
      -2.1,TLGDW501_3800-19.1,TLGDW501_3800-44.1,NMH107-21.1,NMH107-23.1,TLGD904-42.1,TLGD904-42.2,
      TLGD907-63.2,TLGD907-68.1,JHSD1_4000-20,MNIC-221 ,MNIC-283 ,MNIC-292 ,MNIC-294
      ,,,,,,,,,,,,,,,,,,,,,,,,,,,,,,,,,,,,,,,,,,,,,,,,,,,,,,,,,,,,,,,,,,,,,,,,,,,,,,,,,,,,,,,,,,

35,29,0.44664,0.0008,0.00085,4074.1,2.7,2.8,95% conf.,1.09,JH986_4000-22.1,JH54_4000-20-3,JH54_4000
      -40-2,JH54_4000-58-3,JHW74_4000-7-2,JHW74_4000-154-2,JHW74_4000-174-3,JHSD1_4000-43,JH54_4000-31
      ,JHW74_4000-8
      ,,,,,,,,,,,,,,,,,,,,,,,,,,,,,,,,,,,,,,,,,,,,,,,,,,,,,,,,,,,,,,,,,,,,,,,,,,,,,,,,,,,,,,,,,,

36,12,0.27092,0.00036,0.0003,3311.4,2.1,1.7,95% conf.,0.61,TLGDW500-61.1,TLGD904-71.1,MNIC
      -105011.17.1,MNIC-105011.17.2,MNIC-105011.18.1,MNIC-105011.20.1,MNIC-105011.5.1,MNIC-105011.7.1,
      MNIC-105011.8.1,MNIC-105011.9.1,JHIC-116 ,MNIC-256
      ,,,,,,,,,,,,,,,,,,,,,,,,,,,,,,,,,,,,,,,,,,,,,,,,,,,,,,,,,,,,,,,,,,,,,,,,,,,,,,,,,,,,,,,,,,

37,18,0.4735,0.00079,0.00103,4160.7,2.5,3.2,95% conf.,1.6,MA64_4000-31.1,MA03_4000-18.3,JH54_4000
      -17-3,JH54_4000-34-2,JH54_4000-34-3,JH54_4000-66-3,JH54_4000-68-2,JH54_4000-78-2,JHSD2_4000
      -29,,,,,,,,,,,,,,,,,,,,,,,,,,,,,,,,,,,,,,,,,,,,,,,,,,,,,,,,,,,,,,,,,,,,,,,,,,,,,,,,,,,,,,,

39,18,0.41809,0.00105,0.0013,3975.4,3.8,4.7,95% conf.,1.44,JH54_4000-17-4,JHW74_4000-36-2,JHW74_4000
      -134-3,JHSD1_4000-44,JHSD1_4000-69,JHSD2_4000-54,JHW74_4000-11 ,JHW74_4000-27 ,JHW74_4000-87 ,
      JHW74_4000-130
      ,,,,,,,,,,,,,,,,,,,,,,,,,,,,,,,,,,,,,,,,,,,,,,,,,,,,,,,,,,,,,,,,,,,,,,,,,,,,,,,,,,,,,,,,,,

41,20,0.38534,0.00133,0.0016,3852.8,5.2,6.3,95% conf.,1.37,MA07_4000-65.1,MA07_4000-65.2,MH09_4000
      -17.1,MH09_4000-8.1,MA64_4000-14.1,MH178067_3800-2.1,TLGDW501_3800-20.1,JHMG154_3900-B33,
      JHMG154_3900-B65,JHMG154_3900-B77,JHMG154_3900-B21-1,JHW74_4000-7 ,JH47_3800-16 ,JH47_3800-21 ,
      JH43-48
      ,,,,,,,,,,,,,,,,,,,,,,,,,,,,,,,,,,,,,,,,,,,,,,,,,,,,,,,,,,,,,,,,,,,,,,,,,,,,,,,,,,,,,,,,,,

43,16,0.48346,0.00105,0.00169,4191.6,3.2,5.2,95% conf.,2.37,MA07_4000-52.2,MA64_4000.40.1*,MA03_4000
      -44.3,MA03_4000-63.3,MA03_4000-18.1,MNW461_4000-121-1,MNW461_4000-87-1,JHW74_4000-13,JH54_4000
      -66-2,JH54_4000-57
      ,,,,,,,,,,,,,,,,,,,,,,,,,,,,,,,,,,,,,,,,,,,,,,,,,,,,,,,,,,,,,,,,,,,,,,,,,,,,,,,,,,,,,,,,,,
```

A.2 Main run script

Main script which calls other scripts for production of a similarity matrix and associated graphs.

```
#!/bin/bash

#
# $1 is the .csv export from CONCH (edited and exported from openoffice or excel)
#
# $2 is the minimum amount of zircons on each group? (have to double check this) typically 0 or 1 or
     2
#

mkdir $1-$2-DIR
cp $1 $1-$2-DIR/
cp all-parsed-zircon-data-YILGARN-2010.data $1-$2-DIR/

echo "CALCULATING_INITIAL_SIMILARITIES_AND_NORMALIZATIONS"

./calculatesimilarities.sh $1 $2

echo "SIMILARITY_GRAPHING"

./graphsimilarities.sh $1

mkdir $1-$2-DIR/HISTOGRAMS
mv *.png $1-$2-DIR/HISTOGRAMS/
mv *.eps $1-$2-DIR/HISTOGRAMS/
```

```
echo "MATRIX OUTPUT"

./similarityonly.sh $1

echo "CONVERTING MATRIX FOR R PLOTS"

./convert-matrix-output-to-R-MATRIX.sh $1-MATRIXOUTPUT

cp -f RPLOT-MATRIX-$1-MATRIXOUTPUT $1-$2-DIR/

echo "STACKED HISTOGRAM GRAPHING"

./stacked-histograms.sh $1

mv *.png $1-$2-DIR/
mv *.eps $1-$2-DIR/

echo "CREATING R GRAPHS"

./R-graphs.sh RPLOT-MATRIX-$1-MATRIXOUTPUT-EDITED
./R-graphs-PCA.sh RPLOT-MATRIX-$1-MATRIXOUTPUT

cp -f RPLOT-MATRIX-$1-MATRIXOUTPUT-EDITED* $1-$2-DIR/

cp -f SAMPLELABELS $1-$2-DIR/
cp -f SIMILARITYPERCENT $1-$2-DIR/
cp -f SIMILARITYPERCENTSORTED $1-$2-DIR/
cp -f STACKEDHISTOGRAMDATA $1-$2-DIR/
cp -f STACKEDHISTOGRAMDATA2 $1-$2-DIR/
cp -f concentrations $1-$2-DIR/
cp -f GROUPEDOUTPUTGRAPHING $1-$2-DIR/
cp -f GROUPEDOUTPUT $1-$2-DIR/
cp -f $1.tex $1-$2-DIR/
cp -f $1.pdf $1-$2-DIR/
cp -f $1-stacked-histograms.tex $1-$2-DIR/
cp -f $1-stacked-histograms.pdf $1-$2-DIR/
```

A.3 Calculate similarities script

Similarity calculation script, pre-processing for similarity matrices.

```
#!/bin/bash

#
#
#
#
#

#
# VARIABLES
#

# define how many samples need to be in each group before we'll use these groups
# eg. '1' to use "all" groups, best to try this with minimum of '3'
#
groupcutoff=3



#
# non user variables
#
TOTALDATA=$(cat $1 | awk '{ count += gsub(/\,[Aa-Zz][Aa-Zz]/,"_x_") } END {print count}')

TOTALGROUPS=$(grep -v Group $1 | wc -l)

# create sample labels file so we can iterate over this
grep -v Group $1 | awk -F"," '{for (i=11; i < NF; i++) print $i }' | awk -F"\\\-" '{print $1}' | awk
    -F"\\\." '{print $1}' | sed '/^$/d' |sort | uniq > SAMPLELABELS
#
# here's a way to just force a single sample
#
#echo "MH09_4000" > SAMPLELABELS


echo ""
echo "Running analysis for file $1"
echo "Group Cutoff: $groupcutoff , Total Data: $TOTALDATA , Total Groups: $TOTALGROUPS"
echo ""


#
# this gets us our real "TOTALDATA" so that our normalizations will work even when excluding
# samples where there are less than X number of a particular analyses of a particular sample in a
    group
#

echo "" > TOTALDATATEMP1
for sample1 in `cat SAMPLELABELS`; do
for age1 in `cat $1 | grep -v Group | awk -F"," '{print $6}'`; do
        SAMPLECOUNT1=$(grep ",$age1," $1 | awk -v sample=$sample1 '{ count += gsub(x,"b") } END {
            print count}' x=$sample1)
        #
```

```
        # here we limit the sample count in each sample, do we allow for a lower limit of "1" in each
              sample?
        # if so, we may bias samples that have random bits in other samples due to a single zircon
             grain ending up there
        #
        if [ "$SAMPLECOUNT1" -le "$2" ]
                then
                SAMPLECOUNT1="0"
                else
                echo -n ""
        fi
        echo "$sample1,$age1,$SAMPLECOUNT1" ; done; done > TOTALDATATEMP1


echo "Analyzing sample, exporting to file 'GROUPEDOUTPUT'"

#
# goes through each sample and age group and counts up number of that particular sample in each age
     group and exports in .csv format for easy graphing
#

for sample in `cat SAMPLELABELS`; do
        SAMPLETOTAL=$(grep $sample TOTALDATATEMP1 | awk -F"," '{ORS="+"; print $3}' | awk -F"+$" '{
             print $1}' | concalc)
        #echo "$SAMPLETOTAL"
        #SAMPLETOTAL=$(cat $1 | awk -v sample=$sample '{ count += gsub(x,"b") } END {print count}' x=
             $sample)
        GROUPSINSAMPLE=$(grep "$sample," TOTALDATATEMP1 | grep -v "*,0$" | wc -l)
        #echo $GROUPSINSAMPLE
for age in `cat $1 | grep -v Group | awk -F"," '{print $6}'`; do
        THEAGEGROUP=$(grep ",$age," $1 | awk -F"," '{print $1}')
        SAMPLECOUNT=$(grep "$sample,$age," TOTALDATATEMP1 | awk -F"," '{print $3}')
        #echo "SAMPLECOUNT = $SAMPLECOUNT"
        #SAMPLECOUNT=$(grep ",$age," $1 | awk -v sample=$sample '{ count += gsub(x,"b") } END {print
             count}' x=$sample)
        #
        # here we limit the sample count in each sample, do we allow for a lower limit of "1" in each
              sample?
        # if so, we may bias samples that have random bits in other samples due to a single zircon
             grain ending up there
        #
        #if [ "$SAMPLECOUNT" -le "$2" ]
        #       then
        #       SAMPLECOUNT="0"
        #       else
        #       echo -n ""
        #fi
        TOTALGROUPDATA=$(grep ",$age," TOTALDATATEMP1 | awk -F"," '{ORS="+"; print $3}' | awk -F"+$"
             '{print $1}' | concalc)
        #echo "totalgroupdata = $TOTALGROUPDATA"
        #TOTALGROUPDATA=$(grep ",$age," $1 | awk '{ count += gsub(/\,[Aa-Zz][Aa-Zz]/,"_x_") } END {
             print count}')
        #
        # here's where we get the concentration info for U, Th, and Titanium temperatures
        #
        echo "" > concentrations
        for samplelabel in `grep ",$age," $1 | awk -F"," '{ORS="\n"; for (n=11; n<=NF; n++) print $n
             }' | grep $sample | sed 's/_3900//g' | sed 's/_3800//g' | sed 's/_4000//g' | sed 's/\*//g
             ' | sed '/^$/d' | sed -e 's/[ \t]*$//' | grep "[A-Z*]" `; do
                U=$(grep $samplelabel all-parsed-zircon-data-YILGARN-2010.data | awk '{print $2}')
                TH=$(grep $samplelabel all-parsed-zircon-data-YILGARN-2010.data | awk '{print $3}')
                TI=$(grep $samplelabel TI-DATA-FULL.csv | awk -F"," '{print $6}')
                if [ "$TI" > "0" ]
                        then
                        TI=$TI
                        else
                        TI="0"
                fi
                echo "$sample,$U,$TH,$TI,$age"; done >> concentrations
                SAMPLELABELNUMBER=$(grep ",$age," $1 | awk -F"," '{ORS="\n"; for (n=11; n<=NF; n++)
                     print $n}'| grep $sample | sed 's/_3900//g' | sed 's/_3800//g' | sed 's/_4000//g'
                      | sed 's/\*//g' | sed '/^$/d' | grep "[A-Z*]" | wc -l)
                if [ "$SAMPLELABELNUMBER" -le "$2" ]
                        then
                        SAMPLELABELNUMBER="0"
                        else
                        echo -n ""
                fi
                #TISAMPLENUMBER=$(grep $samplelabel TI-DATA-FULL.csv |)
                UCONCENTRATION1=$(grep $sample concentrations | grep $age | awk -F"," '{ORS="+";
                     print $2}' | awk -F"+$" '{print $1}' | concalc)
                THCONCENTRATION1=$(grep $sample concentrations | grep $age | awk -F"," '{ORS="+";
                     print $3}' | awk -F"+$" '{print $1}' | concalc)
                #echo "UCONC: $UCONCENTRATION1 THCONC: $THCONCENTRATION1"
                UCONC=$(echo "$UCONCENTRATION1/$SAMPLELABELNUMBER" |concalc -o 3)
                THCONC=$(echo "$THCONCENTRATION1/$SAMPLELABELNUMBER" |concalc -o 3)
                TISAMPLELABELNUMBER=$(grep $sample concentrations | grep $age | grep -v ",0,$age" |
                     wc -l)
                if [ "$TI" > "2" ]
                        then
                        TITEMP1=$(grep $sample concentrations | grep $age | awk -F"," '{ORS="+";
                             print $4}' | awk -F"+$" '{print $1}' | concalc)
                        TITEMP=$(echo $TITEMP1/$TISAMPLELABELNUMBER |concalc -o 3)
                        else
                        TITEMP=1
                fi
                THU=$(echo "$THCONC/$UCONC" |concalc -o 3)
        #
        #
        NORMALIZED=$(echo $SAMPLECOUNT/$SAMPLETOTAL | concalc -o 3)
        NORMALIZEDPERCENT=$(echo $NORMALIZED*100 | concalc -o 3)
        #
```

```
        # is this right? do we really use totaldata here, or should just use all data in all groups
            of this particular group?
        #
        #NORMALIZEDGROUP=$(echo $TOTALGROUPDATA/$TOTALDATA | concalc -o 3)
        NORMALIZEDGROUP=$(echo $TOTALGROUPDATA/$TOTALDATA | concalc -o 3)
        NORMALIZEDGROUP2=$(echo $NORMALIZEDGROUP*100 | concalc -o 3)
        PERCENTGROUPTOTAL=$(echo $NORMALIZED/$NORMALIZEDGROUP |concalc -o 3)
        if [ "$NORMALIZEDPERCENT" == 0 ]
                then
                SAMPLEMINUSTOTALPERCENT="0"
                else
                SAMPLEMINUSTOTALPERCENT=$(echo abs\($NORMALIZEDGROUP2-$NORMALIZEDPERCENT\) |concalc -
                    o 3)
        fi
        GROUPPERCENTSIMILAR=$(echo $SAMPLEMINUSTOTALPERCENT/$TOTALGROUPS |concalc -o 3)
        echo "$sample,$THEAGEGROUP,$age,$SAMPLECOUNT,$SAMPLETOTAL,$NORMALIZEDPERCENT,
            $NORMALIZEDGROUP2,$PERCENTGROUPTOTAL,$GROUPSINSAMPLE,$TOTALGROUPS,$TOTALGROUPDATA,
            $TOTALDATA,$SAMPLEMINUSTOTALPERCENT,$GROUPPERCENTSIMILAR,$UCONC,$THCONC,$TITEMP,$THU" ;
            done; done > GROUPEDOUTPUT


echo "Calculating Similarity Percentages of each sample compared to All data, exporting to file '
    SIMILARITYPERCENT'"


for sample in `cat SAMPLELABELS`; do
        #
        # add up all calculated 'similarity percentages' per group for each sample...
        #
        CONCALC=$(grep $sample GROUPEDOUTPUT | awk -F"," '{ORS="+"; print $13}' | awk -F"+$" '{print
            $1}' | concalc -o 4)
        #for group in `grep $sample GROUPEDOUTPUT | grep -v Group | awk -F"," '{print $3}'`; do
        #TOTALGROUP=$(grep $sample GROUPEDOUTPUT |grep $group |
        #
        # divide total calculated similarity for each sample and divide by all groups found in "total
            " sample
        #
        CONCALCDIVGROUPS=$(echo "\(100*\($CONCALC\)\)/$TOTALGROUPS" | concalc -o 3)
        NUMBERINGROUP=$(grep $sample GROUPEDOUTPUT | awk -F"," '{print $5}' | tail -1)
        GROUPSINSAMPLE=$(grep $sample GROUPEDOUTPUT | awk -F"," '{print $9}' | tail -1)
        echo "$sample,$CONCALC,$NUMBERINGROUP,$GROUPSINSAMPLE" ; done > SIMILARITYPERCENT
cat SIMILARITYPERCENT | sort -t, -k2 -n > SIMILARITYPERCENTSORTED
echo "sample,similarity,analyses,groups" > SIMILARITYPERCENT
cat SIMILARITYPERCENTSORTED >> SIMILARITYPERCENT
```

A.4 Graph similarities script

Graphing script from previously processed similarity matrix and percentage of similarities scripts.

```
#!/bin/bash


#####
#
# SET THESE VARIABLES


# set start and end date in Ma (fits sample to this area on y-scale, places bins within this area)
startdate=2900
enddate=4400

# set bin size
binwidthset=10

# set x tics labels (what interval to label the x axis?) relates directly to startdate and enddate,
    which is the x size.
xtics=50

# END OF VARIABLES
#
#####


#
# start output for latex document summary graphs
#

#
# initialize the .tex
#
echo "" > $1.tex

echo -E "\documentclass[11pt,a4paper]{article}
\usepackage{fullpage}
\usepackage{float}
\usepackage{textcomp}
\usepackage{graphicx}
\usepackage{amsmath}
\usepackage{verbatim}
\usepackage{alltt}
\usepackage{lscape}
\RequirePackage{longtable}
%\renewcommand{\textfraction{.15}}
%\renewcommand{\floatpagefraction{.85}}
```

```
\begin{document}
\begin{center}

Normalized probability histogram for all samples by Age\\

" >> $1.tex


sed 's/,0$/,/g' GROUPEDOUTPUT | sed 's/,0,/,,/g' > GROUPEDOUTPUTGRAPHING

#
# "overview" plot for ALL data from all samples
#

#TOTALDATA=$(cat $1 | awk '{ count += gsub(/\,[BMPJNEYT1][AHRDINMLG476]/,"_x_") } END {print count}')
TOTALDATA=$(cat GROUPEDOUTPUT | awk -F"," '{print $12}' | tail -1)
TOTALDATA2=$(grep -v labels all-parsed-zircon-data-YILGARN-2010.data | wc -l)
TOTALPERCENT=$(cat GROUPEDOUTPUT | awk -F"," '{ORS="+"; print $7}' | awk -F"+$" '{print $1}' |
    concalc)
USEDANALYSES=$(echo "$TOTALDATA2-$TOTALDATA" | concalc -o 3)
PERCENTUSED=$(echo "($TOTALDATA/$TOTALDATA2)*100" | concalc -o 3)
echo "$USEDANALYSES_$PERCENTUSED"
echo "set title \"ALL Zircon Groups\";
        set ylabel \"Frequency (percent)\";
        set xlabel \"207Pb/206Pb Age (Ma) of Group\";
        set key top Right right enhanced nobox;
        set size 2.0,1.0;
        set terminal postscript eps 22 color solid enhanced;
        set output 'ALL-histogram.eps';
        set yrange [0:20];
        set xrange [$startdate:$enddate];
        set xtics $xtics;
        set xtic rotate by -45;
        set style data histograms;
        set style histogram cluster gap 0;
        set style fill solid border -1;
        set boxwidth $binwidthset;
        total = \"+/-10% conc. analyses = $TOTALDATA\";
        total2 = \"All Analyses = $TOTALDATA2\";
        usedanalyses = \"Unused=$USEDANALYSES\";
        percentused = \"Used=$PERCENTUSED%\";
        totalpercent = \"Total Group % = $TOTALPERCENT\";
        set label 1 sprintf(\"%s %s\",total,totalpercent) at graph 0.02,0.9 ;
        set label 2 sprintf(\"%s %s %s\",total2,usedanalyses,percentused) at graph 0.02,0.8 ;
        plot \"<cat GROUPEDOUTPUT | awk -F',' '{print \$1,\$2,\$3,\$4,\$5,\$6,\$7,\$8,\$9,\$10,\$11,\
    $12,\$13,\$14}'\" using 3:7 notitle with boxes fs solid 0.7 , '' using 3:7:7 with labels rotate by
    -90 right offset 0,2 notitle;
        " | gnuplot
convert ALL-histogram.eps ALL-histogram.png

echo -E "\begin{figure}[H]
\includegraphics[width=7in,height=2.6in]{ALL-histogram.eps}
\end{figure}" >> $1.tex

echo -E "
\clearpage

Normalized Probability histograms by Age\\

" >> $1.tex


#
# individual plots for each sample
#

for samples in `cat SAMPLELABELS`; do
SAMPLETOTAL=$(grep $samples GROUPEDOUTPUT | awk -F"," '{print $5}' | tail -1)
SIMILARITY=$(grep $samples SIMILARITYPERCENT | awk -F"," '{print $2}')
TOTALSAMPLE=$(grep -v labels all-parsed-zircon-data-YILGARN-2010.data |grep $samples | wc -l)
TOTALPERCENT=$(grep "$samples" GROUPEDOUTPUT | awk -F"," '{ORS="+"; print $6}' | awk -F"+$" '{print
    $1}' | concalc)
USEDANALYSES=$(echo "$TOTALSAMPLE-$SAMPLETOTAL" | concalc -o 3)
PERCENTUSED=$(echo "($SAMPLETOTAL/$TOTALSAMPLE)*100" | concalc -o 3)
echo -n "graphing up $samples groups: "

echo ""

echo "set title \"$samples Zircon Group Age\";
        set ylabel \"Frequency (percent)\";
        set xlabel \"207Pb/206Pb Age (Ma) of Group\";
        set key top Right right enhanced nobox;
        set size 2.0,1.0;
        set terminal postscript eps 22 color solid enhanced;
        set output '$samples-histogram.eps';
        set yrange [0:100];
        set xrange [$startdate:$enddate];
        set xtics $xtics;
        set xtic rotate by -45;
        set style data histograms;
        set style histogram cluster gap 0;
        set style fill solid border -1;
        set boxwidth $binwidthset;
        total = \"+/-10% conc. analyses = $SAMPLETOTAL\";
        similarity = \"Dissimilarity: $SIMILARITY %\";
        total2 = \"All Analyses = $TOTALSAMPLE\";
        totalpercent = \"Total Group % = $TOTALPERCENT\";
        usedanalyses = \"Unused=$USEDANALYSES\";
        percentused = \"Used=$PERCENTUSED%\";
        set label 1 sprintf(\"%s %s\",total,totalpercent) at graph 0.02,0.9 ;
        set label 2 sprintf(\"%s %s %s\",total2,usedanalyses,percentused) at graph 0.02,0.8 ;
        set label 3 sprintf(\"%s\",similarity) at graph 0.02,0.7 ;
```

```
        plot \"<cat GROUPEDOUTPUT | grep '$samples' | awk -F',' '{print \$1,\$2,\$3,\$4,\$5,\$6,\$7,\
    $8,\$9,\$10,\$11,\$12,\$13,\$14}'\" using 3:6 notitle with boxes, '' using 3:6:6 with labels
    rotate by -90 right offset 0,2 notitle;
        " | gnuplot
convert $samples-histogram.eps $samples-histogram.png
echo -E "\begin{figure}[H]
\includegraphics[width=7in,height=2.6in]{$samples-histogram.eps}
\end{figure}

" >> $1.tex; done


echo -E "\clearpage

Normalized Probability histograms by group\\

" >> $1.tex


for samples in `cat SAMPLELABELS`; do
SAMPLETOTAL=$(cat $1 | awk -v sample=$samples '{ count += gsub(x,"b") } END {print count}' x=$samples
    )
SIMILARITY=$(grep $samples SIMILARITYPERCENT | awk -F"," '{print $2}')
TOTALSAMPLE=$(grep -v labels all-parsed-zircon-data-YILGARN-2010.data |grep $samples | wc -l)
TOTALPERCENT=$(grep "$samples" GROUPEDOUTPUT | awk -F"," '{ORS="+"; print $6}' | awk -F"+$" '{print
    $1}' | concalc)
USEDANALYSES=$(echo "$TOTALSAMPLE-$SAMPLETOTAL" | concalc -o 3)
PERCENTUSED=$(echo "($SAMPLETOTAL/$TOTALSAMPLE)*100" | concalc -o 3)
echo -n "graphing up $samples groups: "
for groups in `cat $1 |grep $samples`; do echo -n "$groups "; done
echo ""
echo "set title \"$samples Zircon Groups\";
        set ylabel \"Frequency (percent)\";
        set xlabel \"Group Number (CONCH output)\";
        set key top Right right enhanced nobox;
        set size 2.0,1.0;
        set terminal postscript eps 22 color solid enhanced;
        set output '$samples-groups-histogram.eps';
        set yrange [0:100];
        #set xrange [$startdate:$enddate];
        #set xtics $xtics;
        set style data histogram;
        set style histogram rowstacked;
        set style histogram cluster gap 1;
        set style fill solid border 1;
        #set boxwidth $binwidthset;
        total = \"+/-10% conc. analyses = $SAMPLETOTAL\";
        similarity = \"Dissimilarity: $SIMILARITY %\";
        total2 = \"All Analyses = $TOTALSAMPLE\";
        totalpercent = \"Total Group % = $TOTALPERCENT\";
        usedanalyses = \"Unused=$USEDANALYSES\";
        percentused = \"Used=$PERCENTUSED%\";
        set label 1 sprintf(\"%s %s\",total,totalpercent) at graph 0.02,0.9;
        set label 2 sprintf(\"%s %s %s\",total2,usedanalyses,percentused) at graph 0.02,0.8;
        set label 3 sprintf(\"%s\",similarity) at graph 0.02,0.7;
        plot \"<cat GROUPEDOUTPUT | grep '$samples' | awk -F',' '{print \$1,\$2,\$3,\$4,\$5,\$6,\$7,\
    $8,\$9,\$10,\$11,\$12,\$13,\$14}'\" using 2:6 notitle with boxes, '' using 2:6:6 with labels
    rotate by -90 center offset 0,1 notitle;
        " | gnuplot
convert $samples-groups-histogram.eps $samples-groups-histogram.png
echo -E "\begin{figure}[H]
\begin{center}
\includegraphics[width=7in,height=2.6in]{$samples-groups-histogram.eps}
\end{center}
\end{figure}

" >> $1.tex; done


#
# multiplot stacked histograms
#
echo -E "\end{center}
\clearpage
\end{document}" >> $1.tex

#latex $1.tex
#latex $1.tex
#dvipdfm -l $1-$2.tex
#dvipdfm $1.dvi

rm -f *.aux *.dvi *.log
```

A.5 Calculate similarities script for graphing

Simply calculates similarities for graphing purposes.

```
#!/bin/bash


TOTALGROUPS=$(grep -v Group $1 | wc -l)

for sample in `cat SAMPLELABELS`; do
        #
        # add up all calculated 'similarity percentages' per group for each sample...
```

```
        #
        CONCALC=$(grep $sample GROUPEDOUTPUT | awk -F"," '{ORS="+"; print $13}' | awk -F"+$" '{print
             $1}' | concalc -o 4)
        #for group in `grep $sample GROUPEDOUTPUT | grep -v Group | awk -F"," '{print $3}'`; do
        #TOTALGROUP=$(grep $sample GROUPEDOUTPUT |grep $group |
        #
        # divide total calculated similarity for each sample and divide by all groups found in "total
             " sample
        #
        CONCALCDIVGROUPS=$(echo "$CONCALC/$TOTALGROUPS" | concalc -o 3)
        NUMBERINGROUP=$(grep $sample GROUPEDOUTPUT | awk -F"," '{print $5}' | tail -1)
        GROUPSINSAMPLE=$(grep $sample GROUPEDOUTPUT | awk -F"," '{print $9}' | tail -1)
        echo "$sample,$CONCALCDIVGROUPS,$NUMBERINGROUP,$GROUPSINSAMPLE" ; done > SIMILARITYPERCENT
cat SIMILARITYPERCENT | sort -t, -k2 -n > SIMILARITYPERCENTSORTED
echo "sample,similarity,analyses,groups" > SIMILARITYPERCENT
cat SIMILARITYPERCENTSORTED >> SIMILARITYPERCENT


echo "" > $1-MATRIXOUTPUT
sample1count=1
for sample1 in `cat SAMPLELABELS`; do
        #CONCALC=$(grep $sample GROUPEDOUTPUT | awk -F"," '{ORS="+"; print $6}' | awk -F"+$" '{print
             $1}' | concalc -o 4)
        SAMPLE1GROUPCOUNT=$(grep $sample1 GROUPEDOUTPUT | awk -F"," '{print $9}' | tail -1)
        echo "OUTPUT FOR SAMPLE $sample1"
        sample2count=1
        for sample2 in `cat SAMPLELABELS`; do
                SAMPLE2GROUPCOUNT=$(grep $sample2 GROUPEDOUTPUT | awk -F"," '{print $9}' | tail -1)
                        if [ "$SAMPLE1GROUPCOUNT" -gt "$SAMPLE2GROUPCOUNT" ]
                                then
                                GROUPCOUNT="$SAMPLE1GROUPCOUNT"
                                else
                                GROUPCOUNT="$SAMPLE2GROUPCOUNT"
                        fi
                echo "" > tmpcalc
                echo "calculating group differences between $sample1 and $sample2 out of $GROUPCOUNT
                     groups. $SAMPLE1GROUPCOUNT,$SAMPLE2GROUPCOUNT"
                for group in `grep $sample2 GROUPEDOUTPUT | awk -F"," '{print $3}'`; do

                        SAMPLE1GROUPNORM=$(grep $sample1 GROUPEDOUTPUT |grep $group | awk -F"," '{
                             print $6}' | tail -1)
                        SAMPLE2GROUPNORM=$(grep $sample2 GROUPEDOUTPUT |grep $group | awk -F"," '{
                             print $6}' | tail -1)

                        GROUP1MINUSGROUP2=$(echo abs\($SAMPLE1GROUPNORM-$SAMPLE2GROUPNORM\) |concalc
                             -o 3)


#                       NORMALIZEDGROUP=$(echo $TOTALGROUPDATA/$TOTALDATA | concalc -o 3)
#                       NORMALIZEDGROUP2=$(echo $NORMALIZEDGROUP*100 | concalc -o 3)
#                       PERCENTGROUPTOTAL=$(echo $NORMALIZED/$NORMALIZEDGROUP |concalc -o 3)
#                       if [ "$NORMALIZEDPERCENT" == 0 ]
#                               then
#                               SAMPLEMINUSTOTALPERCENT="0"
#                               else
#                               SAMPLEMINUSTOTALPERCENT=$(echo abs\($NORMALIZEDGROUP2-
     $NORMALIZEDPERCENT\) |concalc -o 3)
#                       fi
                        echo "$sample1,$sample2,$group,$SAMPLE1GROUPCOUNT,$SAMPLE2GROUPCOUNT,
                             $GROUP1MINUSGROUP2,$SAMPLE1GROUPNORM,$SAMPLE2GROUPNORM" >> tmpcalc
                        echo -n "."; done
                S1S2=$(grep "$sample1,$sample2" tmpcalc | awk -F"," '{ORS="+"; print $6}' | awk -F"+$
                     " '{print $1}' | concalc -o 4)
                SAMPLEDIFF=$(echo "$S1S2/$GROUPCOUNT" | concalc -o 4)
                echo " calculated diff = $SAMPLEDIFF"
                echo "$sample1count,$sample2count,$sample1,$sample2,$SAMPLEDIFF" >> $1-MATRIXOUTPUT
                let "sample2count += 1"; done
        let "sample1count += 1";
        echo "Finished with sample $sample1"; done

#
# from here, add up each "sample"'s similiarity (like done in office) and add to end of each line.
# graph up in gnuplot with this info on X, %similar on Y, and each sample labelled?
# to do: add math to label "outliers" from the rest, or most similar groups to others based on
     calculating chi-square, or lowest difference from the mean?
#

#CONCALC=$(grep $sample1 GROUPEDOUTPUT | awk -F"," '{ORS="+"; print $13}' | awk -F"+$" '{print $1}' |
      concalc -o 4)
```

A.6 Convert matrix to R format covariance matrix script

Converts similarity matrix from the previous script into an R-compatible covariance matrix for statistical processing with FactoMineR.

```
#!/bin/bash


#
#
#
#

TOTALGROUPS=$(cat $1 | awk -F"," '{print $3}' | uniq | wc -l)
```

```
#
# here's the matrix header
#
rm -f RPLOT_MATRIX_$1
for sample1 in `cat $1 | awk -F"," '{print $3}' | uniq`; do
        echo -n ",$sample1"; done >> RPLOT_MATRIX_$1

echo "" >> RPLOT_MATRIX_$1
#
# here's the lines of similarity index correlation data to populate the matrix
#
for sample1 in `cat $1 | awk -F"," '{print $3}' | uniq`; do
        echo -n "$sample1"
        for sample2 in `cat $1 | grep "^[0-9][0-9]*,*[0-9][0-9]*,$sample1," | awk -F"," '{print $5
             }'`; do
        echo -n ",$sample2"; done
        echo ""; done >> RPLOT_MATRIX_$1

#
# create EDITED matrix for pvclust (without first column of labels)
#

rm -f RPLOT_MATRIX_$1_EDITED
for sample1 in `cat $1 | awk -F"," '{print $3}' | uniq`; do
        echo -n ",$sample1"; done | cut -b 1 --complement >> RPLOT_MATRIX_$1_EDITED

#echo "" >> RPLOT_MATRIX_$1_EDITED
#
# here's the lines of similarity index correlation data to populate the matrix
#
for sample1 in `cat $1 | awk -F"," '{print $3}' | uniq`; do
        #echo -n "$sample1"
        for sample2 in `cat $1 | grep "^[0-9][0-9]*,*[0-9][0-9]*,$sample1," | awk -F"," '{print $5
             }'`; do
        echo -n ",$sample2"; done
        echo ""; done | cut -b 1 --complement >> RPLOT_MATRIX_$1_EDITED
```

A.7 Script to produce stacked histograms

Creates a relatively simple stacked histogram plot from matrix data for a visual representation of percentage of each shared group in each sample.

```
#!/bin/bash

TOTALGROUPS=$(grep -v Group $1 | wc -l)

#
# start output for latex document summary graphs
#

#
# initialize the .tex
#
echo "" > $1-stacked-histograms.tex

echo -E "\documentclass[landscape,11pt,a4paper]{article}
\usepackage{fullpage}
\usepackage{float}
\usepackage{textcomp}
\usepackage{graphicx}
\usepackage{amsmath}
\usepackage{verbatim}
\usepackage{alltt}
\usepackage{lscape}
\RequirePackage{longtable}
%\renewcommand{\textfraction{.15}}
%\renewcommand{\floatpagefraction{.85}}
\begin{document}
\begin{center}

Normalized group percentage per sample plotted as stacked histograms\\

" >> $1-stacked-histograms.tex



#
# create output for stacked histogram data from GROUPEDOUTPUT
#

echo "" > STACKEDHISTOGRAMDATA

for sample in `cat SAMPLELABELS`; do echo -n "$sample"; for group in `grep $sample GROUPEDOUTPUT |
     awk -F"," '{print $3}'`; do echo -n "_$group"; done; echo ""; done | tail -1 | awk '{OFS="\n";
     ORS="_"; print "Sample_SIMILARITY"; for (n=2; n <= NF; n++) print $n}' >> STACKEDHISTOGRAMDATA
echo "" >> STACKEDHISTOGRAMDATA

for sample in `cat SAMPLELABELS`; do SIMILARITY1=$(grep $sample $1_MATRIXOUTPUT | awk -F"," '{ORS="+"
     ; print $5}' | awk -F"+$" '{print $1}' | concalc); SIMILARITY=$(echo "$SIMILARITY1/$TOTALGROUPS"
     | concalc -o 3); echo -n "$sample_$SIMILARITY"; for group in `grep $sample GROUPEDOUTPUT | awk -F
     "," '{print $6}'`; do echo -n "_$group"; done; echo ""; done > STACKEDHISTOGRAMDATA2
```

```
cat STACKEDHISTOGRAMDATA2 | sort -k2 -n >> STACKEDHISTOGRAMDATA
sed -i '/^$/d' STACKEDHISTOGRAMDATA


#XTICS=$(n=1; for sample in `cat SAMPLELABELS`; do echo -n "\\"\"$sample\\"\" $n, "; let "n += 1";
     done | awk -F", $" '{print $1}')
XTICS=$(n=1; for sample in `grep -v Sample STACKEDHISTOGRAMDATA | awk '{print $1}'`; do echo -n "\"
     $sample\" $n, "; let "n+=1"; done | awk -F",$" '{print $1}')

X2TICS=$(n=1; for percent in `grep -v Sample STACKEDHISTOGRAMDATA | awk '{print $2}'`; do echo -n "\"
     $percent\" $n, "; let "n+=1"; done | awk -F", $" '{print $1}')

echo $XTICS
echo $X2TICS

#ie:
# YNWG142986 6.82 0 29.5 0 0 0 0 4.55 0 9.09 0 2.27 0 9.09 2.27 2.27 2.27 2.27 0 2.27 0 11.4 0 0 2.27
     2.27 0 4.55 0 0 0 6.82 0 0 0 0 0 0 0 0 0 0 0 0 0
# YNWG168945 0 0 0 33.3 0 0 0 0 0 0 0 0 66.7 0 0 0 0 0 0 0 0 0 0 0 0 0 0 0 0 0 0 0 0 0 0 0 0 0 0 0 0 0
     0 0 0 0 0
# etc.


#for samples in `cat SAMPLELABELS`; do
#SAMPLETOTAL=$(grep $samples GROUPEDOUTPUT | awk -F"," '{print $5}' | tail -1)
#SIMILARITY=$(grep $samples SIMILARITYPERCENT | awk -F"," '{print $2}')
#TOTALSAMPLE=$(grep -v labels all-parsed-zircon-data-YILGARN-2010.data |grep $samples | wc -l)
#TOTALPERCENT=$(grep "$samples" GROUPEDOUTPUT | awk -F"," '{ORS="+"; print $6}' | awk -F"+$" '{print
     $1}' | concalc)
#USEDANALYSES=$(echo "$TOTALSAMPLE-$SAMPLETOTAL" | concalc -o 3)
#PERCENTUSED=$(echo "($SAMPLETOTAL/$TOTALSAMPLE)*100" | concalc -o 3)

echo "# set terminal png transparent nocrop enhanced font arial 8 size 420,320 ;
# set output 'histograms.5.png';
set size 3.5,2.5;
set terminal postscript eps 22 color solid enhanced;
set output '$1-STACKED-HISTOGRAM.eps';
set border 3 front linetype -1 linewidth 1.000;
set boxwidth 1.00 absolute;
set style fill   pattern 1.00 border -1;
set grid nopolar;
set grid noxtics nomxtics ytics nomytics noztics nomztics nox2tics nomx2tics noy2tics nomy2tics
     nocbtics nomcbtics;
set grid layerdefault   linetype 0 linewidth 1.000,  linetype 0 linewidth 1.000;
set key outside right top vertical Left reverse enhanced autotitles columnhead nobox;
set key invert samplen 5 spacing 0.95 width 0 height 0 ;
set key title \"Group Age (Ma)\";
set style histogram rowstacked title offset character 0, 0, 0;
set datafile missing '-';
set style data histograms;
set xtics border in scale 1,0.5 nomirror rotate by -45  offset character 0, 0, 0 ;
set xtics ($XTICS);
set x2tics border in scale 0,0 nomirror rotate by 45  offset character 0, 0, 0 ;
set x2tics ($X2TICS);
set noytics;
set title \"Normalized group probabilities per sample\" ;
set ylabel \"Percent of total\" ;
set xlabel \"Sample Number (left to right - most similar to most dissimilar to all pooled samples)\";
set x2label \"Percent Dissimilar to all pooled samples\";
set y2label \"Largest groups to smallest groups (Bottom to Top in key)\";
set yrange [0:100] noreverse nowriteback;
i = 48;
plot 'STACKEDHISTOGRAMDATA' using 3:xtic(1) t column(3), for [i=4:48] '' using i:x2tic(2) title
     column(i);" | gnuplot
convert $1-STACKED-HISTOGRAM.eps $1-STACKED-HISTOGRAM.png

echo -E "\begin{figure}[H]
\includegraphics[width=5in,height=3in]{$1-STACKED-HISTOGRAM.eps}
\end{figure}" >> $1-stacked-histograms.tex


echo -E "\end{center}
\clearpage
\end{document}" >> $1-stacked-histograms.tex

#latex $1-stacked-histograms.tex
#latex $1-stacked-histograms.tex
#dvipdfm -l $1-stacked-histograms.dvi

rm -f *.aux *.dvi *.log
```

A.8 R statistical language graph output scripts

R script for generating a set of standard R graphs for visual representation of data.

```
#!/bin/bash

#
# runs R scripts for creation of graphs
#
#

#
#echo "CREATING R GRAPHS"
```

```
#
#./R-graphs.sh RPLOT-MATRIX-$1-EDITED
#

cp -f PVCLUST.R PVCLUST-RUN.R
sed -i "s/TOBEADDEDBYSCRIPT/$1/g" PVCLUST-RUN.R
Rscript PVCLUST-RUN.R
```

A.9 Automated clustering script for R

R script for generating statistically generated clusters from the similarity matrix.

```
SIMILARITYMATRIX <-
read.table("RPLOT-MATRIX-2010-FEB-27-NEWSCRIPTS-NORM-EXCLUDE-3247-OLD.csv-MATRIXOUTPUT-EDITED",
    header=TRUE, sep=",", na.strings="nan", dec=".", strip.white=TRUE)

mydata <- na.omit(SIMILARITYMATRIX) # listwise deletion of missing
mydata <- scale(mydata) # standardize variables


#A4=     8.3     11.7
pdf.options(onefile=TRUE, paper="a4r", pagecentre=TRUE)
pdf(file="RPLOT-MATRIX-2010-FEB-27-NEWSCRIPTS-NORM-EXCLUDE-3247-OLD.csv-MATRIXOUTPUT-EDITED.pdf",
     onefile=TRUE, width=11, height=8, paper="a4r", pagecentre=T
RUE)


#######
# Ward Hierarchical Clustering with Bootstrapped p values

library(pvclust)

#dist(model.matrix(~-1, mydata))
#fit <- pvclust(mydata, method.hclust="mcquitty", method.dist="correlation", nboot=100, use.cor="
     pairwise.complete.obs")
fit <- pvclust(mydata, method.hclust="mcquitty", method.dist="correlation", use.cor="pairwise.
     complete.obs",nboot=100, r=seq(.5,1.4,by=.1), store=FALSE, weig
ht=FALSE)
plot(fit) # dendogram with p values

# add rectangles around groups highly supported by the data
#pvrect(fit, alpha=0.95, pv="au", max.only=FALSE)

plot(fit)
pvrect(fit, alpha=0.95, pv="au", max.only=FALSE)
plot(fit)
pvrect(fit, alpha=0.90, pv="au", max.only=FALSE)

#r=seq(.5,1.4,by=.1)
fit <- pvclust(mydata, method.hclust="mcquitty", r=seq(.1,1.9,by=.1), method.dist="correlation",
     nboot=100)
plot(fit)
pvrect(fit, alpha=0.95, pv="au")
plot(fit)
pvrect(fit, alpha=0.90, pv="au")

library(ca)
fit <- ca(Dataset)
plot(fit) # symmetric map
plot(fit, mass = TRUE, contrib = "absolute", map = "rowgreen", arrows = c(FALSE, TRUE)) # asymmetric
     map

## plot diagnostic for curve fitting
msplot(fit, edges=c(1,2,3,4,5,6,7,8,9))
msplot(fit, edges=c(10,11,12,13,14,15,16,17,18))
msplot(fit, edges=c(19,20,21,22,23,24,25,26,27))
msplot(fit, edges=c(28,29,30,31,32,33,34,35,36))
msplot(fit, edges=c(37,38,39,40,41,42,43,44,45))
msplot(fit, edges=c(46,47,48,49,50,51,52,53,54))

dev.off()
```

A.10 Automated PCA script for R

R script for automatic generation of Principle Component Analysis graphs, including factor maps, from similarity matrix data.

```
Dataset <-
  read.table("RPLOT-MATRIX-2010-FEB-27-NEWSCRIPTS-NORM-EXCLUDE-3247-OLD.csv-MATRIXOUTPUT",
    header=TRUE, sep=",", na.strings="nan", dec=".", strip.white=TRUE)
library(FactoMineR)

pdf.options(onefile=TRUE, paper="a4r", pagecentre=TRUE)
pdf(file="RPLOT-MATRIX-2010-FEB-27-NEWSCRIPTS-NORM-EXCLUDE-3247-OLD.csv-MATRIXOUTPUT.pdf", onefile=
     TRUE, width=11, height=8, paper="a4r", pagecentre=TRUE)
```

```
#
# Principle Component Analysis
#

Dataset.PCA<-Dataset[, c("BH01", "BH02", "BH142999", "JH113", "JH36",
  "JH42", "JH43", "JH47", "JH54", "JH60", "JH63", "JH986", "JHIC", "JHMG152",
  "JHMG154", "JHSD1", "JHSD2", "JHSD3", "JHSD4", "JHW74", "JHYG", "MA01",
  "MA03", "MA04", "MA05", "MA07", "MA11", "MA13", "MA14", "MA178064", "MA64",
  "MH09", "MH169074", "MH169075", "MH178065", "MH178066", "MH178067",
  "MH178068", "MNIC", "MNW461", "NMH107", "NNTX", "NT88_185", "NT88_194",
  "NT89_54", "TLGD901", "TLGD904", "TLGD907", "TLGD908", "TLGDW500",
  "TLGDW501", "YGC")]
res<-PCA(Dataset.PCA , scale.unit=FALSE, ncp=5, graph = FALSE)
#plot.PCA(res, axes=c(1, 2), choix="ind", habillage="none", col.ind="black",
#  col.ind.sup="blue", col.quali="magenta", label=c("ind", "ind.sup", "quali"), new.plot=FALSE)
plot.PCA(res, axes=c(1, 2), choix="var", col.var="black",
  col.quanti.sup="blue", label=c("var", "quanti.sup"), lim.cos2.var=0, new.plot=FALSE)
res<-PCA(Dataset.PCA , scale.unit=TRUE, ncp=5, graph = FALSE)
#plot.PCA(res, axes=c(1, 2), choix="ind", habillage="none", col.ind="black",
#  col.ind.sup="blue", col.quali="magenta", label=c("ind", "ind.sup", "quali"), new.plot=FALSE)
plot.PCA(res, axes=c(1, 2), choix="var", col.var="black",
  col.quanti.sup="blue", label=c("var", "quanti.sup"), lim.cos2.var=0, new.plot=FALSE)
remove(Dataset.PCA)

#
# Multiple Factor Analysis
#


Dataset.MFA<-Dataset[, c("MA01", "MA03", "MA04", "MA05", "MA07", "MA11",
  "MA13", "MA14", "MA178064", "MA64", "TLGD901", "TLGD904", "TLGD907",
  "TLGD908", "TLGDW500", "TLGDW501", "JH113", "JH36", "JH42", "JH43", "JH47",
  "JH54", "JH60", "JH63", "JH986", "JHMG152", "JHMG154", "JHSD1", "JHSD2",
  "JHSD3", "JHSD4", "JHW74", "MNW461", "NT88_185", "NT88_194", "NT89_54",
  "JHIC", "MNIC", "NNTX", "BH01", "BH02", "BH142999", "MH09", "MH169074",
  "MH169075", "MH178065", "MH178066", "MH178067", "MH178068", "NMH107")]
res<-MFA(Dataset.MFA, group=c(10, 6, 16, 4, 3, 3, 8), type=c("s", "s", "s",
  "s", "s", "s", "s"), ncp=5, name.group=c("MTALFRED", "TLGD", "JACKHILLS",
  "NARRYER", "COMPOSITE", "BROOKINGHILLS", "MAYNARDHILLS"), num.group.sup=c(),
   graph=FALSE)

plot.MFA(res, axes=c(1, 2), choix="group", lab.grpe=TRUE, new.plot=FALSE)
plot.MFA(res, axes=c(1, 2), choix="axes", habillage="group", new.plot=FALSE)
plot.MFA(res, axes=c(1, 2), choix="var", lab.var=TRUE, habillage="group",
  lim.cos2.var=0, new.plot=FALSE)
#plot.MFA(res, axes=c(1, 2), choix="ind", lab.ind.moy=TRUE, lab.par=TRUE,
#  habillage="group", new.plot=FALSE)
remove(Dataset.MFA)


#
# Correspondance Analysis
#


Dataset.CA<-Dataset[c("1", "2", "3", "4", "5", "6", "7", "8", "9", "10",
  "11", "12", "13", "14", "15", "16", "17", "18", "19", "20", "21", "22",
  "23", "24", "25", "26", "27", "28", "29", "30", "31", "32", "33", "34",
  "35", "36", "37", "38", "39", "40", "41", "42", "43", "44", "45", "46",
  "47", "48", "49", "50", "51", "52") ,c("BH01", "BH02", "BH142999", "JH113",
  "JH36", "JH42", "JH43", "JH47", "JH54", "JH60", "JH63", "JH986", "JHIC",
  "JHMG152", "JHMG154", "JHSD1", "JHSD2", "JHSD3", "JHSD4", "JHW74", "JHYG",
  "MA01", "MA03", "MA04", "MA05", "MA07", "MA11", "MA13", "MA14", "MA178064",
  "MA64", "MH09", "MH169074", "MH169075", "MH178065", "MH178066", "MH178067",
  "MH178068", "MNIC", "MNW461", "NMH107", "NNTX", "NT88_185", "NT88_194",
  "NT89_54", "TLGD901", "TLGD904", "TLGD907", "TLGD908", "TLGDW500",
  "TLGDW501", "YGC")]

res<-CA(Dataset.CA, ncp=5, row.sup=NULL, col.sup=NULL, graph = FALSE)

plot.CA(res, axes=c(1, 2), col.row="red", col.col="blue", label=c("col", "col.sup", "row.sup"),
     invisible=c("row"), title="Correspondence Analysis Map", new.
plot=FALSE)



#
# GPA Analysis
#

Dataset.GPA<-Dataset[, c("MA01", "MA03", "MA04", "MA05", "MA07", "MA11",
  "MA13", "MA14", "MA178064", "MA64", "TLGD901", "TLGD904", "TLGD907",
  "TLGD908", "TLGDW500", "TLGDW501", "JH113", "JH36", "JH42", "JH43", "JH47",
  "JH54", "JH60", "JH63", "JH986", "JHMG152", "JHMG154", "JHSD1", "JHSD2",
  "JHSD3", "JHSD4", "JHW74", "MNW461", "NT88_185", "NT88_194", "NT89_54",
  "JHIC", "MNIC", "NNTX", "BH01", "BH02", "BH142999", "MH09", "MH169074",
  "MH169075", "MH178065", "MH178066", "MH178067", "MH178068", "NMH107")]
res<-GPA(Dataset.GPA, group=c(10, 6, 16, 4, 3, 3, 8), name.group=c("MTALFRED", "TLGD", "JACKHILLS",
  "NARRYER", "COMPOSITE", "BROOKINGHILLS", "MAYNARDHILLS"), scale=FALSE,
  graph=FALSE)

plot.GPA(res, axes=c(1, 2), lab.ind.moy=TRUE, habillage="group", partial=c("all"), new.plot=FALSE)
#plot.GPA(res, axes=c(1, 2), lab.ind.moy=TRUE, habillage="ind", new.plot=FALSE)

res<-GPA(Dataset.GPA, group=c(5, 6, 5, 7, 7, 4, 8), name.group=c("MA1",
  "MA64", "NARRYER1", "TLGD1", "JHMH1", "JH2", "JACKHILLS2"), scale=TRUE,
  graph=FALSE)

plot.GPA(res, axes=c(1, 2), lab.ind.moy=TRUE, habillage="group", partial=c("all"), new.plot=FALSE)
#plot.GPA(res, axes=c(1, 2), lab.ind.moy=TRUE, habillage="ind", new.plot=FALSE)


library(Rcmdr)
```

```
#
# KMEANS CLUSTER ANALYSIS
#
.cluster <- KMeans(model.matrix(~-1 + BH01 + BH02 + BH142999 + JH36 + JH42
  + JH43 + JH47 + JH54 + JH60 + JH63 + JH113 + JH986 + JHIC + JHMG152 +
  JHMG154 + JHSD1 + JHSD2 + JHSD3 + JHSD4 + JHW74 + JHYG + MA01 + MA03 + MA04
  + MA05 + MA07 + MA11 + MA13 + MA14 + MA64 + MA178064 + MH09 + MH169074 +
  MH169075 + MH178065 + MH178066 + MH178067 + MH178068 + MNIC + MNW461 +
  NMH107 + NNTX + NT88_185 + NT88_194 + NT89_54 + TLGD901 + TLGD904 + TLGD907
  + TLGD908 + TLGDW500 + TLGDW501 + YGC, Dataset), centers = 5, iter.max = 10,
   num.seeds = 10)
.cluster$size # Cluster Sizes
.cluster$centers # Cluster Centroids
.cluster$withinss # Within Cluster Sum of Squares
.cluster$tot.withinss # Total Within Sum of Squares
.cluster$betweenss # Between Cluster Sum of Squares
biplot(princomp(model.matrix(~-1 + BH01 + BH02 + BH142999 + JH36 + JH42 +
  JH43 + JH47 + JH54 + JH60 + JH63 + JH113 + JH986 + JHIC + JHMG152 + JHMG154
  + JHSD1 + JHSD2 + JHSD3 + JHSD4 + JHW74 + JHYG + MA01 + MA03 + MA04 + MA05
  + MA07 + MA11 + MA13 + MA14 + MA64 + MA178064 + MH09 + MH169074 + MH169075
  + MH178065 + MH178066 + MH178067 + MH178068 + MNIC + MNW461 + NMH107 + NNTX
  + NT88_185 + NT88_194 + NT89_54 + TLGD901 + TLGD904 + TLGD907 + TLGD908 +
  TLGDW500 + TLGDW501 + YGC, Dataset)), xlabs =
  as.character(.cluster$cluster))
remove(.cluster)


dev.off()
```

APPENDIX B
SAMPLE MA07 ZIRCON SEM PHOTOS

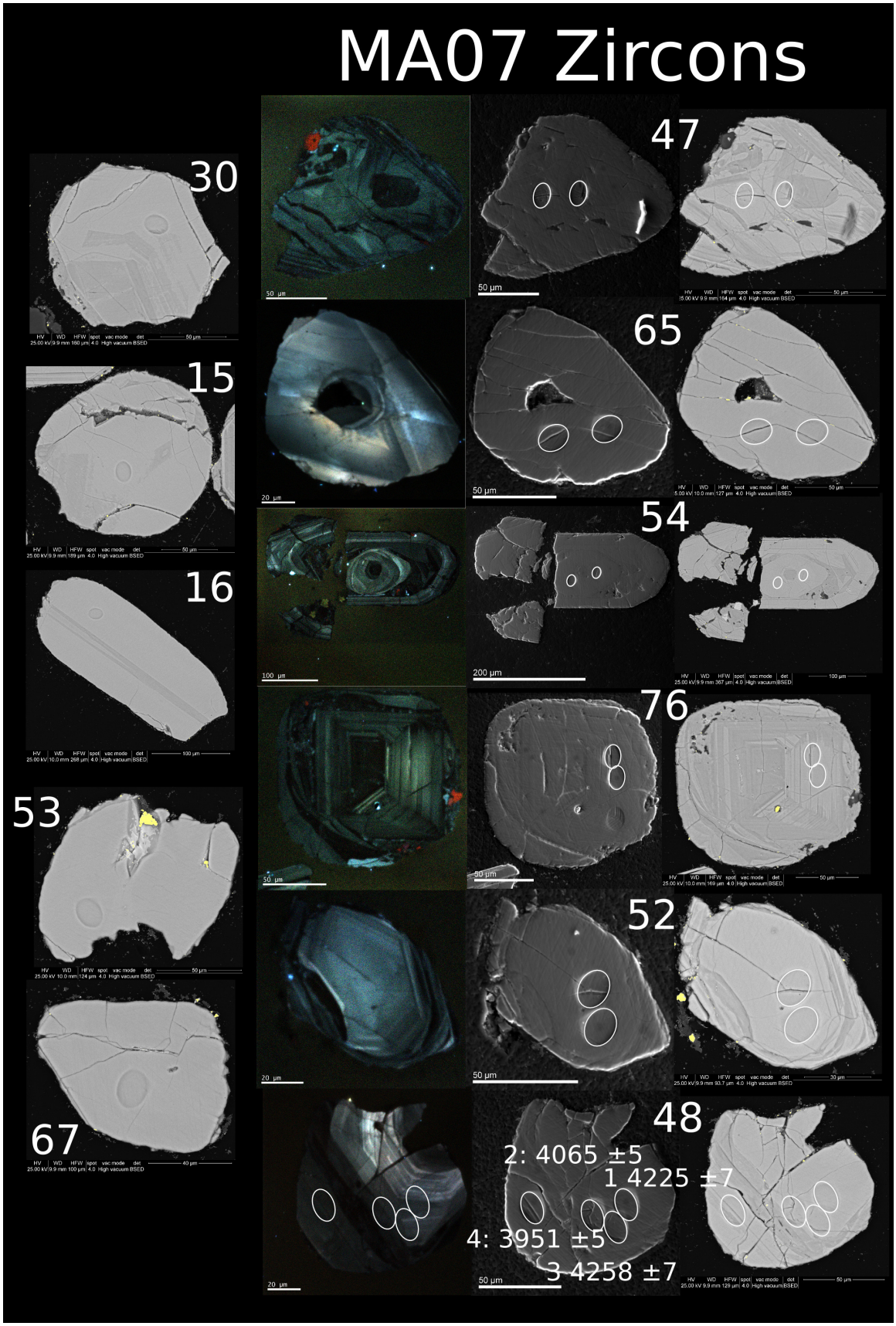

Figure B.1: Sample MA07 CL, SE and BSE (left to right) images showing grain morphology and detrital features with some SHRIMP spots marked.

APPENDIX C
THIN SECTIONS

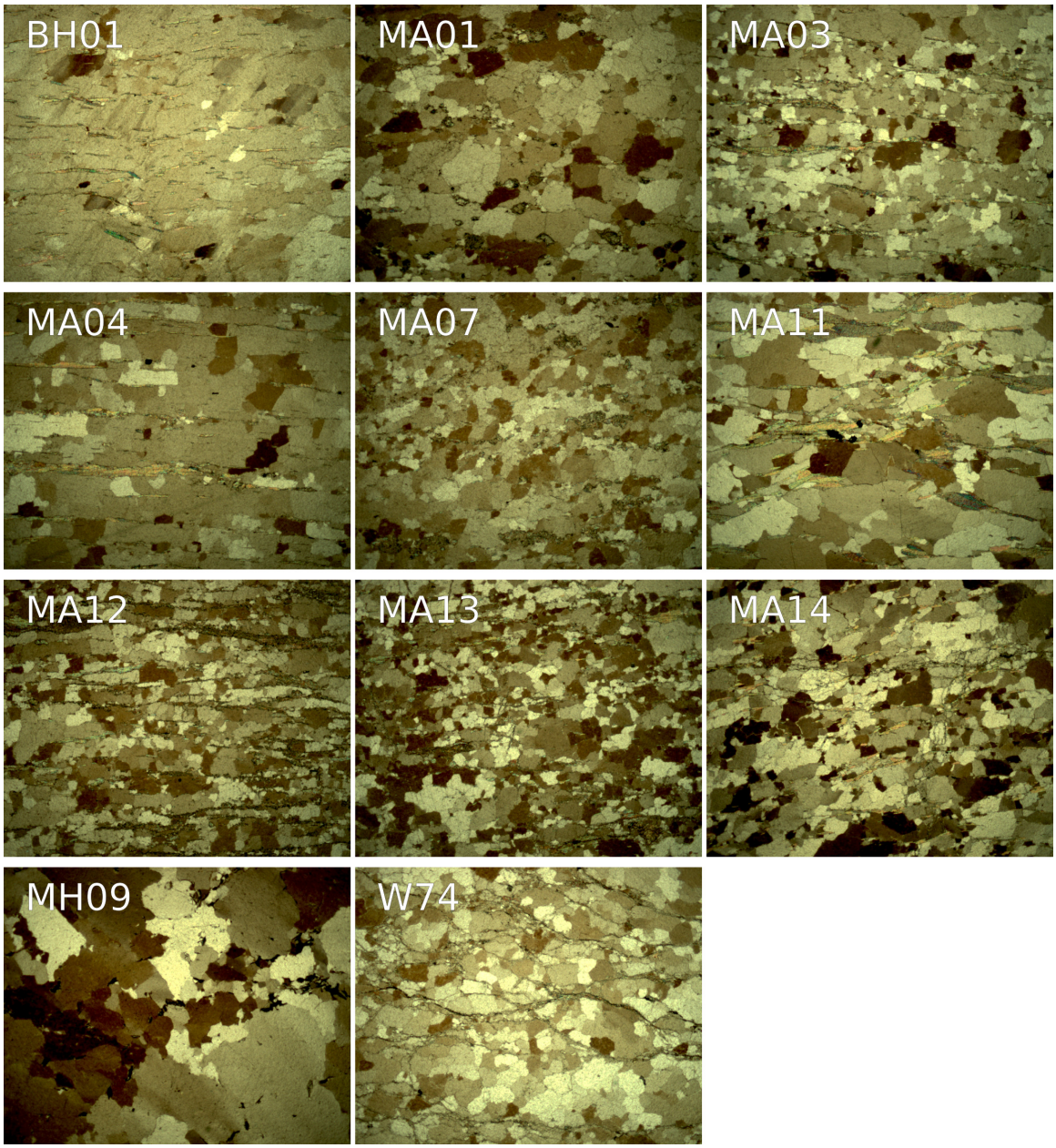

Figure C.1: Thin sections of select samples from the Illaara and Maynard Hills greenstone belts. Sample W74 is a thin section of the Jack Hills W74 sample site for comparison. All thin sections are shown at 45° cross-polar. These all show highly recrystallized features within these quartz-arenite style metasedimentary rocks. Foliation fabrics can be readily seen in some thin sections.

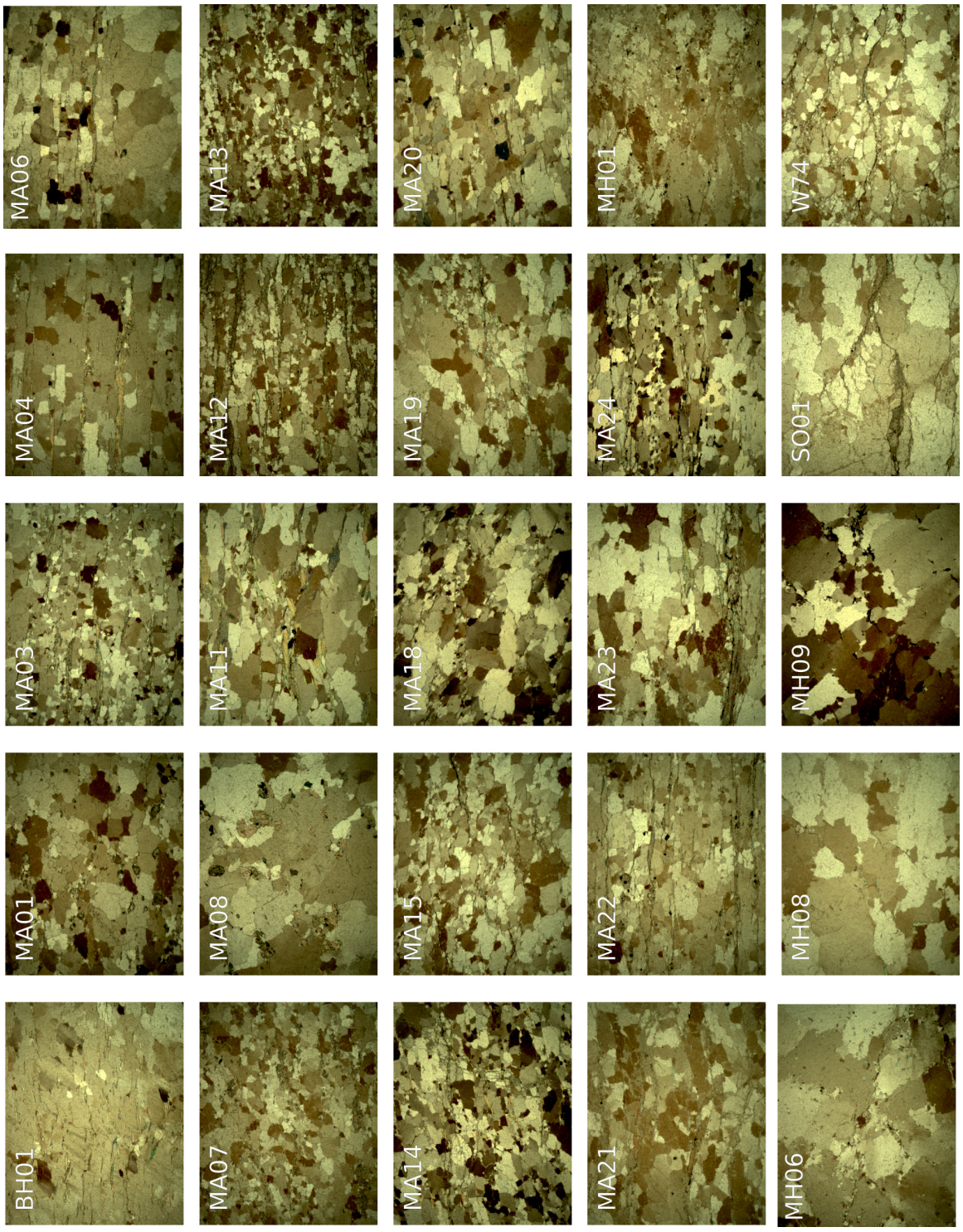

Figure C.2: Extra thin sections, for comparison, of other samples collected during this study. Samples "Ma" are Mt. Alfred, "MH" are Maynard Hills, "SO" is a small outcrop north of Mt. Alfred, "BH" is Brooking Hills, and W74 is the Jack Hills conglomerate for comparison. Maynard Hills sampes show larger, more recrystallized grain sizes. The samples at Mt. Alfred are commonly weathered.

APPENDIX D
TOURMALINE ^{40}AR/^{39}AR DATA

Table D.1: $^{40}Ar/^{39}Ar$ data table for tourmaline samples MA08, MA24, BH04 and BH05

Sample Step	Laser Power	Used*	^{36}Ar	%1σ	^{37}Ar	%1σ	^{38}Ar	%1σ	^{39}Ar	%1σ	^{40}Ar	%1σ	Age (Ma)	±2s	^{40}Ar(r) (%)	^{39}Ar(k) (%)	K/Ca	±2s
Sample Tourmaline-BH01-grain-1																		
1A18442D	56.00 W		0.00011	9.88	0.0019	59.94	0.0000	41.06	0.0000	57.76	0.07	0.163	5853.8	1852.9	53.4	0.25	0.0030	0.0060
1A18443D	56.50 W		0.00002	49.30	0.0013	84.54	0.0000	289.42	0.0003	4.28	0.07	0.295	2078.9	163.3	90.6	4.39	0.0860	0.1460
1A18444D	57.00 W		0.00000	723.78	0.0009	130.84	0.0000	60.07	0.0009	1.58	0.26	0.066	2438.5	50.4	100.2	14.55	0.4350	1.1390
1A18446D	57.50 W		0.00000	264.52	0.0013	88.45	0.0000	68.42	0.0005	1.93	0.19	0.085	2687.0	68.8	100.6	8.84	0.1810	0.3200
1A18447D	58.00 W	4	0.00002	46.02	0.0153	8.30	0.0000	19.78	0.0023	1.06	0.78	0.062	2614.9	31.4	99.3	37.73	0.0630	0.0110
1A18448D	59.00 W	4	0.00001	107.07	0.0063	19.14	0.0000	55.22	0.0009	1.74	0.32	0.071	2591.9	55.1	99.3	15.56	0.0640	0.0250
1A18450D	60.00 W	4	0.00001	115.15	0.0028	39.58	0.0000	110.91	0.0004	3.10	0.15	0.087	2616.8	100.3	98.6	6.97	0.0630	0.0500
1A18451D	70.00 W	4	0.00002	60.20	0.0028	41.38	0.0000	98.49	0.0007	2.10	0.25	0.093	2670.5	67.9	98.1	11.71	0.1070	0.0890
TOTAL			0.00018	15.15	0.0262	12.48	0.0001	19.17	0.0060	0.69	2.09	0.033						
Sample Tourmaline-BH01-grain-2																		
1A18423D	56.50 W		0.00001	120.76	0.0003	511.12	0.0000	148.75	0.0000	12.40	0.06	0.455	4878.2	474.7	95.2	0.39	0.0670	0.6820
1A18424D	57.00 W		0.00003	37.33	0.0007	188.95	0.0000	24.94	0.0005	2.16	0.14	0.239	2376.8	94.3	93.0	4.42	0.2790	1.0560
1A18425D	57.50 W	4	0.00003	44.87	0.0000	11973.12	0.0000	50.62	0.0002	4.14	0.07	0.374	2752.1	197.2	88.9	1.68	6.7330	1612.2650
1A18427D	58.00 W	4	0.00001	126.33	0.0004	297.06	0.0000	39.07	0.0005	1.81	0.18	0.216	2632.8	76.3	98.4	5.10	0.5010	2.9760
1A18428D	58.50 W	4	0.00004	27.77	0.0113	12.18	0.0001	9.34	0.0038	0.90	1.31	0.034	2615.8	26.1	99.1	36.99	0.1440	0.0350
1A18429D	59.00 W	4	0.00002	50.39	0.0177	8.39	0.0000	15.13	0.0019	1.15	0.67	0.071	2641.4	35.5	99.2	18.69	0.0460	0.0080
1A18431D	60.00 W	4	0.00002	80.26	0.0125	11.47	0.0000	25.22	0.0012	1.92	0.43	0.113	2691.5	59.7	99.1	11.61	0.0410	0.0100
1A18432D	70.00 W	4	0.00002	71.26	0.0067	20.65	0.0000	13.31	0.0022	0.86	0.75	0.044	2618.6	27.5	99.4	21.12	0.1400	0.0580
TOTAL			0.00018	19.26	0.0487	7.96	0.0002	7.65	0.0103	0.51	3.62	0.030						
Sample Tourmaline-BH01-grain-3																		
1A18399D	56.00 W		0.00004	18.30	0.0011	32.90	0.0000	10466.02	0.0000	116.78	0.08	0.288	7247.9	3845.6	85.8	0.35	0.0045	0.0101
1A18400D	56.40 W		0.00004	20.60	0.0002	160.72	0.0000	81.62	0.0001	11.99	0.10	0.182	3438.0	380.4	86.6	4.22	0.3577	1.1530
1A18401D	56.70 W		0.00000	357.90	0.0002	148.46	0.0000	162.59	0.0001	11.33	0.06	0.218	2991.9	366.4	98.5	4.21	0.2599	0.7739
1A18403D	57.00 W		0.00001	152.76	0.0005	64.63	0.0000	863.88	0.0001	17.11	0.03	0.424	2776.7	532.6	105.4	2.72	0.0836	0.1118
1A18404D	57.50 W		0.00000	3215.17	0.0039	10.29	0.0000	79.35	0.0005	4.58	0.16	0.209	2632.3	133.3	100.2	14.31	0.0523	0.0118
1A18405D	58.00 W		0.00000	18202.31	0.0101	4.18	0.0000	97.33	0.0009	1.76	0.34	0.134	2798.4	53.0	100.2	26.89	0.0375	0.0034
1A18408D	58.50 W		0.00000	386.82	0.0087	4.47	0.0000	153.69	0.0007	2.83	0.29	0.044	2820.2	89.9	99.9	22.54	0.0365	0.0039
1A18409D	59.00 W		0.00014	5.82	0.0050	8.84	0.0000	41.59	0.0004	3.66	0.21	0.184	2906.9	115.3	79.6	11.94	0.0340	0.0065
1A18410D	59.70 W		0.00001	129.16	0.0010	46.15	0.0000	108.68	0.0001	20.22	0.03	0.244	2999.8	629.0	95.3	2.03	0.0296	0.0299
1A18411D	70.00 W		0.00002	42.25	0.0052	6.72	0.0000	68.78	0.0004	4.32	0.17	0.194	3010.1	136.1	96.6	10.80	0.0294	0.0047
TOTAL			0.00025	11.20	0.0332	3.57	0.0001	39.53	0.0033	1.57	1.47	0.058						
Sample Tourmaline-MA08-pkg-1																		
1A15056D	59.00 W		0.00112	2.63	0.0001	184.66	0.0002	4.41	0.0000	395.50	0.50	0.124	10312.0	14397.9	33.5	0.02	0.0236	0.2086
1A15057D	59.50 W		0.00149	2.52	0.0001	133.87	0.0003	5.33	0.0000	533.98	0.57	0.093	0.0	19810.8	22.6	0.01	0.0121	0.1363
1A15058D	60.00 W		0.00117	2.41	0.0001	293.81	0.0003	4.39	0.0000	74.78	0.50	0.089	7089.5	2654.5	29.5	0.08	0.2031	1.2318
1A15059D	61.00 W		0.00176	2.13	0.0000	552.71	0.0004	4.33	0.0001	20.15	0.74	0.101	5384.6	712.8	28.7	0.32	1.2834	14.1960
1A15061D	61.50 W		0.00056	2.91	0.0001	368.60	0.0001	10.44	0.0001	32.72	0.32	0.161	5697.5	1134.9	48.5	0.20	0.5495	4.0666
1A15062D	62.00 W		0.00022	9.10	0.0001	173.44	0.0000	31.59	0.0000	910.55	0.09	0.446	8071.1	31350.1	24.7	0.01	0.0092	0.1643
1A15063D	63.00 W		0.00152	1.95	0.0001	156.15	0.0003	4.47	0.0000	122.73	0.64	0.075	8325.6	4403.0	29.1	0.05	0.0696	0.2770
1A15064D	64.00 W		0.00038	3.91	0.0001	192.25	0.0001	15.99	0.0000	82.12	0.16	0.274	5393.3	2835.0	30.7	0.08	0.1220	0.5101
1A15066D	65.00 W		0.00112	2.78	0.0000	5358.84	0.0002	6.55	0.0001	42.51	0.46	0.091	5669.1	1490.1	26.5	0.16	6.3951	685.4253
1A15067D	66.00 W		0.00069	2.15	0.0001	142.23	0.0001	9.71	0.0000	57.27	0.25	0.188	4345.4	1917.8	16.5	0.12	0.1218	0.3736
1A15068D	67.00 W		0.00040	4.22	0.0001	138.26	0.0001	15.85	0.0001	38.42	0.17	0.269	4105.7	1281.3	30.1	0.17	0.2023	0.5805
1A15069D	68.00 W		0.00098	3.02	0.0004	47.19	0.0002	6.57	0.0002	13.04	0.45	0.121	3925.0	454.6	35.0	0.58	0.2049	0.2007
1A15071D	69.50 W		0.00019	7.65	0.0007	30.06	0.0000	28.37	0.0002	15.02	0.15	0.307	3057.9	464.1	62.1	0.61	0.1329	0.0894
1A15072D	70.00 W		0.00019	9.28	0.0031	6.93	0.0000	31.73	0.0003	8.71	0.20	0.286	3064.5	278.8	72.6	0.95	0.0435	0.0097
1A15073D	70.50 W		0.00113	2.25	0.0325	2.42	0.0003	6.46	0.0017	2.50	0.99	0.095	2824.4	79.8	66.2	4.99	0.0220	0.0015
1A15074D	70.70 W		0.00119	2.27	0.0537	2.38	0.0003	6.56	0.0024	1.48	1.32	0.075	2885.8	50.0	73.5	7.05	0.0189	0.0011

Continued on Next Page...

Table D.1 – Continued

Sample Step	Laser Power	Used*	^{36}Ar	%1σ	^{37}Ar	%1σ	^{38}Ar	%1σ	^{39}Ar	%1σ	^{40}Ar	%1σ	Age (Ma)	±2s	^{40}Ar(r) (%)	^{39}Ar(k) (%)	K/Ca	±2s
1A15076D	70.80 W	4	0.00225	1.81	0.1012	2.28	0.0005	4.76	0.0042	1.00	2.42	0.113	2946.8	36.6	72.5	12.24	0.0174	0.0009
1A15077D	70.90 W	4	0.00075	2.96	0.1060	2.27	0.0002	6.90	0.0044	1.03	2.05	0.038	2923.0	32.7	89.5	12.99	0.0176	0.0009
1A15078D	71.00 W	4	0.00040	5.68	0.1065	2.24	0.0001	12.66	0.0043	0.93	1.90	0.040	2920.0	30.1	94.2	12.69	0.0171	0.0008
1A15079D	71.10 W	4	0.00016	10.06	0.0772	2.27	0.0001	16.82	0.0031	1.03	1.34	0.046	2917.2	32.8	96.9	9.26	0.0172	0.0009
1A15081D	71.20 W	4	0.00011	19.22	0.0494	2.30	0.0001	25.28	0.0020	1.94	0.86	0.083	2908.8	61.3	96.7	5.99	0.0174	0.0011
1A15082D	71.30 W	4	0.00008	20.06	0.0586	2.49	0.0000	37.49	0.0024	1.13	1.04	0.038	2970.4	36.3	98.3	7.00	0.0171	0.0009
1A15084D	71.40 W	4	0.00001	83.81	0.0396	2.37	0.0000	116.89	0.0016	2.04	0.68	0.088	2990.1	62.8	99.9	4.58	0.0166	0.0011
1A15085D	71.50 W	4	0.00002	67.37	0.0296	2.64	0.0000	87.18	0.0012	2.13	0.53	0.093	2956.9	66.4	99.4	3.66	0.0178	0.0012
1A15086D	71.70 W	4	0.00002	91.22	0.0273	2.34	0.0000	37.56	0.0011	2.49	0.48	0.115	2964.4	78.2	99.5	3.32	0.0175	0.0012
1A15087D	71.90 W	4	0.00000	297.80	0.0132	2.63	0.0000	49.83	0.0005	4.09	0.23	0.223	2970.8	129.8	100.0	1.58	0.0171	0.0017
1A15089D	72.20 W	4	0.00001	146.67	0.0119	3.21	0.0000	492.07	0.0005	4.68	0.22	0.200	3062.0	149.7	99.3	1.41	0.0170	0.0020
1A15090D	72.50 W	4	0.00001	108.12	0.0061	4.18	0.0000	5630.58	0.0002	9.44	0.11	0.354	3177.3	302.8	103.5	0.70	0.0166	0.0035
1A15091D	72.90 W	4	0.00000	493.85	0.0059	4.67	0.0000	1641.35	0.0003	8.28	0.12	0.387	3123.3	266.3	99.8	0.77	0.0186	0.0036
1A15092D	80.00 W		0.00001	194.00	0.0015	14.22	0.0000	387.24	0.0001	36.31	0.04	1.052	3382.4	1192.1	94.3	0.17	0.0170	0.0134
1A15094D	81.00 W		0.00007	20.90	0.0187	2.58	0.0000	44.41	0.0009	2.94	0.42	0.125	3062.7	93.8	95.4	2.60	0.0200	0.0016
1A15095D	81.50 W		0.00035	6.30	0.0330	2.56	0.0001	13.95	0.0019	1.93	1.01	0.059	3137.7	62.0	90.1	5.58	0.0243	0.0016
1A15096D	81.80 W		0.00015	10.98	0.0003	75.85	0.0000	33.58	0.0000	57.66	0.08	0.493	4335.8	1945.5	47.0	0.11	0.0518	0.0989
TOTAL			0.01851	0.69	0.7766	0.70	0.0042	1.86	0.0340	0.48	21.06	0.020						
Sample Tourmaline-MA08-pkg-2																		
1A15293D	60.00 W		0.00031	4.29	0.0000	683.60	0.0000	21.57	0.0000	50.91	0.13	0.160	5531.9	1784.5	29.1	0.05	0.2473	3.3898
1A15294D	61.00 W		0.00230	1.60	0.0000	29541.52	0.0005	3.05	0.0000	28.02	1.02	0.063	8212.8	1006.4	32.9	0.10	23.7828	14051.5832
1A15295D	62.00 W		0.00160	1.72	0.0003	66.86	0.0003	3.86	0.0000	18.31	0.71	0.071	6978.3	655.2	32.8	0.13	0.0661	0.0915
1A15296D	63.00 W		0.00294	1.66	0.0002	80.05	0.0006	2.16	0.0001	8.84	1.11	0.064	5388.5	373.3	20.7	0.32	0.2139	0.3445
1A15298D	65.00 W		0.00257	1.58	0.0020	9.64	0.0005	3.09	0.0002	6.08	1.05	0.044	5057.4	252.7	27.1	0.49	0.0381	0.0087
1A15299D	67.00 W		0.00135	2.83	0.0038	6.24	0.0003	7.21	0.0002	7.08	0.55	0.066	3575.1	330.8	26.5	0.62	0.0250	0.0048
1A15300D	69.00 W		0.00063	3.13	0.0021	10.69	0.0001	9.53	0.0004	6.26	0.37	0.164	2991.1	205.3	49.9	1.17	0.0858	0.0213
1A15301D	69.50 W		0.00115	3.53	0.0110	3.74	0.0002	7.80	0.0009	3.04	0.66	0.127	2642.8	135.7	48.2	2.57	0.0362	0.0035
1A15303D	70.00 W	4	0.00318	1.52	0.0864	2.48	0.0007	2.29	0.0037	1.12	2.49	0.023	2917.4	43.1	62.1	10.21	0.0183	0.0010
1A15348D	70.00 W	4	0.00117	3.14	0.0762	2.62	0.0003	7.05	0.0031	0.74	1.59	0.067	2901.6	34.0	78.5	8.35	0.0169	0.0009
1A15350D	70.00 W	4	0.00076	4.04	0.0470	2.82	0.0002	6.78	0.0018	1.22	1.00	0.076	2962.0	50.2	77.7	5.01	0.0165	0.0010
1A15352D	70.20 W	4	0.00182	2.40	0.1183	2.54	0.0004	5.11	0.0048	0.92	2.52	0.072	2934.5	33.9	78.8	13.00	0.0170	0.0009
1A15353D	70.20 W	4	0.00036	4.71	0.0944	2.58	0.0001	12.50	0.0037	0.81	1.61	0.082	2925.3	26.7	93.8	9.96	0.0163	0.0009
1A15354D	70.30 W	4	0.00020	10.50	0.1089	2.54	0.0001	12.68	0.0044	0.50	1.89	0.056	2941.6	18.8	97.3	11.96	0.0170	0.0009
1A15356D	70.40 W	4	0.00012	13.72	0.0757	2.58	0.0001	16.40	0.0031	1.00	1.33	0.049	2938.1	32.1	97.9	8.51	0.0174	0.0010
1A15357D	70.50 W	4	0.00006	28.16	0.0500	2.60	0.0000	23.22	0.0021	1.11	0.90	0.082	2957.7	37.2	98.5	5.68	0.0176	0.0010
1A15358D	70.70 W	4	0.00006	23.07	0.0450	2.65	0.0001	22.00	0.0020	1.16	0.85	0.094	2971.8	37.9	98.3	5.34	0.0184	0.0011
1A15359D	70.90 W	4	0.00004	31.48	0.0236	3.07	0.0000	34.94	0.0010	1.44	0.47	0.094	2985.9	50.1	97.7	2.87	0.0188	0.0013
1A15361D	71.20 W	4	0.00004	33.54	0.0152	3.77	0.0000	46.17	0.0007	2.04	0.31	0.113	2982.1	74.6	96.2	1.89	0.0192	0.0017
1A15362D	71.60 W	4	0.00011	17.71	0.0222	3.35	0.0000	32.95	0.0011	1.73	0.49	0.082	2968.9	62.3	93.9	2.96	0.0206	0.0016
1A15363D	72.20 W		0.00014	12.85	0.0116	4.25	0.0000	28.61	0.0005	2.56	0.28	0.141	3053.9	100.1	85.8	1.45	0.0194	0.0019
1A15364D	72.90 W		0.00015	11.09	0.0110	4.53	0.0000	35.38	0.0005	2.30	0.28	0.149	2983.4	92.8	84.0	1.48	0.0209	0.0021
1A15366D	80.50 W		0.00017	10.12	0.0083	5.60	0.0000	30.30	0.0005	3.45	0.27	0.129	3050.8	124.8	81.0	1.32	0.0248	0.0033
1A15367D	81.50 W		0.00032	6.04	0.0154	3.89	0.0001	17.56	0.0010	1.71	0.54	0.095	3092.3	64.2	82.5	2.63	0.0264	0.0023
1A15368D	82.00 W		0.00023	6.76	0.0107	4.28	0.0001	15.32	0.0007	1.65	0.46	0.111	3353.4	62.3	85.4	1.94	0.0281	0.0026
TOTAL			0.02178	0.65	0.8387	0.78	0.0048	1.42	0.0366	0.30	22.90	0.016						
Sample Tourmaline-MA08-I9-singlegrain-1																		
1A15878D	55.30 W		0.00002	33.76	0.0002	142.01	0.0000	62.86	0.0000	77.98	0.01	1.084	3505.4	2752.1	45.4	2.88	0.0209	0.0681
1A15880D	56.30 W		0.00003	29.68	0.0015	17.66	0.0000	62.96	0.0001	14.03	0.05	0.324	3712.0	500.6	81.2	18.30	0.0162	0.0074
1A15882D	56.50 W	4	0.00000	1345.64	0.0032	12.06	0.0000	906.55	0.0001	14.89	0.02	0.582	2923.4	544.4	100.3	19.32	0.0079	0.0031
1A15884D	56.80 W	4	0.00001	82.88	0.0011	22.81	0.0000	478.35	0.0000	31.58	0.01	1.184	2359.1	1316.0	69.3	8.14	0.0094	0.0075
1A15886D	57.20 W	4	0.00000	188.04	0.0031	11.01	0.0000	170.53	0.0001	13.63	0.02	0.553	3090.4	497.3	96.5	16.41	0.0069	0.0025
1A15888D	70.00 W	4	0.00000	169.95	0.0048	7.09	0.0000	122.49	0.0001	7.59	0.04	0.492	2586.5	286.5	97.2	34.96	0.0095	0.0020

Continued on Next Page...

Table D.1 – Continued

Sample Step	Laser Power	Used*	^{36}Ar	%1σ	^{37}Ar	%1σ	^{38}Ar	%1σ	^{39}Ar	%1σ	^{40}Ar	%1σ	Age (Ma)	±2s	^{40}Ar(r) (%)	^{39}Ar(k) (%)	K/Ca	±2s
TOTAL			0.00007	27.83	0.0139	5.48	0.0000	52.26	0.0003	6.20	0.16	0.228						
Sample Tourmaline-MA08-I9-singlegrain-2																		
1A15554D	55.50 W		0.00022	8.64	0.0001	399.58	0.0000	36.42	0.0000	57.22	0.08	0.182	5181.8	2238.9	21.2	2.68	0.0771	0.6223
1A15555D	55.70 W		0.00001	272.94	0.0002	108.83	0.0000	104.75	0.0000	115.03	0.01	2.095	0.0	5355.2	133.9	1.38	0.0098	0.0316
1A15556D	56.10 W		0.00000	343.19	0.0004	45.79	0.0000	216.05	0.0000	290.08	0.01	1.851	4283.9	10092.0	85.7	1.94	0.0071	0.0435
1A15557D	56.30 W	4	0.00004	37.93	0.0021	12.04	0.0000	69.09	0.0001	23.05	0.06	0.350	3142.3	751.7	80.3	24.58	0.0190	0.0100
1A15559D	56.80 W	4	0.00001	182.17	0.0025	11.25	0.0000	94.04	0.0001	5.35	0.06	0.239	2844.7	206.9	97.8	38.29	0.0249	0.0062
1A15561D	57.00 W	4	0.00001	53.16	0.0011	28.80	0.0000	1063.50	0.0001	11.73	0.03	0.458	2799.2	428.9	85.5	15.30	0.0219	0.0137
1A15562D	57.50 W	4	0.00001	55.27	0.0011	29.09	0.0000	737.30	0.0000	16.51	0.02	0.347	2929.1	595.0	82.7	11.40	0.0175	0.0117
1A15563D	58.00 W	4	0.00002	64.25	0.0004	87.31	0.0000	1324.39	0.0000	56.59	0.01	1.131	1656.3	2469.6	39.6	5.58	0.0236	0.0493
1A15565D	59.00 W	4	0.00001	149.27	0.0005	47.49	0.0000	133.94	0.0000	50.66	0.02	0.672	4431.1	1899.9	86.0	3.51	0.0112	0.0158
1A15566D	62.00 W		0.00001	131.35	0.0004	55.26	0.0000	494.01	0.0000	100.39	0.01	1.441	0.0	9514.6	46.4	1.89	0.0071	0.0158
TOTAL			0.00032	12.83	0.0085	10.16	0.0001	46.80	0.0004	9.89	0.29	0.141						
Sample Tourmaline-MA08-I9-singlegrain-3																		
1A15731D	55.30 W	4	0.00002	68.02	0.0000	629.46	0.0000	46.71	0.0000	74.59	0.01	0.765	3036.7	3165.2	46.6	3.09	0.0972	1.2321
1A15732D	56.40 W	4	0.00001	444.78	0.0031	9.20	0.0000	74.94	0.0001	15.24	0.04	0.404	3016.6	756.7	96.2	25.20	0.0121	0.0044
1A15734D	56.50 W	4	0.00001	462.75	0.0017	19.56	0.0000	687.57	0.0001	20.44	0.02	0.513	3025.8	1446.8	111.5	14.37	0.0123	0.0071
1A15735D	56.70 W	4	0.00001	353.98	0.0005	61.45	0.0000	380.44	0.0000	55.00	0.01	1.804	3069.8	4039.1	155.9	5.01	0.0139	0.0231
1A15737D	57.50 W	4	0.00002	66.60	0.0057	6.75	0.0000	316.93	0.0002	5.00	0.07	0.205	2913.8	232.4	111.0	52.33	0.0134	0.0023
TOTAL			0.00002	373.06	0.0110	6.65	0.0000	361.21	0.0003	6.55	0.14	0.186						
Sample Tourmaline-MA08-I9-singlegrain-4																		
1A15739D	55.60 W		0.00001	286.23	0.0002	158.08	0.0000	454.65	0.0000	239.37	0.01	0.961	4772.1	8761.9	149.8	2.05	0.0168	0.0974
1A15740D	56.40 W		0.00001	72.81	0.0007	40.69	0.0000	304.93	0.0001	30.42	0.02	0.692	2114.8	990.0	74.5	14.11	0.0326	0.0332
1A15742D	56.60 W	4	0.00000	158.39	0.0007	32.66	0.0000	157.62	0.0001	6.97	0.04	0.448	2856.5	265.1	96.5	22.42	0.0528	0.0353
1A15743D	56.80 W	4	0.00000	55913.11	0.0009	33.03	0.0000	56.21	0.0001	8.25	0.05	0.257	2987.1	272.8	100.2	28.29	0.0520	0.0354
1A15746D	57.00 W	4	0.00001	140.27	0.0003	81.30	0.0000	246.02	0.0000	19.88	0.03	0.715	3113.1	687.1	92.4	13.01	0.0615	0.1030
1A15747D	70.00 W	4	0.00001	216.79	0.0000	634.05	0.0000	71.18	0.0001	12.60	0.04	0.761	2998.1	465.0	95.7	20.12	0.7298	9.2567
TOTAL			0.00002	209.27	0.0028	24.85	0.0000	274.10	0.0004	8.01	0.17	0.242						
Sample Tourmaline-MA08-I11-singlegrain-1																		
1A18481D	55.50 W		0.00069	0.00	0.0000	0.00	0.0233	5764.43	2433.3500	10.19	0.97	0.009	0.0	0.0	0.0	0.00	0.0000	0.0000
1A18482D	56.00 W	4	0.00013	0.00	0.0000	0.00	0.0235	7432.10	5558.9400	37.86	0.38	0.002	0.0	0.0	0.0	0.00	0.0000	0.0000
1A18483D	57.00 W	4	0.00001	0.00	0.0000	0.00	0.0138	3039.49	1190.4900	86.88	3.05	0.016	0.0	0.0	0.0	0.00	0.0000	0.0000
1A18485D	57.50 W	4	0.00003	0.00	0.0000	0.00	0.0538	3186.26	201.5400	84.86	10.81	0.031	0.0	0.0	0.0	0.00	0.0000	0.0000
1A18486D	58.00 W	4	0.00006	0.01	0.0000	0.00	0.2225	2932.30	74.7800	92.65	53.14	0.026	0.0	0.0	0.0	0.00	0.0000	0.0000
1A18488D	59.00 W	4	0.00001	0.00	0.0000	0.00	0.0847	2983.76	156.1100	97.31	19.53	0.037	0.0	0.0	0.0	0.00	0.0000	0.0000
1A18489D	70.00 W	4	0.00000	0.00	0.0000	0.00	0.0603	3187.11	233.9200	101.31	12.11	0.053	0.1	0.0	0.0	0.00	0.0000	0.0000
TOTAL			0.00092	0.02	0.0000	0.00	0.4819	0.00	0.0000	0.00	0.00	0.000						
Sample Tourmaline-MA08-I11-singlegrain-2																		
1A18491D	56.00 W		0.00082	1.59	0.0002	184.10	0.0002	5.92	0.0000	3408.01	0.28	0.095	12620.3	59282.9	13.2	0.05	0.0006	0.0201
1A18492D	57.00 W		0.00023	4.08	0.0034	10.24	0.0001	11.46	0.0002	6.29	0.14	0.171	2917.9	215.7	51.6	25.86	0.0215	0.0052
1A18493D	58.00 W		0.00001	91.72	0.0028	12.37	0.0000	50.22	0.0002	5.16	0.09	0.268	2866.0	168.8	97.4	31.15	0.0309	0.0083
1A18494D	70.00 W		0.00001	66.45	0.0066	6.94	0.0000	91.37	0.0003	3.03	0.14	0.215	3089.6	98.6	98.6	42.94	0.0183	0.0028
TOTAL			0.00106	1.74	0.0126	6.32	0.0002	6.32	0.0007	2.75	0.64	0.080						

Sample Tourmaline-MA08-I11-singlegrain-3
Continued on Next Page...

Table D.1 – Continued

Sample Step	Laser Power	Used*	^{36}Ar	%1σ	^{37}Ar	%1σ	^{38}Ar	%1σ	^{39}Ar	%1σ	^{40}Ar	%1σ	Age (Ma)	±2s	^{40}Ar(r) (%)	^{39}Ar(k) (%)	K/Ca	±2s
1A18497D	56.00 W		0.00007	14.79	0.0001	471.93	0.0000	776.44	0.0000	95.20	0.04	0.640	6044.3	3328.0	50.5	1.64	0.0429	0.4128
1A18498D	57.00 W	4	0.00001	64.94	0.0014	26.45	0.0000	303.30	0.0000	15.61	0.02	0.586	2405.8	608.7	80.4	10.70	0.0136	0.0084
1A18500D	58.00 W	4	0.00030	3.98	0.0179	4.36	0.0001	14.14	0.0004	3.46	0.22	0.154	2816.6	127.8	60.6	80.68	0.0082	0.0009
1A18501D	70.00 W		0.00000	551.73	0.0016	25.44	0.0000	408.74	0.0000	24.70	0.04	0.356	4697.9	873.5	101.3	6.97	0.0082	0.0059
TOTAL			0.00038	4.86	0.0209	4.85	0.0000	34.64	0.0004	3.97	0.32	0.145						
Sample Tourmaline-MA08-I11-singlegrain-4																		
1A18504D	56.00 W		0.00048	3.44	0.0004	284.50	0.0001	15.78	0.0000	38.53	0.18	0.314	5370.3	1459.7	17.9	2.87	0.0170	0.0979
1A18505D	57.00 W		0.00003	29.93	0.0016	66.90	0.0000	10003.99	0.0001	12.28	0.04	0.709	2224.5	417.1	74.3	18.37	0.0278	0.0379
1A18506D	58.00 W	4	0.00001	83.10	0.0071	16.38	0.0000	92.84	0.0003	3.74	0.14	0.259	2972.3	120.8	98.5	54.85	0.0186	0.0063
1A18507D	70.00 W	4	0.00000	1862.29	0.0034	31.71	0.0000	197.68	0.0001	6.24	0.06	0.394	2989.3	216.3	100.3	23.91	0.0169	0.0110
TOTAL			0.00052	4.14	0.0124	17.86	0.0001	25.17	0.0006	3.57	0.41	0.182						
Sample Tourmaline-MA08-I11-singlegrain-4																		
1A18504D	56.00 W		0.00048	3.44	0.0004	284.50	0.0001	15.78	0.0000	38.53	0.18	0.314	5370.3	1459.7	17.9	2.87	0.0170	0.0979
1A18505D	57.00 W		0.00003	29.93	0.0016	66.90	0.0000	10003.99	0.0001	12.28	0.04	0.709	2224.5	417.1	74.3	18.37	0.0278	0.0379
1A18506D	58.00 W	4	0.00001	83.10	0.0071	16.38	0.0000	92.84	0.0003	3.74	0.14	0.259	2972.3	120.8	98.5	54.85	0.0186	0.0063
1A18507D	70.00 W	4	0.00000	1862.29	0.0034	31.71	0.0000	197.68	0.0001	6.24	0.06	0.394	2989.3	216.3	100.3	23.91	0.0169	0.0110
TOTAL			0.00052	4.14	0.0124	17.86	0.0001	25.17	0.0006	3.57	0.41	0.182						
Sample Tourmaline-MA24-singlegrain-1																		
1A18464D	56.00 W		0.00000	1710.12	0.0001	685.93	0.0000	144.40	0.0000	230.85	0.11	0.251	0.0	8301.5	100.2	0.74	0.0340	0.4970
1A18465D	56.30 W		0.00000	218.37	0.0005	104.54	0.0000	35.89	0.0000	130.11	0.01	0.687	0.0	5369.4	110.0	1.27	0.0090	0.0320
1A18466D	57.30 W		0.00000	4989.96	0.0004	155.47	0.0000	7092.98	0.0000	173.23	0.24	0.115	9830.5	6035.0	100.0	1.05	0.0110	0.0480
1A18467D	57.60 W		0.00001	147.87	0.0006	104.33	0.0000	90.51	0.0002	10.33	0.12	0.304	3782.0	337.4	98.4	17.28	0.1200	0.2510
1A18469D	58.00 W	4	0.00000	1022.03	0.0009	65.80	0.0000	453.89	0.0003	5.98	0.13	0.188	3091.6	188.6	99.8	30.19	0.1380	0.1830
1A18470D	58.50 W	4	0.00001	165.11	0.0019	28.12	0.0000	224.06	0.0003	6.51	0.13	0.110	3011.0	201.9	101.5	30.29	0.0630	0.0360
1A18471D	59.00 W	4	0.00000	686.05	0.0008	72.56	0.0000	212.08	0.0001	11.12	0.06	0.192	3002.9	357.1	99.4	15.10	0.0750	0.1100
1A18473D	59.50 W	4	0.00000	460.11	0.0003	232.69	0.0000	299.02	0.0000	46.78	0.01	0.672	2896.3	1515.5	95.3	3.57	0.0550	0.2620
1A18474D	70.00 W	4	0.00000	1012.90	0.0001	883.82	0.0000	88.92	0.0000	37.63	0.02	0.492	3336.4	1204.0	101.2	4.52	0.2590	4.5800
TOTAL			0.00000	10274.72	0.0037	48.05	0.0000	66.53	0.0009	5.26	0.85	0.077						

* Sample steps used for plateau age calculation, denoted by '4'

Table D.2: ^{40}Ar/^{39}Ar data table tourmaline furnace diffusion experiment

Sample Step	Furnace Temp	Used*	^{36}Ar	%1σ	^{37}Ar	%1σ	^{38}Ar	%1σ	^{39}Ar	%1σ	^{40}Ar	%1σ	Age (Ma)	±2s	^{40}Ar(r) (%)	^{39}Ar(k) (%)	K/Ca	±2s
Sample Tourmaline-MA08-Diffusion-Furnace-pkg																		
2A19373D	550 °C		0.00038	3.53	0.0006	313.33	0.0001	13.76	0.0001	21.22	0.15	1.094	3449.4	744.5	24.5	0.28	0.0500	0.2800
2A19374D	600 °C		0.00068	2.57	0.0014	129.59	0.0001	8.34	0.0001	9.55	0.29	0.575	3782.5	366.9	29.0	0.52	0.0300	0.0900
2A19375D	650 °C		0.00039	4.51	0.0001	1486.59	0.0001	9.19	0.0002	5.82	0.20	0.807	3211.0	261.9	42.2	0.78	0.6400	19.1700
2A19376D	700 °C		0.00019	6.27	0.0006	296.36	0.0000	20.61	0.0001	12.26	0.11	1.454	2741.3	395.4	50.2	0.70	0.1000	0.6000
2A19377D	770 °C		0.00020	6.95	0.0007	265.84	0.0000	26.00	0.0001	7.37	0.12	1.385	2812.5	299.8	50.0	0.70	0.0900	0.5000
2A19378D	850 °C		0.00137	1.78	0.0036	49.13	0.0003	2.91	0.0027	0.98	1.30	0.134	2576.7	35.4	68.5	12.61	0.3200	0.3100
2A19379D	870 °C	4	0.00367	1.18	0.0079	24.58	0.0008	2.37	0.0084	0.62	4.69	0.081	2938.4	21.1	76.7	39.29	0.4500	0.2200
2A19380D	880 °C	4	0.00063	2.62	0.0018	102.77	0.0002	4.39	0.0046	0.55	2.16	0.081	2922.9	17.8	91.2	21.78	1.1300	2.3200
2A19381D	890 °C	4	0.00008	13.92	0.0001	3289.01	0.0000	17.78	0.0013	1.15	0.57	0.303	2898.2	39.1	95.6	6.06	9.4600	622.5100
2A19382D	910 °C	4	0.00001	83.15	0.0008	224.54	0.0000	82.39	0.0004	2.63	0.17	0.926	2936.1	96.5	97.9	1.87	0.2200	0.9800
2A19383D	930 °C	4	0.00001	94.77	0.0005	387.19	0.0000	172.12	0.0002	3.60	0.10	1.602	3024.5	148.2	103.4	1.08	0.2100	1.6100
2A19384D	970 °C	4	0.00001	81.76	0.0004	501.16	0.0000	72.85	0.0001	8.41	0.04	3.898	2989.5	335.7	109.0	0.48	0.1100	1.0600
2A19385D	1050 °C	4	0.00023	5.13	0.0021	89.82	0.0001	9.68	0.0004	2.59	0.27	0.607	2990.1	96.2	73.9	2.08	0.0900	0.1600
2A19386D	1130 °C		0.00002	49.10	0.0005	336.68	0.0000	74.16	0.0003	3.32	0.13	1.226	3081.8	129.5	95.2	1.25	0.2100	1.4100
2A19387D	1230 °C		0.00007	16.99	0.0018	94.55	0.0000	17.24	0.0016	1.10	0.88	0.203	3243.5	35.9	97.8	7.67	0.3800	0.7200
2A19388D	1300 °C		0.00004	30.25	0.0016	110.44	0.0000	51.37	0.0007	1.66	0.49	0.344	3649.0	57.6	97.9	3.24	0.1800	0.4000
2A19389D	1400 °C		0.00000	1929.49	0.0007	250.36	0.0000	544.16	0.0001	9.93	0.06	2.754	0.0	507.7	99.8	0.38	0.0500	0.2600
TOTAL			0.00794	0.89	0.0150	50.24	0.0018	1.88	0.0213	0.37	11.74	0.065						

* Sample steps used for plateau age calculation, denoted by '4'

APPENDIX E
BORON ISOTOPIC RESULTS

Table E.1: Tourmaline δ^{11}B analytical results

Sample Label	δ^{11}B	$^{+-}1\sigma$
BH04 Tourmalines (47 analyses)		
BH04-300611-99	0.006	0.956
BH04-300611-114	−0.025	0.968
BH04-1-95	0.038	0.893
BH04-300611-101	0.101	0.767
BH04-300611-105	0.164	0.642
BH04-300611-108	−0.183	0.966
BH04-300611-111	−0.183	0.966
BH04-300611-112	0.227	0.516
BH04-300611-107	−0.246	0.966
BH04-300611-106	−0.278	0.966
BH04-1-91	−0.309	0.965
BH04-300611-113	0.479	0.014
BH04-300611-109	−0.498	0.964
BH04-300611-117	−0.498	0.964
BH04-300611-104	0.574	0.174
BH04-300611-119	−0.656	0.962
BH04-300611-116	−0.719	0.961
BH04-1-96	0.763	0.551
BH04-300611-115	−0.782	0.961
BH04-1-89	−0.845	0.960
BH04-1-90	−0.845	0.960
BH04-300611-100	0.858	0.739
BH04-1-85	−0.908	0.960
BH04-300611-26	−1.003	0.958
BH04-300611-103	1.047	0.978
BH04-1-93	−1.066	0.958
BH04-300611-110	−1.066	0.958
BH04-300611-28	−1.192	0.957
BH04-1-87	−1.255	0.956
BH04-300611-27	−1.318	0.956
BH04-1-92	−1.350	0.955
BH04-1-86	−1.381	0.955
BH04-1-94	−1.381	0.955
BH04-300611-118	−1.381	0.955
BH04-300611-102	1.552	0.984
BH04-1-83	−1.634	0.952
BH04-1-84	−1.665	0.952
BH04-1-81	−1.697	0.952
BH04-300611-25	−1.728	0.952
BH04-1-78	−1.917	0.950
BH04-1-77	−2.485	0.944
BH04-1-82	−2.548	0.944
BH04-1-76	−2.832	0.941
BH04-1-97	−3.147	0.938
BH04-1-88	−3.431	0.935
BH04-1-79	−3.810	0.931
BH04-1-80	−3.841	0.931
MA08 Tourmalines (54 analyses)		
MA08-300611-39	−0.278	0.966
MA08-300611-54	−0.309	0.965
MA08-300611-41	−0.530	0.963
MA08-300611-35	−0.593	0.962
MA08-300611-45	−0.719	0.961
MA08-300611-40	−0.782	0.961
MA08-300611-38	−0.814	0.960
MA08-300611-46	−0.940	0.959
MA08-300611-42	−1.003	0.958
MA08-300611-37	−1.224	0.956
MA08-300611-32	−1.287	0.955
MA08-300611-33	−1.381	0.955
MA08-300611-47	−1.413	0.954
MA08-300611-49	−1.444	0.955
MA08-300611-55	−1.476	0.954
MA08-300611-62	−1.476	0.954
MA08-300611-52	−1.508	0.953
MA08-300611-53	−1.571	0.953
MA08-300611-43	−1.697	0.952
MA08-300611-44	−1.728	0.952
MA08-300611-68	−1.791	0.951
MA08-300611-51	−1.886	0.950
MA08-300611-50	−1.917	0.950

Continued on Next Page...

Table E.1 – Continued

Sample Label	δ^{11}B	$+-1\sigma$
MA08-300611-56	−1.949	0.949
MA08-300611-34	−1.981	0.949
MA08-300611-67	−2.012	0.949
MA08-300611-59	−2.044	0.948
MA08-300611-36	−2.107	0.948
MA08-300611-48	−2.296	0.946
MA08-300611-65	−2.327	0.946
MA08-300611-64	−2.422	0.945
MA08-300611-66	−2.454	0.944
MA08-300611-58	−2.517	0.944
MA08-300611-31	−2.580	0.943
MA08-300611-63	−2.895	0.940
MA08-300611-61	−2.990	0.939
MA08-300611-69	−3.337	0.936
MA08-300611-60	−3.368	0.936
MA08-300611-83	−3.810	0.931
MA08-300611-57	−3.999	0.929
MA08-300611-81	−4.630	0.923
MA08-300611-70	−5.134	0.919
MA08-300611-79	−5.387	0.916
MA08-300611-80	−5.387	0.916
MA08-300611-75	−5.576	0.914
MA08-300611-78	−5.607	0.914
MA08-300611-77	−5.986	0.910
MA08-300611-76	−6.112	0.909
MA08-300611-30	−6.144	0.908
MA08-300611-72	−6.207	0.908
MA08-300611-82	−6.207	0.908
MA08-300611-74	−6.711	0.903
MA08-300611-71	−6.806	0.902
MA08-300611-73	−8.194	0.888
MA24 Tourmalines (104 analyses)		
MA24-1-139	−9.644	0.876
MA24-300611-13	−7.500	0.895
MA24-1-114	−6.490	0.906
MA24-1-138	−6.396	0.906
MA24-300611-12	−6.364	0.907
MA24-1-128	−6.175	0.909
MA24-1-136	−6.017	0.910
MA24-1-56	−5.639	0.914
MA24-1-121	−5.450	0.915
MA24-1-57	−5.229	0.918
MA24-1-131	−5.197	0.918
MA24-1-140	−5.166	0.918
MA24-1-117	−5.040	0.919
MA24-1-51	−5.008	0.920
MA24-1-116	−4.977	0.920
MA24-300611-10	−4.724	0.923
MA24-300611-11	−4.724	0.923
MA24-1-122	−4.630	0.923
MA24-1-59	−4.630	0.923
MA24-1-134	−4.598	0.924
MA24-1-119	−4.567	0.924
MA24-1-135	−4.409	0.925
MA24-1-48	−4.251	0.927
MA24-1-115	−4.157	0.928
MA24-1-123	−4.157	0.928
MA24-1-54	−4.125	0.928
MA24-1-113	−3.936	0.930
MA24-1-125	−3.841	0.931
MA24-1-55	−3.841	0.931
MA24-1-37	−3.684	0.932
MA24-1-132	−3.652	0.933
MA24-1-52	−3.621	0.933
MA24-1-118	−3.526	0.934
MA24-1-126	−3.431	0.935
MA24-1-133	−3.431	0.935
MA24-1-62	−3.431	0.935
MA24-1-43	−3.368	0.936
MA24-1-120	−3.305	0.936
MA24-1-53	−3.211	0.937
MA24-1-47	−3.084	0.939

Continued on Next Page...

Table E.1 – Continued

Sample Label	δ^{11}B	$^{+-}1\sigma$
MA24-1-129	−2.990	0.939
MA24-300611-8	−2.990	0.939
MA24-1-44	−2.958	0.940
MA24-1-49	−2.958	0.940
MA24-300611-9	−2.958	0.940
MA24-1-50	−2.927	0.940
MA24-1-28	−2.895	0.940
MA24-1-109	−2.769	0.941
MA24-1-58	−2.769	0.941
MA24-1-39	−2.737	0.942
MA24-1-64	−2.706	0.942
MA24-1-124	−2.454	0.944
MA24-1-41	−2.454	0.944
MA24-1-46	−2.454	0.944
MA24-1-60	−2.422	0.945
MA24-1-111	−2.170	0.947
MA24-1-26	−2.138	0.948
MA24-1-33	−2.138	0.948
MA24-1-65	−1.886	0.950
MA24-1-35	−1.665	0.952
MA24-300611-7	−1.571	0.953
MA24-1-12	−1.508	0.953
MA24-1-61	−1.287	0.955
MA24-1-13	−1.255	0.956
MA24-1-40	−1.224	0.956
MA24-1-63	−1.224	0.956
MA24-1-110	−1.161	0.957
MA24-1-36	−1.161	0.957
MA24-1-34	−1.129	0.957
MA24-1-137	−1.098	0.957
MA24-1-45	−1.034	0.959
MA24-1-11	−0.877	0.959
MA24-1-23	−0.877	0.959
MA24-1-19	−0.845	0.960
MA24-1-20	−0.845	0.960
MA24-1-38	−0.845	0.960
MA24-1-32	−0.688	0.962
MA24-1-27	−0.656	0.962
MA24-300611-6	−0.656	0.962
MA24-1-29	−0.624	0.963
MA24-1-112	−0.593	0.962
MA24-1-21	−0.498	0.964
MA24-1-66	−0.435	0.964
MA24-1-130	−0.278	0.966
MA24-1-30	−0.246	0.966
MA24-1-16	−0.183	0.966
MA24-300611-4	−0.120	0.967
MA24-300611-1	−0.088	0.968
MA24-1-24	−0.057	0.967
MA24-1-67	0.101	0.767
MA24-300611-3	0.101	0.767
MA24-1-31	0.227	0.516
MA24-300611-2	0.259	0.454
MA24-300611-5	0.448	0.077
MA24-1-127	0.542	0.111
MA24-1-17	0.637	0.300
MA24-1-22	0.637	0.300
MA24-1-14	0.669	0.363
MA24-1-25	0.700	0.425
MA24-1-18	1.299	0.980
MA24-1-15	1.362	0.981
MA24-1-108	1.489	0.983

APPENDIX F
RUTILE STANDARDS DATA TABLE

Table F.1: SHRIMP analytical results for rutile standards

						Ratios							Dates (Ma)							
Grain .spot	U ppm	Th ppm	Th/U	Pb ppm	$f206\%$ ^{208}corr	$\frac{^{207}Pb}{^{206}Pb}$ ^{208}corr	$\pm1\sigma$ %	$\frac{^{206}Pb}{^{238}U}$ ^{208}corr	$\pm1\sigma$ %	$\frac{^{207}Pb}{^{235}U}$ ^{208}corr	$\pm1\sigma$	%conc. ^{208}corr	$\frac{^{206}Pb}{^{238}U}$ ^{208}corr	$\pm1\sigma$	$\frac{^{207}Pb}{^{235}U}$ ^{208}corr	$\pm1\sigma$	$\frac{^{207}Pb}{^{206}Pb}$ ^{204}corr	$\pm1\sigma$	$\frac{^{207}Pb}{^{206}Pb}$ ^{208}corr	$\pm1\sigma$
'RUT' standard rutiles (135 analyses)																				
RUT-14.1	461	1	0.00	251	0.015	0.1736	0.54	0.5396	4.13	12.914	4.24	107	2782	93	2673	40	2584	10	2592	9
RUT-81.2	399	0	0.00	219	0.040	0.1741	0.68	0.5416	5.07	13.000	5.20	107	2790	115	2680	49	2585	13	2597	11
RUT-18.2	722	1	0.00	414	0.035	0.1753	0.52	0.5662	4.76	13.687	4.85	111	2892	111	2728	46	2608	9	2609	9
RUT-81.3	366	0	0.00	193	0.118	0.1756	0.72	0.5184	5.15	12.550	5.29	103	2693	113	2647	50	2608	13	2612	12
RUT-34	77	0	-0.00	43	0.583	0.1760	0.85	0.5372	5.85	13.033	6.01	106	2772	132	2682	57	2638	34	2615	14
RUT-85.2	863	1	0.00	452	0.011	0.1759	0.51	0.5178	4.96	12.559	5.05	103	2690	109	2647	48	2612	9	2615	8
RUT-41	108	0	0.00	59	0.351	0.1763	0.61	0.5358	4.06	13.024	4.18	106	2766	91	2681	39	2617	15	2618	10
RUT-91.2	554	0	0.00	290	0.013	0.1765	0.55	0.5166	4.48	12.569	4.58	102	2685	98	2648	43	2615	10	2620	9
RUT-22.1	132	0	0.00	65	0.088	0.1766	0.42	0.4878	2.74	11.881	2.83	98	2561	58	2595	26	2620	8	2622	7
RUT-24	186	0	0.00	90	0.167	0.1767	0.60	0.4746	5.46	11.565	5.57	95	2504	113	2570	52	2615	17	2622	10
RUT-61	228	0	0.00	111	0.017	0.1767	0.47	0.4827	3.56	11.760	3.64	97	2539	75	2586	34	2619	8	2622	8
RUT-64	85	0	0.00	45	0.085	0.1767	0.65	0.5266	3.90	12.827	4.03	104	2727	87	2667	38	2630	11	2622	11
RUT-2	74	0	0.00	44	0.018	0.1768	0.32	0.5873	2.35	14.318	2.41	114	2979	56	2771	23	2627	15	2623	5
RUT-33	97	0	-0.00	56	0.503	0.1768	0.75	0.5650	5.55	13.772	5.69	110	2887	129	2734	54	2644	17	2623	12
RUT-56	125	1	0.00	65	0.062	0.1768	0.65	0.5160	4.20	12.582	4.33	102	2682	92	2649	41	2619	12	2623	11
RUT-15.1	978	1	0.00	513	0.009	0.1769	0.43	0.5180	4.34	12.637	4.41	103	2691	95	2653	42	2620	7	2624	7
RUT-3	140	0	0.00	71	0.127	0.1769	0.59	0.4961	5.61	12.102	5.71	99	2597	120	2612	54	2632	11	2624	10
RUT-8	95	0	0.00	54	0.004	0.1769	0.29	0.5597	2.21	13.654	2.27	109	2865	51	2726	21	2620	5	2624	5
RUT-92.3	456	0	0.00	242	0.018	0.1769	0.59	0.5252	4.52	12.810	4.64	104	2721	100	2666	44	2622	11	2624	10
RUT-12.1	456	0	0.00	256	0.043	0.1770	0.52	0.5540	4.07	13.521	4.17	108	2842	94	2717	39	2621	9	2625	9
RUT-15	226	0	0.00	103	0.147	0.1771	0.60	0.4482	5.46	10.941	5.56	91	2387	109	2518	52	2617	19	2626	10
RUT-92.2	416	0	0.00	218	0.030	0.1771	0.60	0.5178	4.55	12.648	4.67	102	2690	100	2654	44	2625	10	2626	10
RUT-10	144	0	0.00	86	0.213	0.1772	0.63	0.5846	5.78	14.281	5.90	113	2968	138	2769	56	2629	35	2627	10
RUT-1	166	0	0.00	87	-0.006	0.1773	0.32	0.5183	3.07	12.666	3.12	102	2692	67	2655	29	2625	6	2627	5
RUT-13	97	0	0.00	57	0.000	0.1772	0.30	0.5768	2.69	14.091	2.74	112	2936	63	2756	26	2624	7	2627	5
RUT-5	72	0	0.00	41	0.025	0.1773	0.32	0.5586	2.26	13.653	2.32	109	2861	52	2726	22	2625	7	2627	5
RUT-12.2	444	0	0.00	246	0.027	0.1775	0.55	0.5465	4.19	13.371	4.30	107	2810	96	2706	41	2625	10	2629	9
RUT-1	261	1	0.00	154	0.001	0.1775	0.29	0.5820	3.75	14.240	3.80	112	2957	89	2766	36	2627	5	2629	5
RUT-14	80	0	-0.00	51	0.288	0.1775	0.77	0.6189	6.01	15.144	6.15	118	3106	148	2824	59	2658	52	2629	13
RUT-26	124	0	-0.00	70	0.229	0.1775	0.65	0.5525	6.15	13.526	6.27	108	2836	141	2717	59	2644	11	2630	11
RUT-32	392	0	0.00	200	0.079	0.1775	0.36	0.5041	4.35	12.341	4.41	100	2632	94	2631	41	2634	6	2630	6
RUT-44	498	0	0.00	265	0.033	0.1776	0.29	0.5246	2.44	12.844	2.49	103	2719	54	2668	23	2624	6	2630	5
RUT-7	177	0	0.00	97	-0.011	0.1776	0.27	0.5405	2.77	13.234	2.82	106	2786	63	2697	27	2627	5	2630	5
RUT-80.2	653	1	0.00	358	0.024	0.1775	0.56	0.5416	4.80	13.257	4.90	106	2790	109	2698	46	2625	10	2630	9
RUT-8	214	0	0.00	106	-0.005	0.1775	0.24	0.4878	2.61	11.942	2.65	97	2561	55	2600	25	2630	4	2630	4
RUT-2	199	0	0.00	100	0.061	0.1776	0.30	0.4947	3.53	12.117	3.58	98	2591	75	2613	34	2634	5	2631	5
RUT-51	301	0	-0.00	153	0.052	0.1776	0.38	0.4998	2.83	12.239	2.91	99	2613	61	2623	27	2639	14	2631	6

Continued on Next Page...

Table F.1 – Continued

Grain .spot	U ppm	Th ppm	Th/U	Pb ppm	$f206\%$ ^{208}corr	Ratios $\frac{^{207}Pb}{^{206}Pb}$ ^{208}corr	±1σ %	$\frac{^{206}Pb}{^{238}U}$ ^{208}corr	±1σ %	$\frac{^{207}Pb}{^{235}U}$ ^{208}corr	±1σ	%conc. ^{208}corr	Dates (Ma) $\frac{^{206}Pb}{^{238}U}$ ^{208}corr	±1σ	$\frac{^{207}Pb}{^{235}U}$ ^{208}corr	±1σ	$\frac{^{207}Pb}{^{206}Pb}$ ^{204}corr	±1σ	$\frac{^{207}Pb}{^{206}Pb}$ ^{208}corr	±1σ
RUT-53	363	0	0.00	176	0.048	0.1777	0.37	0.4781	2.75	11.713	2.82	96	2519	57	2582	26	2631	7	2631	6
RUT-6	54	0	0.00	110	0.061	0.1776	0.44	1.9918	6.42	48.776	6.49	269	7064	276	3968	65	2637	8	2631	7
RUT-19	92	0	-0.00	52	0.150	0.1778	0.72	0.5542	5.48	13.581	5.62	108	2842	126	2721	53	2621	21	2632	12
RUT-52	286	0	0.00	145	0.052	0.1777	0.40	0.5002	2.88	12.258	2.96	99	2615	62	2624	28	2638	11	2632	7
RUT-7	100	0	0.00	54	0.246	0.1778	0.64	0.5245	5.86	12.857	5.98	103	2718	130	2669	56	2636	14	2632	11
RUT-90.2	527	0	0.00	289	0.022	0.1777	0.55	0.5420	4.43	13.281	4.54	106	2792	100	2700	43	2628	9	2632	9
RUT-91.3	645	0	0.00	323	0.015	0.1778	0.52	0.4945	4.33	12.120	4.43	98	2590	92	2614	42	2629	9	2632	9
RUT-12	100	0	0.00	58	0.002	0.1779	0.30	0.5778	2.67	14.174	2.73	112	2940	63	2761	26	2634	5	2633	5
RUT-12	152	0	0.00	104	0.237	0.1779	0.60	0.6718	5.58	16.478	5.69	126	3313	145	2905	54	2633	16	2633	10
RUT-22	146	0	0.00	81	0.117	0.1778	0.62	0.5417	5.41	13.283	5.52	106	2791	123	2700	52	2626	14	2633	10
RUT-25.1	143	0	0.00	75	0.108	0.1779	0.36	0.5135	2.44	12.595	2.51	101	2672	53	2650	24	2635	7	2633	6
RUT-30	80	0	-0.00	46	0.330	0.1779	0.73	0.5596	5.65	13.726	5.79	109	2865	131	2731	55	2624	23	2633	12
RUT-3	149	0	0.00	80	0.073	0.1778	0.32	0.5274	3.75	12.932	3.80	104	2730	84	2675	36	2631	6	2633	5
RUT-4	217	0	0.00	106	0.006	0.1778	0.23	0.4821	2.13	11.819	2.17	96	2536	45	2590	20	2633	4	2633	4
RUT-46	201	0	0.00	107	0.032	0.1778	0.50	0.5233	4.02	12.829	4.11	103	2713	89	2667	39	2636	9	2633	8
RUT-13	121	0	0.00	65	0.231	0.1779	0.67	0.5250	5.78	12.882	5.90	103	2721	128	2671	56	2639	19	2634	11
RUT-18.1	183	0	-0.00	107	0.196	0.1780	0.35	0.5712	2.46	14.016	2.53	111	2913	58	2751	24	2639	7	2634	6
RUT-19.1	109	0	-0.00	47	0.071	0.1779	0.42	0.4261	2.41	10.454	2.50	87	2288	46	2476	23	2630	8	2634	7
RUT-57	90	0	0.00	49	0.062	0.1780	0.68	0.5311	3.97	13.034	4.11	104	2746	89	2682	39	2629	14	2634	11
RUT-8	136	0	0.00	77	0.173	0.1780	0.59	0.5544	5.51	13.606	5.62	108	2843	127	2723	53	2644	14	2634	10
RUT-13.2	1254	4	0.00	698	0.117	0.1781	0.45	0.5468	4.68	13.428	4.75	107	2812	107	2710	45	2631	8	2635	8
RUT-2	208	0	0.00	111	-0.001	0.1781	0.30	0.5294	3.18	12.996	3.23	104	2739	71	2679	30	2635	5	2635	5
RUT-25.2	134	0	-0.00	70	0.172	0.1780	0.38	0.5143	2.45	12.625	2.53	102	2675	54	2652	24	2630	8	2635	6
RUT-37	104	0	-0.00	54	0.445	0.1781	0.77	0.5072	5.55	12.455	5.70	100	2644	120	2639	54	2643	18	2635	13
RUT-4	177	0	0.00	91	0.070	0.1781	0.31	0.5049	3.64	12.397	3.69	100	2635	79	2635	35	2633	6	2635	5
RUT-63	108	0	0.00	59	0.069	0.1781	0.59	0.5356	3.65	13.152	3.77	105	2765	82	2691	36	2637	12	2635	10
RUT-10	165	0	0.00	85	-0.018	0.1782	0.29	0.5061	3.02	12.435	3.07	100	2640	65	2638	29	2637	5	2636	5
RUT-15.3	800	1	0.00	438	0.003	0.1782	0.48	0.5401	4.80	13.272	4.88	106	2784	109	2699	46	2634	8	2636	8
RUT-29	555	0	-0.00	325	0.036	0.1781	0.30	0.5783	4.24	14.204	4.29	112	2942	100	2763	41	2642	6	2636	5
RUT-40	241	0	0.00	135	0.297	0.1782	0.51	0.5451	4.72	13.392	4.81	106	2805	107	2708	46	2620	13	2636	8
RUT-50	159	0	0.00	84	0.055	0.1782	0.58	0.5195	4.51	12.765	4.62	102	2697	99	2662	43	2635	12	2636	10
RUT-5	105	0	0.00	55	-0.003	0.1782	0.39	0.5222	3.17	12.833	3.24	103	2709	70	2667	31	2635	7	2636	6
RUT-5	140	0	0.00	72	0.103	0.1782	0.32	0.5042	3.47	12.387	3.53	100	2632	75	2634	33	2636	6	2636	5
RUT-54	158	0	0.00	84	0.101	0.1781	0.58	0.5215	3.91	12.809	4.02	103	2706	86	2666	38	2639	20	2636	10
RUT-6	123	0	0.00	67	0.021	0.1782	0.39	0.5396	3.63	13.259	3.69	106	2782	82	2698	35	2635	7	2636	6
RUT-7	167	0	0.00	82	-0.001	0.1782	0.25	0.4826	2.28	11.857	2.32	96	2538	48	2593	22	2633	5	2636	4
RUT-86.1	708	1	0.00	365	0.018	0.1781	0.53	0.5087	4.56	12.495	4.66	101	2651	99	2642	44	2627	10	2636	9
RUT-9	260	1	0.00	140	0.047	0.1781	0.38	0.5295	4.40	13.005	4.46	104	2739	98	2680	42	2638	6	2636	6
RUT-9	364	1	0.00	178	0.047	0.1781	0.38	0.4807	4.52	11.806	4.58	96	2530	95	2589	43	2638	6	2636	6

Continued on Next Page...

Table F.1 – Continued

						Ratios							Dates (Ma)							
Grain .spot	U ppm	Th ppm	Th/U	Pb ppm	$f206\%$ ^{208}corr	$\frac{^{207}Pb}{^{206}Pb}$ ^{208}corr	$\pm1\sigma$ %	$\frac{^{206}Pb}{^{238}U}$ ^{208}corr	$\pm1\sigma$ %	$\frac{^{207}Pb}{^{235}U}$ ^{208}corr	$\pm1\sigma$	%conc. ^{208}corr	$\frac{^{206}Pb}{^{238}U}$ ^{208}corr	$\pm1\sigma$	$\frac{^{207}Pb}{^{235}U}$ ^{208}corr	$\pm1\sigma$	$\frac{^{207}Pb}{^{206}Pb}$ ^{204}corr	$\pm1\sigma$	$\frac{^{207}Pb}{^{206}Pb}$ ^{208}corr	$\pm1\sigma$
RUT-16	213	0	0.00	104	0.171	0.1782	0.57	0.4791	5.42	11.774	5.52	96	2523	113	2587	52	2642	22	2637	9
RUT-3	101	0	0.00	53	0.008	0.1782	0.28	0.5150	2.22	12.657	2.27	102	2678	49	2654	21	2636	5	2637	5
RUT-90.1	463	0	0.00	254	0.029	0.1783	0.58	0.5401	4.59	13.274	4.70	106	2784	104	2699	44	2628	11	2637	10
RUT-1	203	0	0.00	109	-0.009	0.1784	0.24	0.5309	2.30	13.063	2.34	104	2745	51	2684	22	2636	4	2638	4
RUT-36	749	0	-0.00	405	0.137	0.1784	0.35	0.5318	4.65	13.079	4.71	104	2749	104	2685	44	2643	7	2638	6
RUT-49	175	0	0.00	96	0.082	0.1784	0.53	0.5396	3.95	13.274	4.05	105	2782	89	2699	38	2637	12	2638	9
RUT-55	151	0	0.00	77	0.068	0.1784	0.59	0.5049	3.97	12.419	4.08	100	2635	86	2637	38	2635	11	2638	10
RUT-3	107	0	0.00	59	0.001	0.1785	0.35	0.5441	2.92	13.392	2.99	106	2800	66	2708	28	2636	8	2639	6
RUT-43	460	0	0.00	240	0.019	0.1785	0.32	0.5145	2.55	12.662	2.61	101	2676	56	2655	25	2638	6	2639	5
RUT-45	405	0	0.00	239	0.021	0.1785	0.30	0.5810	2.50	14.304	2.56	112	2953	59	2770	24	2639	5	2639	5
RUT-6	289	1	0.00	161	-0.048	0.1785	0.23	0.5506	2.70	13.554	2.74	107	2828	62	2719	26	2633	4	2639	4
RUT-7	202	0	0.00	120	0.036	0.1785	0.29	0.5867	3.57	14.442	3.61	113	2976	85	2779	34	2638	5	2639	5
RUT-27	284	0	0.00	146	0.094	0.1786	0.43	0.5045	4.57	12.427	4.64	100	2633	99	2637	44	2639	9	2640	7
RUT-35	773	0	-0.00	446	0.148	0.1786	0.31	0.5667	4.56	13.958	4.61	110	2894	106	2747	44	2645	6	2640	5
RUT-48	187	0	0.00	104	0.086	0.1786	0.51	0.5464	3.87	13.454	3.97	106	2810	88	2712	38	2649	19	2640	9
RUT-5	178	0	-0.00	91	0.088	0.1786	0.46	0.5027	4.71	12.378	4.79	99	2625	102	2634	45	2662	11	2640	8
RUT-65	593	1	0.00	336	0.012	0.1786	0.29	0.5599	2.91	13.788	2.96	109	2866	67	2735	28	2642	5	2640	5
RUT-80.1	591	1	0.00	331	0.027	0.1786	0.58	0.5511	4.96	13.568	5.07	107	2830	114	2720	48	2637	10	2640	10
RUT-25	232	0	-0.00	130	0.101	0.1787	0.54	0.5517	5.27	13.594	5.36	107	2832	121	2722	51	2641	15	2641	9
RUT-62	487	0	0.00	230	0.021	0.1787	0.30	0.4658	2.50	11.477	2.55	93	2465	51	2563	24	2643	5	2641	5
RUT-28	306	0	-0.00	153	0.054	0.1788	0.42	0.4927	4.57	12.146	4.64	98	2583	97	2616	44	2641	10	2642	7
RUT-31	216	0	-0.00	111	0.181	0.1789	0.55	0.5044	5.21	12.439	5.31	100	2633	113	2638	50	2652	10	2642	9
RUT-92.1	549	0	0.00	284	0.132	0.1789	0.55	0.5082	4.26	12.533	4.37	100	2649	93	2645	41	2634	11	2642	9
RUT-20	535	1	0.00	293	0.017	0.1789	0.36	0.5404	4.69	13.330	4.74	105	2785	106	2703	45	2643	6	2643	6
RUT-91.1	586	0	0.00	307	0.007	0.1789	0.54	0.5172	4.47	12.760	4.57	102	2687	98	2662	43	2638	11	2643	9
RUT-9	176	0	0.00	85	-0.011	0.1789	0.26	0.4746	2.75	11.706	2.79	95	2504	57	2581	26	2643	5	2643	4
RUT-17.1	674	1	0.00	411	0.009	0.1790	0.49	0.6014	4.66	14.844	4.74	115	3035	113	2805	45	2640	9	2644	8
RUT-17	370	0	0.00	203	1.355	0.1791	1.29	0.5149	4.83	12.715	5.15	101	2678	106	2659	49	2656	27	2644	21
RUT-20.1	224	0	0.00	123	0.082	0.1790	0.32	0.5391	2.55	13.308	2.61	105	2780	58	2702	25	2642	6	2644	5
RUT-11	197	0	0.00	106	-0.011	0.1792	0.26	0.5294	2.87	13.076	2.92	104	2739	64	2685	28	2645	5	2645	4
RUT-21	97	0	0.00	52	0.270	0.1791	0.72	0.5267	5.35	13.008	5.49	103	2727	119	2680	52	2635	21	2645	12
RUT-13.1	1052	1	0.00	565	0.002	0.1793	0.41	0.5299	4.39	13.098	4.46	104	2741	98	2687	42	2644	7	2646	7
RUT-27.1	346	0	0.00	206	0.085	0.1793	0.27	0.5859	2.53	14.483	2.57	112	2973	60	2782	24	2646	5	2646	4
RUT-58	381	0	0.00	197	0.050	0.1792	0.34	0.5084	2.54	12.561	2.60	100	2650	55	2647	24	2652	13	2646	6
RUT-59	190	0	0.00	104	0.054	0.1792	0.52	0.5397	4.00	13.336	4.10	105	2782	90	2704	39	2638	12	2646	9
RUT-2	308	0	0.00	159	0.034	0.1794	0.36	0.5079	4.44	12.562	4.50	100	2648	96	2647	42	2651	9	2647	6
RUT-4	288	0	0.00	175	0.076	0.1795	0.34	0.5992	4.42	14.828	4.47	114	3027	107	2804	43	2649	7	2648	6
RUT-60	476	0	0.00	259	0.032	0.1796	0.34	0.5362	3.12	13.280	3.18	104	2768	70	2700	30	2647	7	2649	6
RUT-42	178	1	0.00	97	0.150	0.1797	0.54	0.5334	4.23	13.213	4.33	104	2756	95	2695	41	2639	14	2650	9

Continued on Next Page...

Table F.1 – Continued

Grain .spot	U ppm	Th ppm	Th/U	Pb ppm	$f206\%$ ^{208}corr	Ratios $\frac{^{207}Pb}{^{206}Pb}$ ^{208}corr	$\pm1\sigma$ %	$\frac{^{206}Pb}{^{238}U}$ ^{208}corr	$\pm1\sigma$ %	$\frac{^{207}Pb}{^{235}U}$ ^{208}corr	$\pm1\sigma$	%conc. ^{208}corr	Dates (Ma) $\frac{^{206}Pb}{^{238}U}$ ^{208}corr	$\pm1\sigma$	$\frac{^{207}Pb}{^{235}U}$ ^{208}corr	$\pm1\sigma$	$\frac{^{207}Pb}{^{206}Pb}$ ^{204}corr	$\pm1\sigma$	$\frac{^{207}Pb}{^{206}Pb}$ ^{208}corr	$\pm1\sigma$
RUT-66	539	1	0.00	315	0.038	0.1798	0.36	0.5747	3.05	14.246	3.11	110	2927	72	2766	30	2646	7	2651	6
RUT-47	320	0	0.00	175	0.024	0.1800	0.36	0.5384	2.62	13.362	2.69	105	2777	59	2706	25	2656	7	2653	6
RUT-85.1	932	1	0.00	467	0.009	0.1801	0.49	0.4931	4.82	12.245	4.91	97	2584	103	2623	46	2648	9	2654	8
RUT-1	390	0	0.00	217	0.057	0.1802	0.32	0.5463	4.38	13.574	4.43	106	2810	100	2720	42	2658	6	2655	5
RUT-15.2	753	0	0.00	435	0.012	0.1803	0.47	0.5698	4.85	14.165	4.93	109	2907	113	2761	47	2650	8	2655	8
RUT-81.4	336	0	0.00	181	0.059	0.1808	0.70	0.5313	5.19	13.245	5.33	103	2747	116	2697	50	2656	13	2660	12
RUT-90.3	439	0	0.00	239	0.023	0.1811	0.59	0.5357	4.71	13.378	4.82	104	2765	106	2707	46	2658	11	2663	10
RUT-39	265	0	-0.00	148	0.140	0.1812	0.49	0.5453	4.79	13.621	4.87	105	2806	109	2724	46	2673	8	2664	8
RUT-23	90	0	0.00	53	0.035	0.1813	0.67	0.5790	5.36	14.474	5.48	111	2945	127	2781	52	2679	19	2665	11
RUT-18.1	655	1	0.00	407	0.047	0.1820	0.51	0.6105	4.81	15.323	4.90	115	3072	118	2836	47	2667	9	2672	9
RUT-81.1	469	0	0.00	250	0.023	0.1823	0.60	0.5236	4.65	13.157	4.76	102	2714	103	2691	45	2670	11	2674	10
RUT-4	92	0	0.00	53	0.003	0.1825	0.38	0.5675	3.04	14.284	3.11	108	2898	71	2769	30	2675	7	2676	6
RUT-18	90	0	0.00	57	4.899	0.1851	2.92	0.5231	6.68	13.354	7.62	100	2713	148	2705	72	2717	81	2699	48
RUT-23	8	0	0.02	81	-0.193	0.1852	0.87	10.3200	14.93	263.466	15.06	579	15643	883	5664	154	2673	11	2700	14
RUT-24	17	1	0.05	111	-0.592	0.1866	1.32	6.4785	15.39	166.701	15.61	478	12970	865	5201	159	2655	14	2713	22
RUT-6	225	0	0.00	119	0.006	0.1902	0.21	0.5176	2.21	13.572	2.25	98	2689	49	2720	21	2744	4	2743	4
RUT-19.1	738	0	0.00	392	0.034	0.1939	0.50	0.5169	4.35	13.817	4.44	97	2686	96	2737	42	2772	9	2775	8
RUT-38	130	13	0.10	79	-0.845	0.1949	0.75	0.5916	5.70	15.901	5.85	108	2996	137	2871	56	2716	15	2784	12
RUT-11	162	0	0.00	144	0.130	0.2194	0.45	0.8415	5.55	25.453	5.62	132	3936	163	3326	55	2983	7	2976	7
RUT-86.2*	389	172	0.44	201	-4.875	0.2196	1.27	0.5278	6.61	15.981	6.89	92	2732	147	2876	66	2378	37	2978	20

$f206\%$ = 100 x (common ^{206}Pb/total ^{206}Pb)
^{207}Pb/^{206}Pb 204corr = ^{204}Pb-corrected ^{207}Pb/^{206}Pb ratio
^{206}Pb/^{238}U 204corr = ^{204}Pb-corrected ^{206}Pb/^{238}U ratio
^{207}Pb/^{235}U 204corr = ^{204}Pb-corrected ^{207}Pb/^{235}U ratio
%c = % Concordance
^{206}Pb/^{238}U date = ^{208}Pb-corrected ^{206}Pb/^{238}U date
^{207}Pb/^{235}U date = ^{208}Pb-corrected ^{207}Pb/^{235}U date
^{207}Pb/^{206}Pb date = ^{208}Pb-corrected ^{207}Pb/^{206}Pb date

APPENDIX G
MUSCOVITE-FUCHSITE $^{40}AR/^{39}AR$ DATA

Table G.1: ^{40}Ar/^{39}Ar data table for muscovite-fuchsites

Sample Step	Laser Power	Used*	^{36}Ar	%1σ	^{37}Ar	%1σ	^{38}Ar	%1σ	^{39}Ar	%1σ	^{40}Ar	%1σ	Age (Ma)	±2s	^{40}Ar(r) (%)	^{39}Ar(k) (%)	K/Ca	±2s
Sample Muscovite-Fuchsite-BH01-I9																		
1A14545D	55.70 W		0.00001	103.12	0.0000	512.22	0.0000	683.71	0.0001	10.77	0.05	0.324	2625.2	297.8	100.0	0.02	1.9000	19.3000
1A14546D	56.50 W		0.00000	481.35	0.0001	173.18	0.0000	558.07	0.0014	1.95	0.48	0.110	2615.8	56.7	99.9	0.20	5.3000	29.4000
1A14547D	56.60 W		0.00001	74.75	0.0000	1348.13	0.0000	299.52	0.0002	10.22	0.05	0.314	2396.2	334.7	91.0	0.02	35.1000	11429.3000
1A14549D	57.20 W		0.00001	140.44	0.0000	882.24	0.0000	112.30	0.0001	18.37	0.03	0.416	2490.0	584.6	92.5	0.01	10.7000	1196.2000
1A14551D	57.70 W		0.00002	39.24	0.0000	438.00	0.0000	83.39	0.0004	4.23	0.13	0.205	2412.4	127.5	94.6	0.06	4.6000	40.2000
1A14552D	57.90 W		0.00001	84.38	0.0002	82.01	0.0000	271.66	0.0003	6.32	0.08	0.193	2425.8	202.1	95.3	0.04	0.7000	1.1000
1A14554D	58.10 W		0.00002	63.18	0.0001	276.56	0.0000	406.43	0.0005	3.92	0.13	0.373	2316.4	129.5	95.4	0.07	2.0000	8.7000
1A14555D	58.30 W		0.00001	203.08	0.0002	104.22	0.0000	288.35	0.0008	2.46	0.22	0.109	2365.6	76.0	99.3	0.11	16.3000	328.4000
1A14574D	58.60 W		0.00001	177.98	0.0002	65.07	0.0000	125.85	0.0006	2.90	0.16	0.156	2412.3	106.5	98.5	0.08	16.5000	241.6000
1A14575D	58.90 W		0.00005	30.27	0.0001	86.65	0.0000	43.39	0.0012	1.67	0.35	0.127	2420.9	56.4	95.9	0.17	10.1000	44.5000
1A14576D	59.20 W		0.00002	76.91	0.0000	2469.95	0.0000	58.73	0.0006	2.42	0.18	0.201	2445.5	89.7	97.1	0.08	46.0000	2271.9000
1A14577D	59.50 W		0.00001	96.08	0.0001	178.91	0.0001	26.31	0.0046	0.63	1.43	0.056	2507.7	18.9	99.7	0.66	10595.3000	15213703.2000
1A14579D	59.60 W		0.00004	36.88	0.0001	155.70	0.0002	7.60	0.0136	0.48	4.44	0.039	2584.6	13.5	99.7	1.93	104.1000	398.1000
1A14580D	59.60 W	4	0.00001	129.91	0.0000	1383.07	0.0001	21.30	0.0046	0.97	1.52	0.057	2620.3	28.0	99.8	0.65	273.6000	10551.4000
1A14581D	59.60 W	4	0.00000	926.13	0.0001	173.81	0.0000	37.56	0.0016	1.77	0.51	0.108	2595.3	55.1	99.9	0.22	18.8000	108.0000
1A14582D	59.70 W	4	0.00002	73.97	0.0000	495.37	0.0000	65.29	0.0021	1.39	0.71	0.116	2619.2	38.4	100.0	0.30	59.3000	1012.4000
1A14584D	59.80 W	4	0.00000	1036.09	0.0001	143.80	0.0000	38.43	0.0027	0.67	0.92	0.083	2622.6	23.9	100.0	0.39	73.6000	1222.0000
1A14585D	59.90 W	4	0.00001	240.91	0.0001	218.54	0.0001	17.99	0.0054	0.60	1.80	0.049	2613.5	18.2	99.9	0.77	73.6000	1222.0000
1A14586D	60.00 W	4	0.00001	241.03	0.0001	153.07	0.0000	64.11	0.0033	1.03	1.10	0.044	2630.4	28.6	100.0	0.46	16.0000	49.1000
1A14587D	60.20 W	4	0.00002	79.71	0.0001	173.04	0.0001	25.84	0.0039	0.81	1.29	0.070	2595.9	24.3	99.6	0.56	10.2000	22.6000
1A14589D	60.50 W	4	0.00000	344.63	0.0000	377.67	0.0001	18.66	0.0057	0.71	1.88	0.054	2606.6	20.6	99.9	0.81	10.2000	22.6000
1A14590D	60.90 W	4	0.00000	849.31	0.0001	190.45	0.0002	7.19	0.0117	0.52	3.86	0.032	2604.4	14.4	100.0	1.66	76.4000	291.1000
1A14591D	61.20 W	4	0.00004	43.44	0.0000	299.28	0.0004	4.10	0.0326	0.33	10.78	0.036	2604.8	9.1	99.9	4.64	308.4000	1846.0000
1A14592D	61.40 W	4	0.00001	203.74	0.0001	180.51	0.0003	5.98	0.0242	0.41	7.99	0.041	2605.4	11.4	100.0	3.44	1001.1000	20518.1000
1A14594D	61.60 W	4	0.00010	47.54	0.0051	4.68	0.0009	2.89	0.0753	0.37	24.92	0.023	2605.5	10.4	99.9	10.71	6.4000	0.6000
1A14595D	62.00 W	4	0.00001	122.59	0.0000	407.29	0.0002	7.66	0.0148	0.47	4.92	0.045	2617.3	13.5	99.9	2.10	198.0000	1613.0000
1A14596D	62.40 W	4	0.00016	35.35	0.0061	7.07	0.0008	8.25	0.0565	0.43	18.60	0.036	2598.3	12.1	99.8	8.03	4.0000	0.6000
1A14609D	62.70 W	4	0.00002	83.51	0.0001	155.15	0.0004	4.51	0.0331	0.38	10.98	0.030	2608.6	10.7	99.9	4.71	4.0000	0.6000
1A14610D	63.00 W	4	0.00010	41.22	0.0060	6.05	0.0006	8.40	0.0445	0.57	14.66	0.052	2597.3	15.9	99.8	6.33	3.2000	0.4000
1A14611D	63.40 W	4	0.00001	284.57	0.0001	95.34	0.0001	13.65	0.0122	0.49	4.04	0.045	2604.7	14.2	100.0	1.74	3.2000	0.4000
1A14612D	63.80 W	4	0.00002	82.54	0.0000	1161.81	0.0003	6.81	0.0248	0.46	8.20	0.027	2605.5	12.7	99.9	3.53	777.0000	18054.9000
1A14614D	64.00 W	4	0.00002	79.78	0.0002	97.67	0.0003	5.91	0.0206	0.42	6.80	0.019	2603.0	11.8	99.9	2.93	200.3000	1669.2000
1A14617D	64.50 W	4	0.00016	20.55	0.0060	3.62	0.0009	4.42	0.0693	0.42	22.91	0.045	2604.1	11.8	99.8	9.85	4.9000	0.4000
1A14618D	64.50 W	4	0.00002	96.69	0.0001	161.84	0.0002	6.77	0.0204	0.43	6.76	0.024	2609.3	12.1	99.9	2.90	2278.0000	146752.0000
1A14619D	64.60 W	4	0.00015	55.87	0.0071	4.90	0.0018	2.15	0.1440	0.40	47.71	0.040	2608.1	11.1	99.9	20.48	8.7000	0.9000
1A14620D	64.60 W	4	0.00003	59.32	0.0000	437.45	0.0004	4.72	0.0321	0.39	10.62	0.035	2606.2	10.8	99.9	4.57	147.3000	468.8000
1A14622D	64.60 W	4	0.00003	56.90	0.0001	168.95	0.0003	7.06	0.0212	0.40	7.00	0.030	2601.8	11.2	99.9	3.01	147.3000	468.8000
1A14623D	64.70 W	4	0.00002	126.18	0.0001	238.23	0.0001	10.88	0.0124	0.44	4.11	0.049	2612.5	12.8	99.9	1.76	147.3000	468.8000
TOTAL			0.00114	13.35	0.0283	4.01	0.0090	1.51	0.7032	0.12	232.32	0.011						
Sample Muscovite-Fuchsite-FCW01-I9																		
1A14698D	56.00 W		0.00000	438.33	0.0002	41.43	0.0000	73.19	0.0015	1.88	0.50	0.062	2641.4	58.9	99.8	1.05	2.9000	2.4000
1A14699D	56.50 W	4	0.00002	59.75	0.0000	1973.67	0.0000	210.57	0.0003	7.50	0.09	0.217	2717.0	240.5	107.5	0.19	21.3000	839.6000
1A14710D	59.00 W	4	0.00002	73.86	0.0001	145.56	0.0002	8.71	0.0201	0.88	6.69	0.050	2603.8	24.4	99.9	14.54	89.9000	261.9000
1A14711D	59.30 W	4	0.00000	619.99	0.0000	1078.93	0.0001	10.20	0.0103	0.63	3.43	0.080	2613.9	17.8	100.0	7.40	222.3000	4796.8000
1A14712D	59.40 W	4	0.00001	118.45	0.0001	90.95	0.0002	6.93	0.0128	0.51	4.28	0.026	2607.8	14.2	99.9	9.28	37.1000	67.4000
1A14713D	59.50 W	4	0.00001	158.16	0.0002	55.03	0.0004	4.11	0.0282	0.41	9.43	0.039	2613.4	11.5	100.0	20.35	51.0000	56.1000
1A14715D	59.50 W	4	0.00002	68.91	0.0002	57.10	0.0003	6.99	0.0222	0.44	7.47	0.021	2620.7	12.3	100.1	16.06	44.5000	50.8000
1A14716D	59.60 W	4	0.00000	414.44	0.0005	29.93	0.0001	11.41	0.0083	0.67	2.78	0.033	2613.2	18.8	100.0	6.01	6.9000	4.1000
1A14717D	59.80 W	4	0.00000	1638.61	0.0002	78.02	0.0001	12.21	0.0090	0.68	3.00	0.029	2606.3	19.0	100.0	6.52	21.3000	33.2000
1A14718D	60.20 W	4	0.00000	816.41	0.0003	43.01	0.0002	6.19	0.0137	0.40	4.56	0.050	2608.7	11.4	100.0	9.89	20.0000	17.2000
1A14720D	60.70 W	4	0.00001	102.38	0.0003	44.32	0.0001	22.06	0.0033	0.87	1.11	0.033	2607.1	26.0	99.6	2.39	4.5000	4.0000
1A14721D	61.70 W	4	0.00000	320.84	0.0004	30.71	0.0000	54.31	0.0022	0.89	0.75	0.087	2619.9	28.3	99.8	1.62	2.2000	1.4000
1A14722D	63.00 W	4	0.00000	585.59	0.0004	39.22	0.0000	106.58	0.0017	1.39	0.56	0.064	2611.3	43.9	99.9	1.22	1.8000	1.4000

Continued on Next Page...

Table G.1 – Continued

Sample Step	Laser Power	Used*	^{36}Ar	%1σ	^{37}Ar	%1σ	^{38}Ar	%1σ	^{39}Ar	%1σ	^{40}Ar	%1σ	Age (Ma)	±2s	^{40}Ar(r) (%)	^{39}Ar(k) (%)	K/Ca	±2s
1A14723D	65.00 W	4	0.00001	103.58	0.0003	51.43	0.0000	2393.47	0.0013	1.06	0.43	0.103	2596.7	38.4	99.1	0.92	2.2000	2.3000
1A14725D	67.00 W	4	0.00001	121.62	0.0000	326.36	0.0000	28.58	0.0035	1.09	1.20	0.041	2630.5	31.5	99.7	2.56	39.1000	255.1000
TOTAL			0.00004	144.47	0.0032	16.98	0.0017	3.05	0.1385	0.20	46.29	0.014						
Sample Muscovite-Fuchsite-MA05-I9																		
1A14644D	60.50 W		0.00004	48.61	0.0000	454.85	0.0000	87.99	0.0002	6.32	0.04	0.456	1712.0	404.5	73.9	0.03	2.1000	19.3000
1A14646D	61.00 W		0.00003	61.34	0.0001	315.69	0.0000	68.71	0.0009	1.60	0.24	0.065	2282.4	74.3	96.3	0.14	6.3000	39.8000
1A14647D	61.30 W		0.00003	73.00	0.0001	182.81	0.0000	34.71	0.0007	2.03	0.23	0.099	2512.6	85.9	96.8	0.12	3.1000	11.5000
1A14648D	61.70 W	4	0.00004	48.62	0.0000	524.82	0.0000	58.28	0.0011	1.64	0.37	0.080	2580.1	60.6	97.0	0.18	13.7000	143.6000
1A14649D	62.10 W	4	0.00003	60.60	0.0000	568.05	0.0001	19.19	0.0035	0.66	1.13	0.048	2583.5	23.3	99.1	0.57	49.0000	556.6000
1A14651D	62.30 W	4	0.00004	42.50	0.0000	682.47	0.0002	5.87	0.0117	0.51	3.87	0.028	2601.8	14.5	99.7	1.93	193.5000	2641.7000
1A14652D	62.40 W	4	0.00001	342.82	0.0001	251.90	0.0001	9.84	0.0084	0.49	2.78	0.016	2606.3	14.5	100.1	1.39	49.7000	250.2000
1A14653D	62.50 W	4	0.00001	142.53	0.0001	243.88	0.0001	10.51	0.0116	0.63	3.87	0.059	2612.3	17.8	99.9	1.92	69.7000	339.9000
1A14654D	62.60 W	4	0.00002	112.26	0.0001	174.49	0.0002	4.29	0.0184	0.46	6.07	0.044	2604.6	12.9	99.9	3.03	76.1000	265.6000
1A14656D	62.70 W	4	0.00000	1035.50	0.0001	272.30	0.0003	6.26	0.0219	0.41	7.26	0.024	2608.8	11.4	100.0	3.62	142.7000	777.2000
1A14657D	62.80 W	4	0.00001	224.70	0.0000	821.14	0.0001	17.00	0.0048	1.07	1.55	0.057	2586.7	30.8	100.2	0.79	85.6000	1405.0000
1A14658D	63.10 W	4	0.00015	35.98	0.0064	6.17	0.0008	7.95	0.0751	0.51	24.77	0.051	2599.9	14.3	99.8	12.39	5.0000	0.6000
1A14662D	63.30 W	4	0.00002	67.07	0.0003	93.49	0.0000	41.54	0.0037	1.33	1.23	0.055	2591.5	38.1	99.4	0.62	5.5000	10.3000
1A14663D	63.60 W	4	0.00003	65.33	0.0002	159.24	0.0001	24.36	0.0056	0.79	1.86	0.051	2601.5	22.9	99.6	0.93	15.0000	47.8000
1A14664D	63.90 W	4	0.00001	259.28	0.0000	2434.67	0.0004	4.70	0.0333	0.42	10.91	0.039	2592.2	11.6	100.0	5.50	1338.1000	65155.9000
1A14665D	64.00 W	4	0.00017	27.62	0.0059	5.43	0.0006	5.59	0.0503	0.43	16.38	0.017	2582.7	12.2	99.7	8.29	3.6000	0.4000
1A14667D	64.00 W	4	0.00017	23.75	0.0060	6.55	0.0010	5.27	0.0696	0.46	22.90	0.025	2596.7	12.7	99.8	11.48	5.0000	0.7000
1A14668D	64.00 W	4	0.00009	45.02	0.0065	6.17	0.0005	6.94	0.0462	0.55	15.10	0.062	2587.7	15.3	99.8	7.62	3.0000	0.4000
1A14669D	64.00 W	4	0.00012	27.52	0.0069	6.84	0.0014	4.02	0.1061	0.43	35.01	0.046	2602.7	12.0	99.9	17.49	6.7000	0.9000
1A14670D	64.00 W	4	0.00001	125.53	0.0001	205.60	0.0001	11.78	0.0126	0.47	4.15	0.026	2603.6	13.1	99.9	2.07	41.0000	168.5000
1A14672D	64.10 W	4	0.00003	56.17	0.0001	504.31	0.0001	11.30	0.0116	0.69	3.83	0.034	2599.3	19.4	99.7	1.91	92.0000	927.4000
1A14673D	64.20 W	4	0.00001	117.77	0.0001	415.60	0.0001	15.65	0.0071	0.73	2.33	0.043	2600.5	20.6	99.8	1.17	47.6000	396.0000
1A14674D	64.20 W	4	0.00001	129.06	0.0001	304.29	0.0000	43.68	0.0030	1.04	0.98	0.068	2589.1	31.1	99.7	0.49	14.8000	89.8000
1A14675D	64.40 W	4	0.00001	134.00	0.0000	796.87	0.0000	67.44	0.0022	1.80	0.71	0.089	2578.5	52.8	99.5	0.36	28.7000	457.3000
1A14677D	64.70 W	4	0.00000	9233.81	0.0001	491.96	0.0000	38.17	0.0031	1.17	1.03	0.079	2608.3	34.8	100.0	0.51	24.8000	243.9000
1A14678D	65.20 W	4	0.00001	239.79	0.0000	1802.96	0.0001	30.54	0.0039	0.95	1.29	0.064	2601.2	27.7	99.9	0.65	114.0000	4110.0000
1A14679D	66.20 W	4	0.00001	295.89	0.0000	3316.01	0.0001	11.84	0.0102	0.53	3.38	0.045	2603.6	15.3	99.9	1.69	552.7000	36656.5000
1A14680D	67.20 W	4	0.00001	165.33	0.0001	229.81	0.0002	8.11	0.0175	0.43	5.79	0.028	2608.2	12.3	100.1	2.89	66.4000	305.1000
1A14682D	68.20 W	4	0.00000	516.73	0.0002	162.92	0.0001	11.90	0.0112	0.61	3.67	0.038	2596.1	17.2	100.0	1.84	30.0000	97.9000
1A14695D	68.70 W	4	0.00002	65.74	0.0001	112.18	0.0001	12.93	0.0096	0.55	3.17	0.060	2607.8	15.6	100.2	1.58	57.0000	127.8000
1A14696D	69.20 W	4	0.00001	158.59	0.0001	87.78	0.0003	4.87	0.0236	0.51	7.79	0.026	2606.1	14.1	100.0	3.89	89.2000	156.7000
1A14697D	69.70 W	4	0.00000	1559.96	0.0001	65.97	0.0002	6.82	0.0177	0.46	5.86	0.048	2609.6	12.9	100.0	2.92	54.8000	72.4000
TOTAL			0.00102	12.96	0.0316	4.57	0.0076	1.77	0.6063	0.14	199.55	0.012						
Sample Muscovite-Fuchsite-MA11-I9																		
115204D	57.00 W		0.00000	335.13	0.0000	302.68	0.0000	371.45	0.0001	12.20	0.04	0.587	2565.9	433.5	97.1	0.04	1.0200	6.2100
115205D	59.00 W		0.00000	20454.51	0.0003	55.40	0.0000	155.12	0.0002	8.52	0.05	0.470	2371.2	292.9	100.0	0.06	0.2200	0.2400
115206D	59.50 W		0.00002	55.78	0.0001	136.46	0.0000	55.64	0.0008	1.87	0.25	0.106	2500.8	64.0	97.5	0.27	2.7300	7.4400
115207D	60.00 W		0.00007	18.60	0.0003	62.91	0.0001	18.01	0.0043	0.58	1.48	0.068	2635.2	17.7	98.7	1.48	5.7900	7.2900
115209D	60.10 W	4	0.00016	21.45	0.0098	3.92	0.0007	4.59	0.0575	0.38	19.18	0.048	2606.8	10.7	99.8	19.79	2.5300	0.2000
115210D	60.10 W	4	0.00000	2664.87	0.0003	69.73	0.0000	119.49	0.0008	1.77	0.26	0.124	2608.2	63.1	100.0	0.27	1.0200	1.4200
115211D	60.30 W	4	0.00001	124.12	0.0001	139.72	0.0000	158.52	0.0012	1.52	0.41	0.100	2639.8	48.7	100.7	0.42	3.9600	11.0800
115212D	60.50 W	4	0.00003	50.13	0.0003	58.48	0.0003	5.36	0.0225	0.39	7.52	0.028	2610.9	10.9	100.1	7.76	34.7900	40.7000
115214D	60.60 W	4	0.00000	564.25	0.0001	117.92	0.0001	15.91	0.0044	0.70	1.48	0.030	2610.4	20.5	100.0	1.52	13.2100	31.1500
115215D	60.80 W	4	0.00000	350.26	0.0004	39.03	0.0000	30.06	0.0029	0.65	0.97	0.087	2615.5	20.7	100.1	1.00	3.2600	2.5500
115216D	61.20 W	4	0.00001	307.30	0.0002	76.64	0.0001	10.64	0.0068	0.47	2.27	0.038	2606.7	14.3	100.1	2.35	12.0700	18.5000
115217D	61.40 W	4	0.00009	34.52	0.0112	6.75	0.0007	8.17	0.0499	0.39	16.60	0.028	2604.8	10.8	99.8	17.17	1.9100	0.2600
115219D	61.40 W	4	0.00007	39.22	0.0121	5.65	0.0007	6.23	0.0520	0.42	17.46	0.028	2618.4	11.8	99.9	17.89	1.8500	0.2100
115220D	61.40 W	4	0.00001	199.02	0.0002	76.14	0.0002	7.15	0.0160	0.40	5.37	0.021	2620.7	11.2	100.0	5.50	30.5200	46.4800
115221D	61.50 W	4	0.00002	94.63	0.0000	3614.51	0.0001	18.86	0.0060	0.63	2.00	0.031	2618.3	18.5	100.2	2.05	548.0000	39614.9500

Continued on Next Page...

Table G.1 – Continued

Sample Step	Laser Power	Used*	^{36}Ar	%1σ	^{37}Ar	%1σ	^{38}Ar	%1σ	^{39}Ar	%1σ	^{40}Ar	%1σ	Age (Ma)	±2s	^{40}Ar(r) (%)	^{39}Ar(k) (%)	K/Ca	±2s
115222D	61.70 W	4	0.00000	2119.05	0.0001	253.18	0.0000	186.71	0.0014	1.45	0.45	0.100	2588.3	48.1	100.0	0.47	8.0700	40.8800
115224D	62.00 W	4	0.00001	123.02	0.0001	132.80	0.0000	40.22	0.0025	1.18	0.84	0.085	2628.9	34.9	100.4	0.86	8.2300	21.8600
115225D	62.40 W	4	0.00001	157.08	0.0003	59.76	0.0001	10.62	0.0109	0.42	3.67	0.023	2618.1	12.2	100.1	3.77	16.8300	20.1100
115226D	63.00 W	4	0.00001	222.22	0.0003	46.44	0.0001	18.98	0.0033	0.68	1.11	0.073	2630.5	20.7	100.1	1.13	4.5000	4.1800
115227D	64.00 W	4	0.00001	234.75	0.0000	5244.20	0.0000	27.70	0.0021	1.28	0.70	0.076	2623.9	38.6	100.2	0.71	242.5900	25443.6600
115229D	65.00 W	4	0.00002	77.07	0.0004	35.08	0.0000	29.54	0.0038	0.65	1.26	0.109	2629.2	19.7	100.4	1.29	3.8200	2.6800
115230D	66.00 W	4	0.00000	5812.76	0.0001	170.60	0.0001	23.44	0.0051	0.65	1.69	0.042	2611.4	18.9	100.0	1.74	21.3900	72.9900
115231D	66.50 W	4	0.00000	521.90	0.0001	237.29	0.0003	4.04	0.0274	0.37	9.22	0.034	2624.1	10.2	100.0	9.42	155.6100	738.5200
115232D	67.00 W	4	0.00001	171.93	0.0001	114.94	0.0001	20.12	0.0051	0.68	1.70	0.059	2610.3	20.0	99.9	1.75	15.3900	35.3900
115234D	68.00 W	4	0.00000	596.77	0.0000	5729.39	0.0000	24.14	0.0038	0.73	1.27	0.044	2633.9	21.7	100.0	1.29	440.1000	50430.2100
TOTAL			0.00031	26.28	0.0296	4.62	0.0038	2.57	0.2904	0.14	97.23	0.013						
Sample Muscovite-Fuchsite-MH08-I9																		
115180D	58.50 W		0.00002	62.50	0.0001	135.74	0.0000	48.25	0.0009	2.01	0.19	0.167	1961.3	74.6	96.3	0.64	2.6000	7.1000
115181D	59.00 W		0.00001	164.66	0.0002	142.81	0.0000	167.89	0.0003	4.72	0.09	0.314	2445.1	197.8	96.7	0.20	0.8000	2.2000
115182D	59.50 W		0.00000	627.32	0.0002	94.00	0.0000	42.97	0.0011	1.62	0.36	0.118	2582.8	51.6	100.1	0.81	2.3000	4.4000
115183D	59.80 W	4	0.00001	117.76	0.0004	57.76	0.0000	17.63	0.0033	0.45	1.07	0.047	2615.6	16.4	100.3	2.34	3.8000	4.4000
115185D	59.90 W	4	0.00002	56.95	0.0003	75.73	0.0001	8.52	0.0075	0.73	2.50	0.040	2627.5	20.7	100.2	5.41	11.5000	17.4000
115186D	60.00 W	4	0.00001	102.36	0.0004	53.90	0.0001	9.88	0.0099	0.66	3.30	0.034	2623.8	18.6	100.1	7.15	11.7000	12.6000
115187D	60.10 W	4	0.00002	85.63	0.0004	54.22	0.0002	3.49	0.0194	0.39	6.37	0.041	2610.7	10.9	100.1	13.91	20.9000	22.6000
115188D	60.20 W	4	0.00000	668.61	0.0006	33.17	0.0003	4.17	0.0270	0.41	8.83	0.043	2604.8	11.3	100.0	19.36	17.9000	11.9000
115190D	60.20 W	4	0.00014	24.90	0.0098	4.75	0.0006	5.05	0.0427	0.52	13.98	0.021	2601.1	14.6	99.7	30.64	1.9000	0.2000
115191D	60.20 W	4	0.00001	127.50	0.0002	101.69	0.0001	12.96	0.0049	0.47	1.59	0.051	2600.9	14.9	99.8	3.49	9.0000	18.4000
115192D	60.30 W	4	0.00000	278.35	0.0002	112.60	0.0000	459.08	0.0009	1.31	0.31	0.127	2637.3	49.6	99.6	0.65	1.8000	4.1000
115193D	60.40 W	4	0.00002	48.46	0.0001	236.00	0.0000	68.37	0.0012	1.81	0.39	0.115	2584.1	56.0	98.1	0.86	5.0000	23.7000
115195D	60.80 W	4	0.00001	120.28	0.0001	137.86	0.0000	47.25	0.0012	1.09	0.40	0.109	2610.2	39.6	99.2	0.86	3.5000	9.5000
115196D	61.50 W	4	0.00001	97.30	0.0002	98.73	0.0001	18.07	0.0044	0.61	1.47	0.032	2613.3	18.2	99.7	3.19	7.9000	15.5000
115197D	62.50 W	4	0.00001	80.42	0.0000	695.42	0.0000	23.16	0.0032	0.64	1.05	0.088	2616.3	20.2	99.6	2.27	45.4000	631.8000
115198D	63.50 W	4	0.00001	221.94	0.0001	240.21	0.0001	13.80	0.0057	0.51	1.89	0.064	2623.5	15.4	100.1	4.10	22.9000	110.0000
115200D	64.50 W	4	0.00002	78.28	0.0001	265.31	0.0000	16.93	0.0044	0.66	1.45	0.028	2612.1	19.4	99.7	3.14	23.5000	124.5000
115201D	70.00 W	4	0.00001	105.26	0.0000	501.69	0.0000	2452.87	0.0014	1.17	0.45	0.075	2626.7	39.1	100.8	0.98	13.5000	135.4000
TOTAL			0.00018	35.86	0.0072	14.21	0.0017	2.70	0.1392	0.20	45.68	0.013						

* Sample steps used for plateau age calculation, denoted by '4'

APPENDIX H
(U−TH)/HE DATA TABLE

Sample Name	Topic	Mineral	Nc	Th (ng)	1 s (%)	U (ng)	1 s (%)	He (ncc)	1 s (%)	TAU (%)	Th/U	raw Age (Ma)	+/- (Ma)	Ft	+/- (%)	Cor. Age (Ma)	+/- (Ma)
Zircon																**230.2**	**13.4**
MA13-Z1	Eric Thern	zircon	1	14.888	3.6%	1.501	3.4%	113.795	1.2	3.0	9.85	185.2	5.5	0.78	5	**237.8**	**13.8**
MA13-Z3*	Eric Thern	zircon	1	12.386	3.6%	1.348	3.4%	129.144	1.2	2.9	9.12	246.0	7.2	0.76	5	**322.6**	**18.7**
MA13-Z4	Eric Thern	zircon	1	20.393	3.6%	1.515	3.0%	117.810	1.2	3.1	13.36	152.3	4.7	0.70	5	**217.3**	**12.7**
MA13-Z5	Eric Thern	zircon	1	15.799	3.6%	2.212	3.2%	131.498	1.2	2.8	7.09	180.5	5.1	0.77	5	**235.7**	**13.5**
Goethite																**24.8**	**1.4**
MA13-GO1	Eric Thern	goethite	1	0.628	3.6%	0.126	2.8%	0.742	1.2	2.6	4.94	22.2	0.6	1.00	5	**22.2**	**1.3**
MA13-GO2	Eric Thern	goethite	1	1.114	3.6%	0.169	2.7%	1.006	1.2	2.7	6.52	19.1	0.5	1.00	5	**19.1**	**1.1**
MA13-GO3*	Eric Thern	goethite	1	1.073	3.6%	0.030	2.9%	1.203	1.2	3.4	35.48	34.9	1.2	1.00	5	**34.9**	**2.1**
MA13-GO4	Eric Thern	goethite	1	3.067	3.6%	0.793	2.7%	4.200	1.2	2.5	3.84	22.7	0.6	1.00	5	**22.7**	**1.3**
Rutile																	
MA13-RU3	Eric Thern	rutile	1	0.129	16.1%	0.432	10.6%	144.792	1.2	10.1	0.30	2065.3	207.9	0.94	5	**2201.0**	**247.4**
MA13-RU4	Eric Thern	rutile	1	0.509	11.3%	0.302	7.6%	112.763	1.2	6.4	1.67	1866.9	120.1	0.94	5	**1990.0**	**162.1**
MA13-RU5	Eric Thern	rutile	1	0.007	12.0%	0.090	7.6%	21.563	1.2	7.6	0.07	1636.0	124.4	0.87	5	**1891.0**	**172.1**
RT-5a*	Eric Thern	rutile	1	0.187	11.3%	0.113	7.7%	66.519	1.3	6.5	1.65	2684.5	175.2	0.84	5	**3199.6**	**263.1**
RT-5b	Eric Thern	rutile	1	0.073	11.3%	0.037	7.8%	21.695	1.3	6.5	1.98	2596.4	169.9	0.93	5	**2797.7**	**230.4**
RT-6a	Eric Thern	rutile	1	0.450	11.3%	0.150	7.6%	42.705	1.3	6.6	2.98	1252.7	82.5	0.86	5	**1457.8**	**120.5**
RT-6b	Eric Thern	rutile	1	0.955	11.3%	0.246	7.7%	68.903	1.3	6.9	3.85	1117.9	76.8	0.78	5	**1430.9**	**121.6**
Tourmaline																	
MA13-1	Eric Thern	turmaline	1	0.083	11.3%	0.017	7.6%	1.267	1.3	7.1	4.79	277.7	19.7	0.80	5	**348.0**	**30.2**
MA13-2	Eric Thern	turmaline	1	0.041	11.3%	0.006	7.8%	2.476	1.3	7.6	6.43	1199.2	91.3	0.80	5	**1496.2**	**136.3**
MA13-3	Eric Thern	turmaline	1	0.023	11.5%	0.006	8.4%	3.116	1.3	7.2	3.95	1970.9	141.1	0.84	5	**2345.8**	**204.8**
MA13-4	Eric Thern	turmaline	1	0.091	11.3%	0.017	7.8%	1.193	1.3	7.3	5.47	253.7	18.6	0.77	5	**328.0**	**29.1**
TUR-1	Eric Thern	turmaline	1	0.906	11.3%	0.106	7.6%	27.665	1.4	8.1	8.52	689.2	55.7	0.87	10	**793.8**	**102.1**
TUR-2*	Eric Thern	turmaline	1	0.148	11.3%	0.011	7.7%	29.339	1.4	8.9	13.28	4061.8	360.7	0.88	10	**4591.6**	**614.0**
TUR-3	Eric Thern	turmaline	1	0.212	11.3%	0.036	7.7%	5.232	1.4	7.4	5.83	485.6	36.1	0.80	10	**605.2**	**75.4**
TUR-4	Eric Thern	turmaline	1	0.471	11.3%	0.083	7.6%	8.668	1.4	7.4	5.65	360.3	26.6	0.88	10	**410.8**	**51.1**

a Nc - number of dated crystals; Th - 232Th; U - 238U; He - 4He at STP; TAU - total analytical uncertainty; Unc. age - uncorrected He age; Ft - alpha recoil correction factor after Farley et al. (1996); Cor. age - corrected He age. Samples marked with asterisk are considered as 'fliers'.

APPENDIX I
POSTERS, ABSTRACTS AND TALKS

Eric Thern, David Nelson (2011) Principal component analysis applied to 3.0-4.35 Ga detrital zircon populations within ca. 3.0 Ga metasediments of the Yilgarn Craton. Goldschmidt conference, Prague 2011: Workshop on Detrital Zircon U-Pb Geochronology 13th-14th August 2011. (Poster)

E. Thern, F. Jourdan, N.J. Evans, B.J., McDonald, M. Danisik, R.A. Frew, D.R. Nelson. (2011) Post-depositional thermal history of the 4364−3060 Ma zircon-bearing metasandstones of the Illaara and Maynard Hills granite greenstone belts Western Australia. Goldschmidt conference, Prague 2011. (Abstract)

B.I.A. McInnes, N.J. Evans1, B.J. McDonald, E. Thern, and D.H. Corbett (2010) U-Th-Pb-He double-dating of zircon from the diamondiferous Ellendale lamproite pipe, Western Australia. Goldschmidt conference, Knoxville 2010. (Abstract)

LUPULESCU, Marian V., CHIARENZELLI, Jeffrey R., COUSENS, Brian, THERN, Eric, and NELSON, David. (2008) Mineralogy and Geochemistry of Mafic-Ultramafic intrusions from Pyrities, Adirondack lowlands, New York, GSA Northeastern Section 43rd Annual Meeting (27-29 March 2008) (Abstract)

CHIARENZELLI, Jeffrey R., LUPULESCU, Marian, COUSENS, Brian, THERN, Eric, and NELSON, David. (2007) Recognition of oceanic crust in the Adirondack lowlands, 2007 GSA Denver Annual Meeting (2831 October 2007), Paper No. 121-7. (Abstract)

CHRAPOWITZKY, Lauren, THERN, Eric, VALENTINO, David, NELSON, David, GEHRELS, George, and CHIARENZELLI, Jeffrey R. (2007) Zircon chronology of the Chimney Mountain metasedimentary sequence, Adirondack Highlands, 2007 GSA Denver Annual Meeting (2831 October 2007) Paper No. 117-16. (Abstract)

Eric R. Thern, David R. Nelson (2007) Geochronology and microstructural studies of zircons from Mt. Alfred and the Maynard Hills, Western Australia; Mumbai SPSS Conference, 2007, (Abstract and Talk).

I.1 Mumbai SPSS Conference (Mumbai, India, 2007)

The SPSS Conference in Mumbai, India, 2007 was of great benefit to this PhD, as it allowed the formation of some key ideas, and the presentation of some initial data.

I.1.1 Mumbai SPSS 2007 Abstract

Geochronology and microstructural studies of zircons from Mt. Alfred and the Maynard Hills, Western Australia

E.R. Thern*, D.R. Nelson
Curtin University of Technology, GPO Box U1987, Perth, WA, 6001, Australia
***Corresponding Author: eric@thern.org**

Recent research into the early Earth (>4000 Ma ago) has been stimulated by the recent finds of >4000 Ma detrital zircons from Western Australia. These zircons older than >4000 Ma have been found in Mt. Narryer (Froude et al., 1983), Jack Hills (Compston et al., 1986a) and the Maynard Hills (Wyche et al., 2004). Zircons older than 4300 Ma have been identified from the Jack Hills (Narryer Terrane) (Wilde et al., 2001; Peck et al., 2001; Cavosie et al., 2004) and Maynard Hills (Barlee Terrane) (Nelson, 2002b; Wyche et al., 2004).

Initial investigations of these >4300 Ma grains strongly imply an igneous origin based on their oscillatory zoning, Th/U ratios and REE abundances (Wilde et al., 2001; Peck et al., 2001; Nelson, 2002b; Cavosie et al., 2004). Further evidence for the formation of evolved continental crust felsic rocks (granites) earlier than 4400 Ma in the Earth's history is made in Wilde et al. (2001), Peck et al. (2001), Valley et al. (2002) and Cavosie et al (2004). Oxygen isotopic evidence of elevated $\delta^{18}O$ in a 4404 Ma zircon from the Jack Hills (Wilde et al., 2001; Peck et al., 2001; Valley et al., 2002) was interpreted to indicate that the igneous source was derived from crustal material that had interacted with a liquid phase hydrosphere. The proposal of Hadean era subduction with a liquid phase hydrosphere has also been proposed by recent research involving titanium concentrations being used to surmise a zircons formation temperature (Watson and Harrison, 2005; Harrison and Schmitt, 2007) and more recently the findings of diamond inclusions within 4.250 Ga zircons (Menneken et al., 2007).

Detailed studies of >4000 Ma zircons have discovered that a number of these have a surprisingly large range of $^{207}Pb/^{206}Pb$ dates (Nelson, 2000c; Wilde et al., 2001; Peck et al., 2001). The range of dates do not correspond with obvious structural features within the grains and even lie on what should be isochemical cathodoluminescence zones. The dates are also significantly larger than can be attributable to analytical uncertainty, which strongly suggests real variations exist. There have been no studies to date that conclusively determine the cause of these variations, and other anomalous behaviors shown within these zircons.

These >4000 Ma zircons are the only known surviving terrestrial material from the early Earth's history (from 4404 Ma to 4030 Ma), and as such are scientifically pertinent to ancient earth studies.

Additional old zircons (>4000 Ma) have recently been found 45km south of the Maynard Hills (Kohler Bore) Location, near Mt. Alfred. These new finds may help elucidate the evolution of the early Earth and further constrain the depositional environment and provenance of these old grains.

I.2 Goldschmidt Geochemistry Conference (Prague, Czech Republic, 2011)

The Goldschmidt Geochemistry conference in 2011 allowed for the discussion of key findings from my research, including attending the Detrital Zircon Workshop, and presenting two posters.

I.2.1 Goldschmidt 2011 Abstract

Post-depositional thermal history of the 43643060Ma zircon-bearing metasandstones of the Illaara and Maynard Hills granite greenstone belts, Western Australia

E.R. Thern[1*], F. Jourdan[2], N.J. Evans[3], B.J. McDonald[3], M. Danisik[3], R.A. Frew[2] and D.R. Nelson[4]

1 DIAP, Curtin Univ., Perth, WA, Australia
2 WA Argon Isotope Facility, Curtin Univ., Perth, Australia
3 CSIRO ESRE, Perth, Australia
4 School of Natural Sciences, Univ. of Western Sydney, Australia
***Corresponding Author: eric@thern.org**

The post-depositional thermal history (spanning 3060 Ma to 26 Ma) of the ca. 3060 Ma Illaara and Maynard Hills granite greenstone belt metastandstones (peak metamorphism of upper greenschist facies) is characterized by a combination of SHRIMP U-Th–Pb, Ar/Ar and (U-Th)/He geochronology. Ar/Ar multi-grain tourmaline results defining two plateau ages of ca. 2940 Ma on a cross-cutting quartz-tourmaline vein provide a minimum depositional age for the metasandstones. Post depositional stratiform qtz-tourmaline veins are a common occurrence in Archean quartzites, and can be useful in assigning minimum depositional ages and timing of hydrothermal fluids.

SHRIMP U-Th–Pb data of >275 rutile analyses from 8 metasandstone samples reveal a complex history of events between deposition of metasandstones (ca. 3060 Ma) and the subsequent folding, thrusting and granitic intrusions (ca. 2730-2630 Ma, regional D1 to D3 events). Some individual rutile grains yield multiple dates which span from before the maximum depositional age of the quartzite at ca. 3060 Ma to the last major metamorphic and granitic event at ca. 2630 Ma. These rutiles exhibit weakly defined core-rim younging profiles which represent multiple stages of metamorphic growth or Pb-loss reset events. These results suggest that under protracted greenschist metamorphic conditions rutile can retain signatures of multiple thermal events and even retain some of their original detrital characteristics.

Ar/Ar plateau ages on muscovites from both greenstone belts show that late to post deformation planar-foliation recrystalization at ca. 2605 Ma (possibly coeval with the end of D3) marks the end of high-grade tectono-thermal events.

(U-Th)/He on zircon at ca. 230 Ma defines exhumation and temperatures <180C for these metasandstones, similar to fission track results throughout the Yilgarn. Goethite (U-Th)/He ages of 26 Ma are likely coeval with Fe-rich meteoric fluid influx and associated zero-age Pb-loss and Fe enrichment in metamict zones of both rutile and zircon within the metasandstones.

I.3 Goldschmidt Geochemistry Conference (Montreal, Canada, 2012)

The following abstract was submitted and accepted for the Goldschmidt Geochemistry Conference in 2012, however due to not attending, it was not published in the proceedings.

I.3.1 Goldschmidt 2012 Abstract

Provenance of Hadean to mid-Archean detrital zircons from siliciclastic metasedimentary rocks of the Illaara and Maynard Hills Greenstone Belts, Western Australia

E.R. Thern[1*], and D.R. Nelson[2]

1 Department of Imaging and Applied Physics, Curtin University, Perth, WA, Australia (*eric@thern.org) (* presenting author)

2 School of Natural Sciences, University of Western Sydney, Australia

SHRIMP U-Pb dating of >1000 detrital zircons from twelve samples within ca. 3.0 Ga siliciclastic metasedimentary rocks of the Illaara and Maynard Hills Greenstone Belts of the Yilgarn Craton, Western Australia, reveal detrital zircon ages up to 4372 Ma [1]. Sedimentary structures are rare and upper-greenschist to middle-amphibolite facies metamorphism and shearing has obscured primary relationships between greenstone sediments and provenance and stratigraphic relationships must be inferred from detrital zircon age spectra and compositional characteristics. Depositional ages are currently constrained by the youngest zircons from Mt. Alfreds eastern (3318 ±6 Ma) and western (3264 ±7 Ma) horizons, and Maynard Hills ca. 3060 to 2960 Ma analyses; and a minimum depositional age of ca. 2940 Ma by Ar/Ar plateau ages from a cross-cutting quartz-tourmaline vein [2].

Increasing age complexity and 'younging' are seen across the East (almost exclusively 3700-3780 Ma) to West (3300-3700 Ma and >3800 Ma) outcrop horizons at the Mt. Alfred locality. The western-most horizon at Mt. Alfred contains abundant >3800 Ma zircons, but lacks the prominent 3500 to 3300 Ma ages common to Jack Hills Hadean-zircon bearing metasedimentary rocks. This horizon at Mt. Alfred is most similar in detrital zircon age characteristics to the metasedimentary rocks at Mt. Narryer, however without the younger zircon ages (of Eurada and Dugel gneiss affinity; 3480-3300 Ma) found in abundance at Mt. Narryer [2,3]. This makes Mt. Alfred a unique source for detrital Hadean zircons.

The detrital zircon age similarities within the metasedimentary rocks of the Illaara, Maynard Hills and Gum Creek Greenstone Belts of the Southern Cross Terrane, the Jack Hills and Mt. Narryer of the Narryer Terrane, and the Toodyay Lake Grace Domain within the South West Terrane strongly suggest a shared provenance of these >2940 Ma metasedimentary rocks throughout the Yilgarn Craton [3]. It is therefore likely they were deposited contemporaneously between ca. 3300-2940 Ma, later separated by multiple younger ca. 2950-2630 Ma granite-greenstone formations during rifting and collision episodes, and occur today as 'rafts' within younger ca. 2730-2640 Ma granite-greenstones.

[1] Thern and Nelson (submitted) Precambrian Research [2] Thern et al. (2011), abstract: Goldschmidt Conf. [3] Thern and Nelson (in press) Precambrian Research

APPENDIX J
STATEMENT OF COPYRIGHT

I warrant that I have obtained, where necessary, permission from the copyright owners to use any third-party copyright material reproduced in the thesis, or to use any of my own published work in which the copyright is held by another party.

APPENDIX K
STATEMENT OF CONTRIBUTION FORMS

Statement of contribution signed forms for authors.

K.1 Chapter 2: first manuscript

Eric R. Thern, David R. Nelson, Greg Hitchen and Chi V. Ly; Age structure within >4300 Ma zircons and implications for conditions on the Hadean Earth.

Statement of Contribution

To Whom It May Concern

I, Eric R. Thern, collected, processed, and analyzed the samples with the exception of the QEMSCAN analyses (Chi V. Ly) and EMPA analyses (Greg Hitchen). With editorial support from David R. Nelson, the manuscripts and figures were entirely produced by the candidate, with scientific discussions and advice in relation to the interpretation of the data therein undertaken with the support of the co-authors.

Publication details:

Eric R. Thern, David R. Nelson, Greg Hitchen and Chi V. Ly; *Interpreting age variations within >4300 Ma zircons and the implications for the early Earth*. For submission to the special issue entitled "The first billion years: assessing the geologic record" of the American Journal of Science in October, 2012.

Eric R. Thern

I, as a Co-Author, endorse that this level of contribution by the candidate indicated above is appropriate.

David R. Nelson

Greg Hitchen

Chi V. Ly

Statement of Contribution

To Whom It May Concern

I, Eric R. Thern, collected, processed, and analyzed the samples with the exception of the QEMSCAN analyses (Chi V. Ly) and EMPA analyses (Greg Hitchen). With editorial support from David R. Nelson, the manuscripts and figures were entirely produced by the candidate, with scientific discussions and advice in relation to the interpretation of the data therein undertaken with the support of the co-authors.

Publication details:

Eric R. Thern, David R. Nelson, Greg Hitchen and Chi V. Ly; *Interpreting age variations within >4300 Ma zircons and the implications for the early Earth*. For submission to the special issue entitled "The first billion years: assessing the geologic record" of the American Journal of Science in October, 2012.

_____

Eric R. Thern

I, as a Co-Author, endorse that this level of contribution by the candidate indicated above is appropriate.

		Chi Vinh Ly
David R. Nelson	Greg Hitchen	Chi V. Ly

Statement of Contribution

To Whom It May Concern

I, Eric R. Thern, collected, processed, and analyzed the samples with the exception of the QEMSCAN analyses (Chi V. Ly) and EMPA analyses (Greg Hitchen). With editorial support from David R. Nelson, the manuscripts and figures were entirely produced by the candidate, with scientific discussions and advice in relation to the interpretation of the data therein undertaken with the support of the co-authors.

Publication details:

Eric R. Thern, David R. Nelson, Greg Hitchen and Chi V. Ly; *Interpreting age variations within >4300 Ma zircons and the implications for the early Earth*. For submission to the special issue entitled "The first billion years: assessing the geologic record" of the American Journal of Science in October, 2012.

Eric R. Thern

I, as a Co-Author, endorse that this level of contribution by the candidate indicated above is appropriate.

David R. Nelson Greg Hitchen Chi V. Ly

K.2 Chapter 3: first paper (in press)

Thern, E. R., Nelson, D. R., (2012). Detrital zircon age structure within ca. 3 Ga metasedimentary rocks, Yilgarn Craton: elucidation of Hadean source terranes by principal component analysis. Precambrian Research; v.214215; p. 2843

Statement of Contribution

To Whom It May Concern

I, Eric R. Thern, collected, processed, and analyzed the samples, and wrote any software associated with the publication. With editorial support from David R. Nelson, the manuscripts and figures were entirely produced by the candidate, with scientific discussions and advice in relation to the interpretation of the data therein undertaken with the support of the co-author.

Publication details:

Eric R. Thern and David R. Nelson (2012) *Detrital zircon age structure within ca. 3 Ga metasedimentary rocks, Yilgarn Craton: elucidation of Hadean source terranes by principal component analysis*. Precambrian Research, Volumes 214–215, September 2012, Pages 28-43

Eric R. Thern

I, as a Co-Author, endorse that this level of contribution by the candidate indicated above is appropriate.

D Nelson

David R. Nelson

K.3 Chapter 4: second paper (in revision)

Thern, E. R., Nelson, D. R., (2012). Provenance of ca. 4372−3000 Ma detrital zircons within Early Archean siliciclastic metasedimentary rocks from the Illaara and Maynard Hills Greenstone Belts, Western Australia, submitted to Precambrian Research

Statement of Contribution

To Whom It May Concern

I, Eric R. Thern, collected, processed, analyzed the samples, and interpreted the data. With editorial support from David R. Nelson, the manuscripts and figures were entirely produced by the candidate, with scientific discussions and advice in relation to the interpretation of the data therein undertaken with the support of the co-author.

Publication details:

Eric R. Thern and David R. Nelson, (Submitted) *Provenance of ca. 3000-4372 Ma detrital zircons within Early Archean siliciclastic metasedimentary rocks from the Illaara and Maynard Hills Greenstone Belts, Western Australia.* Under Review at Precambrian Research

Eric R. Thern

I, as a Co-Author, endorse that this level of contribution by the candidate indicated above is appropriate.

D Nel

David R. Nelson

K.4 Chapter 8: third paper (in press)

Chiarenzelli, J., Lupulescu, M., Cousens, B., Thern, E., Coffin, L., Regan, S. (2010) Enriched Grenvillian Lithospheric Mantle as a Consequence of Long-Lived Subduction Beneath Laurentia. Geology, February 2010; v.38; no. 2; p. 151-154.

K.5 Chapter 8: fourth paper (in press)

J. Chiarenzelli, D. Valentino, M. Lupulescu, E. Thern, and S. Johnston (2011) Differentiating Shawinigan and Ottawan orogenesis in the Central Adirondacks. Geosphere, Feb 2011; 7: 222.

K.6 Chapter 8: fifth paper (in press)

J. Chiarenzelli, M. Lupulescu, E. Thern, and B. Cousens (2011) Tectonic implications of the discovery of a Shawinigan ophiolite (Pyrites Complex) in the Adirondack Lowlands. Geosphere, April 1, 2011; 7(2): 333 356

K.7 Chapter 8: sixth paper (in press)

W. Siebel, C. K. Shang, E. Thern, M. Danišík and J. Rohrmuller (2012) Zircon response to high-grade metamorphism as revealed by U−Pb and cathodoluminescence studies. Int J Earth Sci (Geol Rundsch), 22 April 2012; DOI 10.1007/s00531-012-0772-5

K.8 Chapter 8: seventh paper (in press)

Noreen J. Evans, Brent I. A. McInnes, Brad McDonald, Martin Danišík, Fred Jourdan, Celia Mayers, Eric Thern, Dudley Corbett. (2012) Emplacement age and thermal footprint of the diamondiferous Ellendale E9 lamproite pipe, Western Australia. Miner Deposita, 14 July 2012; DOI 10.1007/s00126-012-0430-7

APPENDIX L
THIS THESIS AND OPEN SOURCE SOFTWARE

L.1 Open Source Software

This entire thesis is written with the freely available open source software package LaTeX(pronounced Lah-Tech). Most graphs have been created with GNUPlot, and code written in GNU Bash and R statistical language.

To avoid any consistency or reproducibility problems with any of the data within this thesis, an outline of all software versions used is given below in Table L.1.

Table L.1: Software used throughout this thesis

Program	Version	website
Ubuntu Linux	12.04	www.ubuntu.com
LaTeXand pdfTeX	3.1415926-1.40.10-2.2	www.latex.org
GNU Awk	3.1.6	www.gnu.org
GNU sed version	4.2.1	www.gnu.org
GNU bash	4.2.24(1)-release	www.gnu.org
sort (coreutils)	8.13	www.gnu.org
Python	2.7.3	www.python.org
gnuplot	4.4 patchlevel 0-rc1	www.gnuplot.info
Inkscape	0.48.3.1 r9886	www.inkscape.org
GNU GIMP	2.6.12	www.gimp.org
ImageMagick	6.6.9-7 2012-08-17	www.imagemagick.org
R	2.14.1 (2011-12-22)	www.r-project.org
FactoMineR	1.14	factominer.free.fr

References

References

Andersen, T., 2005. Detrital zircons as tracers of sedimentary provenance: limiting conditions from statistics and numerical simulation. Chemical Geology 216 (3-4), 249–270.

Blewett, R., Czarnota, K., Henson, P., 2010. Structural-event framework for the eastern Yilgarn Craton, Western Australia, and its implications for orogenic gold. Precambrian Research 183 (2), 203–229.

Bosch, D., Bruguier, O., Pidgeon, R., 1996. Evolution of an Archean metamorphic belt: a conventional and SHRIMP U–Pb study of accessory minerals from the Jimperding metamorphic belt, Yilgarn Craton, West Australia. Journal of Geology 104, 695–711.

Canup, R. M., 2004. Origin of terrestrial planets and the Earth-Moon system. Physics Today, 57–67.

Cavosie, A. J., Valley, J. W., Wilde, S. A., 2006. Correlated microanalysis of zircon: Trace element, δ18O, and U-Th-Pb isotopic constraints on the igneous origin of complex >3900Ma detrital grains. Geochimica et Cosmochimica Acta 70 (22), 5601–5616.

Cavosie, A. J., Wilde, S. A., Liu, D., Weiblen, P. W., Valley, J. W., 2004. Internal zoning and U-Th-Pb chemistry of Jack Hills detrital zircons: a mineral record of early Archean to Mesoproterozoic (4348-1576Ma) magmatism. Precambrian Research 135 (4), 251–279.

Chambers, J. E., Wetherill, G. W., 1998. Making the Terrestrial Planets: N-Body Integrations of Planetary Embryos in Three Dimensions. Icarus 136 (2), 304–327.

Chaussidon, M., Uitterdijk Appel, P. W., 1997. Boron isotopic composition of tourmalines from the 3.8-Ga-old Isua supracrustals, West Greenland: implications on the [delta]11B value of early Archean seawater. Chemical Geology 136 (3-4), 171–180.

Chen, C.-H., Lu, H.-Y., Lin, W., Lee, C.-Y., 2006. Thermal event records in SE China coastal areas: Constraints from Monazite Ages of Beach Sands from two sides of the Taiwan Strait. Chemical Geology 231 (1-2), 118–134.

Chen, S. F., Libby, J. W., Wyche, S., Riganti, A., 2004a. Kinematic nature and origin of regional-scale ductile shear zones in the central Yilgarn Craton, Western Australia. Tectonophysics 394 (3-4), 139–153.

Chen, S. F., Riganti, A., Wyche, S., Greenfield, J. E., Nelson, D. R., 2003. Lithostratigraphy and tectonic evolution of contrasting greenstone successions in the central Yilgarn Craton, Western Australia. Precambrian Research 127 (1-3), 249–266.

Chen, S. F., Witt, W. K., Liu, S., 2001. Transpression and restraining jogs in the northeastern Yilgarn craton, Western Australia. Precambrian Research 106 (3-4), 309–328.

Chen, W.-S., Lee, K.-J., Lee, L.-S., Ponti, D. J., Prentice, C., Chen, Y.-G., Chang, H.-C., Lee, Y.-H., 2004b. Paleoseismology of the Chelungpu Fault during the past 1900 years. Quaternary International 115-116, 167–176.

Cherniak, D. J., 2000. Pb diffusion in rutile. Contributions to Mineralogy and Petrology 139 (2), 198–207.

Clark, D. J., Hensen, B. J., Kinny, P. D., 2000. Geochronological constraints for a two-stage history of the Albany-Fraser Orogen, Western Australia. Precambrian Research 102 (3-4), 155–183.

Compston, W., Froude, D. O., Ireland, T. R., Kinny, P. D., Williams, I. S., Williams, I. R., Myers, J. S., 1985. The age of (a tiny part of) the Australian continent. Nature 317 (6037), 559–560.

Compston, W., Kinny, P. D., Williams, I. S., Foster, J. J., 1986a. The age and Pb loss behaviour of zircons from the Isua supracrustal belt as determined by ion microprobe. Earth and Planetary Science Letters 80 (1-2), 71–81.

Compston, W., Williams, I. S., Campbell, I. H., Gresham, J. J., 1986b. Zircon xenocrysts from the Kambalda volcanics: age constraints and direct evidence for older continental crust below the Kambalda-Norseman greenstones. Earth and Planetary Science Letters 76 (3-4), 299–311.

Compston, W., Williams, I. S., Meyer, C., 1984. U-Pb geochronology of zircons from lunar breccia 73217 using a sensitive high mass-resolution ion microprobe. Journal of Geophysical Research 89, B252–B534.

Condie, K. C., Belousova, E., Griffin, W., Sircombe, K. N., 2009. Granitoid events in space and time: Constraints from igneous and detrital zircon age spectra. Gondwana Research 15 (3-4), 228–242.

Cook, N., Ashley, P., 1992. Meta-evaporite sequence, exhalative chemical sediments and associated rocks in the Proterozoic Willyama Supergroup, South Australia: implications for metallogenesis. Precambrian Research 56 (3-4), 211–226.

Crowley, J. L., Myers, J. S., Sylvester, P. J., Cox, R. A., 2005. Detrital zircon from the Jack Hills and Mount Narryer, Western Australia; evidence for diverse >4.0 Ga source rocks. Journal of Geology 113 (3), 239–263.

Cumming, G., Richards, J., 1975. Ore lead isotope ratios in a continuously changing earth. Earth and Planetary Science Letters 28, 155–171.

de Laeter, J., Fletcher, I., Rosman, K., Williams, I., Gee, R. D., Libby, W., 1981. Early Archaean gneisses from the Yilgarn block, Western Australia. Nature 292, 322–324.

Debaille, V., Brandon, A. D., Yin, Q. Z., Jacobsen, B., 2007. Coupled 142Nd-143Nd evidence for a protracted magma ocean in Mars. Nature 450 (7169), 525–528.

Deliens, M., Delhal, J., Tarte, P., 1977. Metamictization and U-Pb systematics – a study by infrared absorption spectrometry of Precambrian zircons. Earth and Planetary Science Letters 33 (3), 331–344.

Donaldson, J. A., de Kemp, E. A., 1998. Archaean quartz arenites in the Canadian Shield: examples from the Superior and Churchill Provinces. Sedimentary Geology 120 (1-4), 153–176.

Dunn, S. J., Nemchin, A. A., Cawood, P. A., Pidgeon, R. T., 2005. Provenance record of the Jack Hills metasedimentary belt: Source of the Earth's oldest zircons. Precambrian Research 138 (3-4), 235–254.

Eriksson, K. A., Wilde, S. A., 2010. Palaeoenvironmental analysis of Archaean siliciclastic sedimentary rocks in the west–central Jack Hills belt, Western Australia with new constraints on ages and correlations. Journal of the Geological Society 167, 827–840.

Evans, N., Byrne, J., Keegan, J., Dotter, L., 2005. Use of ICP-MS for the determination of uranium and thorium in (U-Th)/He Thermochronology. Analytical Chemistry In press.

Ewing, R. C., Meldrum, A., Wang, L., Weber, William, J., Corrales, L. R., 2003. Radiation Effects in Zircon. Reviews in Mineralogy and Geochemistry 53 (1), 387–425.

Ewing, R. C., Meldrum, A., Wang, L. M., Wang, S. X., 2000. Transformation Processes in Minerals. Mineralogical Society of America, Ch. Radiation-induced amorphization, pp. 319–361.

Farley, K. A., Kohn, B. P., Pillans, B., 2002. The effects of secular disequilibrium on (U-Th)/He systematics and dating of Quaternary volcanic zircon and apatite. Earth and Planetary Science Letters 201 (1), 117–125.

Farley, K. A., Wolf, R. A., Silver, L. T., 1996. The effects of long alpha-stopping distances on (U—Th)/He ages. Geochimica et Cosmochimica Acta 60 (21), 4223–4229.

Force, E. R., 1980. The provenance of rutile. Journal of Sedimentary Petrology 50, 485–488.

Force, E. R., 1991. Geology of Titanium-Mineral Deposits. Geol. Soc. of America, Spec. Publ. 259, 112.

Froude, D. O., Ireland, T. R., Kinny, P. D., Williams, I. S., Compston, W., Williams, I. R., Myers, J. S., 1983. Ion microprobe identification of 4100-4200 Myr-old terrestrial zircons. Nature 304, 616–618.

Geisler, T., Pidgeon, R. T., 2002. Raman scattering from metamict zircon: comments on "Metamictisation of natural zircon: accumulation versus thermal annealing of radioactivity-induced damage" by Nasdala et al. 2001 (¡SMALL¿Contribution to Mineralogy and Petrology¡/SMALL¿ 141: 125-144). Contributions to Mineralogy and Petrology 143 (6), 750–755.

Glasmacher, U., Lang, M., Keppler, H., Langenhorst, F., Neumann, R., Schardt, D., Trautmann, C., Wagner, G., 2006. Phase transitions in solids stimulated by simultaneous exposure to High Pressure and Ion Radiation. Physical Review Letters 96, 195701–1 −− 195701–4.

Grange, M. L., Wilde, S. A., Nemchin, A. A., Pidgeon, R. T., 2010. Proterozoic events recorded in quartzite cobbles at Jack Hills, Western Australia: New constraints on sedimentation and source of >4Ga zircons. Earth and Planetary Science Letters 292 (1-2), 158–169.

Griffin, W. L., Belousova, E. A., Shee, S. R., Pearson, N. J., O'Reilly, S. Y., 2004. Archean crustal evolution in the northern Yilgarn Craton: U-Pb and Hf-isotope evidence from detrital zircons. Precambrian Research 131 (3-4), 231–282.

Halliday, A. N., 2000. Terrestrial accretion rates and the origin of the Moon. Earth and Planetary Science Letters 176, 17–30.

Hanchar, J. M., Miller, C. F., 1993. Zircon zonation patterns as revealed by cathodoluminescence and backscattered electron images: Implications for interpretation of complex crustal histories. Chemical Geology 110 (1-3), 1–13.

Harraz, H., El-Sharkawy, M., 2001. Origin of tourmaline in the metamorphosed Sikait pelitic belt, south Eastern Desert, Egypt. Journal of African Earth Sciences 33 (2), 391–416.

Harrison, T., Trail, D., Schmitt, A., Watson, E., 2007. Rutile 207Pb/206Pb ages in the Jack Hills quartzite, Western Australia. Geochimica et Cosmochimica Acta 71 (15, Supplement 1), A383.

Harrison, T. M., 2005. Heterogeneous Hadean hafnium: evidence of continental crust at 4.4 to 4.5 Ga. Science 310, 1947–1950.

Harrison, T. M., Schmitt, A. K., 2007. High sensitivity mapping of Ti distributions in Hadean zircons. Earth and Planetary Science Letters 261 (1-2), 9–19.

Hartmann, L. A., Pineyro, D., Bossi, J., Leite, J. A. D., McNaughton, N. J., 2000. Zircon U-Pb SHRIMP dating of Palaeoproterozoic Isla Mala granitic magmatism in the Rio de la Plata Craton, Uruguay. Journal of South American Earth Sciences 13 (1-2), 105–113.

Hesse, R., Schacht, U., 2011. Early Diagenesis of Deep-Sea Sediments. In: HuN̈eke, H., Mulder, T. (Eds.), Deep-Sea Sediments. Vol. 63. Elsevier, pp. 557–713.

Holden, P., Lanc, P., Ireland, T. R., Harrison, T. M., Foster, J. J., Bruce, Z., 2009. Mass-spectrometric mining of Hadean zircons by automated SHRIMP multi-collector and single-collector U/Pb zircon age dating: The first 100,000 grains. International Journal of Mass Spectrometry 286 (2-3), 53–63.

Hoskin, P. W., 2005. Trace-element composition of hydrothermal zircon and the alteration of Hadean zircon from the Jack Hills, Australia. Geochimica et Cosmochimica Acta 69 (3), 637–648.

Ivanic, T. J., Wingate, M. T. D., Kirkland, C. L., Van Kranendonk, M. J., Wyche, S., 2010. Age and significance of voluminous mafic-ultramafic magmatic events in the Murchison Domain, Yilgarn Craton. Australian Journal of Earth Sciences 57 (5), 597–614.

Jiang, S.-Y., Palmer, M. R., Yeats, C. J., 2002. Chemical and boron isotopic compositions of tourmaline from the Archean Big Bell and Mount Gibson gold deposits, Murchison Province, Yilgarn Craton, Western Australia. Chemical Geology 188 (3-4), 229–247.

Joly, A., Miller, J., McCuaig, T. C., 2010. Archean polyphase deformation in the Lake Johnston Greenstone Belt area: Implications for the understanding of ore systems of the Yilgarn Craton. Precambrian Research 177 (1-2), 181–198.

King, R. W., Kerrich, R. W., 1989. Strontium isotope compositions of tourmaline from lode gold deposits of the Archean Abitibi Greenstone belt (Ontario-Quebec, Canada): Implications for source reservoirs. Chemical Geology: Isotope Geoscience section 79 (3), 225–240.

Kinny, P. D., Nutman, A. P., 1996. Zirconology of the Meeberrie gneiss, Yilgarn Craton, Western Australia: an early Archaean migmatite. Precambrian Research 78 (1-3), 165–178.

Kinny, P. D., Wijbrans, J. R., Froude, D. O., Williams, I. S., Compston, W., 1990. Age constraints on the geological evolution of the Narryer Gneiss Complex, Western Australia. Australian Journal of Earth Sciences 37 (1), 51–69.

Kinny, P. D., Williams, I. S., Froude, D. O., Ireland, T. R., Compston, W., 1988. Early archaean zircon ages from orthogneisses and anorthosites at Mount Narryer, Western Australia. Precambrian Research 38 (4), 325–341.

Kooijman, E., Mezger, K., Berndt, J., 2010. Constraints on the UPb systematics of metamorphic rutile from in situ LA-ICP-MS analysis. Earth and Planetary Science Letters 293 (34), 321–330.

Koppers, A., 2002. ArArCALC-software for 40Ar/39Ar age calculations. Computers & Geosciences 28, 605?619.

Kositcin, N., Krapez, B., 2004. Relationship between detrital zircon age-spectra and the tectonic evolution of the Late Archaean Witwatersrand Basin, South Africa. Precambrian Research 129 (1-2), 141–168.

Lee, D.-C., Halliday, A. N., Leya, I., Wieler, R., Wiechert, U., 2002. Cosmogenic tungsten and the origin and earliest differentiation of the Moon. Earth and Planetary Science Letters 198 (3-4), 267–274.

Luvizotto, G., Zack, T., 2009. Nb and Zr behavior in rutile during high-grade metamorphism and retrogression: An example from the Ivrea-Verbano Zone. Chemical Geology 261 (3-4), 303–317.

L, S., Josse J., Husson, F., 2008. FactoMineR: An R Package for Multivariate Analysis. Journal of Statistical Software 25(1), 1–18.

Maas, R., Kinny, P. D., Williams, I. S., Froude, D. O., Compston, W., 1992. The Earth's oldest known crust: A geochronological and geochemical study of 3900-4200 Ma old detrital zircons from Mt. Narryer and Jack Hills, Western Australia. Geochimica et Cosmochimica Acta 56 (3), 1281–1300.

Marschall, H. R., Jiang, S.-Y., 2011. Tourmaline Isotopes: No Element Left Behind. Elements 7, 313–319.

Martínez-Martínez, J., Torres-Ruiz, J., Pesquera, A., Gil-Crespo, P., 2010. Geological relationships and U-Pb zircon and 40 Ar/39Ar tourmaline geochronology of gneisses and tourmalinites from the Nevado-Filabride complex (western Sierra Nevada, Spain): Tectonic implications. Lithos 119 (3-4), 238–250.

Mathison, C., Ahmat, A., 1996. The Windimurra Complex, Western Australia. In: Cawthorn, R. G. (Ed.), Layered Intrusions. Vol. 15. Elsevier, pp. 485–510.

McLaren, A. C., Gerald, J. D. F., Williams, I. S., 1994. The microstructure of zircon and its influence on the age determination from Pb/U isotopic ratios measured by ion microprobe. Geochimica et Cosmochimica Acta 58 (2), 993–1005.

Meinhold, G., 2010. Rutile and its applications in earth sciences. Earth-Science Reviews 102 (1-2), 1–28.

Meldrum, A., Boatner, L. A., Weber, W. J., Ewing, R. C., 1998. Radiation damage in zircon and monazite. Geochimica et Cosmochimica Acta 62 (14), 2509–2520.

Melosh, H. J., 1989. Origin of the Earth. Oxford University Press, Oxford, Ch. Giant impacts and the thermal states of the early Earth, pp. 69–83.

Menneken, M., Nemchin, A. A., Geisler, T., Pidgeon, R. T., Wilde, S. A., 2007. Hadean diamonds in zircon from Jack Hills, Western Australia. Nature 448, 917–920.

Mezger, K., Hanson, G. N., Bohlen, S. R., 1989. High-precision U—Pb ages of metamorphic rutile: application to the cooling history of high-grade terranes. Earth and Planetary Science Letters 96 (1-2), 106–118.

Min, K., Mundil, R., Renne12, P. R., Ludwig, K. R., 2000. A test for systematic errors in 40Ar/39Ar geochronology through comparison with U/Pb analysis of a 1.1-Ga rhyolite. Geochimica et Cosmochimica Acta 64 (1), 73–98.

Moroney, M. J., 1984. Facts from Figures. Penguin Books.

Morris, P. A., Riganti, A., Chen, S. F., 2007. Evaluating the provenance of Archean sedimentary rocks of the Diemals Formation (central Yilgarn Craton) using whole-rock chemistry and precise U?Pb zircon chronology. Australian Journal of Earth Sciences: An International Geoscience Journal of the Geological Society of Australia 54 (8), 1123–1136.

Mueller, A. G., McNaughton, N. J., 2000. U-Pb Ages Constraining Batholith Emplacement, ContactMetamorphism, and the Formation of Gold and W-Mo Skarns in the SouthernCross Area, Yilgarn Craton, Western Australia. Economic Geology 95 (6), 1231–1257.

Myers, J. S., 1988a. Early archaean narryer gneiss complex, Yilgarn Craton, Western Australia. Precambrian Research 38 (4), 297–307.

Myers, J. S., 1988b. Oldest known terrestrial anorthosite at mount Narryer, Western Australia. Precambrian Research 38 (4), 309–323.

Myers, J. S., 1997. Preface: Archaean geology of the Eastern Goldfields of Western Australia – regional overview. Precambrian Research 83 (1-3), 1–10.

Myers, J. S., Williams, I. R., 1985. Early Precambrian crustal evolution at Mount Narryer, Western Australia. Precambrian Research 27 (1-3), 153–163.

Nasdala, L., Hofmeister, W., Norberg, N., Martinson, J. M., Corfu, F., Drr, W., Kamo, S. L., Kennedy, A. K., Kronz, A., Reiners, P. W., Frei, D., Kosler, J., Wan, Y., Gtze, J., Hger, T., Krner, A., Valley, J. W., 2008. Zircon M257 - a Homogeneous Natural Reference Material for the Ion Microprobe U-Pb Analysis of Zircon. Geostandards and Geoanalytical Research 32 (3), 247–265.

Nasdala, L., Pidgeon, R. T., Wolf, D., 1996. Heterogeneous metamictization of zircon on a microscale. Geochimica et Cosmochimica Acta 60, 1091–1097.

Nasdala, L., Pidgeon, R. T., Wolf, D., Irmer, G., 1998. Metamictization and U-Pb isotopic discordance in single zircons: a combined Raman microprobe and SHRIMP ion probe study. Mineralogy and Petrology 62, 1–27.

Nasdala, L., Wenzel, T., Pidgeon, R. T., Kronz, A., 1999. Internal structures and dating of complex zircons from Meissen Massif monzonites, Saxony. Chemical Geology 156 (1-4), 331–341.

Nelson, D. R., 1997. Evolution of the Archaean granite-greenstone terranes of the Eastern Goldfields, Western Australia: SHRIMP U—Pb zircon constraints. Precambrian Research 83 (1-3), 57–81.

Nelson, D. R., 2000a. 142986: metasandstone, Eranondoo Hill; in Compilation of geochronology data, 1999. No. Record 2000/2 in 1. Western Australia Geological Survey.

Nelson, D. R., 2000b. 142986: metasandstone, Eranondoo Hill; in Compilation of geochronology data, 1999. No. Record 2000/2 in 1. Western Australia Geological Survey.

Nelson, D. R., 2000c. Compilation of geochronology data, 1999. No. 2000/2 in 1. Western Australia Geological Survey.

Nelson, D. R., 2001. Compilation of geochronology data, 2000. No. 2001/2 in 1. Western Australia Geological Survey.

Nelson, D. R., 2002a. Compilation of geochronology data, 2001. No. 2002/2 in 1. Western Australia Geological Survey.

Nelson, D. R., 2002b. Hadean Earth crust: microanalytical investigation of 4.4 to 4.0 Ga zircons from Western Australia. Geochimica et Cosmochimica Acta 66, A549, abstract.

Nelson, D. R., 2004a. 142986: metasandstone, Eranondoo Hill; Data released: 2004 Geochronology dataset 290; in Compilation of geochronology data, June 2006 update. Western Australia Geological Survey.

Nelson, D. R., 2004b. CONCH: A Visualbasic program for interactive processing of ion-microprobe geochronology data. Geochimica et Cosmochimica Acta 68 (11S), A70, abstract only.

Nelson, D. R., 2004c. The Precambrian Earth: tempos and events. Elsevier, Amsterdam, Ch. Earth's formation and first billion years, pp. 3–27.

Nelson, D. R., 2005. Compilation of geochronology data, 2003. No. 2005/2 in 1. Western Australia Geological Survey.

Nelson, D. R., 2006. CONCH: A Visual Basic program for interactive processing of ion-microprobe analytical data. Computers & Geosciences 32 (9), 1479–1498.

Nemchin, A., Pidgeon, R., Whitehouse, M., 2006. Re-evaluation of the origin and evolution of ¿?4.2 Ga zircons from the Jack Hills metasedimentary rocks. Earth and Planetary Science Letters 244 (1-2), 218–233.

Nutman, A. P., Kinny, P. D., Compston, W., Williams, I. S., 1991. SHRIMP U-Pb zircon geochronology of the Narryer Gneiss Complex, Western Australia. Precambrian Research 52 (3-4), 275–300.

Occhipinti, S. A., Sheppard, S., Passchier, C., Tyler, I. M., Nelson, D. R., 2004. Palaeoproterozoic crustal accretion and collision in the southern Capricorn Orogen: the Glenburgh Orogeny. Precambrian Research 128 (3-4), 237–255.

Peck, W. H., Valley, J. W., Wilde, S. A., Graham, C. M., 2001. Oxygen isotope ratios and rare earth elements in 3.3 to 4.4 Ga zircons: Ion microprobe evidence for high [delta]18O continental crust and oceans in the Early Archean. Geochimica et Cosmochimica Acta 65 (22), 4215–4229.

Pidgeon, R., Nemchin, A., 2006. High abundance of early Archaean grains and the age distribution of detrital zircons in a sillimanite-bearing quartzite from Mt Narryer, Western Australia. Precambrian Research 150 (3-4), 201–220.

Pidgeon, R., Wilde, S., 1990. The distribution of 3.0 Ga and 2.7 Ga volcanic episodes in the Yilgarn Craton of Western Australia. Precambrian Research 48 (3), 309–325.

Pidgeon, R., Wilde, S., 1990. The distribution of 3.0 Ga and 2.7 Ga volcanic episodes in the Yilgarn Craton of Western Australia. Precambrian Research 48 (3), 309–325.

Pidgeon, R. T., Bosch, D., Bruguier, O., 1996. Inherited zircon and titanite U—Pb systems in an Archaean syenite from southwestern Australia: implications for U—Pb stability of titanite. Earth and Planetary Science Letters 141 (1-4), 187–198.

Pidgeon, R. T., Nemchin, A. A., Hitchen, G. J., 1998. Internal structures of zircons from Archaean granites from the Darling Range batholith: implications for zircon stability and the interpretation of zircon U-Pb ages. Contributions to Mineralogy and Petrology 132 (3), 288–299.

Pidgeon, R. T., Wingate, M. T. D., Bodorkos, S., Nelson, D. R., 2010. The age distribution of detrital zircons in quartzites from the Toodyay-Lake Grace Domain, Western Australia: Implications for the early evolution of the Yilgarn Craton. American Journal of Science 310 (9), 1115–1135.

Qiu, Y. M., McNaughton, N. J., Groves, D. I., Dalstra, H. J., 1999. Ages of internal granitoids in the Southern Cross region, Yilgarn Craton, Western Australia, and their crustal evolution and tectonic implications*. Australian Journal of Earth Sciences 46 (6), 971–981.

Rahn, M. K., Brandon, M. T., Batt, G. E., Garver, J. I., 2004. A zero-damage model for fission-track annealing in zircon. American Mineralogist 89 (4), 473–484.

Rasmussen, B., Fletcher, I. R., Muhling, J. R., Wilde, S. A., 2010. In situ U-Th-Pb geochronology of monazite and xenotime from the Jack Hills belt: Implications for the age of deposition and metamorphism of Hadean zircons. Precambrian Research 180 (1-2), 26–46.

Renne, P., Swisher, C., Deino, A., Karner, D., Owens, T., Depaolo, D., 1998. Intercalibration of Standards, absolute ages and uncertainties in 40Ar/39Ar dating. Chemical Geology 145, 117?152.

Renne, P. R., Mundil, R., Balco, G., Min, K., Ludwig, K., 2010. Joint determination of 40K decay constants and 40Ar*/40K for the Fish Canyon sanadine standard, and imrpved accuracy for 40Ar/39Ar geochronology. Geochimica et Cosmochimica Acta 74 (18), 5349–5367.

Riganti, A., 2003. Geology of the Everett Creek 1:100 000 sheet. Geological Survey of Western Australia 1:100 000 Geological Series Explanatory Notes.

Robb, L., Meyer, F., 1990. The nature of the Witwatersrand hinterland: conjecture on the source area problem. Economic Geology 85, 511–536.

Robb, L. J., Meyer, F. M., 1995. The Witwatersrand Basin, South Africa: Geological framework and mineralization processes. Ore Geology Reviews 10 (2), 67–94.

Robinson, B. W., Graham, J., 1992. Advances in electron microprobe trace-element analysis. J. Comput. Assist. Microscopy 4, 263–265.

Schiotte, L., Campbell, I. H., 1996. Chronology of the Mount Magnet granite-greenstone terrain, Yilgarn Craton, Western Australia: implications for field based predictions of the relative timing of granitoid emplacement. Precambrian Research 78 (4), 237–260.

Schuster, B., Lang, M., Klein, R., Trautmann, C., Neumann, R., Benyagoub, A., 2009. Structural phase transition in ZrO2 induced by swift heavy ion irradiation at high-pressure. Nuclear Instruments and Methods in Physics Research Section B: Beam Interactions with Materials and Atoms 267 (6), 964–968.

Sircombe, K., Hazelton, M., 2004. Comparison of detrital zircon age distributions by kernel functional estimation. Sedimentary Geology 171 (1-4), 91–111.

Sircombe, K. N., 1999. Tracing provenance through the isotope ages of littoral and sedimentary detrital zircon, eastern Australia. Sedimentary Geology 124 (1-4), 47–67.

Sircombe, K. N., 2000. Quantitative comparison of large sets of geochronological data using multivariate analysis: a provenance study example from Australia. Geochimica et Cosmochimica Acta 64 (9), 1593–1616.

Sircombe, K. N., Freeman, M. J., 1999. Provenance of detrital zircons on the Western Australia coastline − Implications for the geologic history of the Perth basin and denudation of the Yilgarn craton. Geology 27, 879–882.

Spaggiari, C. V., 2007. The Jack Hills greenstone belt, Western Australia: Part 1: Structural and tectonic evolution over >1.5Ga. Precambrian Research 155 (3-4), 204–228.

Spaggiari, C. V., Pidgeon, R. T., Wilde, S. A., 2007. The Jack Hills greenstone belt, Western Australia; Part 2, Lithological relationships and implications for the deposition of ≥4.0 Ga detrital zircons. Precambrian Research 155 (3-4), 261–286.

Spaggiari, C. V., Pidgeon, R. T., Wilde, S. A., Anonymous, Grimes, C., John, B., Kelemen, P., Mazdab, F., Wooden, J., Cheadle, M., Hanghoj, K., Schwartz, J., 2004. Trace element chemistry of zircons from oceanic crust: A method for distinguishing detrital zircon provenance. Geological Society of America, 2004 annual meeting 36 (5), 207.

Spaggiari, C. V., Wartho, J.-A., Wilde, S. A., 2008. Proterozoic deformation in the northwest of the Archean Yilgarn Craton, Western Australia. Precambrian Research 162 (3-4), 354–384.

Stern, R. A., Bodorkos, S., Kamo, S. L., Hickman, A. H., Corfu, F., 2009. Measurement of SIMS Instrumental Mass Fractionation of Pb Isotopes During Zircon Dating. Geostandards and Geoanalytical Research 33 (2), 145–168.

Sugitani, K., Mimura, K., Suzuki, K., Nagamine, K., Sugisaki, R., 2003. Stratigraphy and sedimentary petrology of an Archean volcanic-sedimentary succession at Mt. Goldsworthy in the Pilbara Block, Western Australia: implications of evaporite (nahcolite) and barite deposition. Precambrian Research 120 (1-2), 55–79.

Taylor, R., Clark, C., Reddy, S., 2012. The effect of grain orientation on the SIMS U-Pb analysis of Rutile. Chemical Geology 300-301, 81–87.

Thern, E., Jourdan, F., Evans, N., Mcdonald, B., Danisik, M., Frew, R., Nelson D.R., 2011. Post-depositional thermal history of the 4364−3060Ma zircon-bearing metasandstones of the Illaara and Maynard Hills granite greenstone belts, Western Australia. Mineralogical Magazine Goldschmidt Conference Abstracts, p.2003.

Thern, E., Nelson, D., 2012a. Provenance of ca. 4372−3000 Ma detrital zircons within Early Archean siliciclastic metasedimentary rocks from the Illaara and Maynard Hills Greenstone Belts, Western Australia. Manuscript Submitted for Publication.

Thern, E. R., Nelson, D. R., 2012b. Detrital zircon age structure within ca. 3 Ga metasedimentary rocks, Yilgarn Craton: elucidation of Hadean source terranes by principal component analysis. Precambrian Research 214-215, 28–43.

Thorsten Geisler, Robert T. Pidgeon, Wilhelm Van Bronswijk, Ron Pleysier, 2001. Kinetics of thermal recovery and recrystallization of partially metamict zircon: a Ramen spectroscopic study. Eur. J. Mineral 13, 1163–1176.

Trail, D., Mojzsis, S. J., Harrison, T. M., 2007. Thermal events documented in Hadean zircons by ion microprobe depth profiles. Geochimica et Cosmochimica Acta 71 (16), 4044–4065.

Utsunomiya, S., Palenik, C. S., Valley, J. W., Cavosie, A. J., Wilde, S. A., Ewing, R. C., 2004. Nanoscale occurrence of Pb in an Archean zircon. Geochimica et Cosmochimica Acta 68 (22), 4679–4686.

Valley, J. W., Peck, W. H., King, E. M., Wilde, S. A., 2002. A cool early Earth. Geology 30 (4), 351–354.

Vermeesch, P., 2005. Statistical uncertainty associated with histograms in the Earth science. Journal of Geophysical Research 110, 15p.

Wang, K., Li, J., Hao, J., Li, J., Shaoping, Z., 1996. The Wutaishan orogenic belt within the Shanxi Province, northern China: a record of late Archaean collision tectonics. Precambrian Research 78 (1-3), 95–103.

Wang, L. G., Qiu, Y. M., McNaughton, N. J., Groves, D. I., Luo, Z. K., Huang, J. Z., Miao, L. C., Liu, Y. K., 1998a. Constraints on crustal evolution and gold metallogeny in the Northwestern Jiaodong Peninsula, China, from SHRIMP U-Pb zircon studies of granitoids. Ore Geology Reviews 13 (1-5), 275–291.

Wang, X. D., Soderlund, U., Lindh, A., Johansson, L., 1998b. U-Pb and Sm-Nd dating of high-pressure granulite- and upper amphibolite facies rocks from SW Sweden. Precambrian Research 92 (4), 319–339.

Watson, E. B., Harrison, T. M., 2005. Zircon Thermometer Reveals Minimum Melting Conditions on Earliest Earth. Science 308, 841–4.

Weber, J., Ricken, W., 2005. Quartz cementation and related sedimentary architecture of the Triassic Solling Formation, Reinhardswald Basin, Germany. Sedimentary Geology 175 (1-4), 459–477.

Weber, U., Kohn, B., Gleadow, A., Nelson, D., 2005. Low temperature Phanerozoic history of the Northern Yilgarn Craton, Western Australia. Tectonophysics 400 (1-4), 127–151.

Weislogel, A., Graham, S., Chang, E., Wooden, J., Gehrels, G., 2010. Detrital zircon provenance from three turbidite depocenters of the Middle-Upper Triassic Songpan-Ganzi complex, central China: Record of collisional tectonics, erosional exhumation, and sediment production. Geological Society of America Bulletin 122 (11-12), 2041–2062.

Wetherill, G. W., 1975. Late heavy bombardment of the Moon and terrestrial planets. Proc. Lunar Sci. Conf. 6th, 1539–1561.

Wetherill, G. W., 1996. The Formation and Habitability of Extra-Solar Planets. Icarus 119 (1), 219–238.

Wiedenbeck, M., Watkins, K. P., 1993. A time scale for granitoid emplacement in the Archean Murchison Province, Western Australia, by single zircon geochronology. Precambrian Research 61 (1-2), 1–26.

Wilde, S. A., 2010. Proterozoic volcanism in the Jack Hills Belt, Western Australia: Some implications and consequences for the World's oldest zircon population. Precambrian Research 183 (1), 9–24.

Wilde, S. A., Valley, J. W., Peck, W. H., Graham, C. M., 2001. Evidence from detrital zircons for the existence of continental crust and oceans on the Earth 4.4 Gyr ago. Nature 409, 175–178.

Williams, I., Myers, J., 1987. Archaean geology of the Mount Narryer region Western Australia. West Australian Geological Survey Report 22 (32).

Wingate, M., Bodorkos, S., Kirkland, C., 2008a. 177901: quartzite, Kowalyou. Geochronology Record 739: Geological Survey of Western Australia, 5p.

Wingate, M., Bodorkos, S., Kirkland, C., 2008b. 177904: quartzite, Windmill Hill. Geochronology Record 739: Geological Survey of Western Australia, 7p.

Wingate, M., Bodorkos, S., Kirkland, C., 2008c. 177907: quartzite, Noondeening Hill. Geochronology Record 739: Geological Survey of Western Australia, 7p.

Wingate, M., Kirkland, C., Bodorkos, S., 2008d. Introduction to geochronology data released in 2008. Geological Survey of Western Australia, 5p.

Wingate, M., Kirkland, C., Bodorkos, S., 2008e. Introduction to geochronology data released in 2008. Geological Survey of Western Australia, 5p.

Wingate, M. T. D., Bodorkos, S., 2007. 184107: metamorphosed quartz sandstone, Christmas Bore. Vol. Geochronology dataset 678. Western Australia Geological Survey.

Wyche, S., 2007. Chapter 2.6 Evidence of Pre-3100 Ma Crust in the Youanmi and South West Terranes, and Eastern Goldfields Superterrane, of the Yilgarn Craton. In: Martin J. van Kranendonk, R. H. S., Bennett, V. C. (Eds.), Earth's Oldest Rocks. Vol. 15. Elsevier, pp. 113–123.

Wyche, S., Nelson, D. R., Riganti, A., 2004. 4350–3130Ma detrital zircons in the Southern Cross Granite?Greenstone Terrane, Western Australia: implications for the early evolution of the Yilgarn Craton. Australian Journal of Earth Sciences 51 (1), 31–45.

Yeats, C. J., McNaughton, N. J., Groves, D. I., 1996. SHRIMP U?Pb geochronological constraints on Archean volcanic-hosted massive sulfide and lode gold mineralization at Mount Gibson, Yilgarn Craton, Western Australia. Economic Geology 91, 1354?1371.

Yutaka Abe, Eiji Ohtani, Takua Okuchi, Kevin Righter, Michael Drake, 2000. Origin of the Earth and Moon. The University of Arizona Press, Ch. Water in the Early Earth, pp. 413–433.